A study of Sandikli Graben, west central Turkiye, using the vertical electrical sounding geophysical method

by © Fethi Tayfun Turanlı

A Thesis submitted

to the School of Graduate Studies in partial fulfillment of the

requirements for the degree of

Master of Science (Geophysics)

Department of Earth Sciences

Memorial University of Newfoundland

May 2022

St. John's Newfoundland and Labrador

Abstract

Turkiye has a wide range of geothermal and agricultural resources. As part of Alpine-Himalayan orogenic belt it has mountainous regions and high heat flow, with the main sources of geothermal energy being recent volcanism. The study area, the Sandikli graben, is located in west central Anatolia, where there are 1500 wells tapping fresh waters from shallow aquifers for domestic and agricultural use and, within a known geothermal field, 23 deeper thermal wells which provide heat to greenhouses and spas. In this study, data from 384 Vertical Electrical Sounding geophysical surveys were analysed. The data were collected in an area of 36 km x 10 km and provided information on resistivity extending to 1.4 km depth. The aim was to delineate the subsurface resistivity structure of the graben including the locations of hot and cold aquifers as well as fault structures that can provide upward transfer of geothermal waters.

It is found that near surface resistivity is associated with topography and drainage. Raw data in the known geothermal field showed large jumps which may be indicative of near surface geothermal activity. Large lateral resistivity variations are related to known faults. Low resistivity subsurface layers, indicating aquifers, can be seen almost everywhere in the graben. Their depth range of 50 to 300 m suggests that they are cold water aquifers, and there was no indication of deeper geothermal resources outside the known geothermal field.

General Summary

Turkiye is among the top ten countries globally in geothermal energy production. Although geothermal energy has various area of utilization, the most important areas are space heating and agricultural use. Turkiye is also the world's 7th largest agricultural producer, and relies on fresh groundwater for irrigation. Hot geothermal water is used in agricultural areas to heat greenhouses to help production. This study was carried out in the Sandikli graben, a large valley in a region of west central Turkiye where there are several geothermal fields. There are geothermally heated greenhouses and thermal resorts in a localized area in the Sandikli graben. Data from 384 Vertical Electrical Soundings (a geophysical survey method where current is pumped into the ground) were analysed to image the subsurface over the entire graben, primarily looking for more geothermal resources. The results of this study indicate that there are layers that contain fresh groundwater (at depths of ~50 to 300 m) throughout most of the graben, but indications of deep (~1 km) hydrothermal resources were found only in the known geothermal field close to the greenhouses.

Acknowledgements

I would like to extend my sincere thanks to the Ministry of National Education of Turkey. This work would not have been possible without their financial support. I also wish to thank all the people who work in the Education Attaché Office at Turkish Consulate General for their support.

I am deeply indebted to my supervisor Dr. Alison Leitch for her invaluable contribution and suggestions. She gave me the chance to be part of her research group. As my supervisor and mentor, she has shared her personal and professional experiences with me. She always supported and nurtured me with her guidance. I will never forget her help on and off campus. Many thanks to Prof. Colin Farquharson, for his practical teaching materials and helpful advice. I am grateful to Zulfikar Erhan for providing the specific data set I needed for my project. I also wish to thank Jason Greenwood for his contributions in data processing.

My final and biggest thanks to my family and friends, for all their incredible and unconditional support throughout my project.

Table of Contents

Abstract ii

General Summary iii

Acknowledgements iv

Table of Contents v

List of Tables viii

List of Figures x

List of Appendices xvii

Chapter 1: Introduction 1

1.1 Overview and objectives 1

1.2 Regional setting 3

1.3 Geothermal energy in the Afyonkarahisar Province 6

1.4 Geology of the Sandikli Basin 8

1.5 The study area and surveys 16

1.6 Following chapters 21

Chapter 2: Background 23

2.1 Geothermal Energy Utilization 23

2.2 Worldwide Geothermal Energy 25

2.3 Geothermal Energy in Canada 27

2.4 Geothermal Energy in Turkiye 30

2.5 Geothermal Exploration Methods 33

2.6 Resistivity and Ground Properties 34

2.7 Previous Studies using Vertical Electric Soundings 37

Chapter 3: Methods 39

3.1 Basic Principle of Resistivity Measurements 39

3.1.1 Induced Polarization (IP) Data 44
3.2 Vertical Electrical Sounding (VES) Method 45
3.2.1 Identifiable Layers 46
3.3 Description of Field Acquisition and Equipment 48
3.4 Preinversion Processing 52
3.4.1 Inspection of Raw Data: Removal of Offsets 52
3.4.2 Inspection of Raw Data: Identification of layering 54
3.4.3 Surface Heterogeneities 55
3.4.4 Omitting Unreliable Data and Smoothing VES Curves 58
3.5 Theory of 1D and 2D Inversion 61
3.5.1 1D Resistivity Inversion Modelling 62
3.5.2 2D Inversion 67
3.6 Inversion Settings for 1D and 2D 70
3.6.1 1D Inversion 70
3.6.2 2D Inversion 72
3.7 1D Rolling Inversions 75
Chapter 4: Results 77
4.1 Near surface properties and features 77
4.2 Characterization of Areas and Sounding Groups 81
4.2.1 Area 1: Group 17 84
4.2.2 Area 2: Groups 1 to 5 85
4.2.3 Area 3: Groups 12 and 13 88
4.2.4 Area 4: Group 6, 7, 11 and 16 90
4.2.5 Area 5: Groups 8, 9, and 10 94
4.2.6 Area 6: Groups 14 and 15 95

4.3 1D VES Models 97
4.4 Resistivity Layer Pattern Map 101
4.5 1D Rolling Inversion and 2D Inversion Models 104
4.5.1 Area 1: Group 17 105
4.5.2 Area 2: Groups 2 and 3 106
4.5.3 Area 3: Groups 12 and 13 109
4.5.4 Area 4: Groups 6 and 11 111
4.5.5 Area 5: Groups 8, 9 and 10 117
4.5.6 Area 6: Groups 14 and 15 119
Chapter 5: Summary and Conclusions 122
References 131
Appendix A: Google Earth Images of Survey Areas 140
Appendix B: Sounding Locations and Acquisition Dates 144
Appendix C: Raw Data and Data after Removal of Offsets & Smoothing 155
Appendix D: Layer Structure of Soundings 208
Appendix E: 1D Inversion Resistivity Models 219
Appendix F: 1D Rolling Inversion and 2D Inversion Models 347

List of Tables

Table 1.1 Physical properties of Sandikli, Omer-Gecek, Gazlıgöl and Heybeli geothermalfields. 8

Table 1.2 English translation of core log in Figure 1.8. 14

Table 1.3 Soundings categories: Areas, Groups and acquisition dates (day/month) in 2011. 20

Table 2.1 Top ten countries in the world and Canada in terms of geothermal energy utilization in 2015. 26

Table 2.2 Number of drilled wells in Turkiye from 2010 to 2015. 30

Table 2.3 Data on some significant geothermal power plants in Turkiye. 31

Table 2.4 Some certain direct uses implementations of geothermal energy in Turkiye. 32

Table 2.5 Porosity ranges for sedimentary materials, soils and rocks (McNeill, 1980). 35

Table 3.1 The first 20 entries in an example data file 49

Table 3.2 Equipment used in VES measurements..... 51

Table 3.3 Weighted average calculation scheme for sounding 338. 60

Table 4.1 Information on time of acquisition, location and orientation of sounding groups, and shapes of sounding curves within the group. For Shapes, see Figure 4.4: ‘x’ indicates flattening or downturn of sounding at highest AB spacing. 82

Table 4.2 Correspondence of sounding shape with 4 layer ground structure. Numbers are the fraction of soundings with shape (A to F) that have layering pattern (a to f). Strongest correspondences bold and underlined. The number of soundings in each category is given by n. 103

Table 4.3 Overlapped lines for 2D inversion. Overlapped soundings are indicated with red. 105

Table B.1 Acquisition date (in 2011), locations (UTM zone 36 S), spacings between

successive soundings in each group, and Group number for the vertical electric soundings in this study.....145

List of Figures

Figure 1.1 The location map of the Afyon-Sandikli geothermal field, red dots showing the chosen sounding points. 2

Figure 1.2 Tectonic map of the Anatolian platform. Modified from Legeay et al. (2019). The location of the field area is indicated by the red rectangle.....4

Figure 1.3 Elevation map of Turkiye. Reprinted from http://en.wikipedia.org. The field area is indicated by the yellow star.....4

Figure 1.4 The fault and graben map in the middle Anatolia. Grabens: AcG: Acigöl, ÇG: Çivril, DG: Dinar, ByG: Beysehir, SkG: Sandikli, DG: Burdur, KdG: Kovada, AAG: Afyon. Reprinted from Caglar et al. 2005. The field area is within the red rectangle. 6

Figure 1.5 Geothermal fields in the Afyonkarahisar province (Başaran et al., 2015)....7

Figure 1.6 Geological map of the Sandikli Basin (Davraz et al., 2016).Hudai spa is near the middle.....9

Figure 1.7 Conceptual model of water flow in a cross section across the Sandikli plain through the Hudai spa (Davraz et al., 2016). See Figure 1.6. 11

Figure 1.8 Left: core log AFS 17 (see Fig. 1.9 for location). Right: expanded temperature log (in ^{o}C) for depths from 600 m to 125 m. 13

Figure 1.9 Top: Sandikli graben field area with VES locations (red dots). Yellow rectangle indicates the area shown in the bottom panel. Bottom: Geothermal greenhouses (red polygons) and thermal resorts and hotels (blue markers) located in Sandikli geothermal field. The yellow star is the location of the drill core in Figure 1.8. The city in the top right is Sandikli. 17

Figure 1.10 Geological map of Sandikli Basin with extent of DCR spreads in this study shown as thin red lines.....18

Figure 1.11 Map with VES soundings where the data were measured. Dots represent the centres of each of the soundings. Sounding group numbers are indicated. Roadside measurements are highlighted with a blue rectangle.....19

Figure 1.12 Maps of six different areas within the Sandikli geothermal field. Grey dashed lines indicate the full extent of the electrode spread. 21

Figure 2.1 Geothermal energy utilization retrieved from Lindal (1992). 23

Figure 2.2 Categories of worldwide direct uses of geothermal energy from Lund & Boyd (2016). 25

Figure 2.3 The distribution of geothermal energy potential in Canada from Grasby et al. (2012). 28

Figure 2.4 Distribution of geothermal resources and active faults within Turkiye (Mertoglu et al ., 2019). 31

Figure 2.5 Geothermal electricity production in Turkiye until 2019 (Mertoglu et al., 2019). 33

Figure 2.6 Typical resistivities of common rocks (Palacky, 1987). 34

Figure 2.7 Electrical resistivity is plotted as a function of salinity and temperature for saline fluids (Unsworth and Rondenay, 2012). 36

Figure 2.8 The temperature and pressure effect on the resistivity of a KCl solution. Salinity values are shown 25%, 13.5%, and 3.6, respectively (Unsworth & Rodenay, 2012). 37

Figure 3.1 Diagram showing the relationship of L and A to current flow direction for equation (3.1) Here, A = h× w (Reynolds, 2011). 40

Figure 3.2 Ohm's Law for a circuit element. Retrieved from https://www.electronics-notes.com/articles/basic_concepts/resistance/what-is-ohms-law-formula-equation.php 40

Figure 3.3 Electrode arrangement for resistivity measurements, Kirsch (2006). 41

Figure 3.4 Current flow and equipotential lines in a homogeneous subsurface from a single current source (left) and from a pair of current electrodes (right) (Wightman, 2004). 42

Figure 3.5 The Schlumberger, Wenner, dipole-dipole, and pole-dipole electrode arrays. Geometric factor is denoted by K for each array, Kirsch (2006). 43

Figure 3.6 Multichannel resistivity measurements. Retrieved from 44

https://www.zzgeo.com/?gclid=CjwKCAjw_JuGBhBkEiwA1xmbRW-1t_3w8-dsm_sEx-I1a1Y1kvemDz5LWQ-ecr9PBxcDH316qO9-FxoClzQQAvD_BwE. 44

Figure 3.7 Two ways of measuring the time domain IP effect (Reynolds, 2011).....45

Figure 3.8 Increased current electrode spacing and depth penetration. Results of the measurement are shown in the logarithmic chart, Kirsch (2006).....46

Figure 3.9 Expected sounding curves over a two layer Earth, where the top layer has a resistivity of 100 Ω.m, the intervace is at 1 m, and the bottom layer has the resistivity indicated on the curve (Unsworth, 2009).....47

Figure 3.10 Sketches illustrating the possible shapes of sounding curves over ground with three layers: h_2 is the thickness of the middle layer (Reynolds, 2011).....48

Figure 3.11 The curve of sounding 21. Red circles show the offsets where the potential electrode spacings are increased.....53

Figure 3.12 The curve of sounding 22. Red circles show the offsets where the potential electrode spacings are increased.....53

Figure 3.13 Soundings 1,2,9 and 11 from Afyon-Sandikli geothermal field. These soundings are located in Area 2. 54

Figure 3.14 Signal contribution sections for Wenner (A) and Schlumberger (B) arrays (Barker, 1979). 55

Figure 3.15 (a) Location of S-57 and S-58 (Area 2) and geothermal greenhouses, outlined in red. (b) and (c) sounding curves for S-57 and S-58, illustrating large jumps associated with moving the potential electrodes over a heterogeneous surface. 57

Figure 3.16 Examples final curves after omitting unreliable data.....58

Figure 3.17 Apparent resistivity curves on the left and smoothed apparent resistivity curves on the right. 59

Figure 3.18 Comparison of the resistivity and IP data. 61

Figure 3.19 The basis of automated interpretation programs (Zohdy, 1989). 64

Figure 3.20 The working principle of automated interpretation programs: (a)

computation of layering, (b) computation of the calculated (theoretical) sounding curve, based on the layered ground structure in (a); (c) layer depths are shifted to reach minimum rms between theoretical and observed data, (d) layer resistivities are adjusted using the differences between theoretical and observed data, and (e) final model (Zohdy, 1989). 66

Figure 3.21 Comparison of initial three-layer model used to calculate a sounding curve, and multilayer model based on the sounding curve, inverted by automated interpretation programs (Zohdy, 1989). 67

Figure 3.22 A model as being made up of cells for 2D resistivity inversion.....68

Figure 3.23 Inversion parameters used for 1D inversion modelling. 71

Figure 3.24 Electrode locations (blue dots) for 4 collinear soundings in Group 17: s365 to s356. 72

Figure 3.25 EarthImager2D model mesh geometry for collinear soundings s365, s366, s355 and s356. Red dots at the top of the domain indicate electrode locations The black bars indicate cells that are narrower than the line thickness of this graph.....73

Figure 3.26 New mesh model for 2D inversion. 73

Figure 3.27 2D inversion result for soundings s365-366-355-356 (see Fig. 3.24). (a): Resd2Dinv; (b) EarthImager2. The three panels for each inversion are, from top to bottom, pseudosection based on data, pseudosection based on inverted model and the inverted model. A close correspondence between the two top panels is a validation of the model. 74

Figure 3.28 Inversion parameters used for 2D inversion modelling. 75

Figure 4.1 Maps of apparent resistivity (left) and IP effect over the surveyed areas in the Sandikli graben for AB/2=25 m. Apparent resistivity values in the most resistive regions are higher than indicated: over 200 Ω.m in the far north and over 600 Ω.m in the south west. Maps produced using Oasis Montaj, with minimum curvature, log, displayed as linear gridding, a cell size of 300 m, and 1 cell extended beyond data. ..78

Figure 4.2 Topography map of the Sandikli graben with sounding groups indicated..79

Figure 4.3 Map of Sandikli graben showing rivers(thin blue lines), main highway (light

brown) and faults (thick coloured lines). Sounding groups are indicated. Map produced using ArcGIS. 80

Figure 4.4 The general shapes of the soundings curves. 83

Figure 4.5 Map of Sandikli graben including faults, rivers (thin blue lines) and main roads (brown lines) with soundings colour coded by shape (see Figure 4.4). Group 5 soundings have too many offsets for classification of shape. 84

Figure 4.6. Maps of (a) ρ_a for AB=50 m, (b) IP for AB=50 m, (c) topography with contour lines of 50m and (d) faults, roads and rivers with soundings colour coded by shape, in Area 1 (Group 17, s342 to s395). Oasis Montaj, log (save as linear) minimum curvature gridding, cell size 300 m. 85

Figure 4.7. Maps of (a) ρ_a for AB=50 m, (b) IP for AB=50 m, and (c) topography and (d) soundings colour coded by shape, in Area 2 (Group 1 to 5). Oasis Montaj, log (save as linear) minimum curvature gridding for ρ_a, and linear for IP, cell size 200 m. 86

Figure 4.8 Geological map of the Hudai Sandikli geothermal field and environs, including geothermal wells (red dots). Blue dots are VES locations, with Group numbers indicated, from Areas 2 and 3. Modified from Demer et al. (2013). 87

Figure 4.9 Maps of Area 3 (Groups 12 and 13). (a) ρ_a for 50 m, (b) IP for AB=50 m, (c) topography (d) soundings classified by shape. Oasis Montaj, log (save as linear) minimum curvature gridding for ρ_a, and linear for IP, cell size 300 m. 89

Figure 4.10 Maps of (a) ρa for AB=50 m, (b) IP for AB=50 m, (c) topography (d) soundings classified by shape, in Area 4 to 6 (Group 6,7,8,9,10,11,14,15 and 16). Oasis Montaj, log (save as linear) minimum curvature gridding for ρa, and linear for IP, cell size 300 m. 92

Figure 4.11. Maps of apparent resistivity (left) and IP effect over the surveyed areas in the Area 6 for AB/2=25 m. Apparent resistivity values in the most resistive regionres are higher than indicated: over over 600 Ω.m in the west. Dashed line indicates the approximate location of the Kiziloren Fault. Maps produced using Oasis Montaj, with minimum curvature, log, displayed as linear gridding, a cell size of 100 m, and 1 cell extended beyond data. 96

Figure 4.12 Apparent resistivity and IP effect for shortest AB/2 spacings for soundings in Groups 14 and 15, illustrating changes associated with crossing the Kiziloren Fault. 97

Figure 4.13 Location map and 1D inversion resistivity models for selected soundings. 101

Figure 4.14 Resistivity 4-layer pattern map. In the legend, ri represents the resistivity of the ith layer, with r1 being the resistivity of the layer closest to the surface.....102

Figure 4.15 Location map of LineGroup2 and LineGroup3 106

Figure 4.16. 1D rolling and 2D EarthImager inversion models of LineGroup2.....107

Figure 4.17. 1D rolling and 2D inversion models of Group 3 soundings.....108

Figure 4.18. 1D rolling inversion models of Group 12 (top) and Group 13 soundings. Oasis Montaj, cell size 25m, kriging. 110

Figure 4.19 Location map of Group 6 and Group 11. 111

Figure 4.20 1D rolling and 2D inversion models of Group 6 soundings. 112

Figure 4.21 1D rolling and 2D inversion models of Group 11-1 soundings. 114

Figure 4.22 1D rolling and 2D inversion models of Group11-2 soundings. 115

Figure 4.23 1D rolling and 2D inversion models of Group11-3 soundings. 116

Figure 4.24 1D rolling inversions for Group 8 (top), Group 9 (bottom left) and Group 10 (bottom right). Oasis Montaj, cell size 25 m, kriging interpolation. 118

Figure 4.25 Location map of Group 14 and 15 soundings. 119

Figure 4.26 1D rolling and 2D inversion models of LineGroup14. 120

Figure 4.27 1D rolling and 2D inversion models of LineGroup15. 121

Figure 5.1 Left: Geological map of the Sandikli basin (Davraz et al., 2016) with surveyed areas 1 to 6 marked with orange rectangles. Right: Highly simplified version of the drill core log (Figure 1.8, Table 1.2). The location of the drill is indicated by the black star. Wavy blue and red symbols indicate possible locations of cold (blue) and hot (red) aquifers. 123

Figure 5.2 Simplified model of the Sandikli-Hudai geothermal system (Memis, 2010). Location of profile lines A-A'-B-B' are given in Figure 4.8. 124

Figure 5.3 1D rolling inversion sections of Groups 2,3 and 4. Distance is measured from NNW to SSE and sections are in order of E to W down the page. The maximum depth for LineGroups 2 and 3 is 750 m, and for LineGroup 4 it is 500 m. 127

Figure 5.4 1D rolling inversion sections of Groups 6,7,8,9,10,11,14 and 15. Sections are in order of N to S across the page and E to W down the page, except Group 9, which is slightly farther to the west than Group 10. The colour method in Oasis Montaj is histogram normalization, and so the resistivity scales vary as shown 129

Figure B.1 Graph of illustrating the acquisition dates of the 384 resistivity soundings, arranged by Group number. Data provided in Table B.1 below. 145

List of Appendices

Appendix A: Google Earth Images of Survey Areas**Error! Bookmark not defined.**40

Appendix B: Sounding Locations and Acquisition Dates**Error! Bookmark not defined.**4

Appendix C: Raw Data and Data after Removal of Offsets & Smoothing .....**Error! Bookmark not defined.**5

Appendix D: Layer Structure of Soundings.....208

Appendix E: 1D Inversion Resistivity Models .....**Error! Bookmark not defined.**19

Appendix F: 1D Rolling Inversion and 2D Inversion Models**Error! Bookmark not defined.**47

Chapter 1: Introduction

1.1 Overview and objectives

Managed properly, geothermal energy is a clean, reliable, and renewable energy source. The source of geothermal energy is the natural heat existing within rocks and water in the Earth's crust (Meju, 2002). In the agricultural Sandikli graben in Turkiye (Figure 1.1), hot water is pumped from depth to heat greenhouses and support tourism through spas. However, open cultivated fields and households require fresh water from shallow aquifers, and contamination of fresh water resources from geothermal waste water can be a concern (Davraz et al., 2016). It is therefore useful to understand the subsurface structure throughout the graben.

The most common uses of geothermal resources are power generation and heating. According to Dickson and Fanelli (1994), geothermal systems are separated into three groups: high temperature geothermal systems (>150 °C) can be used to produce electricity, and it is also possible to generate power in moderate temperature systems (90 °C to 150 °C) by using circulation systems. Low temperature geothermal systems (<90 °C) are used for heating purposes. In general, geothermal systems in Turkiye are moderate and low temperature systems (<150 °C), however, there are a few high temperature systems. Consequently, these geothermal systems can provide both power generation and heat distribution (Gunerhan et al., 2001).

Different geophysical methods currently used in geothermal exploration are based on the investigation depth or the primary targets (Gupta & Roy, 2006). Geoelectrical methods measure resistivity variations in the subsurface. This is important in geothermal exploration because the factors that affect resistivity are primarily temperature, salinity of water, pressure and particularly alteration mineralogy, which

are related to prospectivity of geothermal resources. To measure resistivity, a pair of current electrodes are positioned on the surface, and current flows between the electrodes. Then, potential difference is measured between another two electrodes (potential electrodes). Simply, resistivity can be calculated by using measured electric current and potential difference values and the geometry of the electrodes, using a version of Ohm's Law. In a vertical electric sounding (VES), the electrodes are centered at a given location and moved further apart to sense deeper into the subsurface.

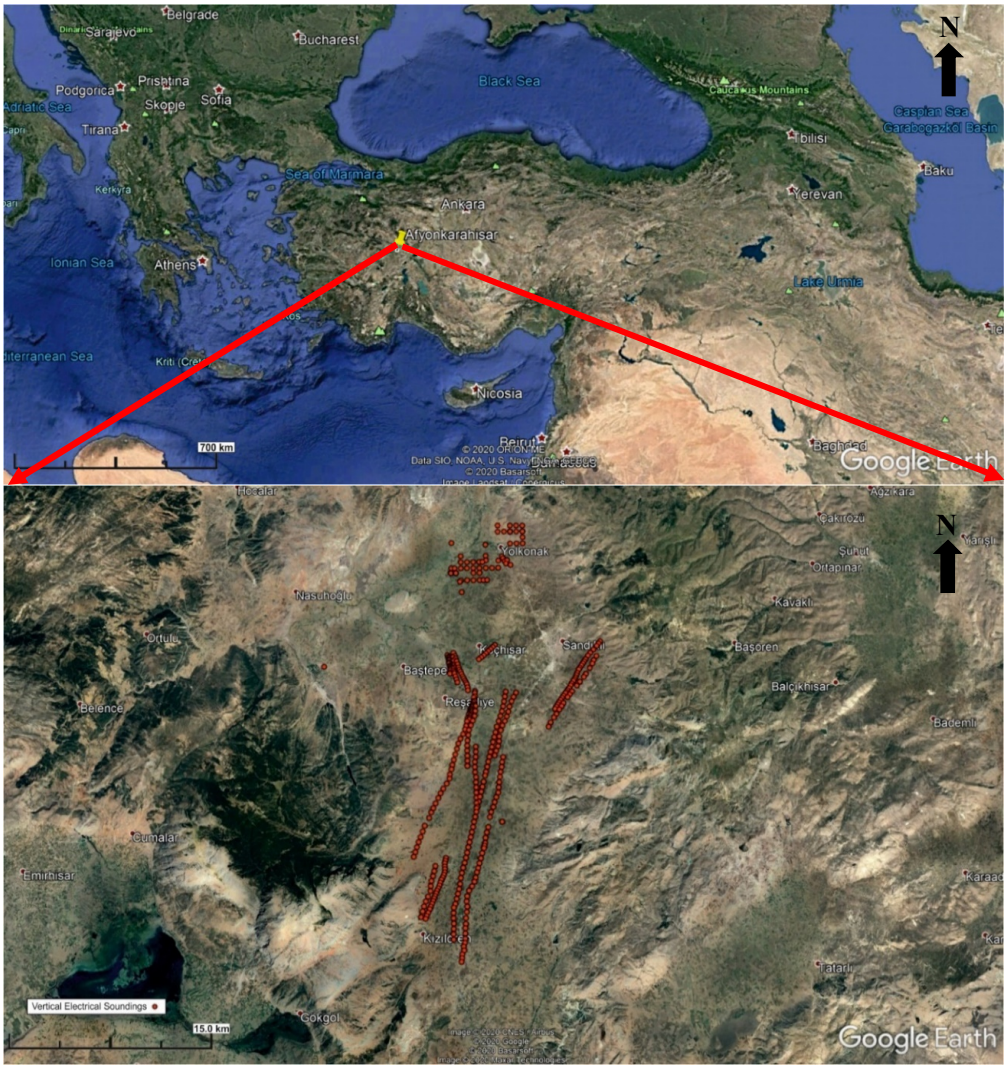

Figure 1.1 The location map of the Afyon-Sandikli geothermal field, red dots showing the chosen sounding points.

The aim of this master's research is to analyse VES resistivity data collected within the Afyon-Sandikli geothermal area, in Turkiye located at about 255000 E, 4250000 N in UTM zone 36 S (30.2° E, 38.375° N, Figure 1.1) and reveal the general characterization of resistivity in the graben, including location of shallow aquifers, while identifying possible areas of geothermal prospectivity. Another aim is to test the utility of the VES method in geothermal exploration. The data consist of three hundred and eighty-four soundings mostly taken along lines in the N-S direction in Afyon-Sandikli geothermal field (Figure 1.1). The scale of the soundings, with current injection spacings from 50 m up to 5000 m, resulted in a range of investigation down to about 1.2 km. Some sounding locations were chosen to investigate spots where fault systems intersect within the Sandikli graben, as faults can be conduits for the transfer of deep hot fluids to the near surface.

In this thesis, 1D and 2D inversion techniques are used to generate resistivity models of the subsurface. The resistivity models are interpreted to understand the general subsurface structure and possible heat sources in the Sandikli graben.

1.2 Regional setting

Turkiye consists of several continental fragments, which were joined together in the Miocene during the ongoing collision of the African and Arabian plate with the Eurasian plate. The different terranes are presented in Figure 1.2. Deep crustal-scale or lithosphere-scale sutures separate these fragments. The structure and tectonics of Turkiye is complex, with an active transform boundary across the north, collision of the Arabian plate in the south-east, and ongoing subduction in the Mediterranean south-west of Turkiye.

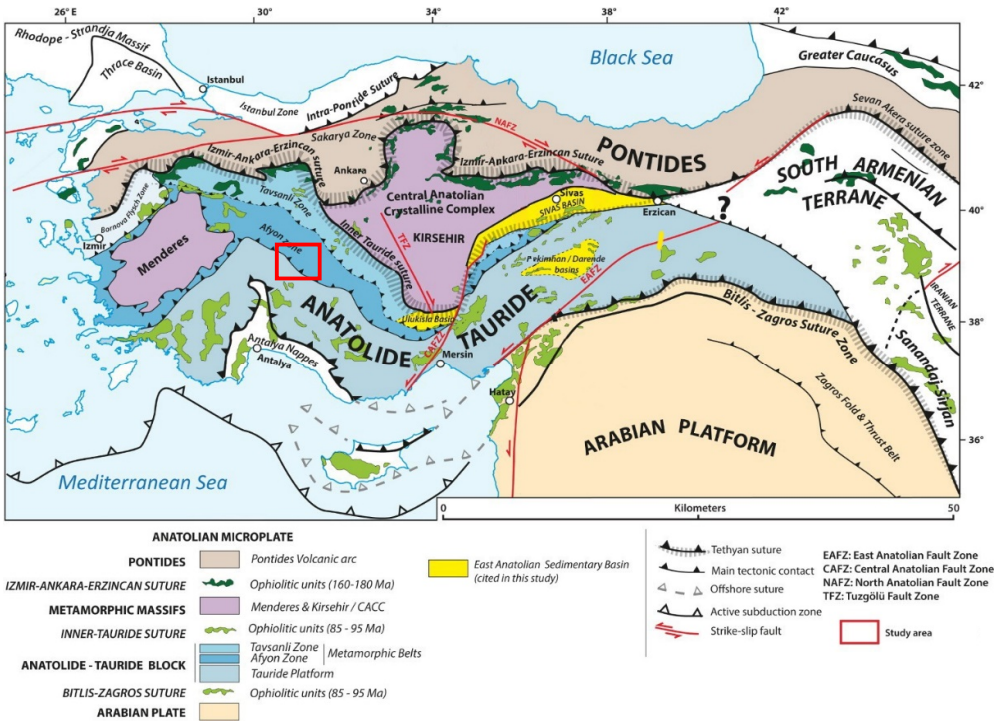

Figure 1.2 Tectonic map of the Anatolian platform. Modified from Legeay et al. (2019). The location of the field area is indicated by the red rectangle.

As shown in Figure 1.3, most of Turkiye has high elevation, and the southeast part of Turkiye has a long mountain range. It can be also seen that Turkiye has rough topography with mountains on the edges and a plateau in the middle.

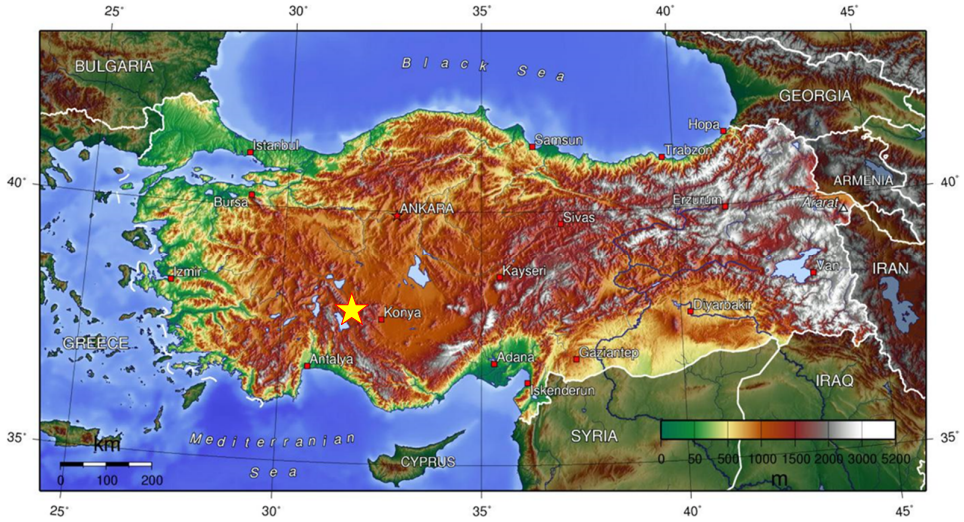

Figure 1.3 Elevation map of Turkiye. Reprinted from http://en.wikipedia.org. The field area is indicated by the yellow star.

The high elevation of Turkiye has been explained by the activities of the bottom of the lithosphere. According to Göğüş et al. (2017), in the last 10 Ma, the bottom part of lithosphere dripped off into the mantle, the hot asthenospheric mantle rose to take the place of the bottom of the lithosphere, and the surface rose by more than 1 km. This mechanism also explains the recent (mostly dormant) volcanism and magmatism in Turkiye, which is related to partial melting of the shallow asthenosphere (Göğüş et al, 2017).

The Sandikli Graben is located in a geologically complicated area known as the Isparta Angle (Caglar et al., 2005). The many fault systems and grabens in this area are represented in Figure 1.4 (see also Figure 1.2): the study area for this project is within the red rectangle.

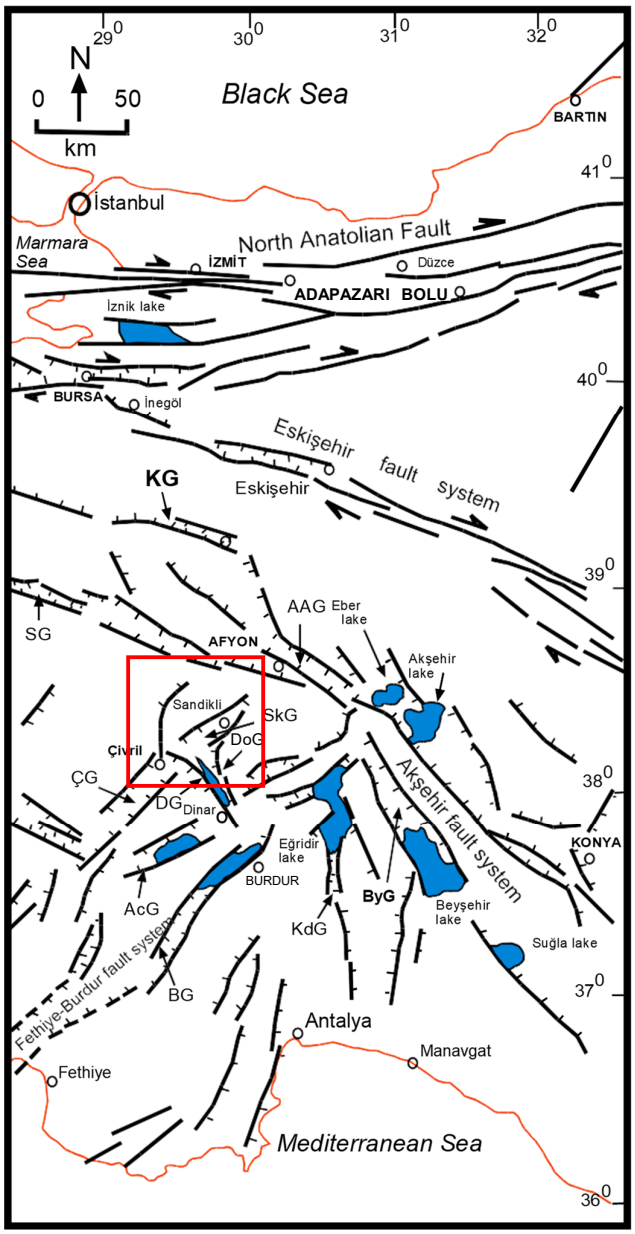

Figure 1.4 The fault and graben map in the middle Anatolia. Grabens: AcG: Acigöl, ÇG: Çivril, DG: Dinar, ByG: Beysehir, SkG: Sandikli, DG: Burdur, KdG: Kovada, AAG: Afyon. Reprinted from Caglar et al. 2005. The field area is within the red rectangle.

1.3 Geothermal energy in the Afyonkarahisar Province

Afyonkarahisar is located in the West Anatolia tectonic zone, and there are various tectonic structures such as grabens, faults and geothermal areas in this region. The major Akşehir Simav Fault System (ASFS) is 3-30 km wide and 500 km long. One of the most significant grabens is Afyon-Akşehir graben with WNW-ESE direction. There are four

major geothermal fields in Afyonkarahisar, and they are Omer-Gecek, Gazlıgöl, Heybeli and Sandikli (Figure 1.5). The Sandikli graben is located southwest of the Afyon-Akşehir graben. Geothermal energy is used for space heating, greenhouse and thermal bathing in Afyonkarahisar.

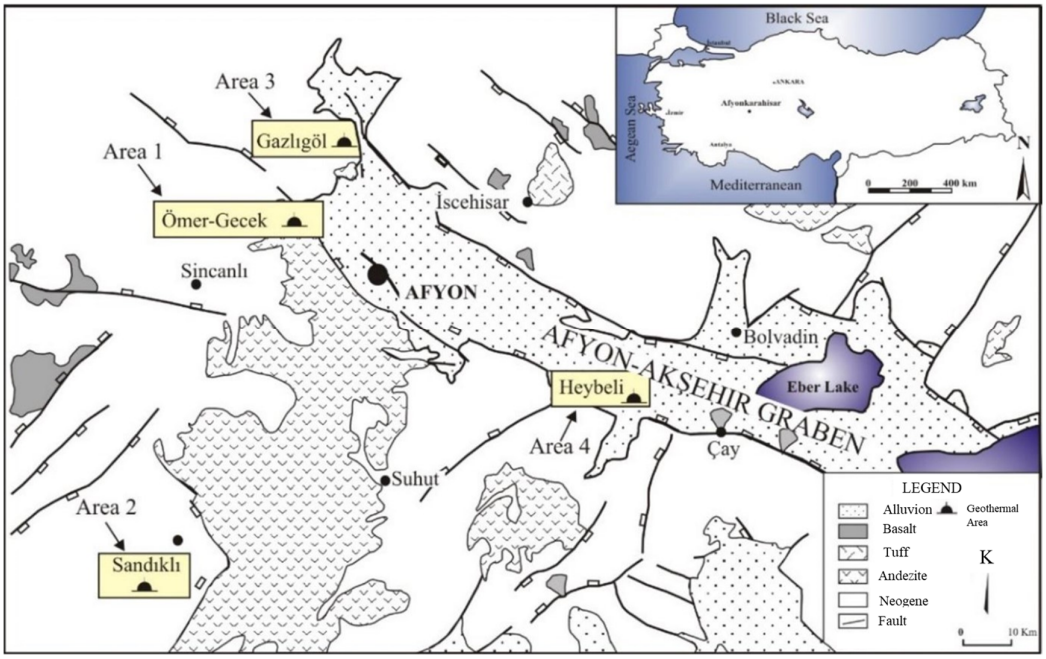

Figure 1.5 Geothermal fields in the Afyonkarahisar province (Başaran et al., 2015).

Geological structure and fault systems have an effect on the geothermal resources in Afyonkarahisar. The heat sources of these geothermal fields area volcanic rocks and the high geothermal gradiant in this region (Başaran et al., 2015). Geothermal resources rise to the surface through Akşehir Simav Fault System (ASFS). As can be seen in Figure 1.5, Afyon-Akşehir graben is located in the Akşehir Simav Fault System. The temperatures of geothermal fields vary from 30°C to 125°C. Different physical and chemical properties are observed in geothermal fields in Afyonkarahisar, depending on reservoir rock, depth and temperature. In Table 1.1, physical properties of four major geothermal fields in Afyonkarahisar are given.

Table 1.1 Physical properties of Sandikli, Omer-Gecek, Gazlıgöl and Heybeli geothermalfields.

	Sandikli	**Omer-Gecek**	**Gazlıgöl**	**Heybeli**
Reservoir rock	Quartzite-Limestone	Marble	Quartzite	Recrystallized limestone
Number of drillings	26	30	56	10
Depths of drillings (m)	49-1200	100-1100	50-800	200-650
Temperatures (°C)	65-85	45-125	43-86	30-55
Total flow rate (l/s)	100	450	260	200
Electrical Resistivity (ohm.m)	4-29	1-4	2.5-3.6	2.8-17
pH	6.4-7.9	7.1-7.9	6.92-8.10	6.4-7.83

Note: Modified from Hydrogeochemical Properties of Geothermal Fluids in Afyon-Akşehir Graben (Akarcay Basin) and the Sustainability of Ömer-Gecek Area, by Başaran et al., (2015), *World Geothermal Congress,* Melbourne, Australia.

1.4 Geology of the Sandikli Basin

Figure 1.6 shows a geological map of the Sandikli Basin, with the Sandikli plain in the northern part and the NS Sandikli graben in the southern part, approximately south from the Hudai spa. The oldest identified unit is the Precambrian Kestel formation, which is overlain in turn by three Paleozoic units: the metamorphic Hudai formation, composed of schists and quartzite, the Caltepe formation of dolomite and limestone, and the Seydişehir formation of sandstones, siltstones and shale (Davraz et al., 2016). The Seydişehir formation is discordantly overlain by Mesozoic sandstones, siltstones and limestones. Cenozoic units, from oldest to youngest, consist of: conglomerates, sandstones, siltstones

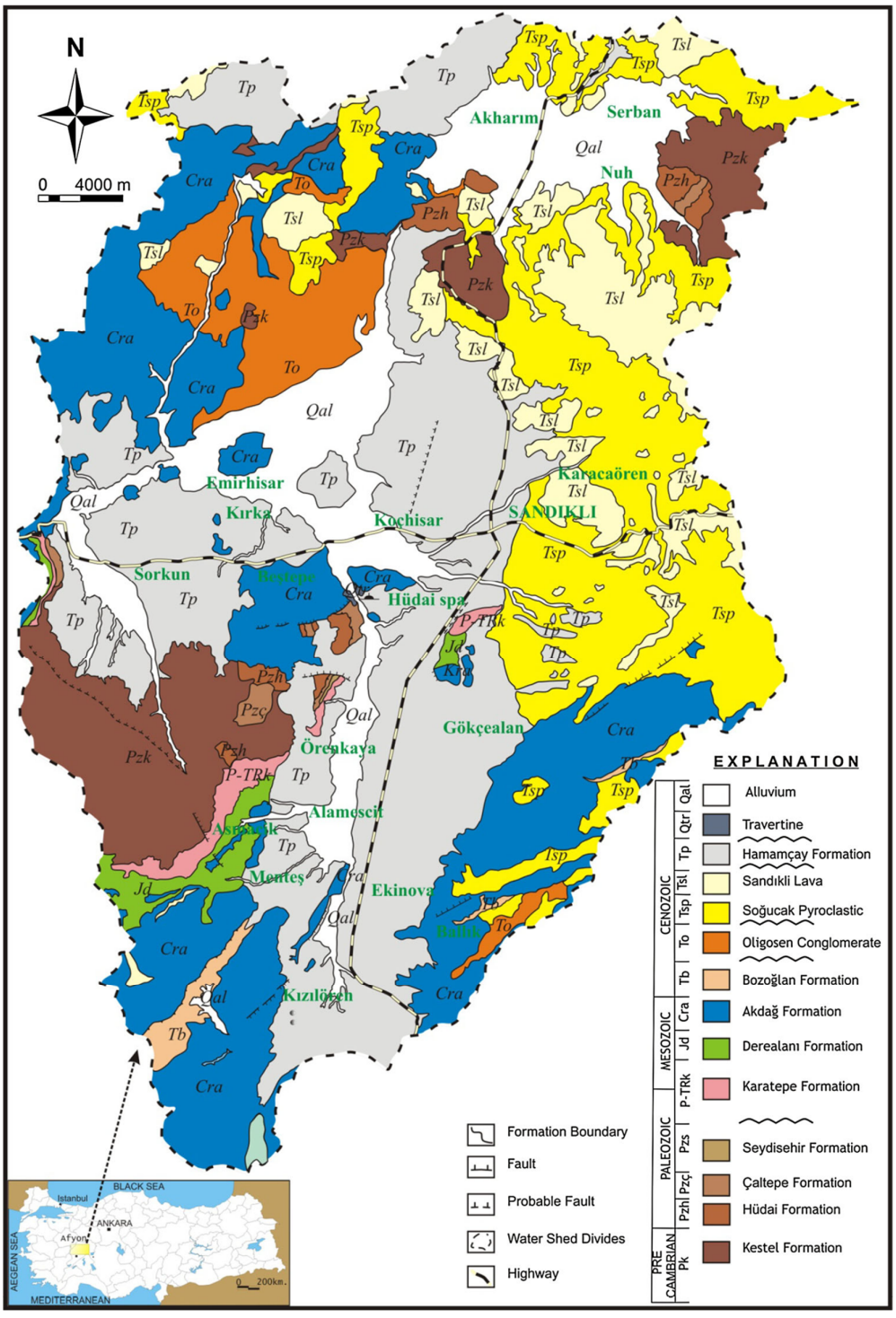

Figure 1.6 Geological map of the Sandikli Basin (Davraz et al., 2016).Hudai spa is near the middle.

and limestones; andesitic to basaltic Sandikli Lavas; pyroclastics; gravels to claystones; alluvium and travertine (Davraz et al., 2016).

There is a recognized geothermal field between Hudai spa and the city of Sandikli. It features 23 geothermal wells and two reinjection wells for waste water. The geothermal wells have depths between 49 and 1053 m, temperatures between 54 and 82 ^{o}C, and a combined discharge of 500 l/s. The reinjection wells are 780 m deep (Davraz et al., 2016).

The alluvium and Pliocene sedimentary Hamamcay units are 200 to 300 m thick in the Sandikli plain. These units host fresh water aquifers which are tapped for domestic and agricultural purposes through 1500 wells (Davraz et al., 2016). The aquifers in the Sandikli Basin are suggested to be unconfined, and drain to the centre and north (Afşin, 1997). The aquifers for the geothermal waters in the Hudai-Sandikli geothermal field are deeper, in the quartzites and limestones of the Mezozoic Akdag formation and older units (Davraz et al., 2016).

Davraz et al. (2016) collected water from wells and springs in the geothermal field and locations mostly in the Sandikli plain in order to assess water quality and the extent of mixing of geothermal water with surface waters. Their cold water samples had temperatures between 10 and 25 ^{o}C, with the lowest temperatures from natural springs, in accordance with the geothermal gradient. Their geothermal well water samples had temperatures between 57 and 80 ^{o}C. Based on oxygen and hydrogen isotopes, all the groundwater is of meteoric origin, though the geothermal waters have a long residence time and deep circulation (Afşin et al., 2012).

The geothermal potential of a region is often assessed from near surface heat flow, which in turn can be estimated from the Curie point depth, found from spectral analysis of magnetic surveys (e.g., Akin et al., 2014) or silica geothermometry. The Curie point depth, the bottom of a magnetic source, corresponds to a temperature of 580

°C where ferromagnetic minerals, particularly magnetite, convert to paramagnetic minerals (Hsieh et al., 2014). Silica geothermometry estimates the source temperature of water based on the concentration of dissolved silica (Güleç, 2003). Using these methods, Maden et al. (2020) calculated for under the Hudai Sandikli geothermal field a geothermal gradient of 49.18 °C km^{-1}, a Curie point depth of about 11.8 km, and an average reservoir depth of 900 m.

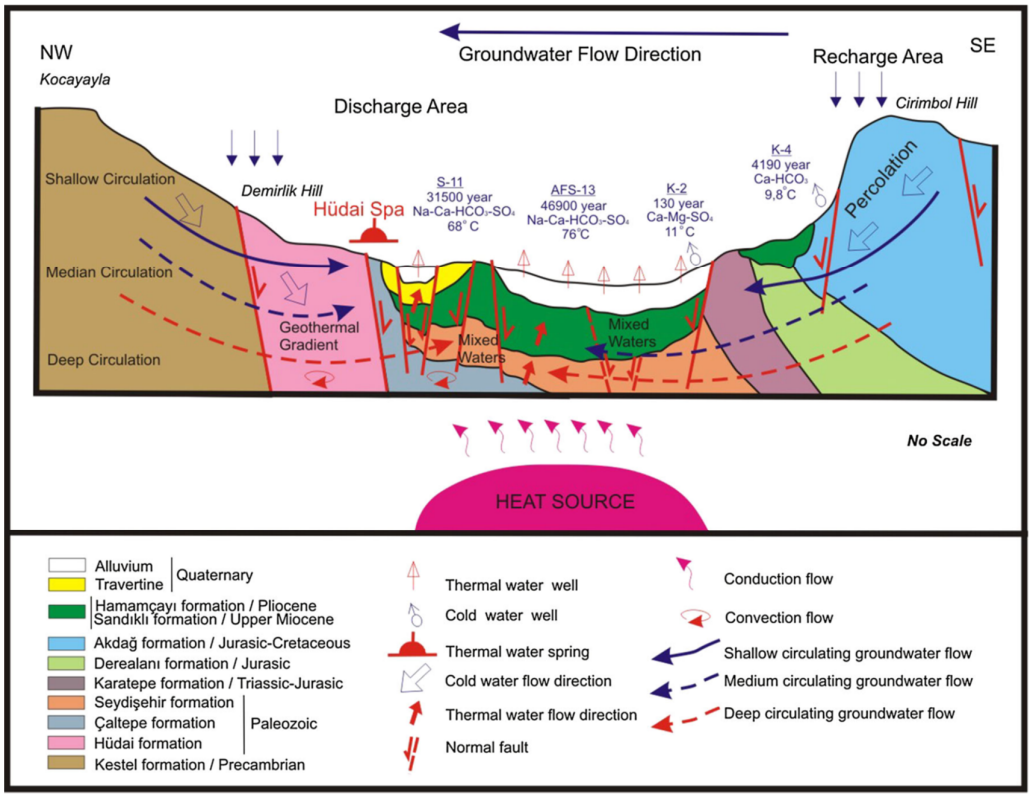

Figure 1.7 Conceptual model of water flow in a cross section across the Sandikli plain through the Hudai spa (Davraz et al., 2016). See Figure 1.6.

Davraz et al. (2016) presented the diagram in Figure 1.7 to illustrate their concept of the structure of the basin near the Hudai spa. They propose that the geothermal water rises to the near surface through faulted regions.

Despite repeated attempts by the author, specific and independent data on electrical resistivities and temperature logs for the area could not be obtained. In Table 1.1 the obtained well temperature information are averages. One core log from the

geothermal field, provided in an internal report by Mr Erhan (see section 3.3) is presented in Figure 1.8. Its location is indicated in Figure 1.9.

Translations of the core log descriptions are given in Table 1.2. The main lithologies are indicated by the different colours: grey is alluvium, green is sedimentary rocks, pinks and purples with 'v' symbols are volcanic rocks, purple with hatch pattern is quartzite, and the pale yellow brick symbol layer is carbonate. There are 22 m of alluvium over Pliocene volcanoclastic sandstones (Hamamcay Formation, Fig. 1.6) to 182 m depth. These layers are identified by Davraz et al. (2016) as hosting unconstrained fresh water aquifers. From 182 m to 330 m there are Lower Pliocene vesicular trachyandesite lava flows (often debris flows), with vesicules filled with zeolite (Sandikli Lava, Fig. 1.6). This is underlain by the Paleozoic Seydişehir Formation of grey green siltstones and fine sandstones. There is no mention in this drill log of the Mesozoic units in Figure 1.6. The Sandikli Lava and Seydişehir Formations were classified by Davraz et al. (2016) as impermeable cap rock. Between 824 and 836 m, there is a transition to the Hudai Quartzite, which extends to the bottom of the well at 1052 m. There is a layer of carbonate within the Hudai Quartzite, between 960 and 976 m depth.

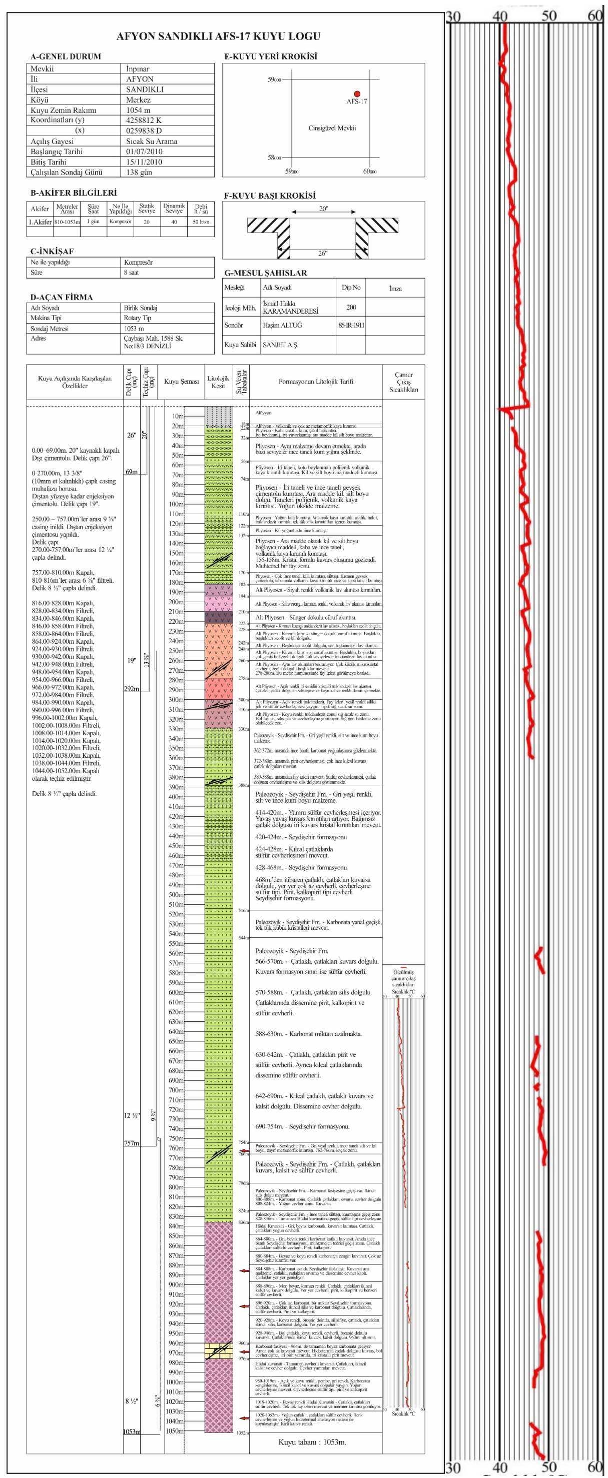

Figure 1.8 Left: core log AFS 17 (see Fig. 1.9 for location). Right: expanded temperature log (in ^{o}C) for depths from 600 m to 125 m.

Table 1.2 English translation of core log in Figure 1.8.

	Depth(m)	Age	Description
	0-18		Alluvium
	18-22		Alluvium - volcanic and small fragments of metamorphic rock
	22-32	Pliocene	Coarse gravel, sand, gravel deposit. Well rounded, intermediate clay and silt size material.
	32-56	Pliocene	As above. Some layers contain lenses of fine grained sand.
	56-74	Pliocene	Coarse-grained, poorly sorted polygenic volcaniclastic sandstone. Sandstone including clay and silt-size particles.
	74-110	Pliocene	Coarse-grained and fine-grained loosely cemented sandstone. Intermediate clay, silt-size filler. Particles of polygenic, volcanic rock. Intensely oxidized material.
	110-122	Pliocene	Dense clayey sandstone. Sandstone with clasts of volcanic rock: trachyte, trachyandesite clastics, isolated siliceous clastics.
	122-132	Pliocene	Clay-rich fine sandstone.
	132-170	Pliocene	Coarse and fine-grained volcaniclastic sandstone with clay and silt-size cement. 156-158 m. A formation of fuzzy quartz was observed. A possible fault zone.
	170-182	Pliocene	Very fine-grained clayey sandstone, siltstone. Fine and coarse-grained sandstone, partly loosely cemented, with igneous rock at the base.
	182-194	Lower Pliocene	Fragmented black volcanic lava flow.
	194-210	Lower Pliocene	Brown, red colored volcanic lava debris flow.
	210-222	Lower Pliocene	Vesicular debris flow.
	222-228	Lower Pliocene	Reddish-brown trachyandesite lava flow, very large vesicules filled with zeolite
	228-242	Lower Pliocene	Brick red vesicular debris flow. Vesicules are filled with zeolite and clay.
	242-248	Lower Pliocene	Consolidated trachyandesite lava flow with zeolite filled cavities
	248-260	Lower Pliocene	Brick red debris flow. A vesicular trachyandesite lava flow, with very large vesicules, filled with zeolite, at lower levels.
	260-278	Lower Pliocene	The same lava flows are repeated. There is very small microcrystalline mineralization and zeolite filled vesicules.
	278-300	Lower Pliocene	278-280 m. Fault traces began to appear in this meter sample. Trachyandesite lava flow with light colored coarse sanidine crystals. Fracture fillings contain silicification and dark brown iron
	300-310	Lower Pliocene	Pale trachyandesite. Fault traces, green silica gel and sulfur mineralization are common. **Typical shallow hot water zone.**
	310-330	Lower Pliocene	Dark colored trachyandesite zone, warm water zone. Abundant fault traces, silica gel and mineralization are observed. May be a recirculation zone.
	330-388	Paleozoic	Seydişehir Fm. Gray green colored silt and fine sand sized material. 362-372 m. Contains a thin layer of carbonate precipitation. 372-380 m. Contains pyrite mineralization and quartz filling very thin capillary fractures.

			380-388 m. Contains traces of faults. Sulfur mineralization and fracture filling mineralization and silica filling are observed.
	338-516	Paleozoic	Seydişehir Fm. Gray green colored silt and fine sand sized material. 414-420 m. Contains bulbous sulfur mineralization. Gradual increase in quartz crystals. Independent fracture filling by coarse quartz crystals. 420-424 m. Seydişehir Fm. 424-428 m. Sulfide mineralization in capillary fractures. 428-468 m. Seydişehir Fm. 468 m. Fractured, fractures filled with quartz, with a very little sulfide mineralization in places. Seydişehir formation with pyrite and chalcopyrite.
	516-544	Paleozoic	Seydişehir Fm. Lateral transition to carbonate with sporadic, isolated cubic crystals.
	544-754	Paleozoic	Seydişehir Fm. 566-570 m. Fractured, quartz filled fractures. Sulfide mineralization at the boundary of the quartz. 570-588 m. Contains fractures filled with silica. There is disseminated sulfide mineralization, including pyrite and chalcopyrite in fractures. 588-630 m. Decreasing amounts of carbonate. 630-642 m. Fractured, fractures with pyrite and sulfide mineralization. Also disseminated sulfide mineralization in capillary veins. 642-690 m. Capillary veining, filled with quartz and calcite and with disseminated mineralization. 690-754 m. Seydişehir Fm.
	754-766	Paleozoic	Gray-green, fine-grained silt and clay-size, weakly metamorphosed sandstone. 762-766 m. Leak zone.
	766-796	Paleozoic	Fissured, broken quartz, calcite and sulfide mineralization.
	796-824	Paleozoic	Seydişehir Fm. There is a transition to carbonate facies. Secondary silica fill occurs. 800-808 m. Carbonate zone. Fractured. Fractures filled with gypsum. 808-824 m. Intensely mineralized quartzite.
	824-836	Paleozoic	Seydişehir Fm. Transition zone from fine-grained siltstone to sandstone 828-836 m. Full transition to Hudai quartzite. Sulfide mineralization.
	836-960	Paleozoic	Hudai quartzite is a gray to white carbonate quartzite fabric. Fractures are strongly mineralized. 864-880 m. Gray, white colored quartzite with carbonate. Interleaved are thin banded Seydişehir formation, possibly a gradual transition zone. Fractured, fractures have sulfide mineralization: pyrite, chalcopyrite. 880-884 m. White and dark colored carbonate-rich quartzite. A very little Seydişehir formation remnant. 884-888 m. Decreased carbonate and increased Seydişehir formation. Quartzite fractured and covered with disseminated mineralization. Fractures widen in places.

			888-896 m. Purple, white, crimson color. Fractured, fractures filled with secondary calcite and quartz. Locally mineralized, with pyrite, chalcopyrite and similar sulfides. 896-920 m. Very little carbonate, some Seydişehir formation. Fractured, fractures filled with secondary silica and carbonate. Sulfide mineralization within fractures. Pyrite and chalcopyrite. 920-928 m. Dark colored, silicified, fractured, Fractures filled with secondary silica and carbonate. Mineralized in places. 928-946 m. Heavily fractured, dark colored, mineralized quartzite. Secondary quartz in fractures, filled with calcite. 960 m. Lower boundary.
	960-976	Paleozoic	White carbonate containing a very little quartzite. **Hydrothermal fracture** filling by quartz, abundant mineralization, coarse pyrite nodules and coarse crystalline pyrite are present.
	976-1052	Paleozoic	Hudai quartzite. Entirely mineralized quartzite. Fractures are filled with secondary calcite and mineralization. Mineralized nodules are present. 980-1019 m. Light and dark colored, pink, gray colored. Carbonate enrichment, secondary calcite and quartz fills are common. There is intense sulfide mineralization. Pyrite and chalcopyrite. 1019-1020 m. White Hudai quartzite. Fractures with sulfide mineralization. There are traces of isolated faults and traces of marble. 1020-1052 m. Intensely fractured with sulphide mineralization in fractures. The color is darkened due to mineralization and **intense hydrothermal alteration**. Dirty brown in color.

From about 300 m depth downward, the rocks often contain disseminated sulfide mineralization, presumably the result of hydrothermal circulation, and both the Seydişehir Formation and the Hudai Quartzite have many intervals which are fractured. The fractures are filled with quartz and/or calcite and often disseminated sulfides.

The temperature increases to nearly 50 °C at about 1 km depth, in agreement with the calculations of Maden et al. (2020).

1.5 The study area and surveys

The locations of the 384 soundings in the Sandikli Basin are shown as red dots in Figure 1.9, with the spas and greenhouses of the geothermal field marked in the bottom panel.

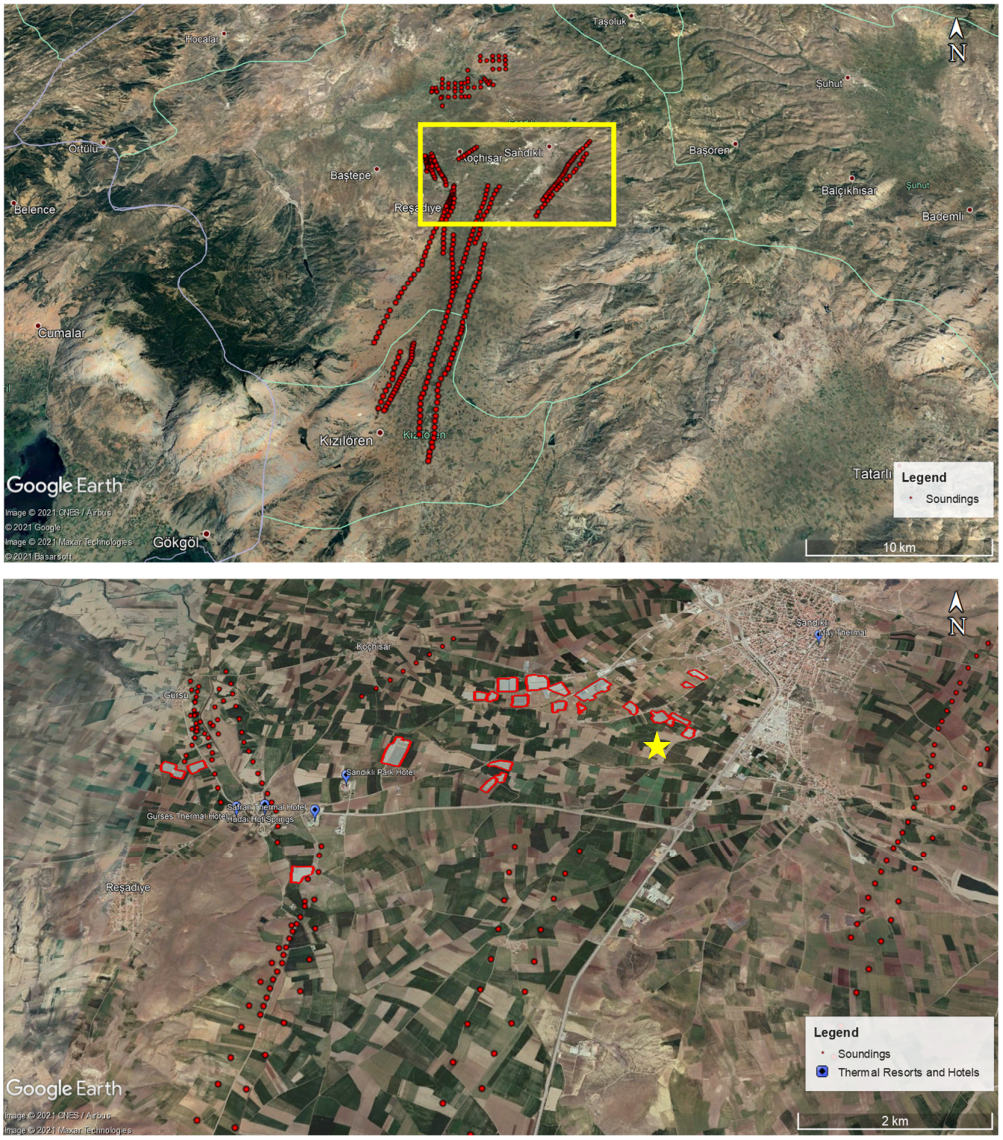

Figure 1.9 Top: Sandikli graben field area with VES locations (red dots). Yellow rectangle indicates the area shown in the bottom panel. Bottom: Geothermal greenhouses (red polygons) and thermal resorts and hotels (blue markers) located in Sandikli geothermal field. The yellow star is the location of the drill core in Figure 1.8. The city in the top right is Sandikli.

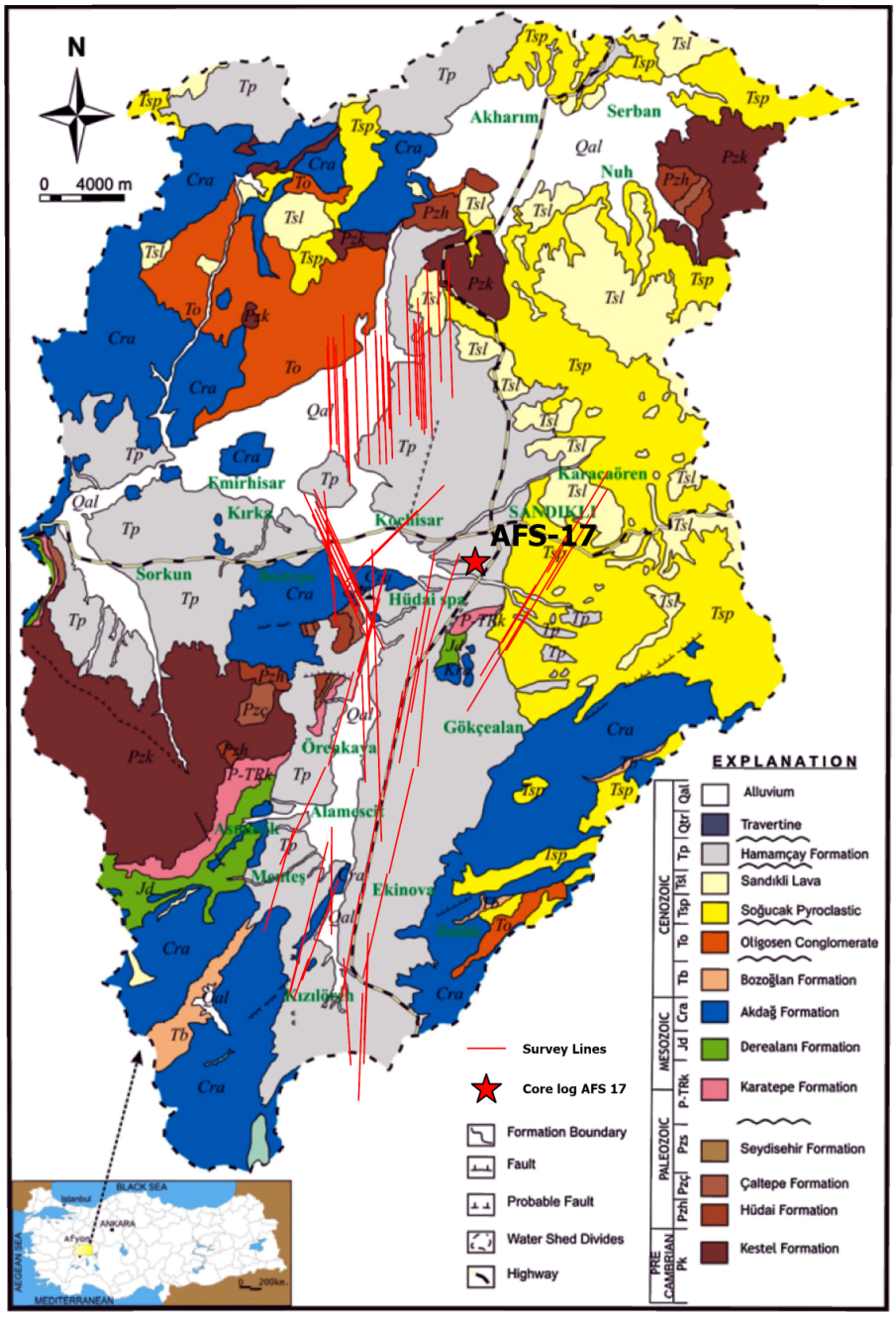

Figure 1.10 Geological map of Sandikli Basin with extent of DCR spreads in this study shown as thin red lines.

The locations of the surveys are superimposed on the geological map in Figure 1.10. Here, the red lines show the extent of the farthest electrodes in the spreads, so they extend outward 2.5 km from the centre of the soundings at the ends of the lines. It is

seen they are mostly over the quaternary alluvium and Pliocene sediments in the basin.

For data analysis, the 384 individual soundings were divided into seventeen groups (Figure 1.11), where each group was a line of soundings or, in the case of Groups 1 and 17, a set of soundings spread over a region. The groups were then allocated into 6 Areas, based on geographic regions. The sounding numbers for the Groups and Areas are given in Table 1.3 and Figure 1.12. The location maps for soundings in each Area, superimposed on Google Earth images, are presented in Appendix A. These maps indicate that most soundings were taken over a patchwork of agricultural fields. Information on the equipment and acquisition method is provided in section 3.3, and descriptions of Groups and soundings are given in Chapter 4.

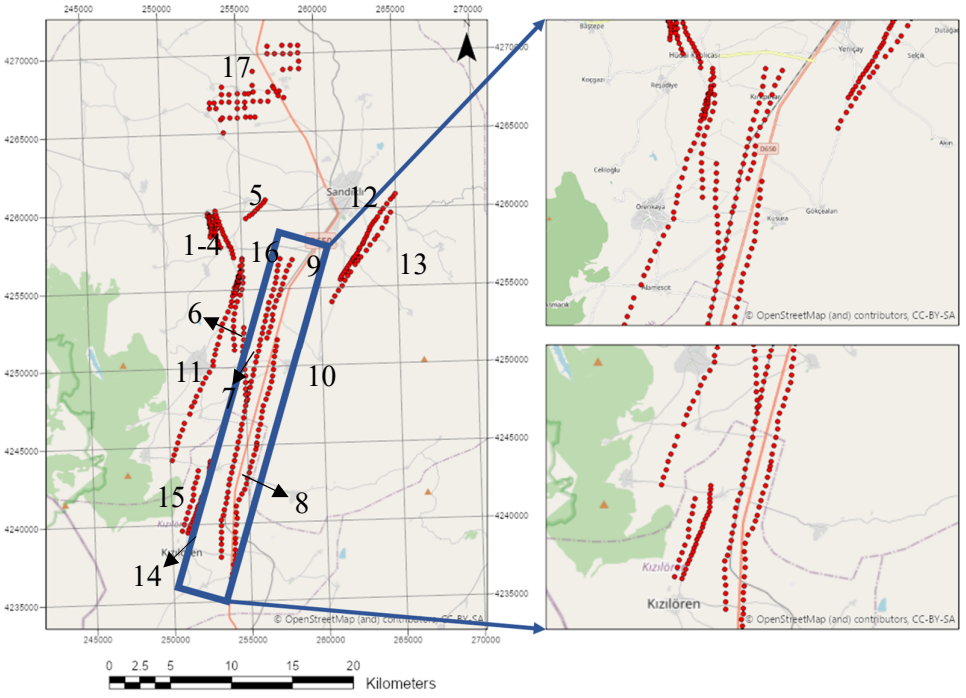

Figure 1.11 Map with VES soundings where the data were measured. Dots represent the centres of each of the soundings. Sounding group numbers are indicated. Roadside measurements are highlighted with a blue rectangle.

Table 1.3 Soundings categories: Areas, Groups and acquisition dates (day/month) in 2011.

Area	Group	Soundings	Acquisition	Area	Group	Soundings	Acquisition
1	17	342-395	22/7-28/8	4	6	64-79	3/3-12/3
2	1	1-16	17/1-2/2		7	80-92	14/3-17/3
	2	17-27	3/2-7/2		11	205-240	4/5-19/5
	3	28-43	7/2-14/2		16	325-338	5/7-11/7
	4	44-55	18/2-28/2	5	8	93-142	27/3-9/4
	5	56-63	28/2-2/3		9	143-150	10/4-12/4
3	12	241-270	25/5-8/6		10	155-204	15/4-3/5
	13	271-288	9/6-20/6	6	14	289-311	20/6-28/6
					15	312-324	29/6-5/7

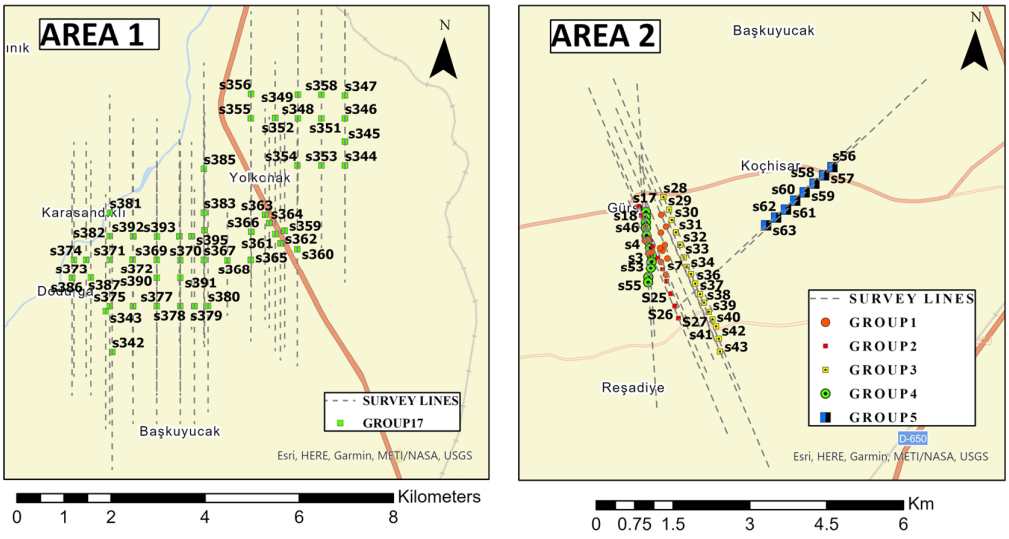

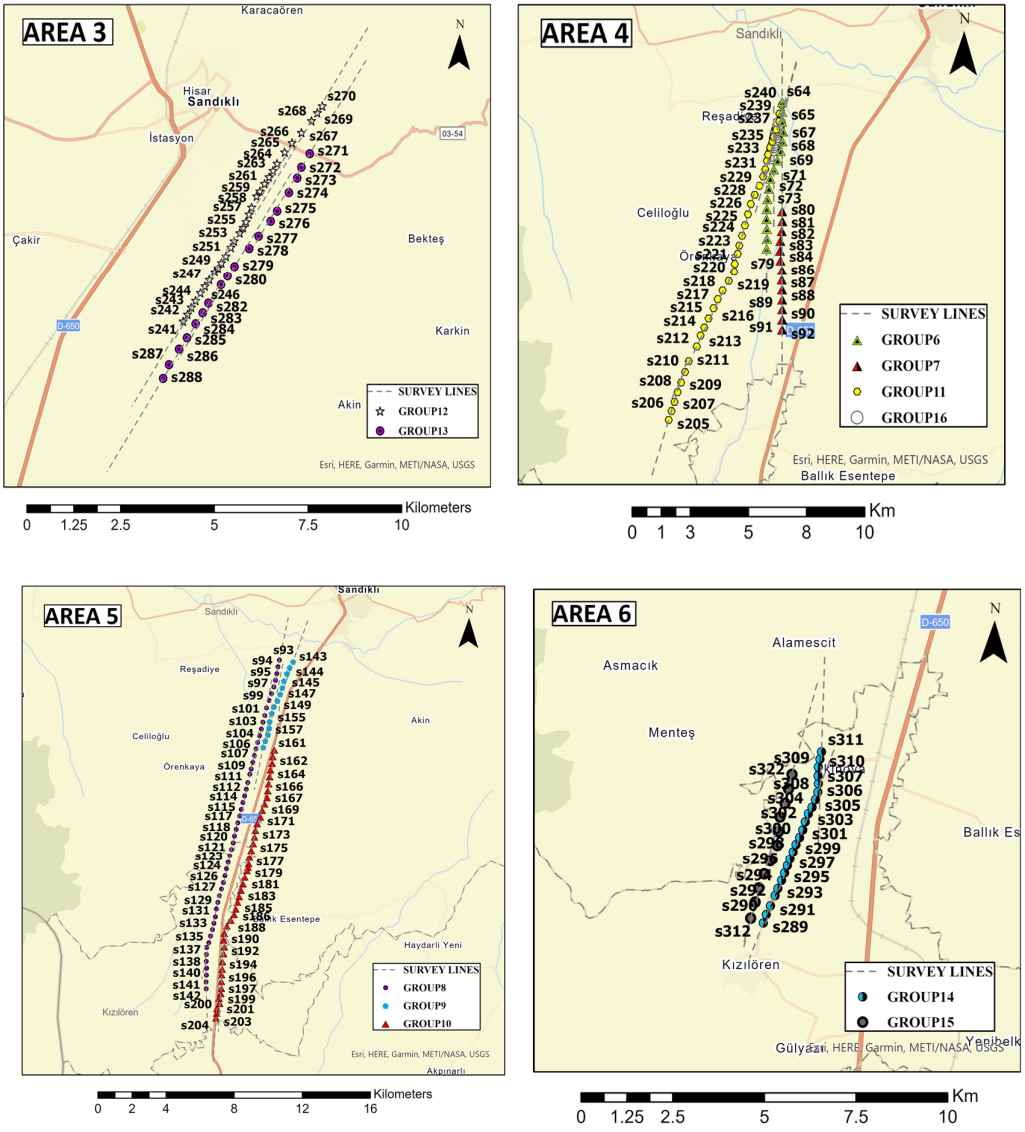

Figure 1.12 Maps of six different areas within the Sandikli geothermal field. Grey dashed lines indicate the full extent of the electrode spread.

The core drill location is about 2 km to the SE of the nearest sounding (s56).

1.6 Following chapters

In Chapter 2, geothermal energy utilization is discussed particularly in Canada and Turkiye. Geothermal exploration methods are briefly mentioned, and resistivity characteristics in geothermal areas are mentioned. Previous studies in the world using Vertical Electrical Sounding method are highlighted. In Chapter 3, the fundamentals of resistivity measurements focusing on the Vertical Electrical Sounding method are

described. Data acquisition and field equipment for this study are described. Inspection and quality control of the raw Vertical Electrical Sounding data and the basic principles of 1D and 2D inversion are explained. Additionally, the chosen inversion parameters are presented. In Chapter 4, the distribution of near-surface apparent resistivity, IP effect and topography are presented and discussed. The characteristics of the soundings are determined, and obtained 1D and 2D models are presented and discussed. Chapter 5 gives a summary and conclusions of the study.

Chapter 2: Background

A considerable amount of literature has been published on geothermal energy and geothermal exploration (Blackwell et al., 1974; Combs, 1978; Muffler, 1979; McNeill, 1980; Fridleifsson, 2001; Barbier, 2002).These studies focus on the utilization of geothermal energy, different types of geothermal resources and systems, and exploration methods including geochemical, geophysical and drilling methods. The aim of this chapter is to emphasize these themes: general status of geothermal energy utilization particularly in Canada and Turkiye; and geothermal exploration techniques.

2.1 Geothermal Energy Utilization

A study such as that established by Lindal (1992) has shown the uses of geothermal resources for particular purposes.

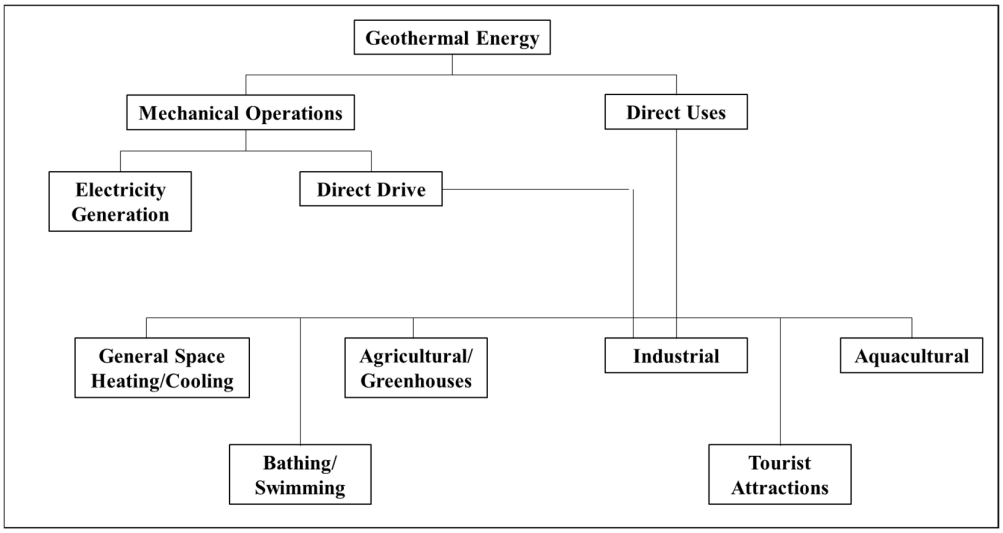

Figure 2.1 Geothermal energy utilization retrieved from Lindal (1992).

Utilization of geothermal energy is categorized into mechanical operations and direct uses in Figure 2.1. In electricity generation, there are three main types of geothermal power plants: dry steam, flash steam and binary cycle power plants. In dry steam power plants steam is directly transferred to a turbine to produce electricity. Flash steam power plants are used where temperatures are higher than 180 °C. Here, fluid is pumped into

a tank at high pressure, and some of the fluid quickly vaporises. Then, electricity is produced by using the expanding vapor in a generator. Binary cycle power plants are used in low and moderate geothermal systems, where geothermal water is not sufficiently hot to produce steam or vapor. Geothermal water flows through a heat exchanger unit, and the heat causes a secondary (binary) fluid, typically a hydrocarbon, to vaporise.

On the other hand, the direct use of geothermal energy is extensively suitable for heating and cooling spaces using geothermal heat pumps. As can be seen from Figure 2.1, there are other fields of application for direct use such as agricultural (e.g., crops and soil heating, and mushroom raising) and greenhouses, industrial (e.g., drying of agricultural products, industrial washing and chemical processing), bathing and swimming. Figure 2.2 shows worldwide direct uses of geothermal energy between 1995 and 2015. Figure 2.2 reveals that geothermal heat pumps, space heating, and bathing/swimming are the most prominent of the direct uses of geothermal energy.

Utilization, TJ/yr					
	2015	**2010**	**2005**	**2000**	**1995**
Geothermal Heat Pumps	325,028	200,149	87,503	23,275	14,617
Space Heating	88,222	63,025	55,256	42,926	38,230
Greenhouse Heating	26,662	23,264	20,661	17,864	15,742
Aquaculture Pond Heating	11,958	11,521	10,976	11,733	13,493
Agricultural Drying	2,030	1,635	2,013	1,038	1,124
Industrial Uses	10,453	11,745	10,868	10,220	10,120
Bathing and Swimming	119,381	109,410	83,018	79,546	15,742
Cooling / Snow Melting	2,600	2,126	2,032	1,063	1,124
Others	1,452	955	1,045	3,034	2,249
Total	**587,786**	**423,830**	**273,372**	**190,699**	**112,441**

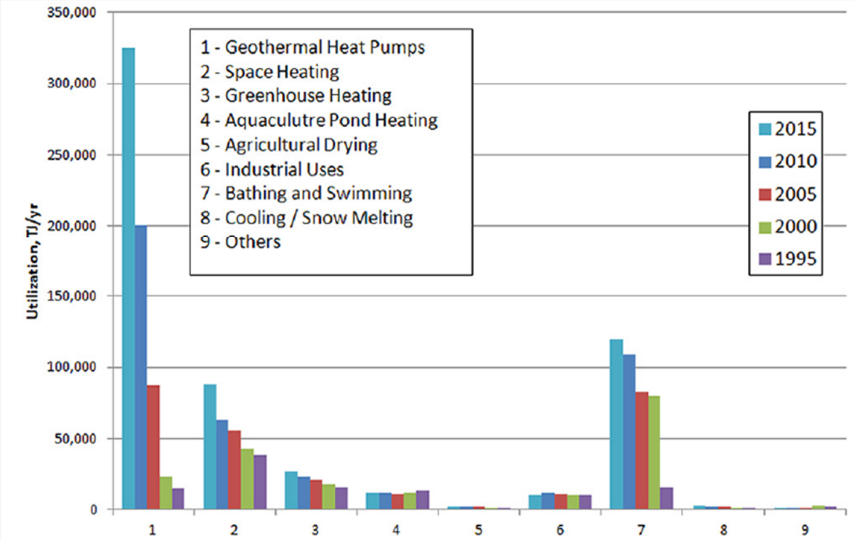

Figure 2.2 Categories of worldwide direct uses of geothermal energy from Lund & Boyd (2016).

2.2 Worldwide Geothermal Energy

Geothermal energy potential is widely spread throughout Canada. Even though Canada has huge geothermal resources, there is no geothermal electricity production in Canada, however, direct use is broadly used. From the data in Table 2.1, it is apparent that Canada is in the top ten countries in geothermal energy utilization.

Table 2.1 Top ten countries in the world and Canada in terms of geothermal energy utilization in 2015.

Electricity Production		Direct Use	
	In GWh electric		In GWh thermal
United States	16,600	China	48,435
Philippines	9,646	UnitedStates	21,074
Indonesia	9,600	Sweden	14,423
New Zealand	7,000	Turkey	12,536
Mexico	6,071	Iceland	7,442
Italy	5,660	Germany	5,426
Iceland	5,245	Finland	5,000
Turkey	3,127	France	4,408
Kenya	2,848	Switzerland	3,288
Japan	2,687	Canada	3,226
Sum of Top 10	68,484	Sum of top 10	125,258
Canada	**0**	**Canada**	**3,226**
All other	5,067	All Other	30,599
World Total	**73,551**	**World Total**	**155,817**

Note: Modified from Geothermal Energy Resource Potential of Canada (Grasby et al., 2012), *Geological Survey of Canada Open File 6914*, Canada, and retrieved from Direct utilization of geothermal energy 2015 worldwide review (Lund and Boyd, 2016).

In geothermal systems, the source of heat is often hot magma, therefore accessible geothermal resources are found in areas where there is magmatism, such as subduction zones, for example, the Cascadian subduction zone in British Columbia (Grasby et al, 2012); hot spots, such as Iceland (Mikhaylov, 2020); or rifts, such as the East African Rift (Kombe and Muguthu, 2019). These are areas where magmatic heat is close to the surface, and where fluids (groundwater) or magmatic fluids given off from magmatic bodies can be tapped for this heat. In the deep sedimentary basins in western Canada, hot fluids are found in areas where the lithosphere is thin and there are porous rock at depth. In this case, the heat is conducted through the associated magmatism.

In the Sandikli geothermal region, deep fracture/sheer zones allow the heat to reach shallow depths, and the Sandikli graben is filled with sediments. There are also

long faults, so there are pathways and reservoirs for hot fluids. The opposite situation is the Canadian Shield in central and northern Canada, where the lithosphere is thick and the rocks are basement rocks (old, cold igneous and metamorphic). There is no volcanic activity and heat flux from the mantle is low, so it must be drilled very deep through impermeable rocks to get to hot rocks. In this case, the only option is fracturing the rock and pumping water down to use geothermal resource (Grasby et al., 2012).

2.3 Geothermal Energy in Canada

Canada has enormous potential for geothermal energy resources. There is a wide range of geological regions that have a significant impact on the potential geothermal resources in Canada. According to Grasby et al. (2012), these regions fall under three main groups: a) the Canadian Cordillera represents mountainous regions in western Canada, b) sedimentary basins, c) the Canadian Shield that extends across central and northern Canada.

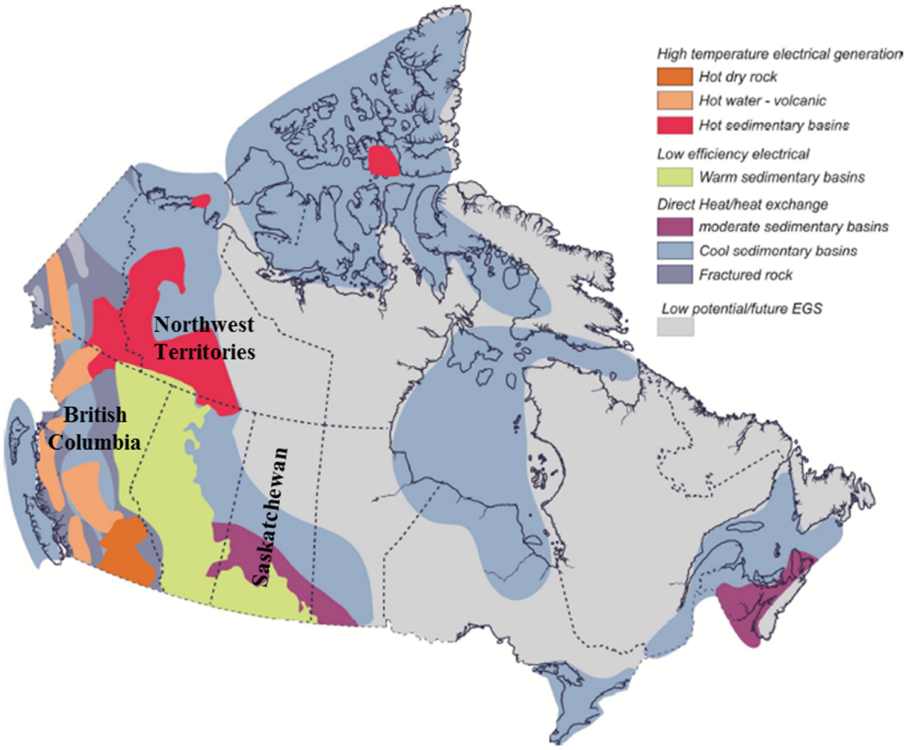

Figure 2.3 The distribution of geothermal energy potential in Canada from Grasby et al. (2012).

As can be seen from Figure 2.3, geothermal energy potential is widely spread throughout Canada, though without the use of EGS (Enhanced Geothermal Systems, basically fracking) potential in Newfoundland and Labrador and the Canadian Shield is limited by slow heat flow. The provinces of British Columbia, Alberta and Saskatchewan, and the Northwest Territories have huge potential geothermal energy resources. A project was deployed as a test electrical site at the Mount Meager massif in British Columbia. Previous research at Mount Meager in the Canadian Cordillera geological region established that temperatures of 200 °C were measured at a depth of 365 m. This system is thought to be an efficient resource to generate electricity, though it has encountered setbacks. According to the latest developments in this research, geothermal energy will be used at Mount Meager by 2025. The new objective is to use a horizontal well to obtain hot water under Mount Meager (Lalonde, 2021). These

systems are limited to the Cordillera region (Richter et al., 2012).

Although there is a wide range of geothermal resources throughout Canada, the direct use applications are limited. A few applications will be mentioned to emphasize geothermal energy potential in Canada. In Springhill, Nova Scotia, geothermal heat was used to heat mine workings. Another project completed to identify the existence of geothermal resources and use the heat energy as a primary source in Fort Liard, the Northwest Territories, which is famous for hot springs in its provincial park. However, the proposal to build a geothermal plant fell through in 2013 (Groundwater, 2013). In the City of Moose Jaw, Saskatchewan, hot geothermal water is used as a source of hot pool spa, and this is a good example of the direct use of geothermal energy in tourism. Additionally, hot springs in Yukon are used to heat hot pools spa, and locals can access this heat source for agricultural use. Besides this, there are on-going projects to take advantage of geothermal energy (Fraser et al., 2019). In 2018, a pilot project was started in Swan Hills, Alberta to assess geothermal energy potential in an active oil field. Construction of the geothermal power plant in Swan Hills is planned to be completed in the first quarter of 2022 (ThinkGeoEnergy, 2021). Another notable example is that the Sustainaville Geopark project is proposed to develop geothermal power for an industrial park in Valemount, British Columbia (Natural Resources Canada, 2018). Furthermore, drilling is currently being operating by Deep Earth Energy Production (DEEP) to draw geothermal heat from very deep wells in Torquay, Saskatchewan (Graney, 2021).

Many organizations play important roles in promoting geothermal research in Canada. One of the most important organizations is Geothermal Canada. This is a non-profit organization where scientists, professionals, students and governments discuss

general aspects of geothermal industry. A considerable number of papers and reports are published on Geothermal Canada's website. For instance, a recent study published by Majorowicz and Grasby (2021) showed that new aquifers were discovered for geothermal heating in western-northwestern Alberta, northeastern British Columbia and southwestern Saskatchewan. In Canada there is an increasing interest in ground source heat pumps for domestic heating and cooling (Government of Canada, 2021). This would be the characterization of low temperature geothermal resources.

2.4 Geothermal Energy in Turkiye

Turkiye is the first in Europe and the 7th in the world for geothermal energy resource use. As of now, several studies have identified more than 470 geothermal fields in Turkiye, and the temperature of geothermal fields varies from 20 to 287 °C. Between 2010 and 2015 a total of 365 production and injection wells were drilled for electricity generation and direct uses (Mertoglu et al., 2015).

Table 2.2 Number of drilled wells in Turkiye from 2010 to 2015.

Purpose	Wellhead Temperature	Wells				Total Depth (km)
		Electric Power	Direct Uses	Combined	Other (gradient)	
Exploration	(all)					
Production	>150 °C	130			20	323
	100-150 °C			20	10	37
	<100 °C		80		15	130
Injection	(all)	70	20			80
Total		200	100	20	45	570

Note: Heat pump wells have been excluded. Modified from Geothermal country update report of Turkiye (2010-2015), Mertoglu et al. (2015).

As seen in Figure 2.4, these wells are primarily located on the major grabens along the Northern Anatolian fault zone and volcanic regions in the west. High temperature geothermal systems such as Kizildere (150-242 °C), Canakkale-Tuzla (165 °C), Aydin-Savatli (172 °C) are mostly located in the West Anatolian region in Turkiye. Table 2.3 shows the list of the total installed capacity of these three power plants and measured temperatures.

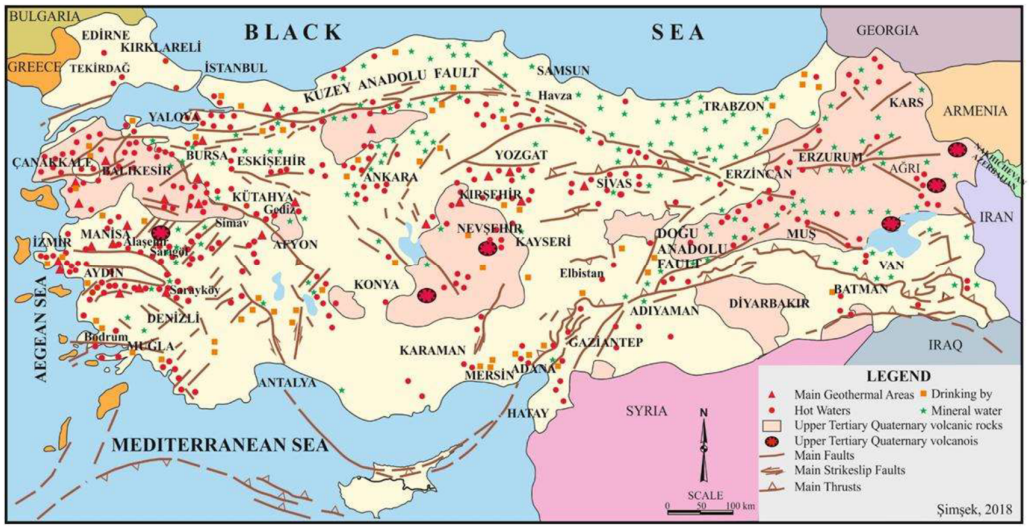

Figure 2.4 Distribution of geothermal resources and active faults within Turkiye (Mertoglu et al ., 2019).

Table 2.3 Data on some significant geothermal power plants in Turkiye.

Place	Unit name	Capacity, MW	Source temperature, °C	Start date
Kizildere-Denizli	Kizildere-I	15	230	1984
	Kizildere-II	60	150	2013
Salavatli-Aydin	Dora-I	7.95	170	2006
	Dora-II	9.5	172	2010
	Dora-IIIa	17	165	2013
	Dora-IIIb	17	170	2014
Tuzla-Canakkale	Enda	7.5	165	2010

Note: Modified from Power generation from geothermal resources in Turkiye (Aksoy, 2014).

On the other hand, direct uses of geothermal energy gradually have increased in the last 40 years. At the beginning of the 1960s, geothermal energy was only used for bathing and medical care (e.g., health spa and therapy center) in Turkiye. The first big space heating implementations started in 1987, and 600 residences in the city of Balikesir were heated by geothermal energy heating systems (Gunerhan et al., 2001). A general summary of the direct uses of geothermal energy in certain places of Turkiye is given in Table 2.4.

Table 2.4 Some certain direct uses implementations of geothermal energy in Turkiye.

System	Capacity, MWt	Implementation	Temperature, °C
Afyon-OmerThermalFacilities	38.875	B-H-G	98
Afyon-Sandikli	37	R	70
Ankara-Kizilcahamam	21.315	R-B-H-G	80
Aydin-Germencik	0.1125	G	35
Balikesir-Gonen	37.45	R-H-B-G-I	80
Canakkale-Ezine-Kestanbol	3.82	R-G	62.5-73
Denizli-Kizildere	2.419	R-G-I	90-147
Izmir-Balcova	87.025	R-G-B-H-S-Ho	40-125
Kutahya-Simav	60	R-G-B-H	137
Manisa-Salihli	0.26	B-H	30-168
Samsun-Havza	0.07	B-H	54
Tokat-Niksar	0.1125	G	27-54
Yozgat-Saraykent	0.45	G	46

Note: B: Bathing, G: Greenhouse, R: Space/district heating, H: Hotel, S: Swimming pool, Ho: hotel, I: Industrial purposes. Reprinted from Geothermal energy utilization in Turkiye (Gunerhan et al., 2001).

As shown in Table 2.4, geothermal energy has various utilization areas, and all types of geothermal systems (high, moderate, and low temperature) are used in Turkiye. According to Mertoglu et al. (2019), installed electricity capacity (see Figure 2.5) and direct use implementations capacity reached 1282.5 MWe (megawatt electric) and 3487 MWt (megawatt thermal), respectively, as by the end of 2018. Estimated installed capacity for direct uses will be 7000 MWt by 2025. As a result, it can be seen from the data in Table 2.1 that direct use of geothermal energy in Turkiye is roughly three times greater than Canada.

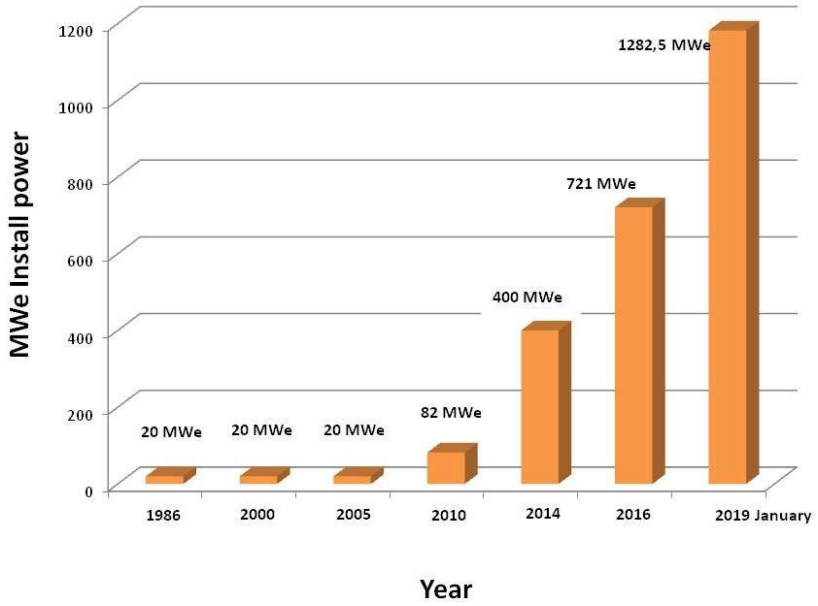

Figure 2.5 Geothermal electricity production in Turkiye until 2019 (Mertoglu et al., 2019).

2.5 Geothermal Exploration Methods

Geothermal resources are mostly located by drilling to test hot water supply in likely locations near plate boundaries or volcanoes (section 2.2), particularly where there is evidence of geothermal activity such as geysers and hot springs (EIA, 2022). Once a potential geothermal field is located, existing exploration methods are used to monitor geothermal resources and determine suitable drilling locations for production. The temperature, volume and permeability parameters must be measured in detail to see whether a well will produce steam or hot water. It is also important to estimate the chemical composition of the fluid that will be produced. There are many available methods to collect this varied information, and these methods are: (a) geological and hydrological methods: the characteristics of a study area can be investigated such as description of local geological units, the existence of shallow or deep aquifers; (b) geochemical methods: flow patterns of geothermal fluid can be identified by making geochemical analysis, and geothermometers are used to determine reservoir

temperature and geothermal fluid chemistry; (c) geophysical methods: physical properties of geothermal systems such as electrical resistivity, density, magnetisation can be measured by using geophysical methods, and geothermal systems can be located and mapped by using differences in physical properties; (d) remote sensing methods: surface effects of geothermal activities can be determined; and (e) drilling methods: locations of drilling are based on geological, hydrological, geochemical and geophysical measurements, and drilling methods are good tools to estimate well productivity. Before employing any of these methods, it will be essential to capitalize on existing literature and data (Gupta & Roy, 2006).

This research set out to investigate a geothermal system using one of the geophysical electrical methods, namely the vertical electrical sounding (VES) method. Thus, the primary objective will be to highlight geophysical methods, and in particular, the VES method in geothermal exploration. In Chapter 3, the details of the VES method will be given.

2.6 Resistivity and Ground Properties

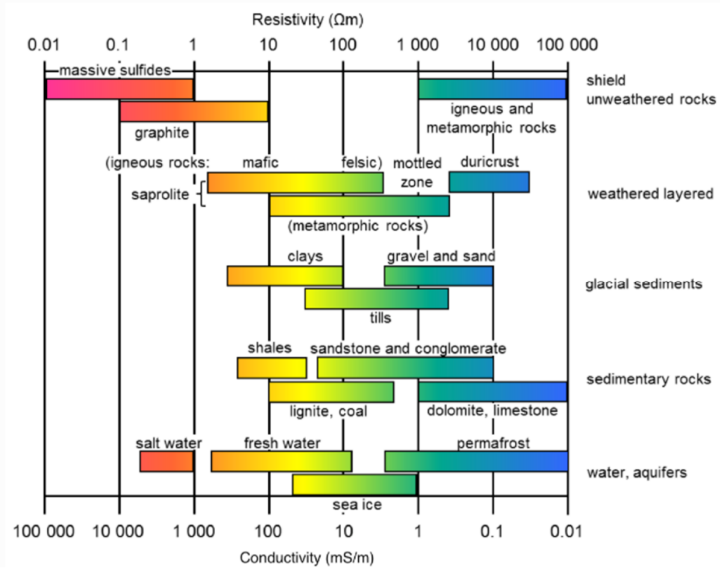

Figure 2.6 Typical resistivities of common rocks (Palacky, 1987).

In order to understand the resistivity distribution in geothermal systems, the factors that affect resistivity should be known. Typical resistivities of earth materials is illustrated in Figure 2.6.There is a wide range of resistivity variability. For instance, unweathered rocks (igneous and metamorphic rocks) have a resistivity range of 1000 to 100000 Ωm. Different types of sedimentary rocks have different resistivity values ranges, such as sandstone and conglomerate from 100 to 10000 Ωm. The resistivity in the Sandikli area is dominated by porosity, permeability, temperature and salinity. Porosity is also an important factor in joints and fractures. Clay tends to have low resistivity, so it can be an important parameter in geothermal exploration. The range of porosities for sedimentary materials, soils and rocks are given in Table 2.5. Data from Figure 2.6 can be compared with the data from Table 2.5 which shows that materials with low porosity show high resistivity, while materials with high porosity show low resistivity.

Table 2.5 Porosity ranges for sedimentary materials, soils and rocks (McNeill, 1980).

Material	Porosity, %
Soils	50–60
Clay	45–55
Silt	40–50
Medium to coarse mixed sand	35–40
Uniform sand	30–40
Fine to medium mixed sand	30–35
Gravel	30–40
Gravel and sand	20–35
Sandstone	10–20
Shale	1–10
Limestone	1–10

Rock or Formation	Porosity, %
Igneous and metamorphic rocks	½– 2
Dense limestones and sandstones	3– 4
Clays and sands in general	8–15
Porous clays, sands, sandstone, cellular limestones, and dolomites	15–40
Marl, loess, clay, and sandy soil	40–75
Peat, diatomaceous earth	80–90

Additionally, the temperature variations of brine resistivity are significant in geothermal exploration. This relation is shown in Figure 2.7 from Unsworth & Rondenay (2012). Resistivity declines at constant salinity between the range of 0 to 300 °C. On the other hand, resistivity increases for temperatures over 300 °C. This is similar to the effect that

is seen in most metals where increasing temperature increases the resistivity (Nesbitt, 1993). Furthermore, increase in salinity decreases resistivity from 0 to 200 °C (Figure 2.6).

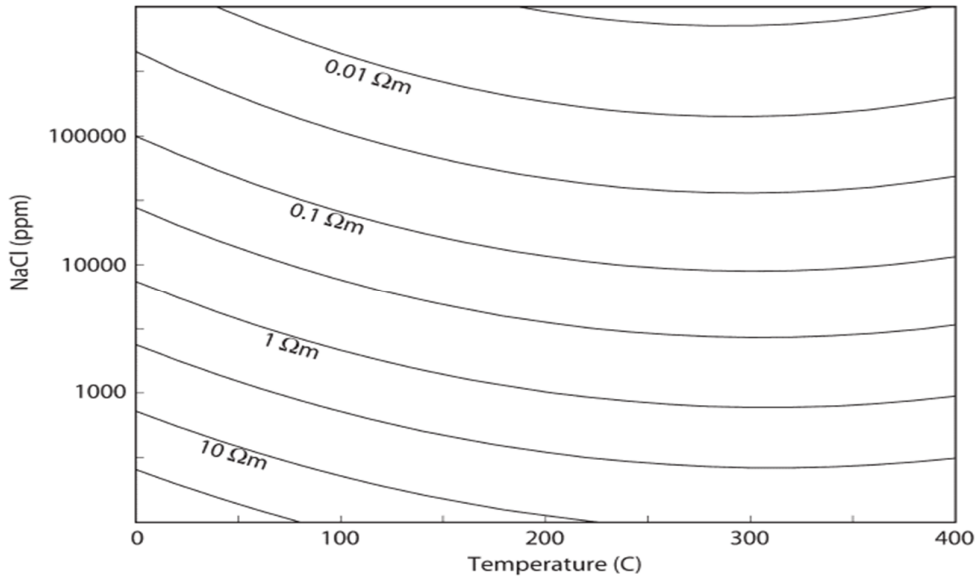

Figure 2.7 Electrical resistivity is plotted as a function of salinity and temperature for saline fluids (Unsworth and Rondenay, 2012).

A study about the fluid resistivity in the Earth's crust was presented by Nesbitt (1993). Figure 2.8 provides the temperature and pressure variation on a KCl solution of different concentrations.

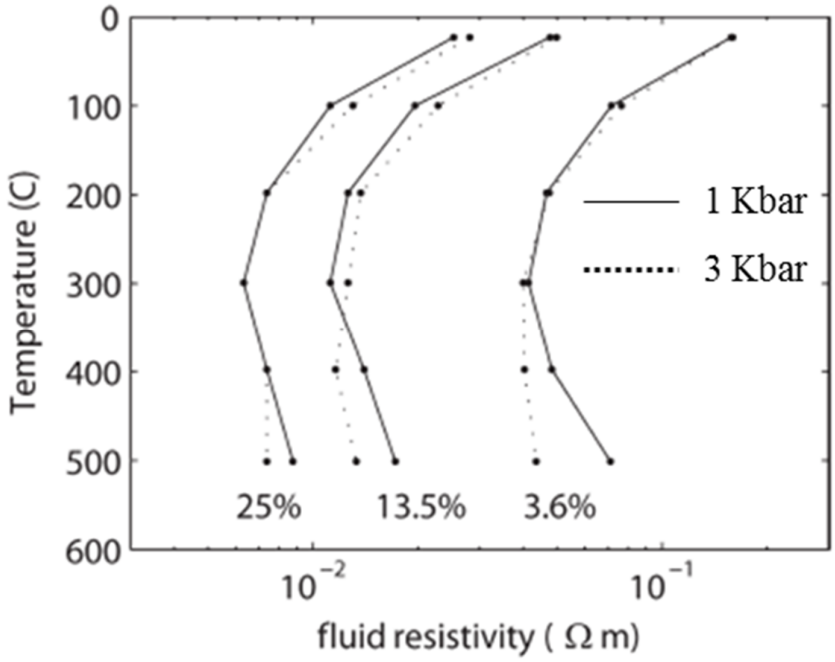

Figure 2.8 The temperature and pressure effect on the resistivity of a KCl solution. Salinity values are shown 25%, 13.5%, and 3.6, respectively (Unsworth & Rodenay, 2012).

From the graph above we can see that, for temperatures below 300°C, pressure has a very small impact and resistivity values decline with increasing temperature. Pressure has an important effect at temperatures over 300°C, where increasing pressure decreases the resistivity by increasing density of the solution.

2.7 Previous Studies using Vertical Electric Soundings

Geophysical electrical methods have a vital role in the exploration of geothermal fields, and large resistivity variations in geothermal systems can be delineated by using these methods. At temperatures between 70 and 200°C (low and moderate temperature geothermal systems), clay alteration causes low resistivity. In high temperature geothermal systems with low and moderate salinity, the resistivity is considerably higher than low and moderate temperature geothermal systems (Ussher et al., 2000).

Zohdy et al. (1973) examined the resistivity distribution using the VES method

at the Mud Volcano vapor-dominated geothermal system in Yellowstone National Park, USA. In the work of Zohdy et al., analysis of the VES data revealed a highly resistive vapor-dominated layer located beneath a very low resistivity layer. This low resistivity layer consists of low porosity rocks with hot water. In a study conducted in the Southern Raft River Valley geothermal area, Idaho, USA, Williams et al. (1975) described geological formations of alluvium tuffaceous sediments and volcanic rocks. Magnetic and gravity data indicate the presence of a buried igneous mass as a possible heat source. Resistivity soundings showed a low resistive layer with 1 km thickness, and the authors reported that this layer might be evidence of hot water. Another study in the Genisea, NE Greece, geothermal field by Thanassoulas et al. (1987) found a low resistive zone that might be related to a heat source, and this was confirmed by temperature data from boreholes. El-Qady (2006) mapped the Hammam Mousa geothermal field in the Sinai, Egypt, using Schlumberger VES. According to 1D and 2D interpretations of the data set, geothermal drilling was recommended, where very low resistivity values are determined. The Sudano-Sahelian region of Cameroon was studied by J.D. Kana et al. (2015). Two potential geothermal reservoirs were mapped at 20 m and 25 m depths with VES method. In a recent study, Schlumberger VES was used over the Kutahya-Hisarcik geothermal field in western Anatolia by Üner et al. (2019). They reported that low resistivity anomalies were associated with the existence of geothermal fluid. Overall, these studies outline the importance of the VES method in geothermal exploration.

Chapter 3: Methods

As was mentioned in the previous chapter, geophysical methods are one of the main tools in geothermal exploration, which also involves geological, geochemical, remote sensing, and drilling methods. Geoelectrical methods are common tools which have considerable impact on investigating geothermal areas. The vertical electrical sounding (VES) method has been applied by many researchers in order to identify large resistivity contrasts in geothermal reservoirs. In this chapter, the basic principle of resistivity measurements, the vertical electrical sounding method, and inspection of raw VES data are presented.

3.1 Basic Principle of Resistivity Measurements

Resistivity ρ (Ωm), like magnetic susceptibility and density, is a property of a material. Resistance R (Ω) is a property of a circuit element (e.g., Reynolds, 2011). In Figure 3.1, the resistance (R) is proportional to the resistivity (ρ), the length (L) of a resistive material in the direction of current flow and cross sectional area (A) perpendicular to current flow. It is expressed as:

$$R=\frac{\rho \times L}{A} \tag{3.1}$$

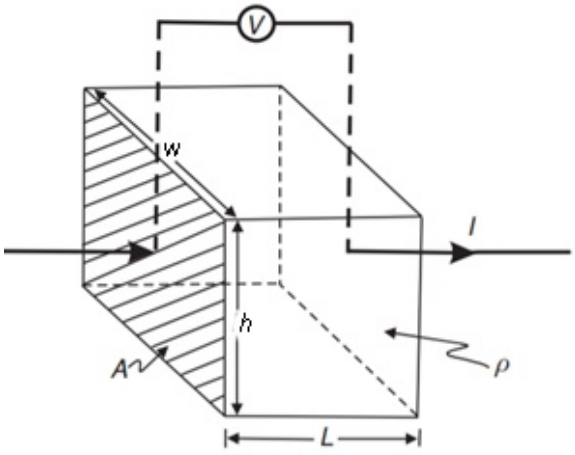

Figure 3.1 Diagram showing the relationship of L and A to current flow direction for equation (3.1) Here, A = h× w (Reynolds, 2011).

The basic relationship in resistance measurements is Ohm's Law:

$$V=IR \tag{3.2}$$

where, the resistance (R) is offered to current flow (I) under an applied voltage (V) (Figure 3.2).

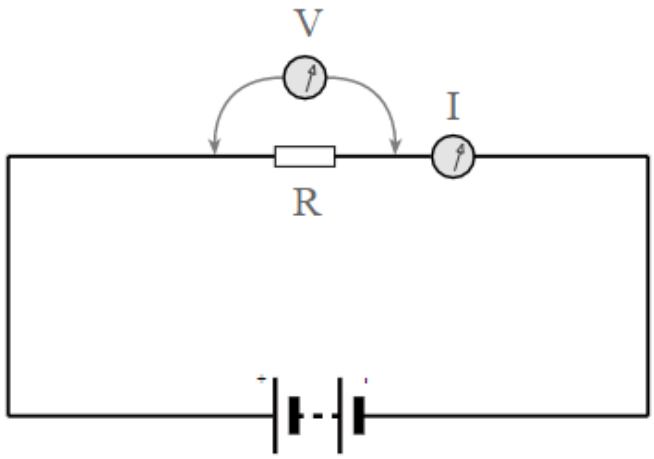

Figure 3.2 Ohm's Law for a circuit element. Retrieved from https://www.electronics-notes.com/articles/basic_concepts/resistance/what-is-ohms-law-formula-equation.php

The principle of resistivity measurement of the Earth's subsurface is that electrical current is injected into the ground through two 'current' electrodes, and that generates a potential difference which is monitored at the surface through two other 'potential' electrodes. In this case, the current does not flow through a simple circuit element with uniform properties like that in Figure 3.1. Instead, the current spreads out through the ground, which is probably inhomogeneous, in 3D. However, by assuming the current follows the path of a dipole electric field set up by the current electrodes, an averaged 'apparent' resistivity of the ground near the electrodes can be calculated as described below.

In resistivity measurements, four electrodes are required; two electrodes A and B are used to inject current and two electrodes M and N are used to observe the potential

difference. The electrodes can be arranged in any way, and some electrode arrangements are shown in Figure 3.3.

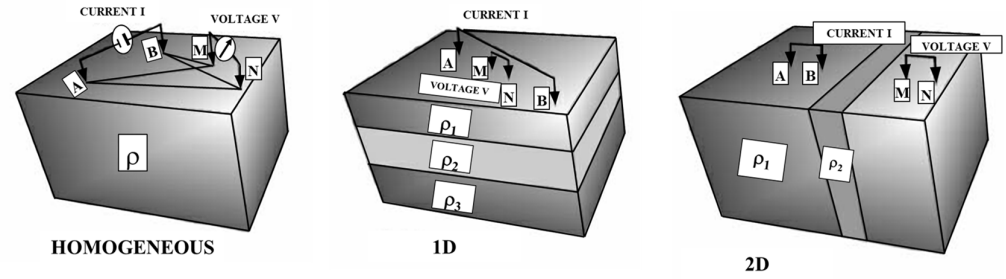

Figure 3.3 Electrode arrangement for resistivity measurements, Kirsch (2006).

The "apparent" resistivity ρ_a (Ωm) can be determined from current I and potential difference ΔV (Figure 3.3) from

$$\rho_a = K \cdot \frac{\Delta V}{I} \tag{3.3}$$

where K depends on the electrode arrangement. In theory, the true resistivity of formations can be obtained by using an electrode arrangement in an isotropic and homogeneous medium. However, anisotropy and heterogeneity are seen more often in reality. Therefore, the resistivity calculated from the measurement is called "apparent resistivity". The apparent resistivity depends on factors such as the thickness and resistivity contrast of the formations and the size and geometry of the array. The geometric factor K (unit: metre) depends on the configuration of electrodes and can be calculated from the distances between current and potential electrodes, and it expressed as:

$$K = 2\pi \left[\frac{1}{|r_A - r_M|} - \frac{1}{|r_A - r_N|} - \frac{1}{|r_B - r_M|} + \frac{1}{|r_B - r_N|} \right]^{-1} \tag{3.4}$$

where the r's refer to the locations of the electrodes. Current flow and equipotentials for a homogeneous medium are shown in Figure 3.4.

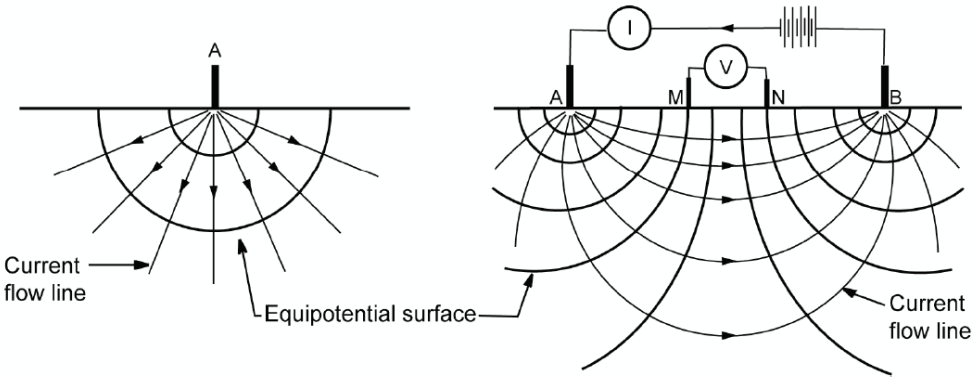

Figure 3.4 Current flow and equipotential lines in a homogeneous subsurface from a single current source (left) and from a pair of current electrodes (right) (Wightman, 2004).

In Figure 3.4 (left), the current flows radially out from an electrode A. The corresponding equipotentials are perpendicular to the current flow, and they form hemispheres. In reality, this perpendicular form will be more complex than hemispheres if the resistivity values change in the subsurface. For the current electrode pair (Figure 3.4, right), a dipole electric field is created in the subsurface. The current is injected from current electrode A and is received by the current electrode B. Then, the potential difference between M and N electrodes can be measured.

In resistivity measurements, some of the most common electrode configurations are the Schlumberger, Wenner, Pole-Dipole, and Dipole-Dipole arrays (Figure 3.5). The measurement point for plotting purposes is typically considered to be in the centre of the array at about half the AB spacing in depth. Individual measurements of apparent resistivity can be combined, by moving the centre of the array along a line to produce a profile, or increasing the AB spacing to produce a sounding. A 2D pseudo section can be made by doing both. A pseudo section is an approximate and distorted view of the subsurface. It can provide a qualitative picture of how resistivity changes with depth and along the profile. However, current flow in the subsurface is totally dependent on the variation of resistivity, and plotting a pseudo section based on the apparent

resistivity value at a depth equal to a half AB spacing can be a poor presentation of the actual ground structure.

The Schlumberger array is mainly used in VES surveys, where the potential electrodes (MN) are located in the center and, to take a sounding, the current electrodes (AB) are moved outwards after each measurement. Thus, the current can flow deeper.

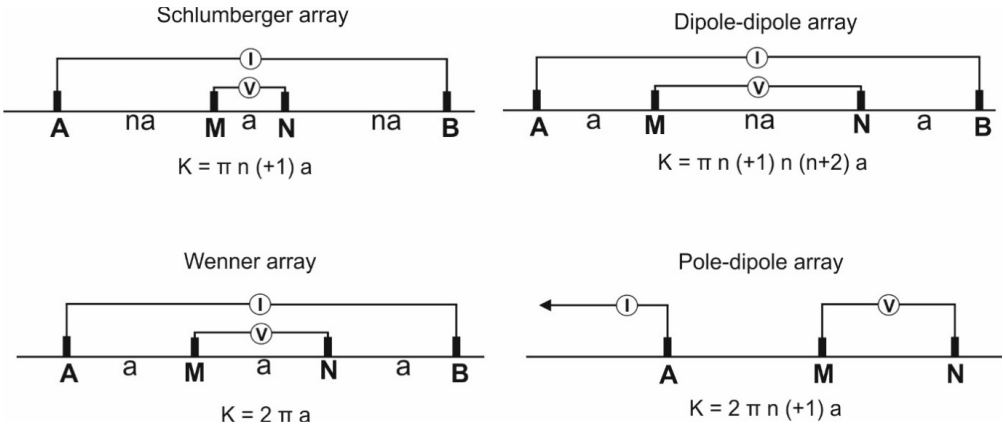

Figure 3.5 The Schlumberger, Wenner, dipole-dipole, and pole-dipole electrode arrays. Geometric factor is denoted by K for each array, Kirsch (2006).

For some surveys (generally Wenner, pole-dipole or dipole-dipole traverses) a number of electrodes are placed on a straight line at equal intervals. The electrodes are connected to a control unit by multicore cables. Electrode positions and electrode types are identified by a computer. More advanced, multichannel systems can measure more than one voltage for each AB. In Figure 3.6, different numbers of voltages are measured depending on the number of electrodes (4-Channel system and Full-Channel system).

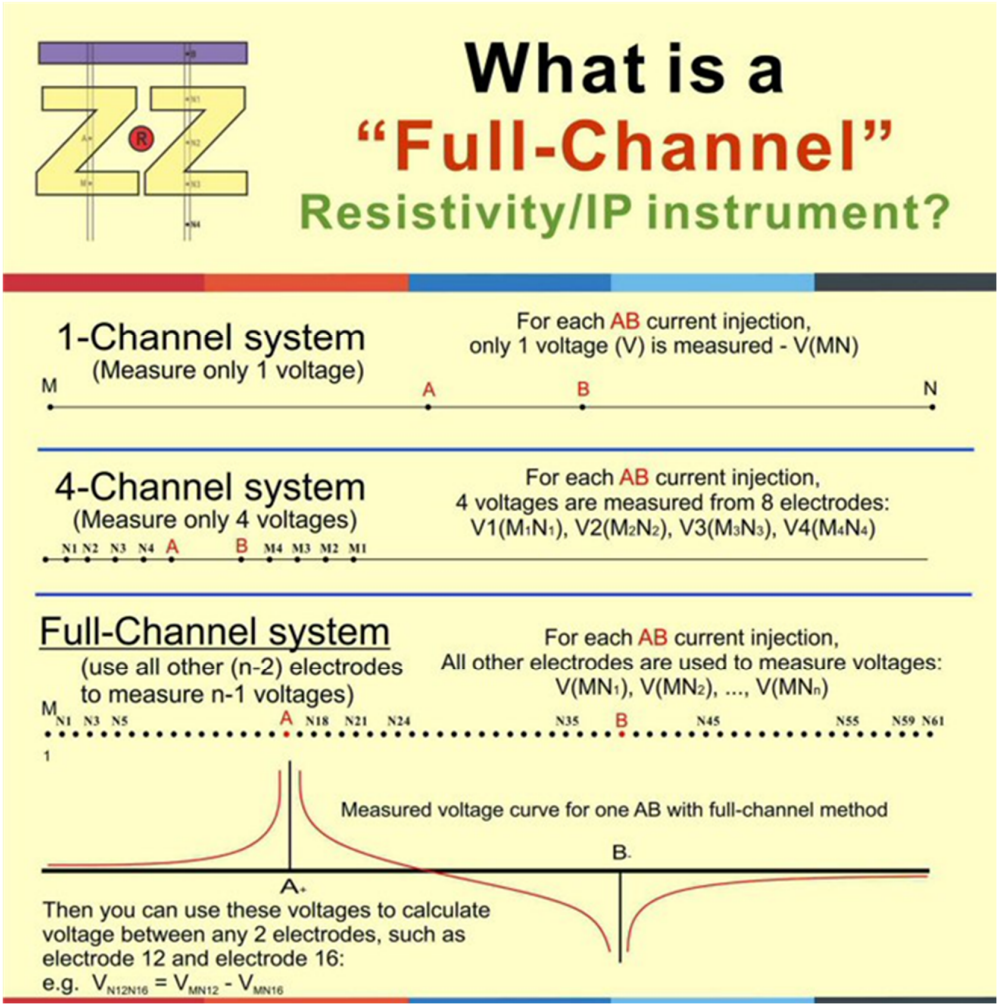

Figure 3.6 Multichannel resistivity measurements. Retrieved from https://www.zzgeo.com/?gclid=CjwKCAjw_JuGBhBkEiwA1xmbRW-1t_3w8-dsm_sEx-I1a1Y1kvemDz5LWQ-ecr9PBxcDH316qO9-FxoClzQQAvD_BwE.

3.1.1 Induced Polarization (IP) Data

The IP method is another geoelectrical method used in geothermal exploration where it is used for the detection of hot brines, alteration zones and faults (Wright et al., 1985). IP is also used in the detection of disseminated mineralization (Reynolds, 2011), and since the geothermal source layer in the drill core near Sandikli contained disseminated mineralization (Table 1.2) this was likely a reason IP was included in the survey data.

While collecting resistivity data, it is possible to collect IP data. In the IP method, injected current into the ground is switched off between resistivity readings.

After the current is switched off, the potential does not immediately drop to zero. The decay with time is measured between the potential electrodes. The measured quantity is called the chargeability, and it can be determined by the voltage existing immediately after the current is switched off (Figure 3.7a), or by an average voltage existing over a time interval after switching off (Figure 3.7b).

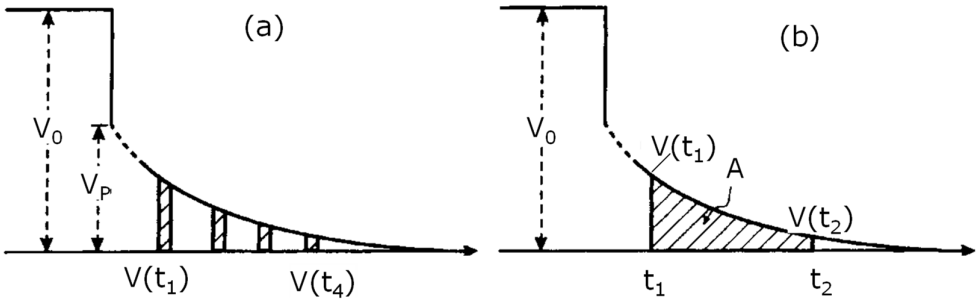

Figure 3.7 Two ways of measuring the time domain IP effect (Reynolds, 2011).

An example of how the IP effect is determined is given in Equation 3.5.

$$M = {}^{V_P}/_{V_0} \text{ (units: mV/V)} \tag{3.5}$$

IP is inherently more subject to noise because the signal is weaker. This is why IP is not used as excessively in geothermal exploration as resistivity.

3.2 Vertical Electrical Sounding (VES) Method

A Vertical Electrical Sounding is used to determine vertical resistivity distribution below the surface of the survey point and is best applied to a horizontally layered medium. In this ideal case, resistivity values and thicknesses of layers are the desired results of VES measurements. In VES measurements, current penetration is increased by increasing the current electrode (AB) spacing. Then, the resistivity values of deeper layers can be seen (Figure 3.8).

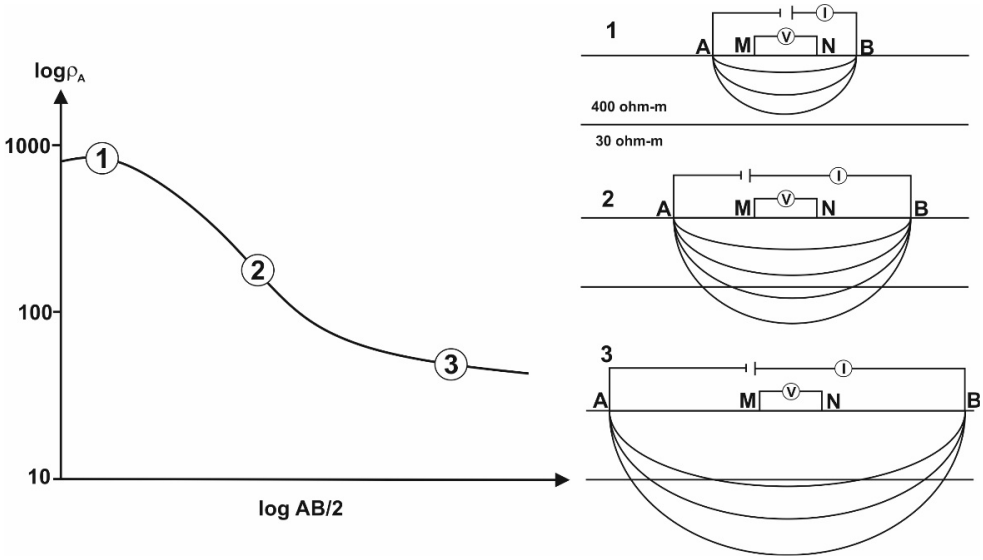

Figure 3.8 Increased current electrode spacing and depth penetration. Results of the measurement are shown in the logarithmic chart, Kirsch (2006).

The raw VES data (apparent resistivity vs current electrode spacing) gives a pseudo depth profile. The first estimate of the number of contrasting layers and their relative resistivities is obtained by inspecting soundings. The inspection of raw VES data provides a qualitative picture of the ground structure and is a helpful guide for developing forward models and predicting the resistivity versus depth in the earth.

3.2.1 Identifiable Layers

Even if the ground is horizontally layered, fine, complex or gradational layering will likely not be resolvable, particularly in the raw data. The number of 'identifiable' layers is equal to the number of identifiable steps in the sounding curve, or to the number of turning points (where the curvature changes sign) plus one (Reynolds, 2011).

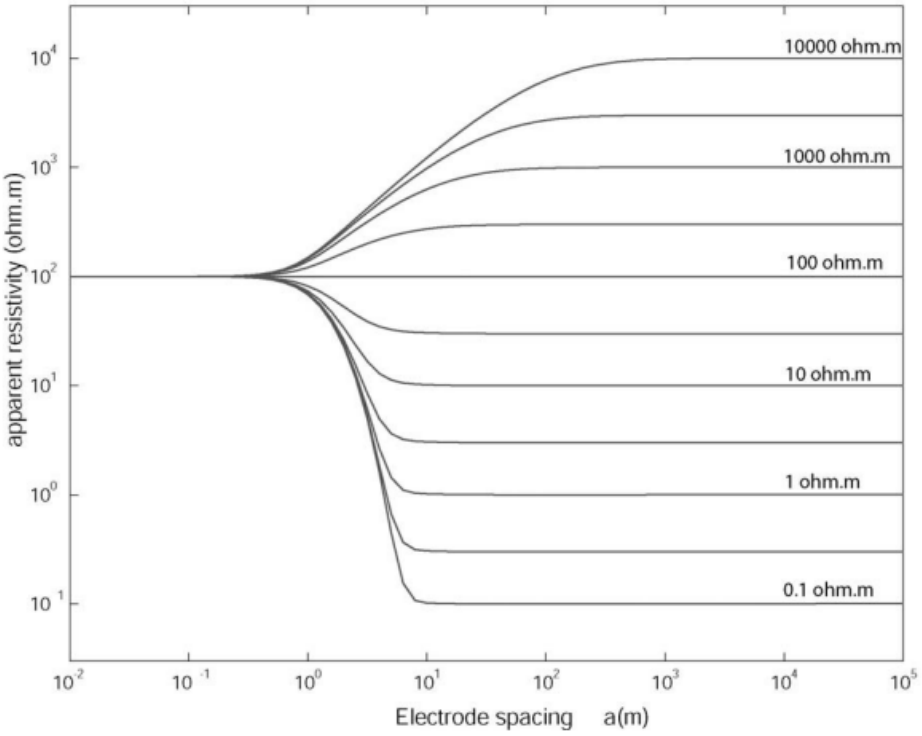

Figure 3.9 Expected sounding curves over a two layer Earth, where the top layer has a resistivity of 100 Ω.m, the intervace is at 1 m, and the bottom layer has the resistivity indicated on the curve (Unsworth, 2009).

If the sounding curve flattens at small current electrode spacings, the resistivity of the top layer can be estimated as the resistivity on the flat part of the curve. In a two-layer system, if the current electrode spacing is wide enough, then the apparent resistivity approaches the resistivity of the lower layer (Figure 3.9). In addition, for a two-layer subsurface, the thickness of the top layer can be roughly calculated from the steepest slope on the sounding curve in a log-log curve. Depending on the resistivity contrast between the layers, the interface occurs at a depth roughly corresponding to a half to $1/10^{th}$ of the AB/2 spacing corresponding to the steepest slope (Figure 3.9). If there are more than 2 layers, the turning points do not provide a reliable depth of the interface.

Figure 3.10 shows general shapes of sounding curves over a 3 layer subsurface, where in each case the resistivity of the first layer is distinguishable. The 45 degree angle for Type H indicates the maximum slope possible for an infinitely resistive third layer. The small h_2 curve for Type Q illustrates that in this situation it may be difficult to identify the middle layer.

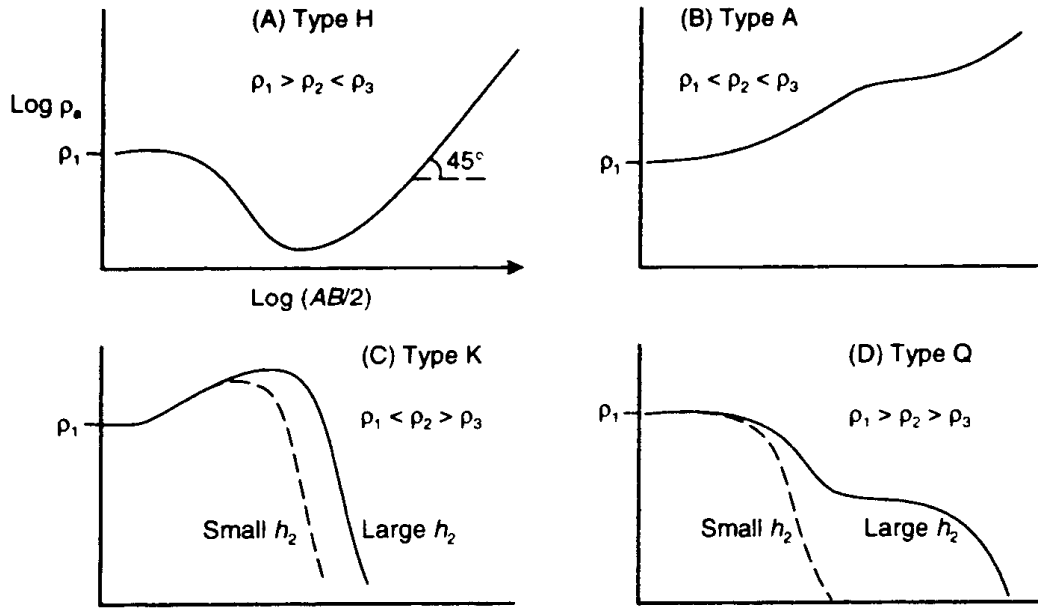

Figure 3.10 Sketches illustrating the possible shapes of sounding curves over ground with three layers: h_2 is the thickness of the middle layer (Reynolds, 2011).

3.3 Description of Field Acquisition and Equipment

The data for this study originates from a survey commissioned by a private company providing geophysical services to determine geothermal heat sources for the greenhouses in the Sandikli region. The data was provided by Mr Zulfikar Erhan, an instructor from the department of geophysical engineering at Dokuz Eylul University, Izmir, Turkiye. The reason why the data has not been previously analysed is that the company was shut down shortly after the data were collected. According to an internal report provided by Mr Zulfikar Erhan, the Vertical Electrical Sounding method was

utilized, where the general sounding locations were chosen based on the high temperature values obtained from drilling in the graben (section 2.4). The provided VES data was in text file format, with one file for each sounding, and an additional location file giving the UTM coordinates of the centre locations of the soundings and the time and date when the data were downloaded from the instrument.

The survey consisting of 384 soundings, labelled s1 through s395 with some omissions. Each sounding data file contains the AB and MN electrode spacings, the apparent resistivity and the IP value (Table 3.1). UTM locations and acquisition dates for each of the soundings can be found in Appendix B, and graphs of the collected raw data (apparent resistivity vs AB spacing) can be seen in Appendix C.

Table 3.1 The first 20 entries in an example data file

DataSet:	Prosys	NORTH:	0	EAST:
Number	AB/2	MN	RESISTIVITY	IP
1	25	10	23.6362	3.6874
2	30	10	24.2259	3.7032
3	35	10	24.5655	3.8912
4	40	10	24.0452	3.8789
5	50	10	21.9239	4.3354
6	60	10	20.239	4.7983
7	70	10	19.3597	5.2968
8	80	10	17.9832	5.0863
9	100	10	16.3851	5.4636
10	120	10	15.3589	4.1313
11	120	40	14.5913	5.8708
12	150	40	10.9733	6.1798
13	180	40	11.719	6.1712
14	200	40	12.9897	5.4069
15	250	40	12.9446	2.8126
16	300	40	11.9219	3.3155
17	300	100	11.5857	4.2256
18	350	100	12.5458	3.3787
19	400	100	13.431	7.4403
20	500	100	17.0033	3.687

Work was carried out between January 2011 and August 2011 (see graph in Appendix B). The study area was mostly over irrigated agricultural lands without dense vegetation (Appendix A). Any areas with dense vegetation and big rocks were cleared. The soundings were arranged so that the centres were located at equal spacings in lines

or grids, with a typical spacing between soundings of ~400 m (Appendix B). The AB spacing for each sounding was varied systematically from 50 to 5000 m for totals of about 35 readings per sounding. The electrodes, expanding outward from the centre for each sounding, were orientated along the lines, such that there was significant overlap between neighbouring soundings. Some measurements were taken by the sides of the main road and railroad for ease of access, however, heavy vehicle traffic was not observed during the measurements.

In the data collection process, the survey team consisted of five workers and one geophysicist. An individual sounding took approximately an hour. Four electrodes of stainless steel were used. During the first 4 months of the surveys, rainfall and snow were observed occasionally. In the hot season, salt water was poured around the electrodes to decrease high contact resistance between soil and electrodes.

To reach the maximum 5000 m spread distance, wire spools each containing 1000 m of wire were spliced together. The current was generated through an IRIS Instruments VIP 5000 electrical transmitter which allows injection parameters such as injection current and voltage to be controlled. The potential difference values were collected and saved by an IRIS Instruments Syscal Pro receiver unit. Syscal Pro can operate with up to 120 electrodes, and the electrode configuration can be configured through the instrument or computer software. An electrical generator was used as a power source. Some detailed features of the equipment are shown in Table 3.2.

Table 3.2 Equipment used in VES measurements.

Transmitter: Resistivity & IP 5 kW VIP 5000 electrical transmitter of IRIS instruments 	**Full microprocessor control Ease-of-use, Standard motor generator** **Outputs: 3000 V - 5000 W - 10 A** **Output power: 5000 W maximum** **Output voltage: 3000 V maximum** **(Automatic voltage range selection)** **Output current: 10 A maximum, current regulated** **Current accuracy: better than 1%** **Current stability: 0.1%**
Receiver: Syscal Pro of IRIS instruments 	**Voltage: 0 - 200 Vpp** **Current: 0 - 50000 mA** **Power: 5000 W** **Input Impedance: 100 MOhms** **Input Voltage: 15V, automatic gain, input protection 1000V**
Generator 	**Single or three-phase** **Output power: 180-220V** **Frequency: 45-800 Hz**

3.4 Preinversion Processing

Before inverting the VES data, it was necessary to inspect the raw data. Unfortunately, the raw data set does not include the currents, voltages, and standard deviations, so this data set could not be used to evaluate the reliability of the data points. For this reason, other criteria are used, such as smoothness, consistency between neighbouring soundings and the magnitude of offsets associated with moving potential electrodes (see below). Curves showing changes correlated with nearness to faults were not considered as reliable, though they were corroboration of the existence of faults. The VES curve of apparent resistivity versus current electrode spacing is plotted from field measurements (Appendix C). This plotted curve is always smooth when it is only affected by vertical variation in resistivity (Van Nostrand and Cook, 1966). If it is not due to an equipment error, irregular readings in the apparent resistivity are an indication of lateral changes in resistivity of the subsurface, particularly if the changes are shallow and close to the electrodes.

3.4.1 Inspection of Raw Data: Removal of Offsets

In the Schlumberger configuration, the sensitivity of the potential difference decreases as the current electrode spacing AB is increased (Van Nostrand and Cook, 1966). To maintain a reasonable signal to noise ratio, the potential electrode spacing MN must be increased periodically as the current electrode spacing increases. Changing the potential electrode spacing usually generates an offset in the VES curve due to lateral inhomogeneity in the near surface environment of the potential electrodes. This offset is observed as a general shift, and it does not change the shape of the VES curve much (Zohdy, 1968). Therefore, by repeating the measurement at the two potential electrode positions, offsets can be calculated and used to obtain smooth curves for the inversion.

The raw data includes such repeat measurements. Figures 3.11 and 3.12 illustrate how offsets were calculated and allowed for. Ideally, these offsets should be small compared with the apparent resistivity values.

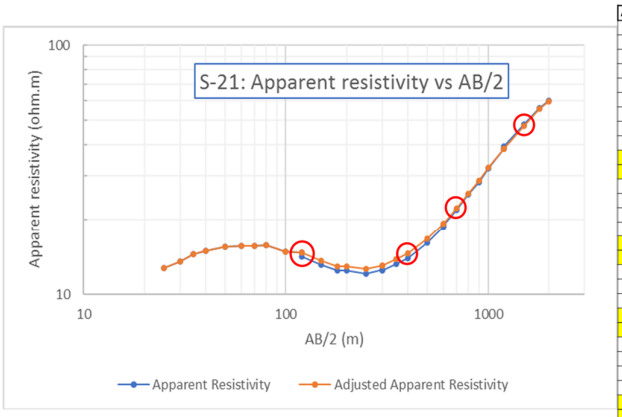

AB/2 (m)	MN (m)	RESISTIVITY (ohm.m)	OFFSET	adjRES
25	10	12.7309		12.7309
30	10	13.5616		13.5616
35	10	14.4953		14.4953
40	10	14.8952		14.8952
50	10	15.5204		15.5204
60	10	15.6501		15.6501
70	10	15.626		15.626
80	10	15.7043		15.7043
100	10	14.8511		14.8511
120	10	14.6843		14.6843
120	40	14.1544	-0.5299	14.6843
150	40	13.0918		13.6217
180	40	12.406		12.9359
200	40	12.4163		12.9462
250	40	12.0764		12.6063
300	40	12.5258		13.0557
300	100	12.4507	-0.0751	13.0557
350	100	13.1808		13.7858
400	100	13.9657		14.5707
500	100	16.1383		16.7433
600	100	18.6344		19.2394
600	200	18.9774	0.343	19.2394
700	200	21.9641		22.2261
800	200	25.2263		25.4883
900	200	28.3788		28.6408
1000	200	32.1283		32.3903
1200	200	38.4112		38.6732
1200	400	39.2829	0.8717	38.6732
1500	400	48.3655		47.7558
1800	400	56.2116		55.6019

Figure 3.11 The curve of sounding 21. Red circles show the offsets where the potential electrode spacings are increased.

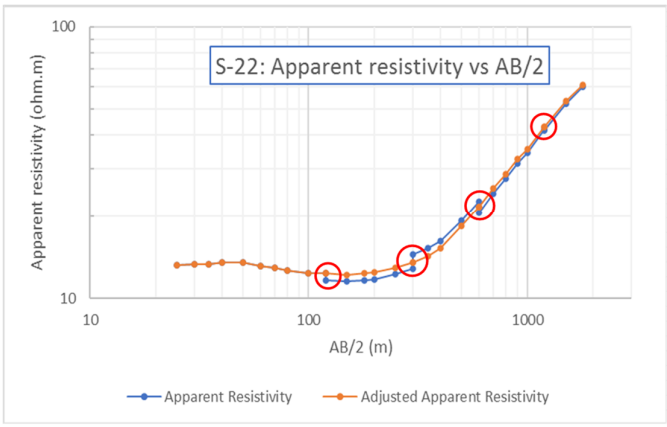

AB/2 (m)	MN (m)	RESISTIVITY (ohm.m)	OFFSET	adjRES
25	10	13.2977		13.2977
30	10	13.3034		13.3034
35	10	13.3762		13.3762
40	10	13.5442		13.5442
50	10	13.5408		13.5408
60	10	13.1048		13.1048
70	10	12.9195		12.9195
80	10	12.671		12.671
100	10	12.4208		12.4208
120	10	12.3374		12.3374
120	40	11.673	-0.6644	12.3374
150	40	11.5526		12.217
180	40	11.671		12.3354
200	40	11.7639		12.4283
250	40	12.278		12.9424
300	40	12.8389		13.5033
300	100	14.4602	1.6213	13.5033
350	100	15.2658		14.3089
400	100	16.2461		15.2892
500	100	19.3511		18.3942
600	100	22.7932		21.8363
600	200	20.7336	-2.0596	21.8363
700	200	24.4684		25.5711
800	200	27.727		28.8297
900	200	31.5541		32.6568
1000	200	34.4267		35.5294
1200	200	41.8382		42.9409
1200	400	41.7119	-0.1263	42.9409
1500	400	51.9975		53.2265
1800	400	59.9928		61.2218

Figure 3.12 The curve of sounding 22. Red circles show the offsets where the potential electrode spacings are increased.

In Figures 3.11 and 3.12, the offsets highlighted in yellow can be seen in the resistivity column. These offsets are determined one by one and subtracted from the resistivity values, respectively. As a result of this adjustment, smoother curves are obtained.

Note that the curves are adjusted to be smooth relative to the measurements at the smallest MN spacing, but there is no reason that the apparent resistivity before an

offset is more reliable than that after the offset. This is not important for a single sounding, where the overall shape is more important than the actual values of resistivity, however when combining soundings in a 2D profile there could be shifts from one sounding to another if the offsets are large. Fortunately, most of the offsets are small (e.g., Figure 3.12) except in particular areas (section 3.4.3).

3.4.2 Inspection of Raw Data: Identification of layering

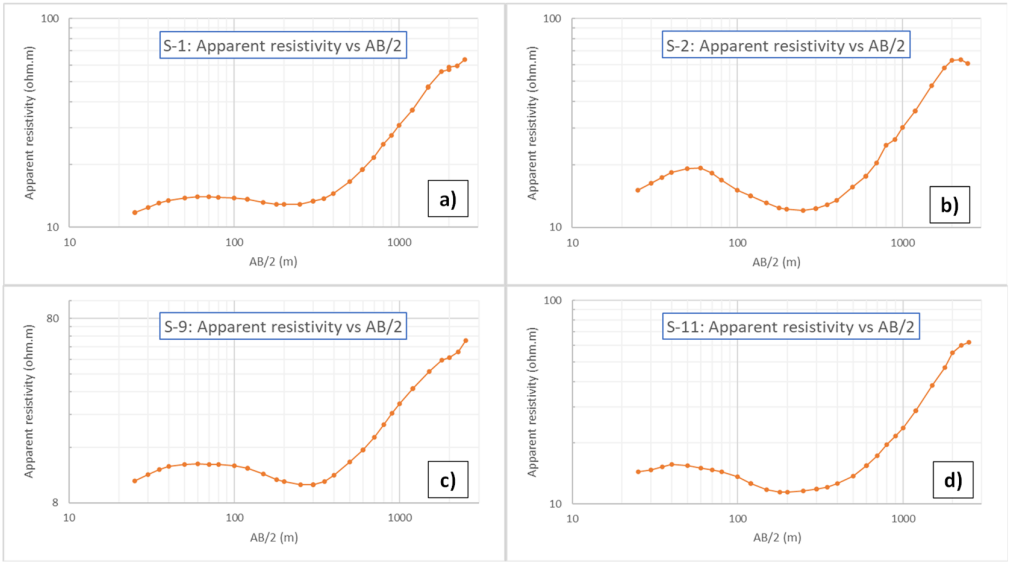

Figure 3.13 Soundings 1,2,9 and 11 from Afyon-Sandikli geothermal field. These soundings are located in Area 2.

As described above (section 3.4.1), an estimate of the number of broad scale contrasting layers can be made from inspection of the sounding curves. In the sounding curve in Figure 3.13(a), there are four identifiable layers. From inspection of this curve, the resistivity of the first layer, $\rho_1 \cong <10$ ohm-m, the second layer has a higher resistivity (>>14 ohm-m), the third layer has a lower resistivity than the second layer, and the fourth layer has considerably higher resistivity. The first turning point occurs at AB/2=<25 m and so the top layer would be less than 8 m thick (25/3). The same number of layers can be identified for the curves of s-2, s-3, and s-11. On the other hand, there

are points where the data become noisy and less reliable. Sharp kinks on the curve where the potential electrode spacing is not changing might a good indication of unreliable data. For example, the resistivity at AB/2~>2000 m changes sharply downward for s-2, so the highest values at this point would likely be omitted from the inversion. More gradual changes, as seen in the other soundings, may be an indication of a deep lower resistivity layer.

3.4.3 Surface Heterogeneities

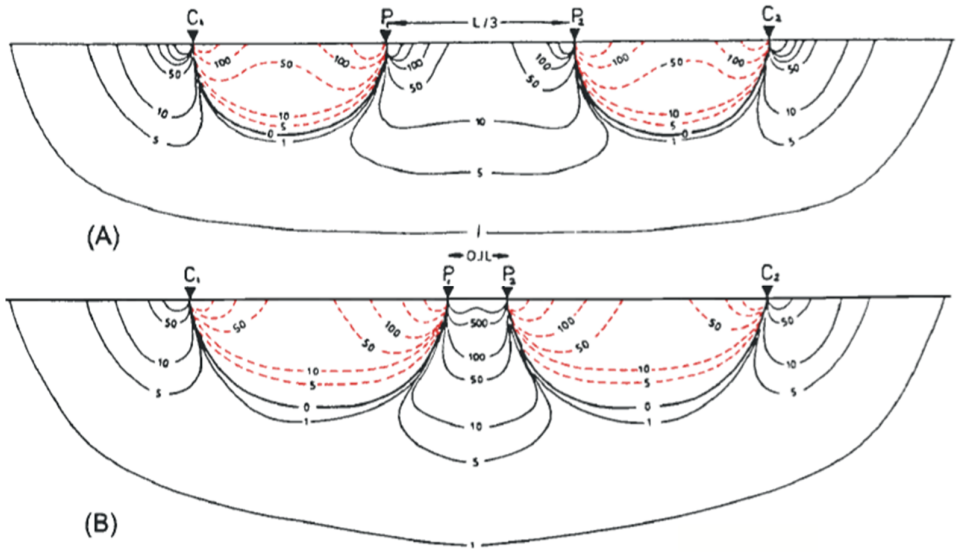

Figure 3.14 Signal contribution sections for Wenner (A) and Schlumberger (B) arrays (Barker, 1979).

Figure 3.14 of 'signal contribution' shows how the resistivity at each location within the subsurface contributes to the measurement of apparent resistivity. The numbers on the contour lines indicate the relative importance of the resistivity values; black contours lines indicate a 'positive' contribution, so that anomalous resistivities in these locations will change the apparent resistivity in the same sense as the anomaly. Red contour lines indicate a 'negative' contribution, so that an anomalous patch of resistivity here will lead to a change in the apparent resistivity in the opposite direction to the

anomaly. The high contours near the electrodes indicate that any variations in resistivity here have a large effect on the reading.

Figure 3.14 indicates that heterogeneities near the surface, and particularly near the electrodes can have large effects on the apparent resistivity values. As the electrodes are moved to new locations on the surface, their location relative to any surface anomalies changes. In the Schlumberger array, the ground between the potential electrodes has a very large effect. This might happen because of the relatively short distance between potential electrodes. Therefore, when the surface is heterogeneous, moving the potential electrodes can lead to large positive or negative jumps in the apparent resistivity readings.

Examples of very large resistivity jumps related to moving the electrodes can be seen in Figure 3.15.

As was mentioned in Chapter 1, there are some geothermal greenhouses in the Afyonkarahisar province. Such geothermal greenhouses are located within the Hudai-Sandikli geothermal field (Figure 3.15a). From the data near the greenhouses, it can be seen that there are significant jumps in resistivity (Figure 3.15b-c) associated with moving the potential electrodes. This result indicates that the near surface in this area is heterogeneous, perhaps as a consequence of shallow hydrothermal activity.

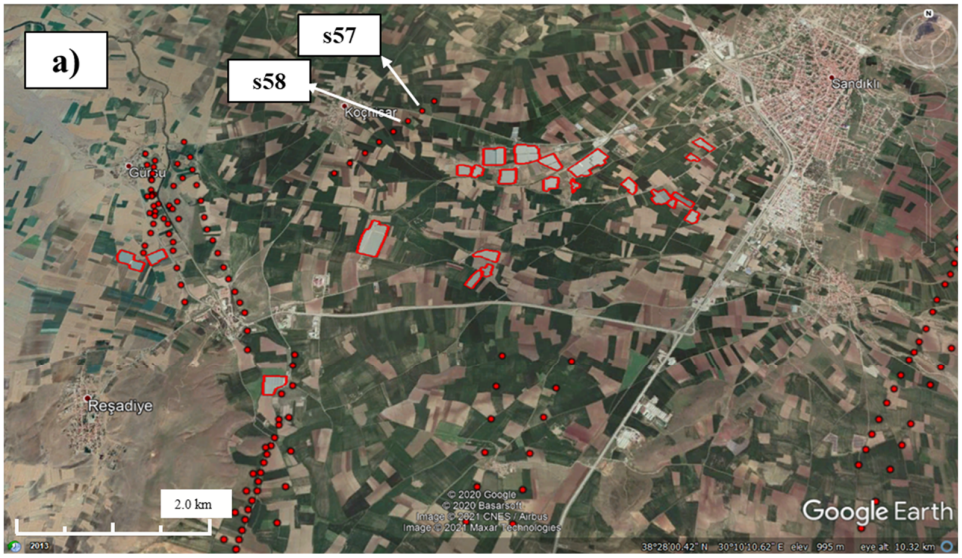

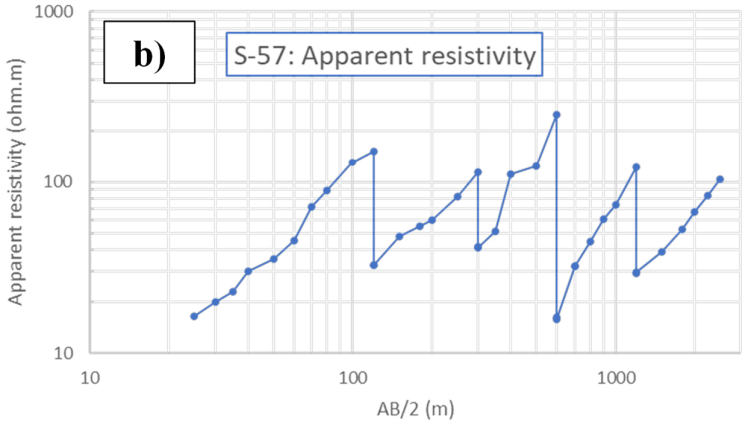

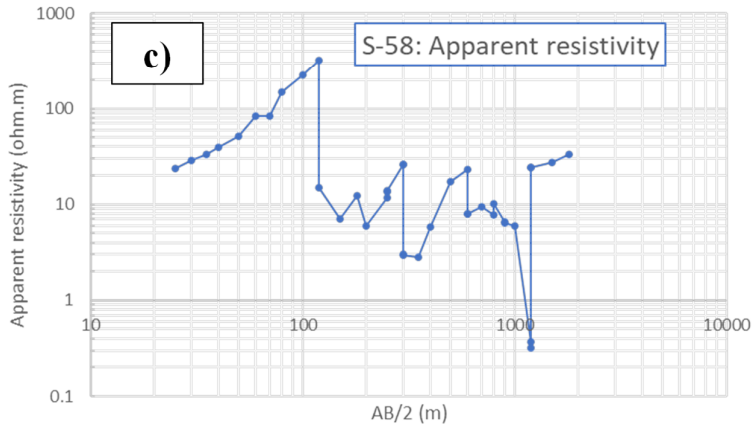

Figure 3.15 (a) Location of S-57 and S-58 (Area 2) and geothermal greenhouses, outlined in red. (b) and (c) sounding curves for S-57 and S-58, illustrating large jumps associated with moving the potential electrodes over a heterogeneous surface.

3.4.4 Omitting Unreliable Data and Smoothing VES Curves

Interpretation methods of VES curves are based on curve matching (theoretical and observed curves) to acquire layer parameters. Before the interpretation of the sounding curves, unreliable and noisy parts of the data, such as single point large resistivity jump or resistivity values that remain constant at the end of sounding curve, should not be included in the interpretation. Examples of data omitted from interpretation are shown in Figure 3.16.

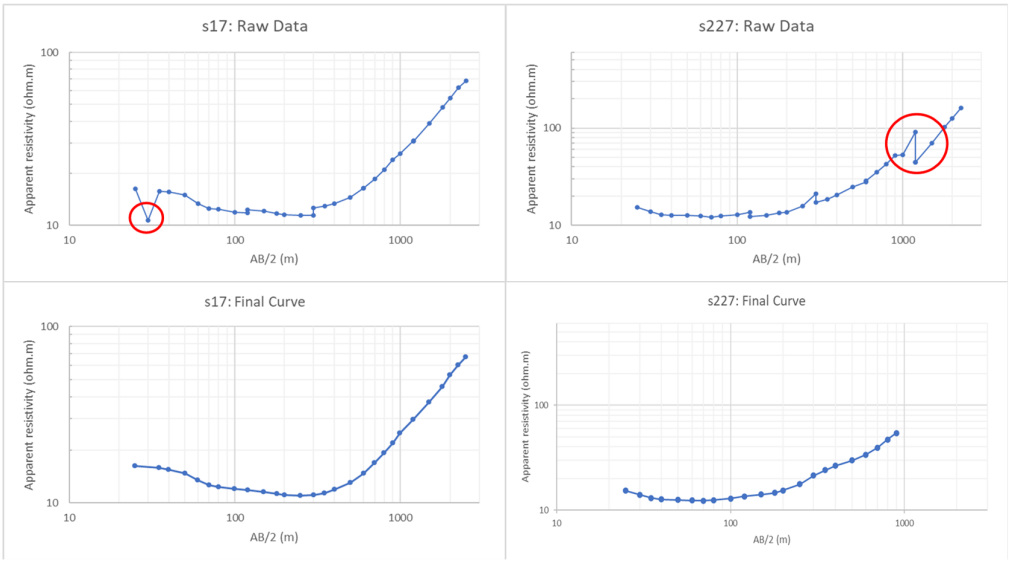

Figure 3.16 Examples final curves after omitting unreliable data.

Additionally, the observed curves should be smoothed before analyses and interpretations to eliminate certain observational errors and the effect of lateral changes. It is important to note that single point anomalies are eliminated, and zigzags are smoothed before the interpretation begins (Figure 3.17). Theoretical and smoothed observed curves should be inspected and compared for distortion in apparent resistivity.

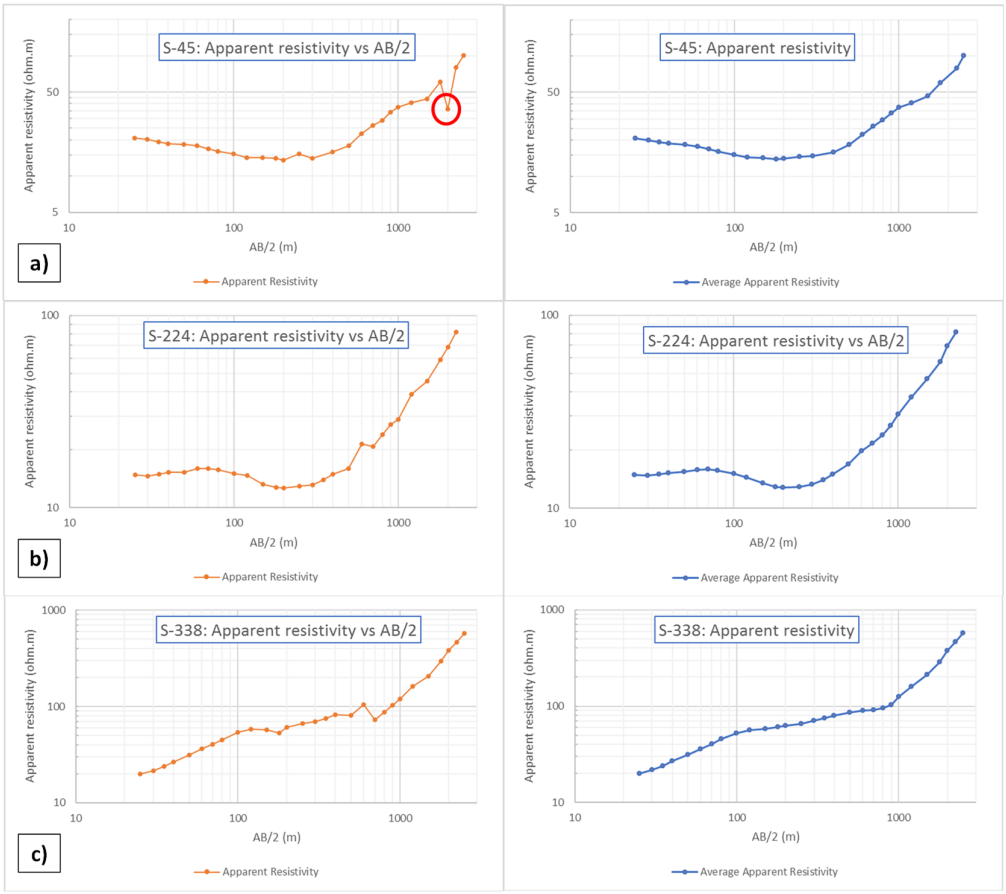

Figure 3.17 Apparent resistivity curves on the left and smoothed apparent resistivity curves on the right.

In Figure 3.17, clear examples of zig-zag effects can be seen in the apparent resistivity graphs on the left. It is assumed that an anomaly shows the approximately equal and opposite effect on neighboring points. The VES curves can be smoothed by replacing apparent resistivity with the weighted average of the measured value at a survey point and the survey points on either side. The images on the right represent smoothed curves using the weighted average.

$$\log(\rho_2') = w_1 \times \log(\rho_2) + w_2 \times \left(\log(\rho_1) + \log(\rho_3)\right) \tag{3.6}$$

$$w_1 + 2w_2 = 1 \tag{3.6a}$$

A weighting scheme of 0.5 (w_1) and 0.25 (w_2) is used to calculate the weighted average of most of the survey points. The weighting w_1 was occasionally varied between 0.48 to 0.52 to achieve a smoother sounding. This smoothing algorithm was applied after eliminating isolated anomalous points. After smoothing, the inverse logarithm of the smoothed values is calculated. For sounding 338 (Figure 3.17c), the weighted average calculation scheme is presented in Table 3.3.

Table 3.3 Weighted average calculation scheme for sounding 338.

	A	B	C	D	E	
Points	**AB/2 (m)**	**ρ_a (ohm.m)**	**Logρ_a**	**Log Average ρ_a**	**Average ρ_a**	
9	100	53.70	1.73	1.72	52.28	⋮
10	120	57.76	1.76	1.75	56.52	D10=0.5*C10+0.25*(C9+C11)
11	150	56.96	1.76	1.77	58.48	D11=0.5*C11+0.25*(C10+C12)
12	180	53.07	1.72	1.78	60.56	D12=0.5*C12+0.25*(C11+C13)
13	200	61.01	1.79	1.80	62.81	D13=0.5*C13+0.25*(C12+C14)
14	250	66.83	1.82	1.82	66.05	D14=0.5*C14+0.25*(C13+C15)
15	300	69.84	1.84	1.85	70.36	D15=0.5*C15+0.25*(C14+C16)
16	350	75.20	1.88	1.88	75.35	D16=0.5*C16+0.25*(C15+C17)
17	400	81.60	1.91	1.90	79.68	D17=0.5*C17+0.25*(C16+C18)
18	500	80.50	1.91	1.94	86.30	D18=0.5*C18+0.25*(C17+C19)
19	600	104.91	2.02	1.95	89.70	D19=0.5*C19+0.25*(C18+C20)
20	700	73.07	1.86	1.96	90.99	D20=0.5*C20+0.25*(C19+C21)
21	800	86.79	1.94	1.98	94.96	D21=0.5*C21+0.25*(C20+C22)
22	900	103.34	2.01	2.01	102.74	D22=0.5*C22+0.25*(C21+C23)
23	1000	120.20	2.08	2.10	124.76	D23=0.5*C23+0.25*(C22+C24)
24	1200	162.27	2.21	2.20	159.83	⋮

In this study, IP data was collected with resistivity method. As illustrated in Figure 3.17, the IP data is much noisier than the resistivity data. In the apparent resistivity curves, it is possible to identify layers with differing resistivities (Figure 3.18). IP results, on the other hand, do not show such patterns due to excessive noise level for AB/2 spacings greater than about 100 m. Therefore, only the near surface IP data is considered in this study.

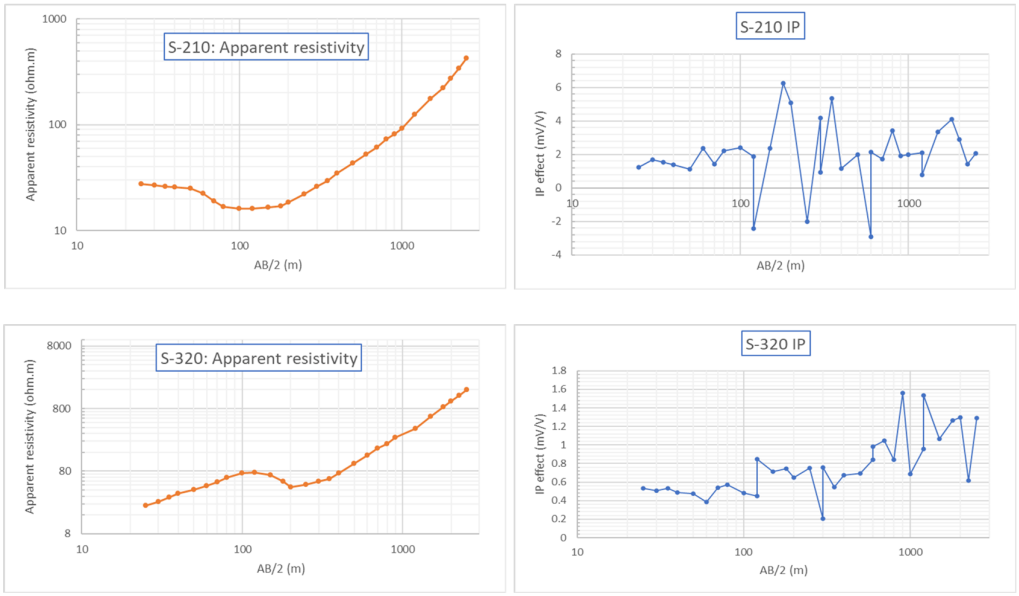

Figure 3.18 Comparison of the resistivity and IP data.

3.5 Theory of 1D and 2D Inversion

Before describing inversion, forward modelling should be described. In forward modelling, the responses to a given model of the subsurface are calculated. The responses (synthetic data) are computed from an array of subsurface cells that have known physical properties (e.g. resistivity, magnetic susceptibility, gravity etc.) Data from a geophysical survey are expressed as:

$$\mathbf{F_j[m]} = \mathbf{d_j^{obs}} \equiv \mathbf{d_j} + \mathbf{n_j} \qquad \mathbf{j}=1, \ldots, N \tag{3.7}$$

where $\mathbf{F_j}$ is the forward modelling operator which is relevant to the survey concept and physical equations, $\mathbf{m}$ describes the physical property distribution, $\mathbf{d_j}$ are the calculated data subject to noise $\mathbf{n_j}$. The N data points $\mathbf{d^{obs}}$ are obtained from a geophysical survey. The results of a forward model are compared with the observed data to see how the model $\mathbf{m}$ can be adjusted to get a better match. In inversion, the adjustment process is automated. The aim of the inversion process is to produce the model $\mathbf{m}$ that best fits the data allowing for noisy observations. Details are presented in Oldenburg and Li (2005).

The Vertical Electrical Sounding method is traditionally used for the exploration of 1D structures in the subsurface. Automated inversion algorithms are used to obtain simple layered earth models in 1D analysis of VES data. In the inversion of VES data, the ground is divided up into a finite number of horizontal layers, with each layer having a constant resistivity within it. Inversion algorithms are performed to determine the optimum number of layers, their true resistivities and thicknesses. In most 1D inversion programs, the interpreter can define the number of layers, and this can be varied to acquire the best model-data fit (Alali and Morgan, 2017). The application of 2D inversion techniques in collinear VES data (that is, a series of soundings taken along a profile) is not common in North America. The reason is that irregular electrode spacing in VES is not suited well to the block (mesh) modelling used by most 2D inversion programs. However, it is possible to use standard 2D inversion algorithms by modifying the block modelling according to the VES electrode positions. In this research, 1D layered models are complemented and combined with 2D inverted models. Before proceeding to examine 1D and 2D models, the theories of inversion programs will be explained in the following section.

3.5.1 1D Resistivity Inversion Modelling

Interpretation methods of vertical electrical sounding data are divided into three groups, and they are known as curve matching methods, direct methods, and iterative methods (Koefoed, 1979). Curve matching methods are where observations are compared with theoretical curves and matched by eye until a desirable measure of misfit is achieved. Currently, they are not widely used because these methods are unsuitable for numerical calculations. In direct methods, a resistivity transformation function is derived from the apparent resistivity values (Başokur, 1990). This transformation function of a VES

curve is used to estimate the layer parameters. However, they are susceptible to noise and are not considered as reliable methods. Iterative methods rely on searching for the best fit between theoretical and observed data using the least-squares approach. First, the theoretical response is calculated using a guess model which is created by the interpreter. Then, observed data and theoretical responses of the model are compared. This operation is then repeated by adjusting guess model parameters until observed and theoretical data sets reach the best-fit (Başokur, 1990). Today, most 1D automated interpretation programs use the iterative method. For 1D inversion modelling, EarthImager 1D software based on iterative method was used. The software uses smoothed model (the Gauss-Newton method) inversion (AGI, 2009). In the section that follows, the procedures of iterative method for EarthImager 1D will be presented.

Iterative Method Procedures

According to Zohdy (1989), one common iterative method is based on the assumptions:

a) The number of layers and the observation points on the VES curve is equal. This assumption will not change during the iterative process.
b) The layer thicknesses correspond to the spacings of the electrodes (usually placed at equal intervals on a logarithmic scale).
c) For the first iteration, the observed apparent resistivities and the true resistivities of the guess model are equal.

Figure 3.19 illustrates the basic working principle of 1D automated interpretation programs. The dots indicate the apparent resistivity values obtained by a sounding, with resistivities given by the solid lines. Panels (a), (b) and (c) illustrate the process over a simple 5 layer subsurface. Close inspection of the figure shows that the calculated layer depths cannot be sufficiently approximated by the electrode spacing (Figure 3.19a). For

this reason, the calculated layer depths are shifted to attain compatibility with the VES curve (Figure 3.19b). The same situation is observed for the true resistivity. The observed resistivities are adjusted to approximate the true resistivities (Figure 3.19c).

The user can define the final number of layers for the model. After the iterative process, the model is further adjusted. As a consequence of these steps, a final model is obtained, the shape of which will depend on the final number of layers specified by the user.

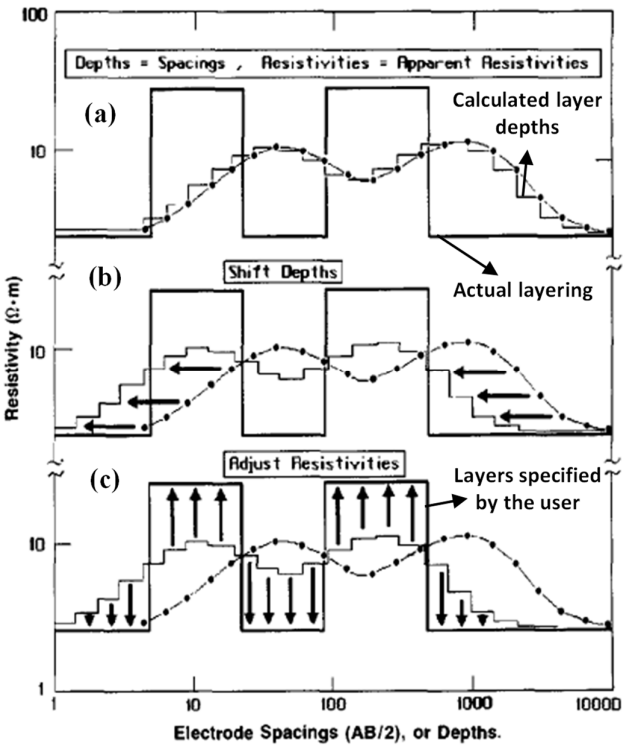

Figure 3.19 The basis of automated interpretation programs (Zohdy, 1989).

Calculation of depths

In practice, it is not possible to obtain perfect accuracy for the resistivity versus depth curve. The iterative process is used to determine the optimum shift amount:

i. A first guess multilayered model is made based on the sounding curve (Figure 3.20a).

ii. A theoretical sounding curve is calculated for a multilayered model by a forward modeling (Figure 3.20b).

iii. The root mean square deviation (RMS) is calculated by the equation:

$$RMS(\%)=\sqrt{\frac{\sum_{j=1}^{N}\left(\frac{\rho_{oj}-\rho_{cj}}{\rho_{oj}}\right)^{2}}{N}}\times 100, \tag{3.8}$$

where ρ_{oj} is the jth observed apparent resistivity and ρ_{cj} is the jth calculated apparent resistivity, and N is the number of observation points.

iv. All depths reduced by a small, arbitrary amount, say, 10% by multiplying them by 0.9 .

v. Steps (ii) and (iii) are repeated, and a new RMS is calculated.

vi. The new and previous rms values are compared. If the new value is lower than the previous rms value, the new calculated layer depths will be closer to their optimum position in terms of the true depths.

vii. All steps are repeated until the minimum rms value is reached. In Figure 3.20c, the shifted depths and calculated theoretical sounding curve for a minimum rms value are presented.

Calculation of Resistivity

After the theoretical depth curve is obtained, resistivities must be adjusted to acquire a better fit between calculated and observed sounding curves. As part of the iterative procedure, the following steps are done:

i. If the calculated resistivity is greater (or less) than the observed resistivity at the same electrode spacing, the corresponding calculated resistivity should be increased (or decreased), so the calculated resistivities are approximated to the

observed resistivities (Figure 3.20d). To obtain a higher or lower layer resistivity value, the layer resistivity is multiplied by the ratio of observed to calculated resistivity, as follows:

$$\rho_{i+1}(j)=\rho_i(j)\times\frac{\rho_o(j)}{\rho_{ci}(j)}, \tag{3.9}$$

where i is the number of iteration, j corresponds to j_{th} layer and j_{th} electrode spacing, $\rho_i(j)$ is j_{th} layer resistivity at i_{th} iteration, $\rho_{ci}(j)$ and $\rho_o(j)$ are calculated and observed apparent resistivity at j_{th} electrode spacing for i_{th} iteration, respectively.

ii. A new sounding curve is calculated using the new layer resistivities.

iii. A new rms is calculated and compared to the previous rms.

iv. Steps (i), (ii), and (iii) are repeated until the best fit is found between the theoretical and observed curve (Figure 3.20e).

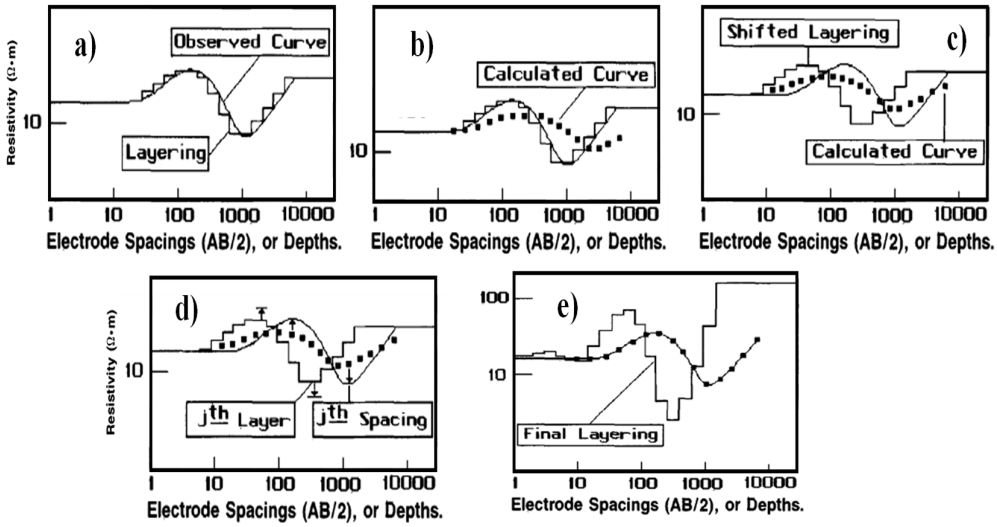

Figure 3.20 The working principle of automated interpretation programs: (a) computation of layering, (b) computation of the calculated (theoretical) sounding curve, based on the layered ground structure in (a); (c) layer depths are shifted to reach minimum rms between theoretical and observed data, (d) layer resistivities are adjusted using the differences between theoretical and observed data, and (e) final model (Zohdy, 1989).

Figure 3.20 shows the results of an automated interpretation program, assuming the same number of layers as data points, operating on a sounding curve originally generated from a three-layer model. It is seen that in the multilayer model the basic structure is recovered, although the sharp interfaces are presented as steps over a wider range of depths, and an artifact is introduced near the surface. This illustrates the danger of overinterpreting small scale features in inversions.

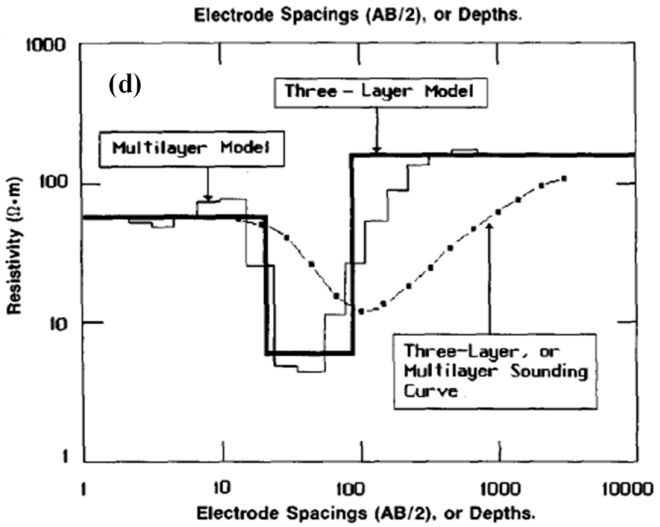

Figure 3.21 Comparison of initial three-layer model used to calculate a sounding curve, and multilayer model based on the sounding curve, inverted by automated interpretation programs (Zohdy, 1989).

3.5.2 2D Inversion

The goal of the geophysical inversion is to produce a model that provides a response similar to the observed data. The subsurface is subdivided into rectangular cells with associated resistivity values (Figure 3.22). An inversion process aims to acquire resistivity values that corresponds to the observed data.

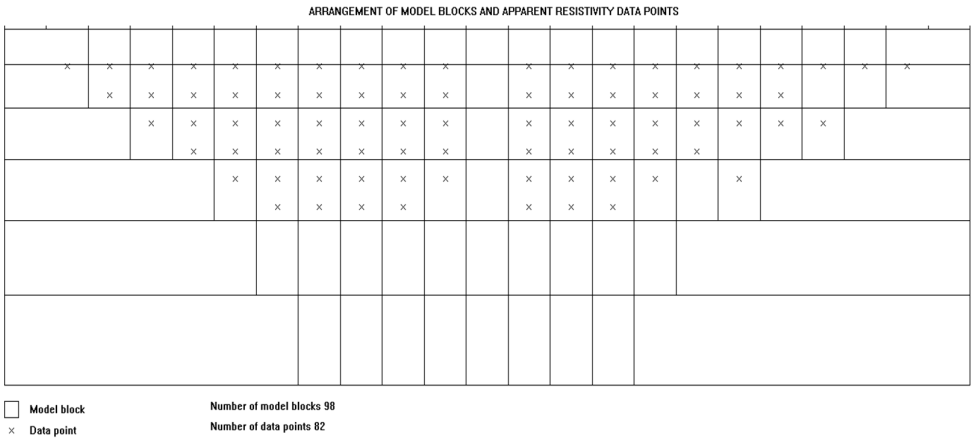

Figure 3.22 A model as being made up of cells for 2D resistivity inversion.

The model has a group of model parameters that can be found using observed data. The observed data is the apparent resistivity values obtained in the field, and the resistivity values of the model cells are called the model parameters. Synthetic data using the model geometry and parameters and calculated with mathematical relationships are defined as the model response. Different optimization methods have been developed to determine model parameters that can be used to calculate the model response. 2D inversion programs (Re2DInv and EarthImager2D) used in this research rely on cell-based modelling methods. In this section, the optimization methods used in inversion programs are briefly explained.

Inverse Theory

A reasonable initial model is created to reduce the first calculated difference between the observed data and the model response: this step is needed for all optimization methods. In eq. (3.10), the observed data (**y**), model response (**f**), and model parameters (**q**) are defined as column vectors:

$$\mathbf{y}=\text{col}(y_1,y_2,\ldots\ldots,y_m) \tag{3.10a}$$

$$\mathbf{f}=\text{col}(f_1,f_2,\ldots\ldots,f_m) \tag{3.10b}$$

$$\mathbf{q}=\mathrm{col}(q_1,q_2,\ldots\ldots,q_n) \tag{3.10c}$$

where m is the number of observation points, and n is the number of model parameters. The discrepancy vector **g** (eq. 3.11) describes the difference between the observed data and the model response.

$$\mathbf{g=y-f} \tag{3.11}$$

According to the least-squares approach, the sum of squares (**E**, error) of the difference between the observed data and the model response is:

$$\mathbf{E=g^T g=}\sum_{i=1}^{n} g_i^2 \tag{3.12}$$

The Gauss-Newton formulation (3.13) is used to minimize eq. (3.12) and modify the changes in the ith model parameter (Lines and Treitel, 1984).

$$\mathbf{J^T J\Delta q=J^T g} \tag{3.13}$$

where **Δq** is the vector that defines the changes in the model parameter, and **J** is the Jacobian matrix (m×n). This matrix consists of partial derivatives.

$$\mathbf{J}_{ij}=\frac{\partial f_i}{\partial q_j} \tag{3.14}$$

Eq. (3.14) represents the change in the ith model response and jth model parameter. After **Δq** is calculated, a new model is obtained:

$$\mathbf{q}_{k+1}=\mathbf{q}_k+\Delta\mathbf{q}_k \tag{3.15}$$

where k is the iteration number in the inversion process. The key problem with eq. (3.13) is that $\mathbf{J^T J}$ might be singular. A poor initial model might cause this. Another drawback is that components of parameter change vector (**Δq**) may have large differences in magnitude, and this can generate non-realistic values. To solve this

problem, a modified version of the Marquardt-Levenberg method is used (Lines and Treitel, 1984). This method is also known as the damped least-squares:

$$\left(\mathbf{J}^{\mathbf{T}}\mathbf{J}+\lambda\mathbf{I}\right)\Delta\mathbf{q}_{k}=\mathbf{J}^{\mathbf{T}}\mathbf{g} \tag{3.16}$$

where the identity matrix is **I**, and the damping or Marquardt factor is λ. The components of the parameter change vector are constrained by the damping factor. Unlike the Gauss-Newton method, the discrepancy vector (**g**) and the parameter change vector (**Δq**) are minimized in the Marquardt-Levenberg method. This method successfully works on resistivity sounding models that have a small number of layers. However, 2D and 3D resistivity models can have a large number of parameters. The method may generate models with unrealistically low and high resistivity values. This problem can be solved using the smoothness-constrained least-squares method (Ellis and Oldenburg, 1994). The method makes gradual and smooth changes in the model resistivity values.

$$\left(\mathbf{J}^{\mathbf{T}}\mathbf{J}+\lambda\mathbf{F}\right)\Delta\mathbf{q}_{k}=\mathbf{J}^{\mathbf{T}}\mathbf{g}-\lambda\mathbf{F}\mathbf{q}_{k} \tag{3.17}$$

where $\mathbf{F} = \alpha_x\mathbf{C}_x^{T}\mathbf{C}_x + \alpha_y\mathbf{C}_y^{T}\mathbf{C}_y + \alpha_z\mathbf{C}_z^{T}\mathbf{C}_z$. $\mathbf{C}_x$, $\mathbf{C}_y$, and $\mathbf{C}_z$ are the smoothing matrices in the x-, y- and z- directions. α_x, α_y, and α_z are weighting factors used in the smoothness filters. If the actual subsurface resistivity changes smoothly and gradually, the smoothness-constrained least-squares method generates a smooth resistivity model.

3.6 Inversion Settings for 1D and 2D

3.6.1 1D Inversion

The AGI EarthImager 1D inversion program is used to interpret 1D electrical resistivity sounding data collected with the Schlumberger array: layered resistivity models are obtained. The program uses the damped least squares inversion method, with some user-

supplied group parameters (Figure 3.25). In this iterative process, the root mean squared (RMS) error, which refers to the discrepancy between observed and calculated data, reduces to a specified maximum value. To avoid wasting computational resources, two other parameters can be set to stop the iteration. One is the maximum allowed number of iterations. The error reduction criteria is used when the RMS error increases or its reduction is extremely small. The inversion is stopped when any of the criteria (number of iteration, max rms error, and error reduction) is reached. The chosen parameters are shown in Figure 3.23. The max RMS error was set to 3%, the maximum number of iterations to 8, and the error reduction criterion was not used.

The default values of the program were used for additional parameters, including the number of layers, the damping and depth factor. The depth factor allows the user to adjust the depth of the model. A default depth factor of 1 is based on expected current penetration, and corresponds to a depth of between 15% and 25% of the array span, depending on the type of array. The number of layers is also a user supplied parameter, discussed in Chapter 4.

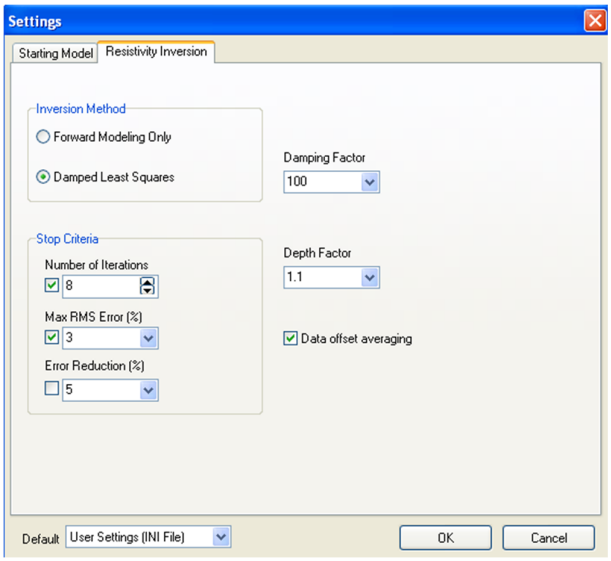

Figure 3.23 Inversion parameters used for 1D inversion modelling.

3.6.2 2D Inversion

Two different programs, EarthImager2D (AGI, 2009) and Res2DInv (Loke, 2003) were used to obtain 2D inversion models. It is observed that there are some fundamental issues with the survey geometry, which are: the very wide spacing of the soundings; the logarithmic progression of current electrode spacings for each sounding; and some overlaps with 'high uniqueness', that is, electrode locations from different soundings that are unique but very close together (Figure 3.24).

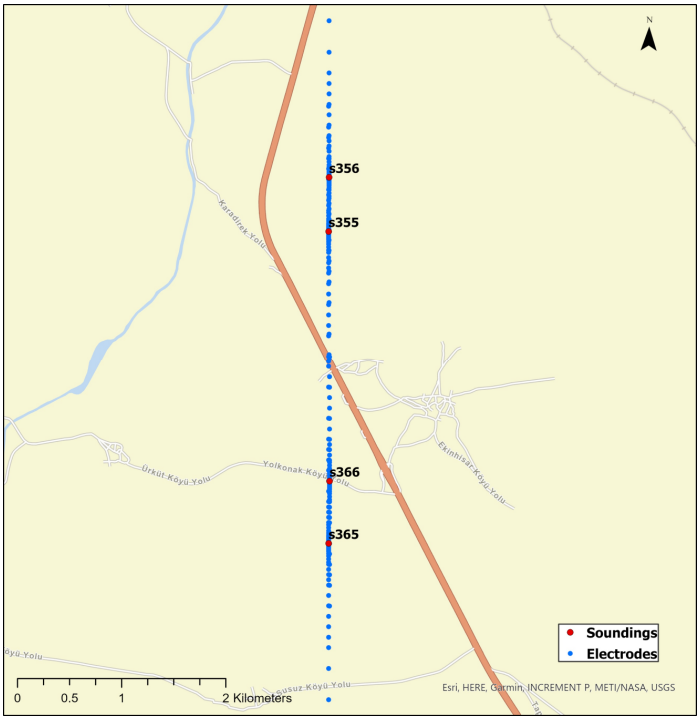

Figure 3.24 Electrode locations (blue dots) for 4 collinear soundings in Group 17: s365 to s356.

The mesh that is set up to perform the inversion is different for EarthImager2D and Res2DInv. For Res2DInv, the mesh has a uniform cell size in the horizontal, and this is set by the minimum electrode spacing. For EarthImager2D, the cell size in the horizontal varies, depending on the individual spacing between the electrodes. This creates an extremely high number of unique model mesh cells. The red dots in Figure 3.25 are electrode positions, and the program creates many cells which are closely

spaced in the horizontal direction due to many, closely spaced but unique electrode positions. A coarse mesh modelling with smooth solution is used to solve this issue. This solution merges parameters from nearby model cells in the x direction to reduce artifacts (Figure 3.26).

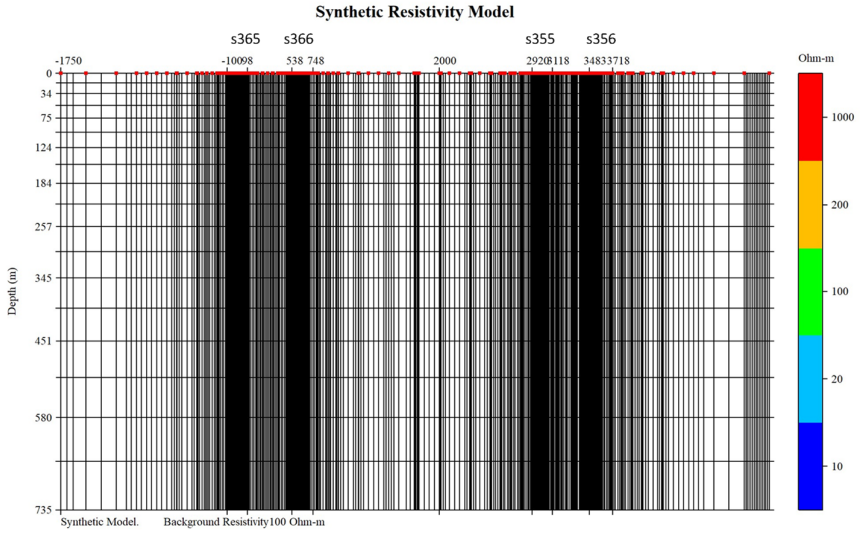

Figure 3.25 EarthImager2D model mesh geometry for collinear soundings s365, s366, s355 and s356. Red dots at the top of the domain indicate electrode locations The black bars indicate cells that are narrower than the line thickness of this graph.

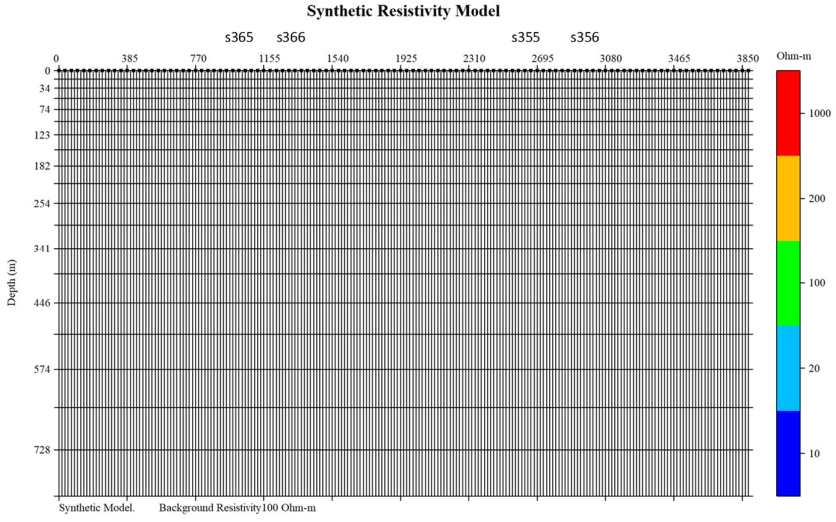

Figure 3.26 New mesh model for 2D inversion.

Because of the problem of the unevenly spaced electrodes, physically unreasonable results were obtained with Res2DInv. However, EarthImager2D works better on this inherited resistivity soundings data. EarthImager2D breaks up all the data into similar sized sections to solve this problem (Figure 3.27).

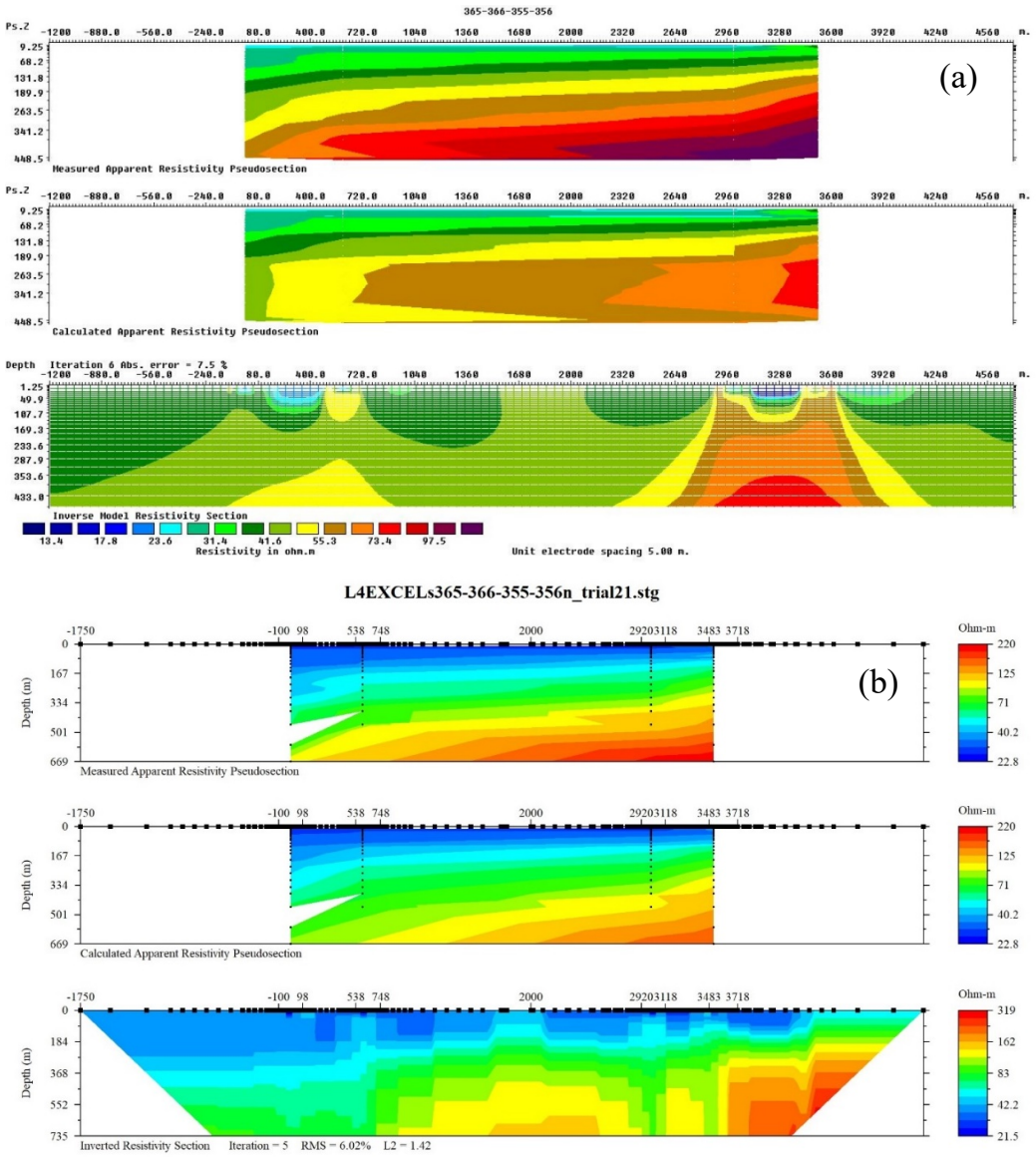

Figure 3.27 2D inversion result for soundings s365-366-355-356 (see Fig. 3.24). (a): Resd2Dinv; (b) EarthImager2. The three panels for each inversion are, from top to bottom, pseudosection based on data, pseudosection based on inverted model and the inverted model. A close correspondence between the two top panels is a validation of the model.

To achieve the more reasonable model in Figure 3.27b, in the inversion settings, the model parameter width was changed. The model parameter width value was taken as 10. This parameter combines the several block models horizontally and creates a single block. Thus, lateral variation in inversion models is suppressed. The software's default values are used for other inversion parameters. The chosen parameters for 2D inversion can be seen in Figure 3.28.

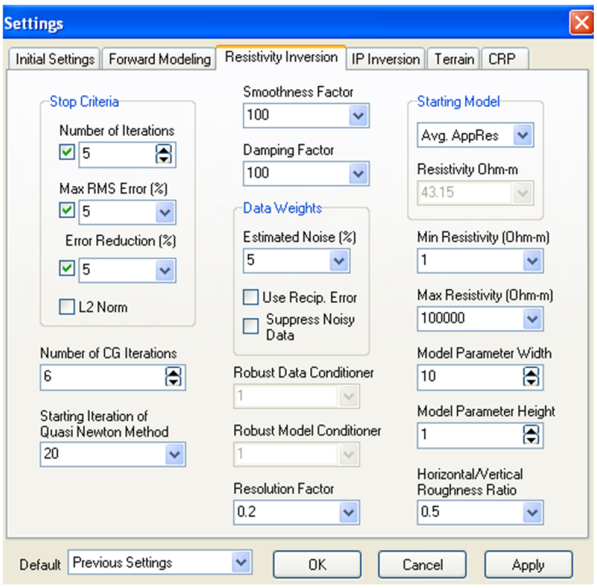

Figure 3.28 Inversion parameters used for 2D inversion modelling.

3.7 1D Rolling Inversions

The first resistivity measurements were performed by Schlumberger brothers in the early 1920s to investigate how electrical current behaves in the ground. For the next 60 years, the resistivity sounding method was used in quantitative interpretation (Loke, 1996). Currently, the resistivity sounding method is actively used in geothermal exploration in Turkiye. To interpret the resistivity sounding data, "1D rolling inversions" can be created. This involves placing the results ρ(z) of 1D inversions adjacent to each other at horizontal locations x corresponding to the centre locations of the soundings, and creating a 2D section ρ(x,z) with graphing software. This method is

widely used in Turkiye and was used in the internal report provided by Mr. Zulfikar Erhan. 1D rolling inversions are a way of displaying 1D resistivity sounding inversions along a profile in an easy-to-interpret manner, since a common color scale is used. Even though it does not reflect the actual ground structure, gradual and rapid changes along the profiles can be easily identified, such as those due to faults.

The mapping program Oasis Montaj was used to obtain 1D rolling inversion sections. Input data for Oasis Montaj was in the form of a table of 1D inversion models. The table had three columns: columns x (the location of the centre of the sounding in metres, the distance from the beginning of the line of soundings), z (proportional to the depth of the centre of the given layer in negative numbers), and ρ (the resistivity of the layer). Because Oasis Montaj uses square cells and the length scales in the horizontal and vertical are so different, it was necessary to multiply the depths of the layers by a factor of 4 to enable smooth interpolation between the soundings. In the resulting maps (section 4.5 and Appendix E) there is therefore a vertical exaggeration of 4. The z axes have been labeled to show the proper depth.

Mapping programs like Oasis Montaj or Surfer are not by default set up to deal with changes over orders of magnitude and where the data points are spaced out in a logarithmic progression. Log scale was used for resistivity to avoid unrealistic overshooting and wiggle to negative numbers.

Chapter 4: Results

As described in Chapter 1, the soundings were divided into 17 groups based on their relationships. The groups are numbered consecutively by time of acquisition, and mostly consist of collinear arrangements of soundings (Figure 1.12). The survey region was divided into 6 geographical areas containing one to a few groups (Figure 1.11, Appendix A).

4.1 Near surface properties and features

As a first step in investigating the distribution of resistivity over the survey area, maps of the apparent resistivity and IP effect for the smallest AB spacing (50 m) were created (Figure 4.1). The values of apparent resistivity would correspond approximately to the weighted average resistivity for the top 10-15 m of the subsurface. The signal contribution is highest near the surface (see Figure 3.14), so the near surface is emphasized in the apparent resistivity value. However, in most of the soundings for the smaller AB spacings, apparent resistivity does not change rapidly with AB spacings so that the apparent resistivities should be a reasonable approximation of the actual resistivities near the surface.

What can be clearly seen in Figure 4.1 is that the resistivity values are mostly low (~10-50 Ω.m). There are cultivated fields and some rivers in the study area, so these low resistivity values fit with overburden-damp to dry soil. Some correlation can be seen between apparent resistivity and topography (Figures 4.1 and 4.2), particularly in northern Area 1 (Group 17). The higher elevations have higher apparent resistivity. This is a reasonable result for the point of view of drainage. It is expected that the water table follows the topography, so the water table is closer to the surface at lower elevations.

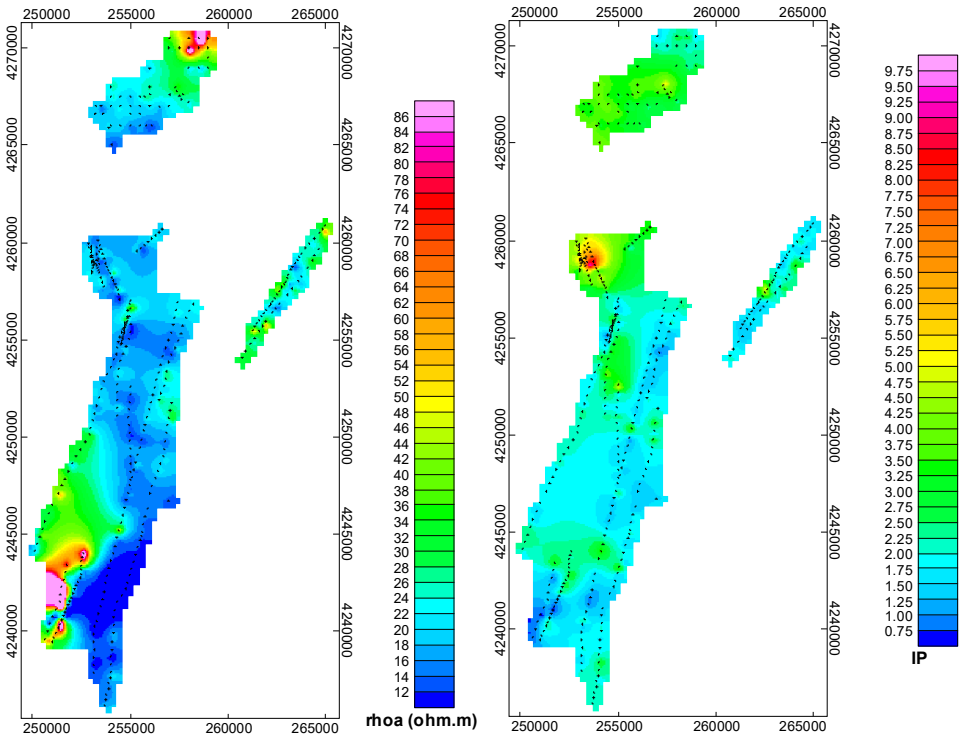

Figure 4.1 Maps of apparent resistivity (left) and IP effect over the surveyed areas in the Sandikli graben for AB/2=25 m. Apparent resistivity values in the most resistive regions are higher than indicated: over 200 Ω.m in the far north and over 600 Ω.m in the south west. Maps produced using Oasis Montaj, with minimum curvature, log, displayed as linear gridding, a cell size of 300 m, and 1 cell extended beyond data.

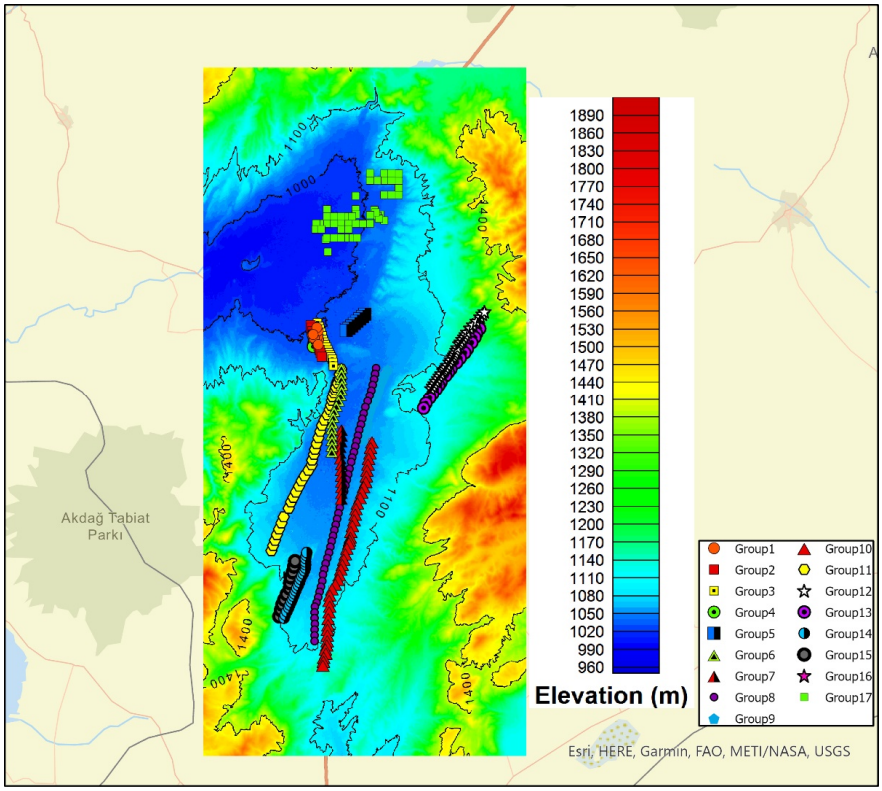

Figure 4.2 Topography map of the Sandikli graben with sounding groups indicated.

The lowest apparent resistivities generally follow the trend of the main rivers across the graben in the north and through the middle of the graben in the centre and the south (Figure 4.3). Additionally, within the central region, there are EW-trending zones where the resistivity is low (Figure 4.1). These might reflect groundwater drainage toward the centre of the graben.

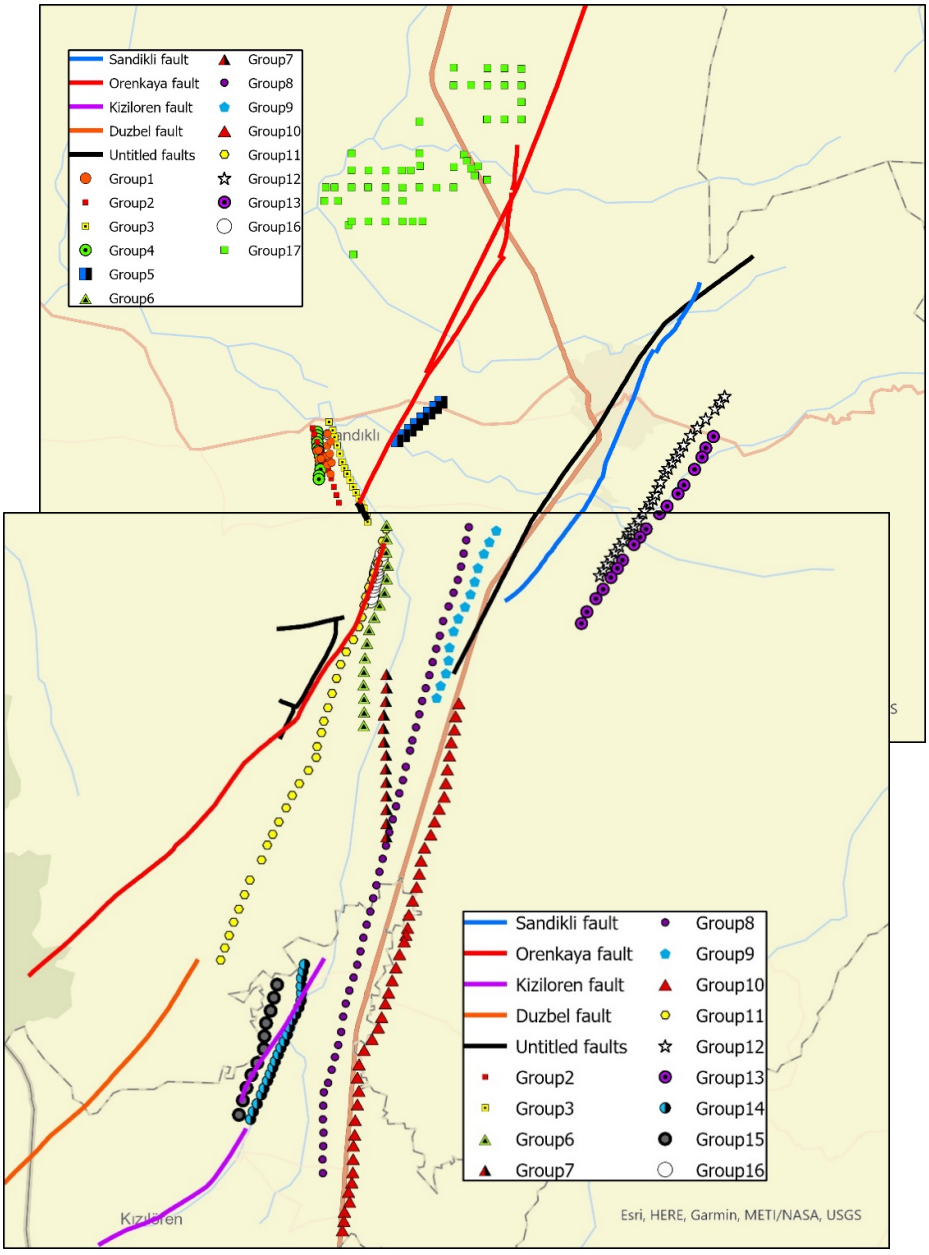

Figure 4.3 Map of Sandikli graben showing rivers(thin blue lines), main highway (light brown) and faults (thick coloured lines). Sounding groups are indicated. Map produced using ArcGIS.

Figure 4.3 also shows principal faults that have been identified in the graben. In general, there are changes in apparent resistivity associated with the faults. For *Group 11*, the apparent resistivity is lower where it is close to the Orenkaya fault. For *Group 9*, the apparent resistivity is a little higher where soundings are closer to an unnamed fault indicated by a black line. The southern part of the map, where Area 6 and the

Kiziloren fault are located, there is a very large change in apparent resistivity across the fault (Figure 4.1).

The near surface IP values are mostly low, between 0.5 and 2.5. There is some correlation with near surface apparent resistivity. IP tends to be low where resistivity is high. Higher IP values could be related to water content, or clay content, both which would be higher at lower elevations.

4.2 Characterization of Areas and Sounding Groups

Main features of the survey area – topography, known faults, and roads and rivers – are presented in Figures 4.2 and 4.3, and basic information on areas and orientations of individual groups are given in Table 4.1. In addition, the shapes of the soundings curves have been categorized into six general shapes, as illustrated in Figure 4.4.

As seen in Figure 4.4, the surface values of apparent resistivity (AB/2 ~ 25 to 50 m) are generally low (10 to 15 Ωm) reflecting the agricultural soil. The deeper values (AB/2 ≥ 500) increase steadily with increasing AB/2 reflecting more resistive bedrock, and there is variation in the shape of the curve at intermediate values of AB/2 reflecting different ground conditions above the bedrock (Figure 4.1). There are a few soundings in Area 2 (near or within the known Hudai-Sandikli geothermal field, see section 4.4.2) where the soundings flatten or turn down at the highest AB/2, however over most of the surveyed region there is no flattening of curves at high AB/2 meaning that the deepest identifiable layer is resistive bedrock and the layers overlying the bedrock are not thin compared with the investigation depth.

Table 4.1 Information on time of acquisition, location and orientation of sounding groups, and shapes of sounding curves within the group. For Shapes, see Figure 4.4: 'x' indicates flattening or downturn of sounding at highest AB spacing.

Area	Group	Soundings	Date (2011)	Type	Location	Shapes
1	17	342 – 395	22 Jul – 28 Aug	Grid	N	A,B,C,E
2	1	1 – 14	3 Jan – 2 Feb	scatter	NW	A, Ax, B, Bx
	2	17 – 27	2 – 7 Feb	NNW–SSE line	NW	A,B,Bx,D
	3	28 – 43	7 – 14 Feb	NS line	NW	A,B,D,F some offsets
	4	44 – 55	7 – 13 Feb	NNW–SSE line	NW	B,D some offsets
	5	56 – 63	28 Feb – 2 Mar	NE–SW line	NW	large offsets
3	12	241 – 270	25 May – 8 Jun	SW– NE line	NE	F,E,B
	13	271 – 288	9 – 20 Jun	NE–SW line	NE	D,F,E
4	6	64 – 79	3 – 13 Mar	NS line	centre	E,D,A
	7	80 – 92	14 – 17 Mar	NS line	centre	E,D
	11	205 – 240	4 – 19 May	SSW–NNE line	centre	F,B,D,E
	16	325 – 338	5 – 11 July	SSW–NNE line	centre	F
5	8	93 – 142	27 Mar – 9 Apr	NS line	Centre S	D,E,F
	9	143 – 150, 155 – 160	10 – 16 Apr	NS line	Centre S	D,E,B
	10	161 – 204	17 Apr – 3 May	NS line	Centre S	D,E,F
6	14	289 – 311	25 May – 7 Jun	SSW–NNE line	SW	C,E,F
	15	312 – 322	29 Jun – 5 Jul	SSW–NNE line	SW	F,C,E

Shapes A, B and C show a distinct decreased apparent resistivity at intermediate depths, indicating the possibility of a low resistivity layer of either a cold aquifer or hydrothermal fluid. Shape D, where the apparent resistivity is flat or decreasing slightly at intermediate depths, is less promising. Shapes E and F, where apparent resistivity increases steadily with AB/2, are least promising for the existence of a cold aquifer.

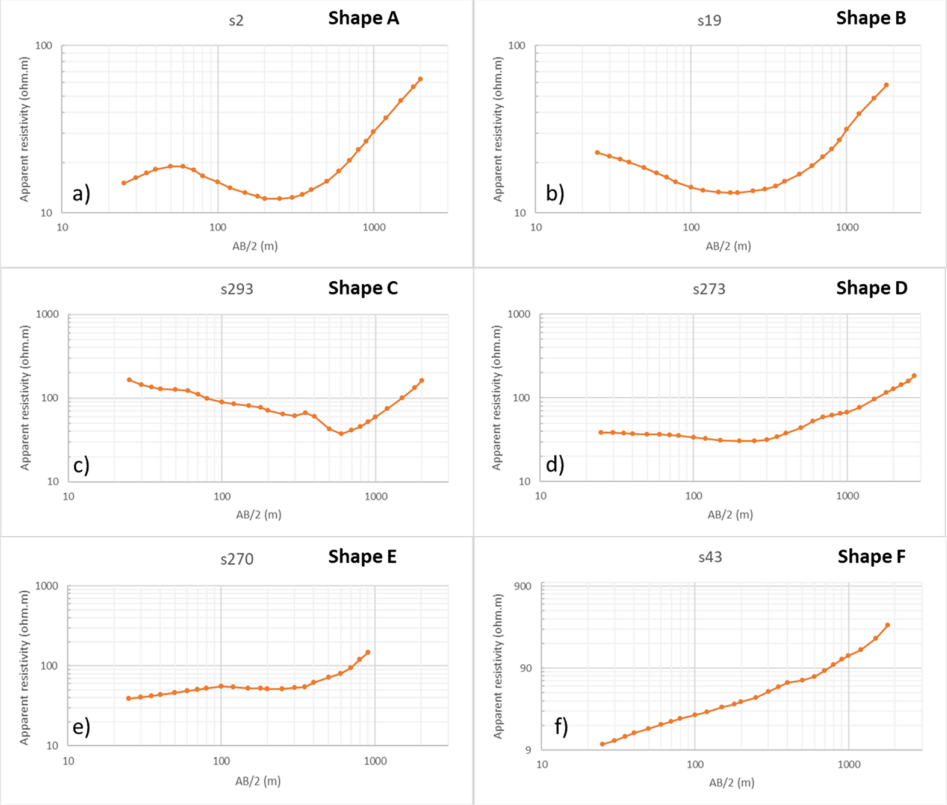

Figure 4.4 The general shapes of the soundings curves.

Characteristics of the sounding curves of the various groups are given below, and sounding shape distribution is presented in Figure 4.5. The sounding curves – both the raw data and curves after smoothing and removal of offsets (sections 3.4.1 and 3.4.4) – are presented in Appendix C, arranged by group number. Large offsets in the raw data (>25% or 50% of the apparent resistivity) are taken to be an indication of surface heterogeneity, and the 'corrected' soundings are therefore considered to be less reliable.

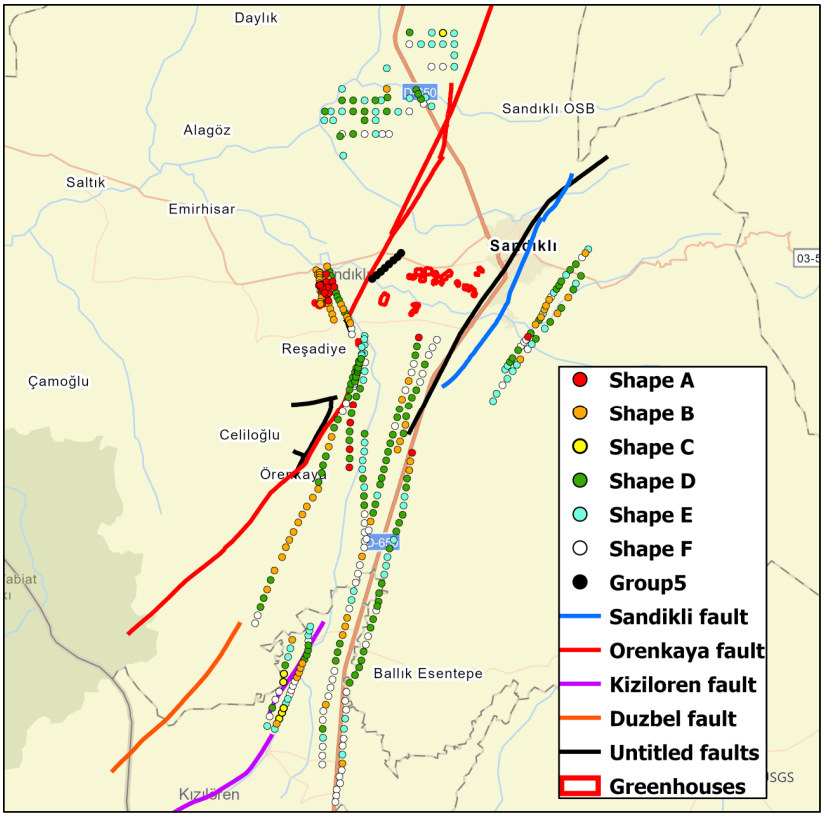

Figure 4.5 Map of Sandikli graben including faults, rivers (thin blue lines) and main roads (brown lines) with soundings colour coded by shape (see Figure 4.4). Group 5 soundings have too many offsets for classification of shape.

4.2.1 Area 1: Group 17

Area 1 is in the northernmost portion of the survey area, in the north part of the Sandikli basin. The soundings here (Group 17, s342 to s395) were collected last, in late July to late August (summer) 2011 in a grid pattern rather than the usual lines. As shown in Figure 4.6, there is a general decrease in apparent resistivity and increase in IP to the SW, following decrease in elevation and increase in alluvium ground cover (Figure 1.10). The highest resistivity and lowest IP is to the NE of the main road. IP is higher near the rivers, and a peak in IP corresponds to a location where the main road crosses a river. The soundings mostly have shapes D and E (see Appendix D), indicating deep surface layers where the resistivity changes little or increases slowly (Figure 4.4).

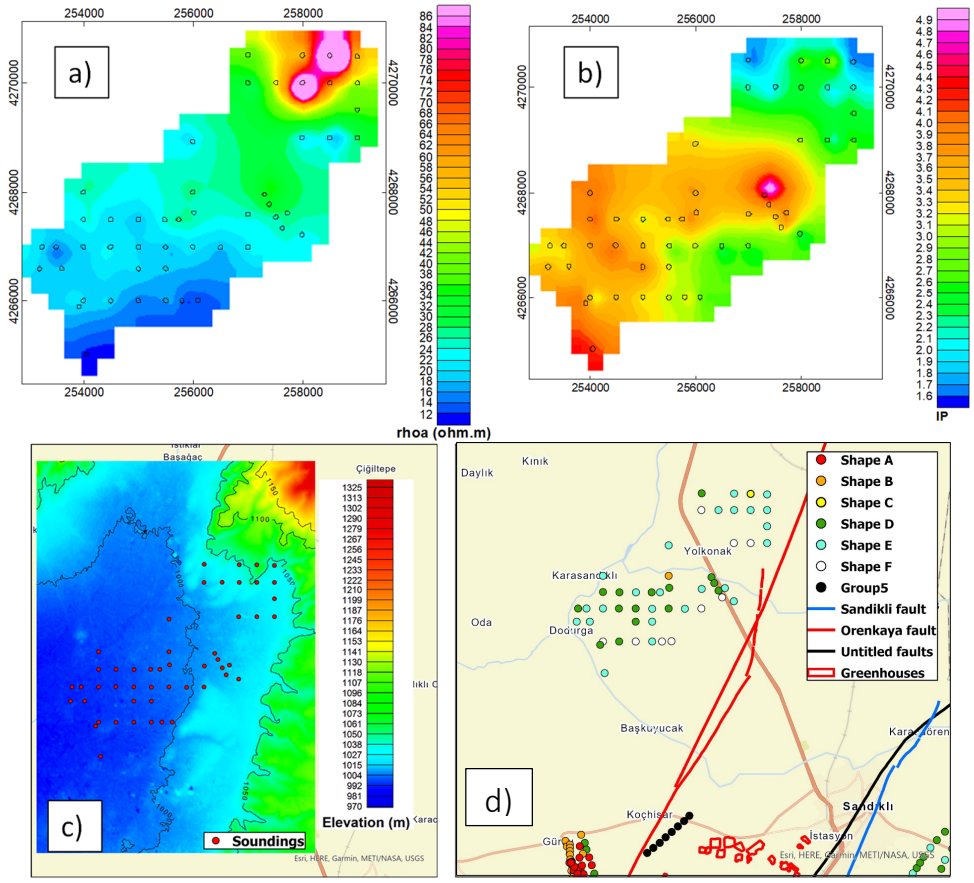

Figure 4.6. Maps of (a) ρ_a for AB=50 m, (b) IP for AB=50 m, (c) topography with contour lines of 50m and (d) faults, roads and rivers with soundings colour coded by shape, in Area 1 (Group 17, s342 to s395). Oasis Montaj, log (save as linear) minimum curvature gridding, cell size 300 m.

4.2.2 Area 2: Groups 1 to 5

Maps of Area 2, to the SW of the town of Sandikli, are shown in Figure 4.7, and the sounding locations are shown as blue dots on a detailed geological map in Figure 4.8.

Group 1 soundings are scattered within a ~500×600 m^2 area between *Groups 3* and *4* in no apparent order. These were the first collected, in the winter (January and February) of 2011. *Groups 2* to *4* consist of collinear soundings trending NNW-SSE subparallel to a river (Hamamcay stream), and *Group 5* soundings form a NE-SW line to the NE. The area features several geothermally heated greenhouses and thermal resorts and hotels (Figure 1.9). In particular, there are geothermally heated greenhouses

near the southern end of *Group 4*, and at the southern end of *Group 3* there are the hot springs of the Hudai spa, near the intersection of Orenkaya and two parallel unnamed faults (Figure 4.7d).

Near surface apparent resistivity, IP, and topography are shown in Figure 4.7a, b and c. As for Area 1, for *Groups 1* to *4* the apparent resistivity and IP are inversely related. Relatively high IP and low resistivity are in the middle between *Groups 3* and *4*, which is near a stream on alluvium (Figure 4.8 and Appendix A). The increase in apparent resistivity and decrease in IP to the west of *Group 4* (Figure 4.7a and b) is an unconstrained extrapolation of the WE trend across the stream.

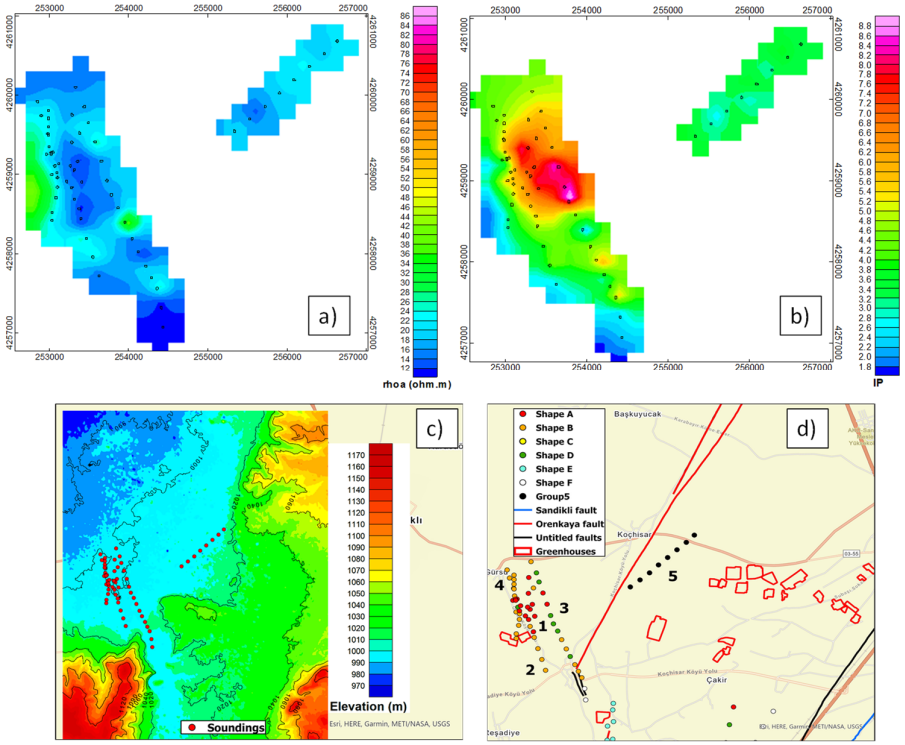

Figure 4.7. Maps of (a) ρ_a for AB=50 m, (b) IP for AB=50 m, and (c) topography and (d) soundings colour coded by shape, in Area 2 (Group 1 to 5). Oasis Montaj, log (save as linear) minimum curvature gridding for ρ_a, and linear for IP, cell size 200 m.

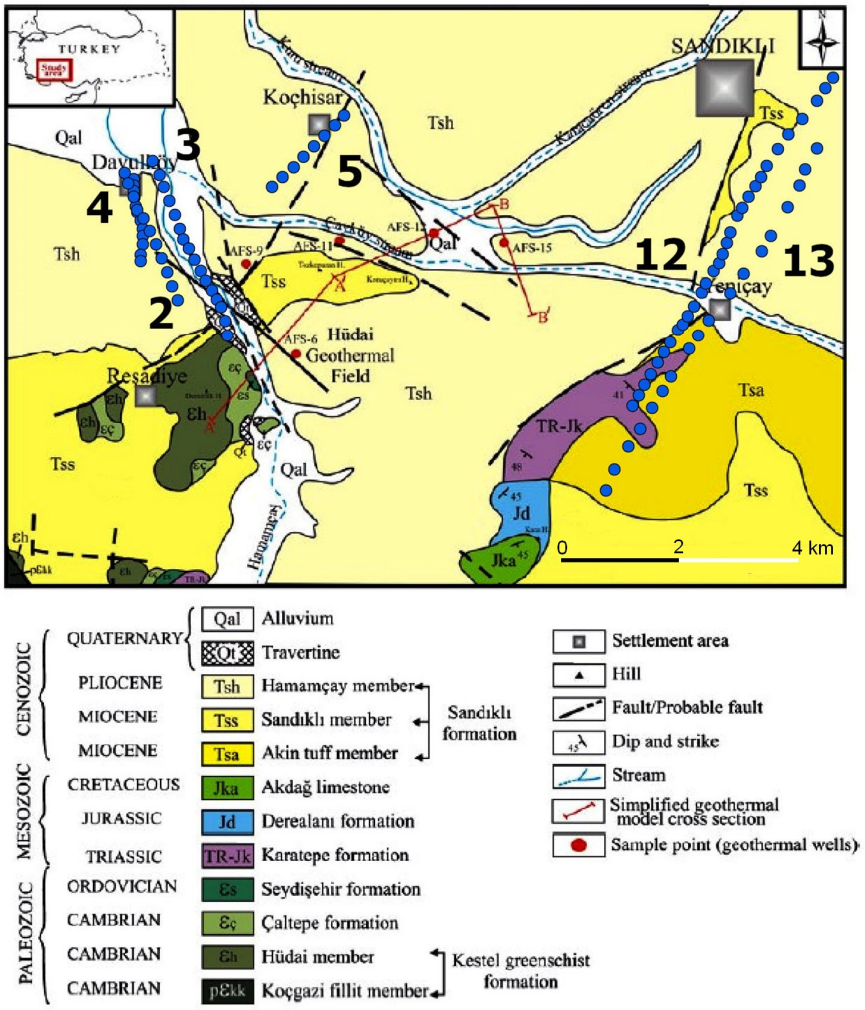

Figure 4.8 Geological map of the Hudai Sandikli geothermal field and environs, including geothermal wells (red dots). Blue dots are VES locations, with Group numbers indicated, from Areas 2 and 3. Modified from Demer et al. (2013).

Groups 1 and *2* show mostly 'A' shapes, which are rare in the rest of the survey area, and 'B' shapes (Figure 4.7d). These shapes may indicate the presence of a relatively shallow aquifer. The southernmost soundings in *Group 2* (s25, s26 and s27, near the Hudai spa) flatten after AB/2 ~ 600 m suggesting the presence of a deeper thermal aquifer.

Group 3 soundings mostly show 'B' and 'D' shapes (Figure 4.4), with 'A' shapes near the cluster of soundings in *Groups 1* and *2* that also have 'A' shapes. In *Group 3*, although sounding curves have different values, the general trend is that the

apparent resistivity decreases until AB/2 ~ 50m and then increases gradually. The northernmost *Group 3* soundings (s28, s29, s30 and s32) have large apparent resistivity jumps in the raw data (Appendix C) when the potential electrode spacing was changed, and measurements collected after these jumps were not included in the inversions.

Most *Group 4* soundings show 'B' shapes (Figure 4.7d). *Group 4* is north-south oriented and has a similar sounding curve pattern to *Group 3*, except for the soundings s51 and s52, near the middle, which show large resistivity offsets.

Almost all *Group 5* soundings show very large apparent resistivity offsets (Figure 3.15, Appendix C). These large apparent resistivity jumps, which appear to be most characteristic of Area 2, are interpreted to be due to near surface heterogeneities (section 3.4.3). Because of the magnitude of the jumps, shapes were not assigned to this group.

4.2.3 Area 3: Groups 12 and 13

Group 12 (s241 to s270) and *Group 13* (s271 to s288) are northeast-southwest oriented, and they are parallel to each other and to the major Sandikli fault to the SE of the town of Sandikli (Figures 4.8 and 4.9). In the region there is a stream, though its location and branching is marked differently in Figures 4.8 and 4.9d. In Figure 4.8, there is a single stream, while Figure 4.9c and 4.9d indicate the stream divides into two branches, with a branch of the stream running NE parallel to 6 soundings of *Group 13*. The discrepancy may be because the streams locations vary seasonally.

The surface resistivity values are higher than in Area 2, though still moderate: ~20 to 40 Ω.m compared with ~10 to 25 Ω.m in Area 2. This is likely related to higher elevation and different surficial geology, with less alluvium under Area 3. The southern part of the area is underlain by older volcanic (Akin tuff) and sedimentary (Karatepe

formation) rocks (Figure 4.8). Although the lines are only 300 to 600 m apart, there is little correlation between the groups to be seen in the surface values of ρ_a and IP (Figure 4.9a and b). These values vary on a small horizontal scale.

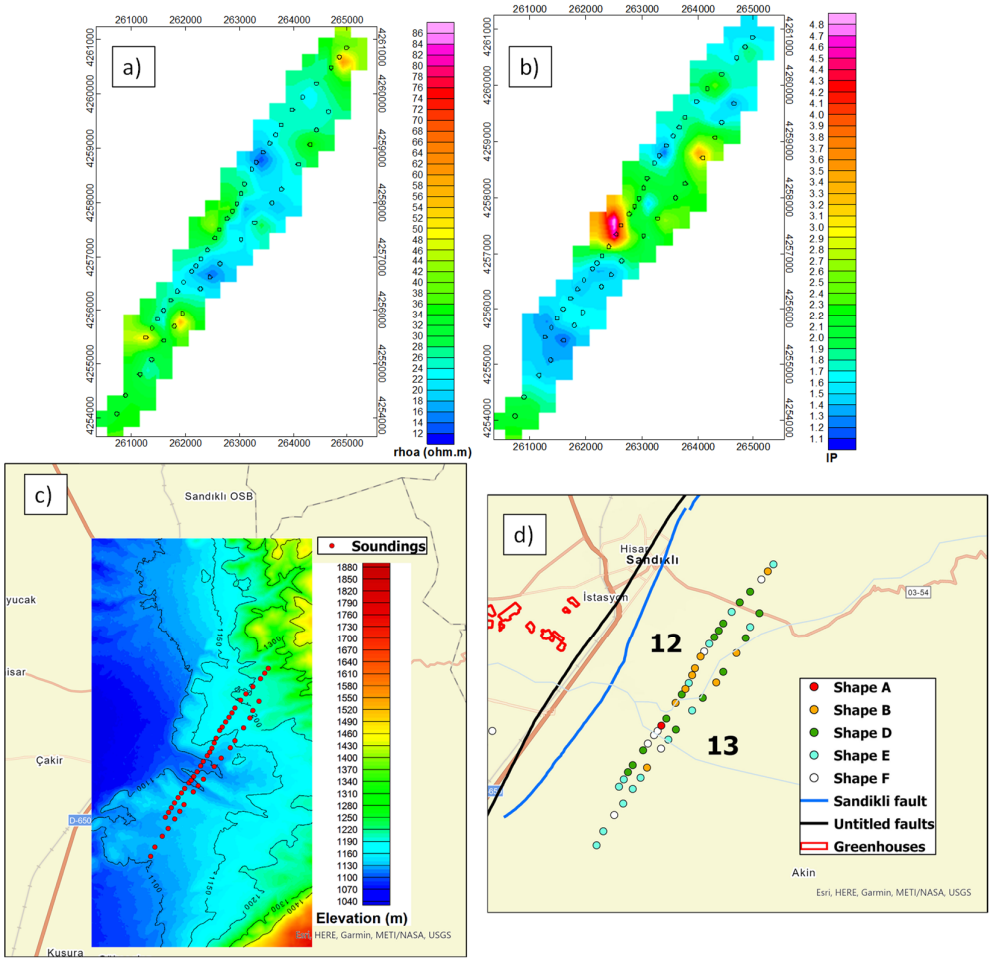

Figure 4.9 Maps of Area 3 (Groups 12 and 13). (a) ρ_a for 50 m, (b) IP for AB=50 m, (c) topography (d) soundings classified by shape. Oasis Montaj, log (save as linear) minimum curvature gridding for ρ_a, and linear for IP, cell size 300 m.

In *Group 12,* there is high IP where this line crosses the NE branch of the stream, and ρ_a is highest toward the NE end of the line into the foothills (Figure 4.9c). The low point in apparent resistivity in *Group 13* corresponds to where the line crosses the southern branch of the stream and the apparent resistivity is relatively low where it runs close to the NE branch.

Similar to the surface values, there is only a weak correlation between the sounding shapes between the groups, and the shapes vary from sounding to sounding. 'B' and 'D' shapes more common near the middle of the lines, and 'E' and 'F' toward the southern end, farther from the stream and over volcanic and carbonate rocks. *Group 12* has mainly 'B', 'D', 'E' and 'F' shapes (Figure 4.1). In *Group 12*, the apparent resistivity values mostly show a steady increase with AB spacing (shape F) or, toward the NE end, they are flat then increase (shape D). The resistivity values of the soundings (s253, s255, s257, s258 and s259) close to the branches of the streams decrease until AB/2 ~ 80 m, and then increase again (shape B). *Group 13* soundings mostly consist of 'E' and 'F' shapes, with some 'B' shapes for soundings parallel to the NE branch of the stream.

Group 13 soundings are well behaved (no unusual high or low resistivities and layer boundaries can be easily distinguished) except s282. This sounding shows unusually high apparent resistivity values until AB/2 ~ 50 m, and then a sudden decrease. This sounding, 7th from the southern end and 800 m from the stream, thus appears to be centred on a patch of relatively resistive surface.

4.2.4 Area 4: Group 6, 7, 11 and 16

Areas 4, 5 and 6 cover the southern part of the Sandikli graben mainly in the lowest elevations (Figures 4.2 and 4.10). Faults running sub parallel to the graben include the major Orenkaya fault on the western edge, the Kiziloren and Duzbel faults to the south, the Sandikli and an unnamed fault to the northeast. There are other unnamed faults close to the Orenkaya fault (Figure 4.10d). A river runs through the centre of the graben, and there are several creeks, not shown in the figure, feeding into the river.

Area 4 is on the west side and central parts of the graben (Figure 4.3) over a NS

extent of about 14 km. Farthest to the north, there is an offset of the Orenkaya fault (Figure 4.3), and there is a large greenhouse in the offset region (Figure 4.3), just to the west of the northernmost soundings of *Group 6*. Here, the near surface resistivities (Figure 4.10a) are moderate. Just south, they are low in a band extending EW across the graben, where *Groups 6, 11* and *16* are close to the fault. Farther to the south, apparent resistivities are low nearer the centre of the graben where the main river flows, and moderate at higher elevations to the west. The surface IP values are mostly low (~2) compared with Area 2, with some higher values near a winding river (best seen in Google Earth, Appendix A) and some variable values close to the fault.

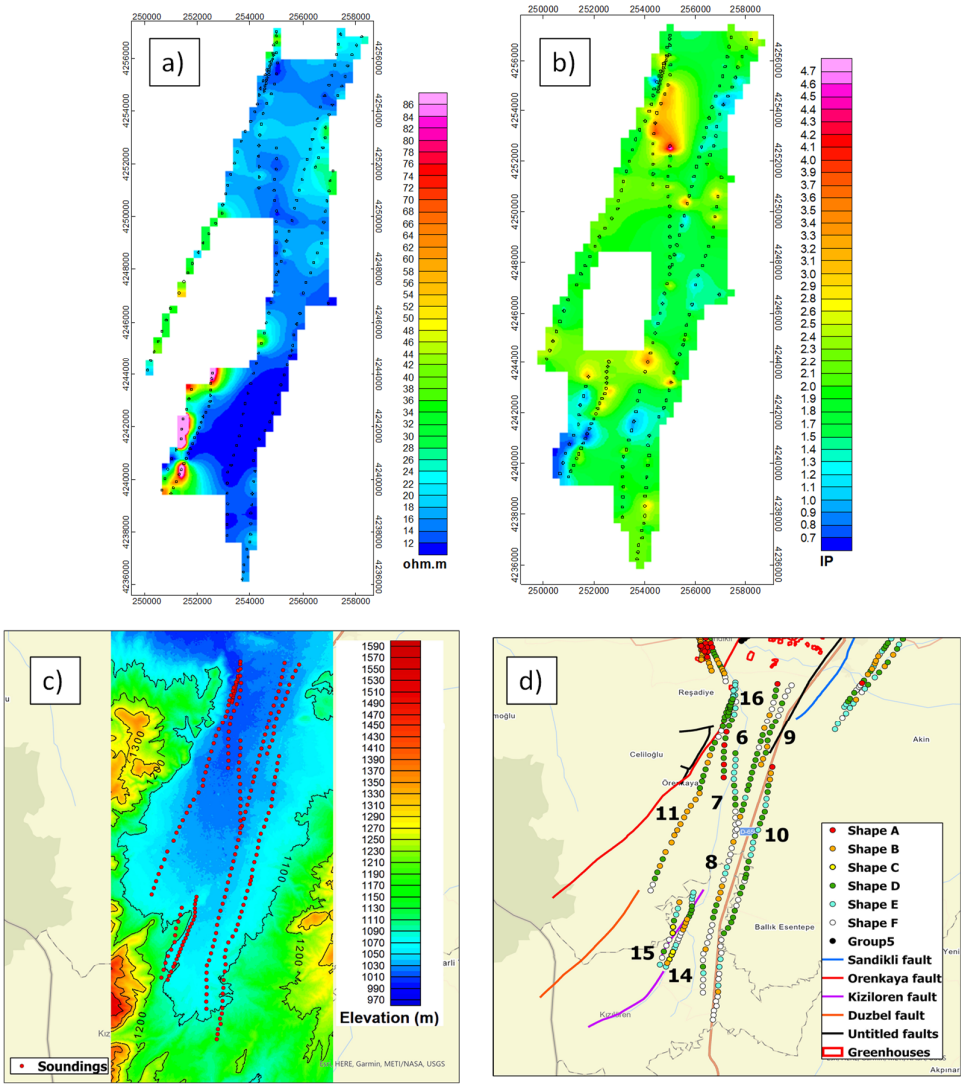

Figure 4.10 Maps of (a) ρa for AB=50 m, (b) IP for AB=50 m, (c) topography (d) soundings classified by shape, in Area 4 to 6 (Group 6,7,8,9,10,11,14,15 and 16). Oasis Montaj, log (save as linear) minimum curvature gridding for ρa, and linear for IP, cell size 300 m.

Group 6 (s64 to s79) soundings make up an approximately 6 km long NS line located between a river and the Orenkaya fault. *Group 6* mostly show 'E' and 'F' shapes in the north and 'A' and 'D' shapes farther south. The northernmost soundings from s64 to s68, have near surface apparent resistivity readings varying between 10 Ωm and 50 Ωm, and a similar large spread in apparent resistivity at large AB/2 (Appendix C). This part is the closest part to the Orenkaya fault and it is thought that the large variation is associated with changing ground conditions near the fault. Other soundings in *Group*

6 have more consistent values, though the soundings closest to the river in the south (s77 to s79) have large offsets presumably associated with heterogeneous surface conditions (Appendix C).

Group 7 soundings (s80 to s92) are in the centre of the graben and follow a line starting on the east side of the river from Group 6 (opposite s75) and progressing almost due south. *Group 7* soundings mostly show 'E' and 'F' shapes. Apart from soundings s80 and s81, farthest north and closest to the river, the soundings are similar, showing low apparent resistivity ρ_a values of 10-20 Ωm up until AB/2 ~ 200m, and then smoothly increasing ρ_a for higher AB/2 (Appendix C). Soundings s80 and s81 show some relatively large jumps in the raw data (e.g., >50% change at AB/2=300 in s80) and are considered less reliable. The other sounding curves suggest the subsurface consists of a thick (several 100 m) of sediment over more resistive bedrock, consistent with the location in the middle of the graben. The proximity of the river to s80 to s84 has no obvious effect on the soundings. The IP effect (Appendix A.7b) is mostly low (~2), with a tendency to increase slightly with AB/2.

Group 11 soundings (s205 to s240) trend SSW to NNE, farthest to the west and next to the Orenkaya fault in the north. They have mostly 'D' shapes close to the fault and 'B' shapes farther south, with some soundings showing 'F' shapes. Soundings from 205 to 229 are mostly consistent, with similar shapes from one sounding to the next. The apparent resistivity values decrease up until AB/2 ~ 250 m, and smoothly increasing for higher AB/2 (Appendix C). Soundings s237, s238, s239 and s240 have a different shape. The apparent resistivity ρ_a increases up until AB/2 ~ 60m and gradually decrease up until AB/2 ~ 600 m. These soundings (s237 to s240) are considerably closer to the Orenkaya fault, and this resistivity variation may be fault related.

Group 16 soundings (s325 to s338) are closely spaced (~100 m rather than ~400 m for other groups) in a ~1.4 km long line along a road very close to s237 to s240 of *Group 11*. Soundings s237 and s238 have 'F' shapes, while s239 and s240 (further north) have 'A' shapes. *Group 16* mostly show 'D' shapes. Soundings s325 to s333 are very similar, the apparent resistivity is almost flat until AB/2~100 then gradually increases. For soundings s334 to s338, the apparent resistivity values are somewhat higher and more irregular. Like the soundings (s237 to s240) located in the north of *Group 11*, it is thought that the irregularity in the apparent resistivity in the soundings s335 to s338 is related to the fault.

4.2.5 Area 5: Groups 8, 9, and 10

Area 5 contains 3 groups which consist of long, SSW to NNE trending lines through the centre and east part of the graben (Figure 4.10). *Groups 8* and *9* are to the west of the main highway, *Group 10* is to the east of the highway at slightly higher elevation. The surface resistivities are mostly low (~10 to 20 Ω.m), with the lowest values toward the southern end. Surface IP values are also low (~2) with patches of slightly higher or lower values (~1 to 3) associated with variations in surface resistivity. In the NE, low IP is associated with higher resistivity, as observed in other areas. However in the south, the opposite occurs.

Groups 8, 9 and *10* mostly show 'D' and 'E' and 'F' shapes, where apparent resistivity is steady or increases with AB/2. There are some places (near the northern end of *Group 10*, and in *Group 8* near the northern end of the Kiziloren fault) where soundings have a 'B' shape, and the northernmost soundings in *Group 8* and *10* have an 'A' shape.

Soundings in *Group 8* (s93 to s142) are mostly well behaved, with similar

resistivity ranges, small offsets and shapes changing consistently between neighbouring soundings, particularly for soundings s125 and farther south. Soundings s123 and s124, about half way along the line, show higher apparent resistivity than the other soundings. There is no obvious associated feature at this location. (The location could correspond to a northeasterly extension of the Kiziloran fault.)

Group 9 (s143 to s160) soundings are parallel to the north part of *Group 8* soundings. In this region, *Group 8* soundings (s93 to s105) and *Group 9* soundings show similar patterns. The apparent resistivity values increase steadily (shape 'F') or increase after being flat or decreasing up to AB/2 ~ 150 m (shapes 'B' and 'D'). In the east of *Group 8* and *Group 9*, there is an untitled fault. However, fault has no obvious effect on the apparent resistivity values.

Group 10 (s161 to s204) is a line located to the right side of the graben. Like *Group 8*, *Group 10* soundings have similar patterns. The raw data of the northernmost soundings s161, s162 and s163, closest to the road and the end of the untitled fault, show some large offsets.

4.2.6 Area 6: Groups 14 and 15

Group 14 and *Group 15* soundings are in the southwest part of the study area, both trending S to N, 4 to 5 km, with *Group 15* to the west and subparallel to *Group 14*. This area is characterized by large variations and the highest values of surface resistivity. The variation of near surface values of apparent resistivity and IP effect along these lines is illustrated in Figures 4.11 and 4.12. In the extreme, soundings s317 to s319, in the middle of *Group 15*, have surface apparent resistivities of 509 to 680 Ωm, while nearby soundings have surface apparent resistivities 100 times less. These resistivity variations are associated with the Kiziloren fault, which crosses the lines, though the

resistivity is not uniform along the estimated location of the fault (Figure 4.11). A similar pattern of variability is seen in the IP, with higher IP mostly associated with higher apparent resistivity.

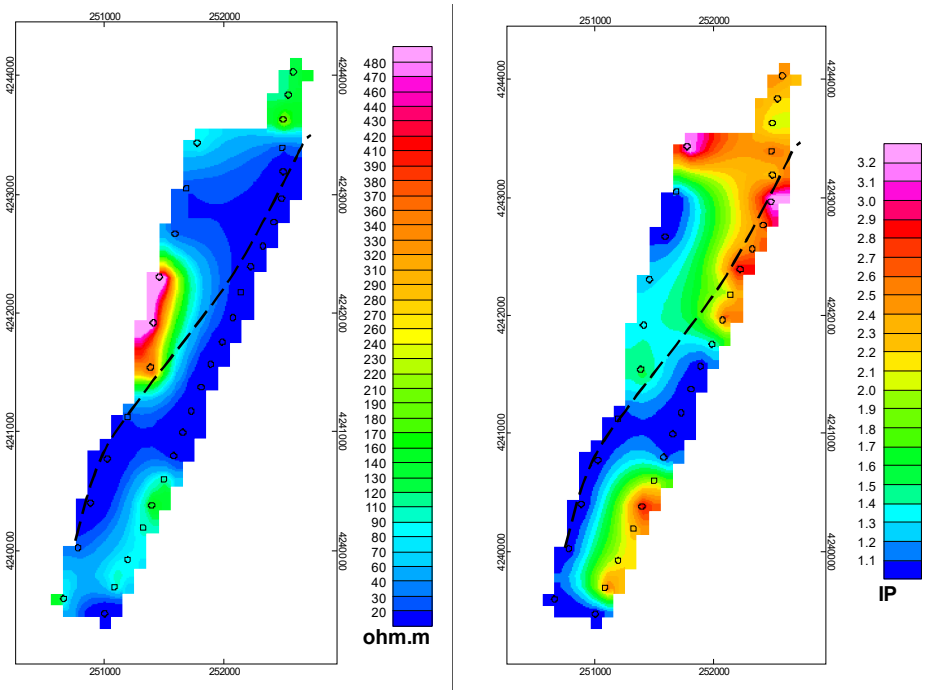

Figure 4.11. Maps of apparent resistivity (left) and IP effect over the surveyed areas in the Area 6 for AB/2=25 m. Apparent resistivity values in the most resistive regionres are higher than indicated: over over 600 Ω.m in the west. Dashed line indicates the approximate location of the Kiziloren Fault. Maps produced using Oasis Montaj, with minimum curvature, log, displayed as linear gridding, a cell size of 100 m, and 1 cell extended beyond data.

Groups 14 and *15* mostly show 'E' and 'F' shapes (a steady increase of apparent resistivity with AB/2), and some soundings have 'B' and 'D' shapes. Because of the existence of the Kiziloren fault, the shapes must be viewed cautiously. Kinks may be associated with electrodes crossing the fault.

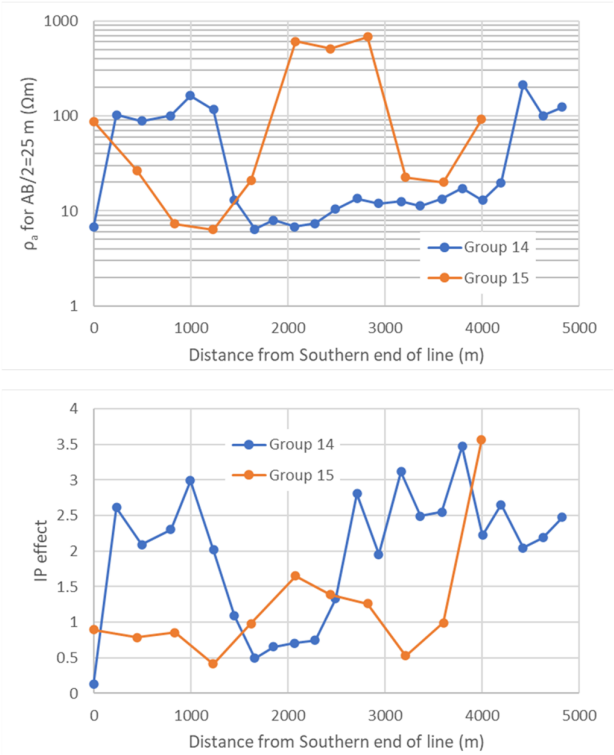

Figure 4.12 Apparent resistivity and IP effect for shortest AB/2 spacings for soundings in Groups 14 and 15, illustrating changes associated with crossing the Kiziloren Fault.

4.3 1D VES Models

370 1D inversion resistivity sounding models were obtained using EarthImager1D software, and these models are presented in Appendix E. As mentioned in section 4.2, the only indication in the sounding shapes of a deep geothermal layer is seen in a few soundings in Area 2, close to the Hudai spa. Therefore elsewhere in the graben the focus was on shallow sources. When looking at the raw data, 4 layers can usually be identified by counting the bends in the sounding curves (section 3.4.2). Very generally, when looking at 1D inversion resistivity models, bedrock is resistive and becomes more resistive with depth as porosity decreases. For shallow source geothermal heating, a zone of hot water is sought above this resistive bedrock. The drill core in the Sandikli plain (Table 1.2) indicates that such a zone might exist at depths of about 300 m. For a 4 layer subsurface, the ideal ground structure for geothermal prospectivity would be:

low resistivity surface, more resistive deeper layer, low resistivity geothermal layer, and consolidated bedrock. It is noted, though, that layers hosting fresh water aquifers could extend to 200 to 300 m depth (Davraz et al., 2016), so a deep low resistivity layer could also result from a fresh water aquifer.

As is well known, the ground is not divided up into sharply defined layers with uniform properties within each layer. Therefore, for the inversions, 8 layers were chosen as a compromise between simplicity and reality. Some examples of inversion models are presented in Figure 4.13.

As described in section 3.5.1, 1D inversion models start with an initial model based on the sounding curves, so the modeled layers are thinnest near the surface and layer thicknesses increase with depth. As can be seen from the models in Figure 4.13 and Appendix E, the 7 interfaces between the layers were typically placed at depths within a few metres of 12, 25, 48, 96, 180, 300 and 480 m respectively, following the approximately logarithmic progression of spacings of the current electrodes. For soundings reaching the maximum AB spacing of 5000 m, the maximum depth of the 1D inversions was 1375 m.

The inversion models are colour coded, with dark blue the least resistive and red the most resistive. As expected, the near surface has low resistivity (from 14 to 17 Ω.m) in this agricultural area. The apparent resistivity map of the top surface also shows fairly low resistivity soil everywhere in the graben (Figure 4.1). Below the topmost layer is a more resistive layer. A low resistivity layer between the bedrock and the surface layers is observed in many models. These observed layers are highlighted with a red circle in Figure 4.13. For s187, below the surface, a low resistivity layer can be seen with thickness roughly 50 m. On the other hand, in some models, for instance s134, the

resistivity constantly increases with depth, and no low resistivity layer is observed above the bedrock. In the section that follows, a resistivity pattern map is provided to see the distribution of the low resistivity layers.

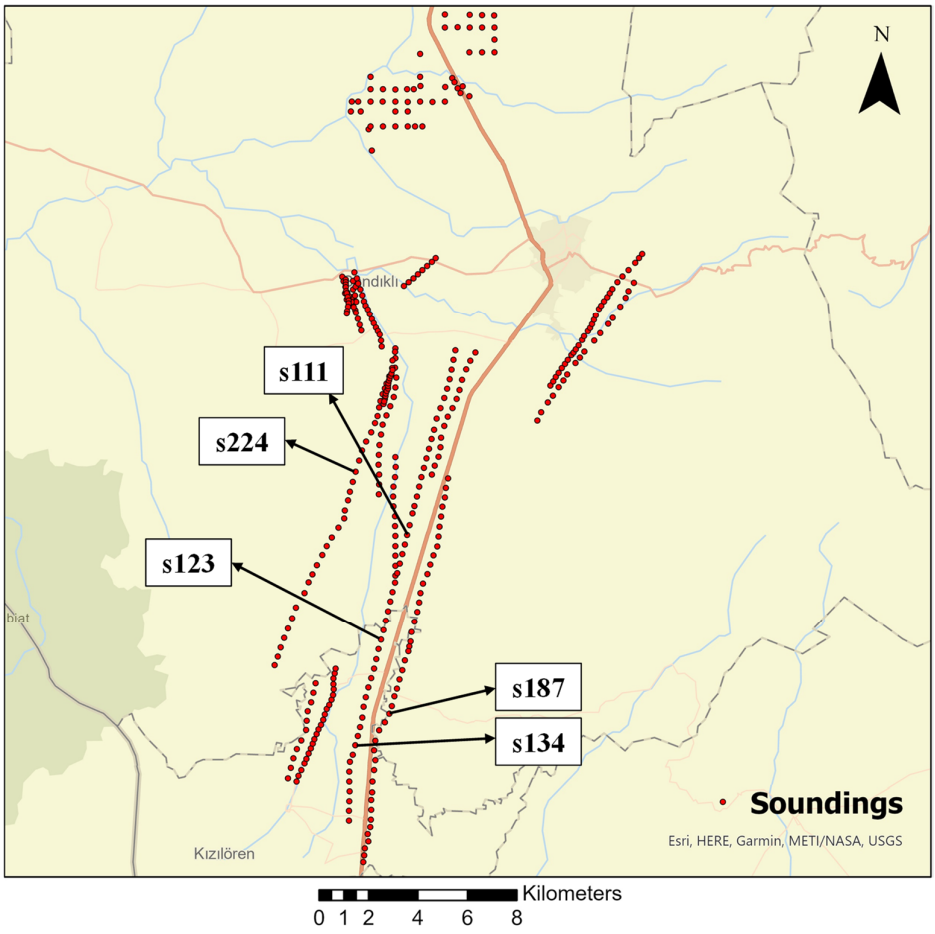

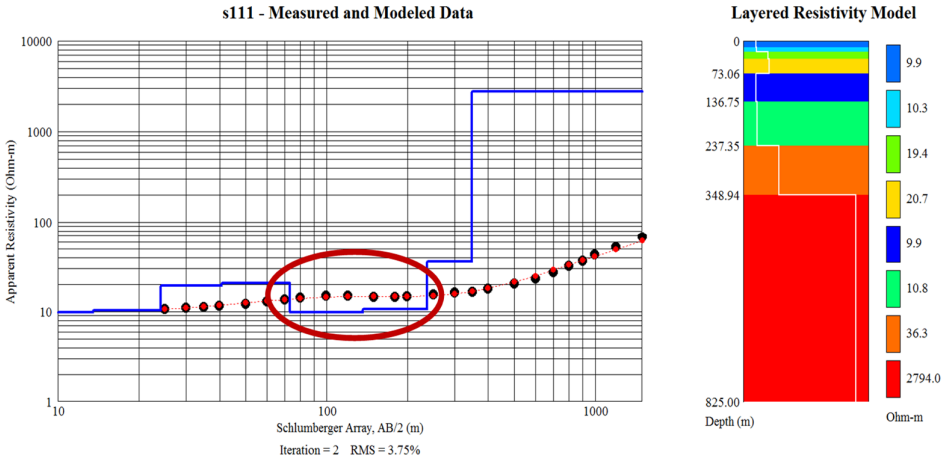

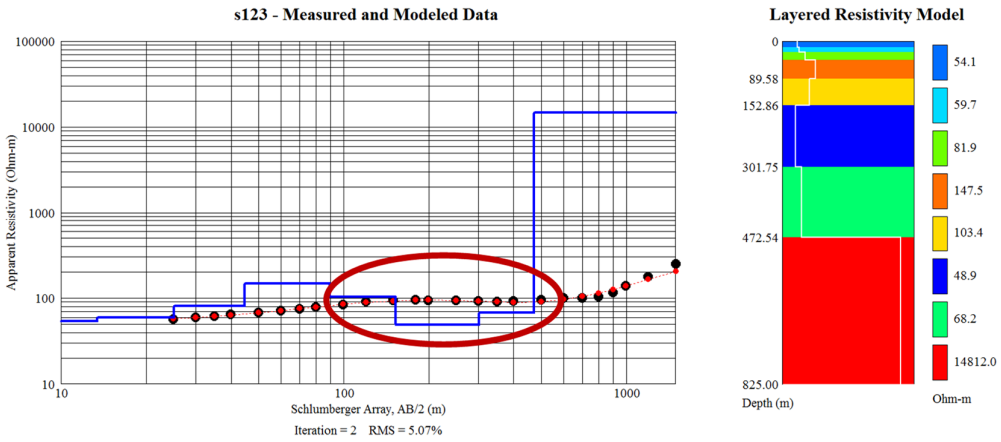
s123 - Measured and Modeled Data
Apparent Resistivity (Ohm-m)
100000
10000
1000
100
10
10
100
1000
Schlumberger Array, AB/2 (m)
Iteration = 2 RMS = 5.07%
Layered Resistivity Model
0
89.58
152.86
301.75
472.54
825.00
Depth (m)
54.1
59.7
81.9
147.5
103.4
48.9
68.2
14812.0
Ohm-m

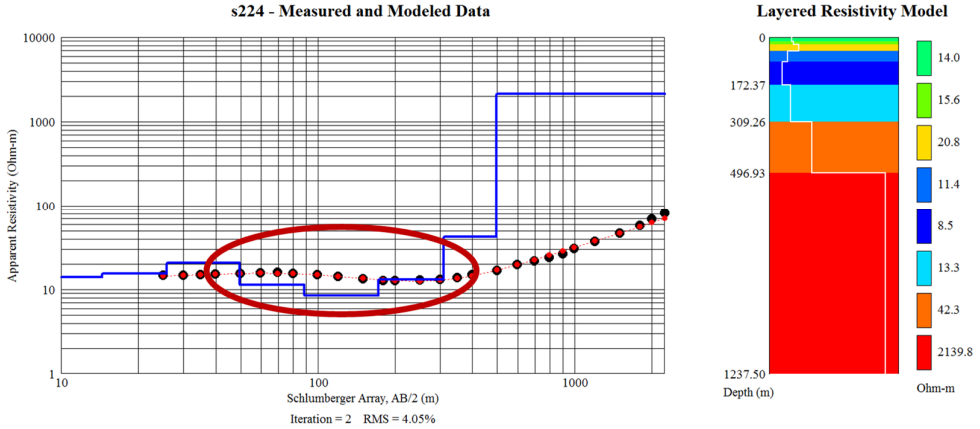
s224 - Measured and Modeled Data
Apparent Resistivity (Ohm-m)
10000
1000
100
10
1
10
100
1000
Schlumberger Array, AB/2 (m)
Iteration = 2 RMS = 4.05%
Layered Resistivity Model
0
172.37
309.26
496.93
1237.50
Depth (m)
14.0
15.6
20.8
11.4
8.5
13.3
42.3
2139.8
Ohm-m

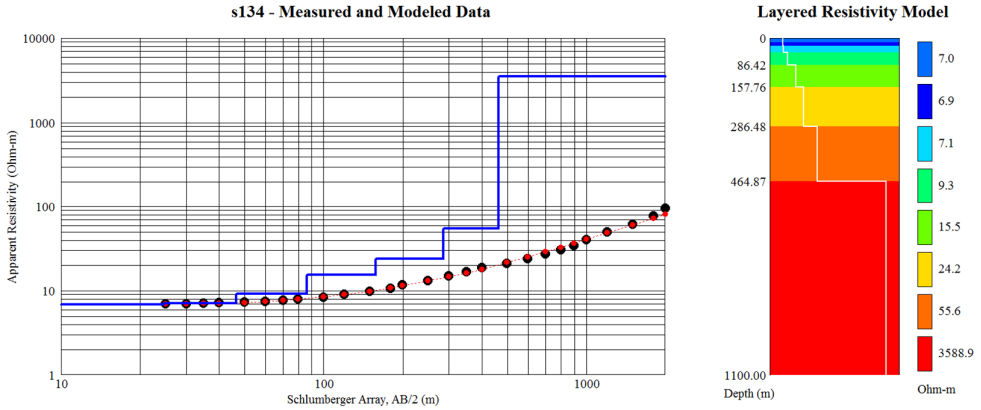
s134 - Measured and Modeled Data
Apparent Resistivity (Ohm-m)
10000
1000
100
10
1
10
100
1000
Schlumberger Array, AB/2 (m)
Layered Resistivity Model
0
86.42
157.76
286.48
464.87
1100.00
Depth (m)
7.0
6.9
7.1
9.3
15.5
24.2
55.6
3588.9
Ohm-m

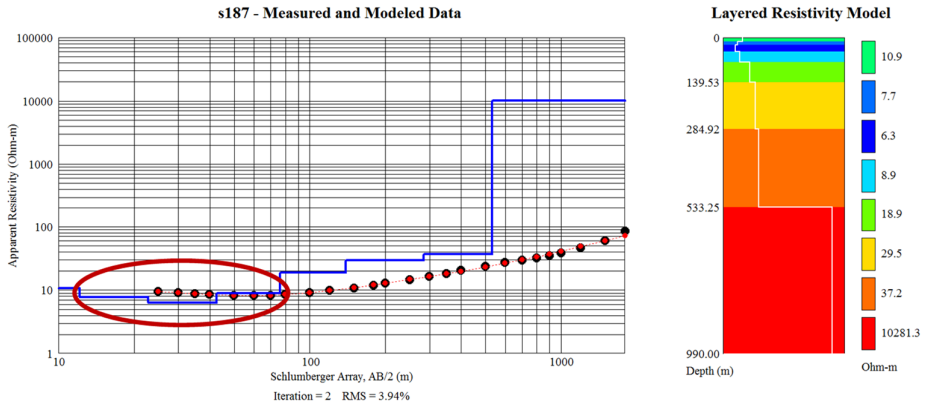

Figure 4.13 Location map and 1D inversion resistivity models for selected soundings.

The surface resistivities match reasonably with the AB/2=25 m results for the apparent resistivity all over the area. The well log in Figure 1.11, located between Area 2 and Area 3, intermediate and deep resistivity values match with the rock types at appropriate depths. Low resistivity values can be seen in the inversion models of Area 2 (see Appendix E) at intermediate depths. In the well log, there are fractured and weathered quartzite formations at the same depths. Deep resistivity values correspond to igneous and metamorphic rocks in the well log.

4.4 Resistivity Layer Pattern Map

To find out whether there was a simple pattern to the ground structure in the surveyed areas, and whether there was a clear relationship between the sounding shapes and the ground structure, the soundings were all inverted assuming 4 layers, and then these 1D models were categorized according to their resistivity structures. 4 different resistivity patterns (type ‘a’, ‘c’, ‘d’ and ‘f’) were observed in the 1D inversion resistivity sections (Figure 4.14). Patterns and shapes for all the soundings are given in Appendix D.

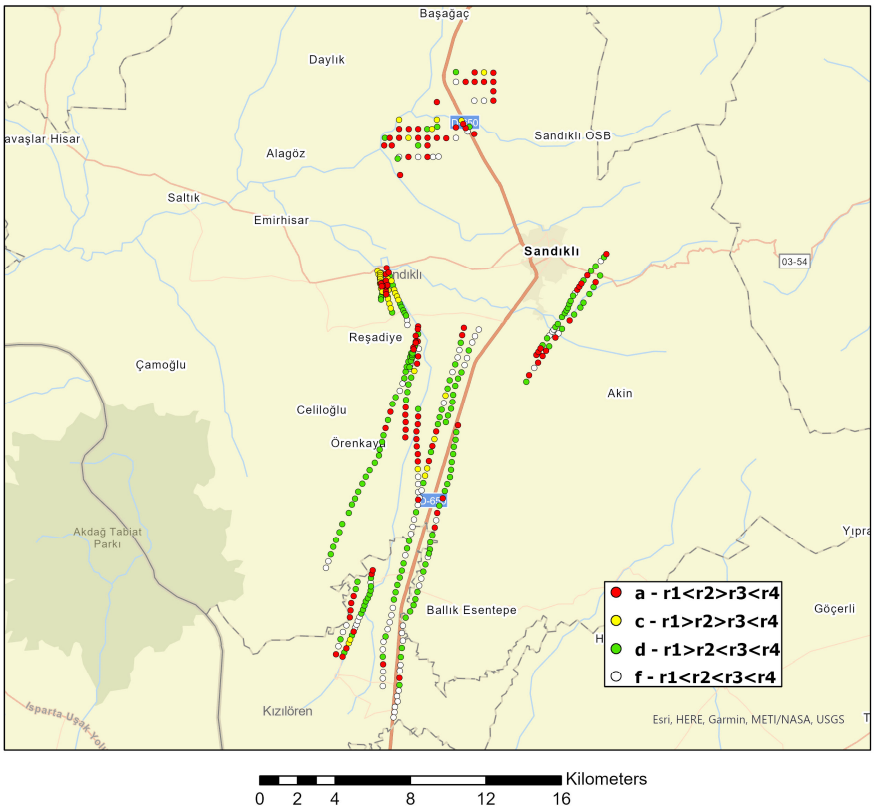

Figure 4.14 Resistivity 4-layer pattern map. In the legend, ri represents the resistivity of the ith layer, with r1 being the resistivity of the layer closest to the surface.

In patterns ‘a’, ‘c’ and ‘d’ there is a low resistivity above the bedrock layer, layer 4. For pattern ‘d’, this low resistivity layer is layer 2, so relatively close to the surface. For a and c it is layer 3, just above the bedrock. Pattern f, like Shape ‘F’ shows a systematic increase of resistivity with depth. A similar naming convention and color scheme as the shape characterization are used to more easily show a correspondence between 4 layer structure and the shape of the soundings. As mentioned before, when 4 layer models are produced in 1D inversion, and the ‘ideal’ ground structure, corresponding to pattern a, is defined as follows;

1) Damp soil = layer 1 = low resistivity
2) Compacted soil/fractured rock = layer 2 = higher resistivity
3) Hot or cold aquifer = layer 3 = low resistivity

4) Bedrock with fewer fractures = layer 4 = high resistivity

Over the map, 80% of the soundings have patterns a, c or d, indicating a low resistivity layer between the bedrock and the surface. Comparing the maps of sounding shape and 4 layer inversion pattern (Figures 4.5 and 4.13), there is not a great deal of correspondence except between Shape 'F' and pattern 'f' (r1<r2<r3<r4), which lacks a low resistivity layer. The relationships are summarized in Table 4.2. It is seen that Shapes 'A' through 'E' (Figure 4.4) all indicate the presence of a low resistivity layer in agreement with layer patterns a, c and d. Inspecting the sounding shapes in Figure 4.4 and the soundings in Appendix C, the lack of a better match is reasonable. Most soundings show low apparent resistivity (often < 50 Ω.m) for the equivalent of a few 100 m's depth, and the 4 layer structure does not consider the thickness or contrast in resistivity of the low resistivity layer with surrounding layers. Shape 'E', for example, may be seen as similar to Shape 'A' but with smaller contrasts between the layers, and comparing Figures 4.5 and 4.14, it is seen that many Shape 'E' soundings have 'a' layer patterns. Sounding 224 (Figure 4.13) is classified as Shape 'D' but has pattern 'a'.

Table 4.2 Correspondence of sounding shape with 4 layer ground structure. Numbers are the fraction of soundings with shape (A to F) that have layering pattern (a to f). Strongest correspondences bold and underlined. The number of soundings in each category is given by n.

Pattern\Shape	**A** (n=25)	**B** (n=69)	**C** (n=6)	**D** (n=115)	**E** (n=76)	**F** (n=79)
a (n=102)	**0.52**	0.04	**0.5**	0.2	**0.76**	0.03
c (n=39)	**0.28**	**0.23**	**0.5**	0.1	0.03	0
d (n=150)	0.2	**0.72**	0	**0.7**	0.18	0.01
f (n=79)	0	0	0	0.01	0.03	**0.96**

Nevertheless, there are some correlations. For example, 70% of the Shape 'D' soundings show layer pattern 'd'. 76% of sounding with 'E' shape, 50% of those with

'C' shape and 52% of those with Shape 'A' all match 4 layer structure 'a' (r1<r2>r3<r4), which we suggest is the most promising indication of a geothermal source layer above the bedrock. 72% of soundings of Shape 'B' and 70% of soundings with Shape 'D' match 4 layer structure 'd', which has the low resistivity layer at a shallower depth. Most notably, almost all the 'F' shapes correspond to layer pattern 'f'.

Pattern 'a' occurs in Area 2, where there is the strongest overlap with Shape 'A', in Area 3, in a band across the graben in Areas 4 and 5. Pattern 'd' (r1>r2<r3<r4) is the most common pattern in Areas 3 to 6 in the graben. Pattern 'f' occurs mainly at the ends of the groups in higher elevations.

Since the Shapes are based on more pronounced characteristics of the sounding curves, they are arguably a better indication of the presence of a significant low resistivity layer than the patterns.

4.5 1D Rolling Inversion and 2D Inversion Models

In this section, inversion models are described for the six Areas, mostly with illustration of the 1D rolling inversions. 2D inversion models are also presented for areas where low resistivity layers are most clearly defined, in Areas 2 and 4, and where the sounding lines cross a major fault, in Area 6. Models from other areas with their location maps are presented in Appendix F. The two panels above the 2D inversion models (e.g., see Figure 4.16) show the pseudosection from observations and the pseudosection based on the inversion model. A close comparison of these two panels indicates a robust inversion. In comparing the rolling inversions and 2D inversion models, note that the rolling inversions have a vertical exaggeration of 4 (section 3.7), a different limiting depth and a different colour scale for resistivity. The resistivity range in the rolling inversions is considerably larger than the range for the 2D inversions.

Due to the high number of sounding in some lines, specifically *Groups 8, 10, 11* and *12*, the lines had to be split into overlapping sections for 2D inversion, because there is a limit to the number of electrode positions allowed in the version of EarthImager that was used. For sounding numbers of overlapped lines see Table 4.3.

Table 4.3 Overlapped lines for 2D inversion. Overlapped soundings are indicated with red.

Line	Sounding Numbers
LineGroup8-1	s93,s94,s95,s96,s97,s98,s99,s100,s101,s102,s103,s104,s105,s106,s107,s108,s109,s110,s111,s112,s113,s114
LineGroup8-2	**s106,s107,s108,s109,s110,s111,s112,s113,s114**,s115,s116,s117,s118,s119,s120,s121,s122,s123,s124,s125,s126,s127,s128,s129
LineGroup8-3	**s120,s121,s122,s123,s124,s125,s126,s127,s128,s129**,s130,s131,s132,s133,s134,s135,s136,s137,s138,s139,s140,s141,s142
LineGroup10-1	s161,s162,s163,s164,s165,s166,s167,s168,s169,s170,s171,s172,s173,s174,s175,s176,s177
LineGroup10-2	**s169,s170,s171,s172,s173,s174,s175,s176,s177**,s178,s179,s180,s181,s182,s183,s184,s185,s186,s187,s188,s189,s190
LineGroup10-3	**s185,s186,s187,s188,s189,s190**,s191,s192,s193,s194,s195,s196,s197,s198,s199,s200,s201,s202,s203,s204
LineGroup11-1	s205,s206,s207,s208,s209,s210,s211,s212,s213,s214,s215,s216,s217,s218,s219
LineGroup11-2	**s214,s215,s216,s217,s218,s219**,s220,s221,s222,s223,s224,s225,s226,s227,s228,s229
LineGroup11-3	**s224,s225,s226,s227,s228,s229**,s230,s231,s232,s233,s234,s235,s236,s237,s238,s239,s240
LineGroup12-1	s241,s242,s243,s244,s245,s246,s247,s248,s249,s250,s251,s252,s253,s254,s255,s256,s257,s258,s259,s260,s261,s262
LineGroup12-2	**s251,s252,s253,s254,s255,s256,s257,s258,s259,s260,s261,s262**,s263,s264,s265,s266,s267,s268,s269,s270

4.5.1 Area 1: Group 17

Rolling 1D inversions were constructed for 3 WE lines of soundings in Area 1, in the northern part of the Sandikli plain (Appendix F). These inversions showed low resistivity areas at the surface and at depths from 50 to >350 m, with the deepest layers toward the western ends of the lines, closer to the river. However, there was little continuity in the ground structure along the lines or from line to line. The variation in resistivity is likely a combination of surface and subsurface heterogeneities, judging from the varied surface features. Area 1 is underlain by alluvium and underlying geology is not mapped (Figure 1.6), there are three creeks, a major highway and three

small towns (Appendix A).

4.5.2 Area 2: Groups 2 and 3

Groups 2 and *3* run NNE to SSW parallel to each other in Area 2 (Figure 4.15). There are greenhouses just to the west, near s23 and s24 of *Group 2*. *Group 3* is longer, extending farther south and a little farther north. A branch of the Orenkaya fault and two unnamed faults lie close to soundings s40 to s43 at the southern end of *Group 3*.

For *Group 2*, the 1D rolling inversion and 2D inversion sections (Figure 4.16) show the same basic structure. In the 1D rolling inversion, there is a zone roughly 2 km long at about 120 m depth with low resistivity (< 10 Ω.m) below a higher resistivity surface layer. Similarly, the 2D resistivity section has a low resistivity zone in the near surface. The rolling inversion section shows that the more resistive surface layer is mostly continuous. The 2D inversion shows some 'bubbling' of resistivity values near the surface around the sounding locations. This is an artifact due to the uneven and overlapping locations of the electrodes (section 3.6.2). High resistivity deeper layers are clearly seen on the right (southern) side of the sections. Additionally, it is seen that the layers all become shallower toward the south in a systematic way.

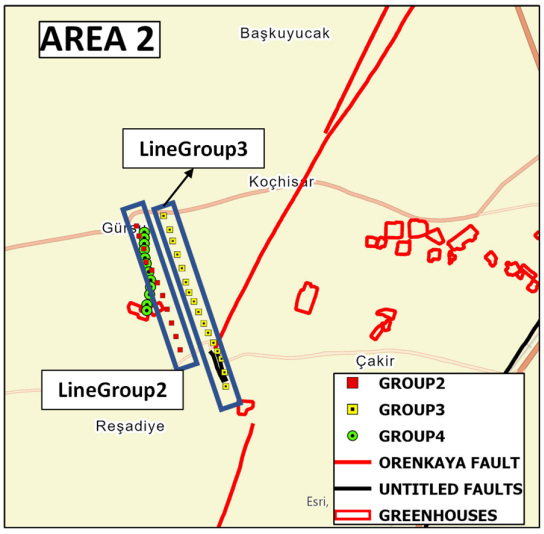

Figure 4.15 Location map of LineGroup2 and LineGroup3

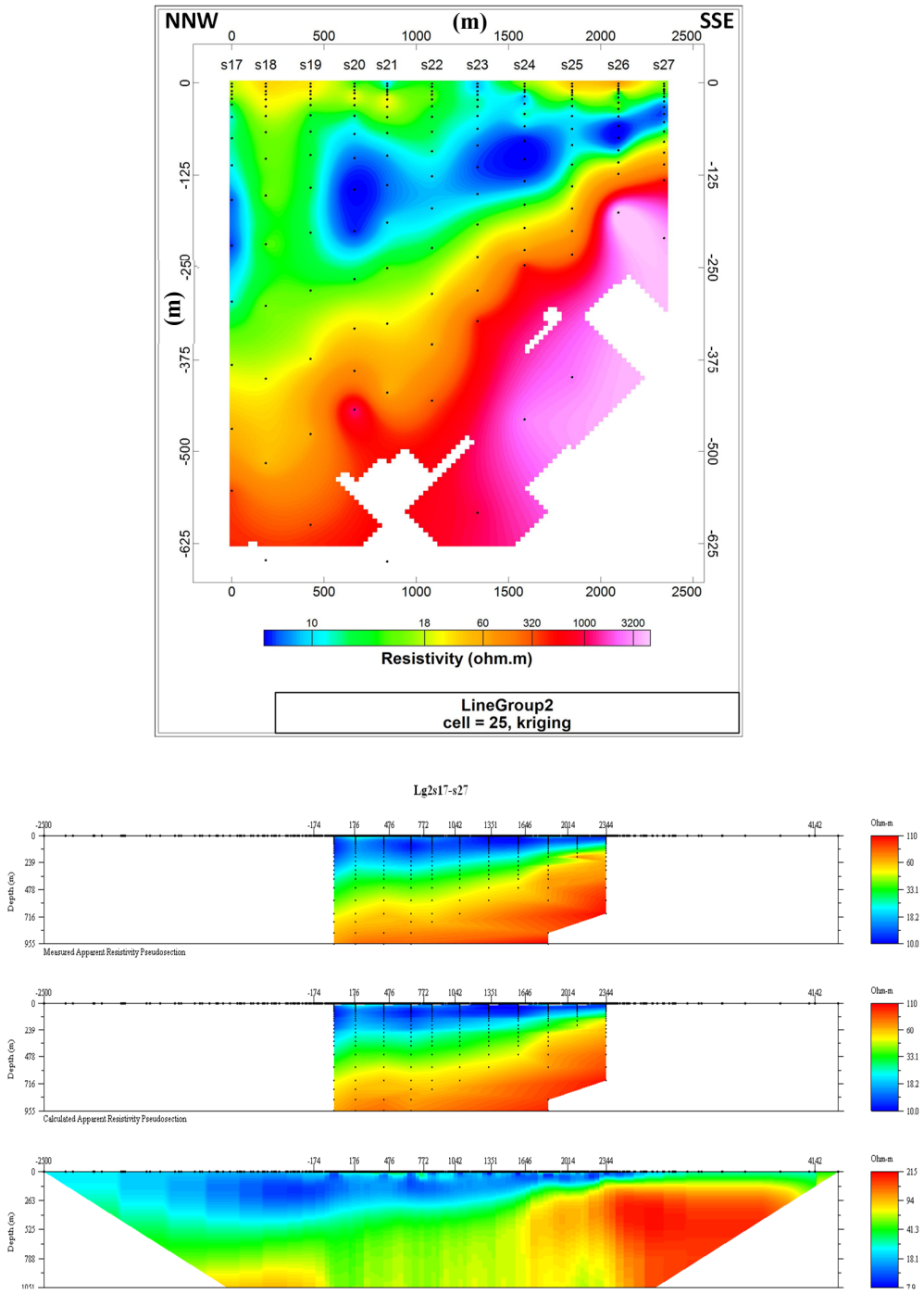

Figure 4.16. 1D rolling and 2D EarthImager inversion models of LineGroup2.

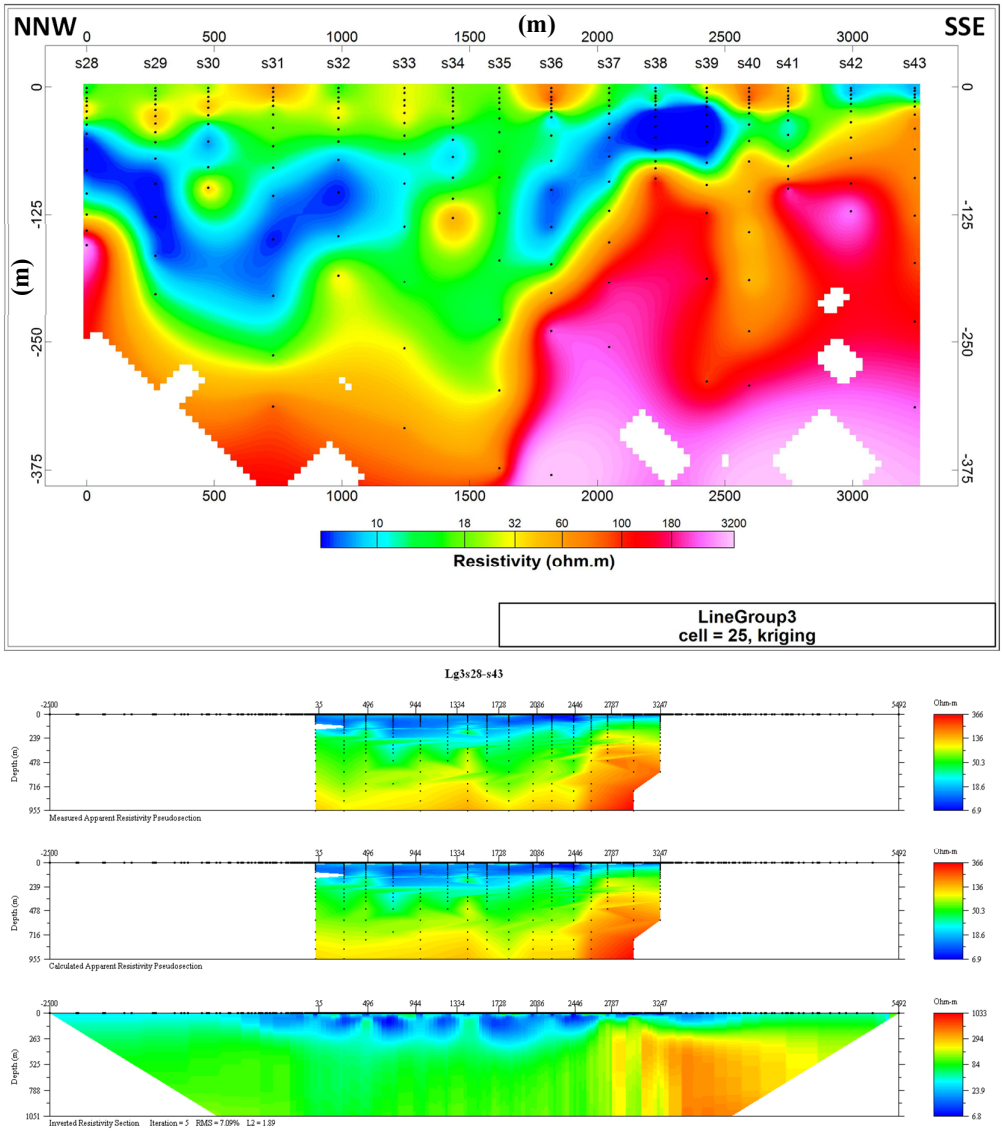

Figure 4.17. 1D rolling and 2D inversion models of Group 3 soundings.

In the 1D rolling section of *Group 3* (Figure 4.17), there is not such a consistency between neighbouring soundings as in the parallel LineGroup2, though for nearly 2 km from s31 to s39 the ground structure is broadly similar to that in LineGroup2. That is, there is a low resistivity (<10 Ω.m) layer, at average depths of 60 to 125 m, sandwiched between higher resistivity layers, there is a deep high resistivity layer in the north, and the layers shallow to the south. The location of the faults between s40 and s43 may be the reason for the variable ground structure in this region. Also, s34 and s35 do not

follow the general pattern. These soundings are near the Hamamcay stream, and s34 shows some significant offsets (Appendix C), so they may be particularly affected by variations in the near surface (section 3.4.3).

In the 2D inversion section, although the location of the low resistivity layer is not as clear, it is observed to be close to the surface. The 'bubbling' near the surface is marked. Both 1D rolling and 2D inversion sections show that resistivity is higher at depth to the south.

Group 4 (Appendix F) shows similar features, with even more sounding-to-sounding variability.

Area 2 is to the east and north of the Hudai Sandikli geothermal field (Figures 4.8 and 1.10), and there are indications of a deep thermal source in soundings to the southern end of *Group 2* and at scattered locations in *Group 1* (Appendices C and D). However, the low resistivity layer is at significantly shallower depths than that proposed for a 'shallow hot water zone' (~300m, Table 1.2) and well within the depth range (up to 200 to 300 m) for cold water aquifers (Davraz et al., 2016). The low resistivity layer deepens and thickens to the NNW as the soundings progress into the thicker alluvium of the Sandikli plain, consistent with cold aquifer draining toward the rivers in that direction. The higher resistivity at depth to the south is consistent with the bedrock being shallower nearer to the graben walls.

4.5.3 Area 3: Groups 12 and 13

Area 3 contains two parallel lines of soundings, *Groups 12* and *13*, to the SE of Sandikli town (Figure 4.9). *Group 13* soundings line is approximately the same length with wider spaced soundings and offset roughly 1350 m to the SW of the *Group 12* soundings line (Figure 4.9). The 1D rolling inversions are given in Figure 4.18. *Group 12* was split

into 2 overlapping sections for 2D inversion (Appendix F, Table 4.3). The inversions showed an irregular low resistivity layer, sometimes reaching the surface, particularly in the middle where the soundings cross the streams at low elevation (Figure 4.9c and d). The high resistivity region is shallower at the NE and SW ends of Area 3, consistent with bedrock being closer to the surface there (Figure 4.18). There is some correspondence in the irregular structure in the middle. Some features line up: s249 in *Group 12* shows a low resistivity column between higher resistivity areas, and so does s281 in *Group 13*.

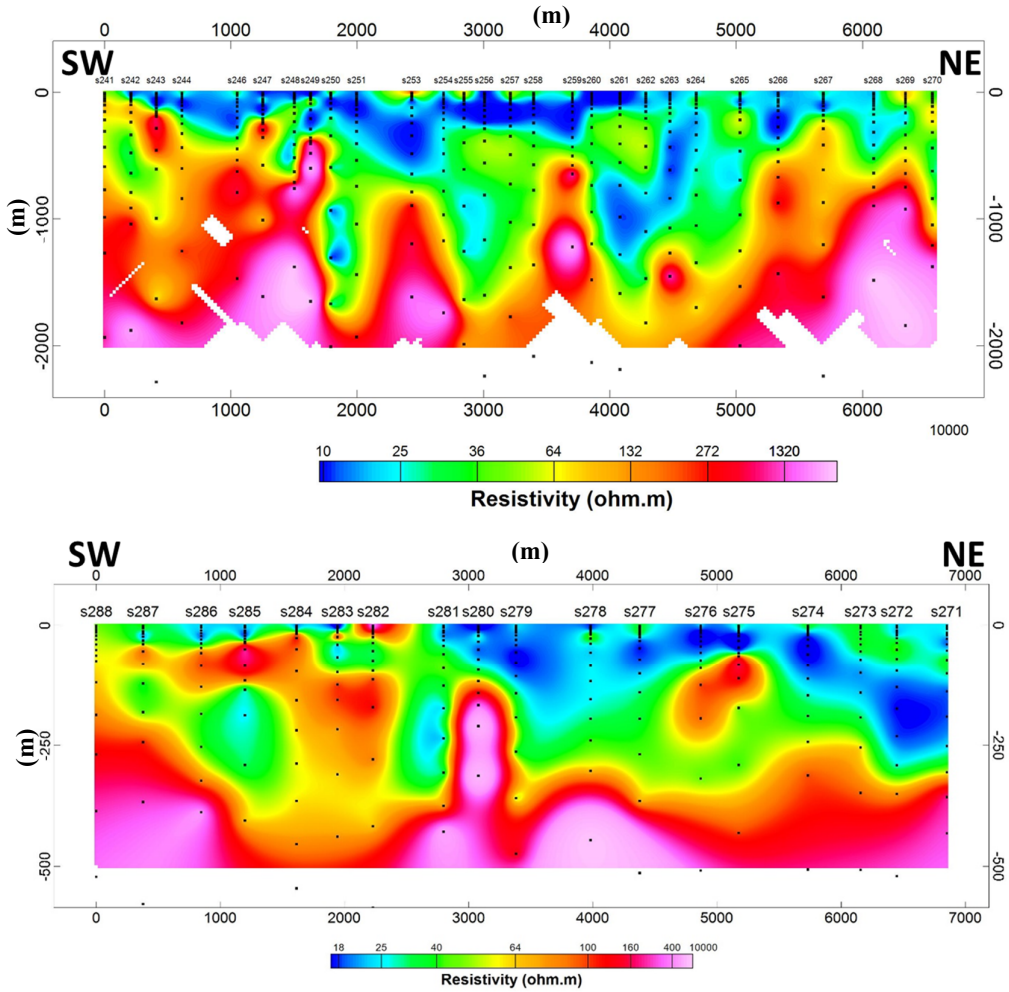

Figure 4.18. 1D rolling inversion models of Group 12 (top) and Group 13 soundings. Oasis Montaj, cell size 25m, kriging.

4.5.4 Area 4: Groups 6 and 11

Area 4 is along the west side of Sandikli graben (Figure 4.19). *Group 6* (s64 to s79) runs N to S, while *Group 11* (s205 to s240) runs from SE to NW. In the north, they are very close together. There is a greenhouse close to the two most northerly soundings of the two groups (s64 and s65, s239 and s240). *Group 6* head toward the centre of the graben from north to south; *Group 11* soundings to the south are at higher elevations (Figure 4.10c).

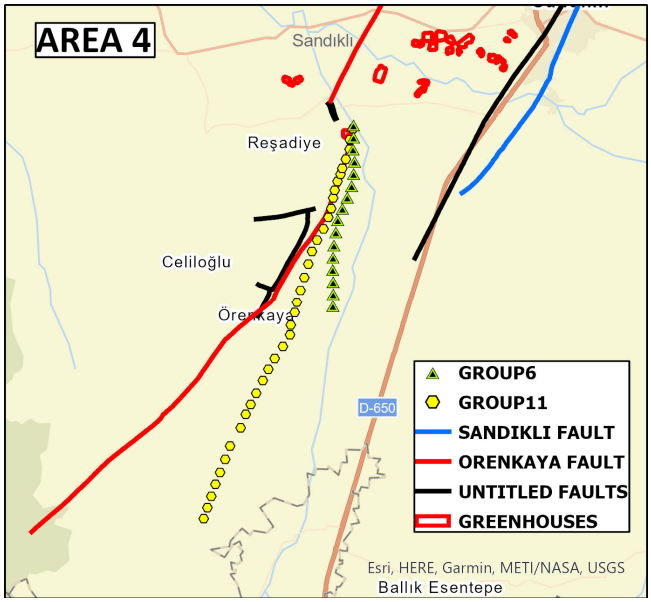

Figure 4.19 Location map of Group 6 and Group 11.

The inversion models for *Group 6* are shown in Figure 4.20. See also Figure 4.10 for the topography and near surface apparent resistivity. In both inversion sections, the northernmost soundings next to the greenhouse show relatively little change in resistivity with depth. Just south, s67 to s72 show the presence of a low resistivity layer with an average depth of 100 m for about 2 km. There is also a high resistivity zone deepening to the south. The high resistivity zone shown in magenta in the 1D rolling inversion model may be related to the closeness to high ground (Figure 4.10c) and/or the closeness of the Orenkaya fault.

Soundings s73 and s78 are anomalous. Inspecting the raw data in Appendix C, this is likely due to the process of removing offsets associated with moving the potential electrodes (see section 3.4.1). For both of these soundings, the apparent resistivity values at high AB (uncorrected for offsets) are similar to those of nearby soundings. Therefore, the breaks in the ground structure associated with s73 and s78 are not considered meaningful.

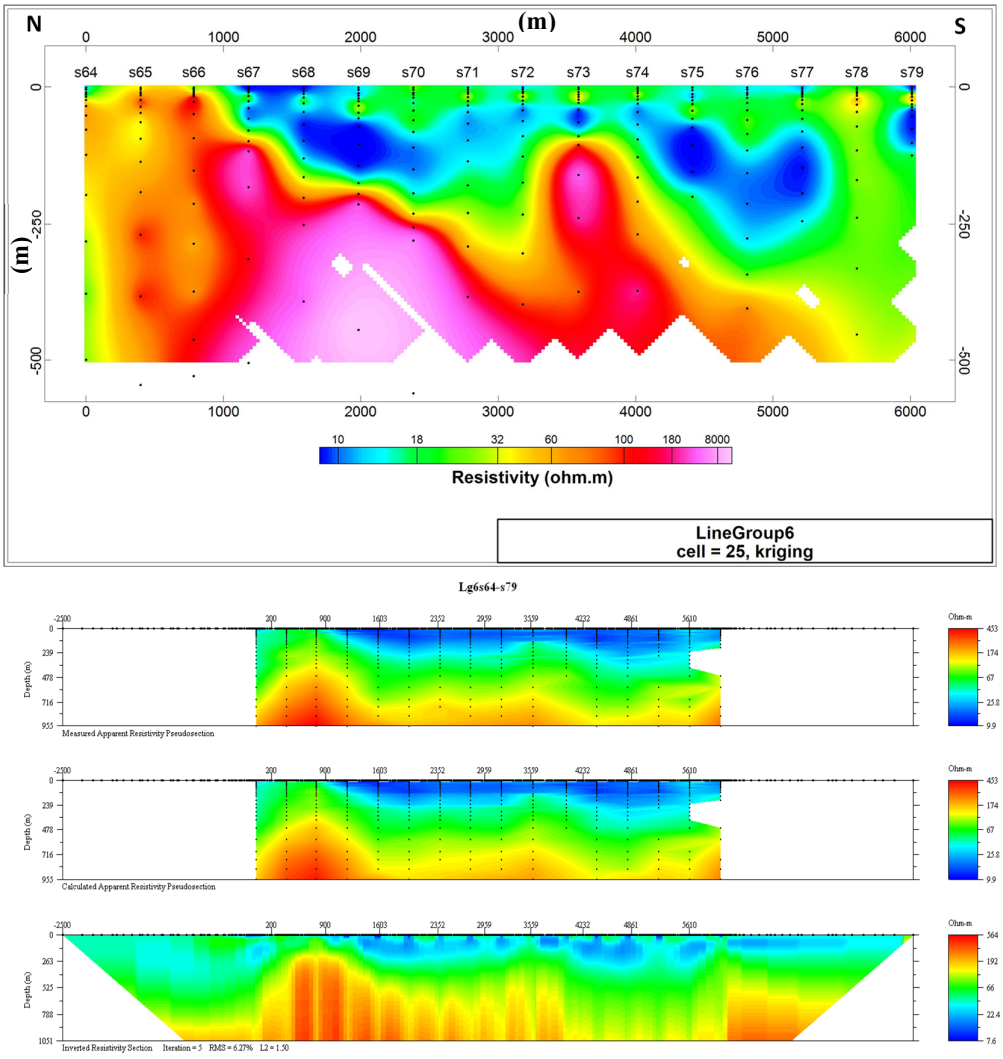

Figure 4.20 1D rolling and 2D inversion models of Group 6 soundings.

Disregarding these two soundings, the models show a ground structure with generally a low to moderate resistivity surface layer, a low resistivity layer and a deeper

layers with increasing resistivity with depth. Toward the south, the surface low and moderate resistivity layers become deeper, consistent with *Group 6*'s soundings becoming closer to the centre of the graben. The near surface resistivity is variable (see also Figure 4.10a), possibly affected by surface or groundwater flow across the graben (section 4.2.4).

The 2D inversion shows a similar structure as the rolling inversion section, including an area of shallow high resistivity to the north. The striping and bubbling are artifacts associated with the non ideal arrangement of electrodes. Apart from that, there is a reasonable agreement between two sections. The region to the south is regarded as unreliable because of the untrusted sounding s78.

It is not known whether the low resistivity layer at ~100 to ~200 m depth is a geothermal source, though the shallow depth suggests a fresh water aquifer. It is possible that the low resistivity area under s68 to s70 is related to the source for the greenhouse near s65 and s66.

Group 11 had to be split into three overlapping sections (Table 4.3). *Group11-1* (Figure 4.21) consists of soundings s205 to s219, covering 6 km from the southernmost location toward the NNE . These sections showcase some issues with both sections. In the 1D rolling inversion section, there is a larger than usual gap between s211 and s212, and because of the Oasis Montaj gridding, the low resistivity layer has been removed there. Looking at the individual soundings it is seen that a resistivity layer in the near surface at 60 to 110 m depth is present for all soundings from s207 to s219, though its depth and resistivity vary. The 2D inversion section shows bubbling and striping.

The sections indicate that the low resistivity layer at about 90 m deep is a

stronger feature to the north and the bedrock deepens as the sounding locations move toward lower elevations.

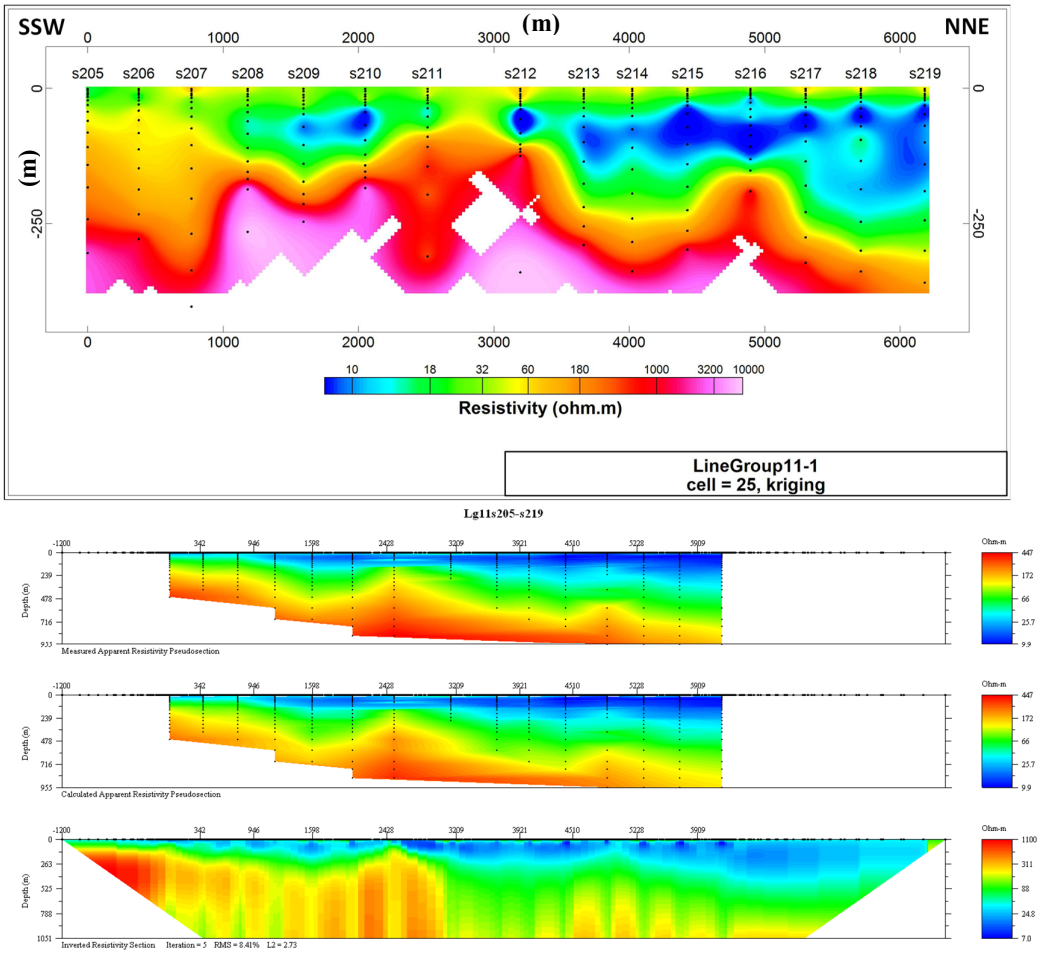

Figure 4.21 1D rolling and 2D inversion models of Group 11-1 soundings.

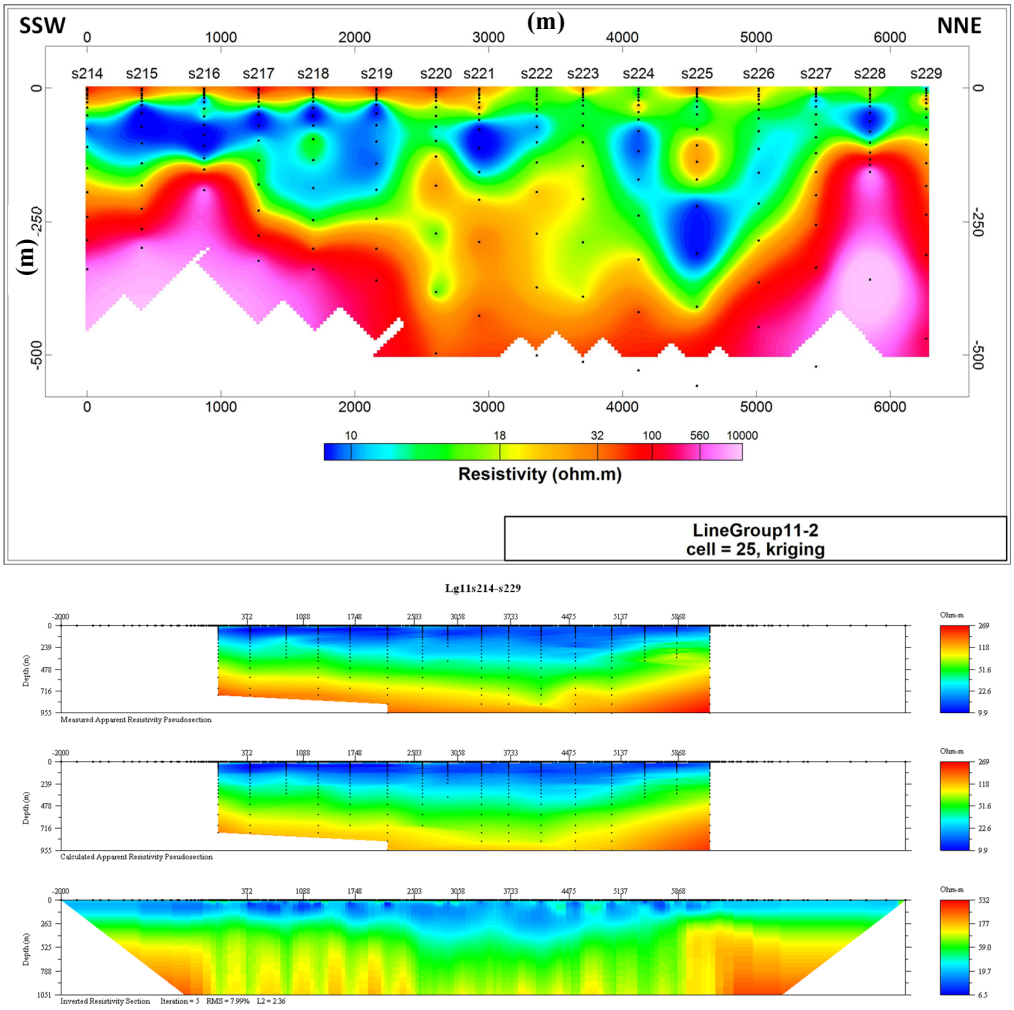

Figure 4.22 1D rolling and 2D inversion models of Group11-2 soundings.

Figure 4.22 shows sections for inversions of south to north *Group 11-2* soundings. These sections overlap those in Figure 4.21, such that the southern half of sections in Figure 4.22 corresponds to the northern half of sections in Figure 4.21. They do not look exactly the same because the colour scales are different. The resistivity and depth ranges for 1D rolling and 2D inversion panels are different, but the resistivity values at similar depths are comparable except at the deepest levels. At the deepest levels, the resistivity in the 1D inversions is significantly higher. This is presumably related to differences in the inversion methods. The low resistivity on the north in Figure 4.20 is seen on the south in Figure 4.21. The length of this low resistivity layer is roughly

4.7 km. There is a deeper layer of moderate resistivity (green colours in the 2D section) between s220 and s225, indicating a thicker layer of material above resistive bedrock. This roughly correlates to a valley in the nearby west shoulder of the graben, seen in the 1100 m contour in Figure 4.2 (see also Appendix A).

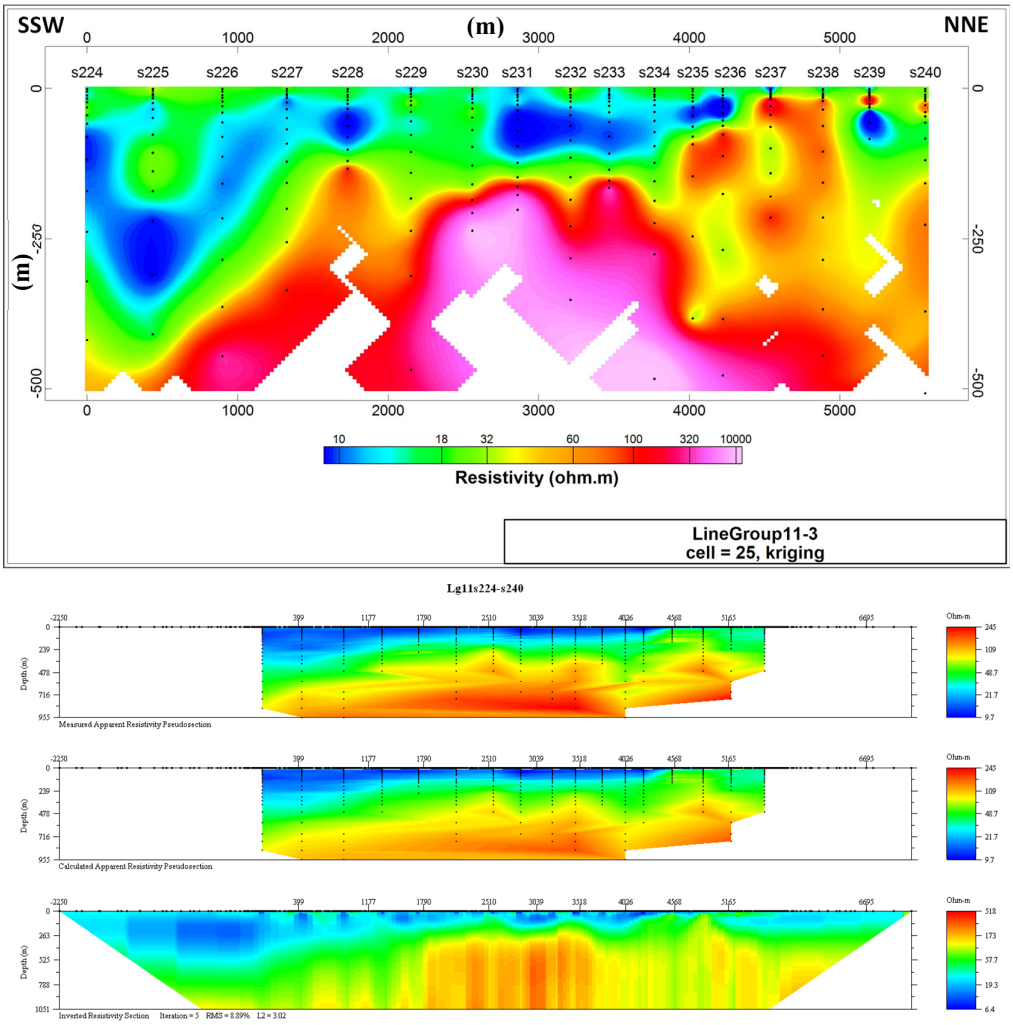

Figure 4.23 1D rolling and 2D inversion models of Group11-3 soundings.

Inversions for the final, northmost, section of *Group 11* are given in Figure 4.23. From s29 to s34 (2 to 4 km) there is high resistivity with depth, likely reflecting the closeness of the graben shoulder. The most northerly soundings are consistent with the overlapping soundings of the northern portion of Group 6 soundings (Figure 4.20). They

show high resistivity near the surface, perhaps related to the Orenkaya fault.

4.5.5 Area 5: Groups 8, 9 and 10

Area 5 consists of long lines of soundings down the east side of the graben (Figure 4.10). *Group 8* extends for about 20 km from north to south, and *Groups 9* and *10* are subparallel to it, from about 700 m to 1.3 km to the east. *Groups 8* and *10* had to be split into sections for 2D inversion (Table 4.3). North to south 1D rolling inversions of the three groups are shown in Figure 4.24 and the 2D inversions in Appendix F. The lines show a similar ground structure, with an irregular low resistivity layer from about 50 to 200 m depth for the northern ~9 km, then a thin, near surface low resistivity layer for the next 1 or 2 km. For Group 8, this pinches out. To the south, there is a low resistivity layer at the surface for about 5 km. Farthest south, bedrock rises closer to the surface (*Group 10* panel).

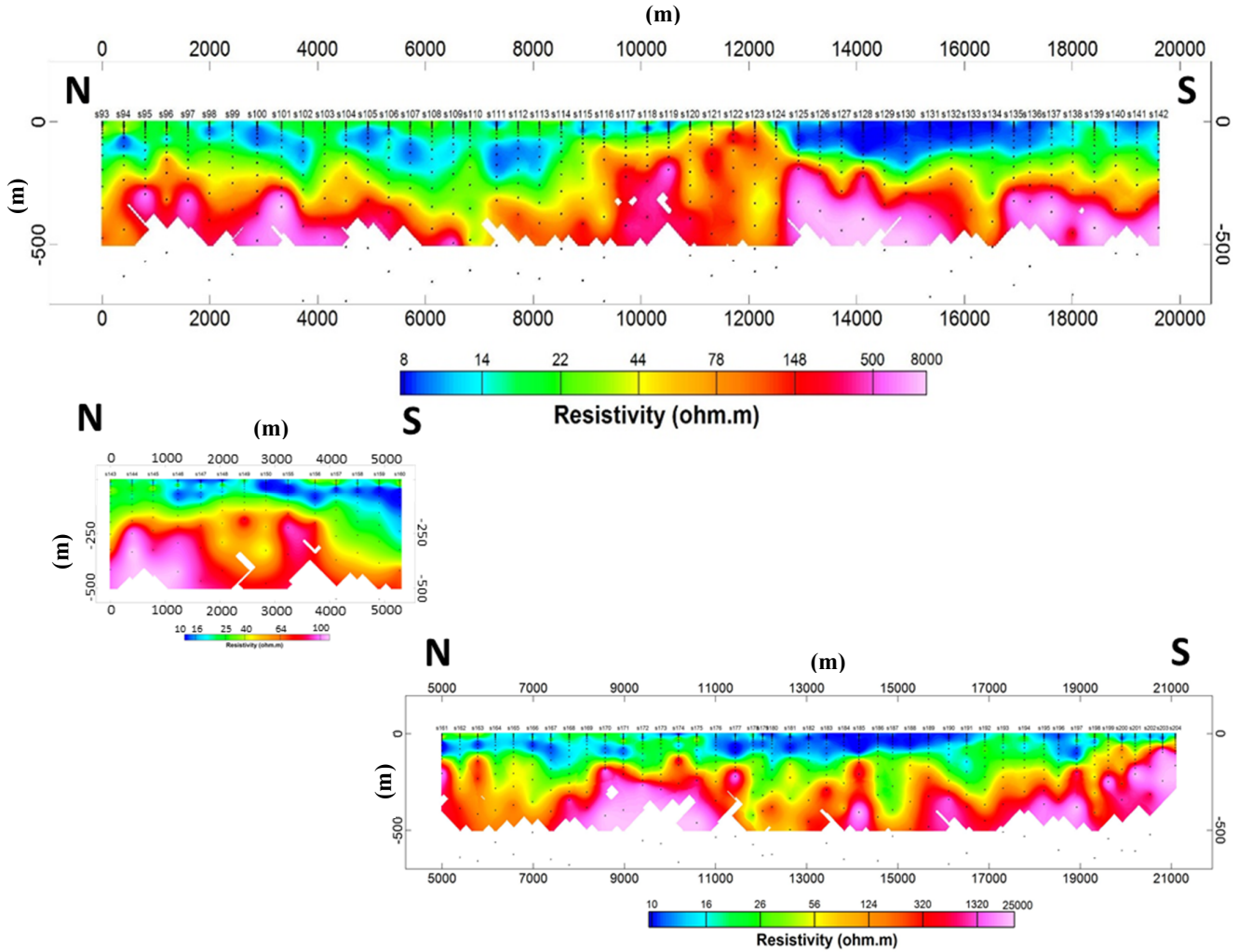

Figure 4.24 1D rolling inversions for Group 8 (top), Group 9 (bottom left) and Group 10 (bottom right). Oasis Montaj, cell size 25 m, kriging interpolation.

4.5.6 Area 6: Groups 14 and 15

Groups 14 and *15*, in the far south west of the graben, are sub parallel to each other and the Kiziloren Fault (Figure 4.25). Both sounding locations progress from south to north. There is an offset to the fault near the southern end of these sounding lines, and several soundings lie very close to the fault and/or cross it. Large changes in the surface resistivity are observed here (Figures 4.10a and 4.11).

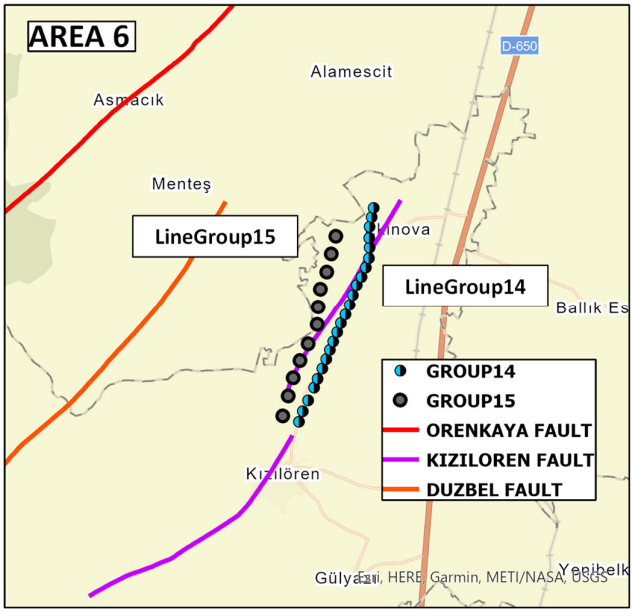

Figure 4.25 Location map of Group 14 and 15 soundings.

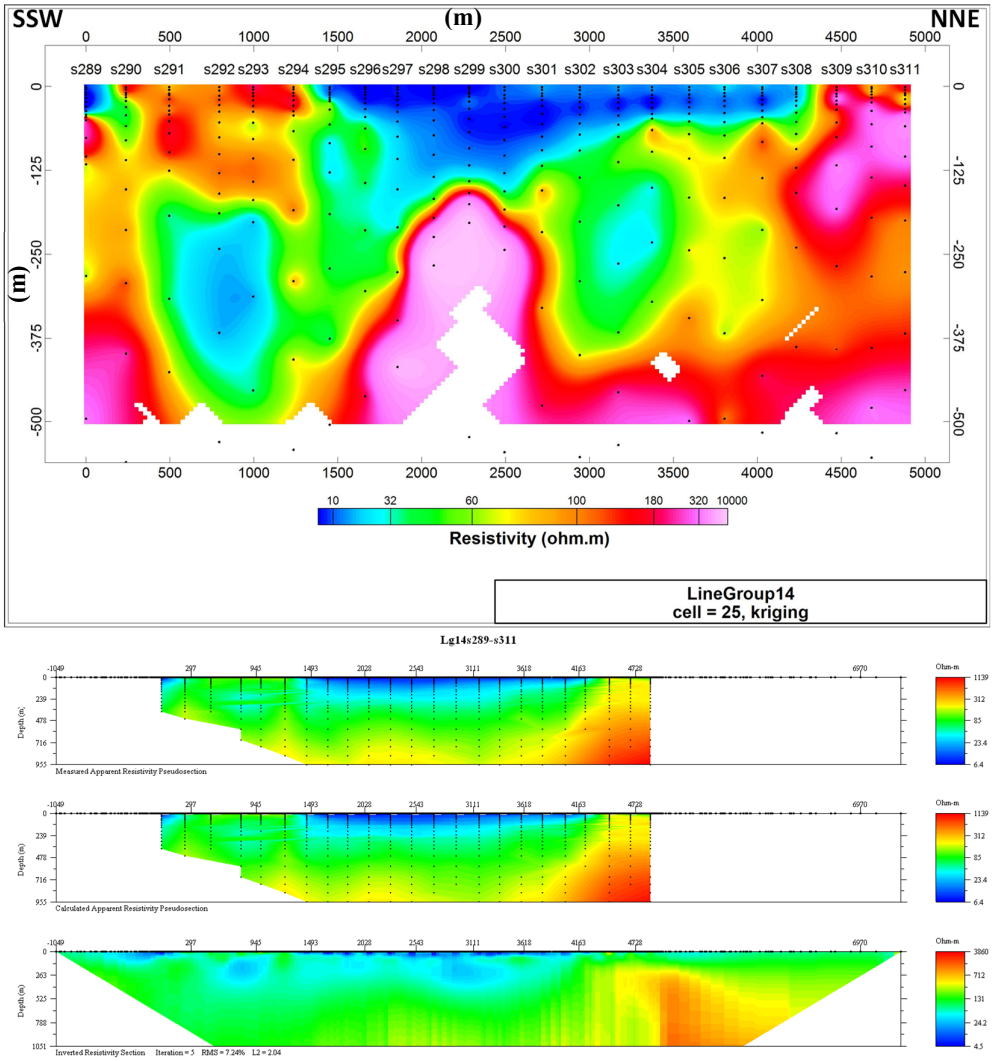

Figure 4.26 1D rolling and 2D inversion models of LineGroup14.

The large changes in the surface resistivity values are seen in the sections, particularly well in the 1D rolling inversion sections (Figures 4.26 and 4.27, top panels). The reason why these two high resistivity layers are observed in the near surface is likely to be related to the fault located in the region (Figure 4.11, section 4.2). The large variations on the surface means that it is difficult to interpret the ground structure at depth. Given the large differences observed in the surface properties of the two parallel sounding lines (Figure 4.11), the ground structure likely varies significantly in 3 dimensions. A low resistivity feature, seen at an apparent depth of 150 to 300 m in s318

of *Group 15* (at distance 2500 m along the line), may be the result of current flowing sideways through the low resistivity region at the same distance along the *Group 14* line (see Chapter 5).

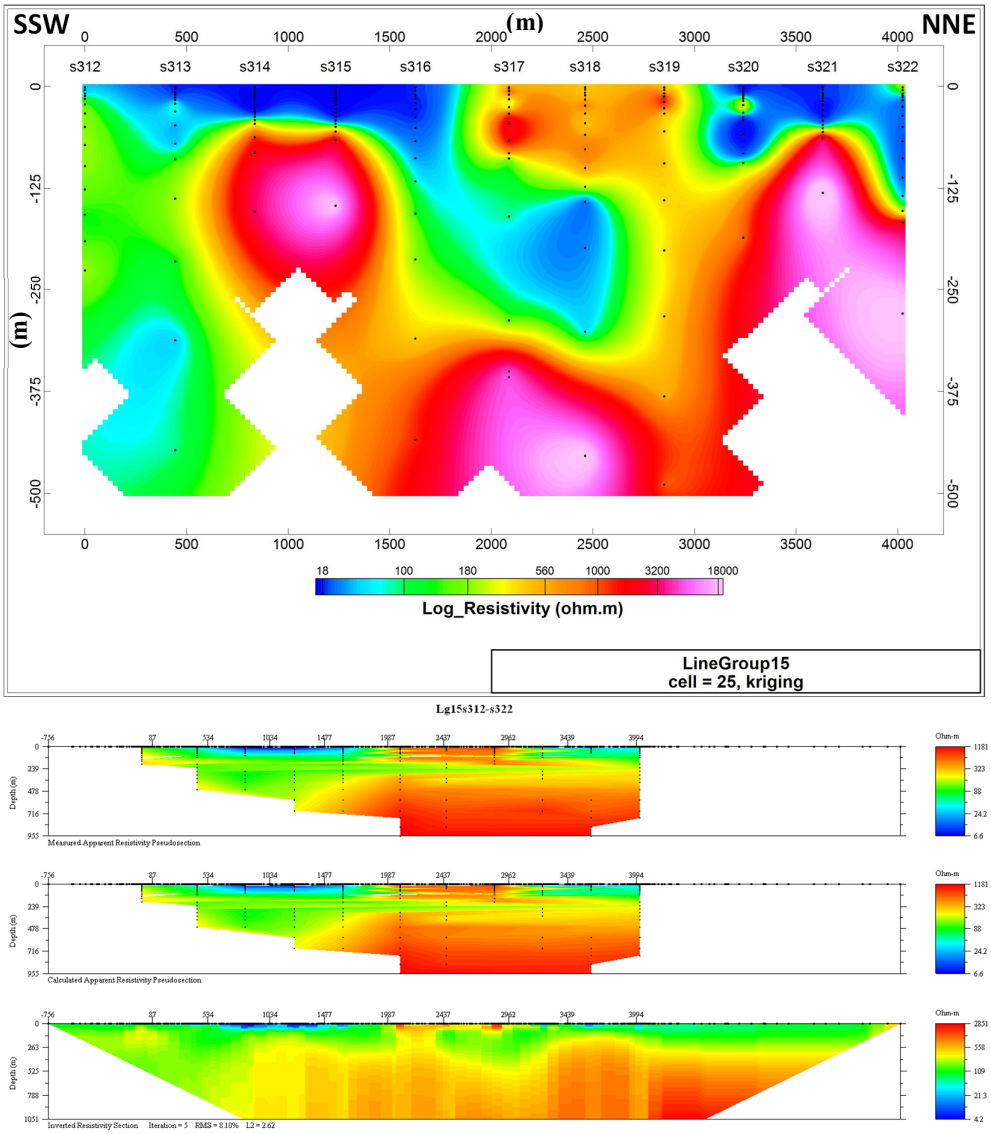

Figure 4.27 1D rolling and 2D inversion models of LineGroup15.

Chapter 5: Summary and Conclusions

The study area is located in the Sandikli district of Afyonkarahisar province in west-central Turkiye. The Afyonkarahisar region has various fault systems and grabens where geothermal resources are utilized. The first geothermal district heating system in the region was started in 1996. Since then, many drillings (observation, production and reinjection wells) have been conducted to capitalize on geothermal energy.

The VES surveys were undertaken to reveal the resistivity characteristics of the Sandikli graben, to seek more geothermal resources for heating greenhouses, and to test the utility of the vertical electric sounding (VES) resistivity method. The data consist of 384 VES surveys with a maximum spread of 5 km and so a depth penetration of about 1.4 km. They were carried out within 6 areas within the graben (Figure 5.1) in 2011. The data included measurements of apparent resistivity and IP effect. However, except for the shallowest measurements, the IP data were too noisy to use.

The Sandikli graben is a major agricultural area in the Afyonkarahisar region, featuring both open air fields and greenhouses. The graben contains cold water aquifers used for domestic and agricultural purposes, while hot water from a recognized geothermal field is used for heating greenhouses and spas. The geothermal field is located between the Hudai spa and the town of Sandikli (Figure 5.1). A core log from a drill over 1 km deep, SE of Sandikli and within the geothermal field (black star in Figure 5.1) shows about 20 m of alluvium (white) underlain by 160 m of Pliocene sediments and porous sedimentary rocks in gray. These units, which can be 200 to 300 m deep, host cold water aquifers. Underneath there are lava and debris flows down to 330 m, and the bottom ~20 m of these are labeled ‘typical shallow hot water zone’ in the drill core log. The degree of hydrothermal alteration increases with depth in the core. The

main reservoir rocks for the geothermal field are taken to be the deeper Hudai quartzite (e.g., Memis et al., 2010), or carbonate units within it (Figure 5.1). In looking for geothermal sources in the graben, characterized by a low resistivity layer in the subsurface, the most prospective depths were ~300 m and ~900 m. However, cold water aquifers would also produce a low resistivity layer.

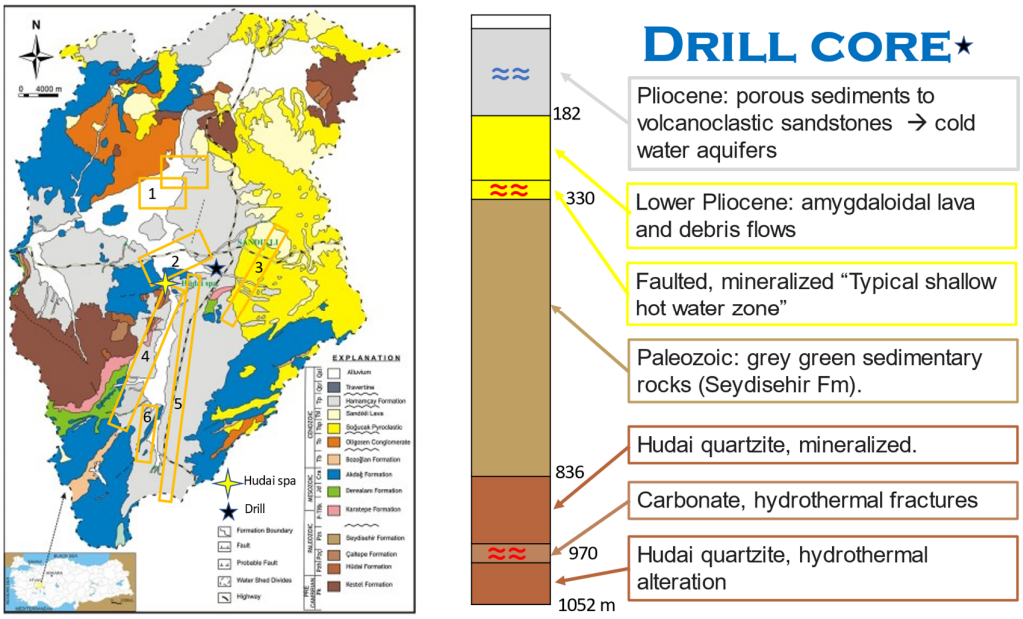

Figure 5.1 Left: Geological map of the Sandikli basin (Davraz et al., 2016) with surveyed areas 1 to 6 marked with orange rectangles. Right: Highly simplified version of the drill core log (Figure 1.8, Table 1.2). The location of the drill is indicated by the black star. Wavy blue and red symbols indicate possible locations of cold (blue) and hot (red) aquifers.

The greatest interest in the Sandikli basin has been in the hydrogeology due to concerns about finding or overusing geothermal waters, and contamination of fresh water aquifers by contaminants such as arsenic from geothermal water (e.g., Memis et al., 2010; Demer et al., 2013; Davraz et al., 2016). Models generally show geothermal areas associated with faults (Figures 1.7 and 5.2), so some VES survey lines were located near known faults (Figure 4.3).

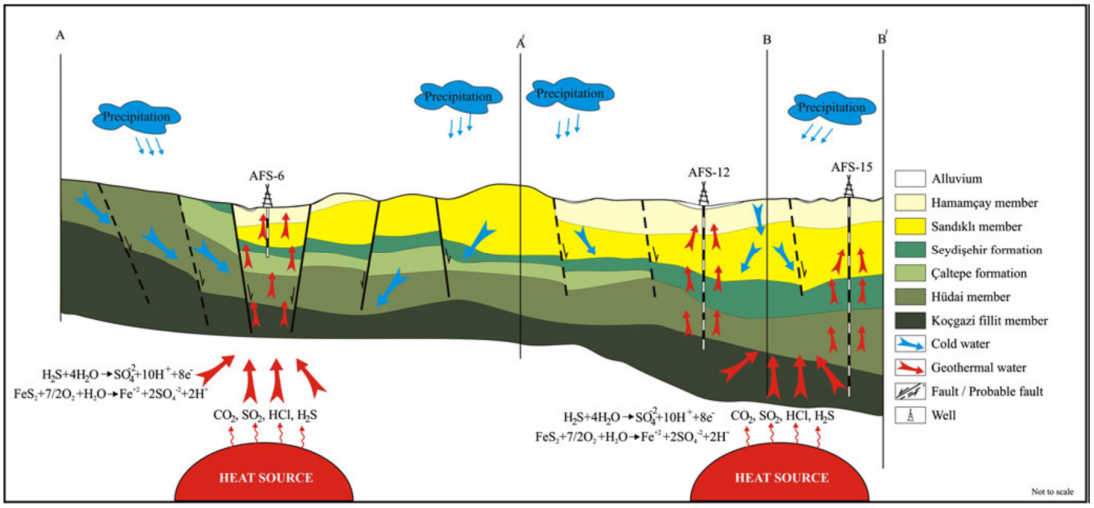

Figure 5.2 Simplified model of the Sandikli-Hudai geothermal system (Memis, 2010). Location of profile lines A-A'-B-B' are given in Figure 4.8.

The first steps of data analysis were inspection of the raw data, omission of unreliable parts of the data such as single anomalous resistivity readings or zigzags, removal of offsets created when changing the potential electrode spacing, and smoothing (section 3.4). Usually the offsets were small, but very large offsets were observed in some sounding curves, particularly in *Group 5*, near the greenhouses in Area 2. The reason for this effect is surface heterogeneities (section 3.4.3), which may be related to faulting (Figure 5.2) and therefore could be an indication of near-surface geothermal activity.

Next, the correlation of near surface measurements (resistivity and IP) with surface features (topography and faults) was examined. High near surface resistivity values are seen mostly in places where the elevation is high (see Figure 4.2) and attributed to a deeper water table with higher elevation. A correlation was found between near surface resistivity and IP values. The surface resistivity is mostly low where the IP values are high, and is likely due to a higher clay content at lower elevations. Surface IP values near the creek in Area 2 are considerably higher than the rest of the region (Figure 4.1b). The most important resistivity change associated with

faults is located in the southern part of the region. There is a significant resistivity variation across the Kiziloren Fault located in Area 6 (Figures 4.1 and 4.11).

The general shapes of the sounding curves were categorized and described, and a map of curve shapes was created (section 4.2). The number of major layers (typically 3 or 4) was identified by looking at the turning points on the soundings curves. The only evidence of a deep low resistivity (geothermal) layer was found in a few soundings in Area 2 (see Appendix D), where there is a leveling or decrease in resistivity at the largest electrode spacings (i.e. greatest depth penetration of current). Most of the soundings showed a steady increase in apparent resistivity at the largest electrode spacings, indicating that the ground deeper than a few hundred metres was resistive bedrock. There was significant variability in shapes throughout the graben (Figure 4.5). Shapes 'A' to 'D', indicating a subsurface low resistivity layer (an aquifer), were very common. Shapes 'E' and 'F', where resistivity increased with depth, occurred sometimes over higher elevations, suggesting no aquifer, and sometimes near streams where a low resistivity layer was at the surface.

1D inversion models were produced for each sounding using software EarthImager1D (Figure 4.13 and Appendix E). These commonly showed a low resistivity layer between 50 and 300 m depth, so likely cold water aquifers. Looking at the 1D inversion models, it was determined that the ground structure has 4 layers. To define ground structure of study area, resistivity patterns of the sounding curves, based on a 4-layer subsurface, were categorized (Figure 4.14). Like the sounding shapes map, resistivity patterns change quickly from sounding to sounding in many places. Except one pattern ('f'), the low resistivity layers are seen almost everywhere. These patterns showed reasonable correspondence with the Shape categories (Table 4.2).

Then, the 1D resistivity models were placed adjacent to each other to create '1D rolling inversions', that is, 2D cross-sections of the subsurface along the survey lines using the mapping program Oasis Montaj. For a better interpretation, 2D inversion based on the Gauss-Newton method was carried out using software EarthImager2D. The low resistivity layers can be seen in the 1D rolling inversion sections in detail. As was mentioned, these are thought to be cold water aquifers and it is not possible to relate low resistivity layers with a geothermal resource (e.g. an aquifer of hot water). As opposed to 1D rolling inversion models, in the 2D inversion models low resistivity layers sandwiched between the bedrock and surface were harder to identify due to 'bubbling' near the surface and 'streaking' at depth (e.g., Figure 4.20). This is due to the poor spacing of electrodes from the point of view of the inversion algorithm (section 3.6.2). However, apart from this, the 2D inversions showed smoother profiles, with similar ground structure and less sounding to sounding variability.

The survey was carried out using the VES method because of practical reasons, including ease of acquisition and time constraints. The surveyors were able to cover a lot of the graben with a small crew using this method. Given this survey geometry, creating sections using 1D rolling inversions makes sense because the difficulty in carrying out 2D inversions (the striping and bubbling). The sections gave similar results, at least qualitatively, even though the 1D inversions make unrealistic assumptions about the ground structure. In the 1D rolling inversions, partly because of the vertical exaggeration, it is easier to see the depth of the aquifers. In the 2D inversions the bubbling at the surface made it more difficult to see that the low resistivity regions were continuous.

In order to visualize the resistivity distribution in the graben in three

dimensions, panels were formed by bringing subparallel 1D rolling inversion sections together (Figures 5.3 and 5.4). Groups 2, 3 and 4 (Figure 5.3) are located in Area 2, in the northern part of the graben, on the western side of the geothermal field (Figures 5.1 and 1.11).

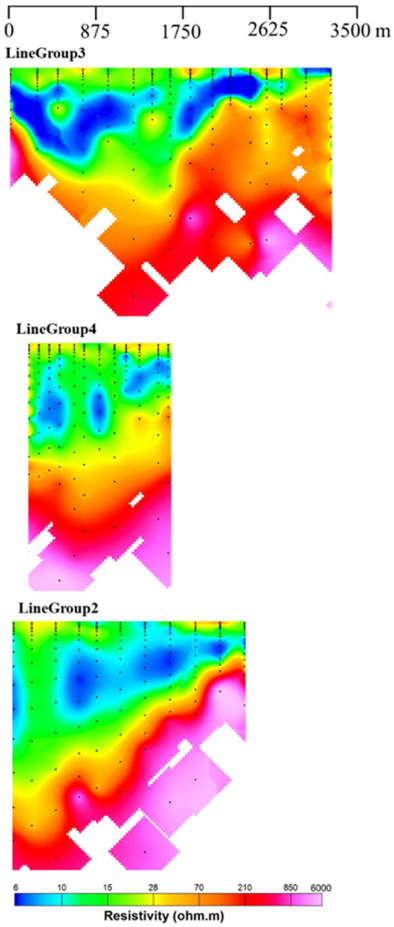

Figure 5.3 1D rolling inversion sections of Groups 2,3 and 4. Distance is measured from NNW to SSE and sections are in order of E to W down the page. The maximum depth for LineGroups 2 and 3 is 750 m, and for LineGroup 4 it is 500 m.

In Figure 5.3 it is seen that the bedrock (high resistivity layer, magenta) is closest to the surface in the south, closer to the graben wall. The aquifer region (low resistivity layers, blue) is irregular but continuous from east to west and generally deepens to the north, toward the centre of the Sandikli plain following drainage patterns there (Memis, 2010).

Figure 5.4 shows a panel of subparallel groups in Areas 4, 5 and 6 (Figure 5.1) south of the geothermal field, from north to south along the graben. Lines of Groups 8, 9 and 10 show some consistency in the ground structure from east to west. Lines of Groups 6 and 7 also show this similar structure. The bedrock is relatively close to the surface in the north, especially to the west (LineGroup 11). Just to the south, there is a continuous aquifer, which is deeper in the middle of the graben (LineGroup 6 and 7), and appears to follow some irregularities in the bedrock. About half way down the sections at distances ~8 to 11 km, the bedrock is close to surface and to the south of this a low resistivity layer can be seen at the surface in LineGroups 10 and 11. This surface layer has a length of about 5 km along LineGroup 10. This layer is also seen clearly in Figure 4.1 as having the lowest surface resistivities in the entire survey area. Bedrock is closer to the surface at the southern end of the graben. The resistivity distribution for LineGroup14 and 15 (Area 6, near the southwest end of the graben) is irregular and high in general, and it is associated with a fault crossing between the two lines. In the middle of LineGroup11 the bedrock is deeper than the other sections. This may be related to fault structure in the region. It is here that the major Orenkaya is intersected by unnamed faults and bends to the west, as seen in Figure 4.3.

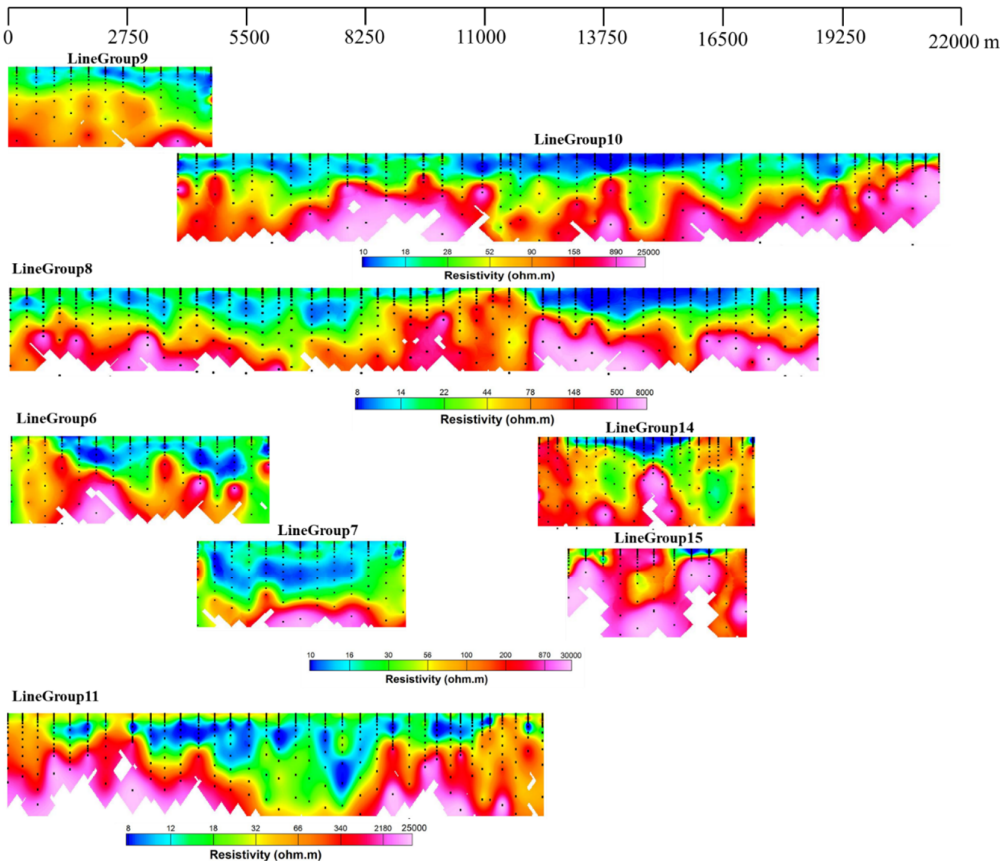

Figure 5.4 1D rolling inversion sections of Groups 6,7,8,9,10,11,14 and 15. Sections are in order of N to S across the page and E to W down the page, except Group 9, which is slightly farther to the west than Group 10. The colour method in Oasis Montaj is histogram normalization, and so the resistivity scales vary as shown.

Considering the inversion results, sounding curve shapes and resistivity pattern map, there are not any extensive areas of particularly prospective ground for geothermal resources. The most prospective ground is Area 2, where there are already hot springs and greenhouses. In Area 2, high surface IP values might be an indication of clay content, which can be the cause of a low resistivity zone in geothermal areas.

Regarding the utility of the VES method, the VES is a relatively fast and cheap method over large areas, and its use enabled the first ever resistivity maps of the graben. However, there are significant issues with this electrode arrangement: VES surveys are particularly susceptible to noise due to surface heterogeneities, and collinear soundings are unsuitable for 2D and 3D inversions, as can be seen from the EarthImager results.

Though the data were noisy, the VES surveys was successful in showing the general ground structure of the graben, including the varying depth to bedrock and the common existence of aquifers at 50 to 300 m depth. With VES method, more precise results can be obtained by using supportive data such as borehole temperatures and lithologies and geochemical data.

References

Advanced Geosciences Inc. (AGI). (2009). *Instruction manual for EarthImager 1D*. Austin, TX.

Afşin, M. (1997). Hydrochemical evolution and water quality along the groundwater flow path in the Sandıklı plain, Afyon, Turkey. *Environmental Geology*, *31*, 221-230. https://doi.org/10.1007/s002540050183

Afşin, M., Dağ, T., Davraz, A., Aksever, F., & Karakaş, Z. (2012, September). *The origin and sustainability of Hudai geothermal waters, Sandikli, Afyonkarahisar, Turkey* [Conference session]. 39th IAH (International Association of Hydrogeologists) Congress, Toronto, Canada.

Akin, U., Ulugergerli, E. U., & Kutlu, S. (2014). The assessment of geothermal potential of Turkey by means of heat flow estimation. *Bulletin Of The Mineral Research and Exploration*, *149*(149), 201-210. https://dergipark.org.tr/en/download/article-file/44040

Aksoy, N. (2014). Power generation from geothermal resources in Turkey. *Renewable Energy*, *68*, 595-601. https://doi.org/10.1016/j.renene.2014.02.049

Alali, A., & Morgan, F. (2017). Novel approach for 1D resistivity inversion using the systematically determined optimum number of layers. *SEG Technical Program Expanded Abstracts 2017*. https://doi.org/10.1190/segam2017-17783083.1

Barbier, E. (2002). Geothermal energy technology and current status: An overview. *Renewable and Sustainable Energy Reviews*, *6*(1-2), 3-65. https://doi.org/10.1016/s1364-0321(02)00002-3

Barker, R. D. (1979). Signal contribution sections and their use in resistivity studies. *Geophysical Journal International, 59*(1), 123-129. https://doi.org/10.1111/j.1365-246x.1979.tb02555.x

Başaran, C., Yıldız, A., Ulutürk, Y., & Bağcı, M. (2015). Hydrogeochemical properties of geothermal fluids in Afyon-Akşehir graben (Akarcay basin) and the sustainability of Ömer-Gecek area. *Proceedings World Geothermal Congress 2015*, 19-25. https://pangea.stanford.edu/ERE/db/WGC/papers/WGC/2015/15021.pdf

Başokur, A. T. (1990). Microcomputer program for the direct interpretation of resistivity sounding data. *Computers & Geosciences, 16*(4), 587-601. https://doi.org/10.1016/0098-3004(90)90016-m

Blackwell, D., Brott, C., Goforth, T., Holdaway, M., Morgan, P., Friedline, R., & Smith, R. (1974). Marysville, Montana, geothermal project: Geological and geophysical exploration at Marysville geothermal area: 1973 results (with a section on "contemporary seismicity in the Helena, Montana region"). https://doi.org/10.2172/7333082

Caglar, I., Tuncer, V., Kaypak, B., & Avsar, U. (2005). A high conductive zone associated with a possible geothermal activity around Afyon, northern part of Tauride zone, Southwest Anatolia. *Proceedings World Geothermal Congress 2005*, 24-29. https://www.geothermal-energy.org/pdf/IGAstandard/WGC/2005/0763.pdf

Combs, J. (1978). Geothermal exploration techniques: A case study. Final report. [Coso geothermal area]. https://doi.org/10.2172/5131609

Davraz, A., Afsin, M., Aksever, F., Karakaş, Z., & Ali Hınıs, M. (2016). The interference of a deep thermal system with a shallow aquifer and health risk assessment: The case of Sandıklı (Afyonkarahisar) basin, Turkey. *Environmental Earth Sciences*, *75*, 1-20. https://doi.org/10.1007/s12665-015-5144-6

Demer, S., Memiş, Ü., & Özgür, N. (2013). Investigation of hydrogeochemical properties of the Hüdai (afyon-sandıklı) geothermal systems, SW Turkey.

Journal of Earth System Science, *122*(4), 1081-1089. https://doi.org/10.1007/s12040-013-0328-5

Dickson, M. H., & Fanelli, M. (1994). Small geothermal resources: A review. *Energy Sources*, *16*(3), 349-376. https://doi.org/10.1080/00908319408909083

Ellis, R. G., & Oldenburg, D. W. (1994). Applied geophysical inversion. *Geophysical Journal International, 116*(1), 5-11. https://doi.org/10.1111/j.1365-246x.1994.tb02122.x

El-Qady, G. (2006). Exploration of a geothermal reservoir using geoelectrical resistivity inversion: Case study at hammam Mousa, Sinai, Egypt. *Journal of Geophysics and Engineering*, *3*(2), 114-121. https://doi.org/10.1088/1742-2132/3/2/002

Energy Information Administration (EIA). (2022). *Where geothermal energy is found*. https://www.eia.gov/energyexplained/geothermal/where-geothermal-energy-is-found.php

Fraser, T., Colpron, M., & Relf, C. (2019). Evaluating geothermal potential in Yukon through temperature gradient drilling. Yukon Exploration and Geology 2018, 75-90. https://www.cangea.ca/uploads/3/0/9/7/30973335/5_fraser_etal.pdf

Fridleifsson, I. B. (2001). Geothermal energy for the benefit of the people. *Renewable and Sustainable Energy Reviews*, *5*(3), 299-312. https://doi.org/10.1016/s1364-0321(01)00002-8

Göğüş, O. H., Pysklywec, R. N., Şengör, A. M., & Gün, E. (2017). Drip tectonics and the enigmatic uplift of the Central Anatolian Plateau. *Nature Communications*, *8*. https://doi.org/10.1038/s41467-017-01611-3

Government of Canada. (2021, February 11). *Heating and cooling with a heat pump*. https://www.nrcan.gc.ca/energy-efficiency/energy-star-canada/about/energy-

star-announcements/publications/heating-and-cooling-heat-pump/6817#b

Graney, E. (2021, September 29). From Black gold to hot water: Inside Western Canada's geothermal push. *The Globe and Mail*. https://www.theglobeandmail.com/business/article-from-black-gold-to-hot-water-inside-western-canadas-geothermal-push/

Grasby, S. E., Allen, D. M., Bell, S., Chen, Z., Ferguson, G., Jessop, A., Kelman, M., Ko, M., Majorowicz, J., Moore, M., Raymond, J., & Therrien, R. (2012). Geothermal energy resource potential of Canada. https://doi.org/10.4095/291488

Groundwater. (2013, May 21). *No geothermal for Fort Liard*. https://www.groundwatercanada.com/no-geothermal-for-fort-liard-2087/

Güleç, N. (2003). Applications of geothermometry. https://www.geothermal-energy.org/pdf/IGAstandard/ISS/2003Turkey/n_lgun_g.pdf

Gunerhan, G. G., Kocar, G., & Hepbasli, A. (2001). Geothermal energy utilization in Turkey. *International Journal of Energy Research*, *25*(9), 769-784. https://doi.org/10.1002/er.718

Gupta, H. K., & Roy, S. (2006). *Geothermal energy: An alternative resource for the 21st century*. Elsevier.

Hsieh, H., Chen, C., Lin, P., & Yen, H. (2014). Curie point depth from spectral analysis of magnetic data in Taiwan. *Journal of Asian Earth Sciences*, *90*, 26-33. https://doi.org/10.1016/j.jseaes.2014.04.007

Kana, J. D., Djongyang, N., Raïdandi, D., Njandjock Nouck, P., Nouayou, R., Tabod, T. C., & Sanda, O. (2015). Geophysical investigation of low enthalpy geothermal potential and ground water reservoirs in the sudano-sahelian region of Cameroon. *Journal of African Earth Sciences*, *110*, 81-91.

https://doi.org/10.1016/j.jafrearsci.2015.06.007

Kirsch, R. (2006). *Groundwater geophysics: A tool for hydrogeology*. Springer Science & Business Media.

Koefoed, O. (1979). Resistivity sounding on an earth model containing transition layers with linear change of resistivity with depth*. *Geophysical Prospecting*, *27*(4), 862-868. https://doi.org/10.1111/j.1365-2478.1979.tb01003.x

Kombe, E. Y., & Muguthu, J. (2018). Geothermal energy development in East Africa: Barriers and strategies. *Journal of Energy Research and Reviews*, 1-6. https://doi.org/10.9734/jenrr/2019/v2i129722

Lalonde, M. (2021, July 31). New Meager Creek Development Corporation looks to turn geothermal energy into hydrogen near Pemberton. *Pique Newsmagazine*. https://www.piquenewsmagazine.com/local-news/new-meager-creek development-corporation-looks-to-turn-geothermal-energy-into-hydrogen-near-pemberton-4175591

Legeay, E., Pichat, A., Kergaravat, C., Ribes, C., Callot, J. P., Ringenbach, J. C., Bonnel, C., Hoareau, G., Poisson, A., Mohn, G., Crumeyrolle, P., Kavak, K. S., & Temiz, H. (2019). Geology of the Central Sivas Basin. *Journal of Maps*, *15*(2). https://doi.org/10.1080/17445647.2018.1514539

Lindal, B. (1992). Review of industrial applications of geothermal energy and future considerations. *Geothermics*, *21*(5-6), 591-604. https://doi.org/10.1016/0375-6505(92)90012-x

Lines, L., & Treitel, S. (1984). A review of least-squares inversion and its application to geophysical problems*. *Geophysical Prospecting, 32*(2), 159-186. https://doi.org/10.1111/j.1365-2478.1984.tb00726.x

Loke, M.H. (1996). 2-D and 3-D electrical imaging surveys: *Tutorial*.

Loke, M.H. (2003). RES2DINV-Rapid 2D Resistivity and IP inversion using the least-squares method. *Geotomo Software Manual,* Malaysia.

Lund, J. W., & Boyd, T. L. (2016). Direct utilization of geothermal energy 2015 worldwide review. *Geothermics*, *60*, 66-93. https://doi.org/10.1016/j.geothermics.2015.11.004

Maden, N., Afşin, M., Aksever, F., & Davraz, A. (2020). Geothermal potential and circulation depth of Hüdai thermal springs (Sandıklı-Afyonkarahisar, Türkiye) using magnetic, geothermometry and heat flow data. *Springer Geophysics*, 335-362. https://doi.org/10.1007/978-3-030-28909-6_12

Majorowicz, J., & Grasby, S. E. (2021). Deep geothermal heating potential for the communities of the western Canadian sedimentary basin. *Energies*, *14*(3), 706. https://doi.org/10.3390/en14030706

McNeill, J. D. (1980). *Electrical conductivity of soils and rocks*. Geonics Limited. http://www.geonics.com/pdfs/technicalnotes/tn5.pdf

Meju, M. A. (2002). Geoelectromagnetic exploration for natural resources: Models, case studies and challenges. *Surveys in Geophysics*, *23*, 133-206. https://doi.org/10.1023/a:1015052419222

Memiş, Ü., Demer, S., & Özgür, N. (2010). Investigation of reservoir temperature of the Afyon-Sandikli Hüdai geothermal system. *Journal of Natural and Applied Sciences*, *14*(3), 293-299.

Mertoglu, O., Sakir, S., & Basarir, N. (2015). Geothermal country update report of Turkey (2010-2015). *Proceedings World Geothermal Congress 2015*, 19-25. https://pangea.stanford.edu/ERE/db/WGC/papers/WGC/2015/01046.pdf

Mertoglu, O., Simsek, S., Basarir, N., & Paksoy, H. (2019). Geothermal energy use, country

update for Turkey. *European Geothermal Congress 2019*. https://europeangeothermalcongress.eu/wp-content/uploads/2019/07/CUR-30-Turkey.pdf

Mikhaylov, A. (2020). Geothermal energy development in Iceland. *International Journal of Energy Economics and Policy*, *10*(4), 31-35. https://doi.org/10.32479/ijeep.9047

Muffler, L. J. (1979). Assessment of geothermal resources of the United States: 1978. *Circular*. https://doi.org/10.3133/cir790

Natural Resources Canada. (2018, September 25). Canada's geothermal village – "Sustainaville" GeoPark. Retrieved from https://www.nrcan.gc.ca/science-and-data/funding-partnerships/funding-opportunities/current-investments/canadas-geothermal-village-sustainaville-geopark/20923

Nesbitt, B. E. (1993). Electrical resistivities of crustal fluids. *Journal of Geophysical Research: Solid Earth*, *98*(B3), 4301-4310. https://doi.org/10.1029/92jb02576

Oldenburg, D. W., & Li, Y. (2005). 5. Inversion for applied geophysics: A tutorial. *Near-Surface Geophysics*, 89-150. https://doi.org/10.1190/1.9781560801719.ch5

Palacky, G. J. (1988). 3. Resistivity characteristics of geologic targets. *Electromagnetic Methods in Applied Geophysics, 1*, 52-129. https://doi.org/10.1190/1.9781560802631.ch3

Reynolds, J. M. (2011). *An introduction to applied and environmental geophysics* (2nd ed.). John Wiley & Sons. https://www.geokniga.org/bookfiles/geokniga-introduction-applied-and-environmental-geophysics_1.pdf

Richter, A., Ko, M., & Thompson, A. (2012). Geothermal energy development in Canada - Country update 2012. *GRC Transactions*, *36,* 757-760. https://publications.mygeoenergynow.org/grc/1030313.pdf

Thanassoulas, C., Tselentis, G., & Kolios, N. (1987). Geothermal prospecting by

geoelectric soundings in NE Greece*. *Geophysical Prospecting*, *35*(1), 83-97. https://doi.org/10.1111/j.1365-2478.1987.tb00804.x

ThinkGeoEnergy. (2021, September 5). Construction started on geothermal project at swan hills, Alberta. Retrieved from https://www.thinkgeoenergy.com/construction-started-on-geothermal-project-at-swan-hills-alberta

Topographic map of Turkey. (2005, June 30). In *Wikipedia*. Retrieved March 10, 2020, from https://en.wikipedia.org/wiki/Geography_of_Turkey#/media/File:Turkey_top.jpg

Üner, S., Ağaçgözgü, G. Ö., & Düşünür Doğan, D. (2019). Hydrogeophysical modelling of Hisarcik (Kütahya) geothermal field, western Turkey. *Geophysical Prospecting*, *67*(8), 2176-2195. https://doi.org/10.1111/1365-2478.12826

Unsworth, M. (2009, January). *Depth-sounding with DC resistivity* [PDF]. University of Alberta. https://sites.ualberta.ca/~unsworth/UA-classes/223/notes223/223B3-2009.pdf

Unsworth, M., & Rondenay, S. (2012). Mapping the distribution of fluids in the crust and lithospheric mantle utilizing geophysical methods. *Lecture Notes in Earth System Sciences*, 535-598. https://doi.org/10.1007/978-3-642-28394-9_13

Ussher, G., Harvey, C., Johnstone, R., & Anderson, E. (2000). Understanding the resistivities observed in geothermal systems. *Proceedings World Geothermal Congress 2000*, 1915-1920. https://www.geothermal energy.org/pdf/IGAstandard/WGC/2000/R0279.PDF

Van Nostrand, R. G., & Cook, K. L. (1966). Interpretation of resistivity data. *Professional Paper*. https://doi.org/10.3133/pp499

What is Ohms Law – formula, equation & triangle. (2008, April 6). Electronics-notes. https://www.electronics-notes.com/articles/basic_concepts/resistance/what-is-

ohms-law-formula-equation.php

Wightman, W. E., Jalinoos, F., Sirles, P., & Hanna, K. (2004). *Application of geophysical methods to highway related problems*. http://www.ce.memphis.edu/7137/PDFs/Geophysical/geotechPdf.pdf

Williams, P. L., Mabey, D. R., Zohdy, A. A. R., Ackermann, H. D., Hoover, D. B., Pierce, K. L., & Oriel, S. S. (1975). Geology and geophysics of the southern raft river Valley geothermal area, Idaho, U.S.A. *Open-File Report*. https://doi.org/10.3133/ofr75322

Wright, P. M., Ward, S. H., Ross, H. P., & West, R. C. (1985). State-of-the-art geophysical exploration for geothermal resources. *GEOPHYSICS*, *50*(12), 2666-2696. https://doi.org/10.1190/1.1441889

Zohdy, A. A. R. (1968). An evaluation of some geophysical methods for water exploration in the Piedmont area by T. J. Joiner, J. C. Warman, and W. L. Scarbrough January-February, 1968. *Groundwater, 6*(4), 38-39. https://doi.org/10.1111/j.1745-6584.1968.tb01655.x

Zohdy, A. A. R. (1989). A new method for the automatic interpretation of Schlumberger and Wenner sounding curves. *GEOPHYSICS, 54*(2), 245-253. https://doi.org/10.1190/1.1442648

Zohdy, A. A. R., Anderson, L. A., & Muffler, L. J. (1973). Resistivity, self-potential, and induced-polarization surveys of a vapor-dominated geothermal system. *GEOPHYSICS*, *38*(6), 1130-1144. https://doi.org/10.1190/1.1440400

ZZ Resistivity Imaging Pty. Ltd. (2020, May 28). *Full-Channel Resistivity/IP*. https://www.zzgeo.com/index.php?p=news_show&id=96&c_id=5&lanmu=2

Appendix A: Google Earth Images of Survey Areas

Area 1: Group 17
Google Earth
2 km
N

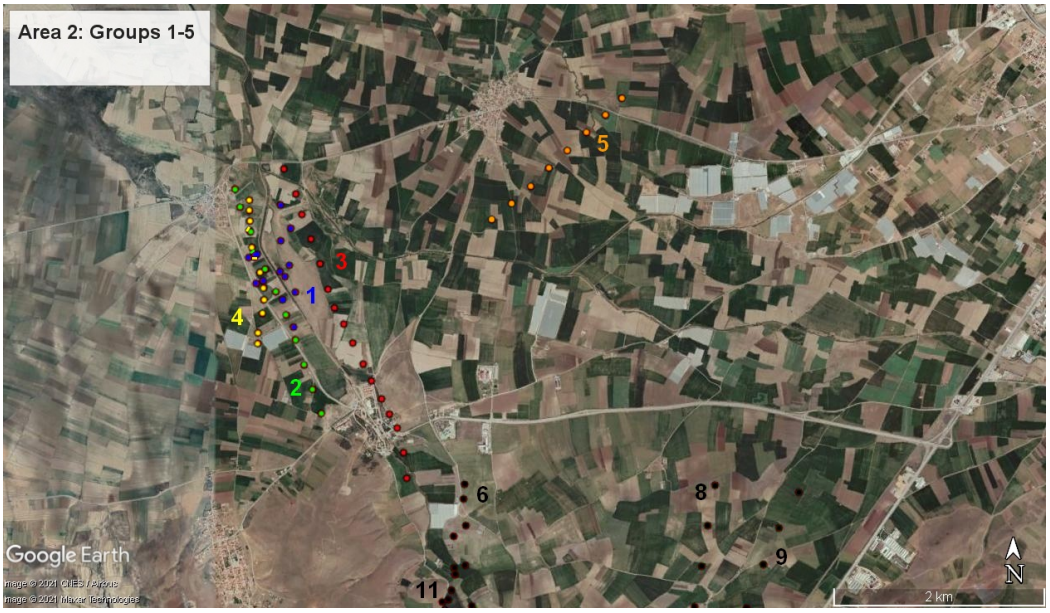
Area 2: Groups 1-5
5
3
1
4
2
6
8
9
11
Google Earth
2 km
N

Area 3: Groups 12,13
12
13
8
9
Google Earth
4 km
N

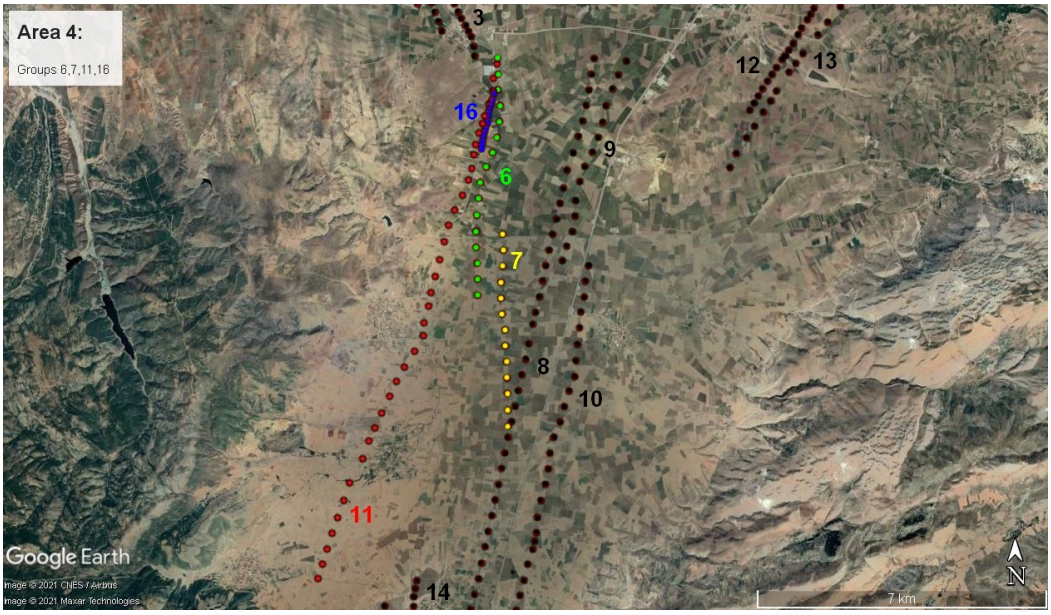
Area 4:
Groups 6,7,11,16
3
12
13
16
9
6
7
8
10
11
14
Google Earth
7 km
N

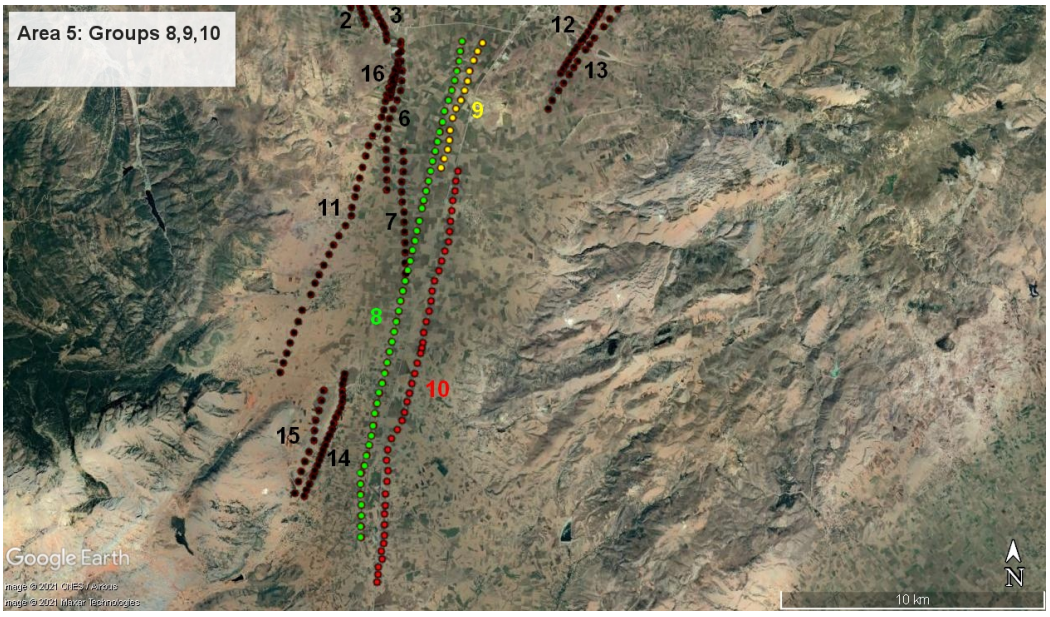
Area 5: Groups 8,9,10
2
3
12
16
13
9
6
11
7
8
10
15
14
Google Earth
10 km
N

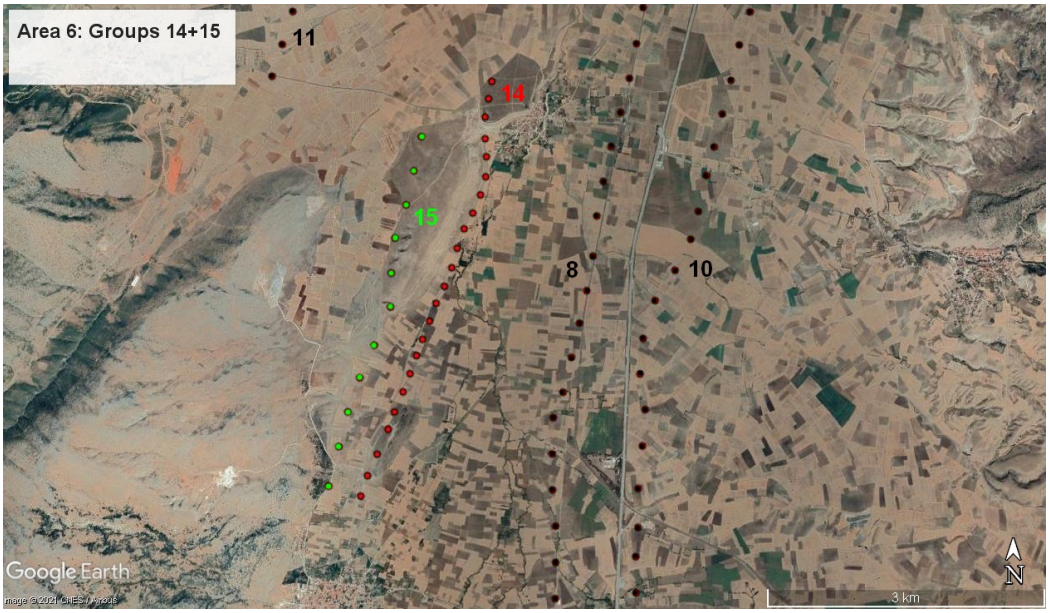
Area 6: Groups 14+15
11
14
15
8
10
Google Earth
3 km
N

Appendix B: Sounding Locations and Acquisition Dates

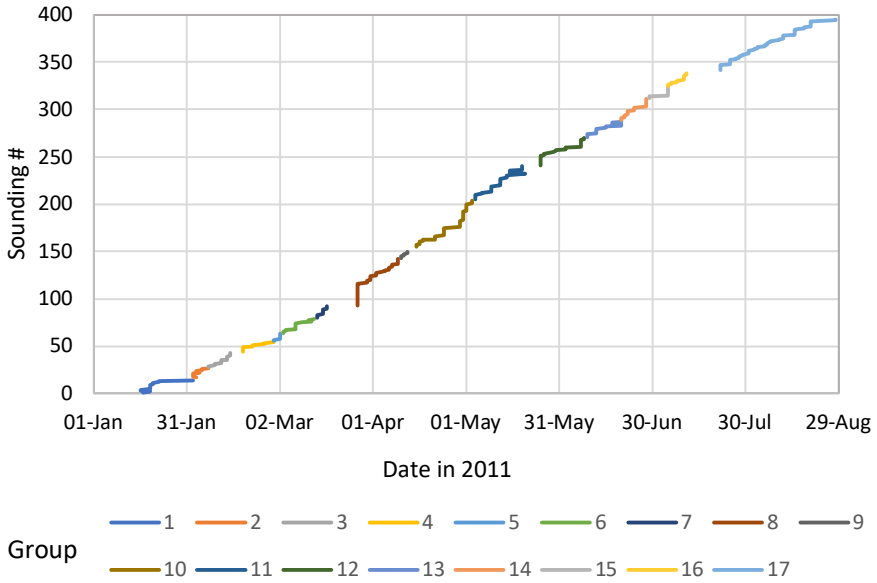

Figure B.1 Graph of illustrating the acquisition dates of the 384 resistivity soundings, arranged by Group number. Data provided in Table B.1 below.

Table B.1 Acquisition date (in 2011), locations (UTM zone 36 S), spacings between successive soundings in each group, and Group number for the vertical electric soundings in this study.

Sounding #	Date	Easting	Northing	spacing (m)	Range	Group
1	17-Jan	253317	4259060		s1-s14	1
2	19-Jan	253054	4259285	346	s1-s14	1
3	16-Jan	253036	4259003	283	s1-s14	1
4	16-Jan	252972	4259255	260	s1-s14	1
5	19-Jan	253287	4258838	523	s1-s14	1
6	19-Jan	253270	4259109	272	s1-s14	1
7	19-Jan	253414	4258907	248	s1-s14	1
8	19-Jan	253286	4259409	518	s1-s14	1
9	19-Jan	253363	4259168	253	s1-s14	1
10	20-Jan	253388	4259527	360	s1-s14	1
11	20-Jan	253293	4259756	248	s1-s14	1
12	22-Jan	253103	4259026	754	s1-s14	1
13	22-Jan	253031	4259273	257	s1-s14	1
14	2-Feb	253385	4258570	787	s1-s14	1
17	3-Feb	252856	4259923		s17-s27	2
18	2-Feb	252902	4259745	184	s17-s27	2
19	2-Feb	252987	4259518	242	s17-s27	2
20	2-Feb	253026	4259283	238	s17-s27	2
21	2-Feb	253128	4259138	177	s17-s27	2
22	4-Feb	253225	4258916	242	s17-s27	2
Sounding #	**Date**	**Easting**	**Northing**	**spacing (m)**	**Range**	**Group**
23	3-Feb	253320	4258688	247	s17-s27	2
24	3-Feb	253400	4258446	255	s17-s27	2

25	5-Feb	253477	4258200	258	s17-s27	2
26	5-Feb	253556	4257962	251	s17-s27	2
27	7-Feb	253630	4257726	247	s17-s27	2
28	7-Feb	253337	4260103		s28-s43	3
29	7-Feb	253446	4259857	269	s28-s43	3
30	9-Feb	253499	4259657	207	s28-s43	3
31	9-Feb	253580	4259416	254	s28-s43	3
32	11-Feb	253662	4259174	256	s28-s43	3
33	11-Feb	253732	4258925	259	s28-s43	3
34	11-Feb	253788	4258744	189	s28-s43	3
35	11-Feb	253875	4258584	182	s28-s43	3
36	13-Feb	253957	4258398	203	s28-s43	3
37	13-Feb	254051	4258192	226	s28-s43	3
38	13-Feb	254127	4258027	182	s28-s43	3
39	13-Feb	254221	4257850	200	s28-s43	3
40	14-Feb	254294	4257701	166	s28-s43	3
41	14-Feb	254364	4257565	153	s28-s43	3
42	14-Feb	254417	4257325	246	s28-s43	3
43	14-Feb	254441	4257076	250	s28-s43	3
44	18-Feb	252995	4259810		s44-s55	4
45	18-Feb	252993	4259710	100	s44-s55	4
46	18-Feb	252993	4259608	102	s44-s55	4
47	18-Feb	252994	4259504	104	s44-s55	4
48	18-Feb	253006	4259354	150	s44-s55	4
49	18-Feb	253028	4259257	99	s44-s55	4
50	21-Feb	253074	4259108	156	s44-s55	4
51	21-Feb	253107	4258960	152	s44-s55	4
52	25-Feb	253105	4258842	118	s44-s55	4
53	25-Feb	253089	4258708	135	s44-s55	4
54	28-Feb	253041	4258525	189	s44-s55	4
55	28-Feb	253038	4258423	102	s44-s55	4
56	28-Feb	256636	4260685		s56-s63	5
57	28-Feb	256474	4260526	227	s56-s63	5
58	2-Mar	256286	4260363	249	s56-s63	5
59	2-Mar	256094	4260195	255	s56-s63	5
60	2-Mar	255910	4260032	246	s56-s63	5
61	2-Mar	255730	4259858	250	s56-s63	5
62	2-Mar	255537	4259702	248	s56-s63	5
63	2-Mar	255342	4259551	247	s56-s63	5
64	3-Mar	255000	4257000		s64-s79	6
Sounding #	**Date**	**Easting**	**Northing**	**spacing (m)**	**Range**	**Group**
65	3-Mar	255002	4256603	397	s64-s79	6
66	4-Mar	254986	4256217	386	s64-s79	6
67	4-Mar	255034	4255821	399	s64-s79	6
68	7-Mar	255004	4255421	401	s64-s79	6
69	7-Mar	254940	4255027	399	s64-s79	6

70	7-Mar	254798	4254654	399	s64-s79	6
71	7-Mar	254639	4254290	397	s64-s79	6
72	7-Mar	254487	4253921	399	s64-s79	6
73	7-Mar	254426	4253520	406	s64-s79	6
74	7-Mar	254362	4253094	431	s64-s79	6
75	9-Mar	254333	4252697	398	s64-s79	6
76	12-Mar	254324	4252298	399	s64-s79	6
77		254338	4251898	400	s64-s79	6
78	11-Mar	254340	4251500	398	s64-s79	6
79	13-Mar	254329	4251100	400	s64-s79	6
80	14-Mar	255000	4252600		s80-s92	7
81	14-Mar	255006	4252202	398	s80-s92	7
82	14-Mar	254983	4251802	401	s80-s92	7
83	14-Mar	254920	4251406	401	s80-s92	7
84	16-Mar	254908	4251008	398	s80-s92	7
85	16-Mar	254926	4250610	398	s80-s92	7
86	16-Mar	254990	4250217	398	s80-s92	7
87		254981	4249819	398	s80-s92	7
88	16-Mar	254994	4249420	399	s80-s92	7
89	16-Mar	254998	4249014	406	s80-s92	7
90	17-Mar	255000	4248624	390	s80-s92	7
91	17-Mar	255001	4248211	413	s80-s92	7
92	17-Mar	254996	4247812	399	s80-s92	7
93	27-Mar	257425	4256922		s93-s142	8
94	27-Mar	257343	4256534	397	s93-s142	8
95	27-Mar	257273	4256141	399	s93-s142	8
96	27-Mar	257193	4255753	396	s93-s142	8
97	27-Mar	257098	4255366	398	s93-s142	8
98	27-Mar	256971	4254989	398	s93-s142	8
99	27-Mar	256825	4254584	431	s93-s142	8
100	27-Mar	256668	4254155	457	s93-s142	8
101	27-Mar	256565	4253715	452	s93-s142	8
102	27-Mar	256461	4253331	398	s93-s142	8
103	27-Mar	256356	4252943	402	s93-s142	8
104	27-Mar	256257	4252559	397	s93-s142	8
105	27-Mar	256152	4252171	402	s93-s142	8
106	27-Mar	256053	4251793	391	s93-s142	8
Sounding #	**Date**	**Easting**	**Northing**	**spacing (m)**	**Range**	**Group**
107	27-Mar	255960	4251406	398	s93-s142	8
108	27-Mar	255870	4251013	403	s93-s142	8
109	27-Mar	255765	4250630	397	s93-s142	8
110	27-Mar	255692	4250332	307	s93-s142	8
111	27-Mar	255573	4249853	494	s93-s142	8
112	27-Mar	255479	4249462	402	s93-s142	8
113	27-Mar	255379	4249079	396	s93-s142	8
114	27-Mar	255278	4248691	401	s93-s142	8

115	27-Mar	255183	4248303	399	s93-s142	8
116	27-Mar	255082	4247920	396	s93-s142	8
117	30-Mar	254982	4247530	403	s93-s142	8
118	30-Mar	254886	4247144	398	s93-s142	8
119	30-Mar	254790	4246758	398	s93-s142	8
120	31-Mar	254708	4246366	400	s93-s142	8
121	31-Mar	254610	4245977	401	s93-s142	8
122	31-Mar	254518	4245589	399	s93-s142	8
123	31-Mar	254419	4245202	399	s93-s142	8
124	31-Mar	254318	4244819	396	s93-s142	8
125	2-Apr	254230	4244411	417	s93-s142	8
126	2-Apr	254136	4244024	398	s93-s142	8
127	2-Apr	254027	4243642	397	s93-s142	8
128	3-Apr	253906	4243263	398	s93-s142	8
129	5-Apr	253805	4242873	403	s93-s142	8
130	5-Apr	253720	4242490	392	s93-s142	8
131	6-Apr	253662	4242043	451	s93-s142	8
132	6-Apr	253579	4241660	392	s93-s142	8
133	6-Apr	253487	4241302	370	s93-s142	8
134	7-Apr	253385	4240925	391	s93-s142	8
135	7-Apr	253279	4240542	397	s93-s142	8
136	7-Apr	253161	4240266	300	s93-s142	8
137	9-Apr	253136	4239865	402	s93-s142	8
138	9-Apr	253130	4239470	395	s93-s142	8
139	9-Apr	253151	4239071	400	s93-s142	8
140	9-Apr	253138	4238674	397	s93-s142	8
141	9-Apr	253121	4238280	394	s93-s142	8
142	9-Apr	253128	4237880	400	s93-s142	8
143	10-Apr	258230	4256830		s143-s150	9
144	10-Apr	258028	4256493	393	s143-s150	9
145	10-Apr	257867	4256145	383	s143-s150	9
146	11-Apr	257691	4255727	454	s143-s150	9
147	11-Apr	257595	4255321	417	s143-s150	9
148	12-Apr	257472	4254949	392	s143-s150	9
Sounding #	**Date**	**Easting**	**Northing**	**spacing (m)**	**Range**	**Group**
149	12-Apr	257311	4254579	404	s143-s150	9
150	12-Apr	257112	4254239	394	s143-s150	9
155	15-Apr	256976	4253860		s155-s204	10
156	15-Apr	256853	4253382	494	s155-s204	10
157	15-Apr	256827	4252999	384	s155-s204	10
158	16-Apr	256750	4252616	391	s155-s204	10
159	16-Apr	256593	4252253	395	s155-s204	10
160	16-Apr	256475	4251897	375	s155-s204	10
161	17-Apr	257127	4251748	669	s155-s204	10
162	17-Apr	257035	4251365	394	s155-s204	10
163	21-Apr	256997	4250976	391	s155-s204	10

164	21-Apr	256901	4250601	387	s155-s204	10
165	21-Apr	256852	4250208	396	s155-s204	10
166	21-Apr	256789	4249795	418	s155-s204	10
167	24-Apr	256745	4249394	403	s155-s204	10
168	24-Apr	256698	4248995	402	s155-s204	10
169	24-Apr	256546	4248638	388	s155-s204	10
170	24-Apr	256413	4248259	402	s155-s204	10
171	24-Apr	256301	4247878	397	s155-s204	10
172	24-Apr	256118	4247495	424	s155-s204	10
173	24-Apr	256016	4247108	400	s155-s204	10
174	24-Apr	255964	4246724	388	s155-s204	10
175	24-Apr	255883	4246333	399	s155-s204	10
176	29-Apr	255764	4245933	417	s155-s204	10
177	29-Apr	255656	4245517	430	s155-s204	10
178	29-Apr	255620	4245130	389	s155-s204	10
179	29-Apr	255570	4244926	210	s155-s204	10
180	29-Apr	255520	4244728	204	s155-s204	10
181	29-Apr	255382	4244356	397	s155-s204	10
182	29-Apr	255277	4243961	409	s155-s204	10
183	30-Apr	255164	4243587	391	s155-s204	10
184	30-Apr	255061	4243220	381	s155-s204	10
185	30-Apr	254963	4242903	332	s155-s204	10
186	30-Apr	254856	4242504	413	s155-s204	10
187	30-Apr	254758	4242195	324	s155-s204	10
188	30-Apr	254572	4241856	387	s155-s204	10
189	30-Apr	254339	4241527	403	s155-s204	10
190	30-Apr	254190	4241110	443	s155-s204	10
191	30-Apr	254141	4240719	394	s155-s204	10
192	30-Apr	254186	4240324	398	s155-s204	10
193	1-May	254142	4239927	399	s155-s204	10
194	1-May	254077	4239463	469	s155-s204	10
Sounding #	**Date**	**Easting**	**Northing**	**spacing (m)**	**Range**	**Group**
195	1-May	254063	4239032	431	s155-s204	10
196	1-May	254025	4238715	319	s155-s204	10
197	1-May	254017	4238317	398	s155-s204	10
198	1-May	254008	4237924	393	s155-s204	10
199	1-May	253979	4237627	298	s155-s204	10
200	1-May	253881	4237346	298	s155-s204	10
201	3-May	253913	4237056	292	s155-s204	10
202	3-May	253763	4236765	327	s155-s204	10
203	3-May	253746	4236492	274	s155-s204	10
204	3-May	253703	4236215	280	s155-s204	10
205	4-May	250120	4244160		s205-s240	11
206	4-May	250241	4244517	377	s205-s240	11
207	4-May	250368	4244885	389	s205-s240	11
208	4-May	250503	4245277	415	s205-s240	11

209	4-May	250653	4245661	412	s205-s240	11
210	4-May	250821	4246085	456	s205-s240	11
211	6-May	250979	4246518	461	s205-s240	11
212	6-May	251324	4247109	684	s205-s240	11
213	9-May	251490	4247547	468	s205-s240	11
214	9-May	251651	4247867	358	s205-s240	11
215	9-May	251831	4248232	407	s205-s240	11
216	9-May	252047	4248645	466	s205-s240	11
217	9-May	252226	4249011	407	s205-s240	11
218	9-May	252434	4249361	407	s205-s240	11
219	9-May	252702	4249750	472	s205-s240	11
220	12-May	252933	4250131	446	s205-s240	11
221	12-May	252958	4250452	322	s205-s240	11
222	12-May	253087	4250863	431	s205-s240	11
223	12-May	253156	4251201	345	s205-s240	11
224	12-May	253276	4251598	415	s205-s240	11
225	12-May	253399	4252017	437	s205-s240	11
226	12-May	253530	4252460	462	s205-s240	11
227	12-May	253649	4252871	428	s205-s240	11
228	14-May	253815	4253239	404	s205-s240	11
229	14-May	254025	4253603	420	s205-s240	11
230	14-May	254183	4253979	408	s205-s240	11
231	15-May	254275	4254265	300	s205-s240	11
232	20-May	254340	4254610	351	s205-s240	11
233	15-May	254390	4254862	257	s205-s240	11
234	15-May	254480	4255149	301	s205-s240	11
235	15-May	254580	4255382	254	s205-s240	11
236	19-May	254637	4255574	200	s205-s240	11
Sounding #	**Date**	**Easting**	**Northing**	**spacing (m)**	**Range**	**Group**
237	19-May	254751	4255870	317	s205-s240	11
238	19-May	254874	4256195	347	s205-s240	11
239	19-May	254881	4256504	309	s205-s240	11
240	19-May	254986	4256859	370	s205-s240	11
241	25-May	261271	4255493		s241-s270	12
242	25-May	261386	4255665	207	s241-s270	12
243	25-May	261489	4255837	200	s241-s270	12
244	25-May	261602	4256007	204	s241-s270	12
245	25-May	261732	4256198	231	s241-s270	12
246	25-May	261852	4256365	206	s241-s270	12
247	25-May	261968	4256530	202	s241-s270	12
248	25-May	262116	4256731	250	s241-s270	12
249	25-May	262200	4256828	128	s241-s270	12
250	25-May	262292	4256961	162	s241-s270	12
251	25-May	262413	4257126	205	s241-s270	12
252	26-May	262546	4257346	257	s241-s270	12
253	26-May	262632	4257503	179	s241-s270	12

254	27-May	262779	4257707	251	s241-s270	12
255	29-May	262871	4257838	160	s241-s270	12
256	30-May	262950	4257982	164	s241-s270	12
257	30-May	263030	4258170	204	s241-s270	12
258	2-Jun	263098	4258341	184	s241-s270	12
259	2-Jun	263231	4258618	307	s241-s270	12
260	2-Jun	263318	4258743	152	s241-s270	12
261	7-Jun	263442	4258928	223	s241-s270	12
262	7-Jun	263563	4259095	206	s241-s270	12
263	7-Jun	263669	4259253	190	s241-s270	12
264	7-Jun	263777	4259430	207	s241-s270	12
265	7-Jun	263981	4259711	347	s241-s270	12
266	7-Jun	264176	4259942	302	s241-s270	12
267	7-Jun	264427	4260196	357	s241-s270	12
268	7-Jun	264697	4260489	398	s241-s270	12
269	8-Jun	264851	4260688	252	s241-s270	12
270	8-Jun	264983	4260857	214	s241-s270	12
271	9-Jun	264649	4259676		s271-s288	13
272	9-Jun	264426	4259340	403	s271-s288	13
273	9-Jun	264315	4259070	292	s271-s288	13
274	9-Jun	264093	4258710	423	s271-s288	13
275	12-Jun	263779	4258249	558	s271-s288	13
276	12-Jun	263607	4257997	305	s271-s288	13
277	12-Jun	263285	4257626	491	s271-s288	13
278	12-Jun	263034	4257318	397	s271-s288	13
Sounding #	**Date**	**Easting**	**Northing**	**spacing (m)**	**Range**	**Group**
279	12-Jun	262641	4256866	599	s271-s288	13
280	12-Jun	262456	4256624	305	s271-s288	13
281	15-Jun	262281	4256407	279	s271-s288	13
282	15-Jun	261946	4255947	569	s271-s288	13
283	20-Jun	261793	4255704	287	s271-s288	13
284	20-Jun	261604	4255434	330	s271-s288	13
285	17-Jun	261373	4255088	416	s271-s288	13
286	17-Jun	261161	4254808	351	s271-s288	13
287	20-Jun	260895	4254422	469	s271-s288	13
288	20-Jun	260737	4254081	376	s271-s288	13
289	20-Jun	251000	4239470		s289-s311	14
290	20-Jun	251081	4239693	237	s289-s311	14
291	20-Jun	251195	4239924	258	s289-s311	14
292	21-Jun	251322	4240194	298	s289-s311	14
293	21-Jun	251396	4240382	202	s289-s311	14
294	21-Jun	251497	4240600	240	s289-s311	14
295	22-Jun	251580	4240799	216	s289-s311	14
296	22-Jun	251657	4240996	212	s289-s311	14
297	22-Jun	251728	4241175	193	s289-s311	14
298	22-Jun	251812	4241374	216	s289-s311	14

299	24-Jun	251891	4241570	211	s289-s311	14
300	24-Jun	251989	4241756	210	s289-s311	14
301	24-Jun	252077	4241961	223	s289-s311	14
302	24-Jun	252144	4242176	225	s289-s311	14
303	28-Jun	252228	4242390	230	s289-s311	14
304	28-Jun	252330	4242563	201	s289-s311	14
305	28-Jun	252422	4242764	221	s289-s311	14
306	28-Jun	252487	4242964	210	s289-s311	14
307	28-Jun	252501	4243189	225	s289-s311	14
308	28-Jun	252493	4243391	202	s289-s311	14
309	28-Jun	252500	4243631	240	s289-s311	14
310	28-Jun	252545	4243835	209	s289-s311	14
311	28-Jun	252587	4244030	199	s289-s311	14
312	29-Jun	250654	4239596		s312-s324	15
313	29-Jun	250775	4240023	444	s312-s324	15
314	29-Jun	250881	4240400	392	s312-s324	15
315	5-Jul	251022	4240772	398	s312-s324	15
316	5-Jul	251192	4241126	393	s312-s324	15
317	5-Jul	251385	4241544	460	s312-s324	15
318	5-Jul	251409	4241918	375	s312-s324	15
319	5-Jul	251459	4242304	389	s312-s324	15
320	5-Jul	251592	4242669	388	s312-s324	15
Sounding #	**Date**	**Easting**	**Northing**	**spacing (m)**	**Range**	**Group**
321	5-Jul	251687	4243049	392	s312-s324	15
322	5-Jul	251778	4243431	393	s312-s324	15
324	5-Jul	251779	4243431	1	s312-s324	15
325	5-Jul	254528	4254755		s325-s338	16
326	5-Jul	254572	4254955	205	s325-s338	16
327	6-Jul	254549	4254856	102	s325-s338	16
328	6-Jul	254595	4255068	217	s325-s338	16
329	8-Jul	254617	4255177	111	s325-s338	16
330	8-Jul	254651	4255275	104	s325-s338	16
331	10-Jul	254697	4255381	116	s325-s338	16
332	10-Jul	254700	4255486	105	s325-s338	16
333	10-Jul	254718	4255584	100	s325-s338	16
334	10-Jul	254744	4255697	116	s325-s338	16
335	10-Jul	254771	4255791	98	s325-s338	16
336	10-Jul	254809	4255889	105	s325-s338	16
337	11-Jul	254842	4255981	98	s325-s338	16
338	11-Jul	254880	4256129	153	s325-s338	16
342	22-Jul	254053	4265029		s342-s395	17
343	22-Jul	253915	4265892	874	s342-s395	17
344	22-Jul	259000	4269000	5960	s342-s395	17
345	22-Jul	259000	4269508	508	s342-s395	17
346	22-Jul	259000	4270000	492	s342-s395	17
347	22-Jul	258999	4270483	483	s342-s395	17

348	25-Jul	258000	4270000	1110	s342-s395	17
349	25-Jul	258000	4270504	504	s342-s395	17
350	25-Jul	259000	4270000	1120	s342-s395	17
351	25-Jul	258500	4270000	500	s342-s395	17
352	25-Jul	257516	4270006	984	s342-s395	17
353	27-Jul	258500	4269000	1407	s342-s395	17
354	27-Jul	257986	4269000	514	s342-s395	17
355	28-Jul	257000	4270000	1404	s342-s395	17
356	28-Jul	257005	4270518	518	s342-s395	17
357	29-Jul	258000	4270000	1122	s342-s395	17
358	29-Jul	258500	4270500	707	s342-s395	17
359	31-Jul	257719	4267621	2983	s342-s395	17
360	31-Jul	257986	4267224	478	s342-s395	17
361	31-Jul	257518	4267547	569	s342-s395	17
362	31-Jul	257628	4267347	228	s342-s395	17
363	2-Aug	257303	4267958	692	s342-s395	17
364	2-Aug	257392	4267782	197	s342-s395	17
365	3-Aug	257000	4267000	875	s342-s395	17
366	3-Aug	257009	4267598	598	s342-s395	17
Sounding #	**Date**	**Easting**	**Northing**	**spacing (m)**	**Range**	**Group**
367	5-Aug	256000	4267000	1173	s342-s395	17
368	5-Aug	256500	4266991	500	s342-s395	17
369	6-Aug	255000	4267000	1500	s342-s395	17
370	6-Aug	255500	4266994	500	s342-s395	17
371	7-Aug	254000	4267000	1500	s342-s395	17
372	7-Aug	254487	4267004	487	s342-s395	17
373	10-Aug	253500	4267000	987	s342-s395	17
374	10-Aug	253240	4267001	260	s342-s395	17
375	11-Aug	254000	4266000	1257	s342-s395	17
376	11-Aug	254496	4266000	496	s342-s395	17
377	11-Aug	255000	4266000	504	s342-s395	17
378	11-Aug	255500	4266000	500	s342-s395	17
379	15-Aug	255800	4266000	300	s342-s395	17
380	15-Aug	256090	4266003	290	s342-s395	17
381	15-Aug	254000	4268000	2891	s342-s395	17
382	15-Aug	254000	4267503	497	s342-s395	17
383	15-Aug	256000	4268000	2061	s342-s395	17
384	15-Aug	256015	4267630	370	s342-s395	17
385	16-Aug	256000	4268930	1300	s342-s395	17
386	18-Aug	253200	4266600	3643	s342-s395	17
387	18-Aug	253600	4266605	400	s342-s395	17
388	20-Aug	253200	4266600	400	s342-s395	17
389	20-Aug	253600	4266605	400	s342-s395	17
390	20-Aug	255000	4266600	1400	s342-s395	17
391	20-Aug	255500	4266601	500	s342-s395	17
392	20-Aug	254500	4267500	1345	s342-s395	17

393	20-Aug	255005	4267497	505	s342-s395	17
394	28-Aug	255480	4267500	475	s342-s395	17
395	28-Aug	255740	4267500	260	s342-s395	17

Appendix C: Raw Data and Data after Removal of Offsets & Smoothing

RAW DATA

Group 1:

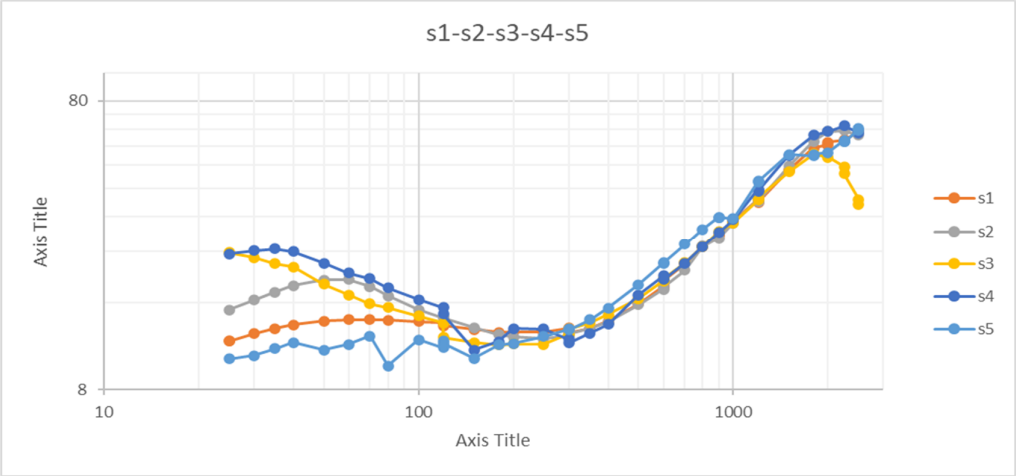

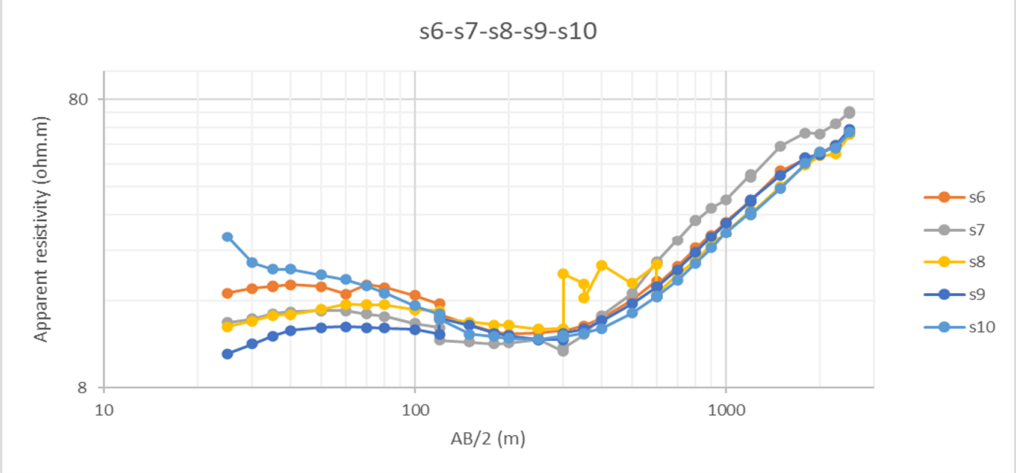

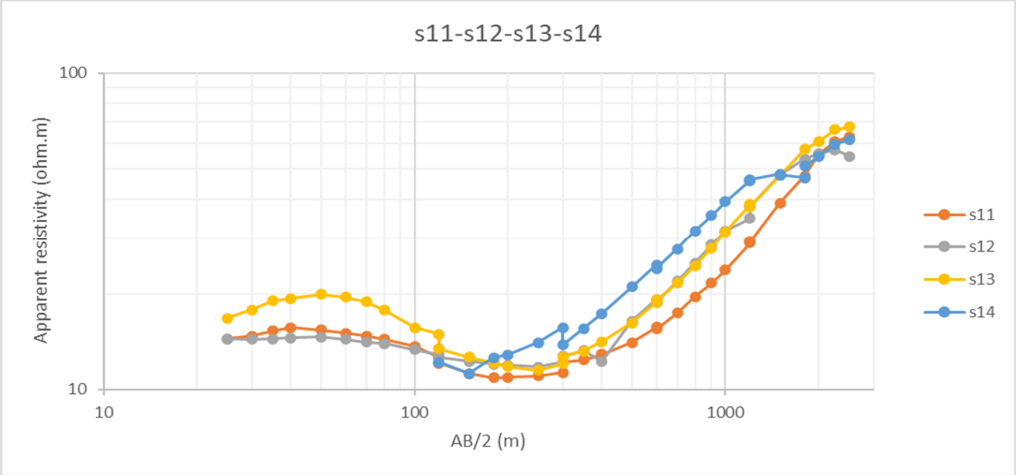

Group 2:

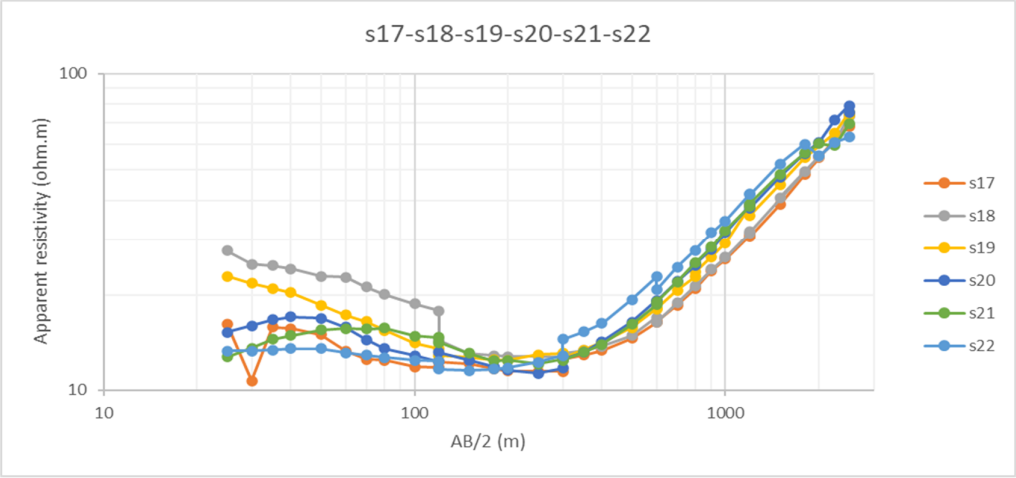

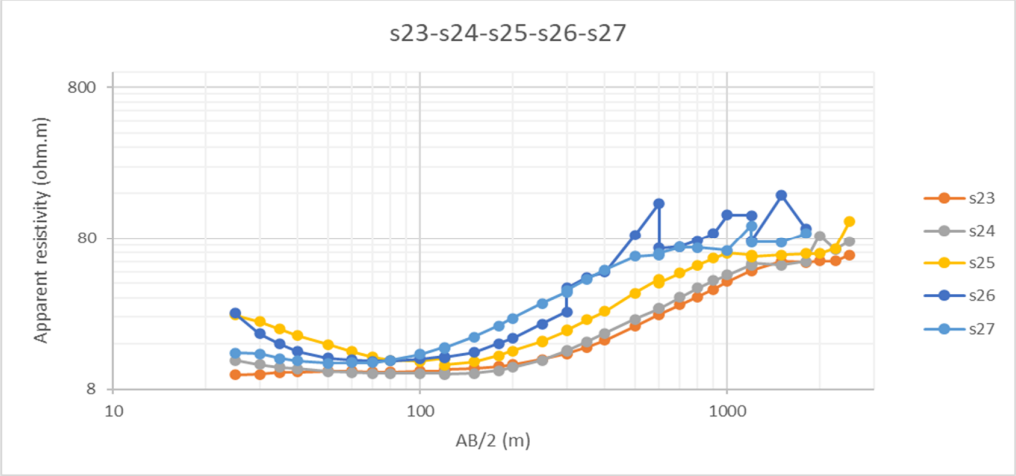

Group 3:

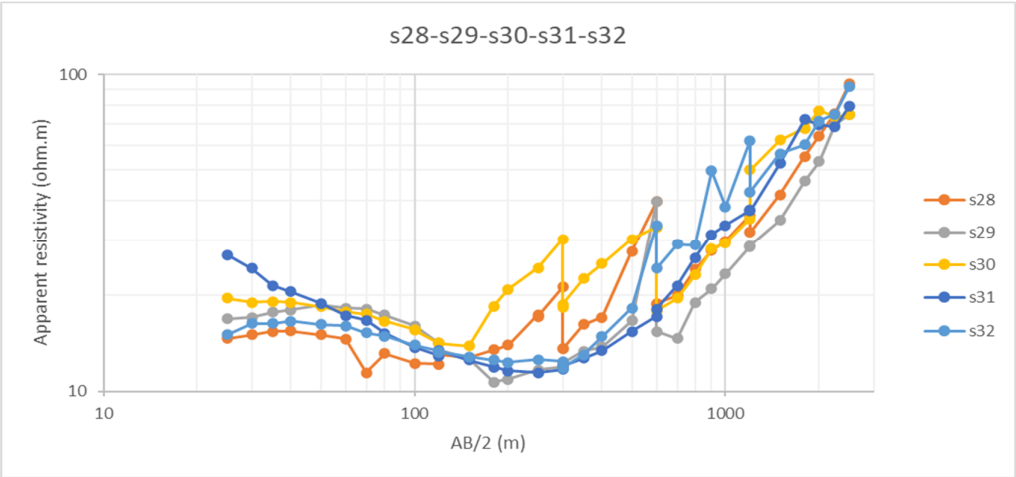

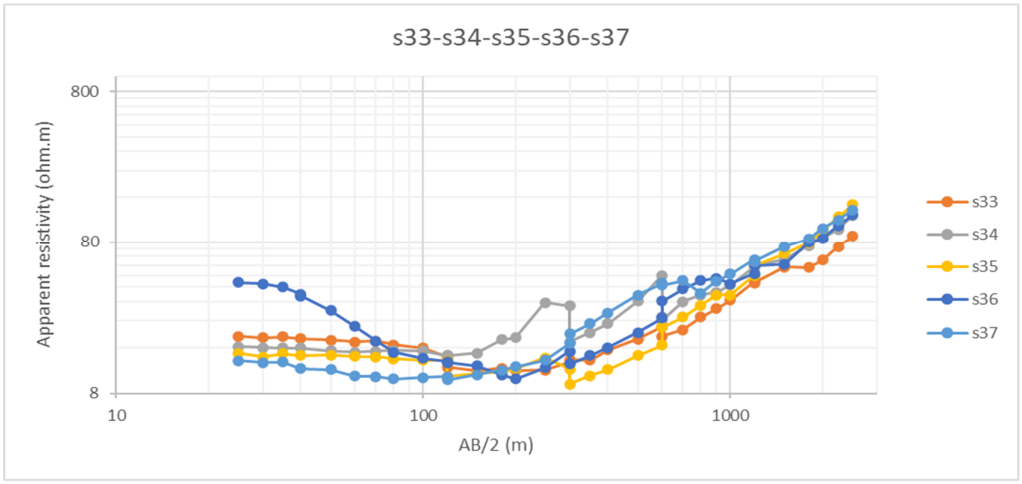
s33-s34-s35-s36-s37
800
80
8
Apparent resistivity (ohm.m)
10
100
1000
AB/2 (m)
s33
s34
s35
s36
s37

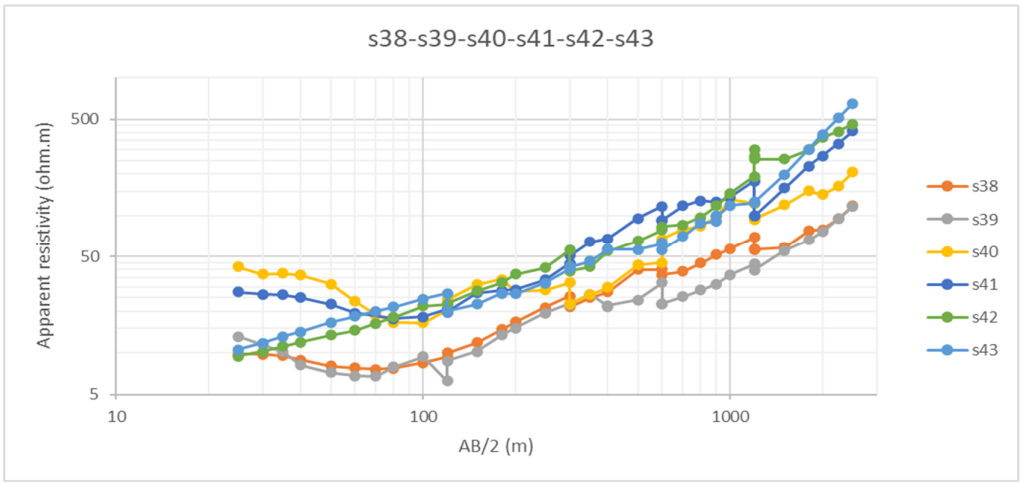
s38-s39-s40-s41-s42-s43
500
50
5
Apparent resistivity (ohm.m)
10
100
1000
AB/2 (m)
s38
s39
s40
s41
s42
s43

Group 4:

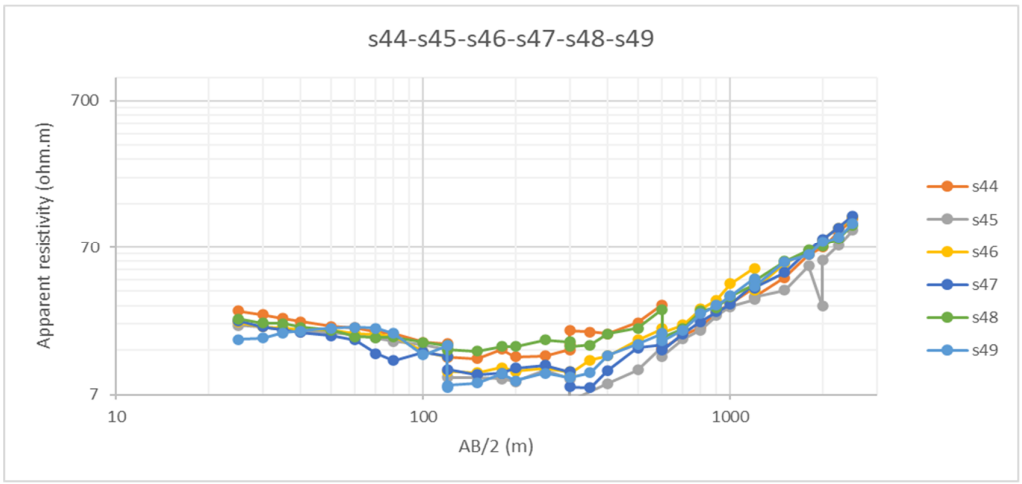
s44-s45-s46-s47-s48-s49
700
70
7
Apparent resistivity (ohm.m)
10
100
1000
AB/2 (m)
s44
s45
s46
s47
s48
s49

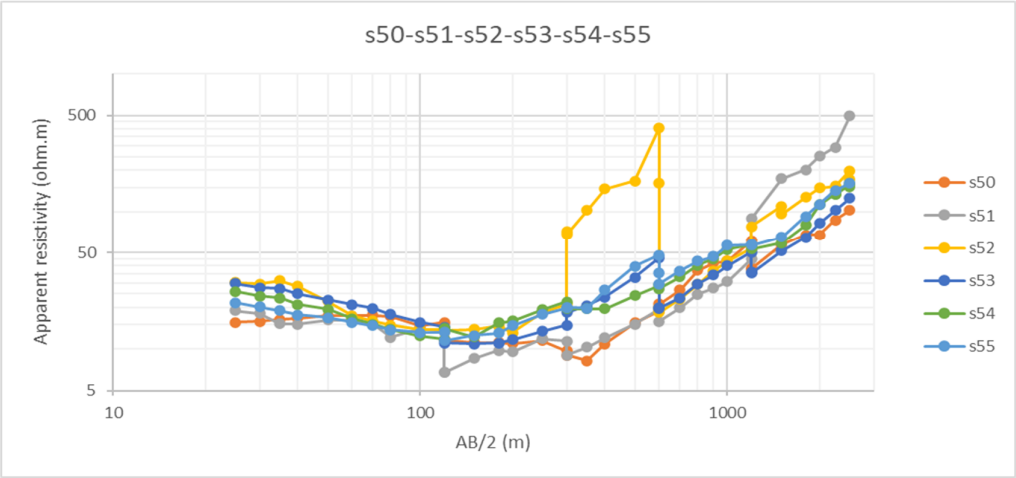
s50-s51-s52-s53-s54-s55
Apparent resistivity (ohm.m)
500
50
5
10
100
1000
AB/2 (m)
s50
s51
s52
s53
s54
s55

Group 5:

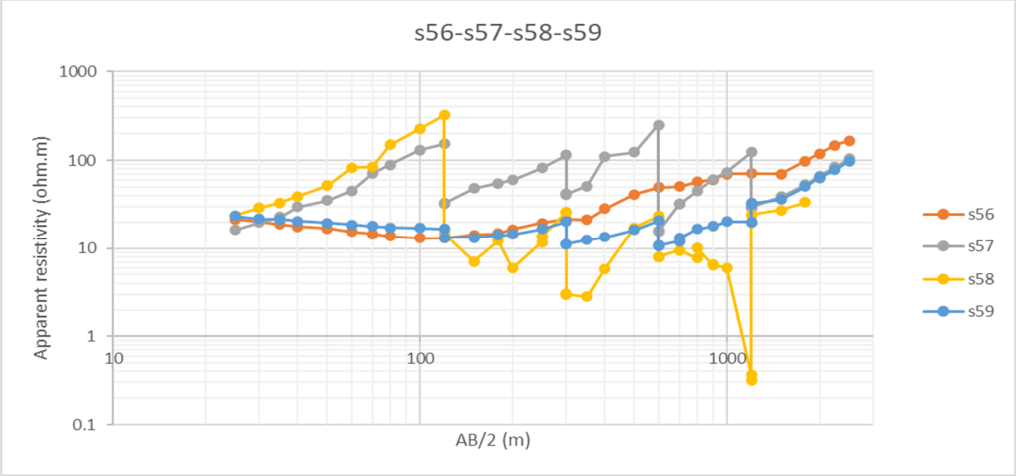
s56-s57-s58-s59
Apparent resistivity (ohm.m)
1000
100
10
1
0.1
10
100
1000
AB/2 (m)
s56
s57
s58
s59

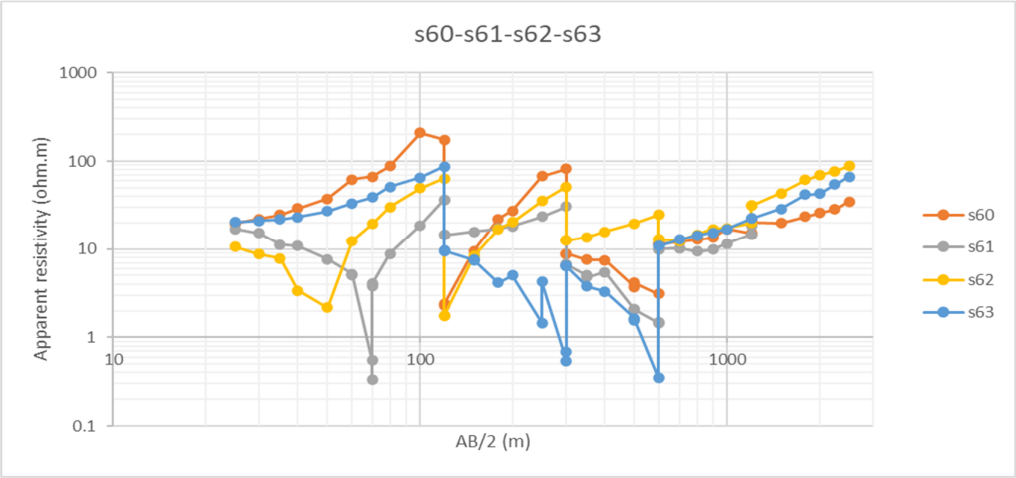
s60-s61-s62-s63
Apparent resistivity (ohm.m)
1000
100
10
1
0.1
10
100
1000
AB/2 (m)
s60
s61
s62
s63

Group 6:

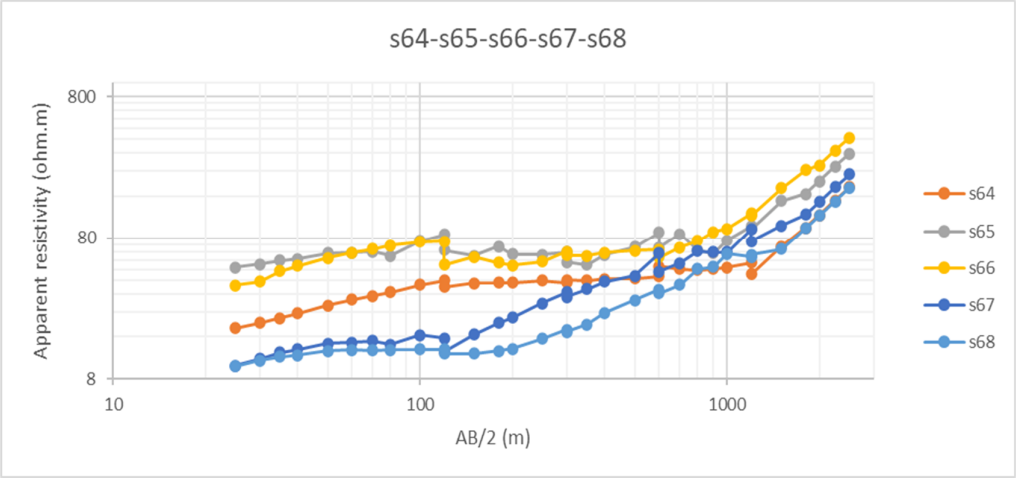
s64-s65-s66-s67-s68
Apparent resistivity (ohm.m)
800
80
8
10
100
1000
AB/2 (m)
s64
s65
s66
s67
s68

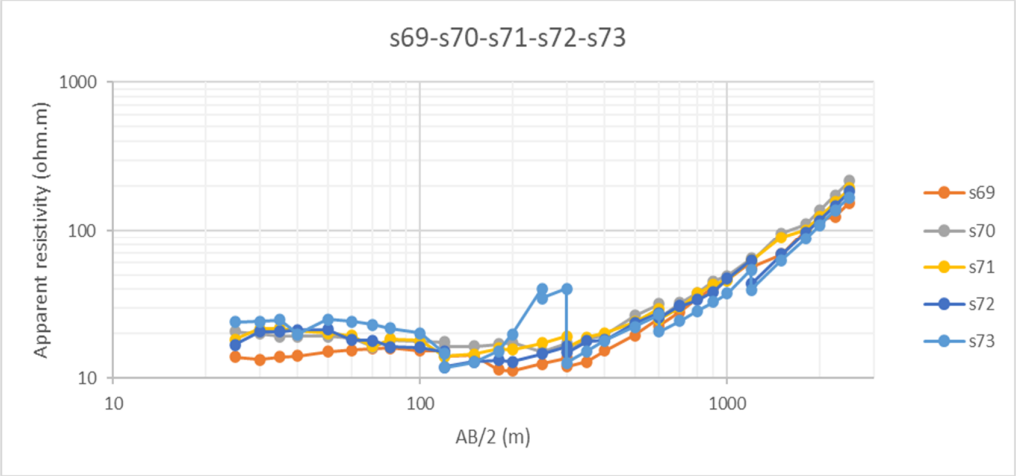
s69-s70-s71-s72-s73
Apparent resistivity (ohm.m)
1000
100
10
10
100
1000
AB/2 (m)
s69
s70
s71
s72
s73

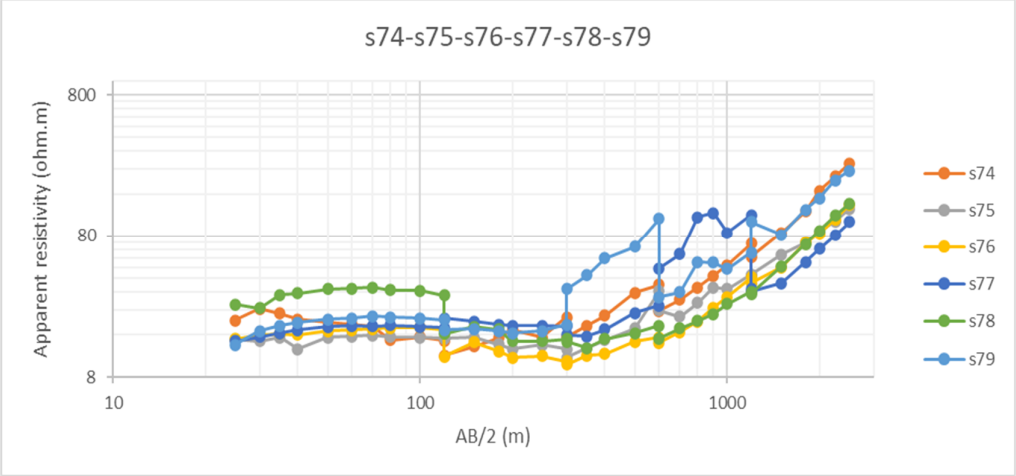
s74-s75-s76-s77-s78-s79
Apparent resistivity (ohm.m)
800
80
8
10
100
1000
AB/2 (m)
s74
s75
s76
s77
s78
s79

Group 7:

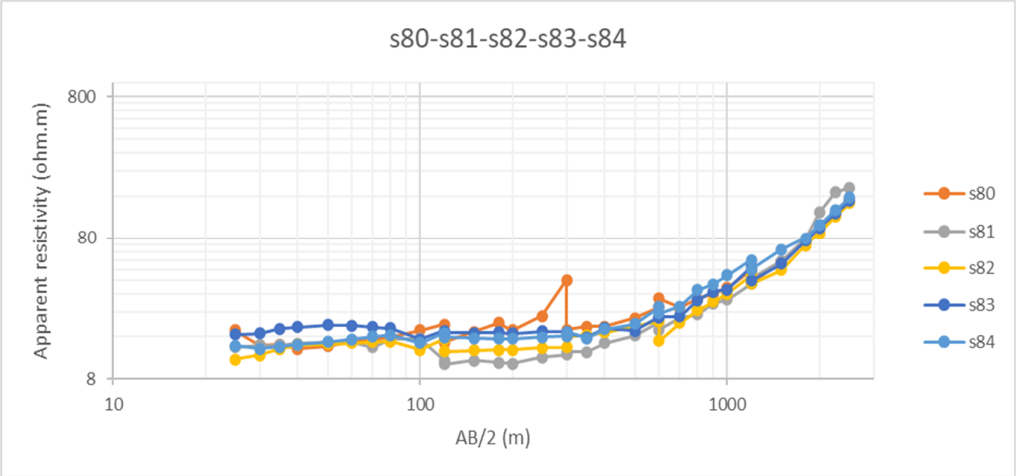
s80-s81-s82-s83-s84
Apparent resistivity (ohm.m)
800
80
8
10
100
1000
AB/2 (m)
s80
s81
s82
s83
s84

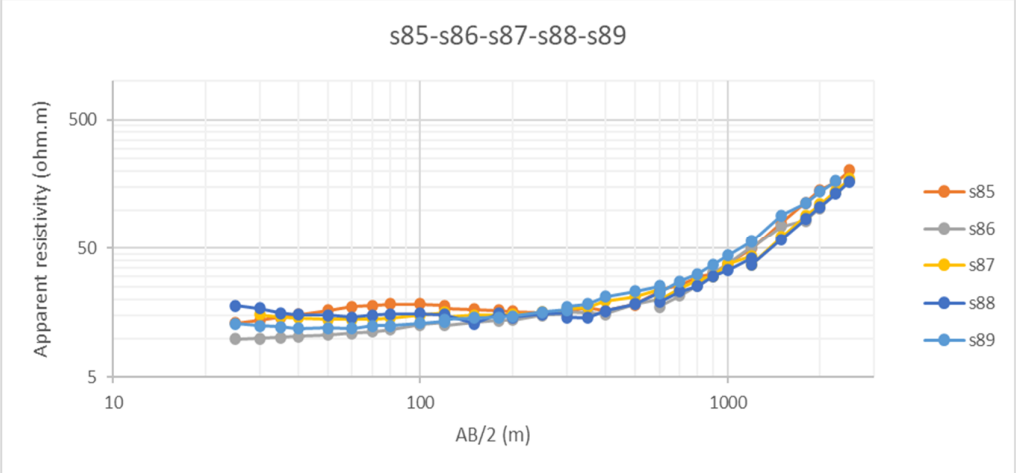
s85-s86-s87-s88-s89
Apparent resistivity (ohm.m)
500
50
5
10
100
1000
AB/2 (m)
s85
s86
s87
s88
s89

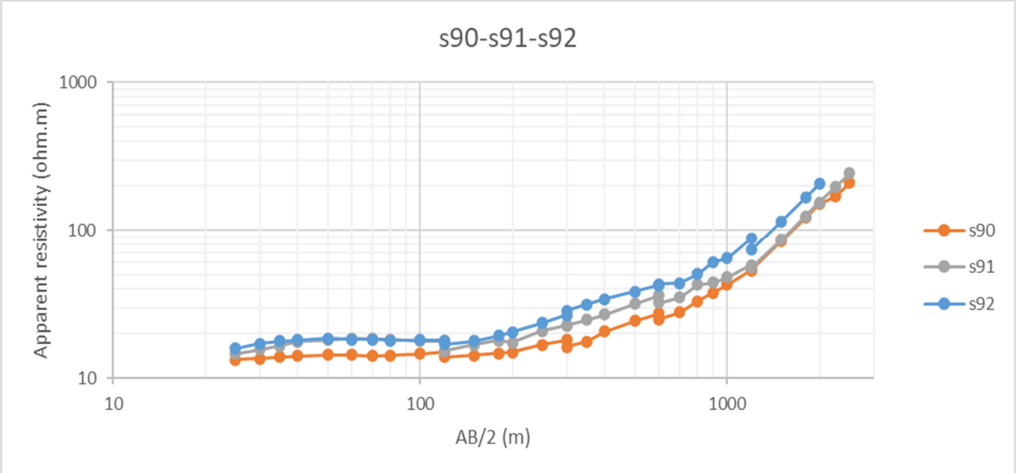
s90-s91-s92
Apparent resistivity (ohm.m)
1000
100
10
10
100
1000
AB/2 (m)
s90
s91
s92

Group 8:

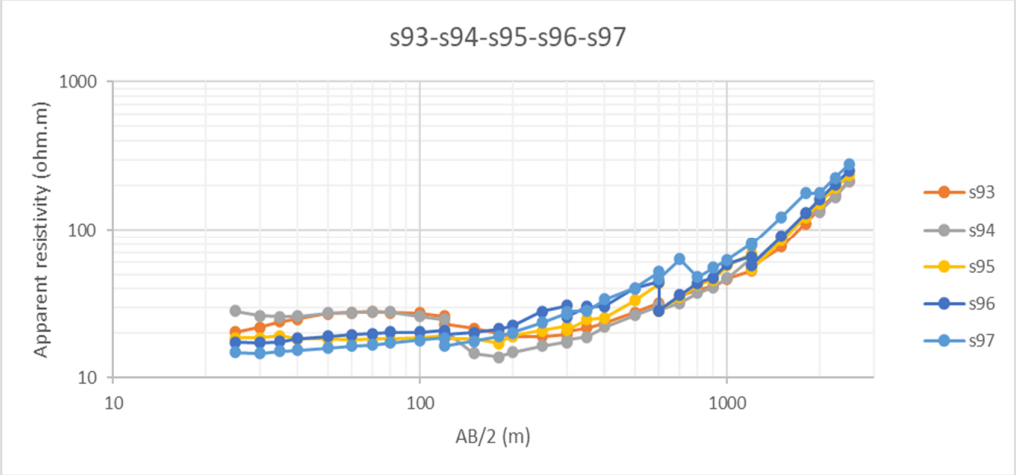
s93-s94-s95-s96-s97
Apparent resistivity (ohm.m)
1000
100
10
10
100
1000
AB/2 (m)
s93
s94
s95
s96
s97

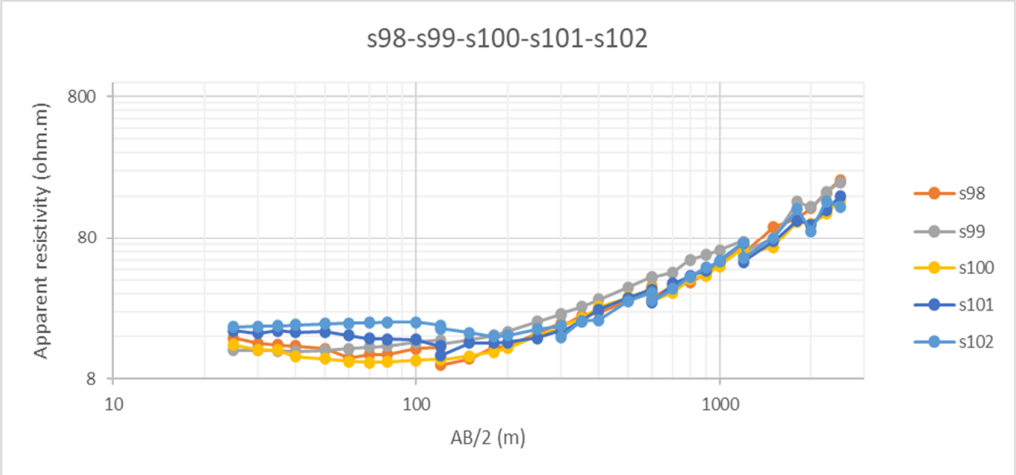
s98-s99-s100-s101-s102
Apparent resistivity (ohm.m)
800
80
8
10
100
1000
AB/2 (m)
s98
s99
s100
s101
s102

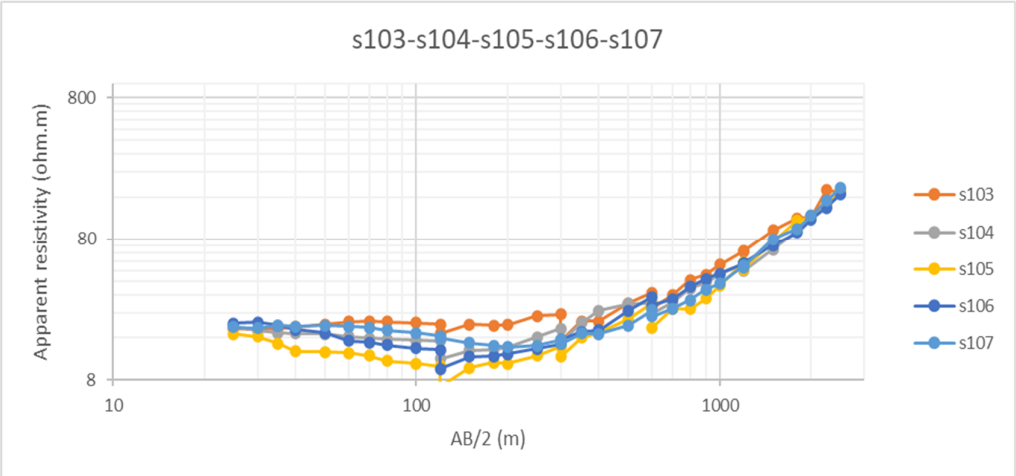
s103-s104-s105-s106-s107
Apparent resistivity (ohm.m)
800
80
8
10
100
1000
AB/2 (m)
s103
s104
s105
s106
s107

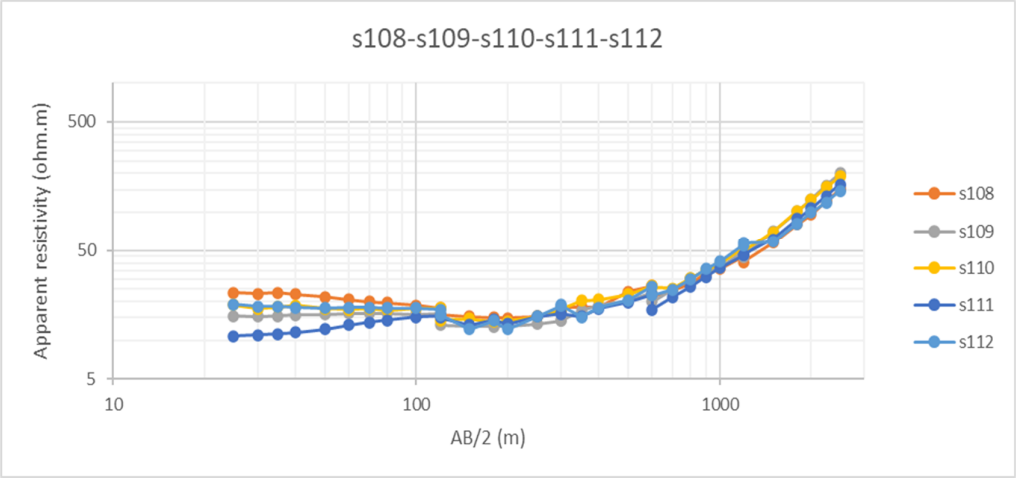
s108-s109-s110-s111-s112
Apparent resistivity (ohm.m)
500
50
5
10
100
1000
AB/2 (m)
s108
s109
s110
s111
s112

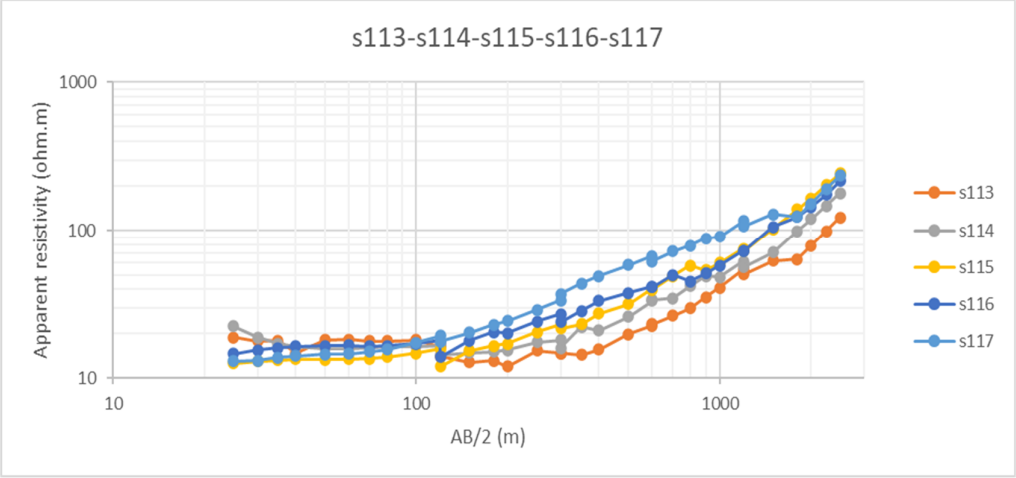
s113-s114-s115-s116-s117
Apparent resistivity (ohm.m)
1000
100
10
10
100
1000
AB/2 (m)
s113
s114
s115
s116
s117

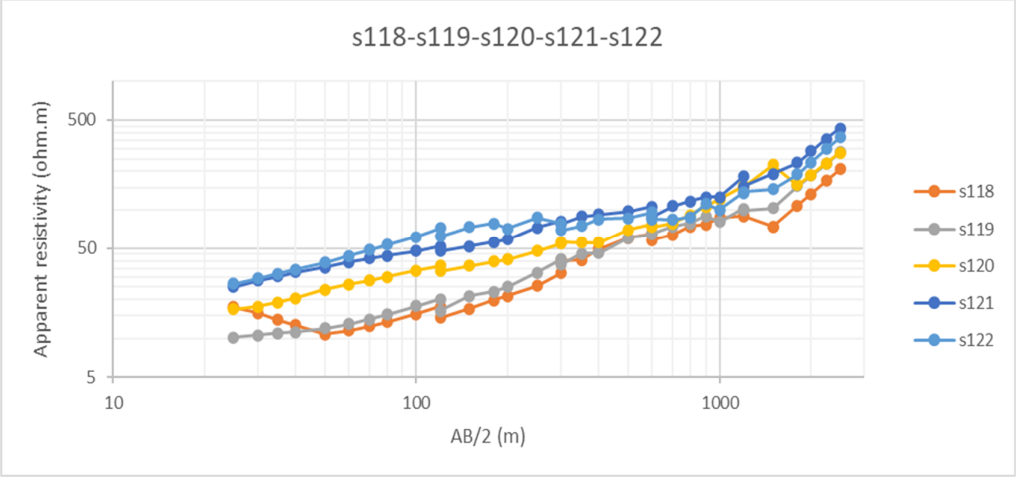
s118-s119-s120-s121-s122
Apparent resistivity (ohm.m)
500
50
5
10
100
1000
AB/2 (m)
s118
s119
s120
s121
s122

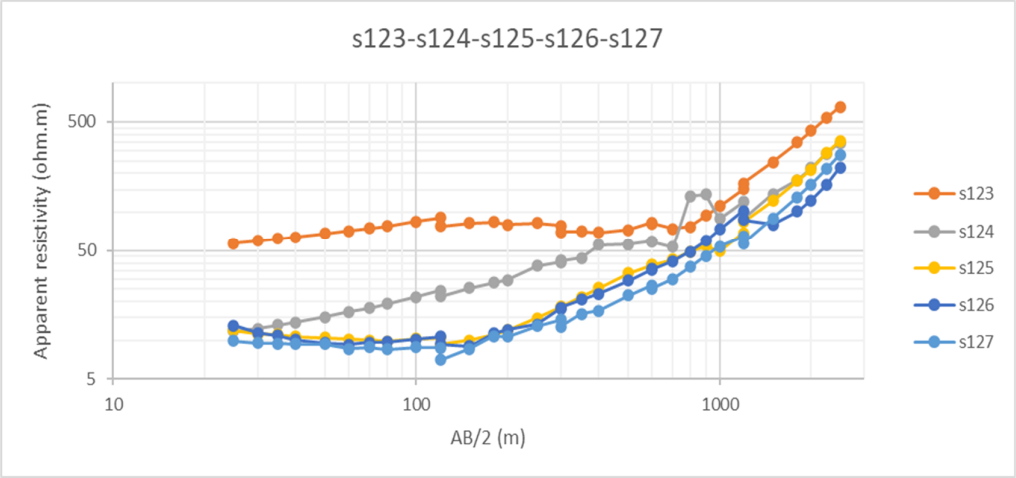
s123-s124-s125-s126-s127
Apparent resistivity (ohm.m)
500
50
5
10
100
1000
AB/2 (m)
s123
s124
s125
s126
s127

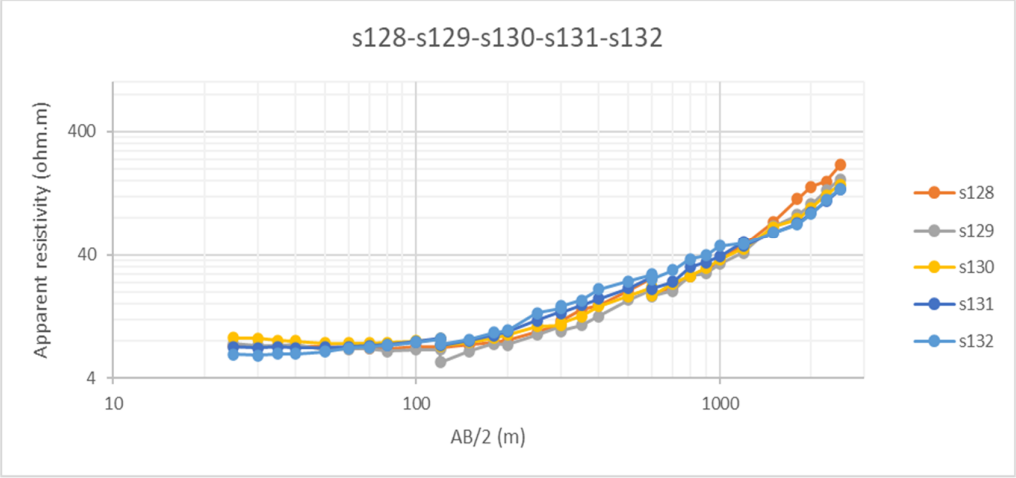
s128-s129-s130-s131-s132
Apparent resistivity (ohm.m)
400
40
4
10
100
1000
AB/2 (m)
s128
s129
s130
s131
s132

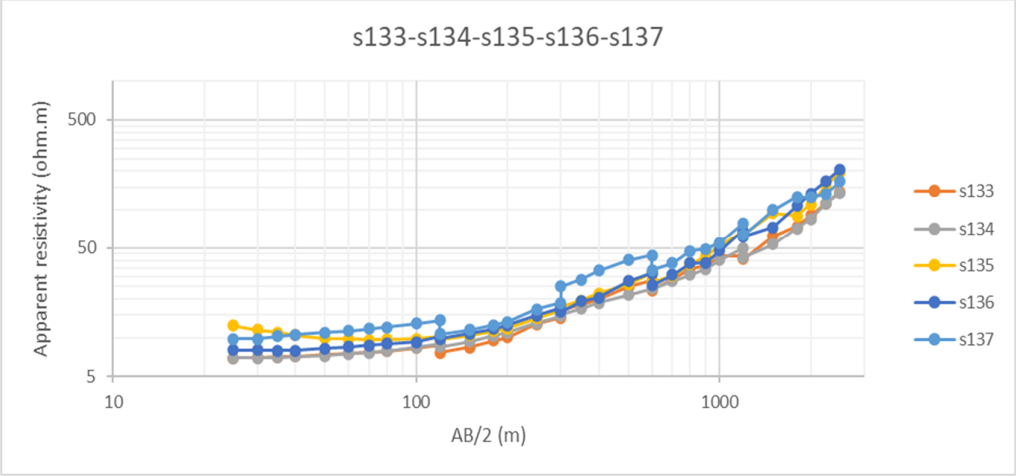
s133-s134-s135-s136-s137
Apparent resistivity (ohm.m)
500
50
5
10
100
1000
AB/2 (m)
s133
s134
s135
s136
s137

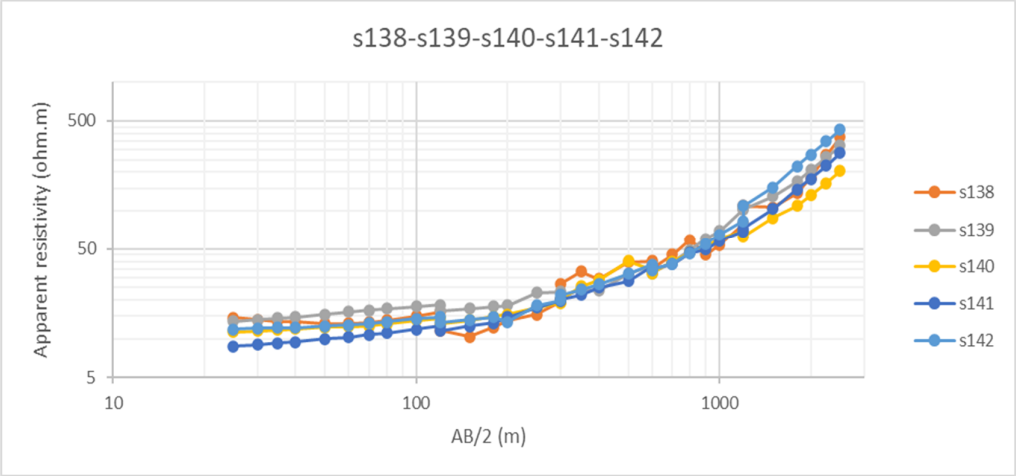
s138-s139-s140-s141-s142
Apparent resistivity (ohm.m)
500
50
5
10
100
1000
AB/2 (m)
s138
s139
s140
s141
s142

Group 9:

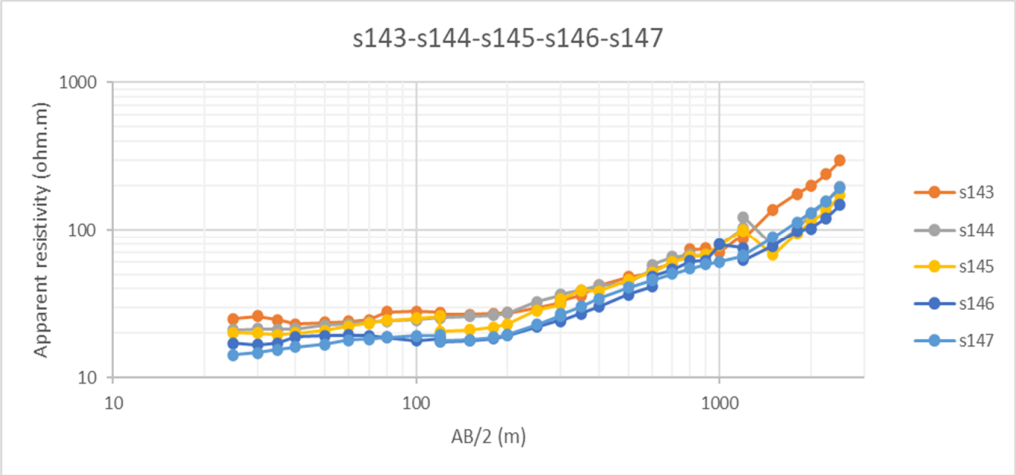
s143-s144-s145-s146-s147
Apparent resistivity (ohm.m)
1000
100
10
10
100
1000
AB/2 (m)
s143
s144
s145
s146
s147

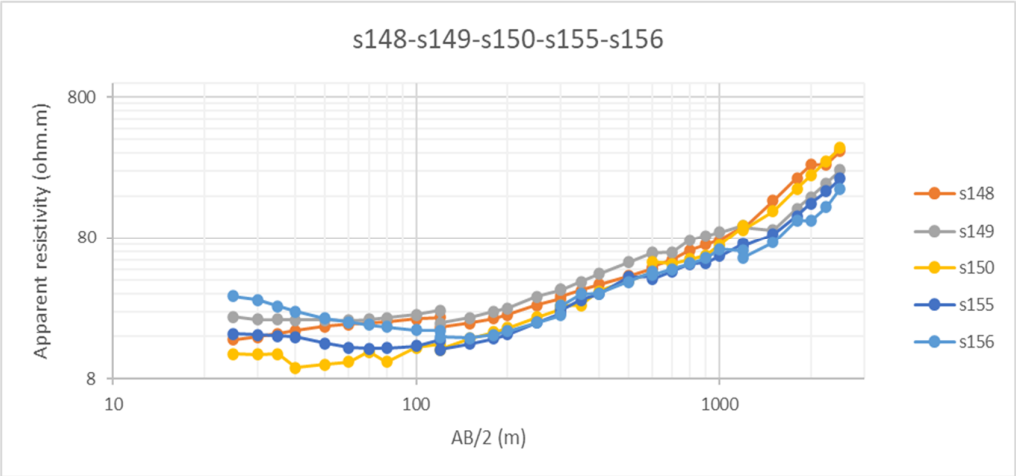
s148-s149-s150-s155-s156
Apparent resistivity (ohm.m)
800
80
8
10
100
1000
AB/2 (m)
s148
s149
s150
s155
s156

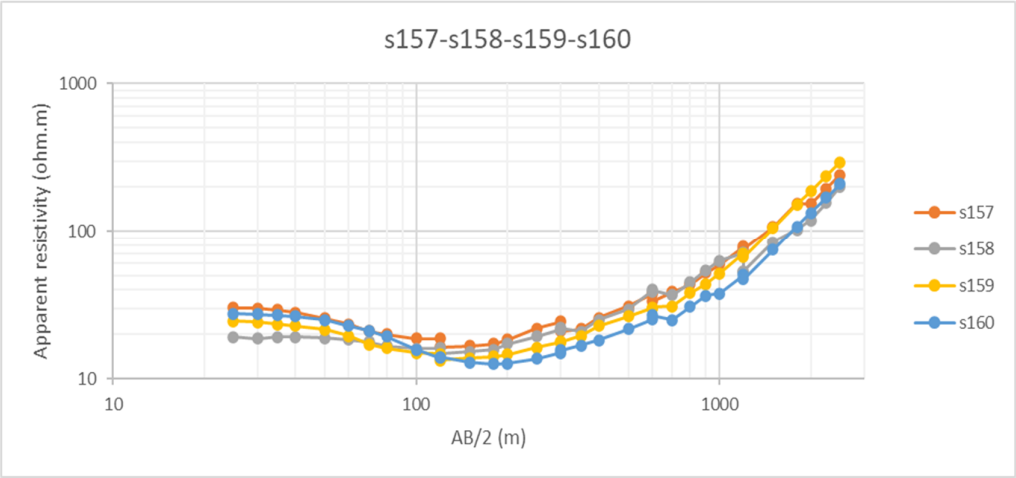
s157-s158-s159-s160
Apparent resistivity (ohm.m)
1000
100
10
10
100
1000
AB/2 (m)
s157
s158
s159
s160

Group 10:

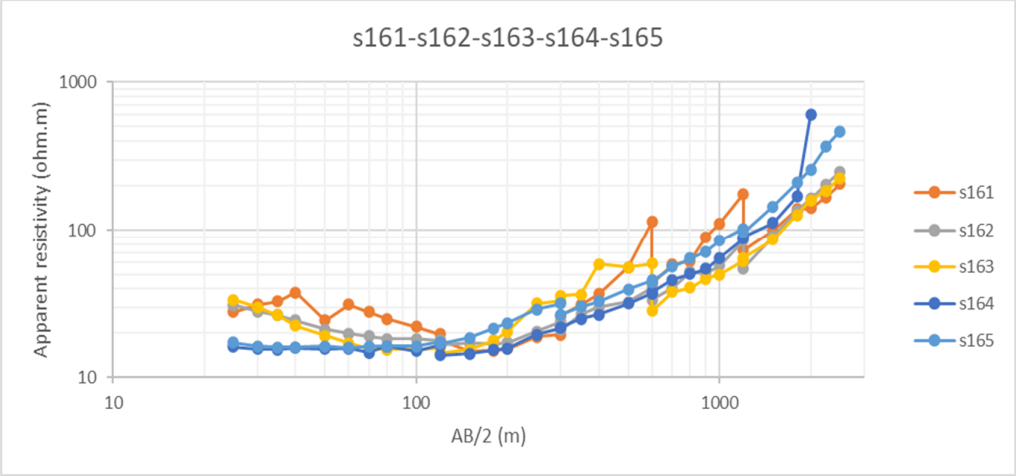
s161-s162-s163-s164-s165
Apparent resistivity (ohm.m)
1000
100
10
10
100
1000
AB/2 (m)
s161
s162
s163
s164
s165

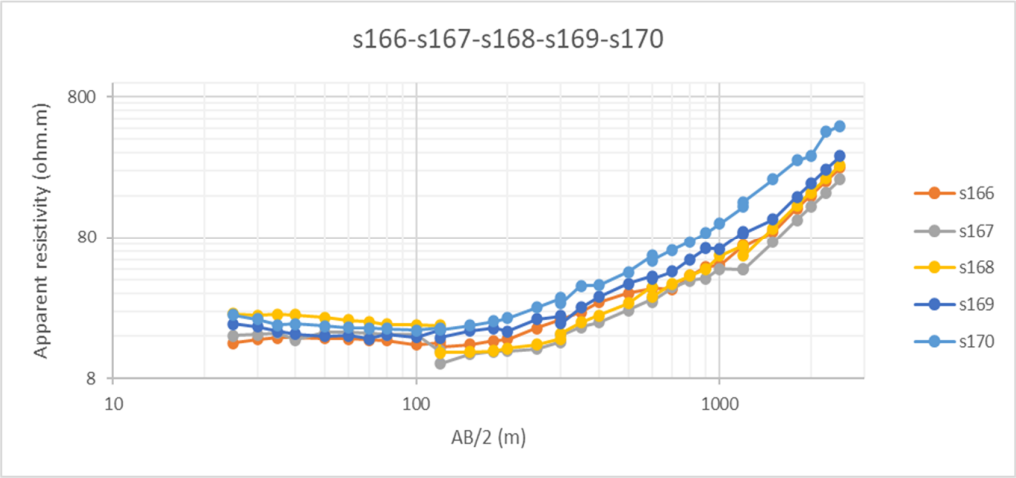
s166-s167-s168-s169-s170
Apparent resistivity (ohm.m)
800
80
8
10
100
1000
AB/2 (m)
s166
s167
s168
s169
s170

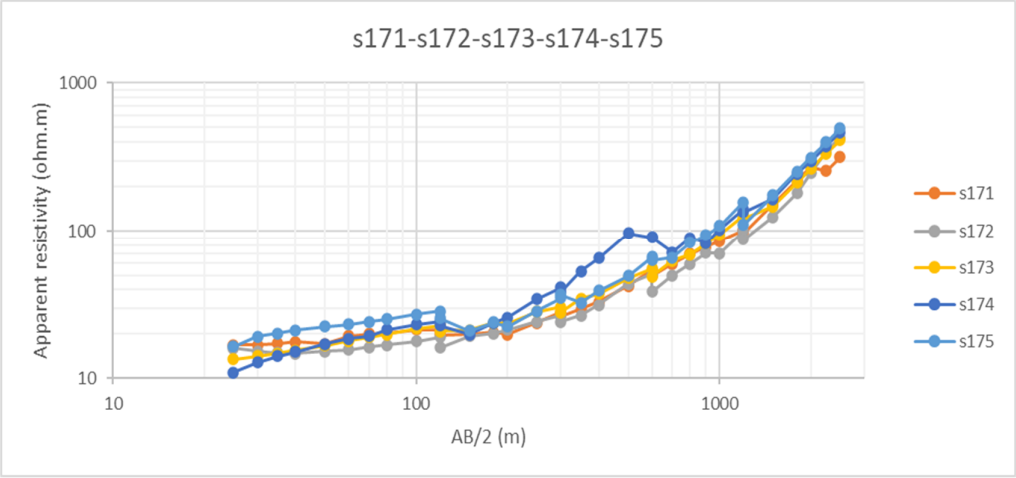
s171-s172-s173-s174-s175
Apparent resistivity (ohm.m)
1000
100
10
10
100
1000
AB/2 (m)
s171
s172
s173
s174
s175

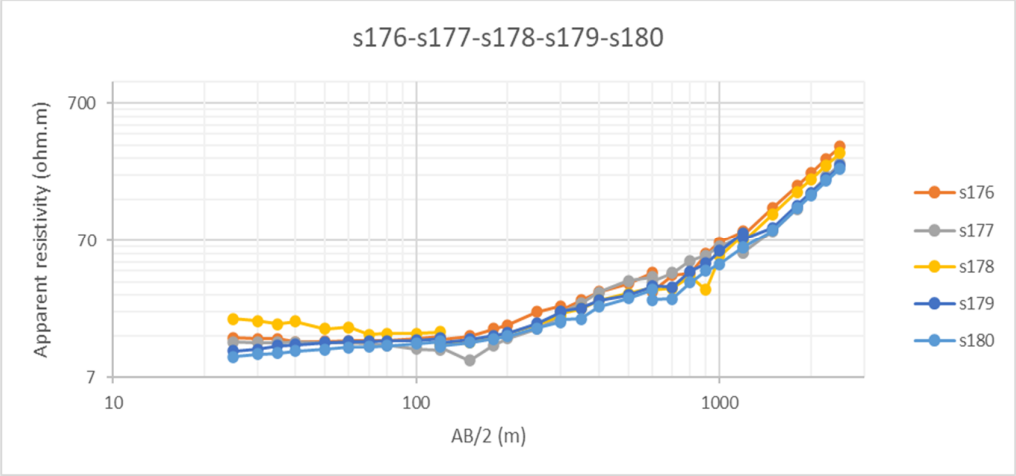
s176-s177-s178-s179-s180
Apparent resistivity (ohm.m)
700
70
7
10
100
1000
AB/2 (m)
s176
s177
s178
s179
s180

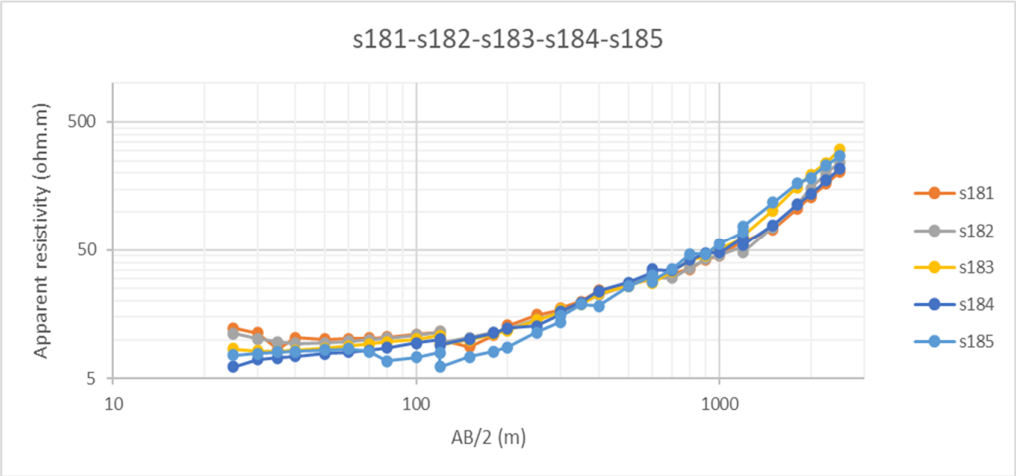
s181-s182-s183-s184-s185
Apparent resistivity (ohm.m)
500
50
5
10
100
1000
AB/2 (m)
s181
s182
s183
s184
s185

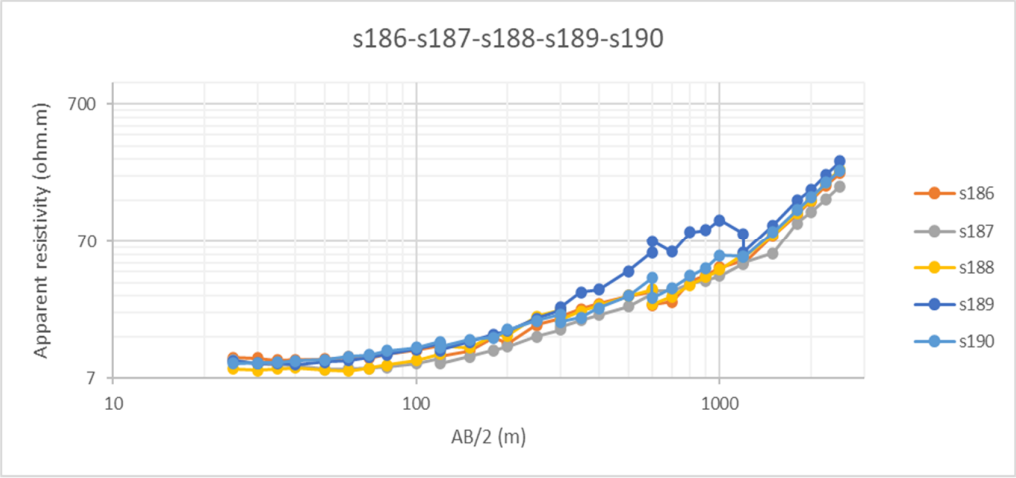
s186-s187-s188-s189-s190
Apparent resistivity (ohm.m)
700
70
7
10
100
1000
AB/2 (m)
s186
s187
s188
s189
s190

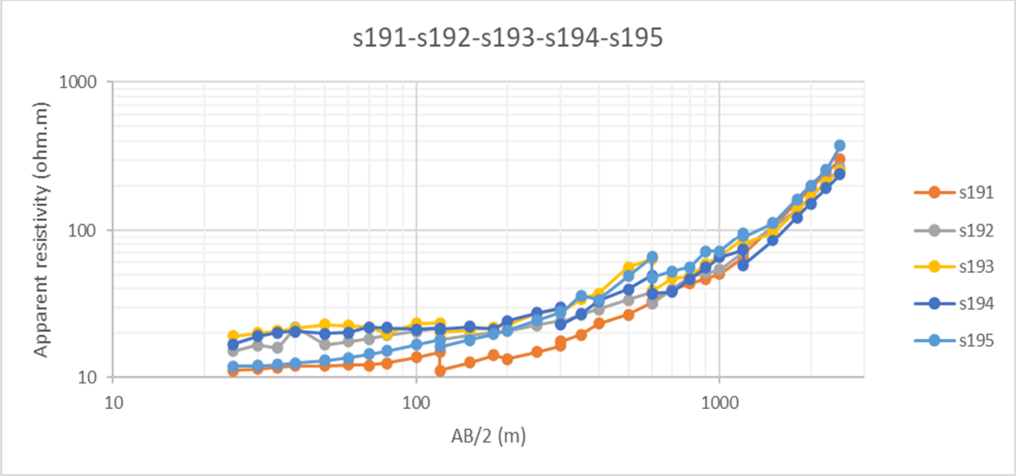
s191-s192-s193-s194-s195
Apparent resistivity (ohm.m)
1000
100
10
10
100
1000
AB/2 (m)
s191
s192
s193
s194
s195

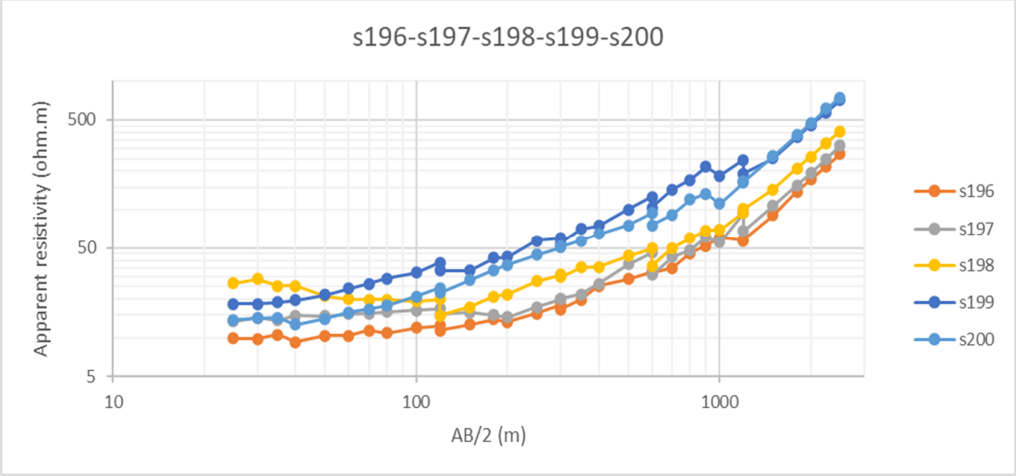
s196-s197-s198-s199-s200
Apparent resistivity (ohm.m)
500
50
5
10
100
1000
AB/2 (m)
s196
s197
s198
s199
s200

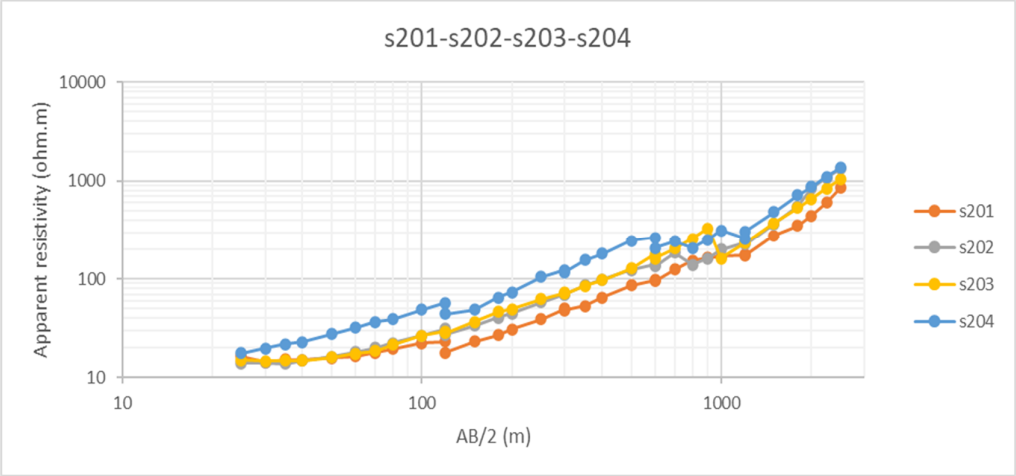
s201-s202-s203-s204
Apparent resistivity (ohm.m)
10000
1000
100
10
10
100
1000
AB/2 (m)
s201
s202
s203
s204

Group 11:

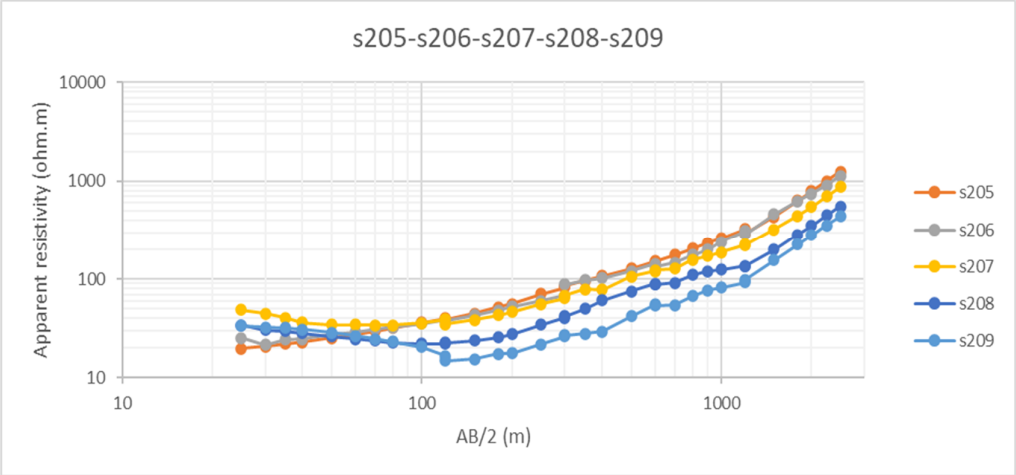
s205-s206-s207-s208-s209
Apparent resistivity (ohm.m)
10000
1000
100
10
10
100
1000
AB/2 (m)
s205
s206
s207
s208
s209

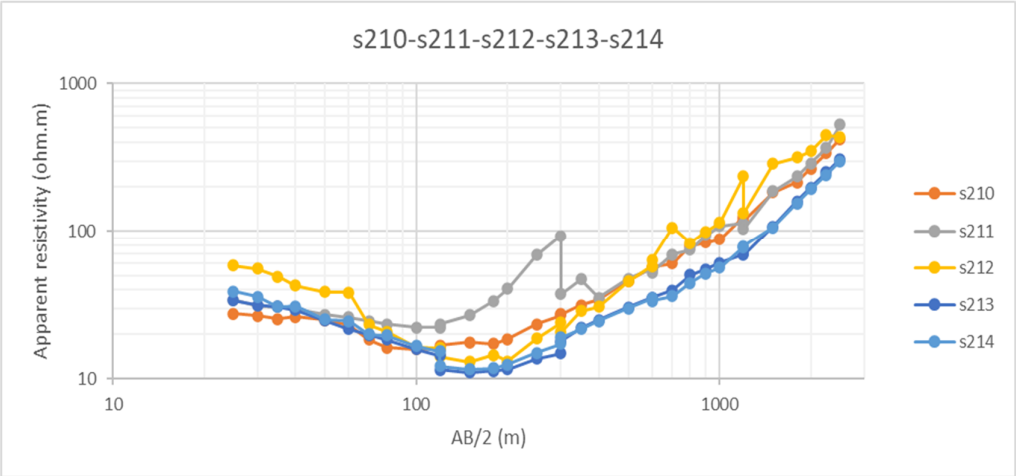
s210-s211-s212-s213-s214
Apparent resistivity (ohm.m)
1000
100
10
10
100
1000
AB/2 (m)
s210
s211
s212
s213
s214

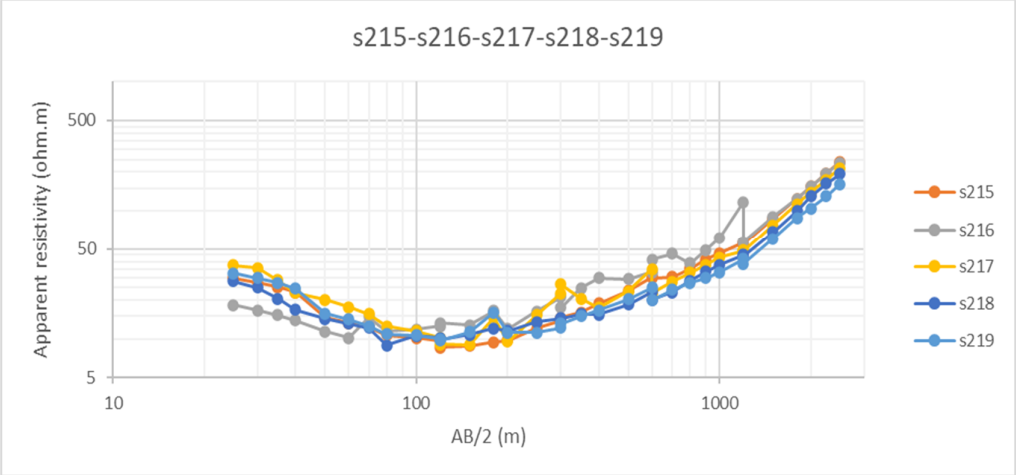
s215-s216-s217-s218-s219
Apparent resistivity (ohm.m)
500
50
5
10
100
1000
AB/2 (m)
s215
s216
s217
s218
s219

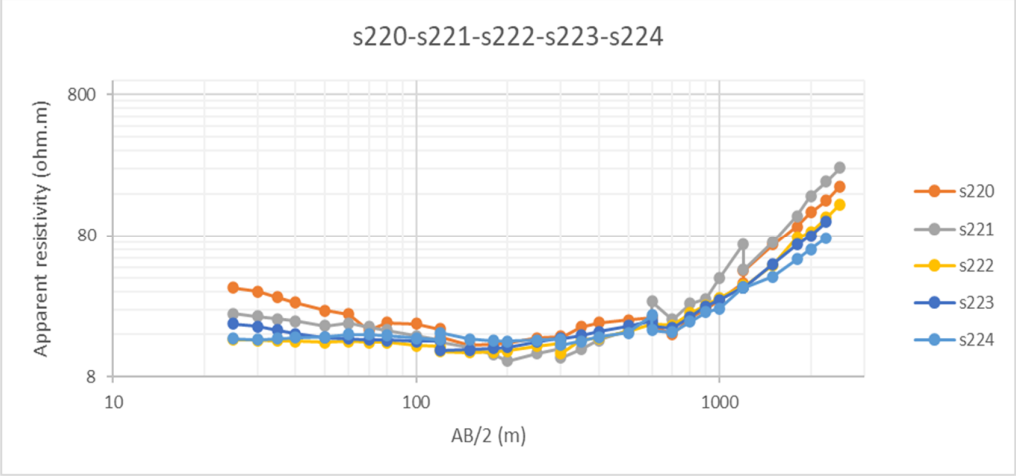
s220-s221-s222-s223-s224
Apparent resistivity (ohm.m)
800
80
8
10
100
1000
AB/2 (m)
s220
s221
s222
s223
s224

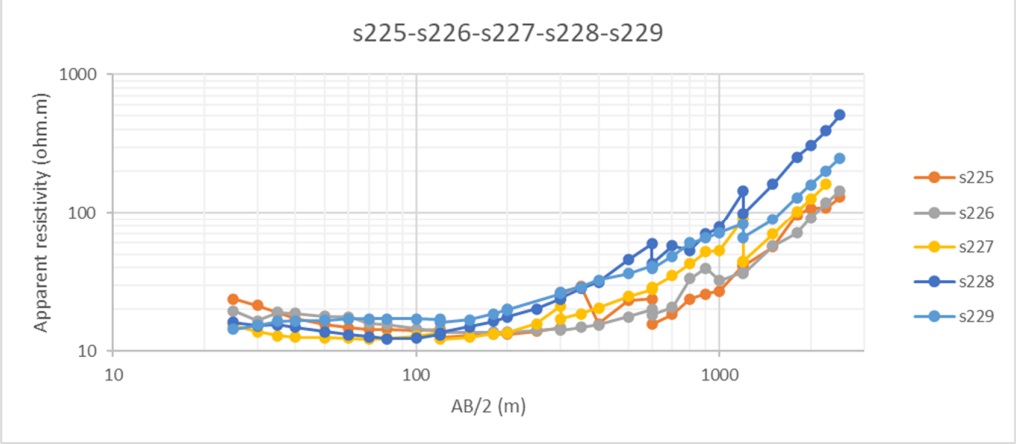
s225-s226-s227-s228-s229
Apparent resistivity (ohm.m)
1000
100
10
10
100
1000
AB/2 (m)
s225
s226
s227
s228
s229

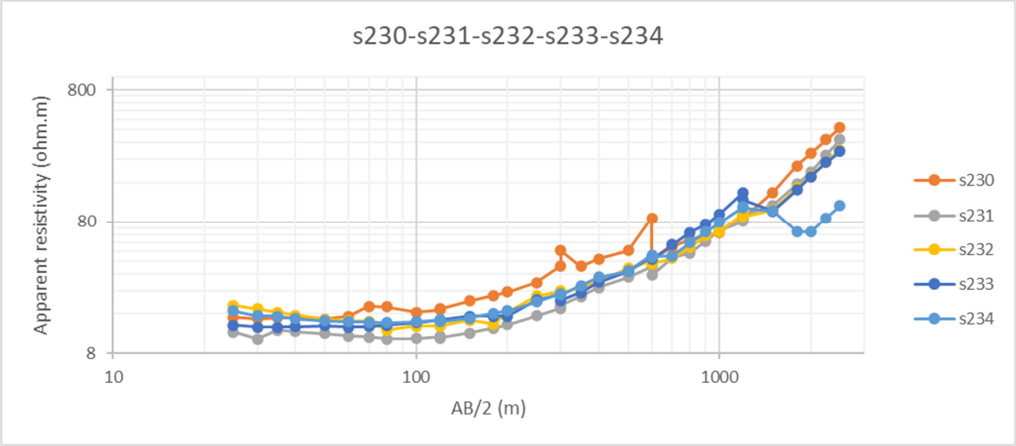
s230-s231-s232-s233-s234
Apparent resistivity (ohm.m)
800
80
8
10
100
1000
AB/2 (m)
s230
s231
s232
s233
s234

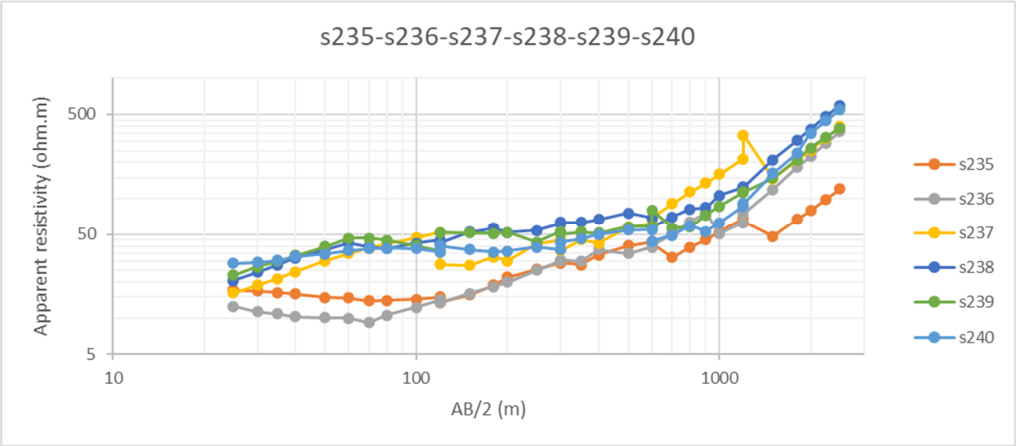
s235-s236-s237-s238-s239-s240
Apparent resistivity (ohm.m)
500
50
5
10
100
1000
AB/2 (m)
s235
s236
s237
s238
s239
s240

Group 12:

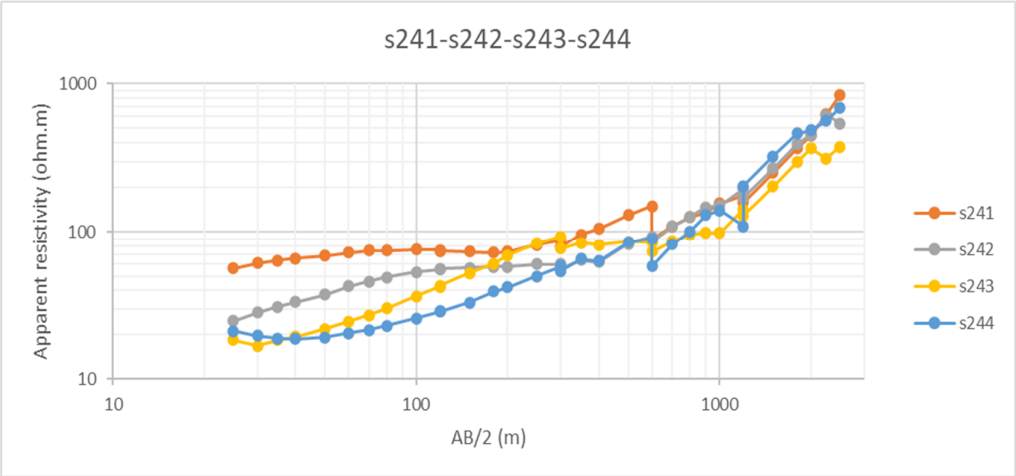
s241-s242-s243-s244
Apparent resistivity (ohm.m)
1000
100
10
10
100
1000
AB/2 (m)
s241
s242
s243
s244

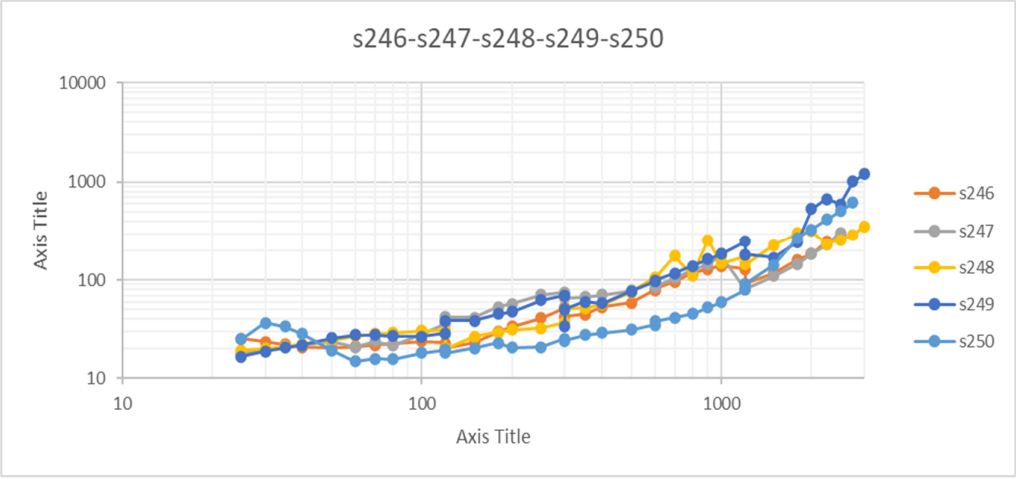
s246-s247-s248-s249-s250
10000
1000
100
10
Axis Title
10
100
1000
Axis Title
s246
s247
s248
s249
s250

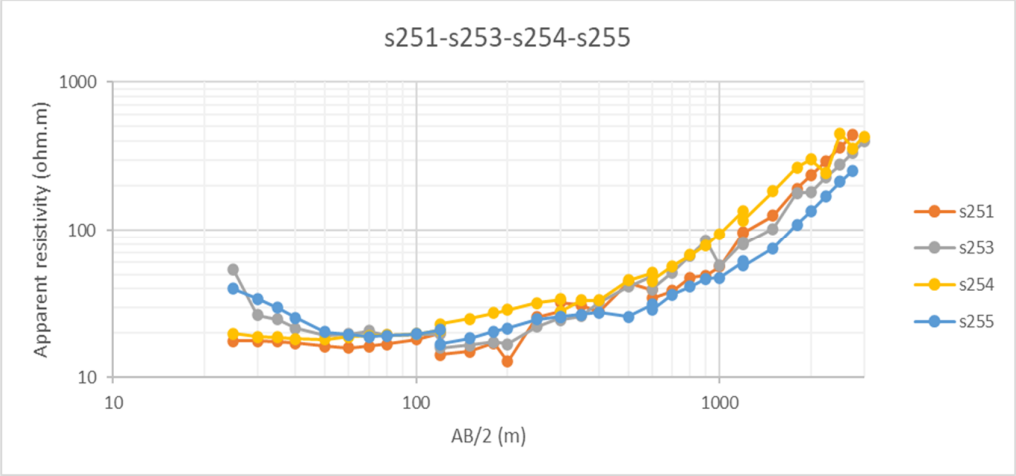
s251-s253-s254-s255
1000
100
10
Apparent resistivity (ohm.m)
10
100
1000
AB/2 (m)
s251
s253
s254
s255

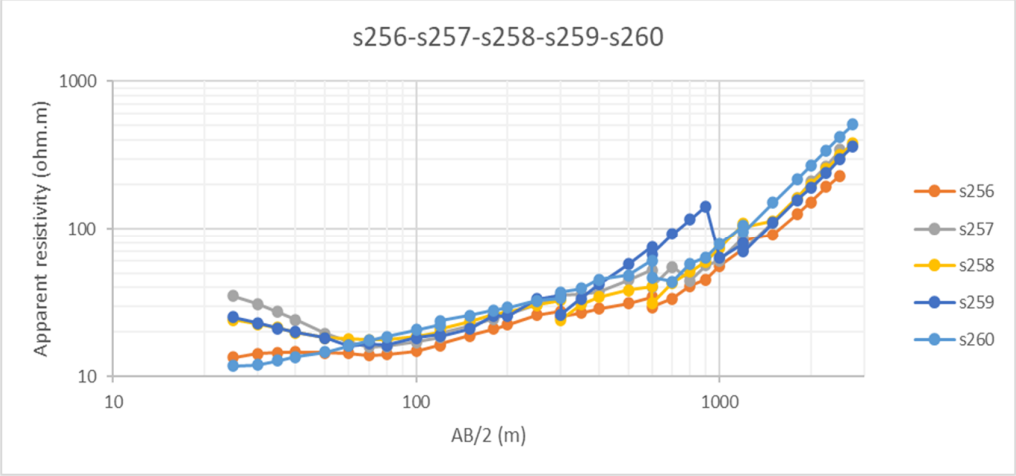
s256-s257-s258-s259-s260
1000
100
10
Apparent resistivity (ohm.m)
10
100
1000
AB/2 (m)
s256
s257
s258
s259
s260

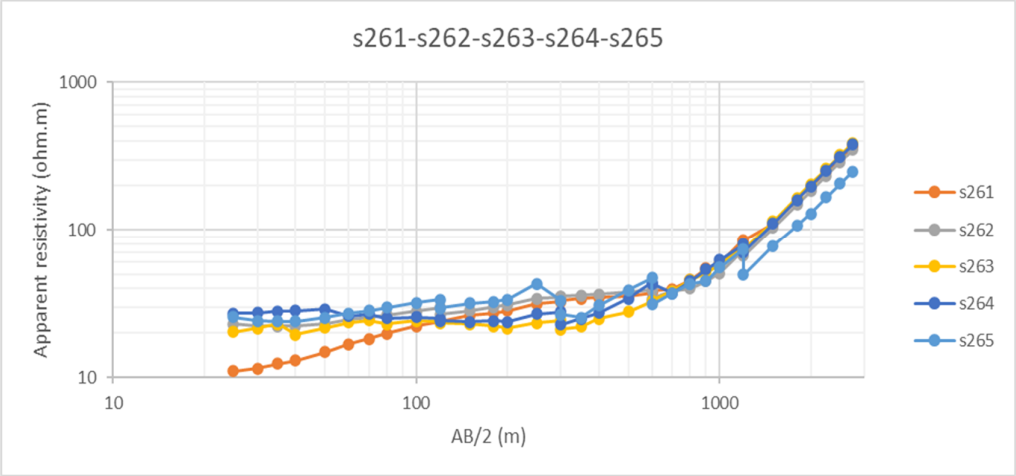
s261-s262-s263-s264-s265
Apparent resistivity (ohm.m)
1000
100
10
10
100
1000
AB/2 (m)
s261
s262
s263
s264
s265

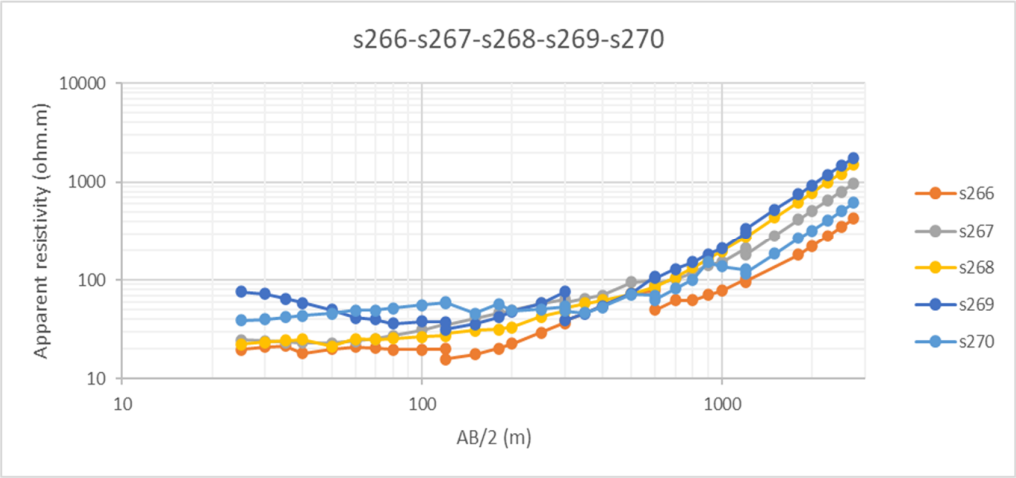
s266-s267-s268-s269-s270
Apparent resistivity (ohm.m)
10000
1000
100
10
10
100
1000
AB/2 (m)
s266
s267
s268
s269
s270

Group 13:

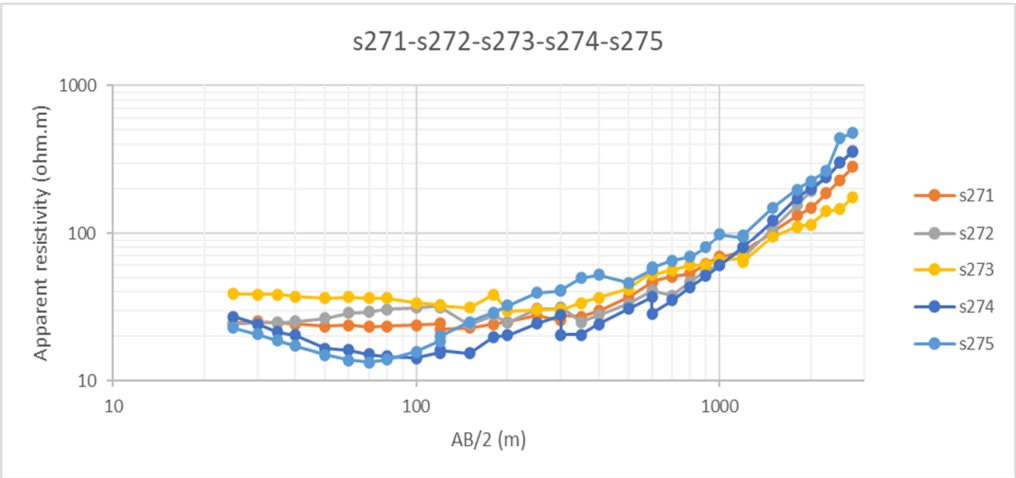
s271-s272-s273-s274-s275
Apparent resistivity (ohm.m)
1000
100
10
10
100
1000
AB/2 (m)
s271
s272
s273
s274
s275

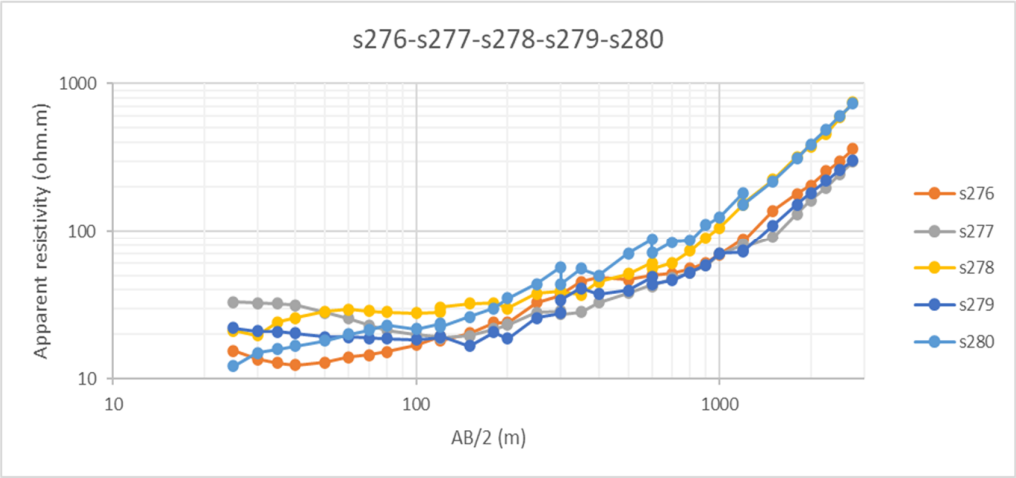
s276-s277-s278-s279-s280
Apparent resistivity (ohm.m)
1000
100
10
10
100
1000
AB/2 (m)
s276
s277
s278
s279
s280

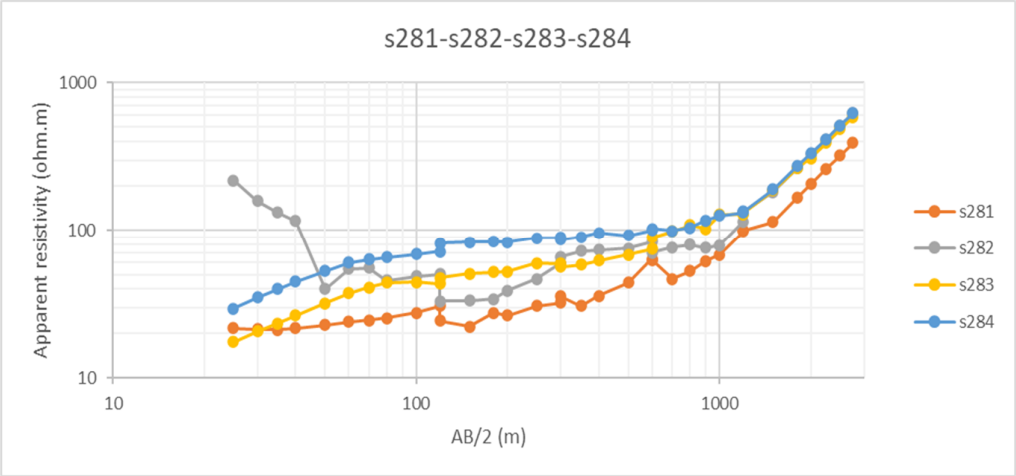
s281-s282-s283-s284
Apparent resistivity (ohm.m)
1000
100
10
10
100
1000
AB/2 (m)
s281
s282
s283
s284

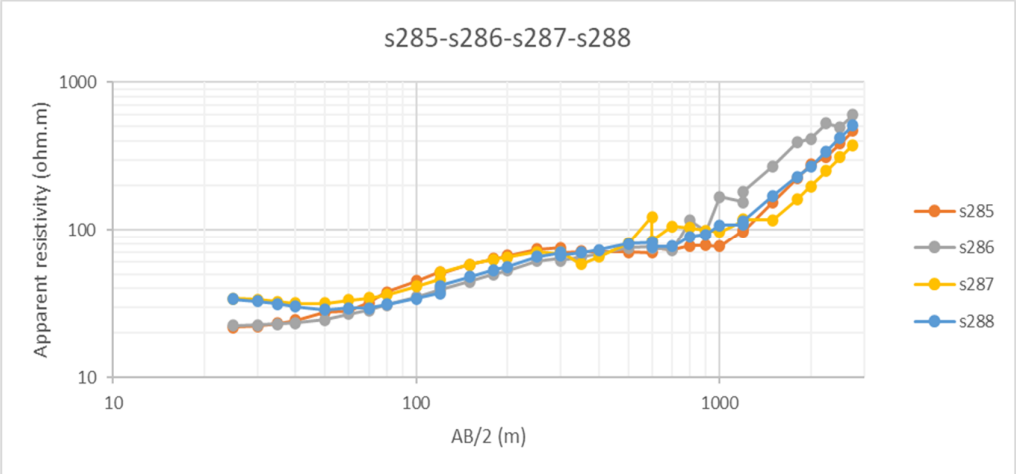
s285-s286-s287-s288
Apparent resistivity (ohm.m)
1000
100
10
10
100
1000
AB/2 (m)
s285
s286
s287
s288

Group 14:

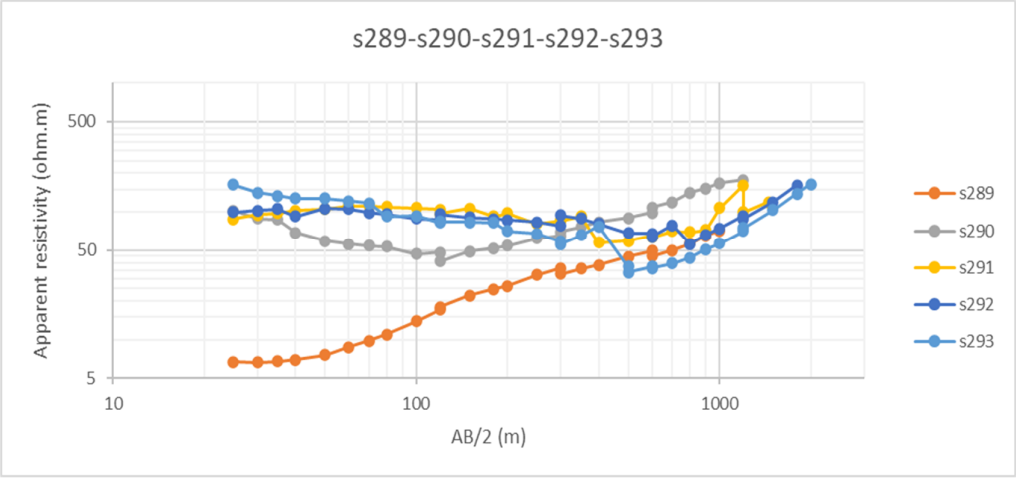
s289-s290-s291-s292-s293
Apparent resistivity (ohm.m)
500
50
5
10
100
1000
AB/2 (m)
s289
s290
s291
s292
s293

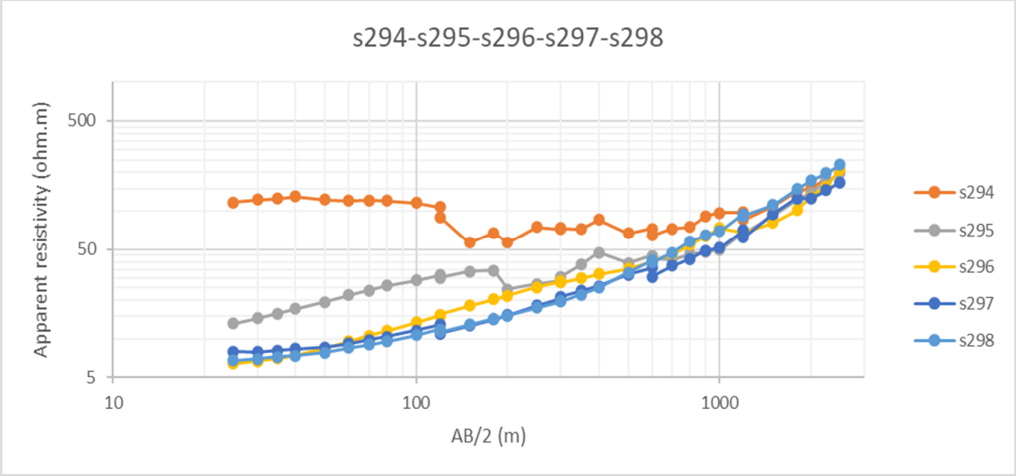
s294-s295-s296-s297-s298
Apparent resistivity (ohm.m)
500
50
5
10
100
1000
AB/2 (m)
s294
s295
s296
s297
s298

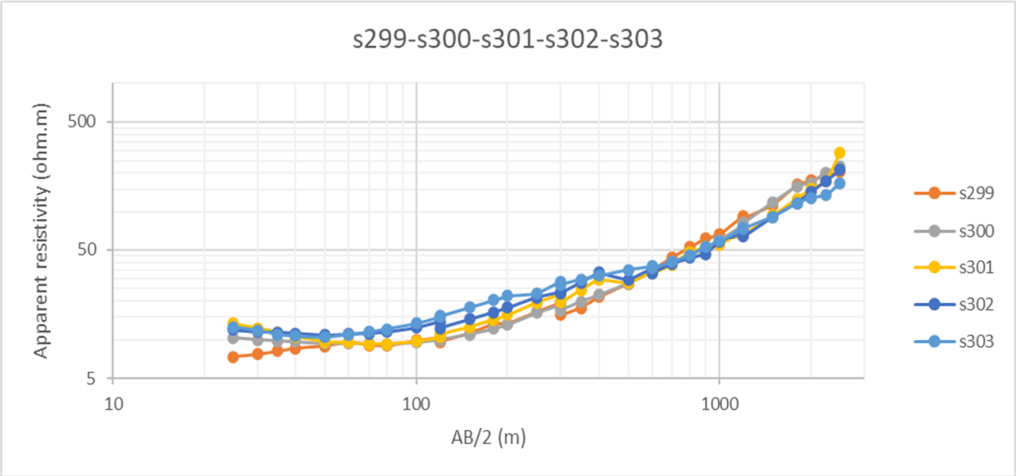
s299-s300-s301-s302-s303
Apparent resistivity (ohm.m)
500
50
5
10
100
1000
AB/2 (m)
s299
s300
s301
s302
s303

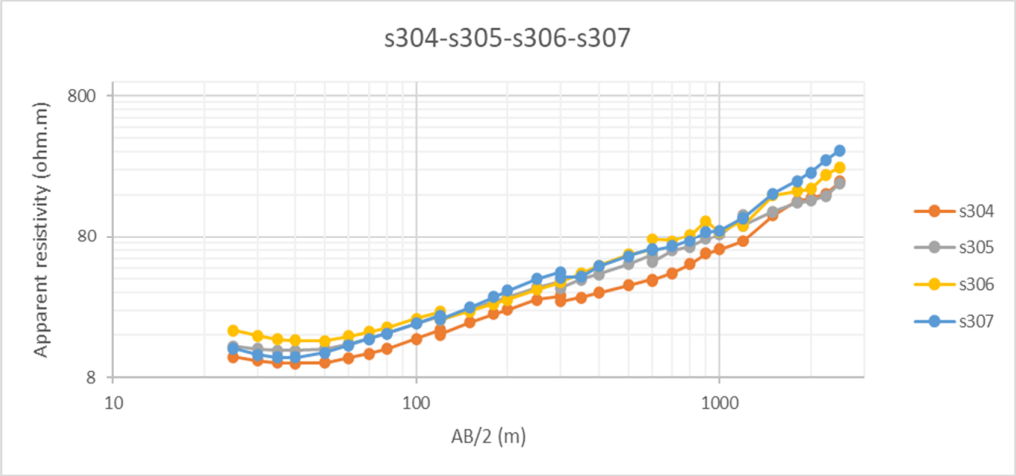
s304-s305-s306-s307
Apparent resistivity (ohm.m)
800
80
8
10
100
1000
AB/2 (m)
s304
s305
s306
s307

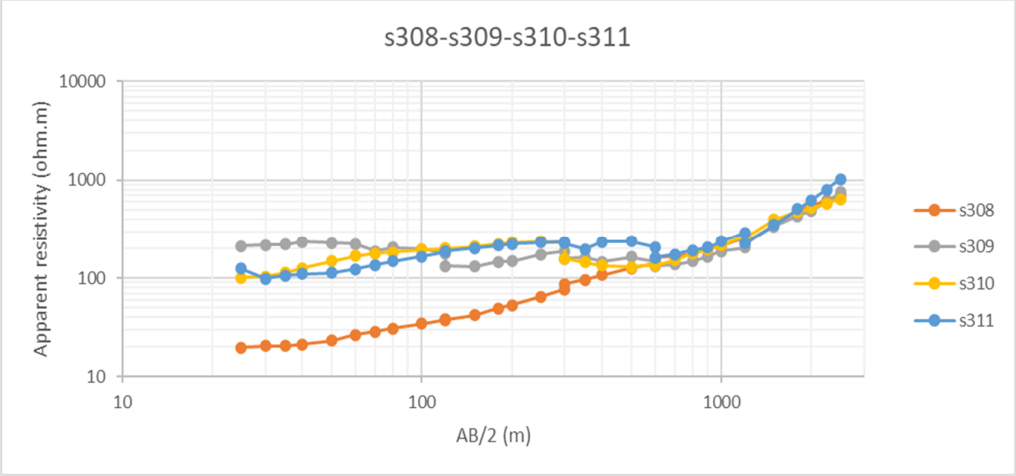
s308-s309-s310-s311
Apparent resistivity (ohm.m)
10000
1000
100
10
10
100
1000
AB/2 (m)
s308
s309
s310
s311

Group 15:

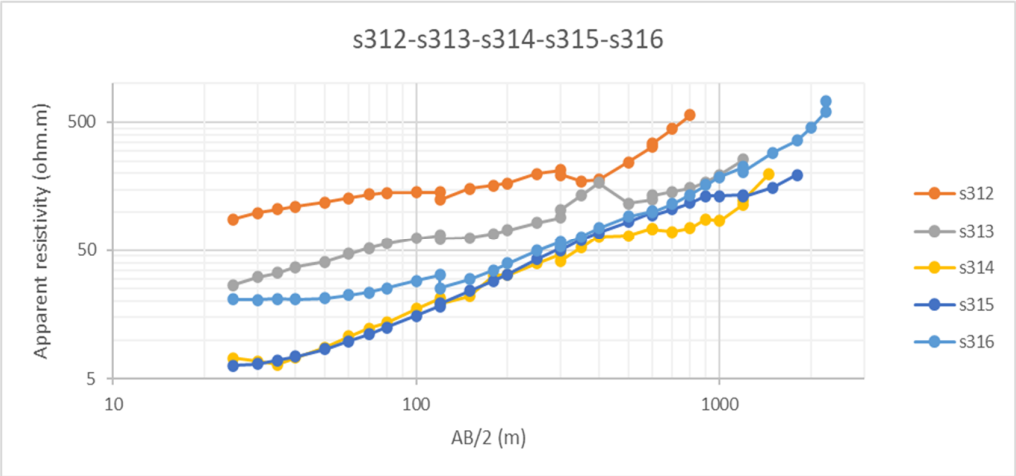
s312-s313-s314-s315-s316
Apparent resistivity (ohm.m)
500
50
5
10
100
1000
AB/2 (m)
s312
s313
s314
s315
s316

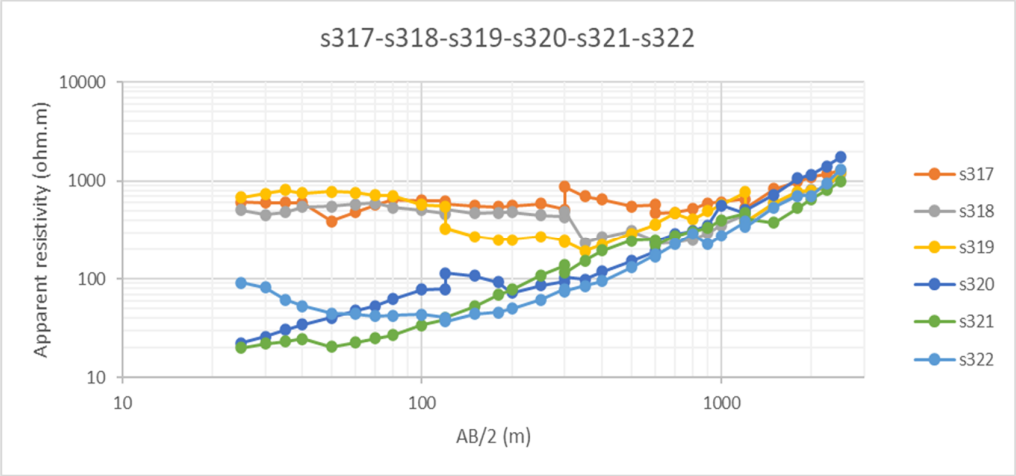
s317-s318-s319-s320-s321-s322
Apparent resistivity (ohm.m)
10000
1000
100
10
10
100
1000
AB/2 (m)
s317
s318
s319
s320
s321
s322

Group 16:

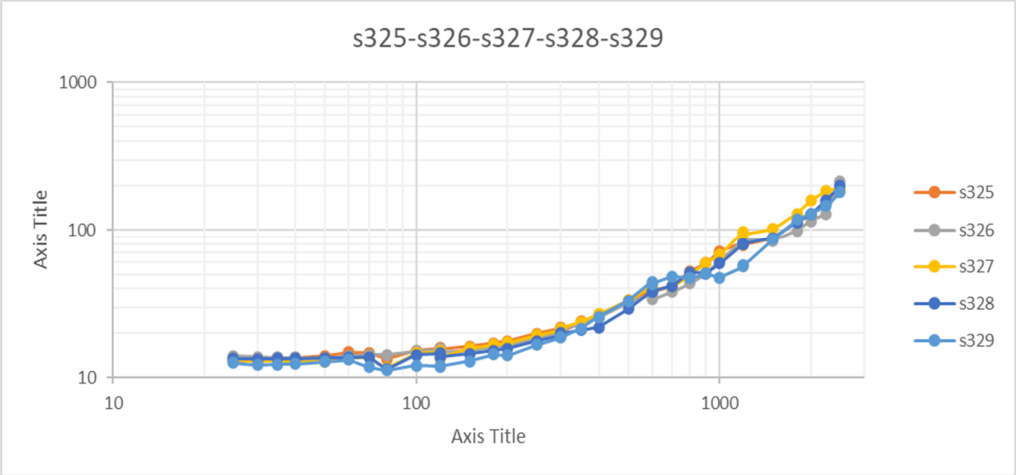
s325-s326-s327-s328-s329
Axis Title
1000
100
10
10
100
1000
Axis Title
s325
s326
s327
s328
s329

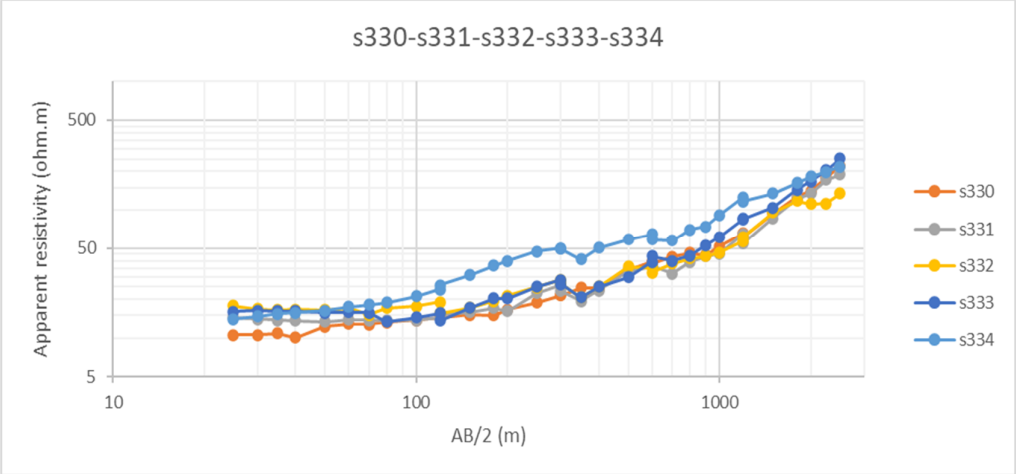
s330-s331-s332-s333-s334
Apparent resistivity (ohm.m)
500
50
5
10
100
1000
AB/2 (m)
s330
s331
s332
s333
s334

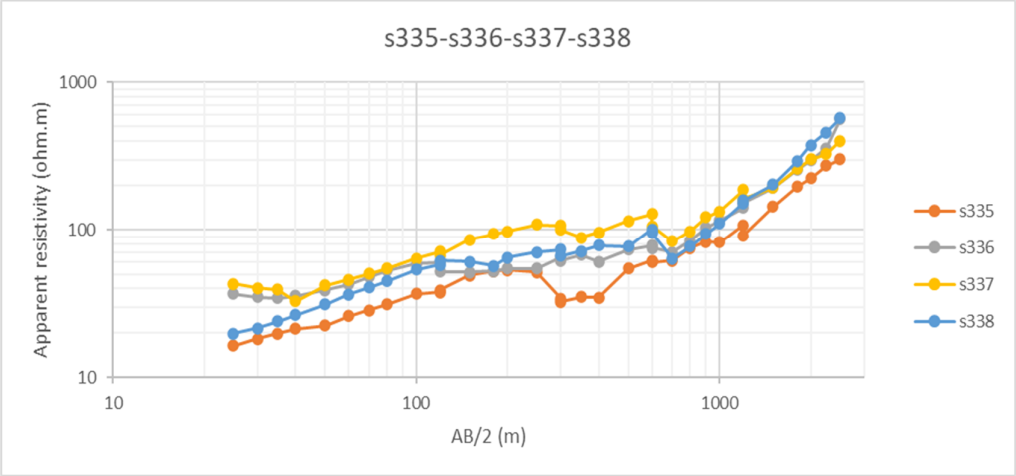
s335-s336-s337-s338
Apparent resistivity (ohm.m)
1000
100
10
10
100
1000
AB/2 (m)
s335
s336
s337
s338

Group 17:

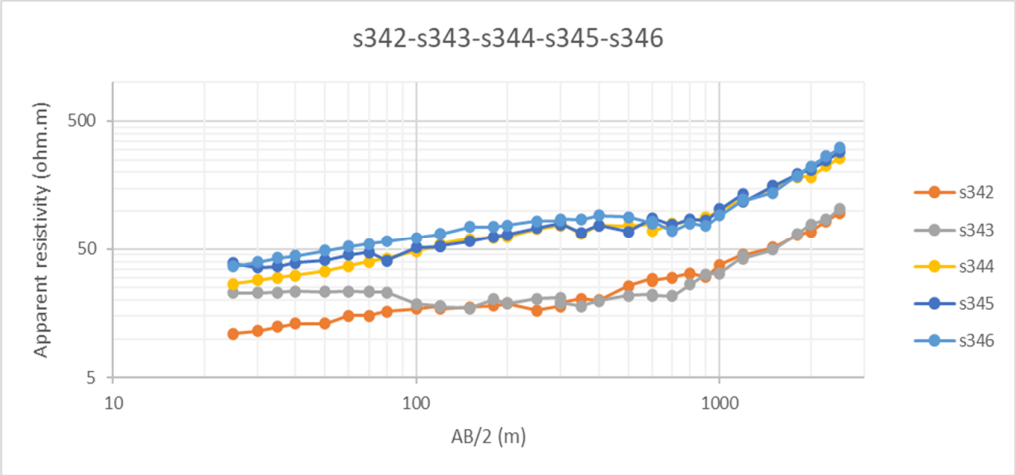
s342-s343-s344-s345-s346
Apparent resistivity (ohm.m)
500
50
5
10
100
1000
AB/2 (m)
s342
s343
s344
s345
s346

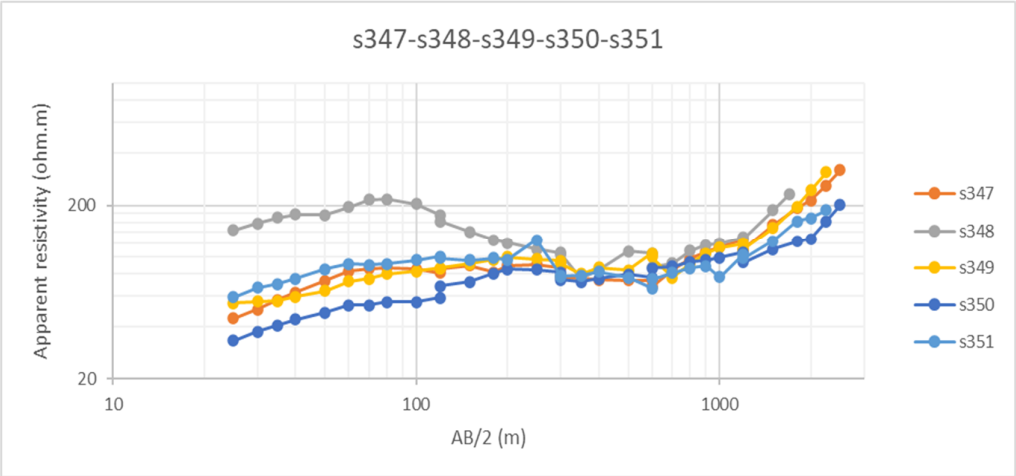
s347-s348-s349-s350-s351
Apparent resistivity (ohm.m)
200
20
10
100
1000
AB/2 (m)
s347
s348
s349
s350
s351

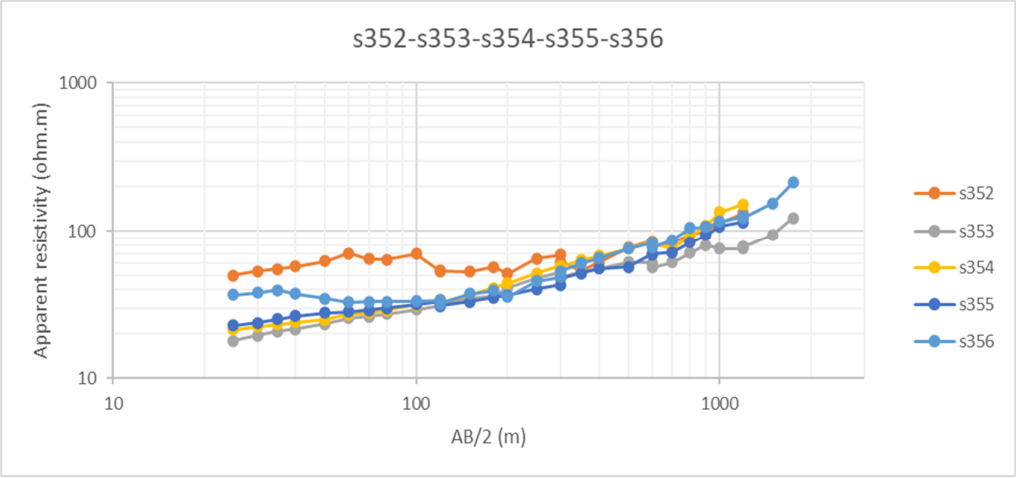
s352-s353-s354-s355-s356
Apparent resistivity (ohm.m)
1000
100
10
10
100
1000
AB/2 (m)
s352
s353
s354
s355
s356

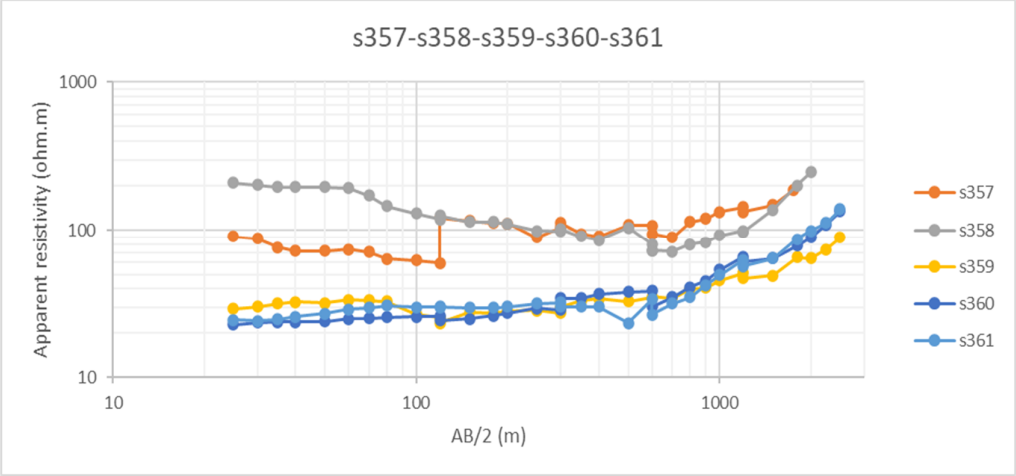
s357-s358-s359-s360-s361
Apparent resistivity (ohm.m)
1000
100
10
10
100
1000
AB/2 (m)
s357
s358
s359
s360
s361

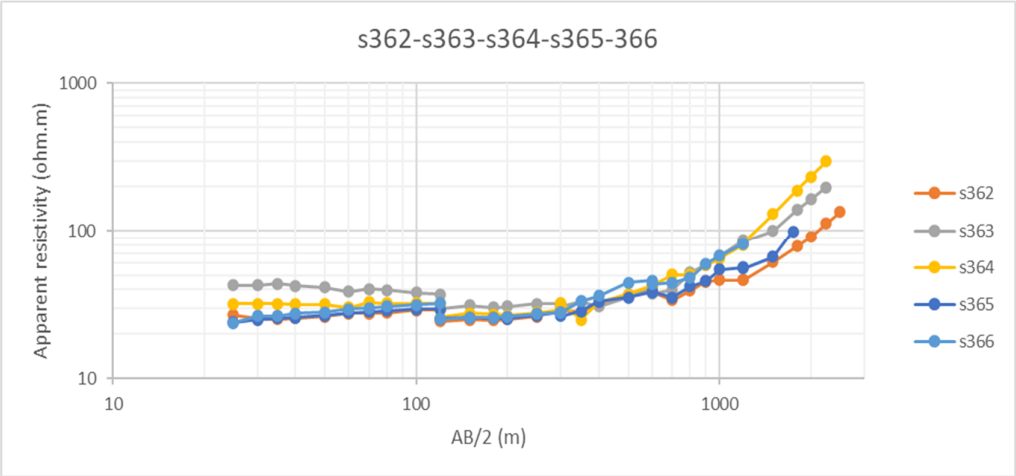
s362-s363-s364-s365-366
Apparent resistivity (ohm.m)
1000
100
10
10
100
1000
AB/2 (m)
s362
s363
s364
s365
s366

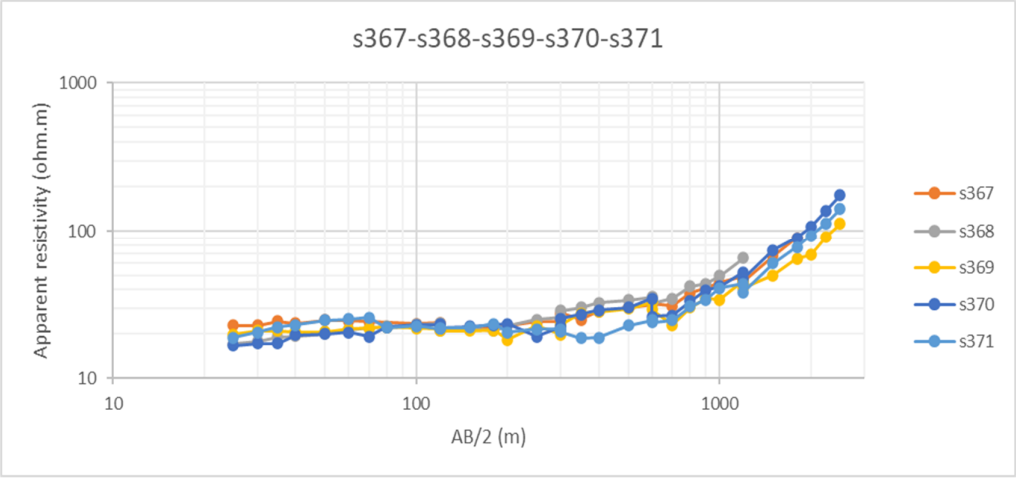
s367-s368-s369-s370-s371
Apparent resistivity (ohm.m)
1000
100
10
10
100
1000
AB/2 (m)
s367
s368
s369
s370
s371

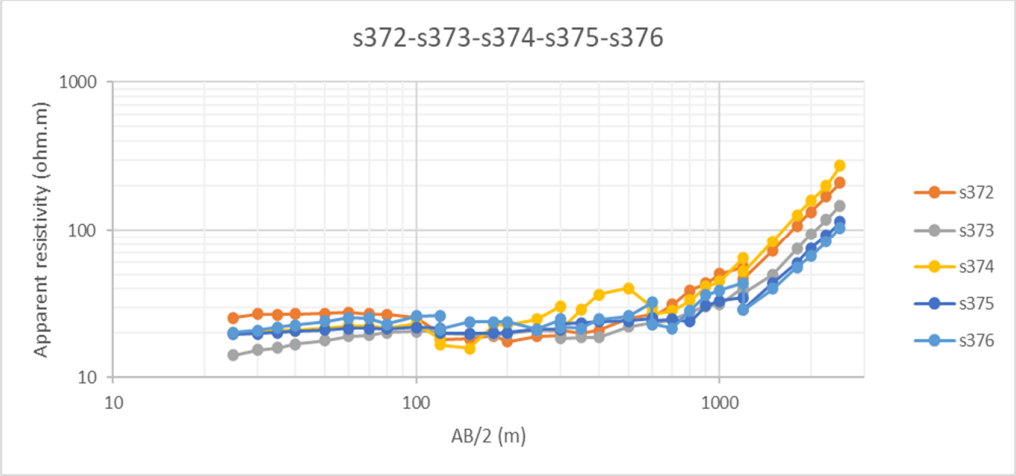
s372-s373-s374-s375-s376
Apparent resistivity (ohm.m)
1000
100
10
10
100
1000
AB/2 (m)
s372
s373
s374
s375
s376

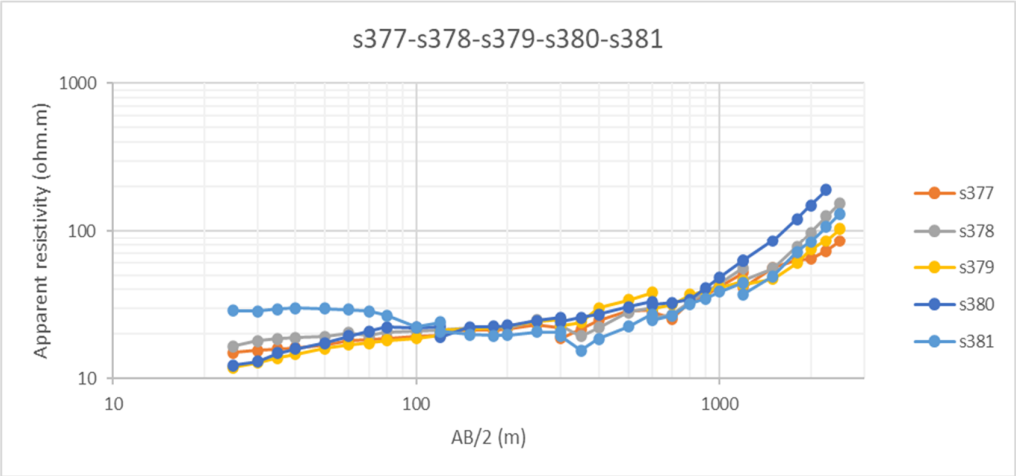
s377-s378-s379-s380-s381
Apparent resistivity (ohm.m)
1000
100
10
10
100
1000
AB/2 (m)
s377
s378
s379
s380
s381

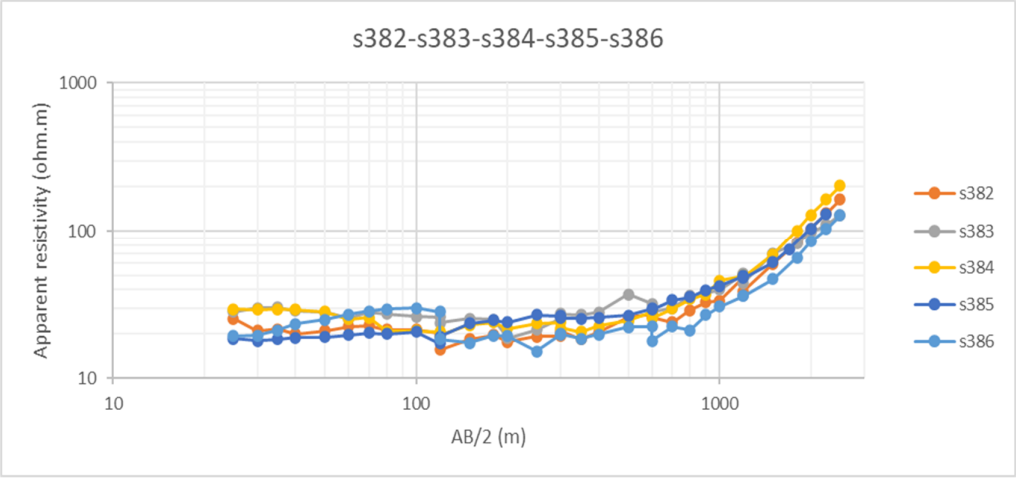
s382-s383-s384-s385-s386
Apparent resistivity (ohm.m)
1000
100
10
10
100
1000
AB/2 (m)
s382
s383
s384
s385
s386

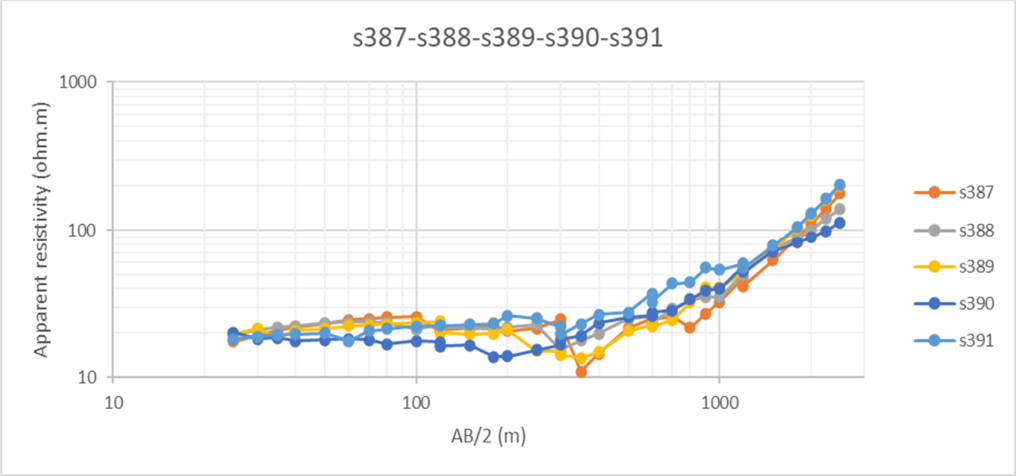
s387-s388-s389-s390-s391
Apparent resistivity (ohm.m)
1000
100
10
10
100
1000
AB/2 (m)
s387
s388
s389
s390
s391

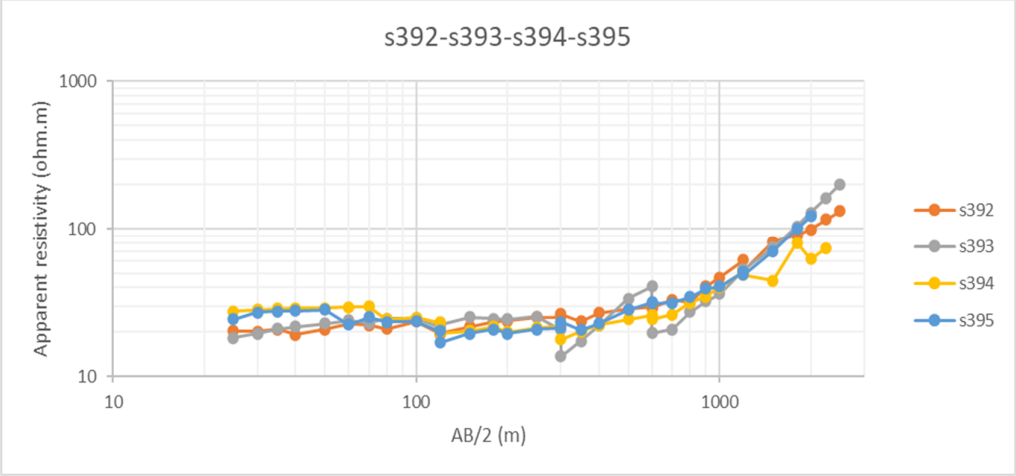
s392-s393-s394-s395
Apparent resistivity (ohm.m)
1000
100
10
10
100
1000
AB/2 (m)
s392
s393
s394
s395

REMOVAL OFFSETS&SMOOTHING DATA

Group 1:

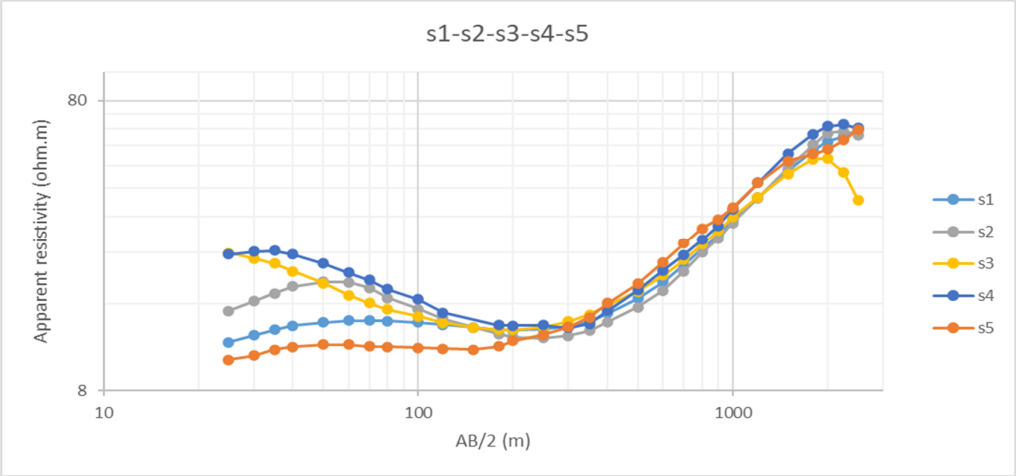

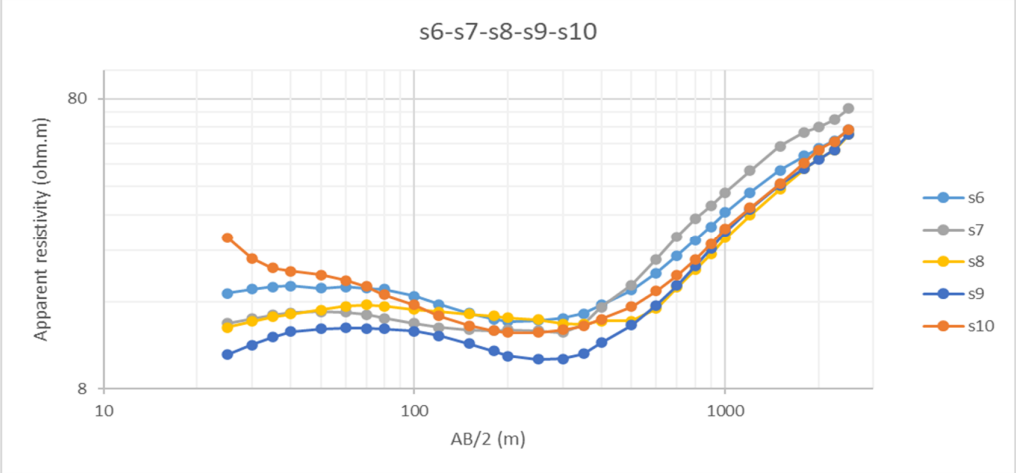

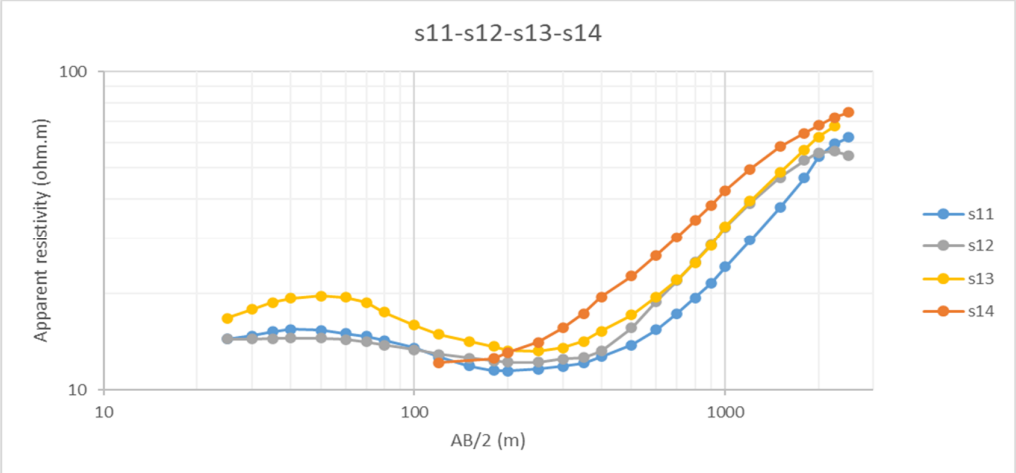

Group 2:

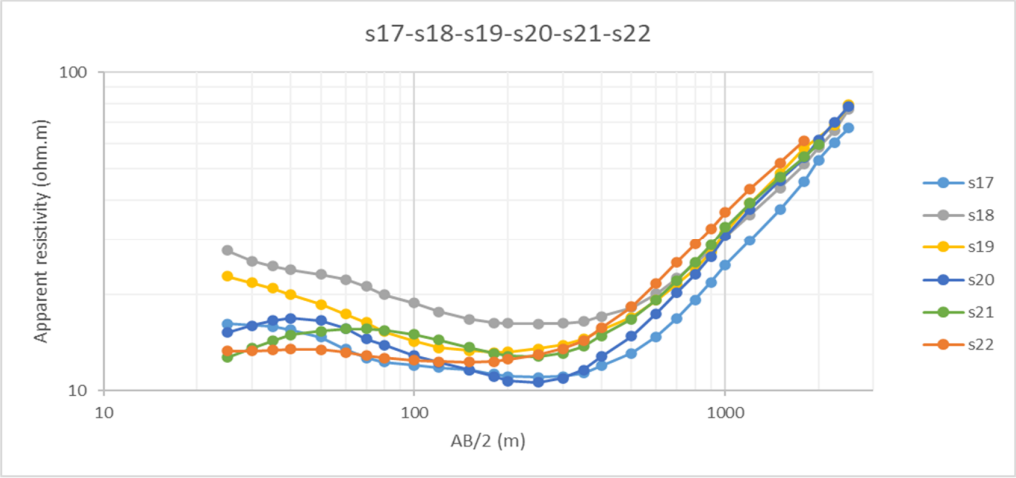

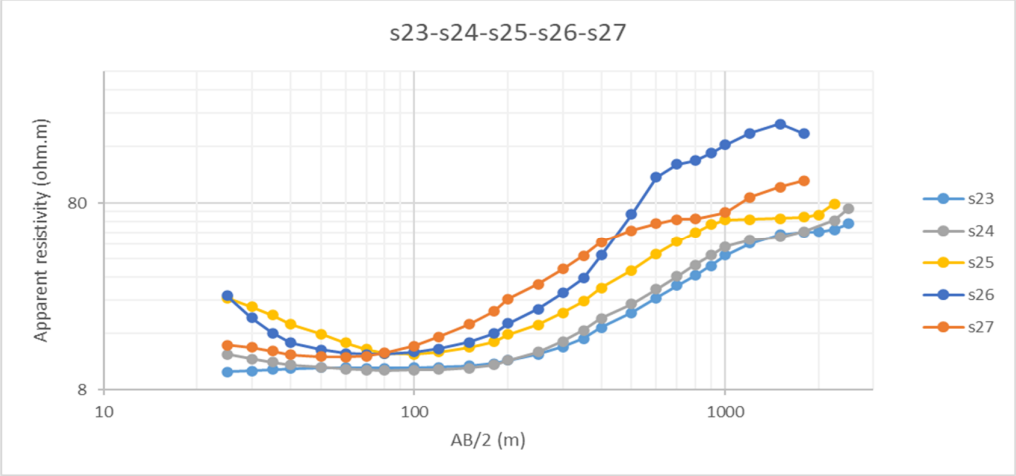

Group 3:

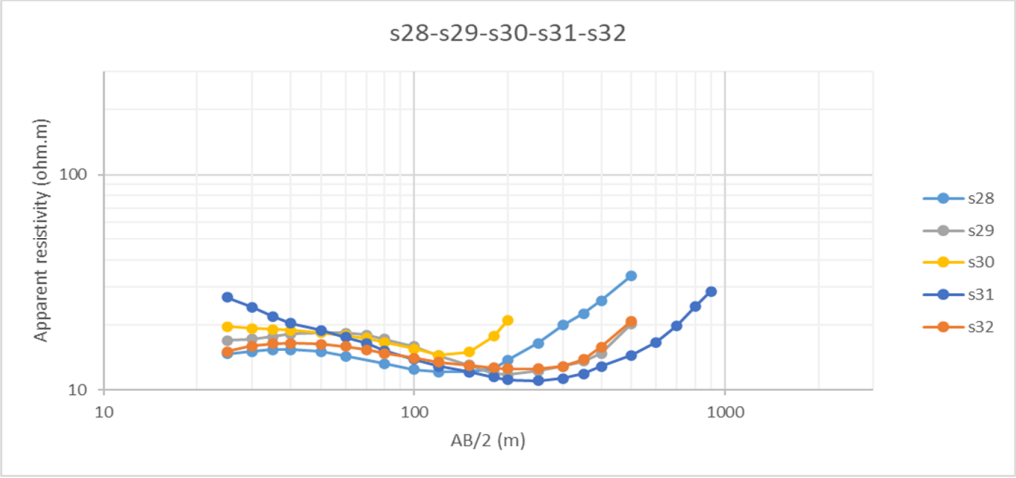

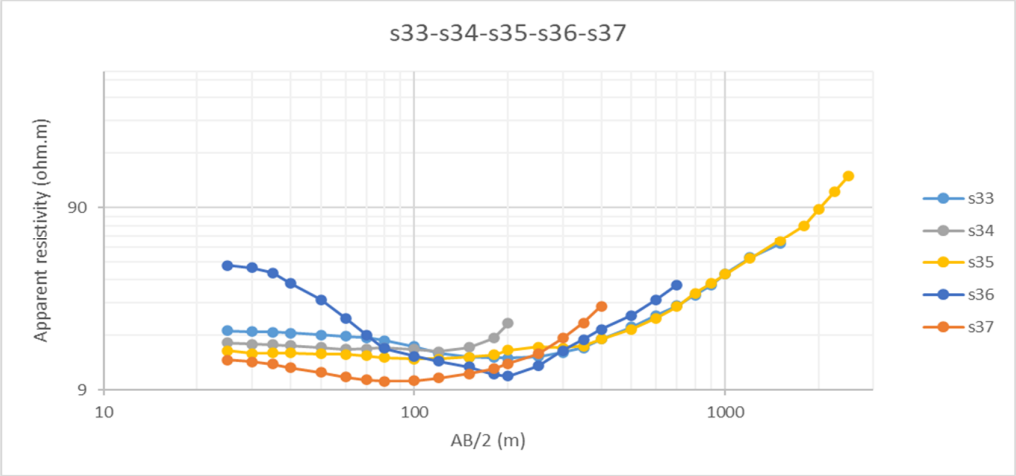
s33-s34-s35-s36-s37
Apparent resistivity (ohm.m)
90
9
10
100
1000
AB/2 (m)
s33
s34
s35
s36
s37

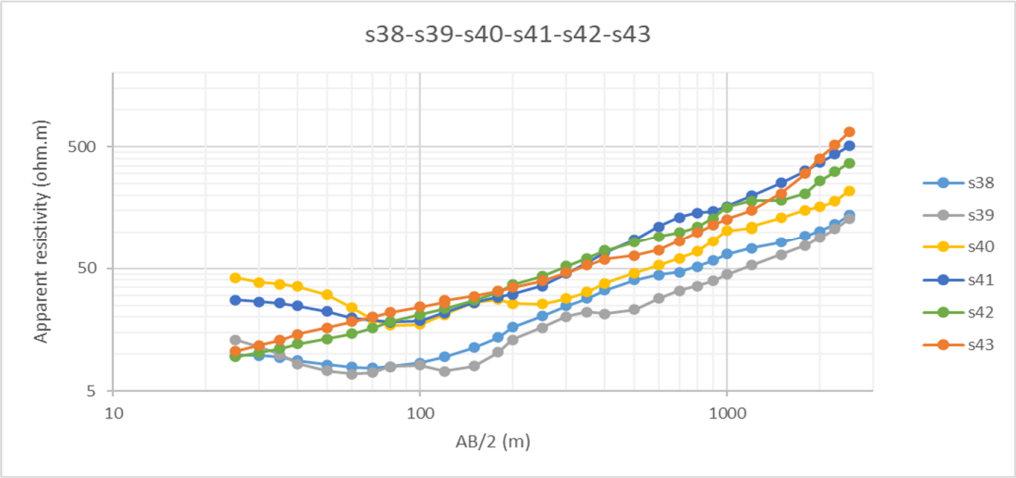
s38-s39-s40-s41-s42-s43
Apparent resistivity (ohm.m)
500
50
5
10
100
1000
AB/2 (m)
s38
s39
s40
s41
s42
s43

Group 4:

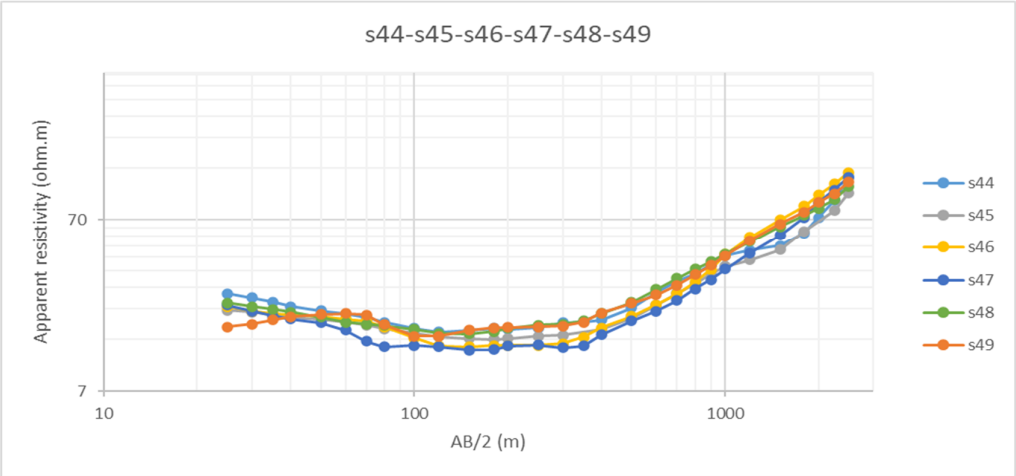
s44-s45-s46-s47-s48-s49
Apparent resistivity (ohm.m)
70
7
10
100
1000
AB/2 (m)
s44
s45
s46
s47
s48
s49

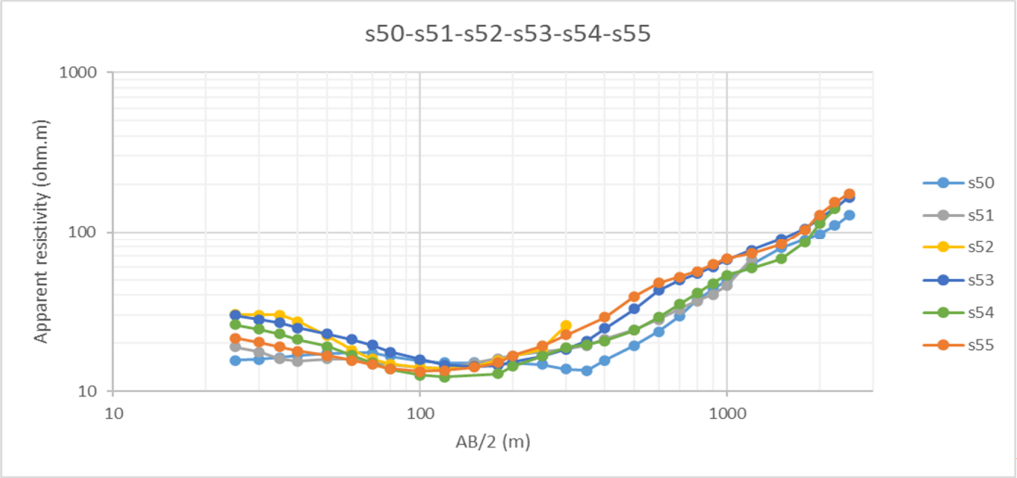
s50-s51-s52-s53-s54-s55
Apparent resistivity (ohm.m)
1000
100
10
10
100
1000
AB/2 (m)
s50
s51
s52
s53
s54
s55

Group 6:

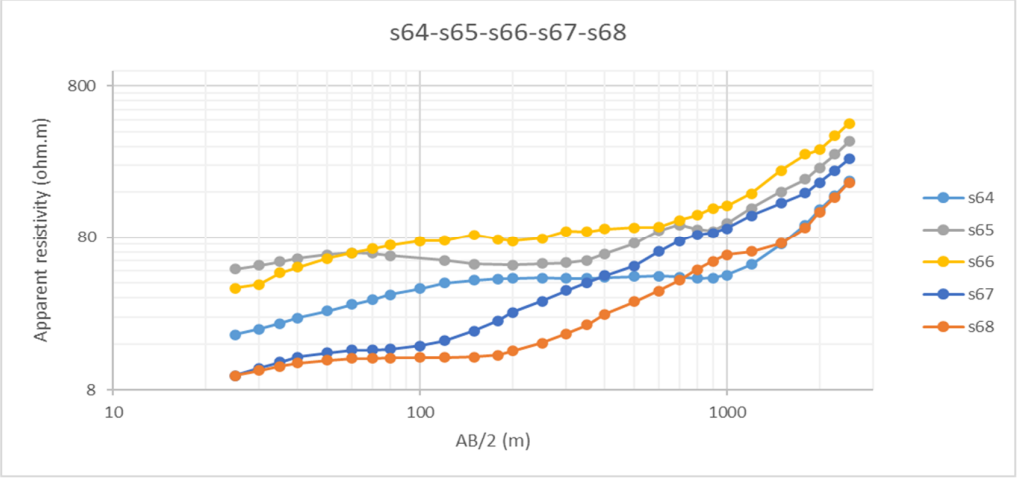
s64-s65-s66-s67-s68
Apparent resistivity (ohm.m)
800
80
8
10
100
1000
AB/2 (m)
s64
s65
s66
s67
s68

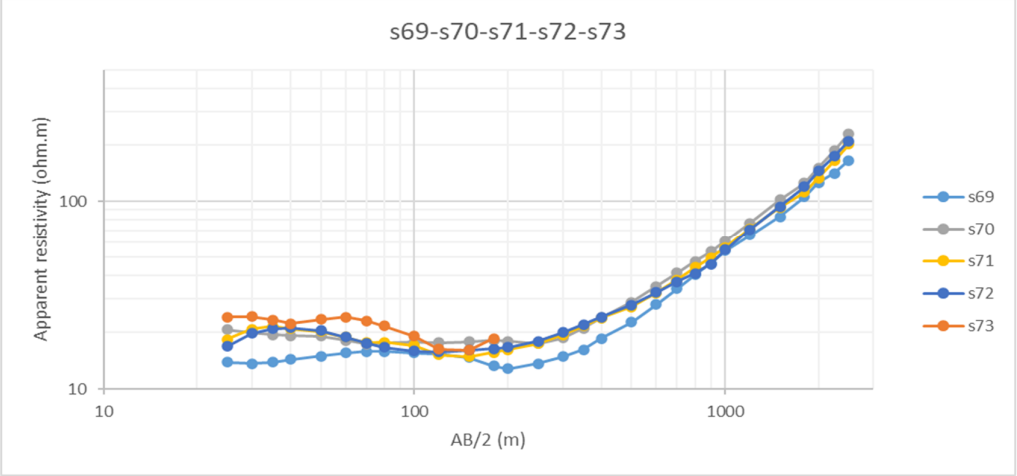
s69-s70-s71-s72-s73
Apparent resistivity (ohm.m)
100
10
10
100
1000
AB/2 (m)
s69
s70
s71
s72
s73

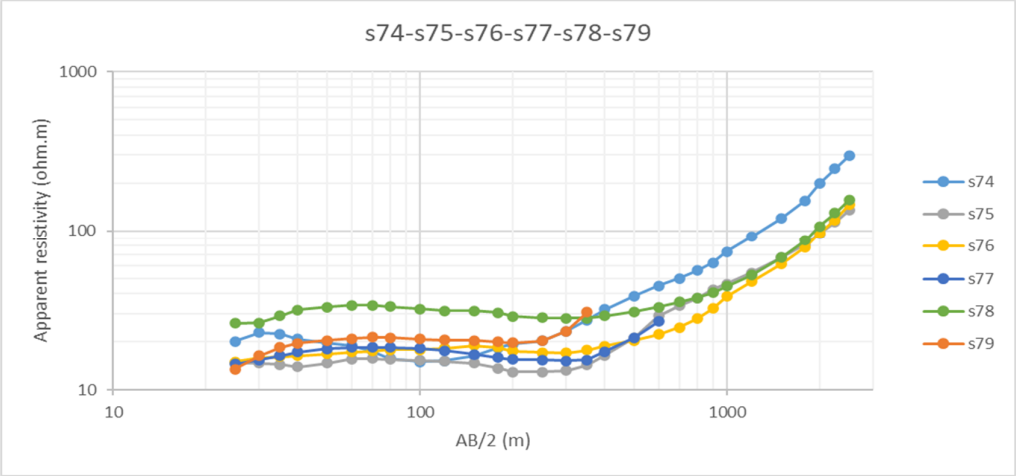
s74-s75-s76-s77-s78-s79
Apparent resistivity (ohm.m)
1000
100
10
10
100
1000
AB/2 (m)
s74
s75
s76
s77
s78
s79

Group 7:

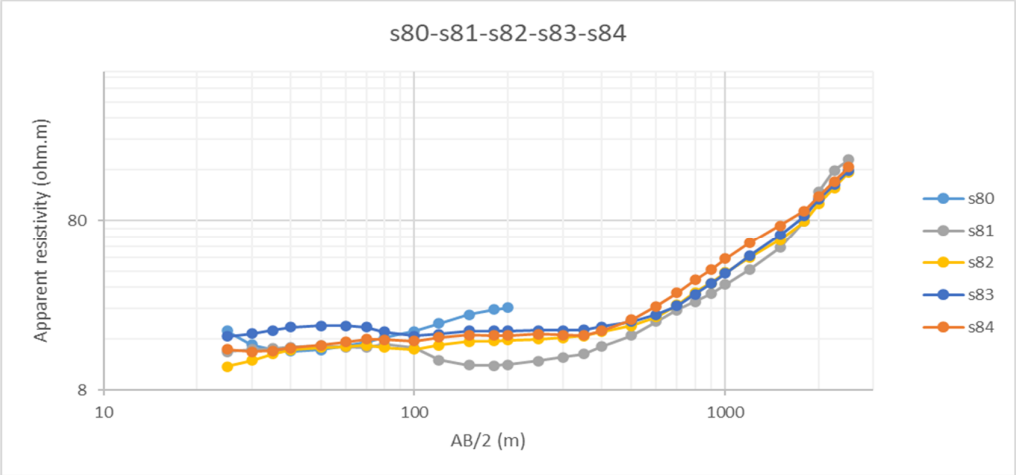
s80-s81-s82-s83-s84
Apparent resistivity (ohm.m)
80
8
10
100
1000
AB/2 (m)
s80
s81
s82
s83
s84

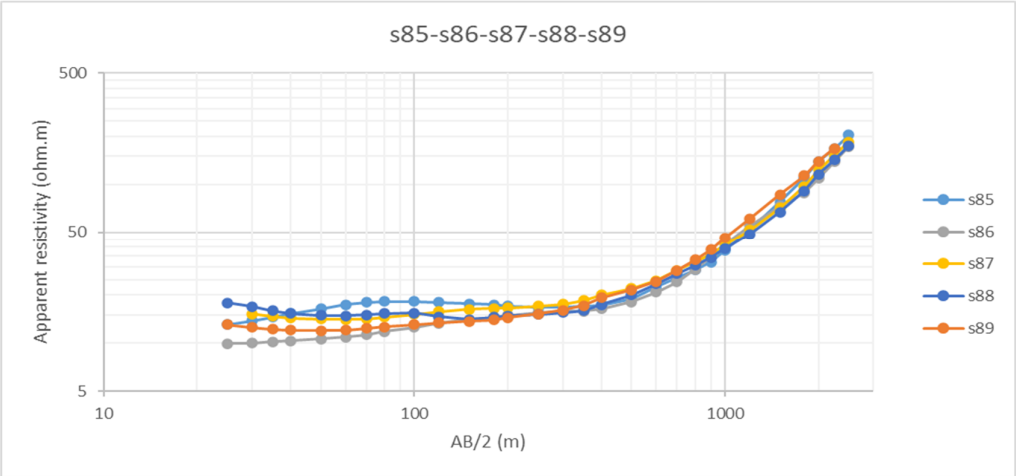
s85-s86-s87-s88-s89
Apparent resistivity (ohm.m)
500
50
5
10
100
1000
AB/2 (m)
s85
s86
s87
s88
s89

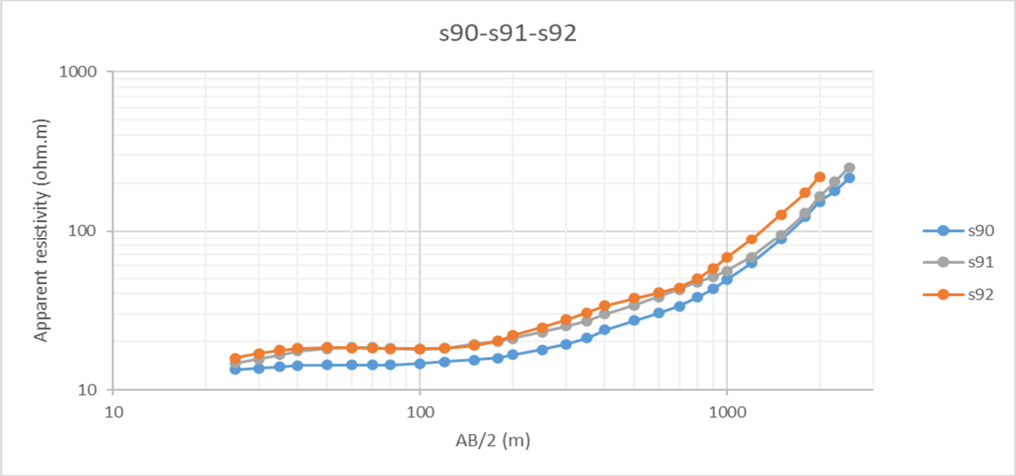
s90-s91-s92
Apparent resistivity (ohm.m)
1000
100
10
10
100
1000
AB/2 (m)
s90
s91
s92

Group 8:

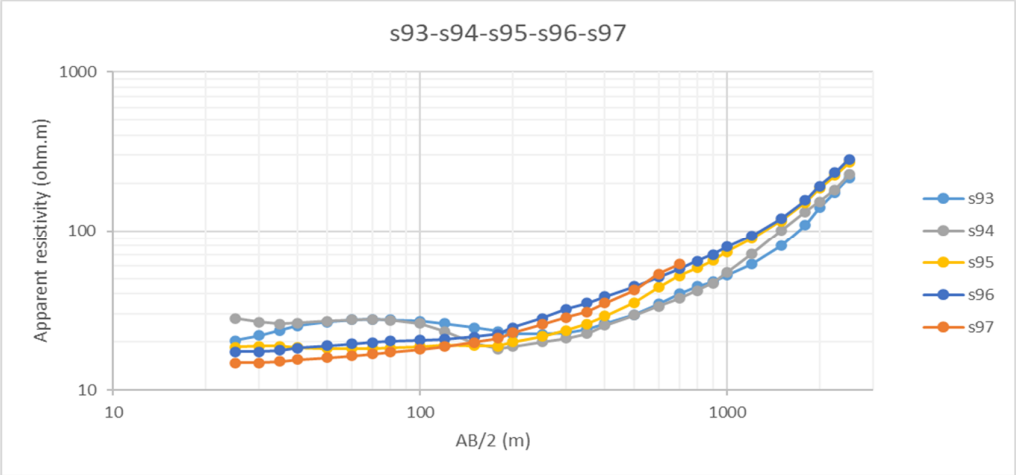
s93-s94-s95-s96-s97
Apparent resistivity (ohm.m)
1000
100
10
10
100
1000
AB/2 (m)
s93
s94
s95
s96
s97

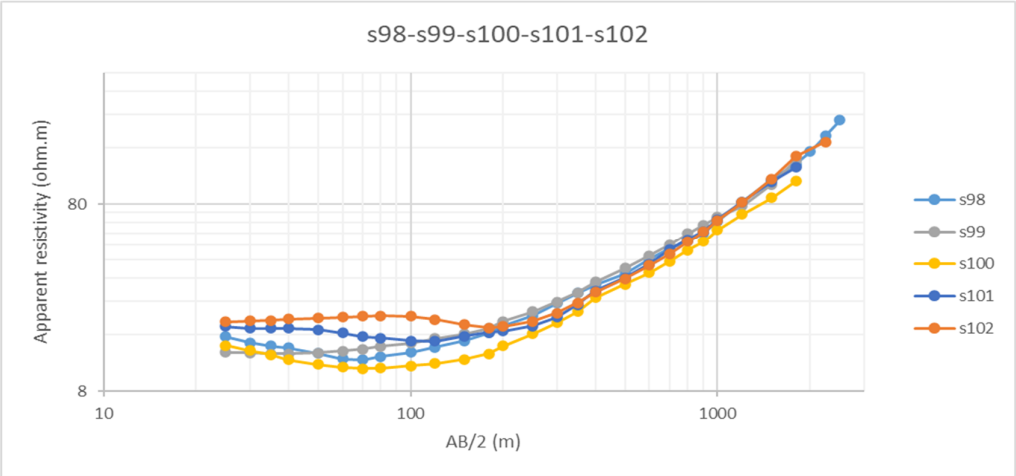
s98-s99-s100-s101-s102
Apparent resistivity (ohm.m)
80
8
10
100
1000
AB/2 (m)
s98
s99
s100
s101
s102

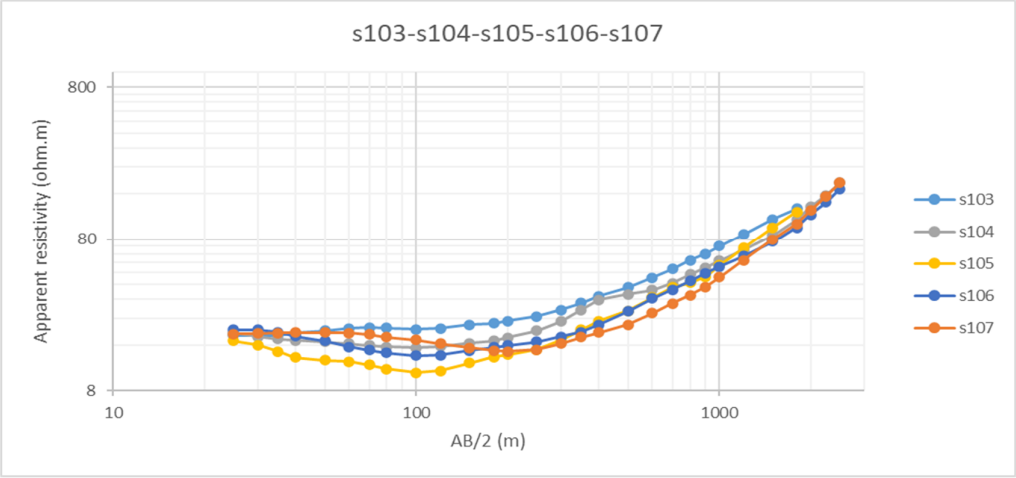
s103-s104-s105-s106-s107
800
80
8
Apparent resistivity (ohm.m)
10
100
1000
AB/2 (m)
s103
s104
s105
s106
s107

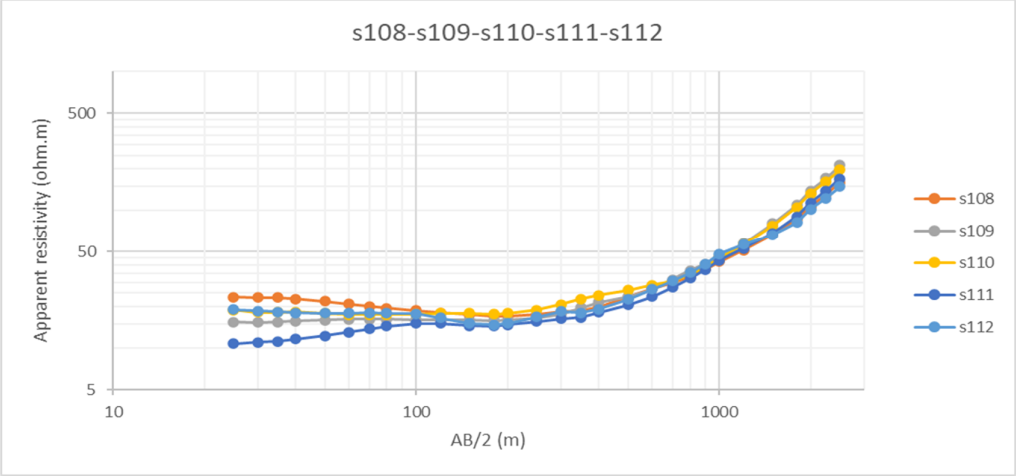
s108-s109-s110-s111-s112
500
50
5
Apparent resistivity (ohm.m)
10
100
1000
AB/2 (m)
s108
s109
s110
s111
s112

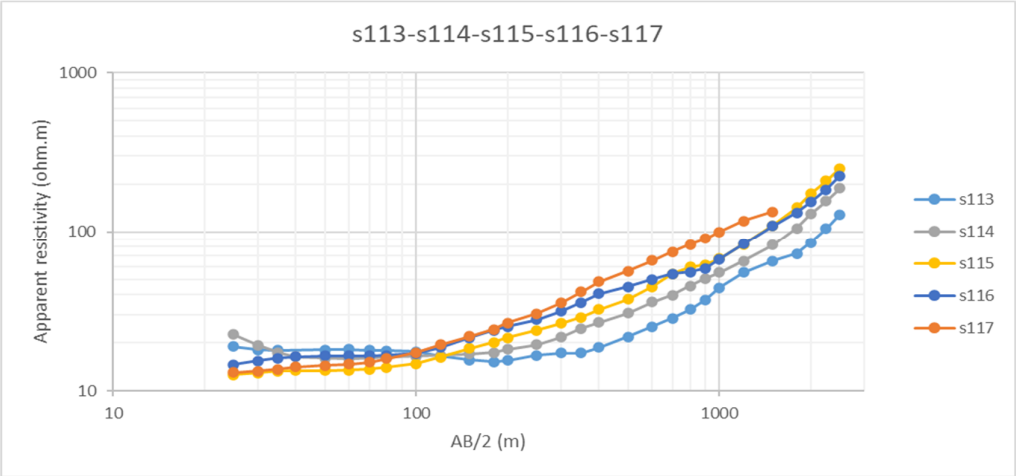
s113-s114-s115-s116-s117
1000
100
10
Apparent resistivity (ohm.m)
10
100
1000
AB/2 (m)
s113
s114
s115
s116
s117

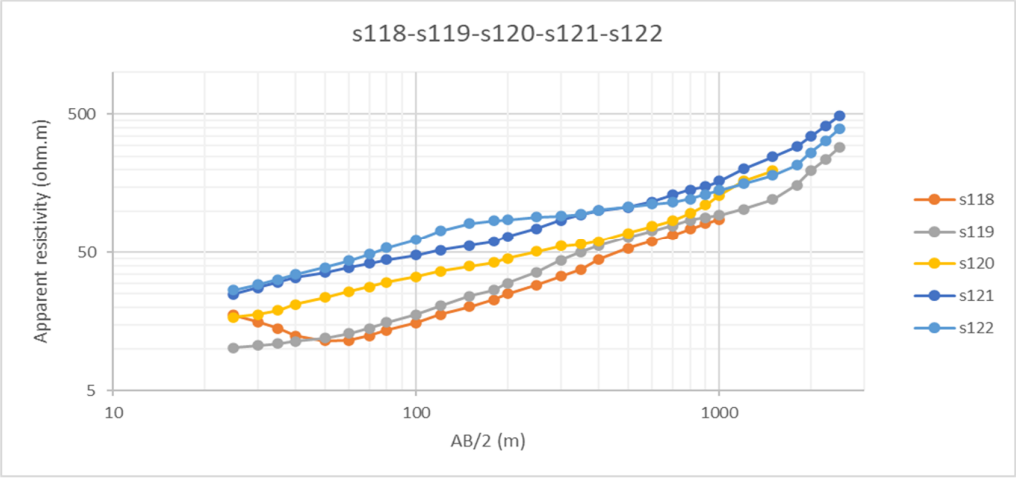
s118-s119-s120-s121-s122
Apparent resistivity (ohm.m)
500
50
5
10
100
1000
AB/2 (m)
s118
s119
s120
s121
s122

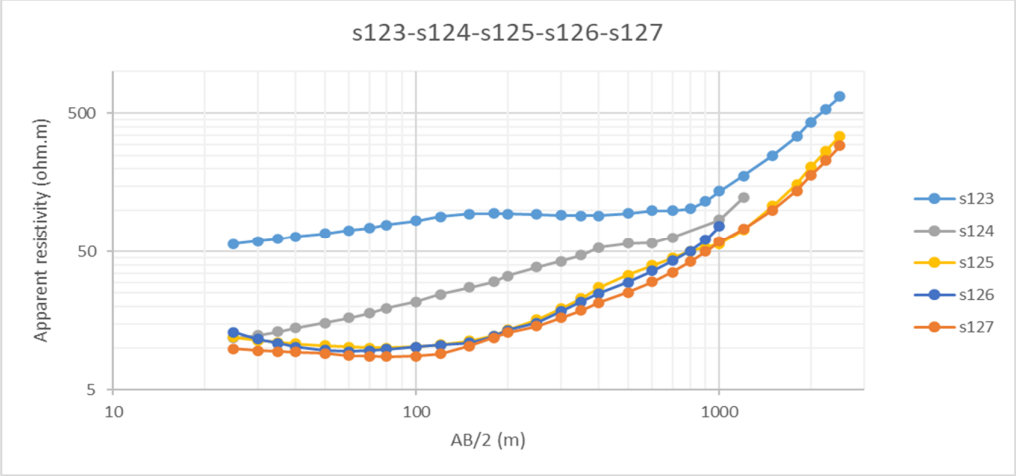
s123-s124-s125-s126-s127
Apparent resistivity (ohm.m)
500
50
5
10
100
1000
AB/2 (m)
s123
s124
s125
s126
s127

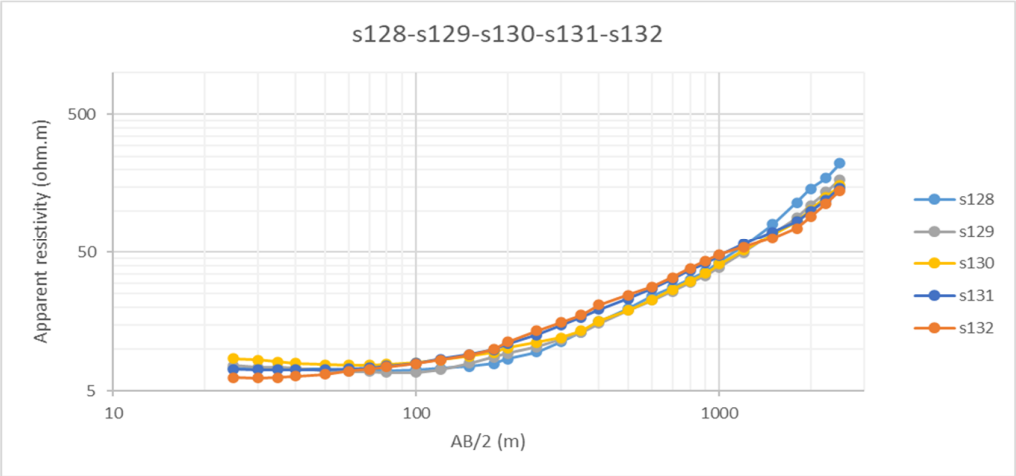
s128-s129-s130-s131-s132
Apparent resistivity (ohm.m)
500
50
5
10
100
1000
AB/2 (m)
s128
s129
s130
s131
s132

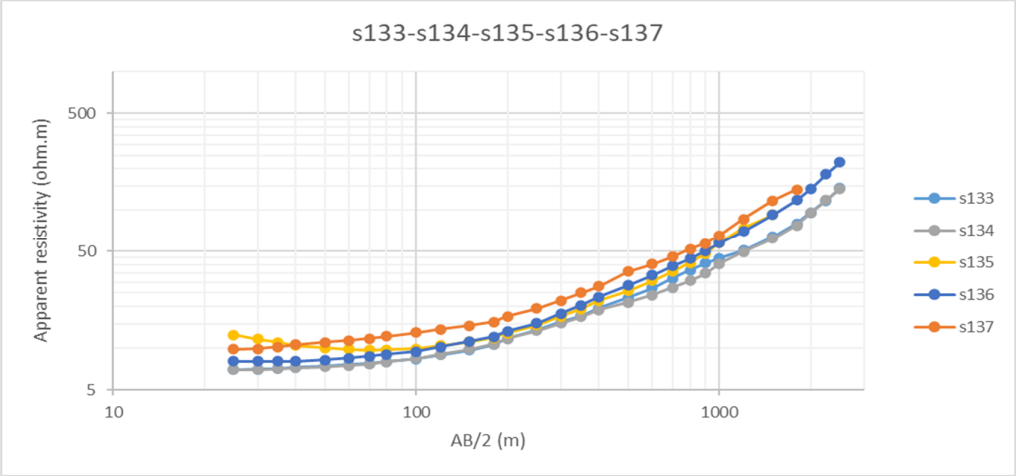
s133-s134-s135-s136-s137
Apparent resistivity (ohm.m)
500
50
5
10
100
1000
AB/2 (m)
s133
s134
s135
s136
s137

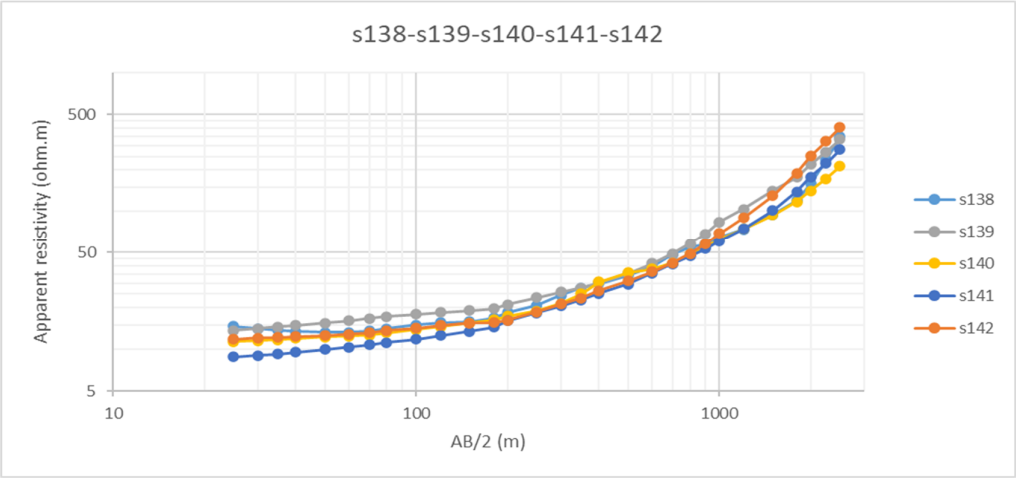
s138-s139-s140-s141-s142
Apparent resistivity (ohm.m)
500
50
5
10
100
1000
AB/2 (m)
s138
s139
s140
s141
s142

Group 9:

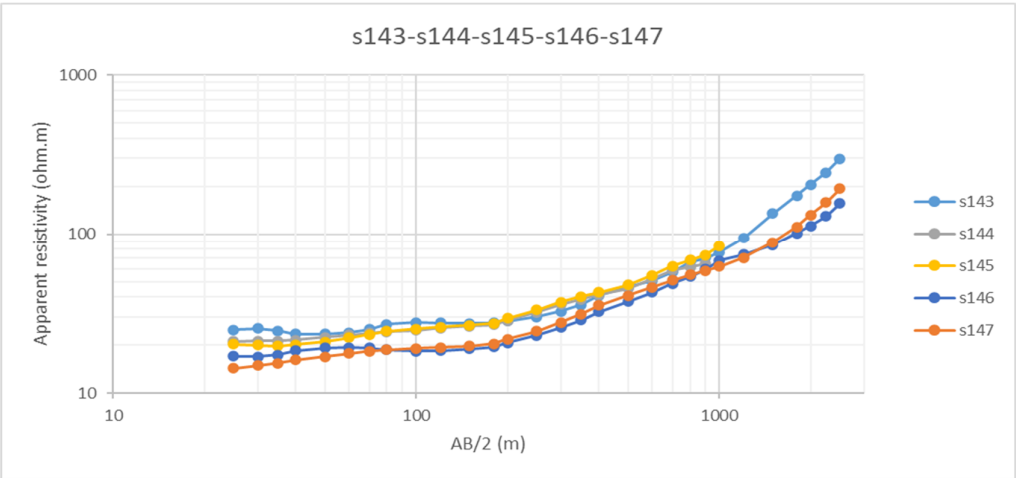
s143-s144-s145-s146-s147
Apparent resistivity (ohm.m)
1000
100
10
10
100
1000
AB/2 (m)
s143
s144
s145
s146
s147

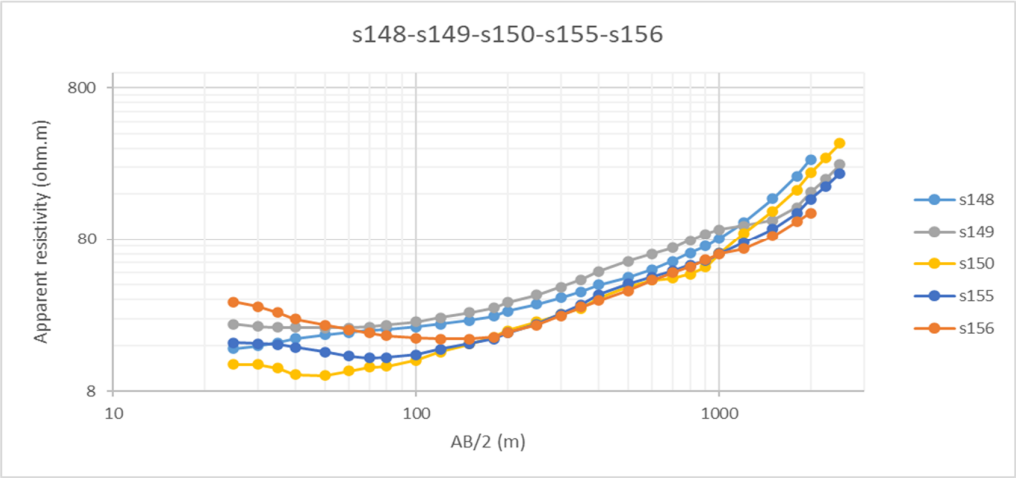
s148-s149-s150-s155-s156
800
80
8
Apparent resistivity (ohm.m)
10
100
1000
AB/2 (m)
s148
s149
s150
s155
s156

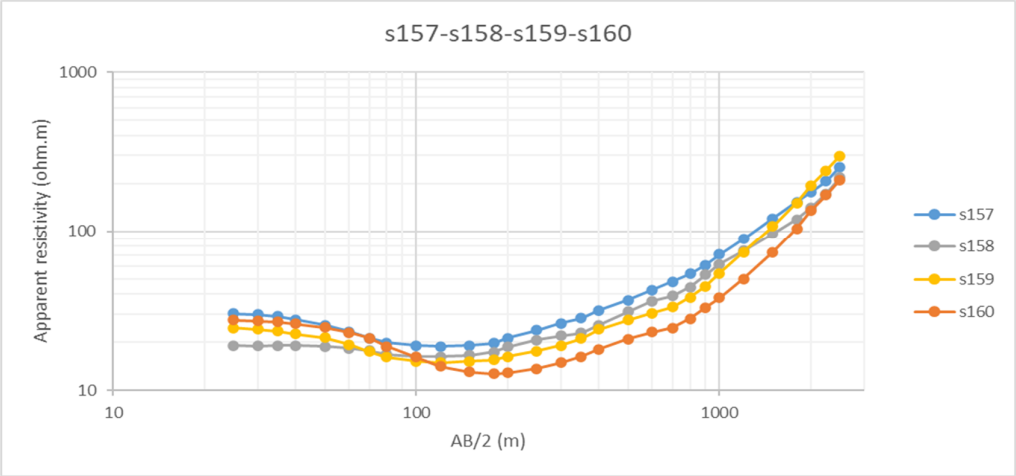
s157-s158-s159-s160
1000
100
10
Apparent resistivity (ohm.m)
10
100
1000
AB/2 (m)
s157
s158
s159
s160

Group 10:

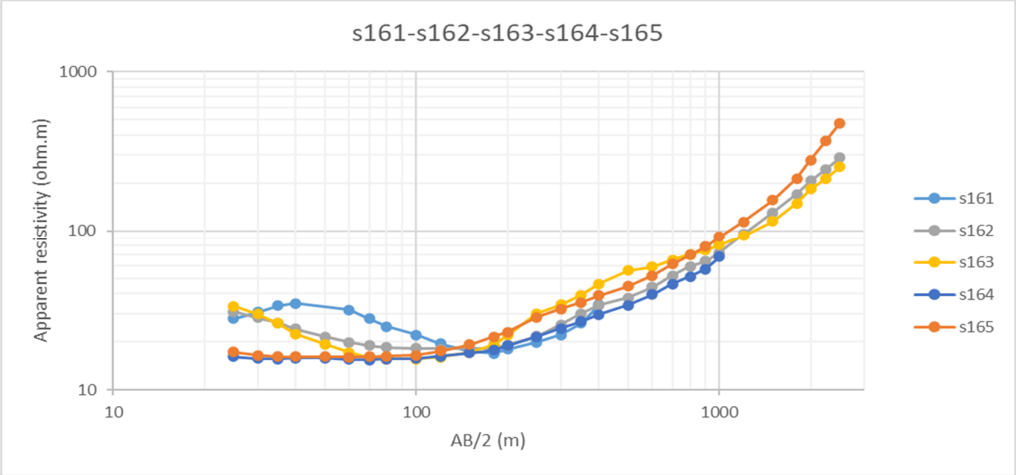
s161-s162-s163-s164-s165
1000
100
10
Apparent resistivity (ohm.m)
10
100
1000
AB/2 (m)
s161
s162
s163
s164
s165

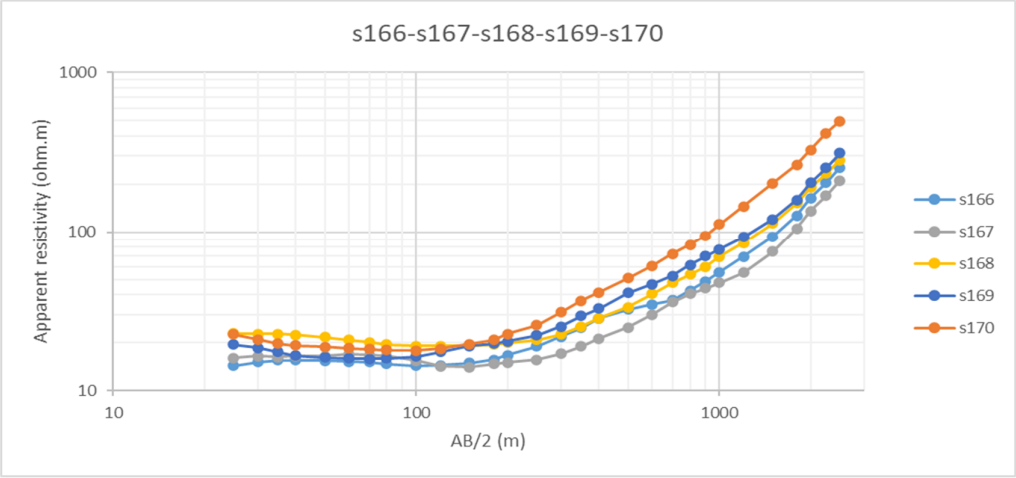
s166-s167-s168-s169-s170
Apparent resistivity (ohm.m)
1000
100
10
10
100
1000
AB/2 (m)
s166
s167
s168
s169
s170

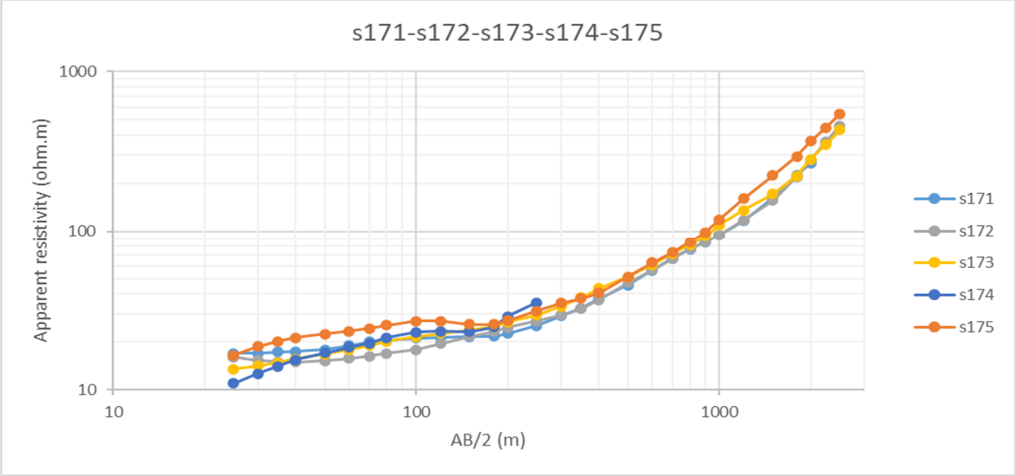
s171-s172-s173-s174-s175
Apparent resistivity (ohm.m)
1000
100
10
10
100
1000
AB/2 (m)
s171
s172
s173
s174
s175

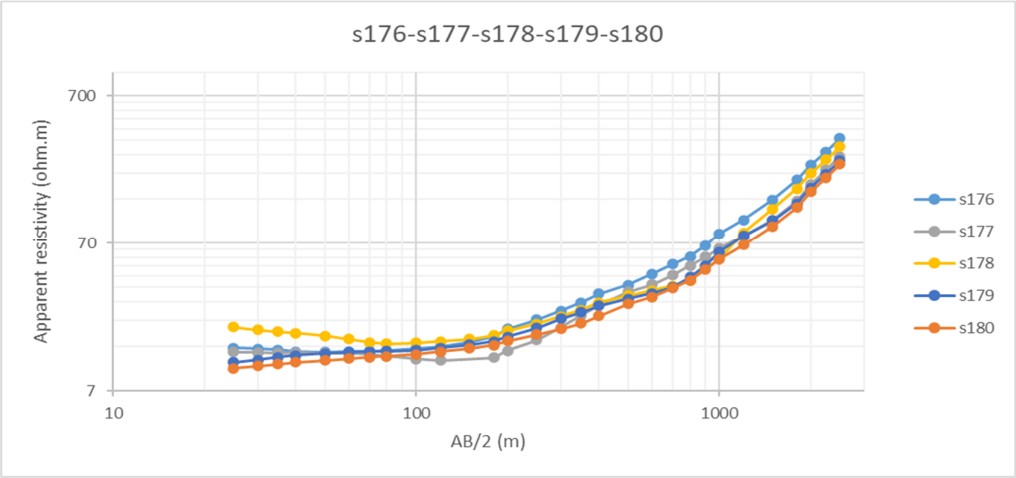
s176-s177-s178-s179-s180
Apparent resistivity (ohm.m)
700
70
7
10
100
1000
AB/2 (m)
s176
s177
s178
s179
s180

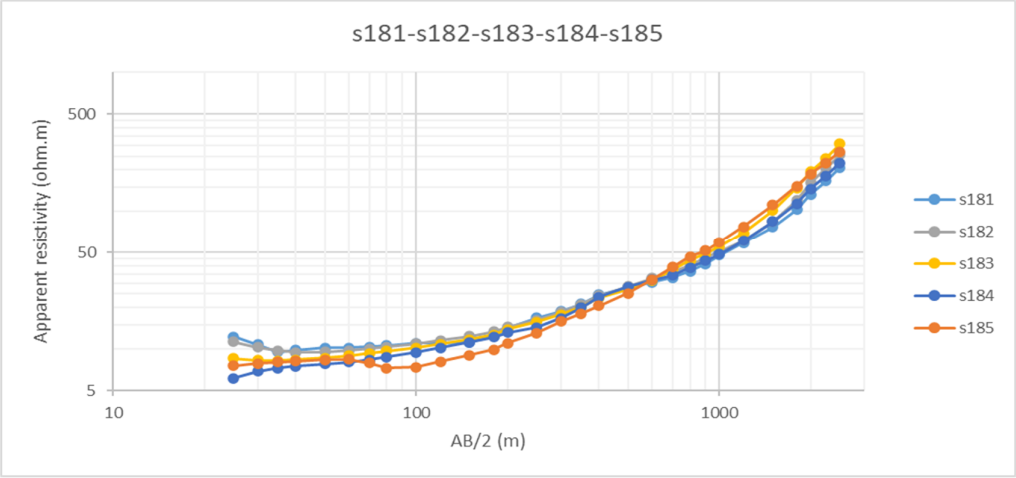
s181-s182-s183-s184-s185
Apparent resistivity (ohm.m)
500
50
5
10
100
1000
AB/2 (m)
s181
s182
s183
s184
s185

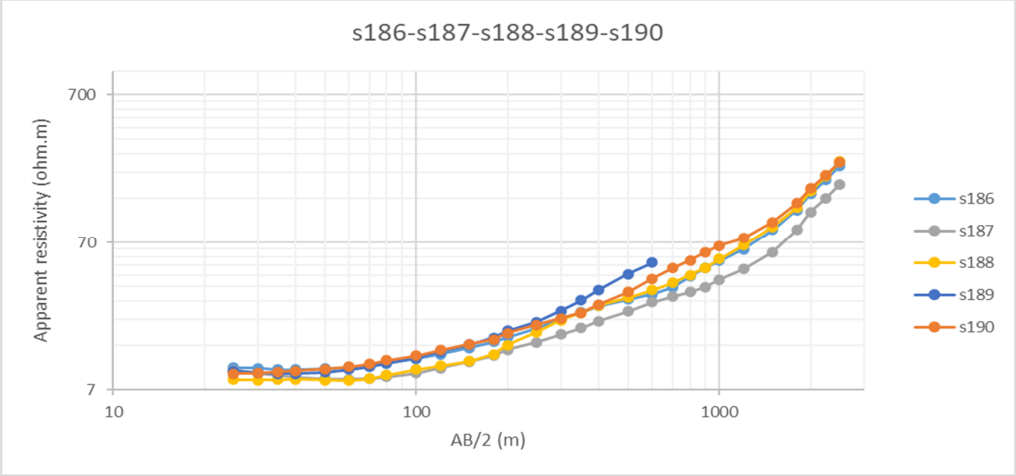
s186-s187-s188-s189-s190
Apparent resistivity (ohm.m)
700
70
7
10
100
1000
AB/2 (m)
s186
s187
s188
s189
s190

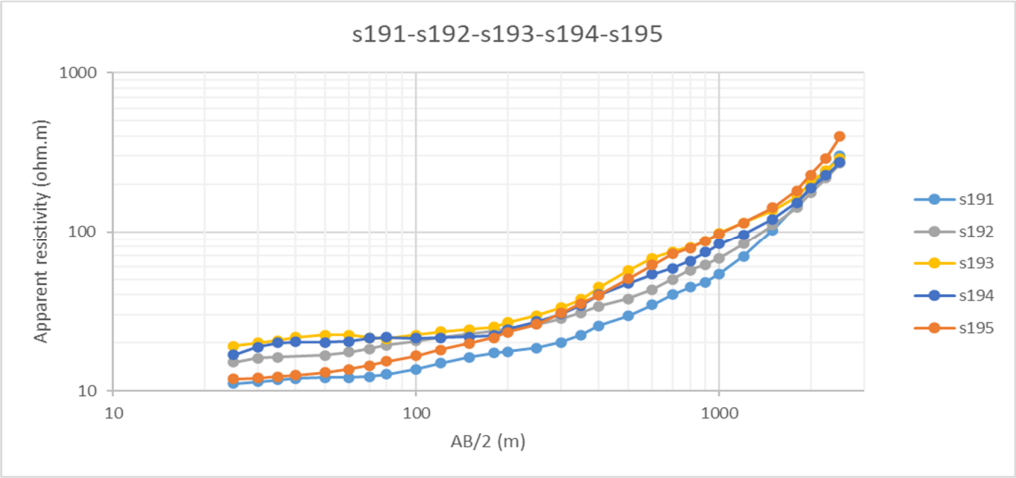
s191-s192-s193-s194-s195
Apparent resistivity (ohm.m)
1000
100
10
10
100
1000
AB/2 (m)
s191
s192
s193
s194
s195

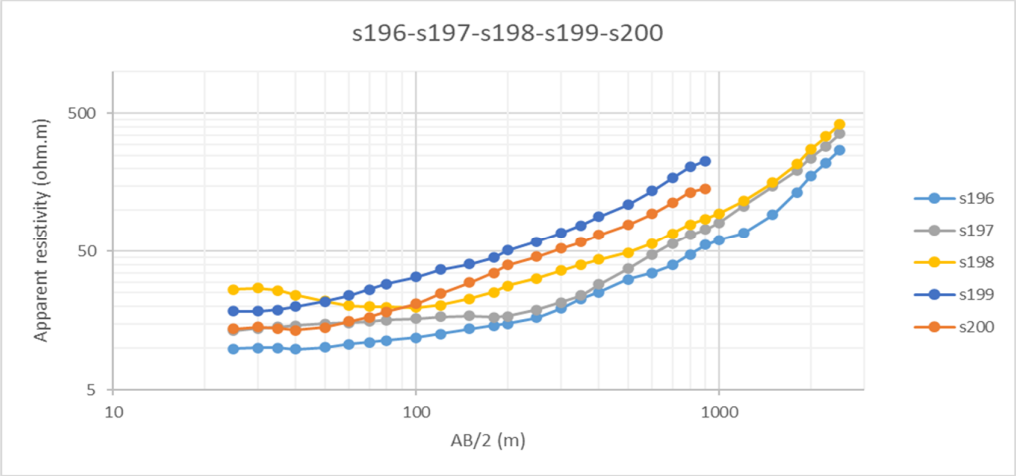
s196-s197-s198-s199-s200
Apparent resistivity (ohm.m)
500
50
5
10
100
1000
AB/2 (m)
s196
s197
s198
s199
s200

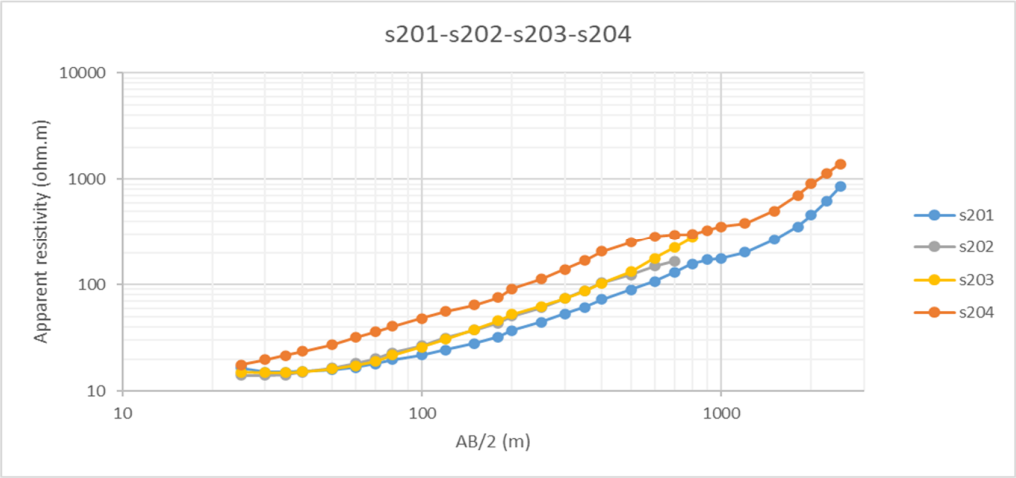
s201-s202-s203-s204
Apparent resistivity (ohm.m)
10000
1000
100
10
10
100
1000
AB/2 (m)
s201
s202
s203
s204

Group 11:

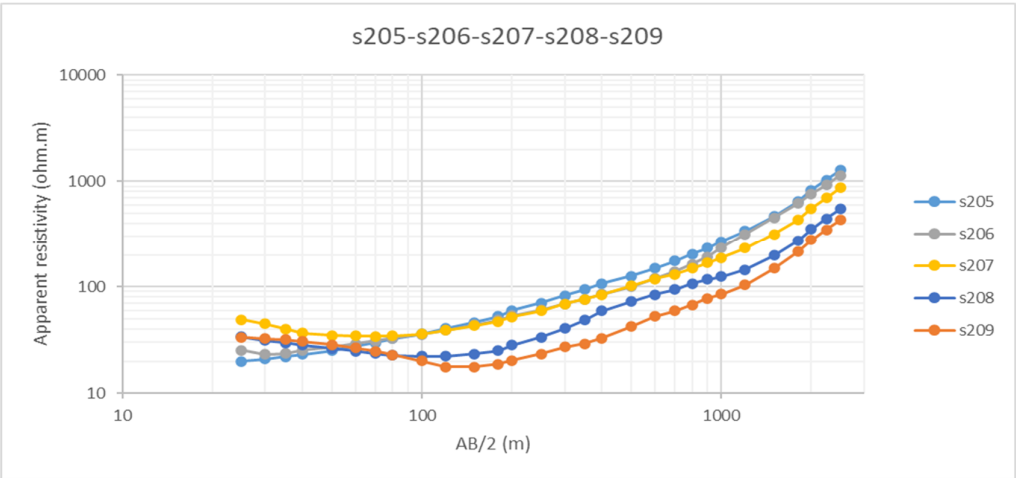
s205-s206-s207-s208-s209
Apparent resistivity (ohm.m)
10000
1000
100
10
10
100
1000
AB/2 (m)
s205
s206
s207
s208
s209

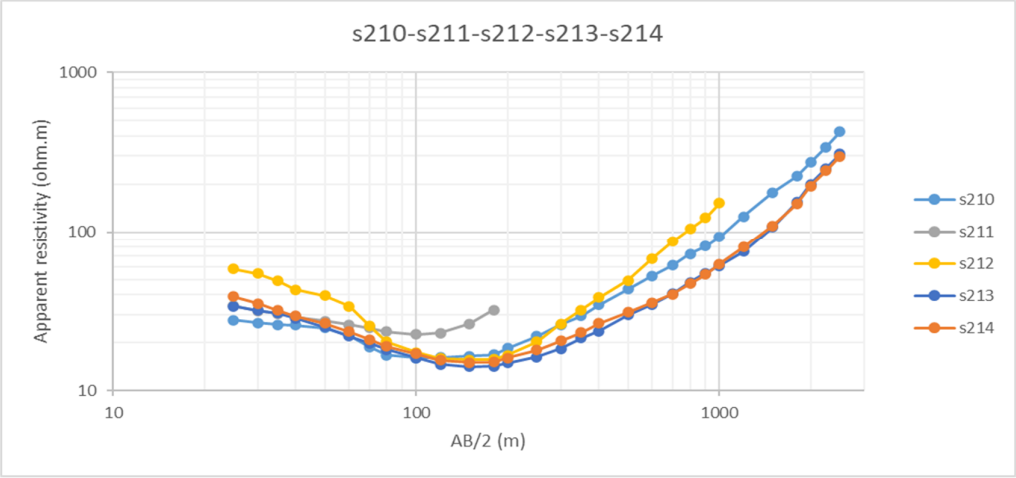
s210-s211-s212-s213-s214
Apparent resistivity (ohm.m)
1000
100
10
10
100
1000
AB/2 (m)
s210
s211
s212
s213
s214

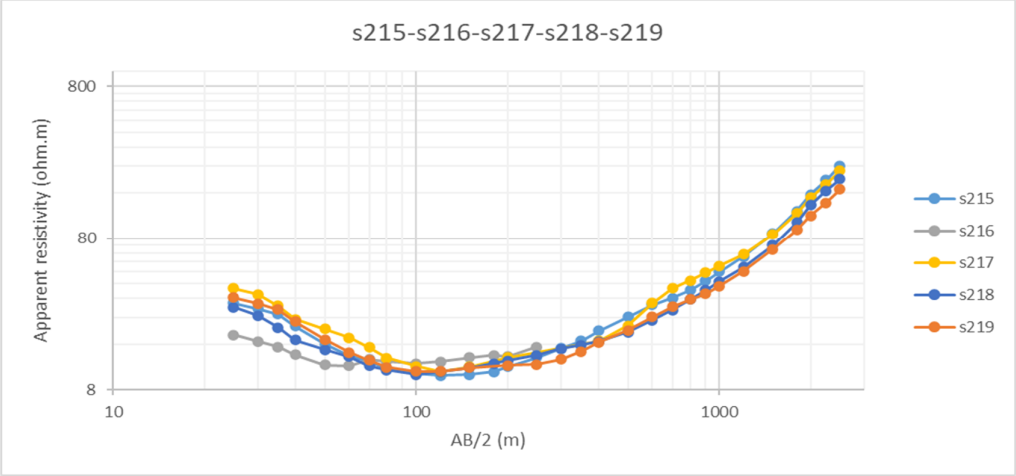
s215-s216-s217-s218-s219
Apparent resistivity (ohm.m)
800
80
8
10
100
1000
AB/2 (m)
s215
s216
s217
s218
s219

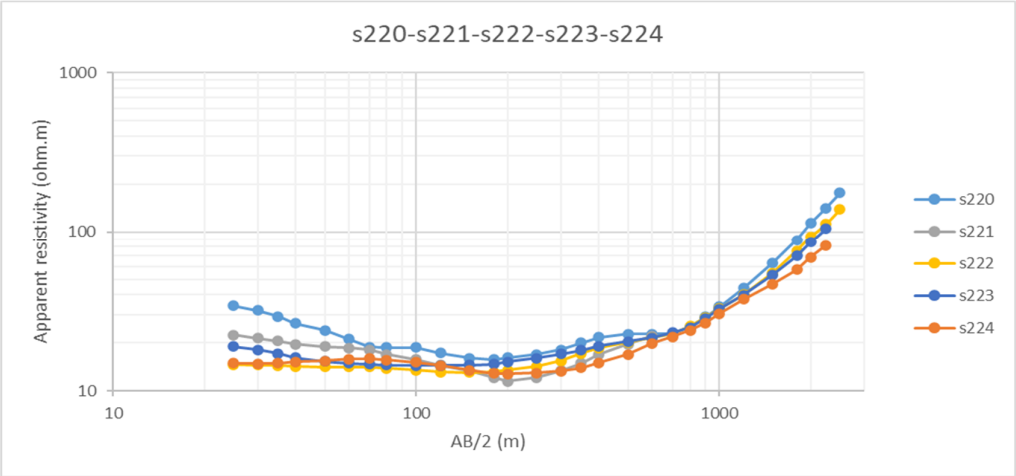
s220-s221-s222-s223-s224
Apparent resistivity (ohm.m)
1000
100
10
10
100
1000
AB/2 (m)
s220
s221
s222
s223
s224

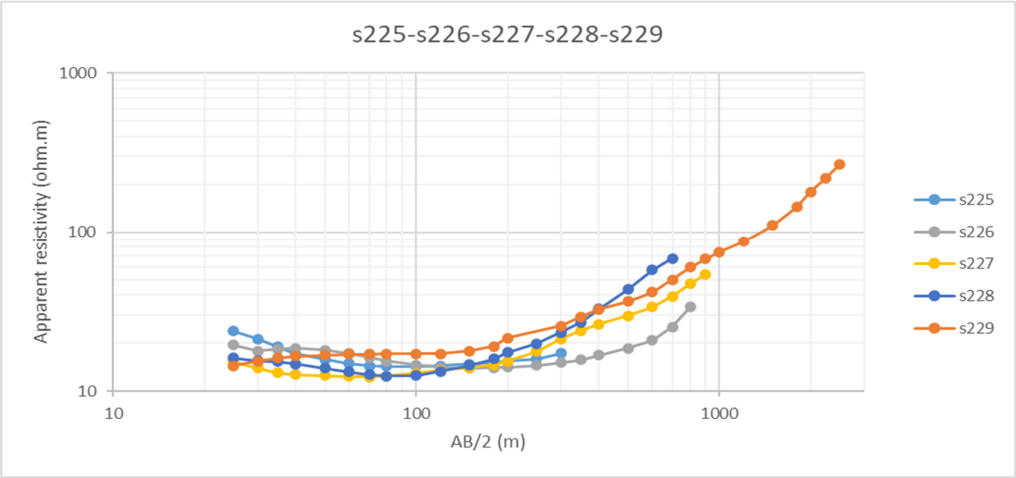
s225-s226-s227-s228-s229
Apparent resistivity (ohm.m)
1000
100
10
10
100
1000
AB/2 (m)
s225
s226
s227
s228
s229

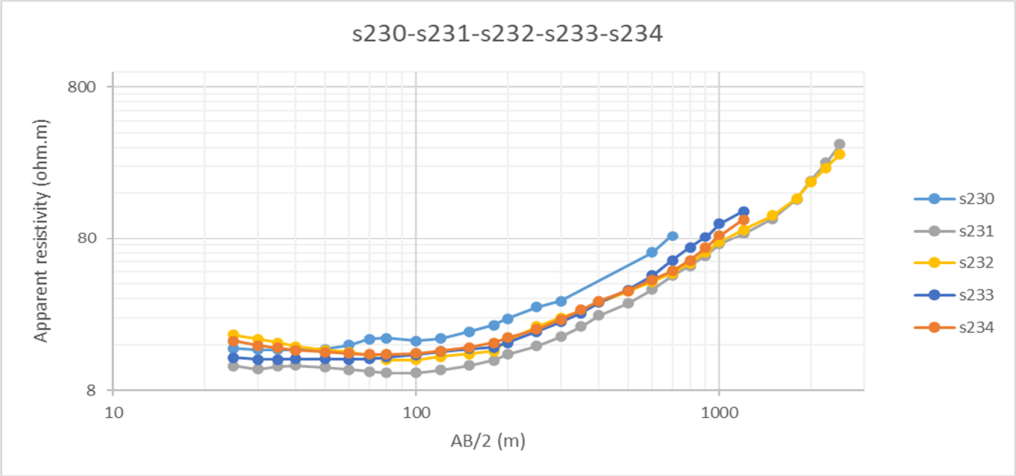
s230-s231-s232-s233-s234
Apparent resistivity (ohm.m)
800
80
8
10
100
1000
AB/2 (m)
s230
s231
s232
s233
s234

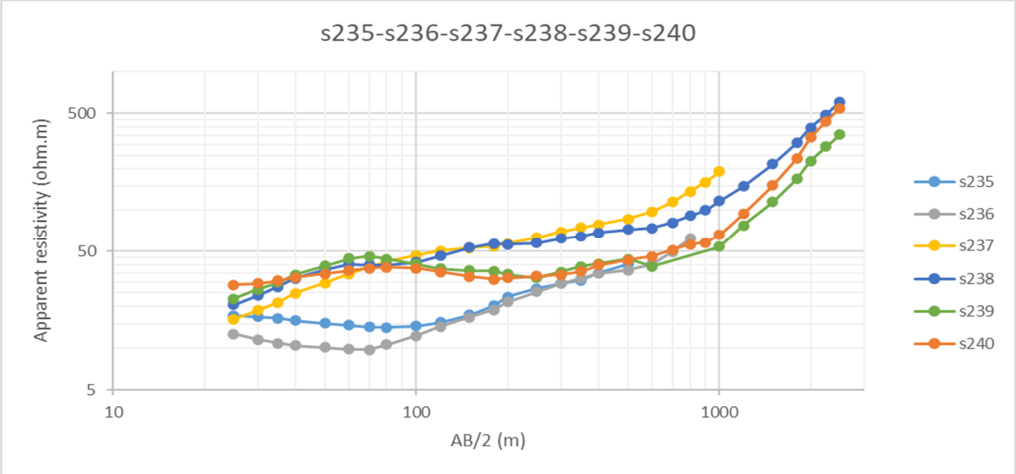
s235-s236-s237-s238-s239-s240
Apparent resistivity (ohm.m)
500
50
5
10
100
1000
AB/2 (m)
s235
s236
s237
s238
s239
s240

Group 12:

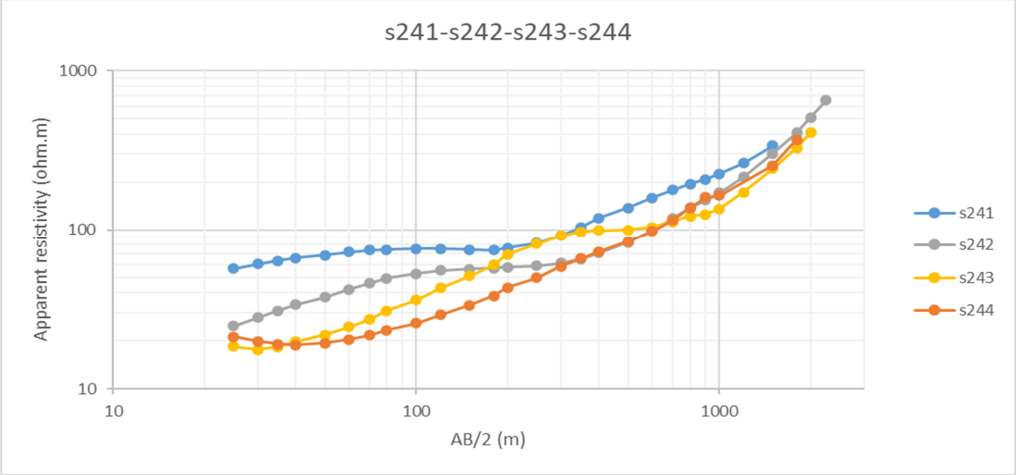
s241-s242-s243-s244
Apparent resistivity (ohm.m)
1000
100
10
10
100
1000
AB/2 (m)
s241
s242
s243
s244

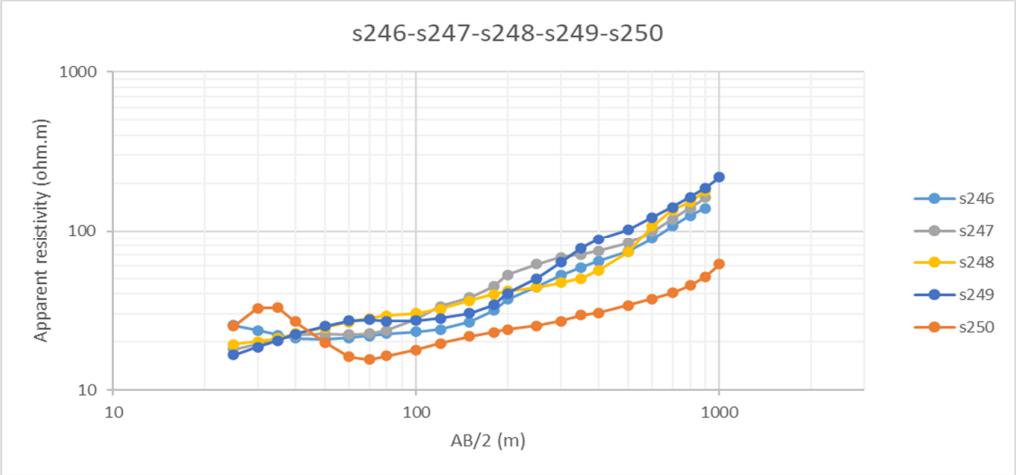
s246-s247-s248-s249-s250
Apparent resistivity (ohm.m)
1000
100
10
10
100
1000
AB/2 (m)
s246
s247
s248
s249
s250

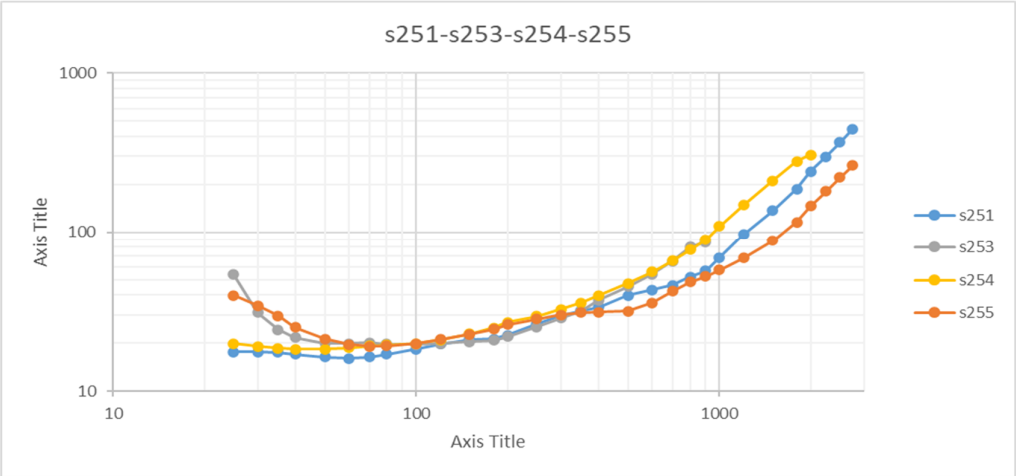
s251-s253-s254-s255
Axis Title
1000
100
10
10
100
1000
Axis Title
s251
s253
s254
s255

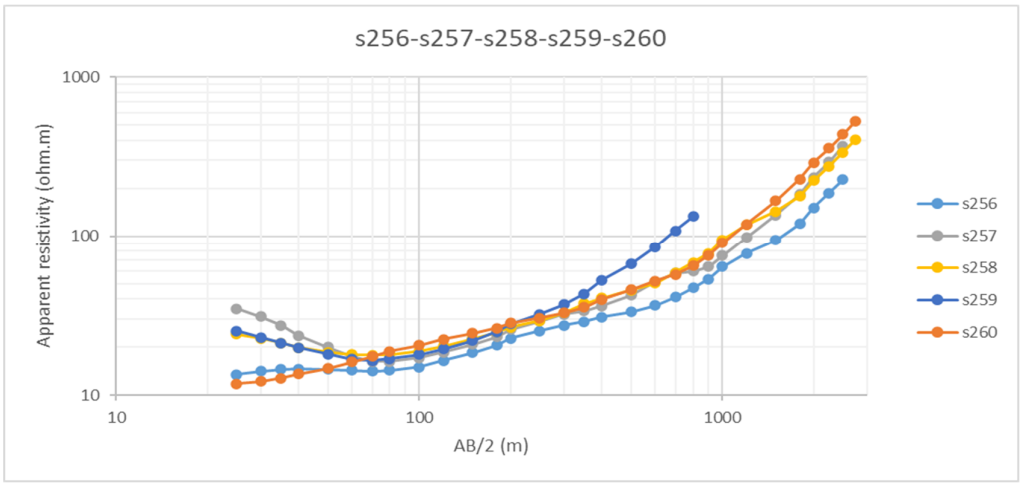
s256-s257-s258-s259-s260
Apparent resistivity (ohm.m)
1000
100
10
10
100
1000
AB/2 (m)
s256
s257
s258
s259
s260

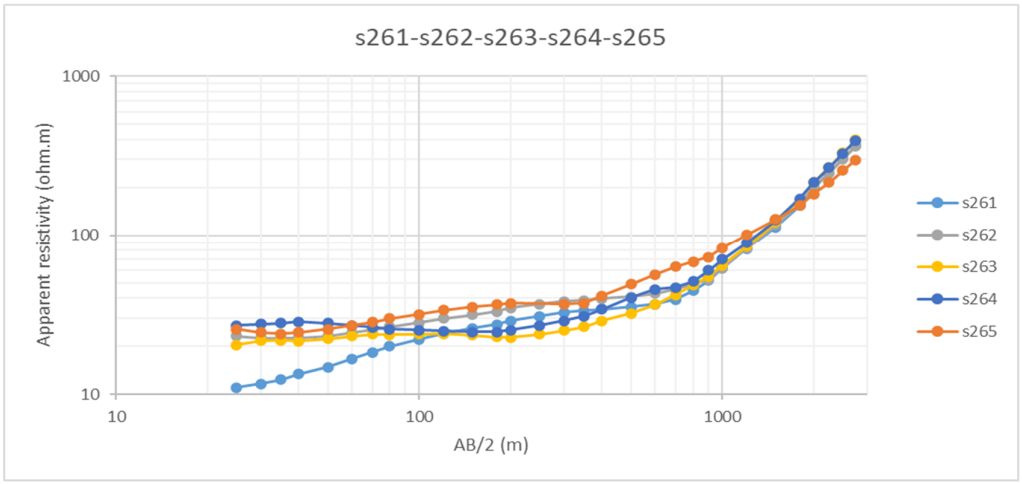
s261-s262-s263-s264-s265
Apparent resistivity (ohm.m)
1000
100
10
10
100
1000
AB/2 (m)
s261
s262
s263
s264
s265

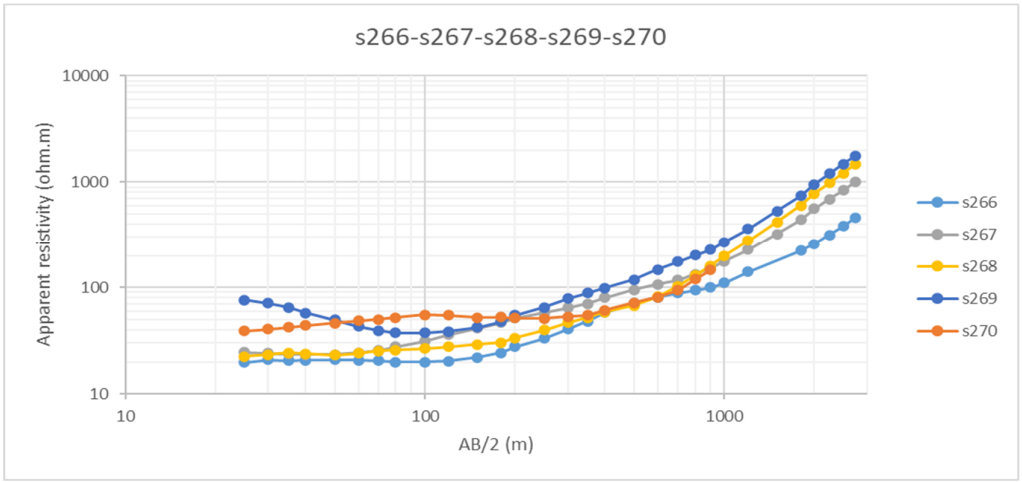
s266-s267-s268-s269-s270
Apparent resistivity (ohm.m)
10000
1000
100
10
10
100
1000
AB/2 (m)
s266
s267
s268
s269
s270

Group 13:

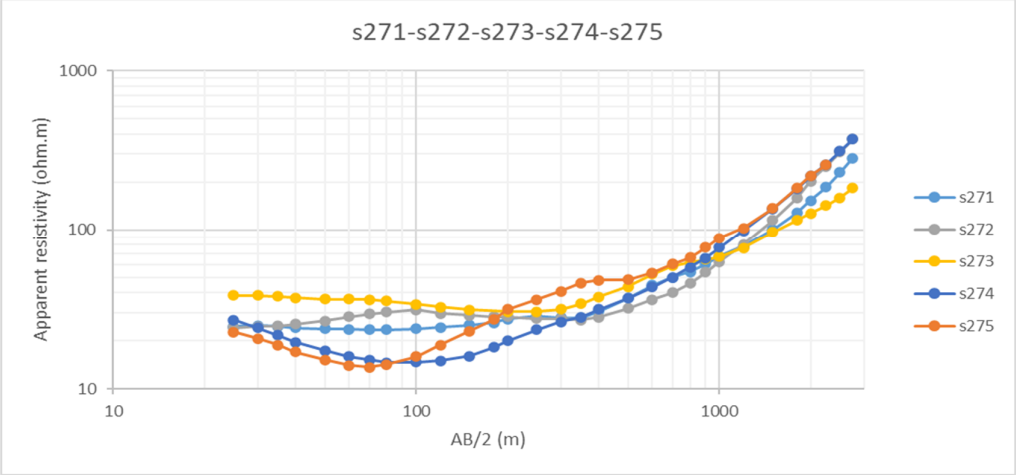
s271-s272-s273-s274-s275
Apparent resistivity (ohm.m)
1000
100
10
10
100
1000
AB/2 (m)
s271
s272
s273
s274
s275

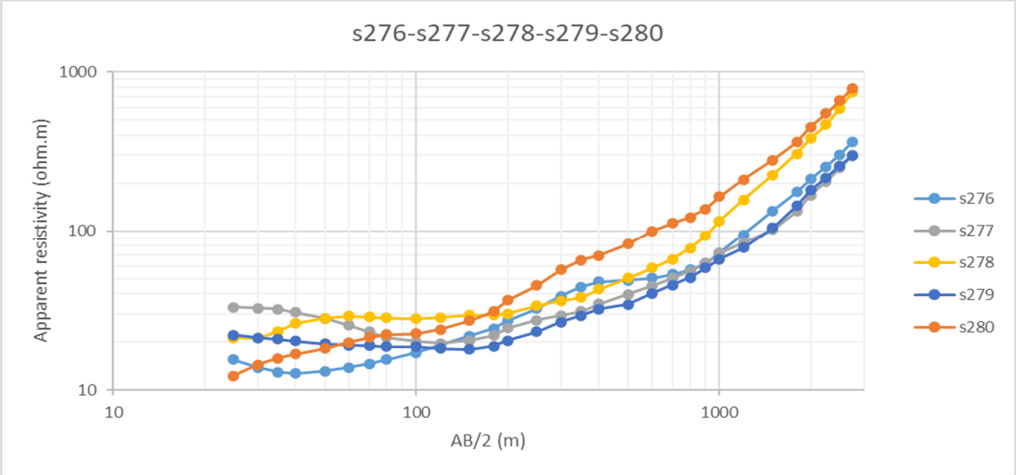
s276-s277-s278-s279-s280
Apparent resistivity (ohm.m)
1000
100
10
10
100
1000
AB/2 (m)
s276
s277
s278
s279
s280

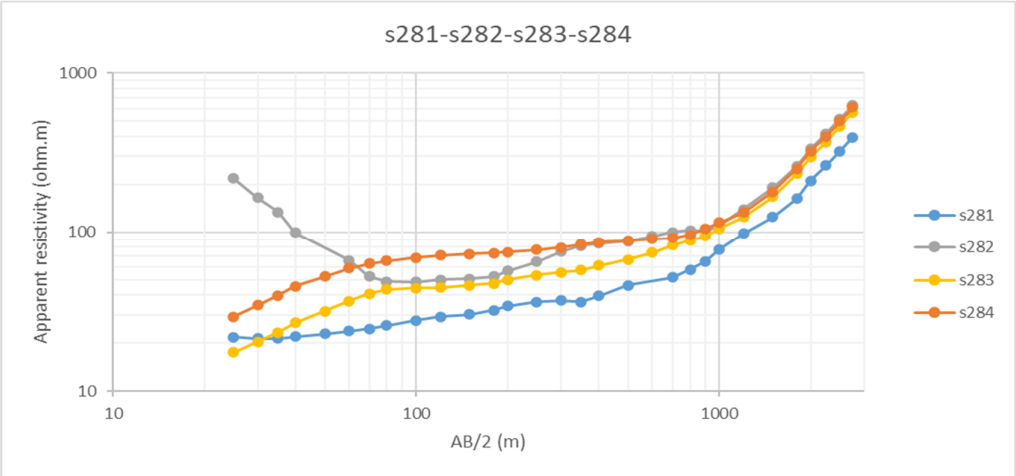
s281-s282-s283-s284
Apparent resistivity (ohm.m)
1000
100
10
10
100
1000
AB/2 (m)
s281
s282
s283
s284

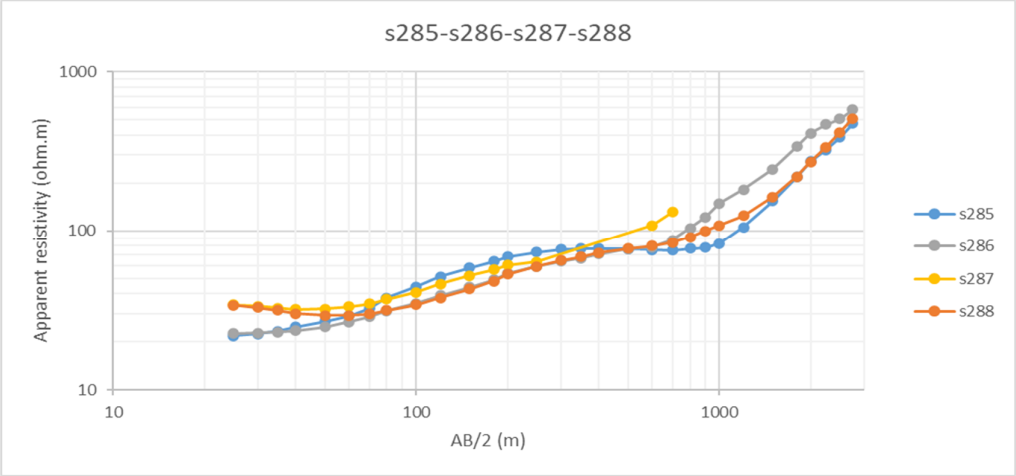
s285-s286-s287-s288
Apparent resistivity (ohm.m)
1000
100
10
10
100
1000
AB/2 (m)
s285
s286
s287
s288

Group 14:

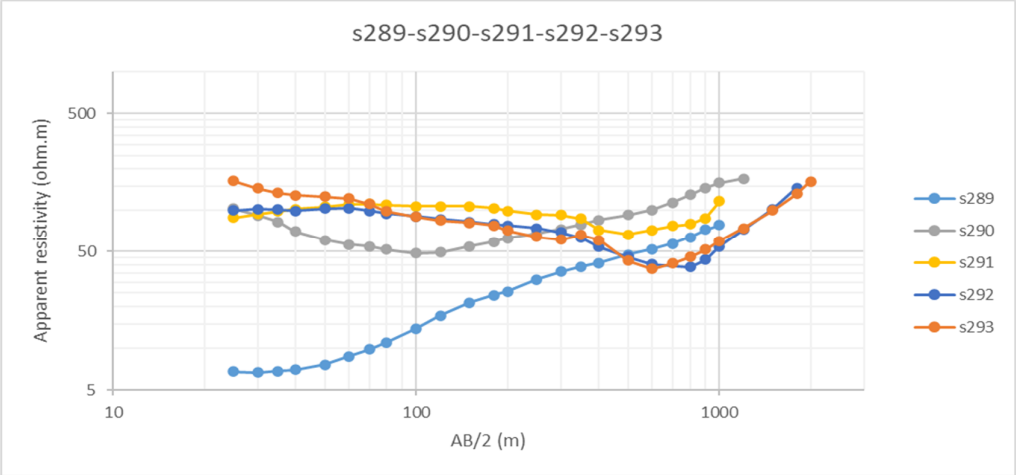
s289-s290-s291-s292-s293
Apparent resistivity (ohm.m)
500
50
5
10
100
1000
AB/2 (m)
s289
s290
s291
s292
s293

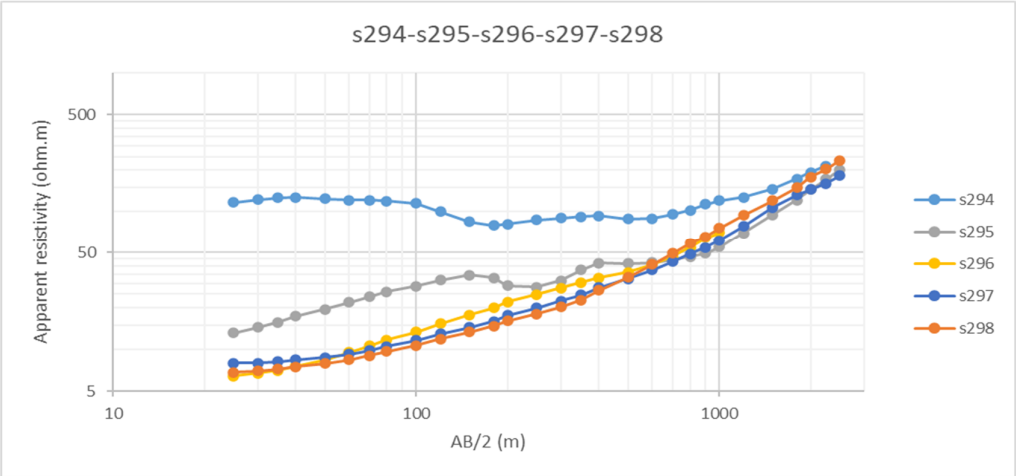
s294-s295-s296-s297-s298
Apparent resistivity (ohm.m)
500
50
5
10
100
1000
AB/2 (m)
s294
s295
s296
s297
s298

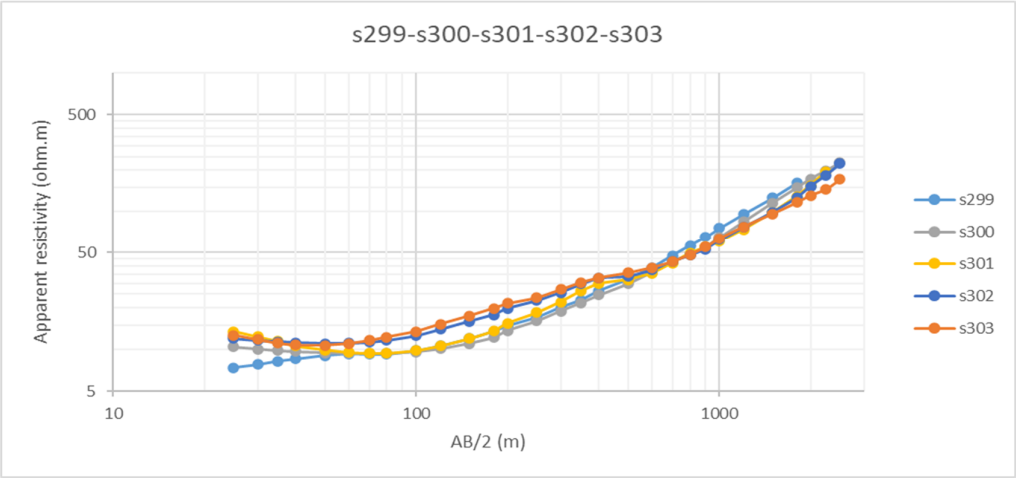
s299-s300-s301-s302-s303
Apparent resistivity (ohm.m)
500
50
5
10
100
1000
AB/2 (m)
s299
s300
s301
s302
s303

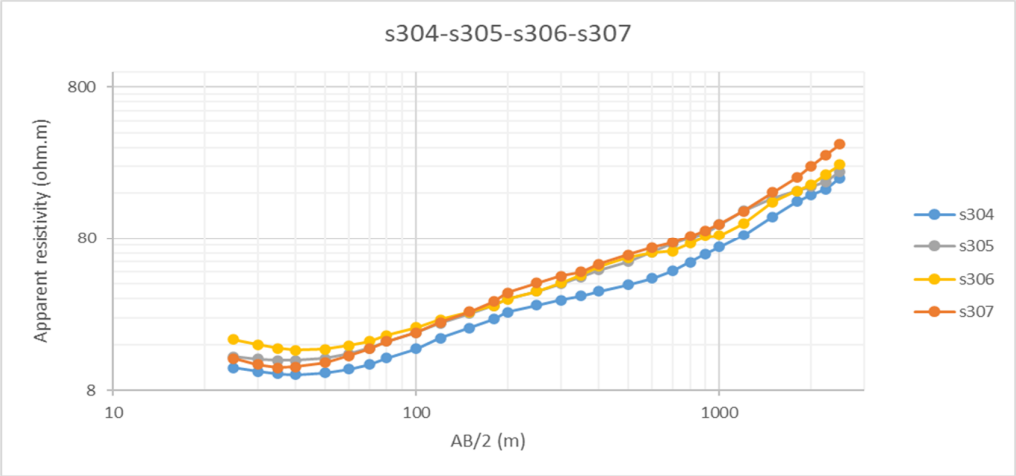
s304-s305-s306-s307
Apparent resistivity (ohm.m)
800
80
8
10
100
1000
AB/2 (m)
s304
s305
s306
s307

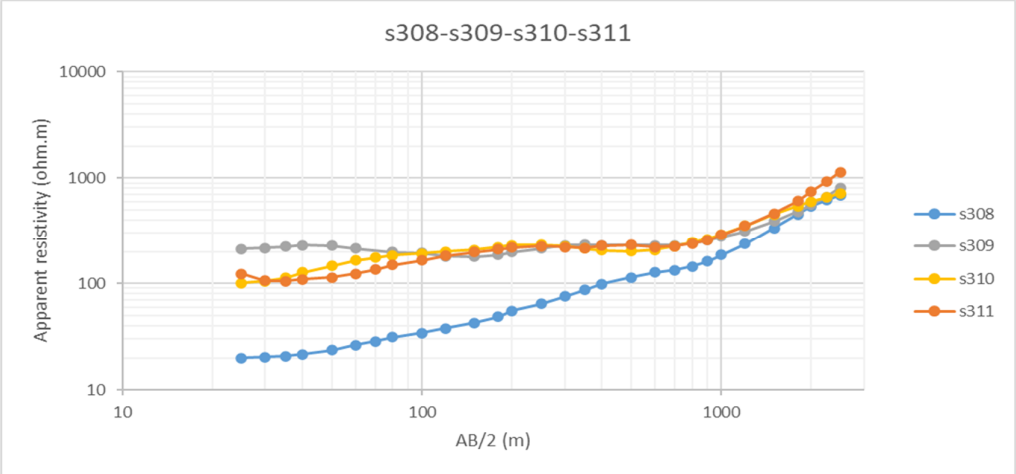
s308-s309-s310-s311
Apparent resistivity (ohm.m)
10000
1000
100
10
10
100
1000
AB/2 (m)
s308
s309
s310
s311

Group 15:

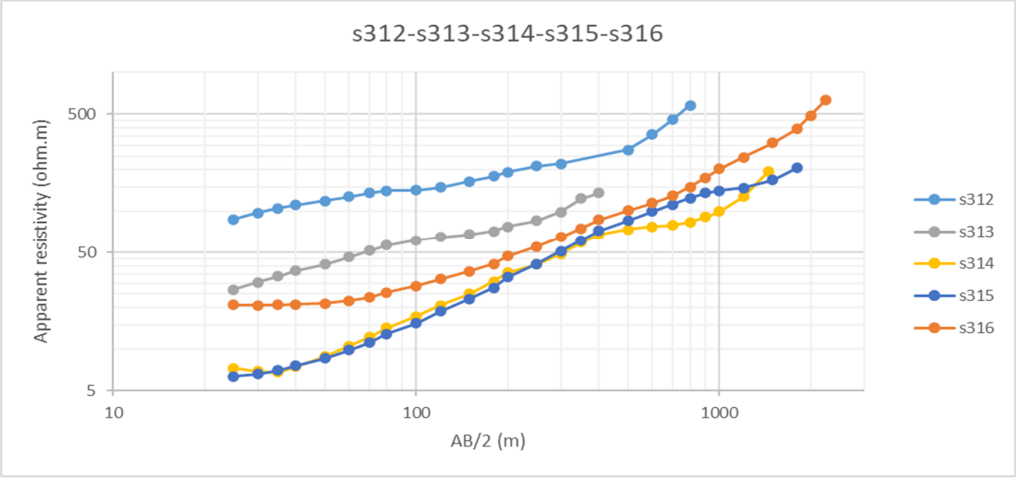

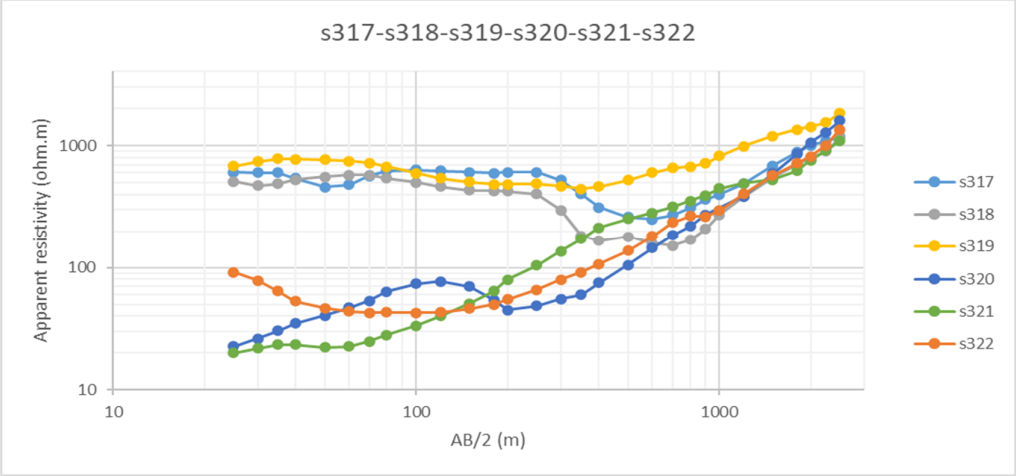

Group 16:

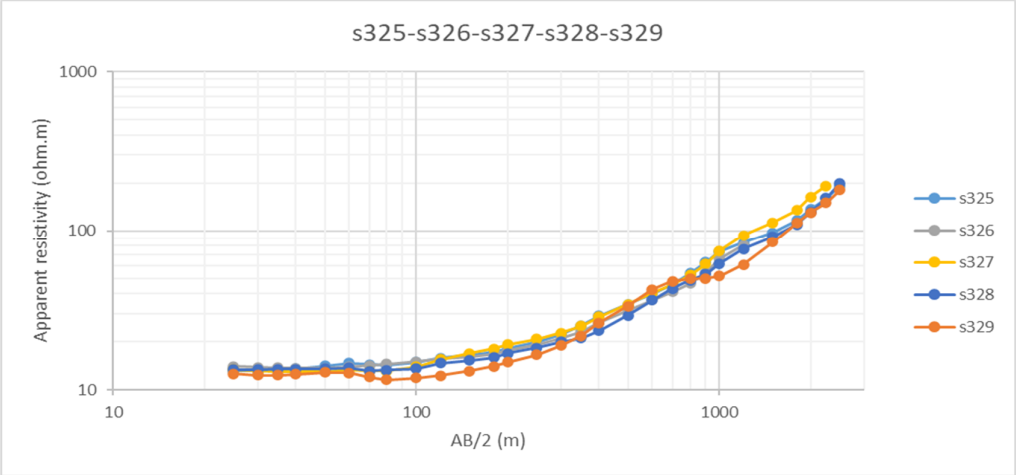

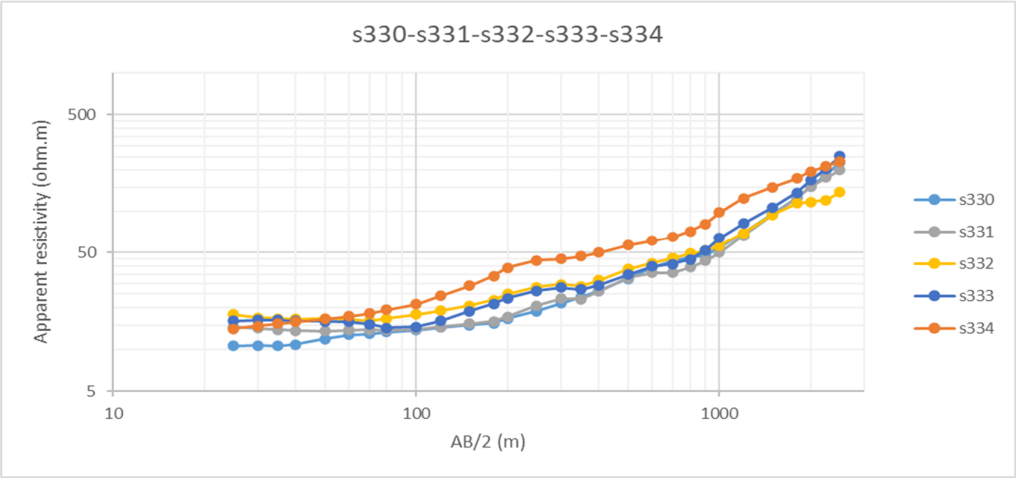
s330-s331-s332-s333-s334
Apparent resistivity (ohm.m)
500
50
5
10
100
1000
AB/2 (m)
s330
s331
s332
s333
s334

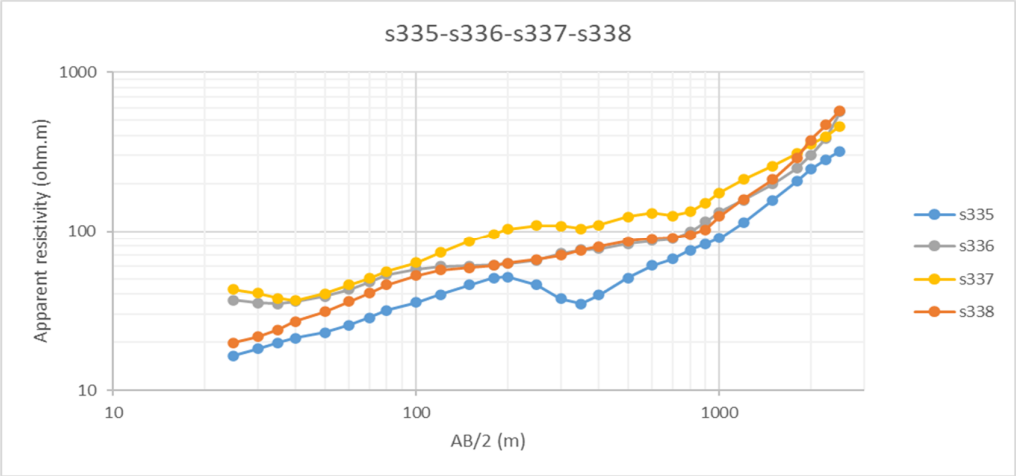
s335-s336-s337-s338
Apparent resistivity (ohm.m)
1000
100
10
10
100
1000
AB/2 (m)
s335
s336
s337
s338

Group 17:

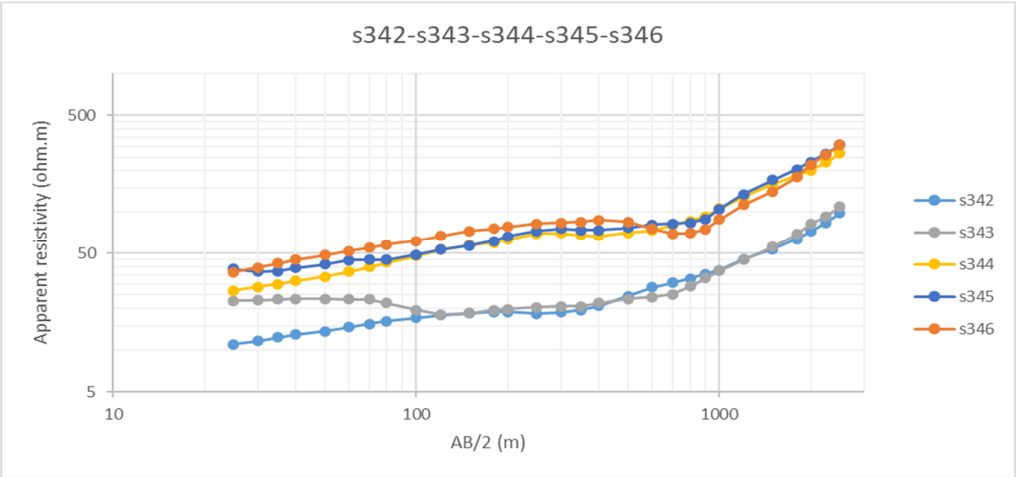
s342-s343-s344-s345-s346
Apparent resistivity (ohm.m)
500
50
5
10
100
1000
AB/2 (m)
s342
s343
s344
s345
s346

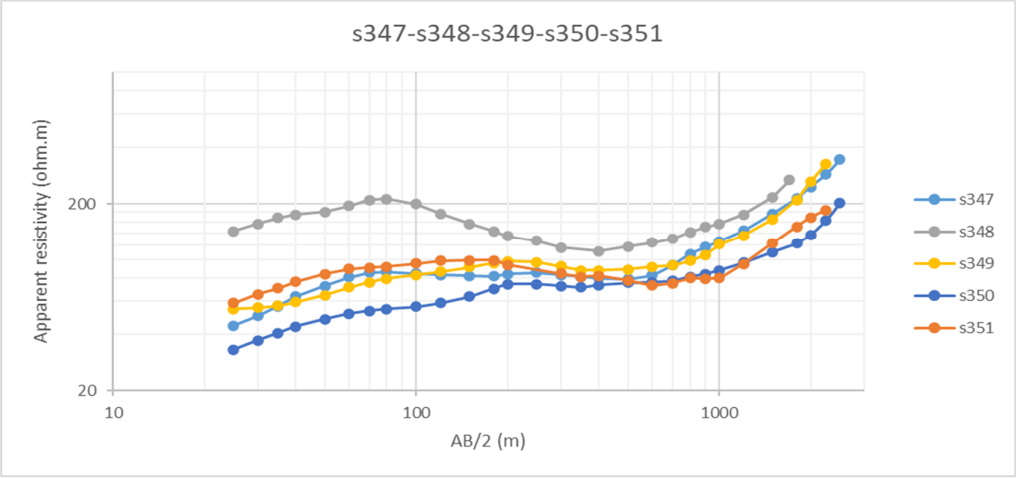
s347-s348-s349-s350-s351
Apparent resistivity (ohm.m)
200
20
10
100
1000
AB/2 (m)
s347
s348
s349
s350
s351

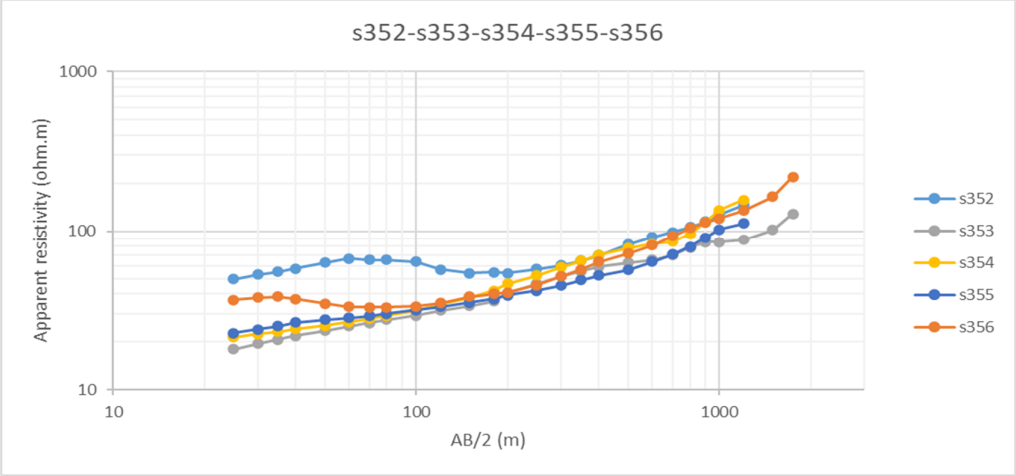
s352-s353-s354-s355-s356
Apparent resistivity (ohm.m)
1000
100
10
10
100
1000
AB/2 (m)
s352
s353
s354
s355
s356

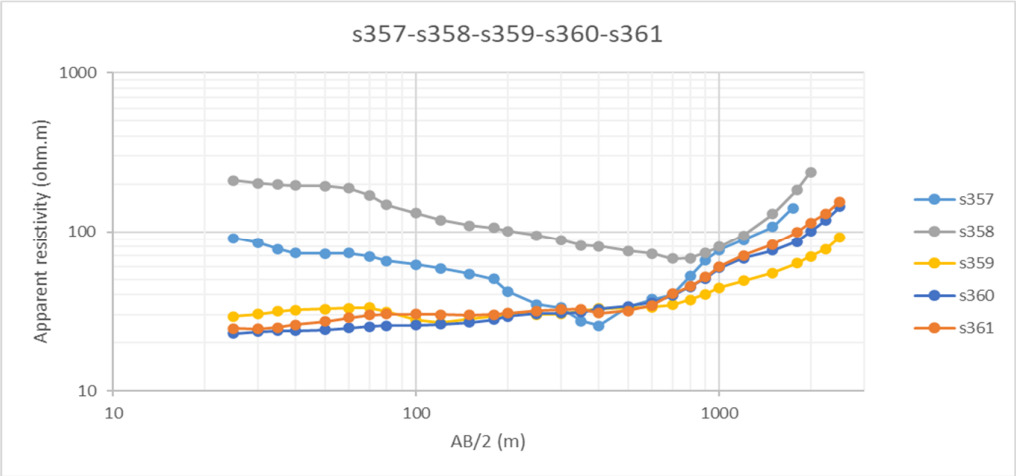
s357-s358-s359-s360-s361
Apparent resistivity (ohm.m)
1000
100
10
10
100
1000
AB/2 (m)
s357
s358
s359
s360
s361

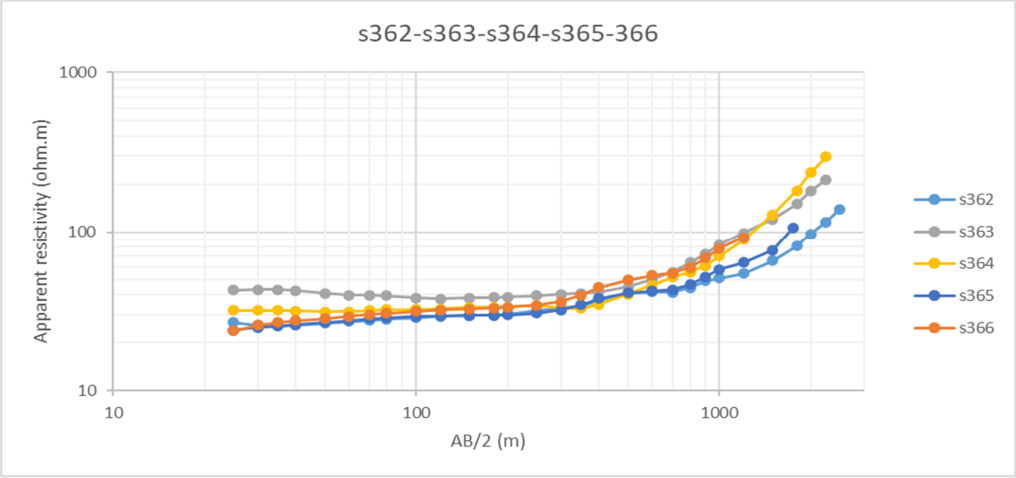
s362-s363-s364-s365-366
Apparent resistivity (ohm.m)
1000
100
10
10
100
1000
AB/2 (m)
s362
s363
s364
s365
s366

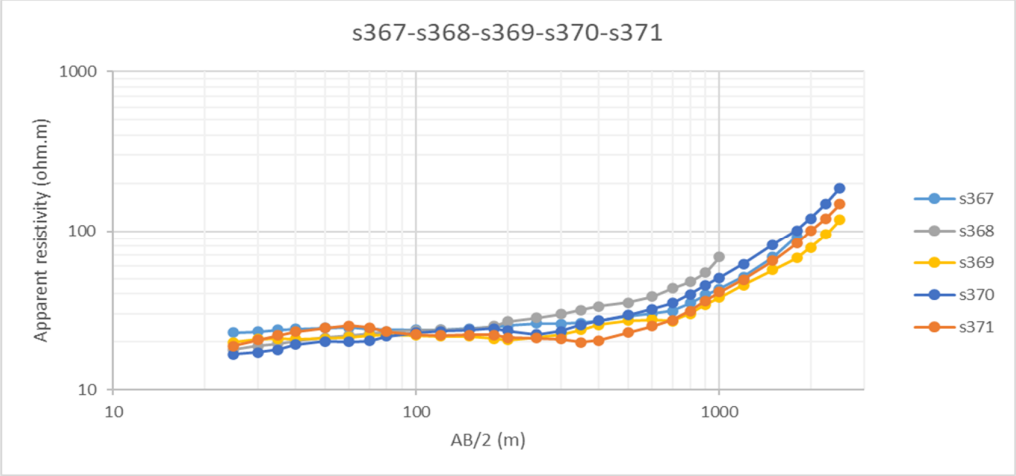
s367-s368-s369-s370-s371
Apparent resistivity (ohm.m)
1000
100
10
10
100
1000
AB/2 (m)
s367
s368
s369
s370
s371

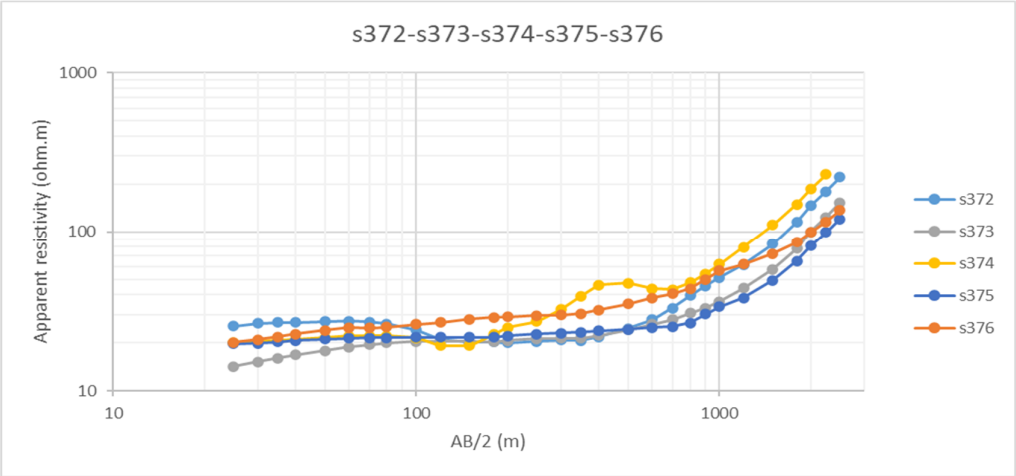
s372-s373-s374-s375-s376
Apparent resistivity (ohm.m)
1000
100
10
10
100
1000
AB/2 (m)
s372
s373
s374
s375
s376

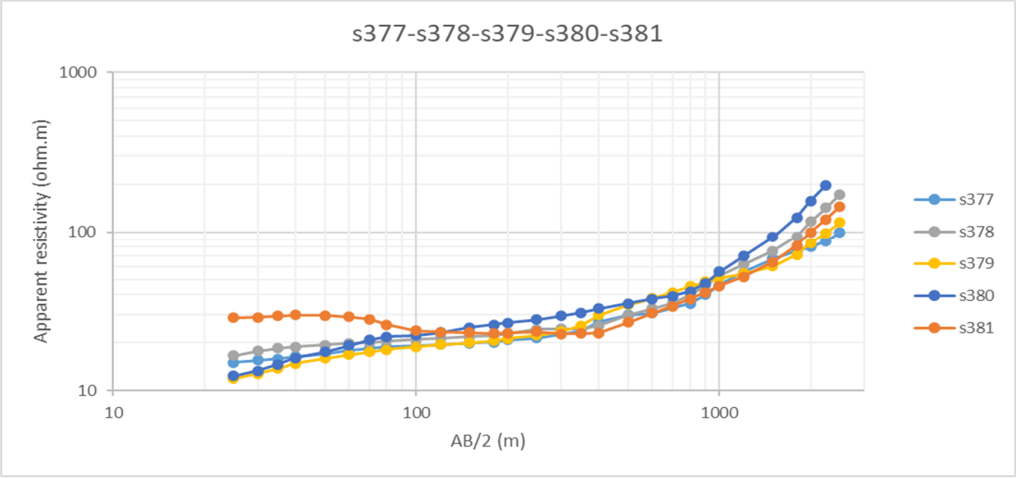
s377-s378-s379-s380-s381
Apparent resistivity (ohm.m)
1000
100
10
10
100
1000
AB/2 (m)
s377
s378
s379
s380
s381

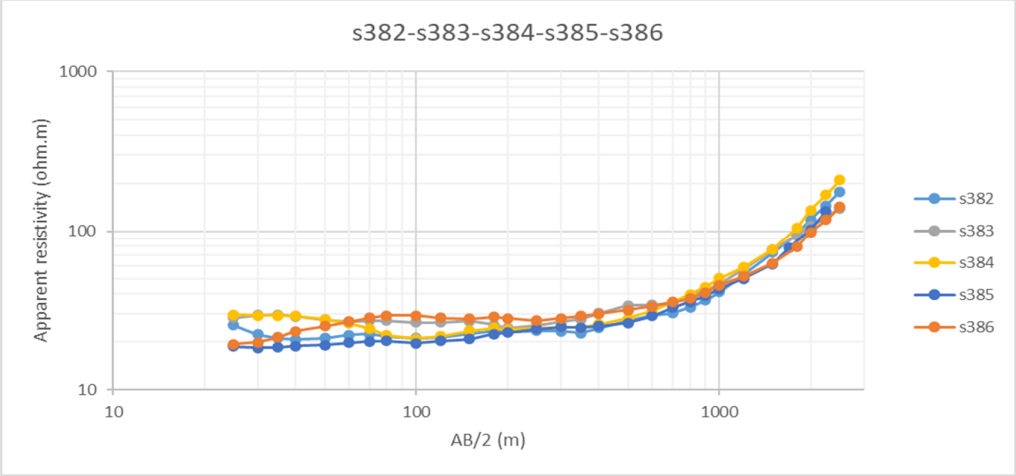
s382-s383-s384-s385-s386
Apparent resistivity (ohm.m)
1000
100
10
10
100
1000
AB/2 (m)
s382
s383
s384
s385
s386

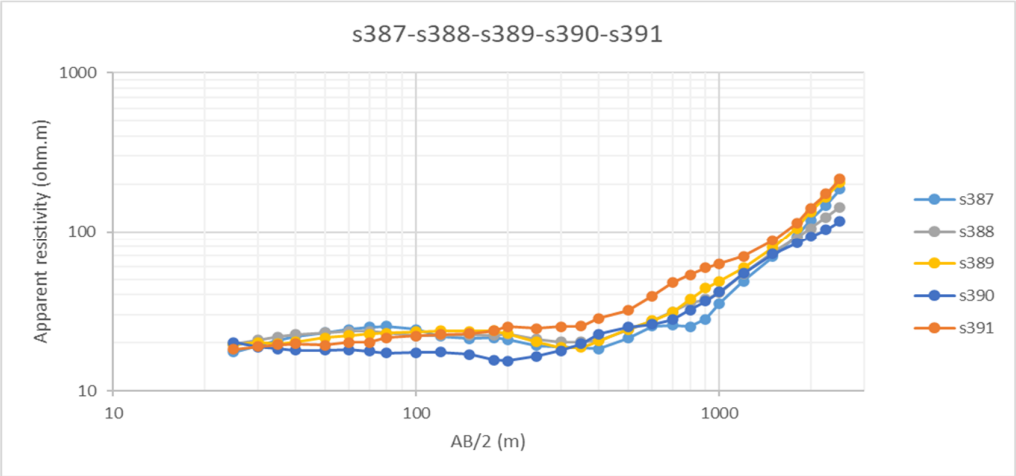
s387-s388-s389-s390-s391
Apparent resistivity (ohm.m)
1000
100
10
10
100
1000
AB/2 (m)
s387
s388
s389
s390
s391

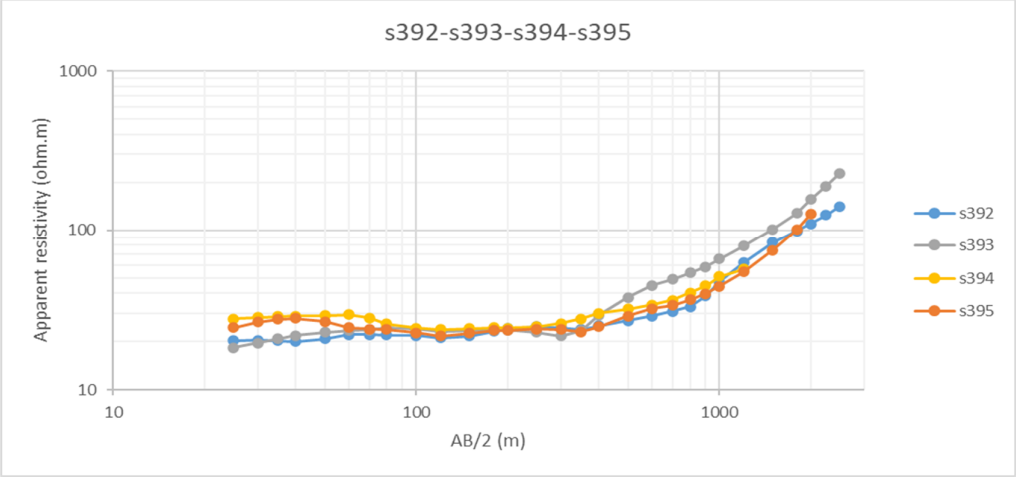
s392-s393-s394-s395
1000
100
10
Apparent resistivity (ohm.m)
10
100
1000
AB/2 (m)
s392
s393
s394
s395

Appendix D: Layer Structure of Soundings

Area	Group	Sounding	Rhoa(25)	IP(25)	Shape*	4 layer structure**
1	17	s342	11.0	4.2	E	a - r1<r2>r3<r4
1	17	s343	22.7	4.2	D	d - r1>r2<r3<r4
1	17	s344	26.8	2.6	E	a - r1<r2>r3<r4
1	17	s345	38.5	2.6	E	a - r1<r2>r3<r4
1	17	s346	36.4	2.2	E	a - r1<r2>r3<r4
1	17	s347	44.5	1.5	E	a - r1<r2>r3<r4
1	17	s348	143.3	2.4	E	a - r1<r2>r3<r4
1	17	s349	54.5	2.7	E	a - r1<r2>r3<r4
1	17	s351	58.7	1.8	E	a - r1<r2>r3<r4
1	17	s352	49.7	1.8	E	a - r1<r2>r3<r4
1	17	s353	18.0	2.2	F	f - r1<r2<r3<r4
1	17	s354	21.4	3.0	F	f - r1<r2<r3<r4
1	17	s355	22.8	2.1	F	f - r1<r2<r3<r4
1	17	s356	36.7	1.5	D	d - r1>r2<r3<r4
1	17	s358	210.5	2.9	C	c - r1>r2>r3<r4
1	17	s359	29.2	4.3	E	d - r1>r2<r3<r4
1	17	s360	22.9	2.3	E	a - r1<r2>r3<r4
1	17	s361	24.6	3.2	D	a - r1<r2>r3<r4
1	17	s362	26.9	3.4	F	f - r1<r2<r3<r4
1	17	s363	42.8	6.4	D	c - r1>r2>r3<r4
1	17	s364	32.0	3.8	D	a - r1<r2>r3<r4
1	17	s365	24.0	2.3	F	f - r1<r2<r3<r4
1	17	s366	23.8	3.5	E	a - r1<r2>r3<r4
1	17	s367	22.8	3.1	D	a - r1<r2>r3<r4
1	17	s368	17.1	2.4	E	a - r1<r2>r3<r4
1	17	s369	19.9	3.5	D	a - r1<r2>r3<r4
1	17	s370	16.7	2.6	E	a - r1<r2>r3<r4
1	17	s371	18.8	3.7	E	a - r1<r2>r3<r4
1	17	s372	25.4	4.3	D	c - r1>r2>r3<r4
1	17	s373	14.2	3.3	E	a - r1<r2>r3<r4
1	17	s374	20.2	3.2	D	d - r1>r2<r3<r4
1	17	s375	19.7	3.2	F	f - r1<r2<r3<r4
1	17	s376	20.1	3.5	D	a - r1<r2>r3<r4
1	17	s377	15.0	3.2	F	f - r1<r2<r3<r4
1	17	s378	16.6	3.0	E	a - r1<r2>r3<r4
1	17	s379	11.9	3.2	F	f - r1<r2<r3<r4
1	17	s380	12.3	2.6	F	f - r1<r2<r3<r4
1	17	s381	28.7	4.2	E	c - r1>r2>r3<r4
1	17	s382	25.4	4.2	D	a - r1<r2>r3<r4
Area	**Group**	**Sounding**	**Rhoa(25)**	**IP(25)**	**Shape**	**4 layer structure**
1	17	s383	28.3	3.9	B	c - r1>r2>r3<r4
1	17	s384	29.6	4.2	D	d - r1>r2<r3<r4

1	17	s385	18.7	3.4	E	a - r1<r2>r3<r4
1	17	s386	19.4	3.6	E	a - r1<r2>r3<r4
1	17	s387	17.5	3.4	E	a - r1<r2>r3<r4
1	17	s390	20.2	3.8	D	d - r1>r2<r3<r4
1	17	s391	18.3	3.1	E	a - r1<r2>r3<r4
1	17	s392	20.3	3.5	D	a - r1<r2>r3<r4
1	17	s393	18.3	3.1	E	a - r1<r2>r3<r4
1	17	s394	27.7	3.5	D	d - r1>r2<r3<r4
1	17	s395	24.4	3.3	E	c - r1>r2>r3<r4
2	1	s1	11.8	4.9	Ax	a - r1<r2>r3<r4
2	1	s2	15.1	31.4	Ax	c - r1>r2>r3<r4
2	1	s3	23.9	5.9	Bx	c - r1>r2>r3<r4
2	1	s4	23.6	3.7	Ax	c - r1>r2>r3<r4
2	1	s5	10.2	8.6	Ax	a - r1<r2>r3<r4
2	1	s6	17.0	8.6	A	a - r1<r2>r3<r4
2	1	s7	13.5	11.3	A	c - r1>r2>r3<r4
2	1	s8	13.0	8.9	A	a - r1<r2>r3<r4
2	1	s9	10.5	7.1	A	a - r1<r2>r3<r4
2	1	s10	26.7	7.1	B	c - r1>r2>r3<r4
2	1	s11	14.4	5.5	A	a - r1<r2>r3<r4
2	1	s12	14.4	4.6	Ax	c - r1>r2>r3<r4
2	1	s13	16.8	2.9	A	a - r1<r2>r3<r4
2	1	s14	12.2	-	A	d - r1>r2<r3<r4
2	2	s17	16.2	4.2	B	c - r1>r2>r3<r4
2	2	s18	27.5	5.4	B	c - r1>r2>r3<r4
2	2	s19	22.9	5.7	B	c - r1>r2>r3<r4
2	2	s20	15.2	3.4	A	c - r1>r2>r3<r4
2	2	s21	12.7	6.5	A	a - r1<r2>r3<r4
2	2	s22	13.3	5.6	A	c - r1>r2>r3<r4
2	2	s23	10.0	6.6	Bx	a - r1<r2>r3<r4
2	2	s24	12.4	4.7	Bx	c - r1>r2>r3<r4
2	2	s25	24.7	3.7	Bx	c - r1>r2>r3<r4
2	2	s26	25.5	4.6	Bx	c - r1>r2>r3<r4
2	2	s27	13.9	2.4	Bx	d - r1>r2<r3<r4
2	3	s28	14.7	4.8	B	a - r1<r2>r3<r4
2	3	s29	16.9	5.8	D	a - r1<r2>r3<r4
2	3	s30	19.6	5.6	D	d - r1>r2<r3<r4
Area	**Group**	**Sounding**	**Rhoa(25)**	**IP(25)**	**Shape**	**4 layer structure**
2	3	s31	26.9	5.8	A	c - r1>r2>r3<r4
2	3	s32	15.1	9.2	A	d - r1>r2<r3<r4
2	3	s33	19.0	9.0	D	c - r1>r2>r3<r4
2	3	s34	16.3	9.5	D	c - r1>r2>r3<r4
2	3	s35	14.7	3.3	D	c - r1>r2>r3<r4
2	3	s36	43.0	1.9	B	c - r1>r2>r3<r4

2	3	s37	13.1	5.0	B	d - r1>r2<r3<r4
2	3	s38	9.8	6.6	D	d - r1>r2<r3<r4
2	3	s39	13.1	2.7	B	d - r1>r2<r3<r4
2	3	s40	42.1	2.2	B	d - r1>r2<r3<r4
2	3	s41	27.6	5.9	B	d - r1>r2<r3<r4
2	3	s42	9.5	1.9	F	f - r1<r2<r3<r4
2	3	s43	10.5	2.1	F	f - r1<r2<r3<r4
2	4	s44	25.8	4.7	B	c - r1>r2>r3<r4
2	4	s45	20.6	4.1	B	c - r1>r2>r3<r4
2	4	s46	21.6	5.4	B	c - r1>r2>r3<r4
2	4	s47	22.2	5.2	B	c - r1>r2>r3<r4
2	4	s48	22.8	6.0	B	c - r1>r2>r3<r4
2	4	s49	16.6	3.3	A	a - r1<r2>r3<r4
2	4	s50	15.6	3.6	D	a - r1<r2>r3<r4
2	4	s51	19.0	5.0	B	d - r1>r2<r3<r4
2	4	s52	30.2	3.9	B	c - r1>r2>r3<r4
2	4	s53	29.9	3.7	B	d - r1>r2<r3<r4
2	4	s54	26.1	2.6	B	d - r1>r2<r3<r4
2	4	s55	21.6	3.1	B	d - r1>r2<r3<r4
2	5	s56	21.6	3.1	-	-
2	5	s57	16.4	4.0	-	-
2	5	s58	23.9	2.9	-	-
2	5	s59	23.4	3.6	-	-
2	5	s60	19.6	2.7	-	-
2	5	s61	17.0	3.5	-	-
2	5	s62	10.6	2.0	-	-
2	5	s63	20.3	3.2	-	-
3	12	s241	56.6	1.4	E	a - r1<r2>r3<r4
3	12	s242	24.8	1.1	E	a - r1<r2>r3<r4
3	12	s243	18.4	1.7	D	a - r1<r2>r3<r4
3	12	s244	21.3	1.6	D	d - r1>r2<r3<r4
3	12	s246	25.4	1.7	D	d - r1>r2<r3<r4
3	12	s247	18.0	1.1	F	f - r1<r2<r3<r4
Area	**Group**	**Sounding**	**Rhoa(25)**	**IP(25)**	**Shape**	**4 layer structure**
3	12	s248	19.3	1.9	F	f - r1<r2<r3<r4
3	12	s249	16.6	0.8	F	f - r1<r2<r3<r4
3	12	s250	25.0	1.7	A	d - r1>r2<r3<r4
3	12	s251	17.7	1.9	D	d - r1>r2<r3<r4
3	12	s253	53.9	6.5	B	d - r1>r2<r3<r4
3	12	s254	19.8	1.6	D	d - r1>r2<r3<r4
3	12	s255	39.8	2.4	B	d - r1>r2<r3<r4
3	12	s256	13.5	1.0	E	d - r1>r2<r3<r4
3	12	s257	34.9	2.1	B	d - r1>r2<r3<r4
3	12	s258	24.1	2.2	B	d - r1>r2<r3<r4

3	12	s259	25.3	1.7	B	d - r1>r2<r3<r4
3	12	s260	11.8	1.2	F	f - r1<r2<r3<r4
3	12	s261	11.1	0.9	E	a - r1<r2>r3<r4
3	12	s262	23.1	1.4	D	a - r1<r2>r3<r4
3	12	s263	20.4	1.8	D	a - r1<r2>r3<r4
3	12	s264	27.1	1.8	D	d - r1>r2<r3<r4
3	12	s265	25.7	1.6	E	a - r1<r2>r3<r4
3	12	s266	19.8	2.9	D	d - r1>r2<r3<r4
3	12	s267	24.7	1.8	D	d - r1>r2<r3<r4
3	12	s268	22.4	1.5	F	f - r1<r2<r3<r4
3	12	s269	76.0	2.0	B	d - r1>r2<r3<r4
3	12	s270	38.9	1.5	E	a - r1<r2>r3<r4
3	13	s271	24.7	1.3	D	d - r1>r2<r3<r4
3	13	s272	24.2	1.2	E	a - r1<r2>r3<r4
3	13	s273	38.6	2.4	D	d - r1>r2<r3<r4
3	13	s274	27.1	4.3	B	d - r1>r2<r3<r4
3	13	s275	22.8	2.0	D	d - r1>r2<r3<r4
3	13	s276	15.6	2.2	B	d - r1>r2<r3<r4
3	13	s277	33.0	2.8	D	d - r1>r2<r3<r4
3	13	s278	21.3	1.8	E	a - r1<r2>r3<r4
3	13	s279	22.2	1.6	D	d - r1>r2<r3<r4
3	13	s280	12.3	1.3	E	f - r1<r2<r3<r4
3	13	s281	21.8	1.6	F	a - r1<r2>r3<r4
3	13	s282	218.9	2.6	B	d - r1>r2<r3<r4
3	13	s283	17.5	0.9	E	a - r1<r2>r3<r4
3	13	s284	29.3	1.1	E	a - r1<r2>r3<r4
3	13	s285	21.9	1.4	E	a - r1<r2>r3<r4
3	13	s286	22.5	1.4	F	f - r1<r2<r3<r4
3	13	s287	34.1	2.0	E	a - r1<r2>r3<r4
Area	**Group**	**Sounding**	**Rhoa(25)**	**IP(25)**	**Shape**	**4 layer structure**
3	13	s288	33.9	2.1	E	d - r1>r2<r3<r4
4	6	s64	18.4	1.8	E	a - r1<r2>r3<r4
4	6	s65	49.3	1.5	E	d - r1>r2<r3<r4
4	6	s66	37.0	1.3	E	a - r1<r2>r3<r4
4	6	s67	10.0	1.4	F	f - r1<r2<r3<r4
4	6	s68	9.9	2.1	E	a - r1<r2>r3<r4
4	6	s69	13.9	3.5	E	a - r1<r2>r3<r4
4	6	s70	20.6	3.4	D	c - r1>r2>r3<r4
4	6	s71	18.3	3.4	D	d - r1>r2<r3<r4
4	6	s72	16.9	3.2	A	d - r1>r2<r3<r4
4	6	s73	24.0	3.8	D	d - r1>r2<r3<r4
4	6	s74	20.2	3.9	A	d - r1>r2<r3<r4
4	6	s75	14.8	1.9	D	a - r1<r2>r3<r4
4	6	s76	15.0	2.7	D	a - r1<r2>r3<r4

4	6	s77	14.5	2.4	A	a - r1<r2>r3<r4
4	6	s78	26.2	1.4	D	a - r1<r2>r3<r4
4	6	s79	13.5	2.6	A	a - r1<r2>r3<r4
4	7	s80	17.8	4.9	D	d - r1>r2<r3<r4
4	7	s81	13.5	1.8	E	a - r1<r2>r3<r4
4	7	s82	11.0	2.0	E	a - r1<r2>r3<r4
4	7	s83	16.5	1.5	E	a - r1<r2>r3<r4
4	7	s84	13.8	2.8	E	a - r1<r2>r3<r4
4	7	s85	13.1	1.7	D	a - r1<r2>r3<r4
4	7	s86	9.9	1.9	E	a - r1<r2>r3<r4
4	7	s87	15.2	2.0	D	a - r1<r2>r3<r4
4	7	s88	17.9	1.5	D	c - r1>r2>r3<r4
4	7	s89	13.0	1.5	F	f - r1<r2<r3<r4
4	7	s90	13.4	1.6	F	f - r1<r2<r3<r4
4	7	s91	14.7	2.0	F	f - r1<r2<r3<r4
4	7	s92	15.9	1.8	F	a - r1<r2>r3<r4
4	11	s205	19.9	1.9	F	f - r1<r2<r3<r4
4	11	s206	25.3	2.6	F	f - r1<r2<r3<r4
4	11	s207	49.0	2.7	D	d - r1>r2<r3<r4
4	11	s208	34.0	2.3	D	d - r1>r2<r3<r4
4	11	s209	33.5	1.5	B	d - r1>r2<r3<r4
4	11	s210	27.7	1.2	D	d - r1>r2<r3<r4
4	11	s211	34.0	1.9	B	d - r1>r2<r3<r4
4	11	s212	58.4	2.0	B	d - r1>r2<r3<r4
4	11	s213	33.8	1.6	B	d - r1>r2<r3<r4
Area	**Group**	**Sounding**	**Rhoa(25)**	**IP(25)**	**Shape**	**4 layer structure**
4	11	s214	38.9	1.9	B	d - r1>r2<r3<r4
4	11	s215	29.8	1.7	B	d - r1>r2<r3<r4
4	11	s216	18.4	2.2	B	d - r1>r2<r3<r4
4	11	s217	37.3	1.9	B	d - r1>r2<r3<r4
4	11	s218	28.0	2.4	B	d - r1>r2<r3<r4
4	11	s219	32.4	2.0	B	d - r1>r2<r3<r4
4	11	s220	34.2	2.0	B	d - r1>r2<r3<r4
4	11	s221	22.3	2.1	D	d - r1>r2<r3<r4
4	11	s222	14.7	2.4	D	d - r1>r2<r3<r4
4	11	s223	19.0	2.5	D	d - r1>r2<r3<r4
4	11	s224	14.9	1.6	D	a - r1<r2>r3<r4
4	11	s225	23.7	2.1	B	d - r1>r2<r3<r4
4	11	s226	19.5	1.8	B	a - r1<r2>r3<r4
4	11	s227	15.4	1.7	D	d - r1>r2<r3<r4
4	11	s228	16.2	1.5	D	d - r1>r2<r3<r4
4	11	s229	14.5	1.6	F	f - r1<r2<r3<r4
4	11	s230	15.1	2.9	F	f - r1<r2<r3<r4
4	11	s231	11.6	2.0	D	d - r1>r2<r3<r4

4	11	s232	18.6	1.4	D	d - r1>r2<r3<r4
4	11	s233	13.1	1.6	D	d - r1>r2<r3<r4
4	11	s234	16.9	0.3	D	d - r1>r2<r3<r4
4	11	s235	17.2	1.6	D	d - r1>r2<r3<r4
4	11	s236	12.6	2.1	D	d - r1>r2<r3<r4
4	11	s237	16.2	2.8	E	a - r1<r2>r3<r4
4	11	s238	20.5	3.4	E	a - r1<r2>r3<r4
4	11	s239	22.8	0.9	E	a - r1<r2>r3<r4
4	11	s240	28.5	1.6	E	a - r1<r2>r3<r4
4	16	s325	13.1	1.6	F	f - r1<r2<r3<r4
4	16	s326	14.0	1.8	D	f - r1<r2<r3<r4
4	16	s327	13.4	1.6	F	d - r1>r2<r3<r4
4	16	s328	13.4	2.2	F	f - r1<r2<r3<r4
4	16	s329	12.6	1.9	D	d - r1>r2<r3<r4
4	16	s330	10.6	2.4	F	f - r1<r2<r3<r4
4	16	s331	14.5	2.3	D	d - r1>r2<r3<r4
4	16	s332	17.8	2.5	D	d - r1>r2<r3<r4
4	16	s333	16.0	2.7	D	d - r1>r2<r3<r4
4	16	s334	14.1	1.8	F	f - r1<r2<r3<r4
4	16	s335	16.5	2.7	D	a - r1<r2>r3<r4
4	16	s336	36.8	3.8	E	d - r1>r2<r3<r4
Area	**Group**	**Sounding**	**Rhoa(25)**	**IP(25)**	**Shape**	**4 layer structure**
4	16	s337	42.8	3.5	D	d - r1>r2<r3<r4
4	16	s338	19.9	3.6	E	a - r1<r2>r3<r4
5	8	s93	20.4	2.1	A	a - r1<r2>r3<r4
5	8	s94	28.2	2.1	D	a - r1<r2>r3<r4
5	8	s95	18.6	1.8	D	d - r1>r2<r3<r4
5	8	s96	17.4	1.3	F	f - r1<r2<r3<r4
5	8	s97	14.8	1.6	F	f - r1<r2<r3<r4
5	8	s98	15.6	2.0	B	d - r1>r2<r3<r4
5	8	s99	12.8	1.3	F	f - r1<r2<r3<r4
5	8	s100	14.0	1.3	B	d - r1>r2<r3<r4
5	8	s101	17.6	1.9	D	d - r1>r2<r3<r4
5	8	s102	18.7	1.3	D	c - r1>r2>r3<r4
5	8	s103	18.5	1.2	F	f - r1<r2<r3<r4
5	8	s104	19.3	1.0	D	d - r1>r2<r3<r4
5	8	s105	17.0	1.7	D	d - r1>r2<r3<r4
5	8	s106	20.1	1.4	D	d - r1>r2<r3<r4
5	8	s107	19.0	1.1	D	a - r1<r2>r3<r4
5	8	s108	23.4	1.6	D	c - r1>r2>r3<r4
5	8	s109	15.4	1.3	D	a - r1<r2>r3<r4
5	8	s110	18.8	4.1	D	d - r1>r2<r3<r4
5	8	s111	10.8	1.0	E	a - r1<r2>r3<r4
5	8	s112	19.0	1.3	D	c - r1>r2>r3<r4

5	8	s113	18.9	1.5	D	c - r1>r2>r3<r4
5	8	s114	22.5	1.9	B	d - r1>r2<r3<r4
5	8	s115	12.6	1.2	F	f - r1<r2<r3<r4
5	8	s116	14.6	1.5	F	f - r1<r2<r3<r4
5	8	s117	13.0	1.5	F	f - r1<r2<r3<r4
5	8	s118	17.5	2.9	B	d - r1>r2<r3<r4
5	8	s119	10.2	1.4	F	f - r1<r2<r3<r4
5	8	s120	16.9	1.2	F	f - r1<r2<r3<r4
5	8	s121	25.0	1.4	F	f - r1<r2<r3<r4
5	8	s122	26.6	1.2	E	d - r1>r2<r3<r4
5	8	s123	57.1	1.6	E	d - r1>r2<r3<r4
5	8	s124	11.8	2.0	F	f - r1<r2<r3<r4
5	8	s125	12.0	3.0	B	d - r1>r2<r3<r4
5	8	s126	13.1	3.8	B	d - r1>r2<r3<r4
5	8	s127	9.9	2.4	B	d - r1>r2<r3<r4
5	8	s128	7.3	-	D	d - r1>r2<r3<r4
5	8	s129	7.6	1.4	D	d - r1>r2<r3<r4
Area	**Group**	**Sounding**	**Rhoa(25)**	**IP(25)**	**Shape**	**4 layer structure**
5	8	s130	8.5	1.5	D	d - r1>r2<r3<r4
5	8	s131	7.2	1.0	F	f - r1<r2<r3<r4
5	8	s132	6.2	0.8	F	f - r1<r2<r3<r4
5	8	s133	7.0	0.9	F	f - r1<r2<r3<r4
5	8	s134	7.0	1.2	F	f - r1<r2<r3<r4
5	8	s135	12.4	2.7	B	d - r1>r2<r3<r4
5	8	s136	8.0	1.2	F	f - r1<r2<r3<r4
5	8	s137	9.8	1.8	F	f - r1<r2<r3<r4
5	8	s138	14.6	2.1	D	d - r1>r2<r3<r4
5	8	s139	13.7	2.1	E	a - r1<r2>r3<r4
5	8	s140	11.4	1.6	F	f - r1<r2<r3<r4
5	8	s141	8.8	1.5	F	f - r1<r2<r3<r4
5	8	s142	11.8	2.3	F	f - r1<r2<r3<r4
5	9	s143	25.0	2.8	F	f - r1<r2<r3<r4
5	9	s144	21.1	2.0	F	f - r1<r2<r3<r4
5	9	s145	20.2	1.8	F	f - r1<r2<r3<r4
5	9	s146	17.1	2.2	D	d - r1>r2<r3<r4
5	9	s147	14.3	1.0	F	f - r1<r2<r3<r4
5	9	s148	15.2	1.7	F	f - r1<r2<r3<r4
5	9	s149	22.1	1.0	D	d - r1>r2<r3<r4
5	9	s150	12.0	0.8	D	d - r1>r2<r3<r4
5	9	s155	16.7	1.6	D	d - r1>r2<r3<r4
5	9	s156	30.9	1.3	D	d - r1>r2<r3<r4
5	9	s157	30.2	1.5	B	d - r1>r2<r3<r4
5	9	s158	19.1	1.4	D	d - r1>r2<r3<r4
5	9	s159	24.7	1.7	B	d - r1>r2<r3<r4

5	9	s160	27.5	2.1	B	d - r1>r2<r3<r4
5	10	s161	27.9	-	A	a - r1<r2>r3<r4
5	10	s162	30.9	2.0	B	d - r1>r2<r3<r4
5	10	s163	33.5	-	B	d - r1>r2<r3<r4
5	10	s164	16.2	3.4	D	d - r1>r2<r3<r4
5	10	s165	17.2	1.5	D	d - r1>r2<r3<r4
5	10	s166	14.3	2.9	E	d - r1>r2<r3<r4
5	10	s167	16.1	1.9	E	d - r1>r2<r3<r4
5	10	s168	22.9	1.9	D	d - r1>r2<r3<r4
5	10	s169	19.5	1.9	D	d - r1>r2<r3<r4
5	10	s170	22.5	1.7	D	d - r1>r2<r3<r4
5	10	s171	16.9	1.5	E	a - r1<r2>r3<r4
5	10	s172	16.0	1.4	D	d - r1>r2<r3<r4
Area	**Group**	**Sounding**	**Rhoa(25)**	**IP(25)**	**Shape**	**4 layer structure**
5	10	s173	13.5	1.1	E	a - r1<r2>r3<r4
5	10	s174	11.0	1.4	E	f - r1<r2<r3<r4
5	10	s175	16.5	1.1	E	a - r1<r2>r3<r4
5	10	s176	13.7	2.1	D	d - r1>r2<r3<r4
5	10	s177	12.8	1.6	D	d - r1>r2<r3<r4
5	10	s178	18.8	2.5	D	d - r1>r2<r3<r4
5	10	s179	10.9	1.8	D	d - r1>r2<r3<r4
5	10	s180	10.0	1.6	F	f - r1<r2<r3<r4
5	10	s181	12.3	1.4	D	d - r1>r2<r3<r4
5	10	s182	11.2	2.1	D	d - r1>r2<r3<r4
5	10	s183	8.6	1.3	F	f - r1<r2<r3<r4
5	10	s184	6.2	3.9	F	f - r1<r2<r3<r4
5	10	s185	7.6	1.4	D	d - r1>r2<r3<r4
5	10	s186	9.9	1.7	D	d - r1>r2<r3<r4
5	10	s187	9.5	1.5	D	d - r1>r2<r3<r4
5	10	s188	8.2	1.2	D	d - r1>r2<r3<r4
5	10	s189	9.4	-	D	d - r1>r2<r3<r4
5	10	s190	9.0	1.5	F	f - r1<r2<r3<r4
5	10	s191	11.1	1.4	F	f - r1<r2<r3<r4
5	10	s192	15.1	2.2	F	f - r1<r2<r3<r4
5	10	s193	19.1	2.0	E	d - r1>r2<r3<r4
5	10	s194	16.8	1.5	E	d - r1>r2<r3<r4
5	10	s195	11.9	1.8	F	f - r1<r2<r3<r4
5	10	s196	9.9	2.0	F	f - r1<r2<r3<r4
5	10	s197	13.4	3.3	E	a - r1<r2>r3<r4
5	10	s198	26.4	2.8	B	d - r1>r2<r3<r4
5	10	s199	18.4	1.5	F	f - r1<r2<r3<r4
5	10	s200	13.8	1.9	F	f - r1<r2<r3<r4
5	10	s201	16.4	2.3	F	f - r1<r2<r3<r4
5	10	s202	14.1	2.4	F	f - r1<r2<r3<r4

5	10	s203	15.0	2.1	F	f - r1<r2<r3<r4
5	10	s204	17.8	2.2	F	f - r1<r2<r3<r4
6	14	s289	6.8	0.1	E	a - r1<r2>r3<r4
6	14	s290	102.7	2.6	B	d - r1>r2<r3<r4
6	14	s291	88.3	2.1	C	a - r1<r2>r3<r4
6	14	s292	100.0	2.3	C	c - r1>r2>r3<r4
6	14	s293	163.0	3.0	C	c - r1>r2>r3<r4
6	14	s294	116.8	2.0	E	d - r1>r2<r3<r4
6	14	s295	13.1	1.1	E	a - r1<r2>r3<r4
Area	**Group**	**Sounding**	**Rhoa(25)**	**IP(25)**	**Shape**	**4 layer structure**
6	14	s296	6.4	0.5	F	f - r1<r2<r3<r4
6	14	s297	8.0	0.7	F	f - r1<r2<r3<r4
6	14	s298	6.8	0.7	F	f - r1<r2<r3<r4
6	14	s299	7.4	0.7	F	f - r1<r2<r3<r4
6	14	s300	10.4	1.3	B	d - r1>r2<r3<r4
6	14	s301	13.5	2.8	B	d - r1>r2<r3<r4
6	14	s302	12.0	2.0	B	d - r1>r2<r3<r4
6	14	s303	12.6	3.1	B	d - r1>r2<r3<r4
6	14	s304	11.2	2.5	D	d - r1>r2<r3<r4
6	14	s305	13.3	2.6	D	d - r1>r2<r3<r4
6	14	s306	17.3	3.5	D	d - r1>r2<r3<r4
6	14	s307	12.9	2.2	D	d - r1>r2<r3<r4
6	14	s308	19.9	2.7	F	f - r1<r2<r3<r4
6	14	s309	212.3	2.0	E	d - r1>r2<r3<r4
6	14	s310	100.5	2.2	E	a - r1<r2>r3<r4
6	14	s311	123.8	2.5	E	a - r1<r2>r3<r4
6	15	s312	87.9	0.9	E	a - r1<r2>r3<r4
6	15	s313	26.8	0.8	F	f - r1<r2<r3<r4
6	15	s314	7.3	0.9	D	d - r1>r2<r3<r4
6	15	s315	6.3	0.4	F	f - r1<r2<r3<r4
6	15	s316	20.8	1.0	F	f - r1<r2<r3<r4
6	15	s317	607.4	1.6	C	a - r1<r2>r3<r4
6	15	s318	509.3	1.4	C	a - r1<r2>r3<r4
6	15	s319	679.5	1.3	D	a - r1<r2>r3<r4
6	15	s320	22.5	0.5	E	a - r1<r2>r3<r4
6	15	s321	20.0	1.0	E	d - r1>r2<r3<r4
6	15	s322	91.9	3.6	B	d - r1>r2<r3<r4

* Sounding shape is classified A to E based on example general shapes illustrated in Figure 4.4. An ‘x’ after the classification indicates that the curve flattened or turned downward at the highest AB spacings.

** Ground structure based on 1D inversions where only 4 layers were permitted: ri is the resistivity of the ith layer. There were 4 patterns identified, labeled a, c, d and f to correspond approximately to the sounding shapes A,C, D and F. The 4th layer always had the highest resistivity.

Appendix E: 1D Inversion Resistivity Models

Group 1

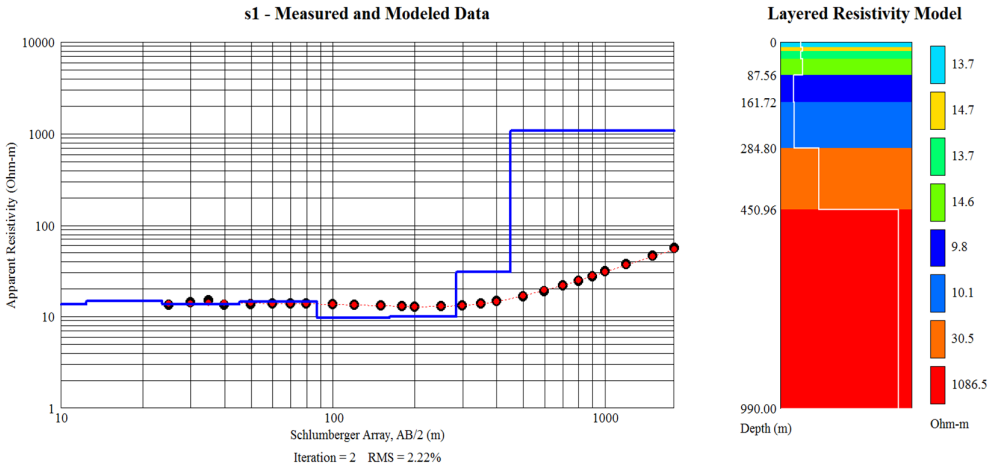
s1 - Measured and Modeled Data
Apparent Resistivity (Ohm-m)
10000
1000
100
10
1
10
100
1000
Schlumberger Array, AB/2 (m)
Iteration = 2 RMS = 2.22%
Layered Resistivity Model
0
87.56
161.72
284.80
450.96
990.00
Depth (m)
13.7
14.7
13.7
14.6
9.8
10.1
30.5
1086.5
Ohm-m

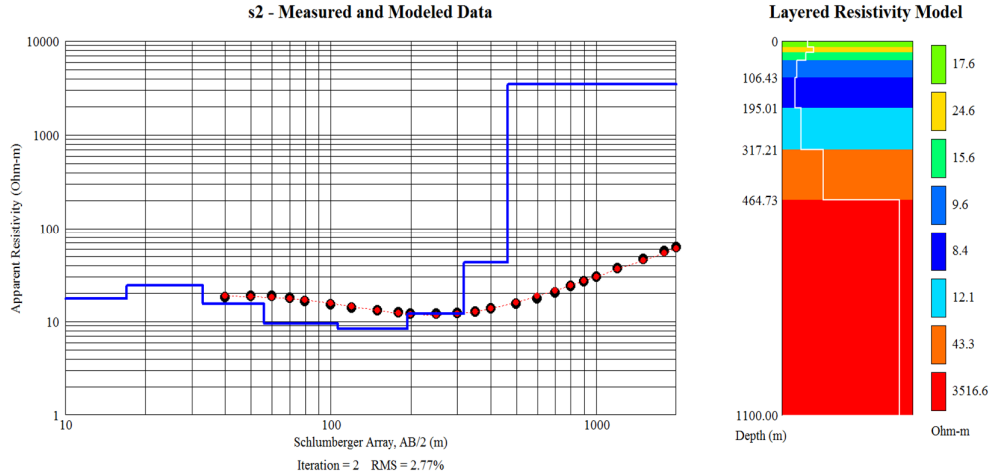
s2 - Measured and Modeled Data
Apparent Resistivity (Ohm-m)
10000
1000
100
10
1
10
100
1000
Schlumberger Array, AB/2 (m)
Iteration = 2 RMS = 2.77%
Layered Resistivity Model
0
106.43
195.01
317.21
464.73
1100.00
Depth (m)
17.6
24.6
15.6
9.6
8.4
12.1
43.3
3516.6
Ohm-m

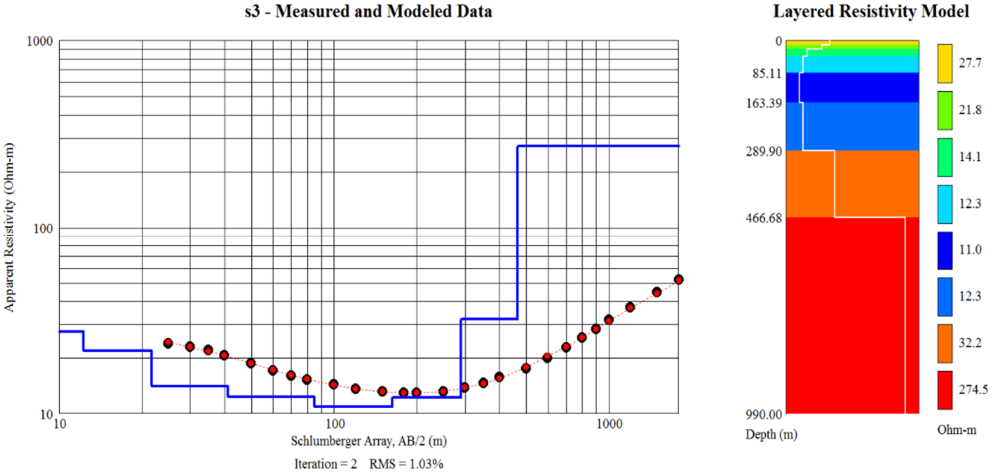
s3 - Measured and Modeled Data
Apparent Resistivity (Ohm-m)
1000
100
10
10
100
1000
Schlumberger Array, AB/2 (m)
Iteration = 2 RMS = 1.03%
Layered Resistivity Model
0
85.11
163.39
289.90
466.68
990.00
Depth (m)
27.7
21.8
14.1
12.3
11.0
12.3
32.2
274.5
Ohm-m

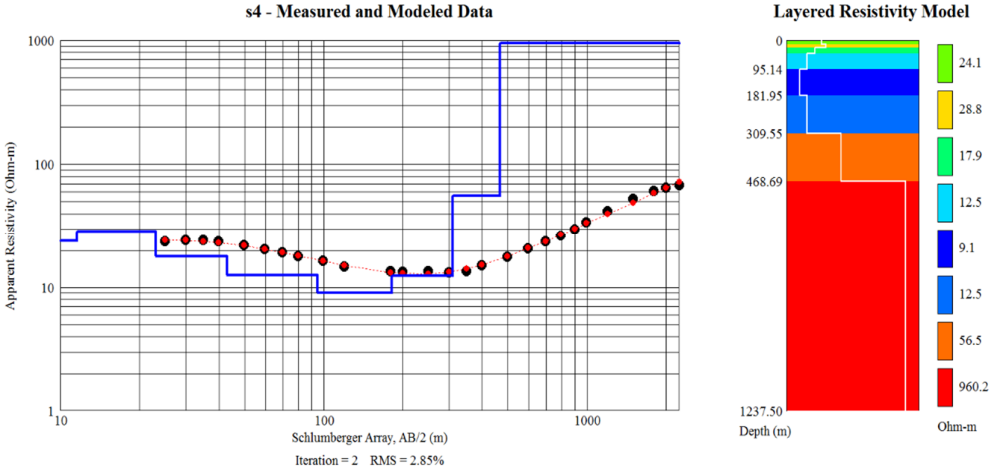
s4 - Measured and Modeled Data
Apparent Resistivity (Ohm-m)
1000
100
10
1
10
100
1000
Schlumberger Array, AB/2 (m)
Iteration = 2 RMS = 2.85%
Layered Resistivity Model
0
95.14
181.95
309.55
468.69
1237.50
Depth (m)
24.1
28.8
17.9
12.5
9.1
12.5
56.5
960.2
Ohm-m

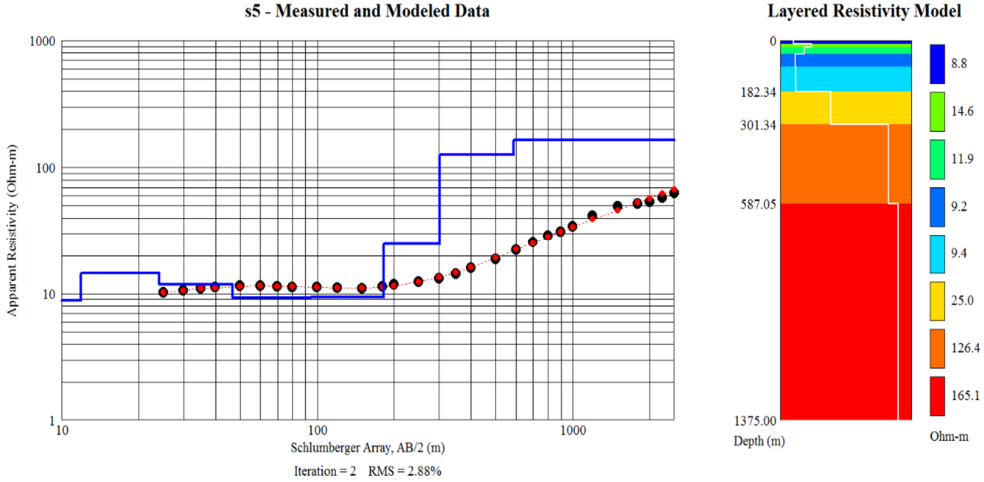
s5 - Measured and Modeled Data
Apparent Resistivity (Ohm-m)
1000
100
10
1
10
100
1000
Schlumberger Array, AB/2 (m)
Iteration = 2 RMS = 2.88%
Layered Resistivity Model
0
182.34
301.34
587.05
1375.00
Depth (m)
8.8
14.6
11.9
9.2
9.4
25.0
126.4
165.1
Ohm-m

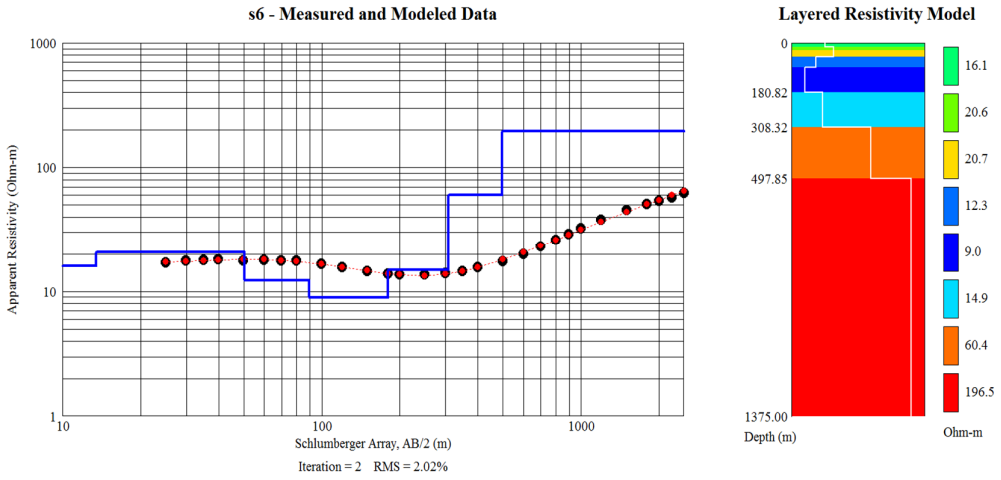
s6 - Measured and Modeled Data
Apparent Resistivity (Ohm-m)
1000
100
10
1
10
100
1000
Schlumberger Array, AB/2 (m)
Iteration = 2 RMS = 2.02%
Layered Resistivity Model
0
180.82
308.32
497.85
1375.00
Depth (m)
16.1
20.6
20.7
12.3
9.0
14.9
60.4
196.5
Ohm-m

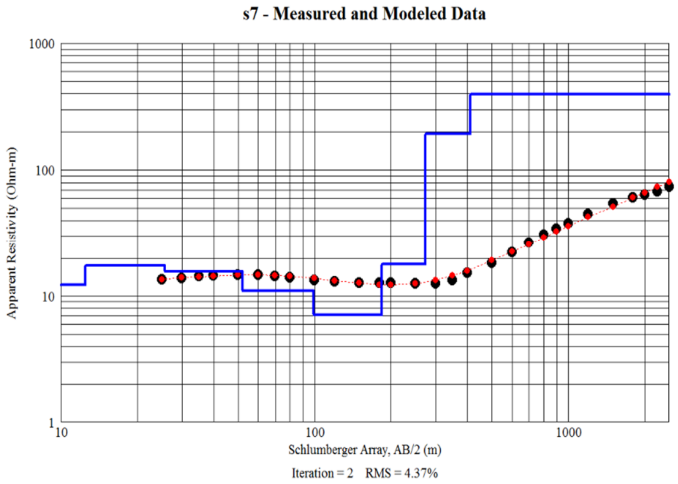
s7 - Measured and Modeled Data
Apparent Resistivity (Ohm-m)
1000
100
10
1
10
100
1000
Schlumberger Array, AB/2 (m)
Iteration = 2 RMS = 4.37%

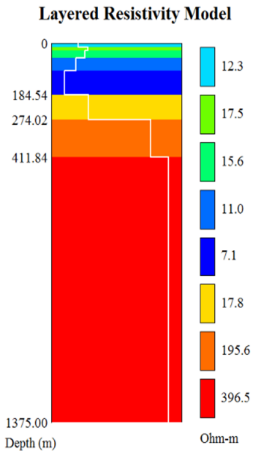
Layered Resistivity Model
0
184.54
274.02
411.84
1375.00
Depth (m)
12.3
17.5
15.6
11.0
7.1
17.8
195.6
396.5
Ohm-m

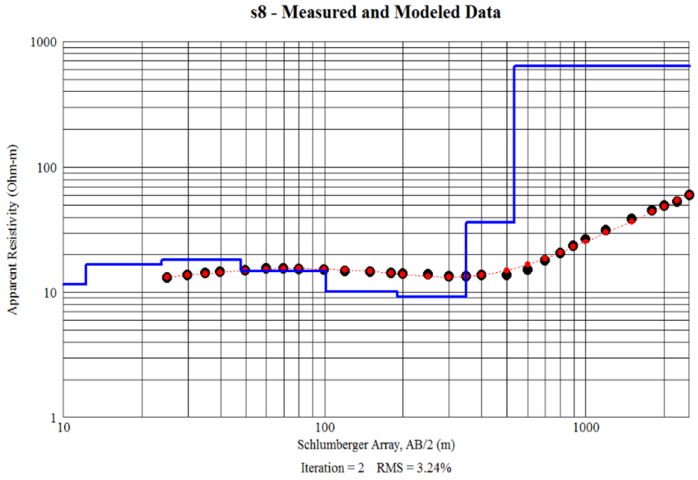
s8 - Measured and Modeled Data
Apparent Resistivity (Ohm-m)
1000
100
10
1
10
100
1000
Schlumberger Array, AB/2 (m)
Iteration = 2 RMS = 3.24%

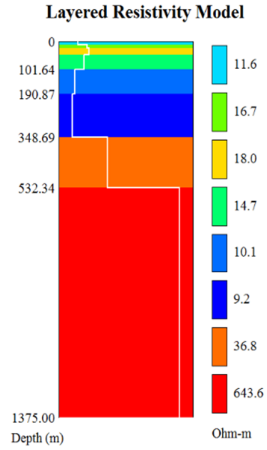
Layered Resistivity Model
0
101.64
190.87
348.69
532.34
1375.00
Depth (m)
11.6
16.7
18.0
14.7
10.1
9.2
36.8
643.6
Ohm-m

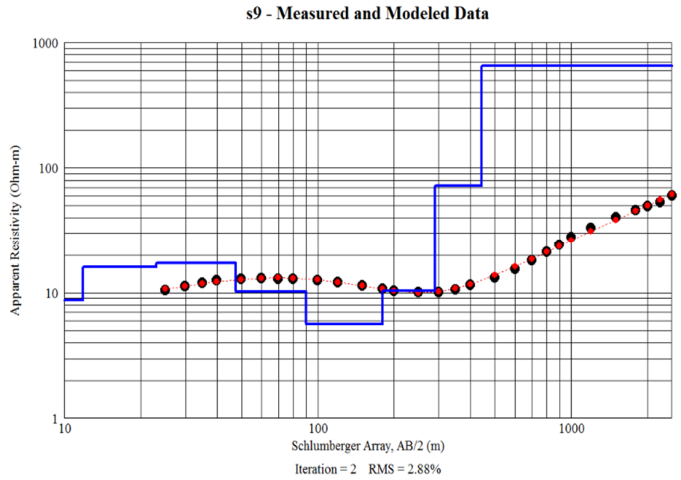
s9 - Measured and Modeled Data
Apparent Resistivity (Ohm-m)
1000
100
10
1
10
100
1000
Schlumberger Array, AB/2 (m)
Iteration = 2 RMS = 2.88%

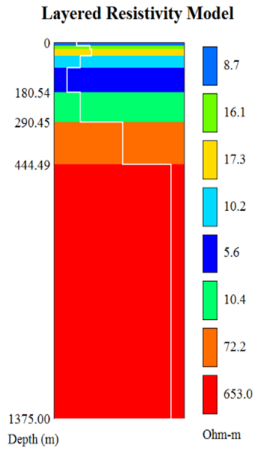
Layered Resistivity Model
0
180.54
290.45
444.49
1375.00
Depth (m)
8.7
16.1
17.3
10.2
5.6
10.4
72.2
653.0
Ohm-m

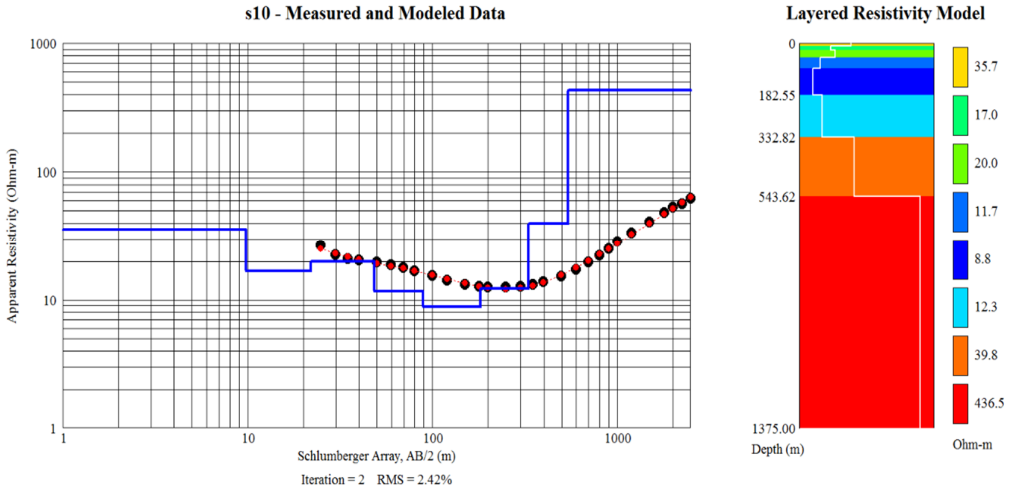
s10 - Measured and Modeled Data
Apparent Resistivity (Ohm-m)
1000
100
10
1
1
10
100
1000
Schlumberger Array, AB/2 (m)
Iteration = 2 RMS = 2.42%
Layered Resistivity Model
0
182.55
332.82
543.62
1375.00
Depth (m)
35.7
17.0
20.0
11.7
8.8
12.3
39.8
436.5
Ohm-m

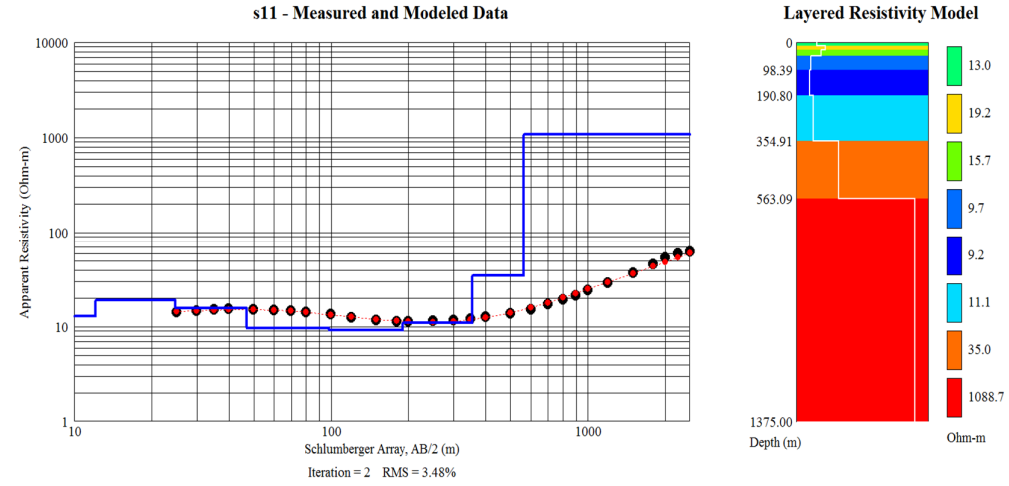
s11 - Measured and Modeled Data
Apparent Resistivity (Ohm-m)
10000
1000
100
10
1
10
100
1000
Schlumberger Array, AB/2 (m)
Iteration = 2 RMS = 3.48%
Layered Resistivity Model
0
98.39
190.80
354.91
563.09
1375.00
Depth (m)
13.0
19.2
15.7
9.7
9.2
11.1
35.0
1088.7
Ohm-m

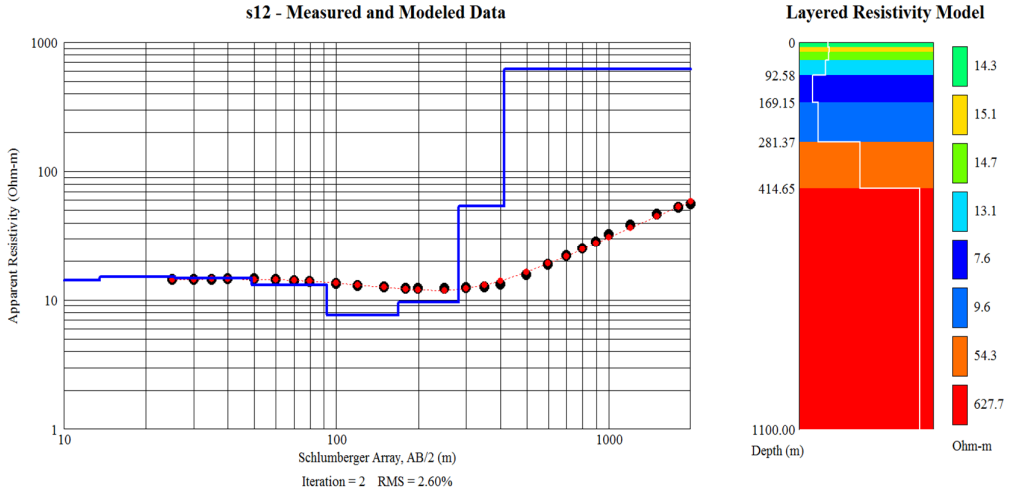
s12 - Measured and Modeled Data
Apparent Resistivity (Ohm-m)
1000
100
10
1
10
100
1000
Schlumberger Array, AB/2 (m)
Iteration = 2 RMS = 2.60%
Layered Resistivity Model
0
92.58
169.15
281.37
414.65
1100.00
Depth (m)
14.3
15.1
14.7
13.1
7.6
9.6
54.3
627.7
Ohm-m

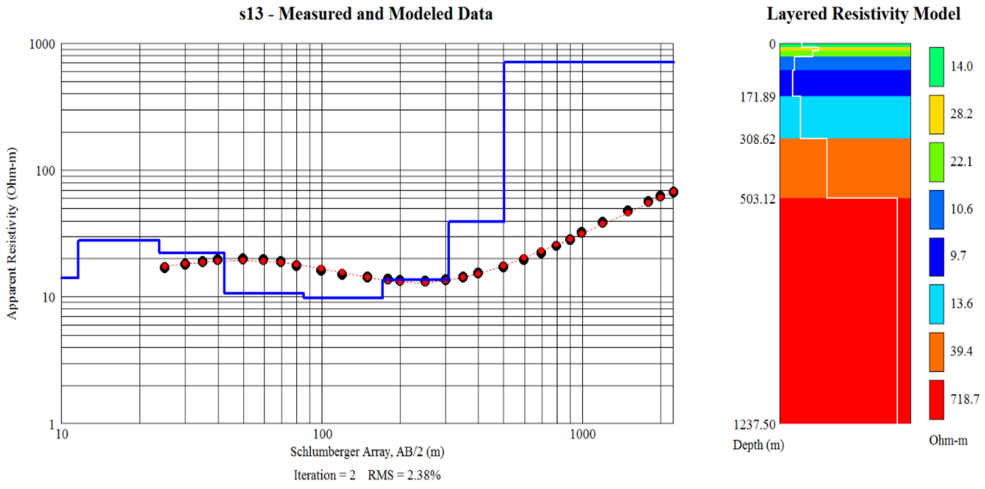
s13 - Measured and Modeled Data
Apparent Resistivity (Ohm-m)
1000
100
10
1
10
100
1000
Schlumberger Array, AB/2 (m)
Iteration = 2 RMS = 2.38%
Layered Resistivity Model
0
171.89
308.62
503.12
1237.50
Depth (m)
14.0
28.2
22.1
10.6
9.7
13.6
39.4
718.7
Ohm-m

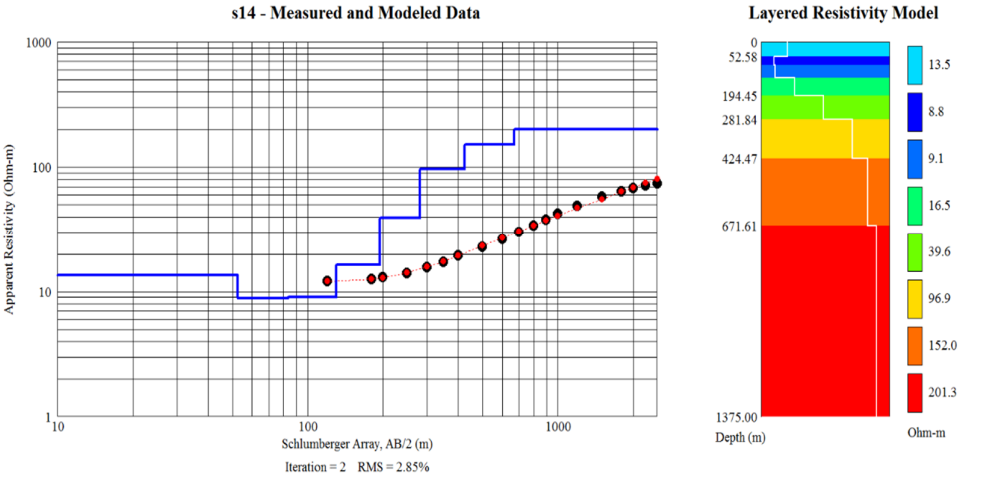
s14 - Measured and Modeled Data
Apparent Resistivity (Ohm-m)
1000
100
10
1
10
100
1000
Schlumberger Array, AB/2 (m)
Iteration = 2 RMS = 2.85%
Layered Resistivity Model
0
52.58
194.45
281.84
424.47
671.61
1375.00
Depth (m)
13.5
8.8
9.1
16.5
39.6
96.9
152.0
201.3
Ohm-m

Group 2

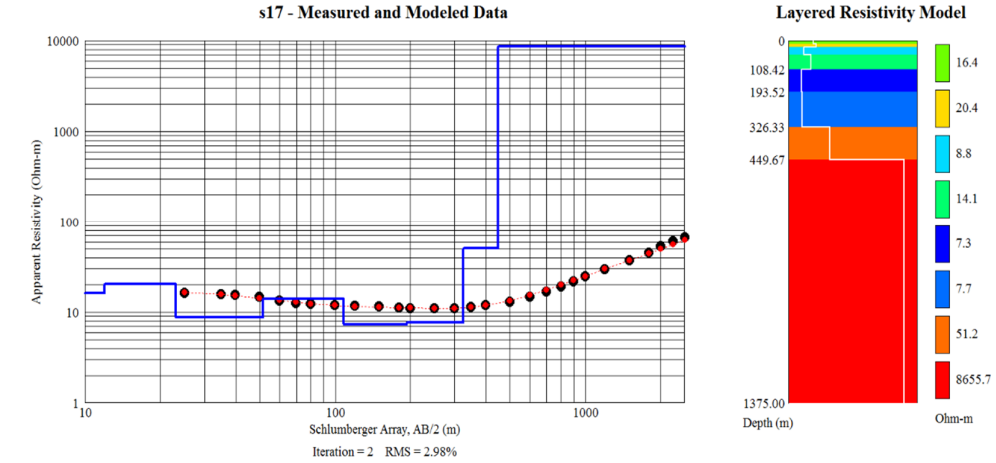
s17 - Measured and Modeled Data
Apparent Resistivity (Ohm-m)
10000
1000
100
10
1
10
100
1000
Schlumberger Array, AB/2 (m)
Iteration = 2 RMS = 2.98%
Layered Resistivity Model
0
108.42
193.52
326.33
449.67
1375.00
Depth (m)
16.4
20.4
8.8
14.1
7.3
7.7
51.2
8655.7
Ohm-m

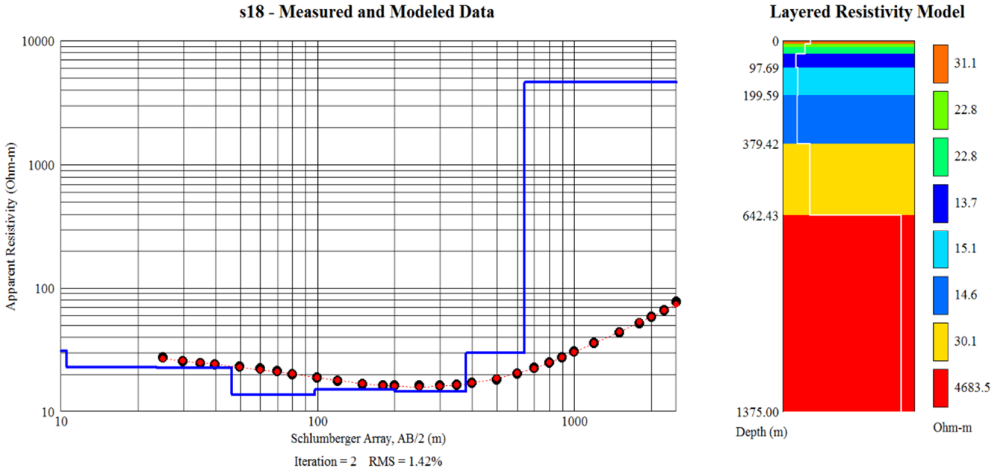
s18 - Measured and Modeled Data
Apparent Resistivity (Ohm-m)
10000
1000
100
10
10
100
1000
Schlumberger Array, AB/2 (m)
Iteration = 2 RMS = 1.42%
Layered Resistivity Model
0
97.69
199.59
379.42
642.43
1375.00
Depth (m)
31.1
22.8
22.8
13.7
15.1
14.6
30.1
4683.5
Ohm-m

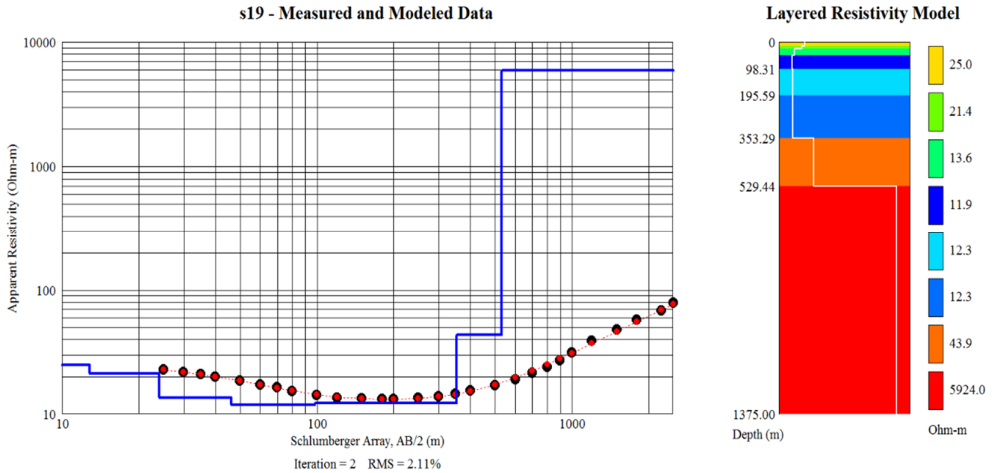
s19 - Measured and Modeled Data
Apparent Resistivity (Ohm-m)
10000
1000
100
10
10
100
1000
Schlumberger Array, AB/2 (m)
Iteration = 2 RMS = 2.11%
Layered Resistivity Model
0
98.31
195.59
353.29
529.44
1375.00
Depth (m)
25.0
21.4
13.6
11.9
12.3
12.3
43.9
5924.0
Ohm-m

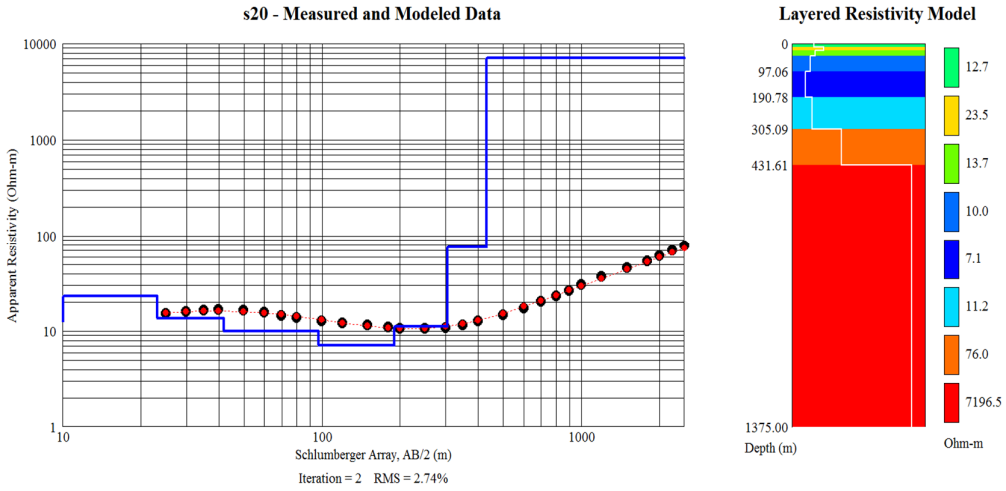
s20 - Measured and Modeled Data
Apparent Resistivity (Ohm-m)
10000
1000
100
10
1
10
100
1000
Schlumberger Array, AB/2 (m)
Iteration = 2 RMS = 2.74%
Layered Resistivity Model
0
97.06
190.78
305.09
431.61
1375.00
Depth (m)
12.7
23.5
13.7
10.0
7.1
11.2
76.0
7196.5
Ohm-m

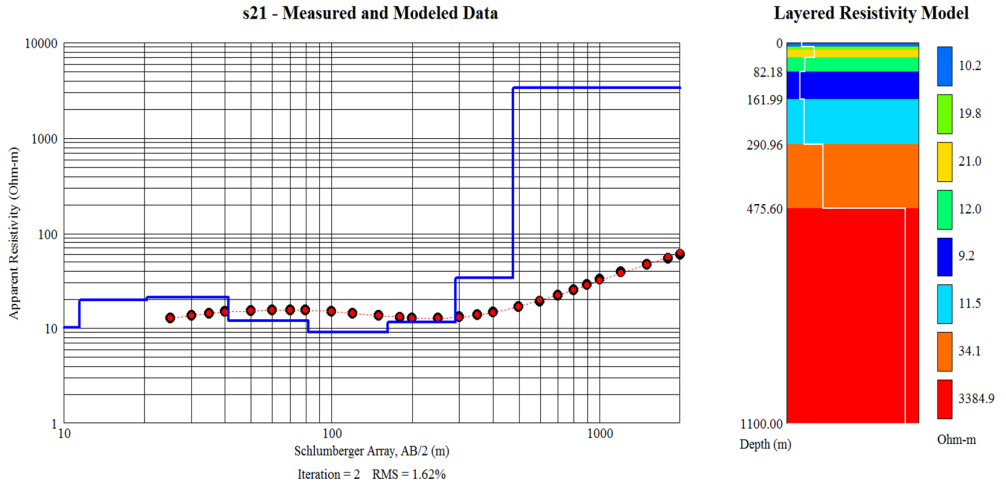
s21 - Measured and Modeled Data
Apparent Resistivity (Ohm-m)
10000
1000
100
10
1
10
100
1000
Schlumberger Array, AB/2 (m)
Iteration = 2 RMS = 1.62%
Layered Resistivity Model
0
82.18
161.99
290.96
475.60
1100.00
Depth (m)
10.2
19.8
21.0
12.0
9.2
11.5
34.1
3384.9
Ohm-m

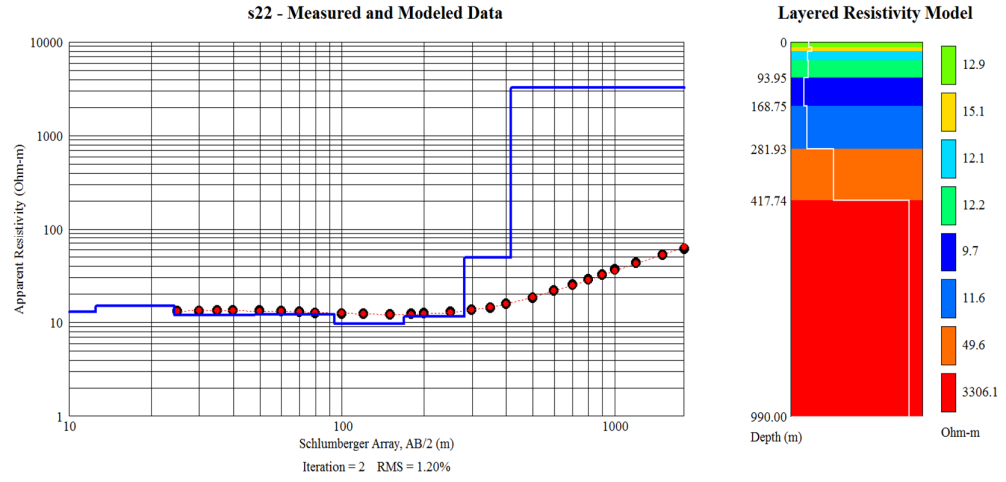
s22 - Measured and Modeled Data
Apparent Resistivity (Ohm-m)
10000
1000
100
10
1
10
100
1000
Schlumberger Array, AB/2 (m)
Iteration = 2 RMS = 1.20%
Layered Resistivity Model
0
93.95
168.75
281.93
417.74
990.00
Depth (m)
12.9
15.1
12.1
12.2
9.7
11.6
49.6
3306.1
Ohm-m

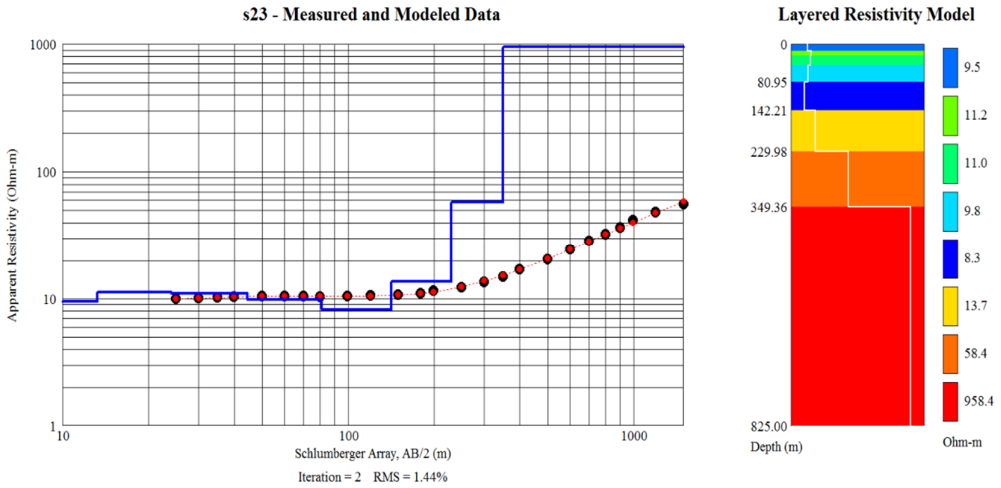
s23 - Measured and Modeled Data
Apparent Resistivity (Ohm-m)
1000
100
10
1
10
100
1000
Schlumberger Array, AB/2 (m)
Iteration = 2 RMS = 1.44%
Layered Resistivity Model
0
80.95
142.21
229.98
349.36
825.00
Depth (m)
9.5
11.2
11.0
9.8
8.3
13.7
58.4
958.4
Ohm-m

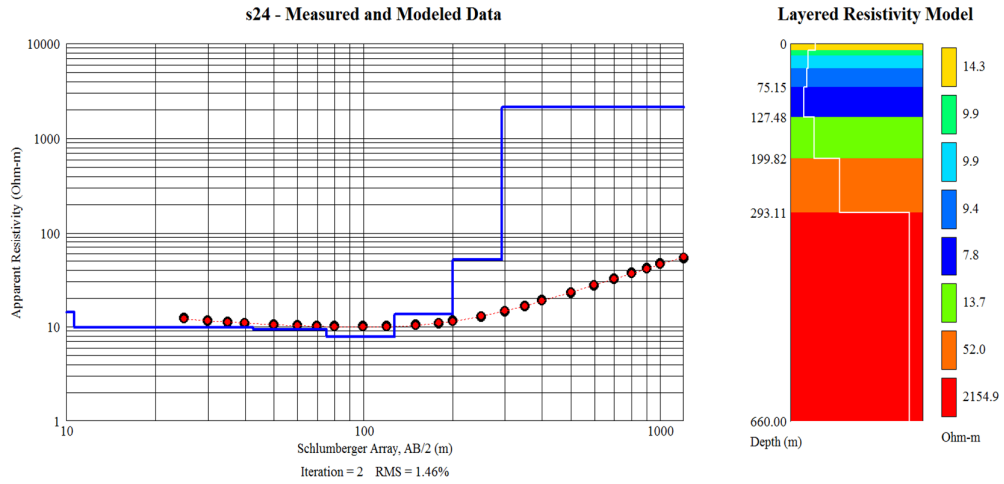
s24 - Measured and Modeled Data
Apparent Resistivity (Ohm-m)
10000
1000
100
10
1
10
100
1000
Schlumberger Array, AB/2 (m)
Iteration = 2 RMS = 1.46%
Layered Resistivity Model
0
75.15
127.48
199.82
293.11
660.00
Depth (m)
14.3
9.9
9.9
9.4
7.8
13.7
52.0
2154.9
Ohm-m

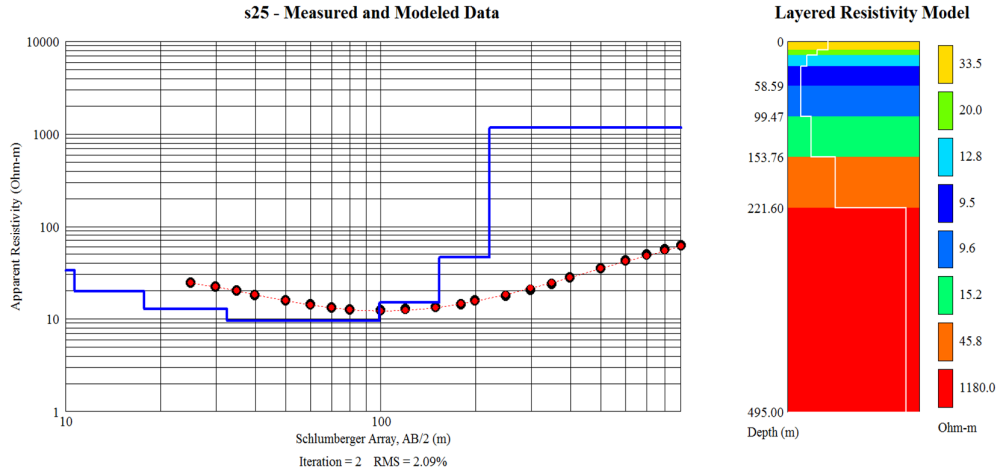
s25 - Measured and Modeled Data
Apparent Resistivity (Ohm-m)
10000
1000
100
10
1
10
100
Schlumberger Array, AB/2 (m)
Iteration = 2 RMS = 2.09%
Layered Resistivity Model
0
58.59
99.47
153.76
221.60
495.00
Depth (m)
33.5
20.0
12.8
9.5
9.6
15.2
45.8
1180.0
Ohm-m

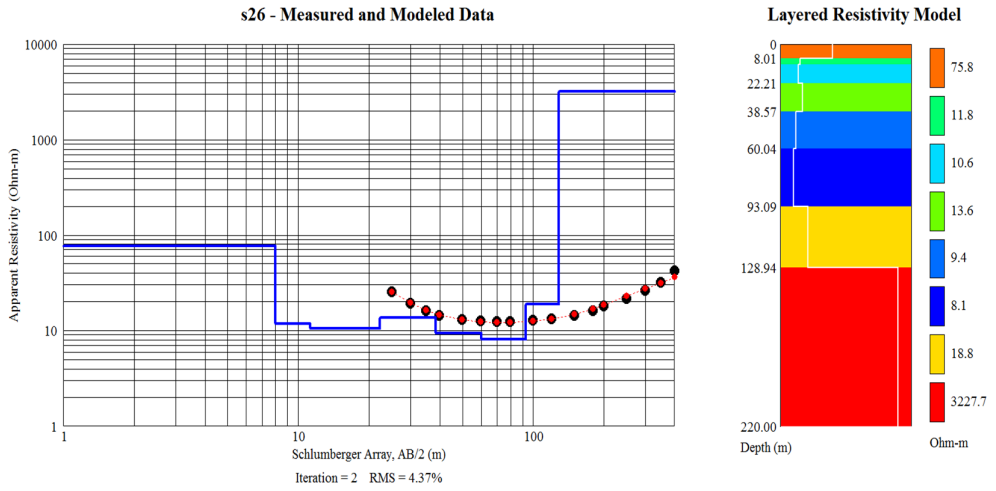
s26 - Measured and Modeled Data
Apparent Resistivity (Ohm-m)
10000
1000
100
10
1
1
10
100
Schlumberger Array, AB/2 (m)
Iteration = 2 RMS = 4.37%
Layered Resistivity Model
0
8.01
22.21
38.57
60.04
93.09
128.94
220.00
Depth (m)
75.8
11.8
10.6
13.6
9.4
8.1
18.8
3227.7
Ohm-m

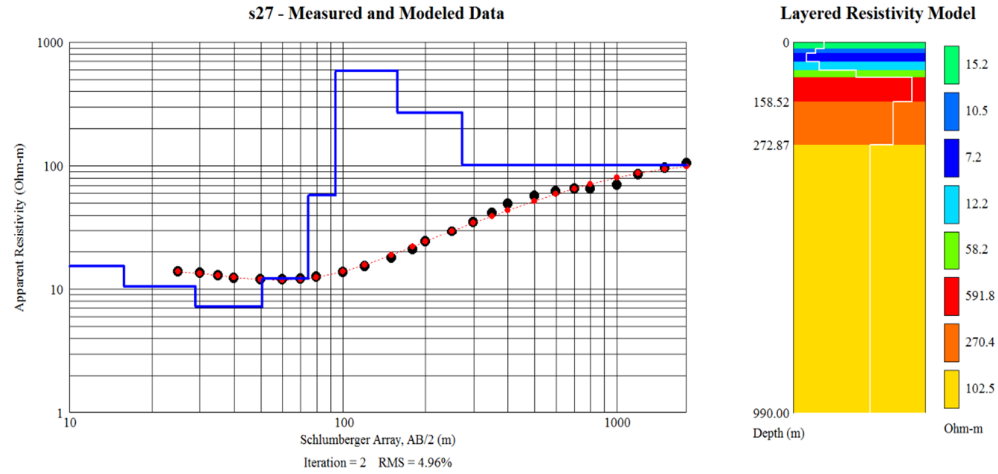
s27 - Measured and Modeled Data
Apparent Resistivity (Ohm-m)
1000
100
10
1
10
100
1000
Schlumberger Array, AB/2 (m)
Iteration = 2 RMS = 4.96%
Layered Resistivity Model
0
158.52
272.87
990.00
Depth (m)
15.2
10.5
7.2
12.2
58.2
591.8
270.4
102.5
Ohm-m

Group 3

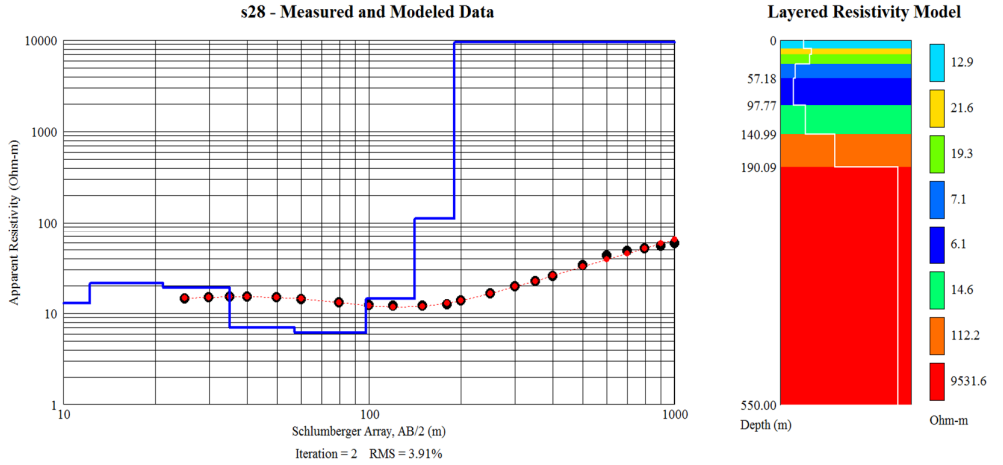
s28 - Measured and Modeled Data
Apparent Resistivity (Ohm-m)
10000
1000
100
10
1
10
100
1000
Schlumberger Array, AB/2 (m)
Iteration = 2 RMS = 3.91%
Layered Resistivity Model
0
57.18
97.77
140.99
190.09
550.00
Depth (m)
12.9
21.6
19.3
7.1
6.1
14.6
112.2
9531.6
Ohm-m

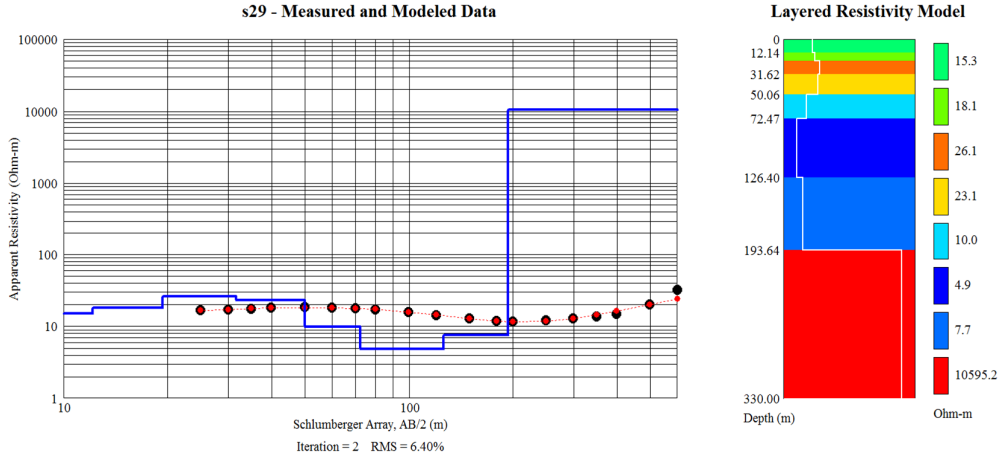
s29 - Measured and Modeled Data
Apparent Resistivity (Ohm-m)
100000
10000
1000
100
10
1
10
100
Schlumberger Array, AB/2 (m)
Iteration = 2 RMS = 6.40%
Layered Resistivity Model
0
12.14
31.62
50.06
72.47
126.40
193.64
330.00
Depth (m)
15.3
18.1
26.1
23.1
10.0
4.9
7.7
10595.2
Ohm-m

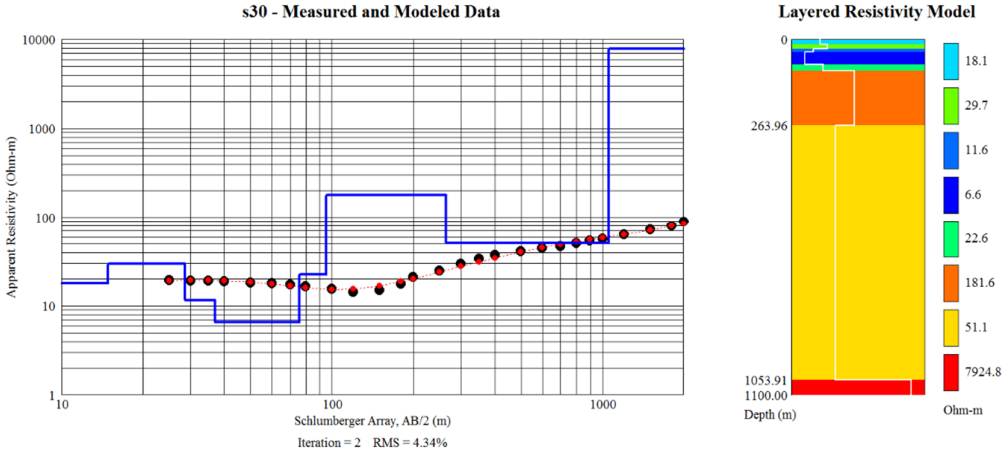
s30 - Measured and Modeled Data
Apparent Resistivity (Ohm-m)
10000
1000
100
10
1
10
100
1000
Schlumberger Array, AB/2 (m)
Iteration = 2 RMS = 4.34%
Layered Resistivity Model
0
263.96
1053.91
1100.00
Depth (m)
18.1
29.7
11.6
6.6
22.6
181.6
51.1
7924.8
Ohm-m

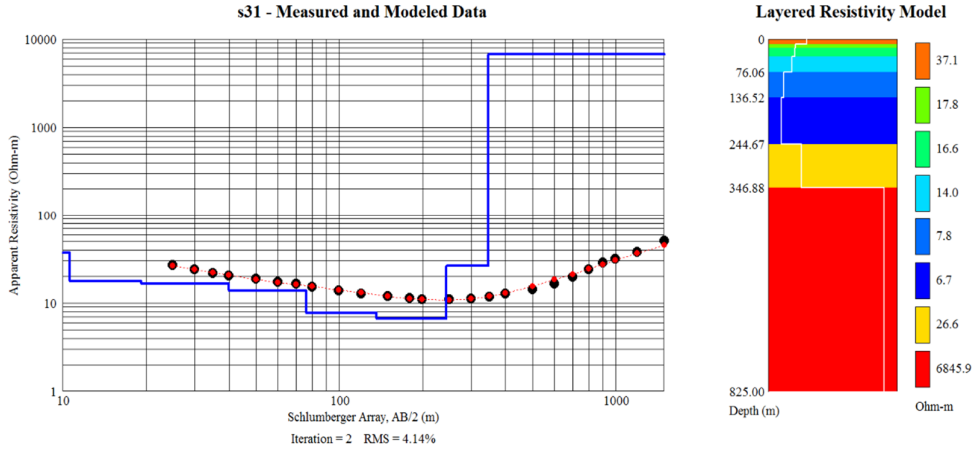
s31 - Measured and Modeled Data
Apparent Resistivity (Ohm-m)
10000
1000
100
10
1
10
100
1000
Schlumberger Array, AB/2 (m)
Iteration = 2 RMS = 4.14%
Layered Resistivity Model
0
76.06
136.52
244.67
346.88
825.00
Depth (m)
37.1
17.8
16.6
14.0
7.8
6.7
26.6
6845.9
Ohm-m

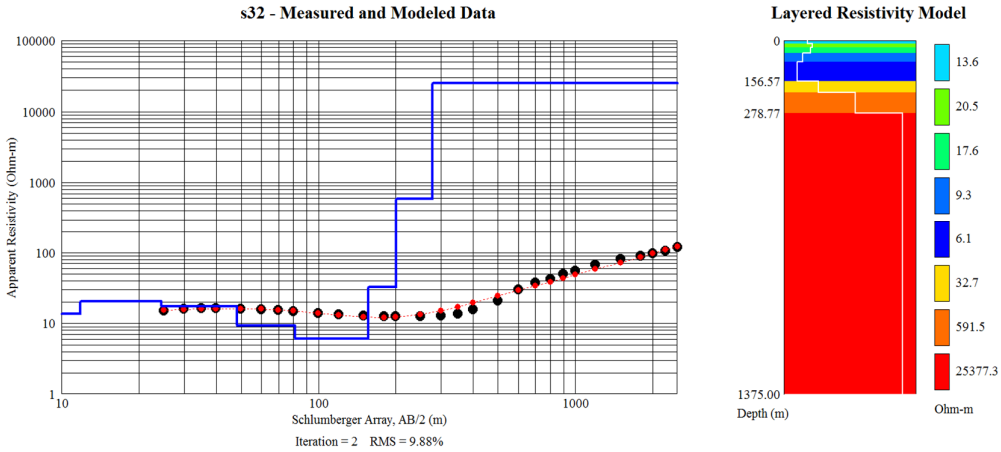
s32 - Measured and Modeled Data
Apparent Resistivity (Ohm-m)
100000
10000
1000
100
10
1
10
100
1000
Schlumberger Array, AB/2 (m)
Iteration = 2 RMS = 9.88%
Layered Resistivity Model
0
156.57
278.77
1375.00
Depth (m)
13.6
20.5
17.6
9.3
6.1
32.7
591.5
25377.3
Ohm-m

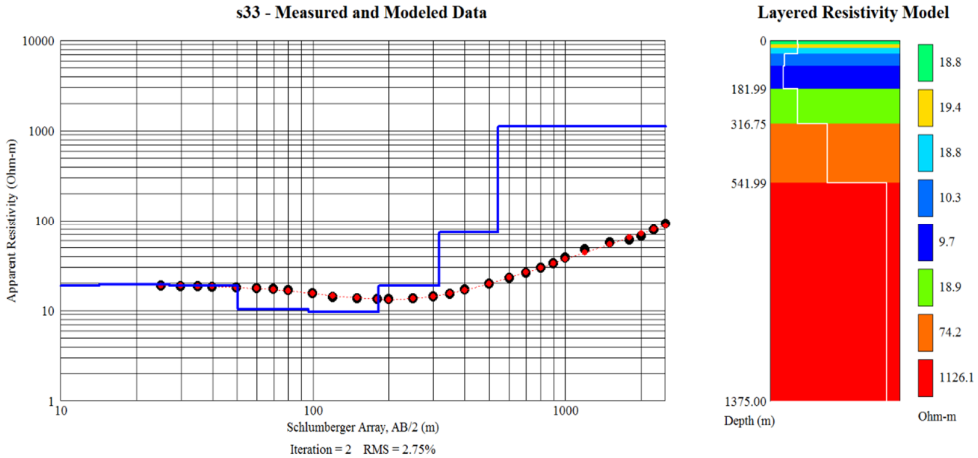
s33 - Measured and Modeled Data
Apparent Resistivity (Ohm-m)
10000
1000
100
10
1
10
100
1000
Schlumberger Array, AB/2 (m)
Iteration = 2 RMS = 2.75%
Layered Resistivity Model
0
181.99
316.75
541.99
1375.00
Depth (m)
18.8
19.4
18.8
10.3
9.7
18.9
74.2
1126.1
Ohm-m

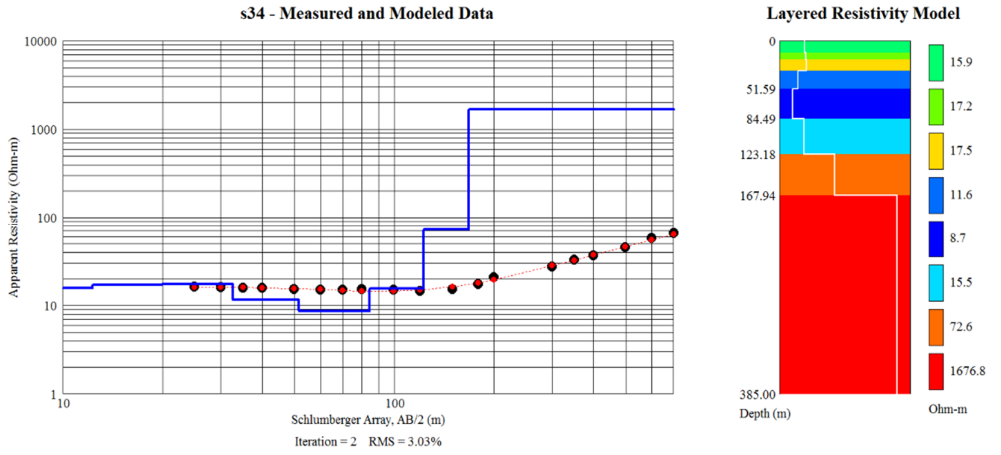
s34 - Measured and Modeled Data
Apparent Resistivity (Ohm-m)
10000
1000
100
10
1
10
100
Schlumberger Array, AB/2 (m)
Iteration = 2 RMS = 3.03%
Layered Resistivity Model
0
51.59
84.49
123.18
167.94
385.00
Depth (m)
15.9
17.2
17.5
11.6
8.7
15.5
72.6
1676.8
Ohm-m

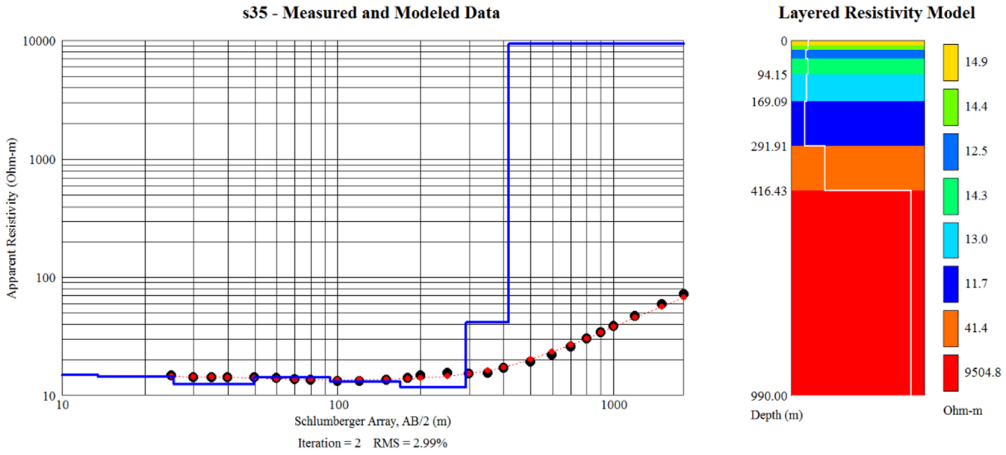
s35 - Measured and Modeled Data
Apparent Resistivity (Ohm-m)
10000
1000
100
10
10
100
1000
Schlumberger Array, AB/2 (m)
Iteration = 2 RMS = 2.99%
Layered Resistivity Model
0
94.15
169.09
291.91
416.43
990.00
Depth (m)
14.9
14.4
12.5
14.3
13.0
11.7
41.4
9504.8
Ohm-m

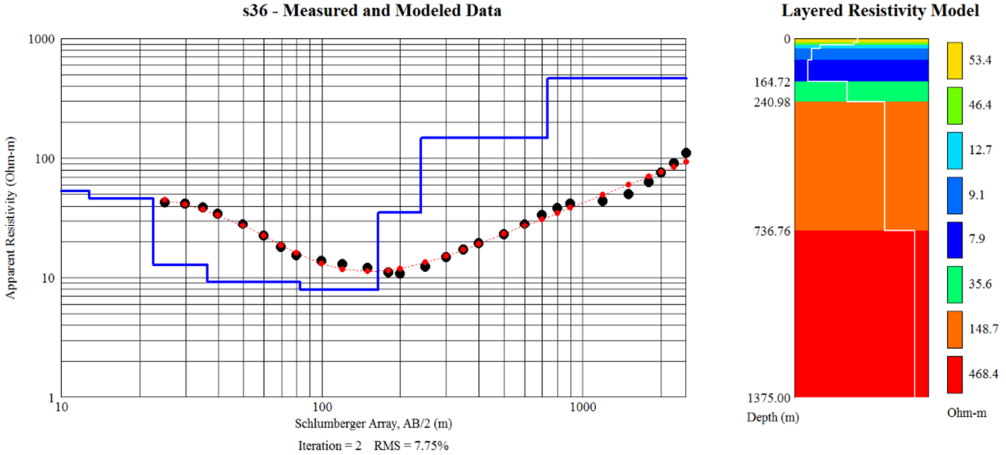
s36 - Measured and Modeled Data
Apparent Resistivity (Ohm-m)
1000
100
10
1
10
100
1000
Schlumberger Array, AB/2 (m)
Iteration = 2 RMS = 7.75%
Layered Resistivity Model
0
164.72
240.98
736.76
1375.00
Depth (m)
53.4
46.4
12.7
9.1
7.9
35.6
148.7
468.4
Ohm-m

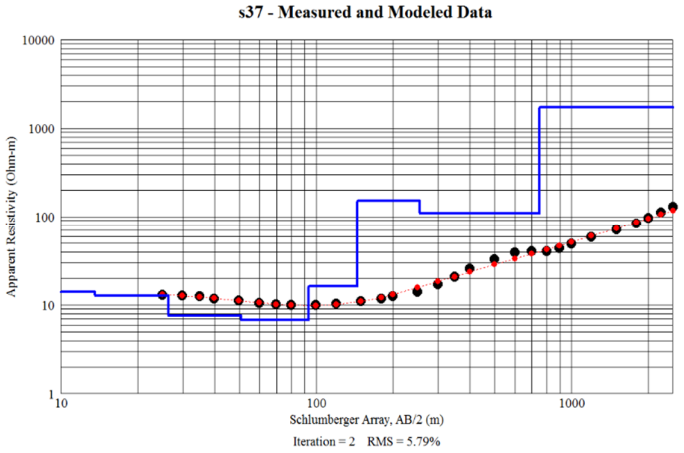
s37 - Measured and Modeled Data
Apparent Resistivity (Ohm-m)
10000
1000
100
10
1
10
100
1000
Schlumberger Array, AB/2 (m)
Iteration = 2 RMS = 5.79%

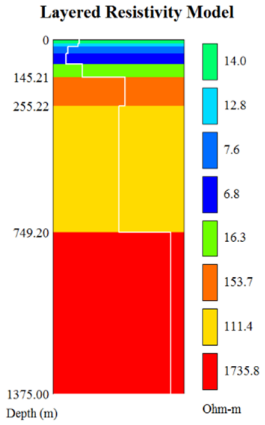
Layered Resistivity Model
0
145.21
255.22
749.20
1375.00
Depth (m)
14.0
12.8
7.6
6.8
16.3
153.7
111.4
1735.8
Ohm-m

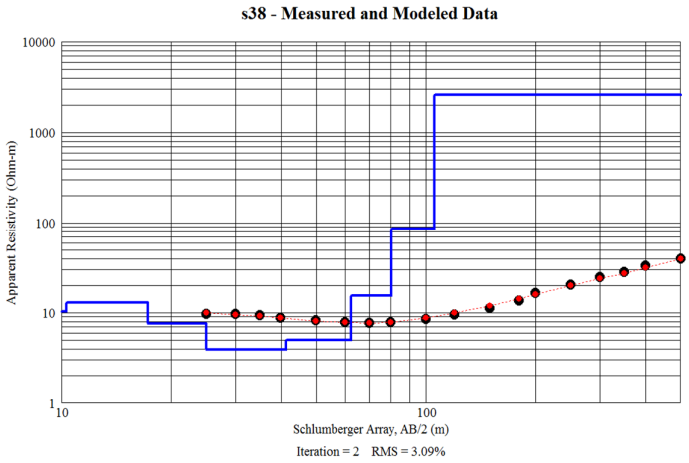
s38 - Measured and Modeled Data
Apparent Resistivity (Ohm-m)
10000
1000
100
10
1
10
100
Schlumberger Array, AB/2 (m)
Iteration = 2 RMS = 3.09%

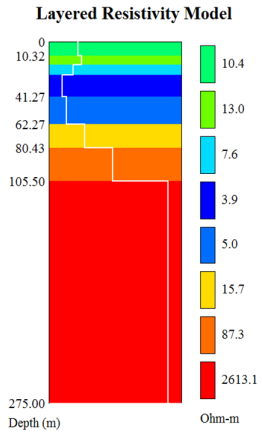
Layered Resistivity Model
0
10.32
41.27
62.27
80.43
105.50
275.00
Depth (m)
10.4
13.0
7.6
3.9
5.0
15.7
87.3
2613.1
Ohm-m

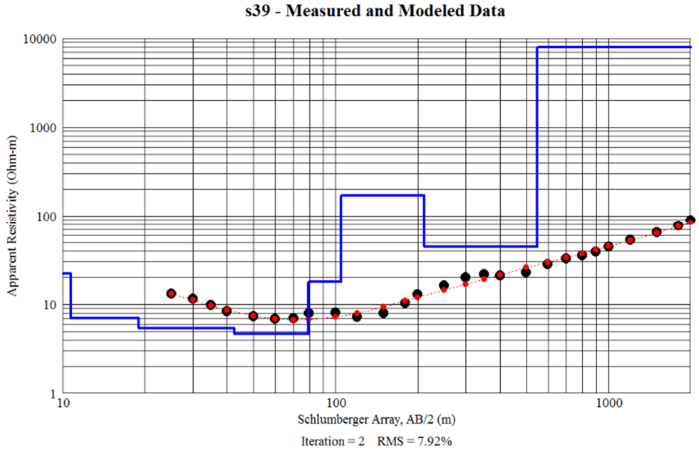
s39 - Measured and Modeled Data
Apparent Resistivity (Ohm-m)
10000
1000
100
10
1
10
100
1000
Schlumberger Array, AB/2 (m)
Iteration = 2 RMS = 7.92%

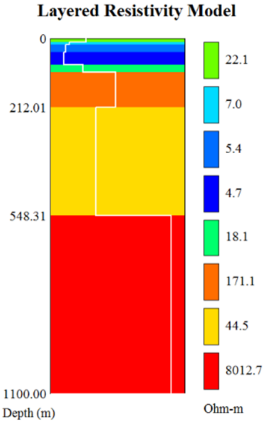
Layered Resistivity Model
0
212.01
548.31
1100.00
Depth (m)
22.1
7.0
5.4
4.7
18.1
171.1
44.5
8012.7
Ohm-m

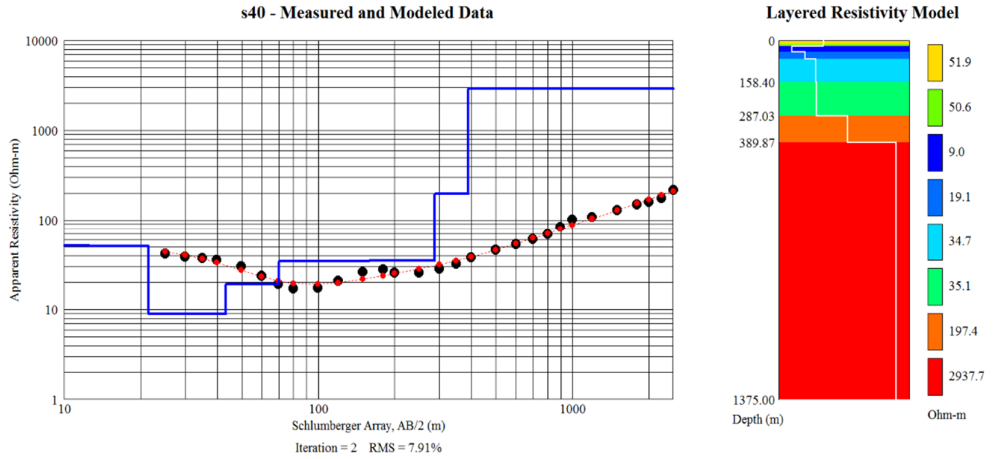
s40 - Measured and Modeled Data
Apparent Resistivity (Ohm-m)
10000
1000
100
10
1
10
100
1000
Schlumberger Array, AB/2 (m)
Iteration = 2 RMS = 7.91%
Layered Resistivity Model
0
158.40
287.03
389.87
1375.00
Depth (m)
51.9
50.6
9.0
19.1
34.7
35.1
197.4
2937.7
Ohm-m

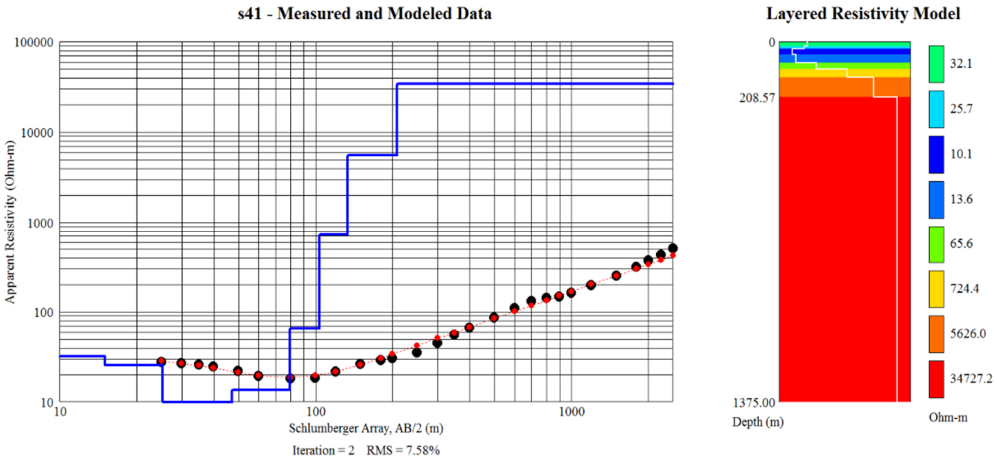
s41 - Measured and Modeled Data
Apparent Resistivity (Ohm-m)
100000
10000
1000
100
10
10
100
1000
Schlumberger Array, AB/2 (m)
Iteration = 2 RMS = 7.58%
Layered Resistivity Model
0
208.57
1375.00
Depth (m)
32.1
25.7
10.1
13.6
65.6
724.4
5626.0
34727.2
Ohm-m

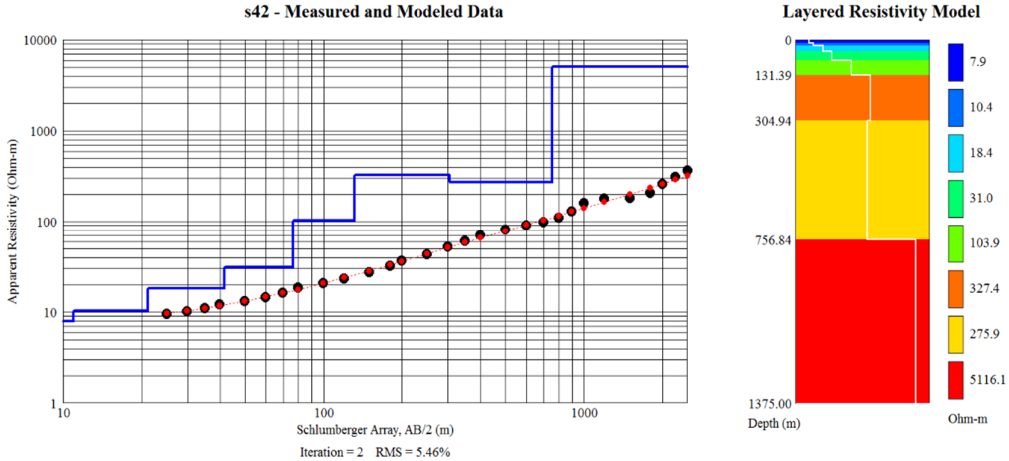
s42 - Measured and Modeled Data
Apparent Resistivity (Ohm-m)
10000
1000
100
10
1
10
100
1000
Schlumberger Array, AB/2 (m)
Iteration = 2 RMS = 5.46%
Layered Resistivity Model
0
131.39
304.94
756.84
1375.00
Depth (m)
7.9
10.4
18.4
31.0
103.9
327.4
275.9
5116.1
Ohm-m

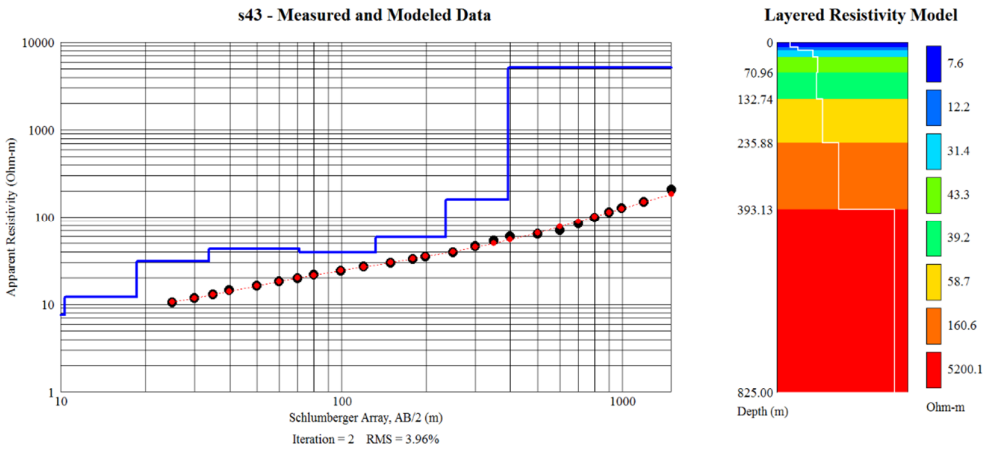
s43 - Measured and Modeled Data
Apparent Resistivity (Ohm-m)
10000
1000
100
10
1
10
100
1000
Schlumberger Array, AB/2 (m)
Iteration = 2 RMS = 3.96%
Layered Resistivity Model
0
70.96
132.74
235.88
393.13
825.00
Depth (m)
7.6
12.2
31.4
43.3
39.2
58.7
160.6
5200.1
Ohm-m

Group 4

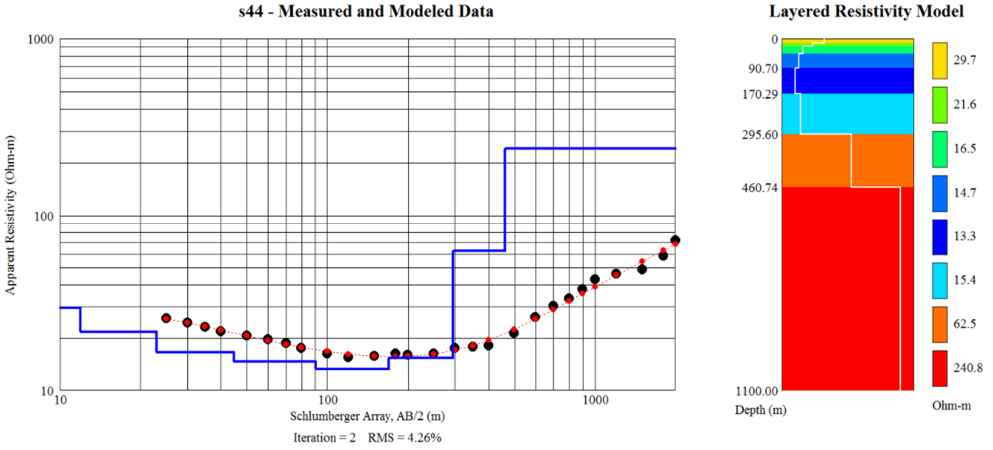
s44 - Measured and Modeled Data
Apparent Resistivity (Ohm-m)
1000
100
10
10
100
1000
Schlumberger Array, AB/2 (m)
Iteration = 2 RMS = 4.26%
Layered Resistivity Model
0
90.70
170.29
295.60
460.74
1100.00
Depth (m)
29.7
21.6
16.5
14.7
13.3
15.4
62.5
240.8
Ohm-m

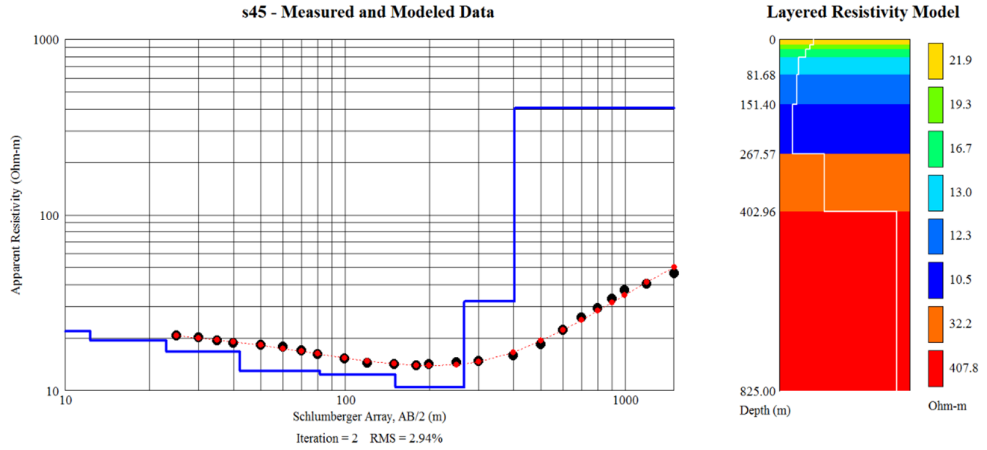
s45 - Measured and Modeled Data
Apparent Resistivity (Ohm-m)
1000
100
10
10
100
1000
Schlumberger Array, AB/2 (m)
Iteration = 2 RMS = 2.94%
Layered Resistivity Model
0
81.68
151.40
267.57
402.96
825.00
Depth (m)
21.9
19.3
16.7
13.0
12.3
10.5
32.2
407.8
Ohm-m

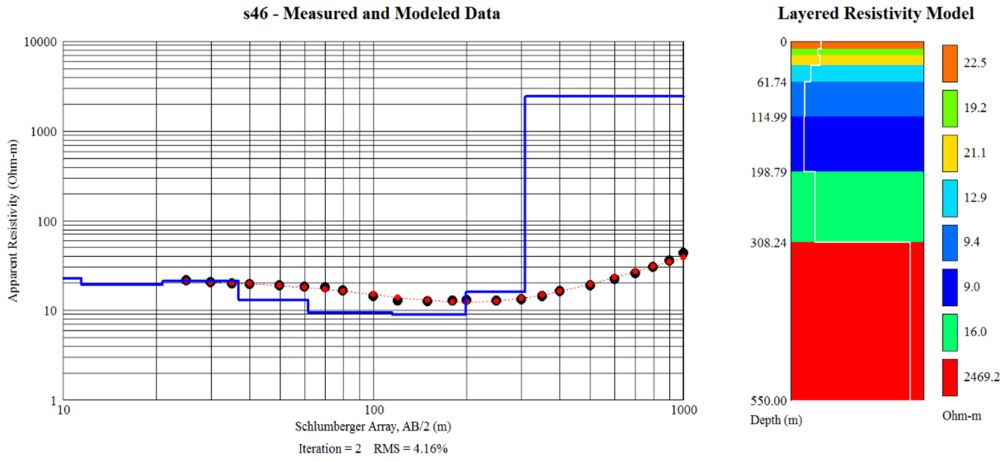
s46 - Measured and Modeled Data
Apparent Resistivity (Ohm-m)
10000
1000
100
10
1
10
100
1000
Schlumberger Array, AB/2 (m)
Iteration = 2 RMS = 4.16%
Layered Resistivity Model
0
61.74
114.99
198.79
308.24
550.00
Depth (m)
22.5
19.2
21.1
12.9
9.4
9.0
16.0
2469.2
Ohm-m

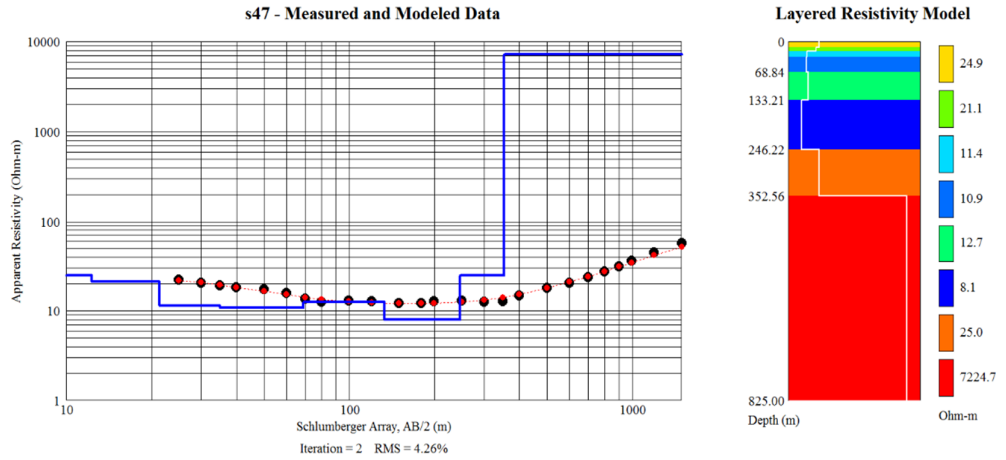
s47 - Measured and Modeled Data
Apparent Resistivity (Ohm-m)
10000
1000
100
10
1
10
100
1000
Schlumberger Array, AB/2 (m)
Iteration = 2 RMS = 4.26%
Layered Resistivity Model
0
68.84
133.21
246.22
352.56
825.00
Depth (m)
24.9
21.1
11.4
10.9
12.7
8.1
25.0
7224.7
Ohm-m

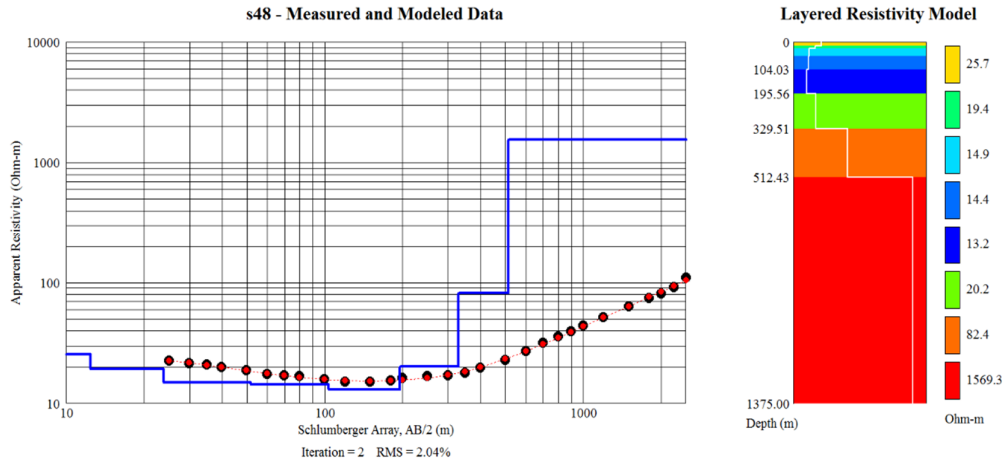
s48 - Measured and Modeled Data
Apparent Resistivity (Ohm-m)
10000
1000
100
10
10
100
1000
Schlumberger Array, AB/2 (m)
Iteration = 2 RMS = 2.04%
Layered Resistivity Model
0
104.03
195.56
329.51
512.43
1375.00
Depth (m)
25.7
19.4
14.9
14.4
13.2
20.2
82.4
1569.3
Ohm-m

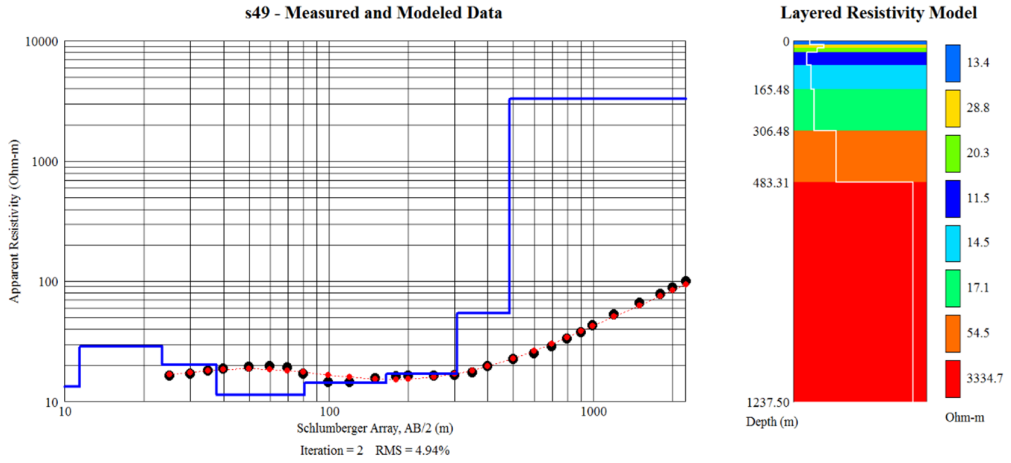
s49 - Measured and Modeled Data
Apparent Resistivity (Ohm-m)
10000
1000
100
10
10
100
1000
Schlumberger Array, AB/2 (m)
Iteration = 2 RMS = 4.94%
Layered Resistivity Model
0
165.48
306.48
483.31
1237.50
Depth (m)
13.4
28.8
20.3
11.5
14.5
17.1
54.5
3334.7
Ohm-m

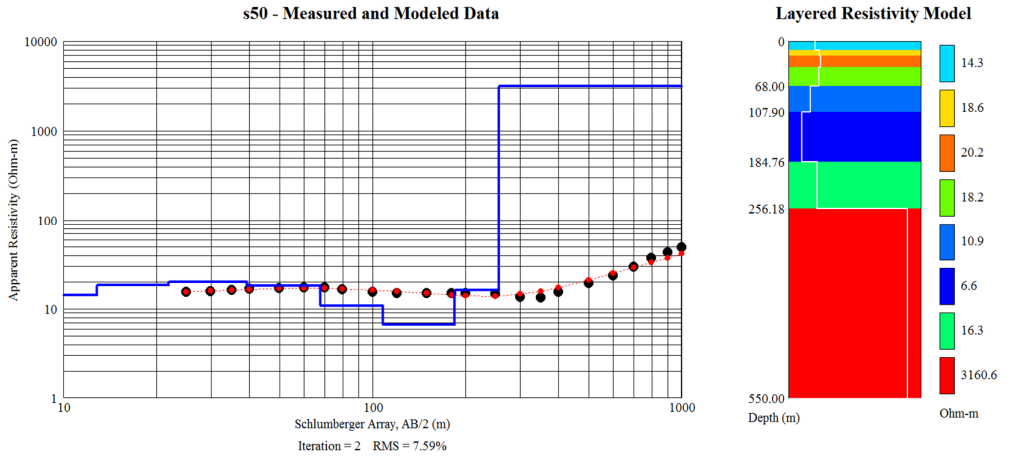
s50 - Measured and Modeled Data
Apparent Resistivity (Ohm-m)
10000
1000
100
10
1
10
100
1000
Schlumberger Array, AB/2 (m)
Iteration = 2 RMS = 7.59%
Layered Resistivity Model
0
68.00
107.90
184.76
256.18
550.00
Depth (m)
14.3
18.6
20.2
18.2
10.9
6.6
16.3
3160.6
Ohm-m

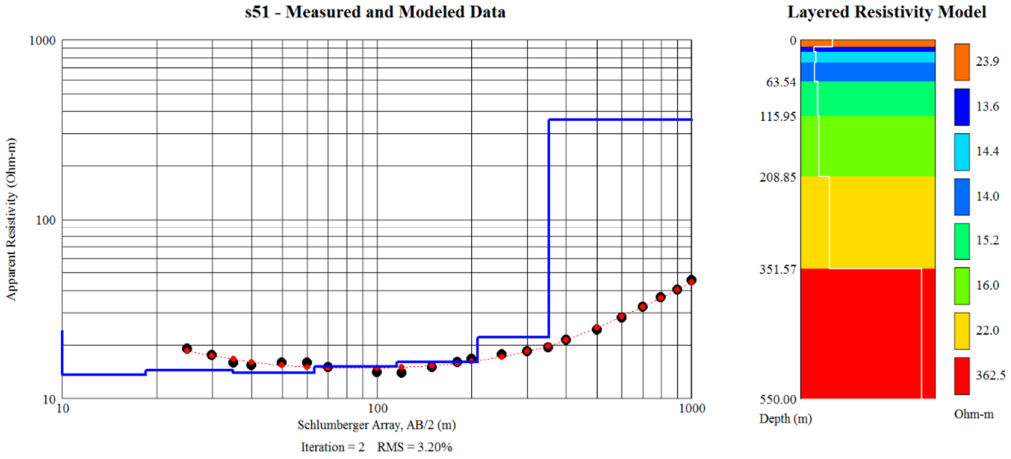
s51 - Measured and Modeled Data
Apparent Resistivity (Ohm-m)
1000
100
10
10
100
1000
Schlumberger Array, AB/2 (m)
Iteration = 2 RMS = 3.20%
Layered Resistivity Model
0
63.54
115.95
208.85
351.57
550.00
Depth (m)
23.9
13.6
14.4
14.0
15.2
16.0
22.0
362.5
Ohm-m

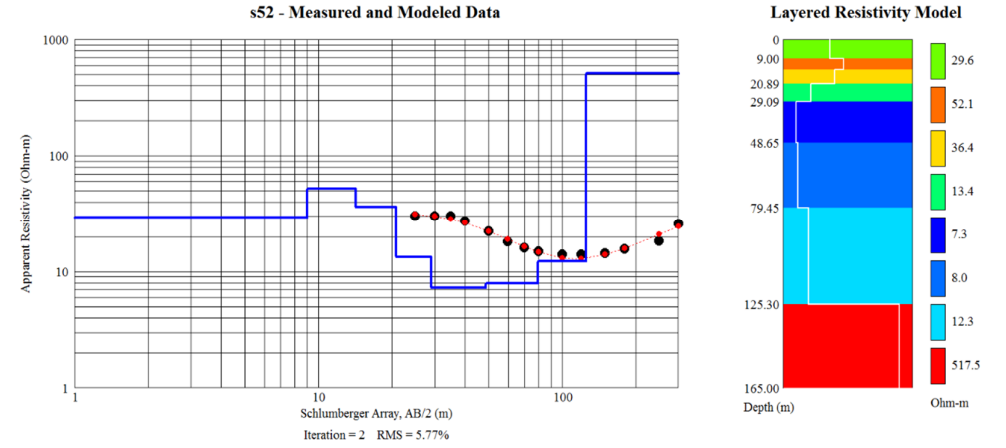
s52 - Measured and Modeled Data
Apparent Resistivity (Ohm-m)
1000
100
10
1
1
10
100
Schlumberger Array, AB/2 (m)
Iteration = 2 RMS = 5.77%
Layered Resistivity Model
0
9.00
20.89
29.09
48.65
79.45
125.30
165.00
Depth (m)
29.6
52.1
36.4
13.4
7.3
8.0
12.3
517.5
Ohm-m

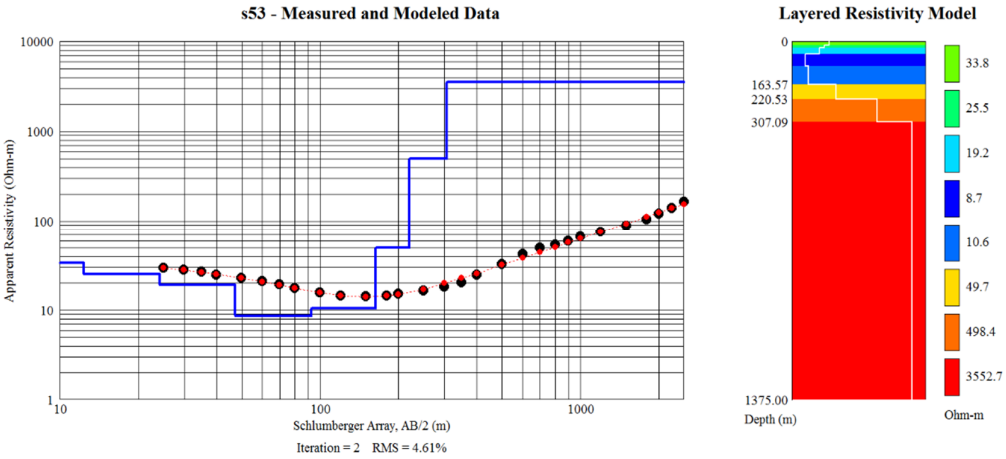
s53 - Measured and Modeled Data
Apparent Resistivity (Ohm-m)
10000
1000
100
10
1
10
100
1000
Schlumberger Array, AB/2 (m)
Iteration = 2 RMS = 4.61%
Layered Resistivity Model
0
163.57
220.53
307.09
1375.00
Depth (m)
33.8
25.5
19.2
8.7
10.6
49.7
498.4
3552.7
Ohm-m

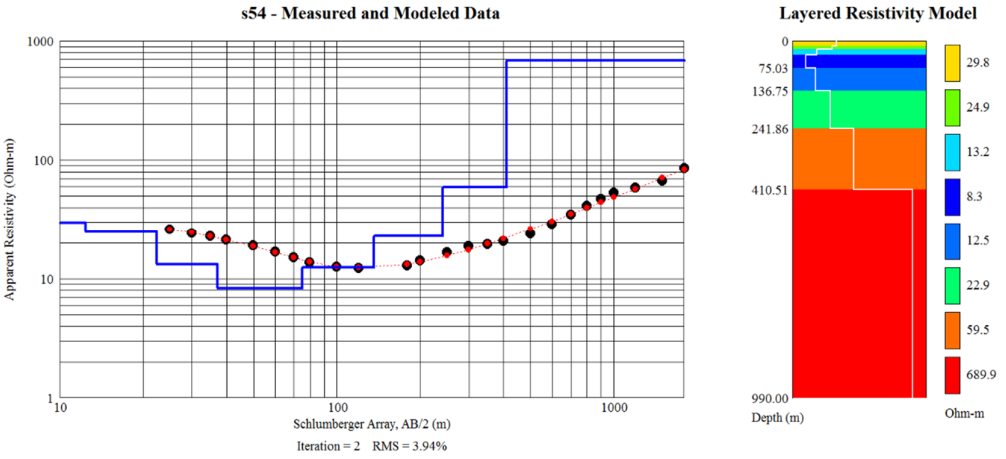
s54 - Measured and Modeled Data
Apparent Resistivity (Ohm-m)
1000
100
10
1
10
100
1000
Schlumberger Array, AB/2 (m)
Iteration = 2 RMS = 3.94%
Layered Resistivity Model
0
75.03
136.75
241.86
410.51
990.00
Depth (m)
29.8
24.9
13.2
8.3
12.5
22.9
59.5
689.9
Ohm-m

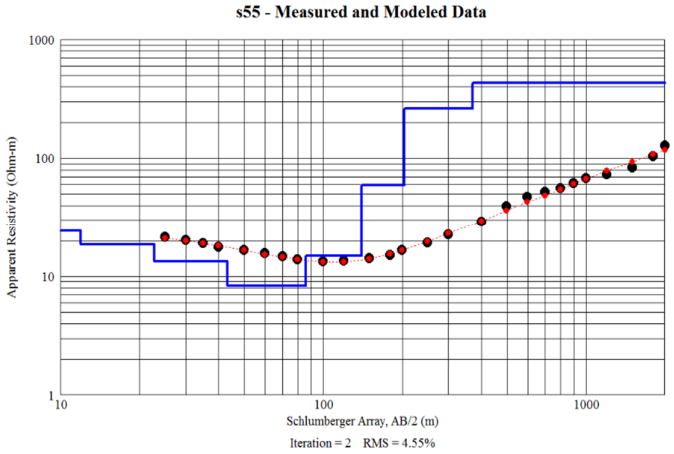
s55 - Measured and Modeled Data
Apparent Resistivity (Ohm-m)
1000
100
10
1
10
100
1000
Schlumberger Array, AB/2 (m)
Iteration = 2 RMS = 4.55%

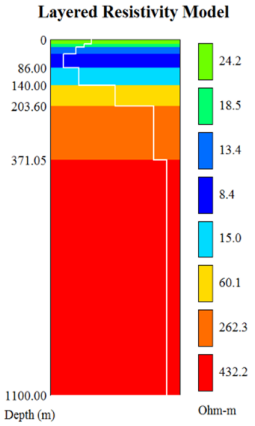
Layered Resistivity Model
0
86.00
140.00
203.60
371.05
1100.00
Depth (m)
24.2
18.5
13.4
8.4
15.0
60.1
262.3
432.2
Ohm-m

Group 6

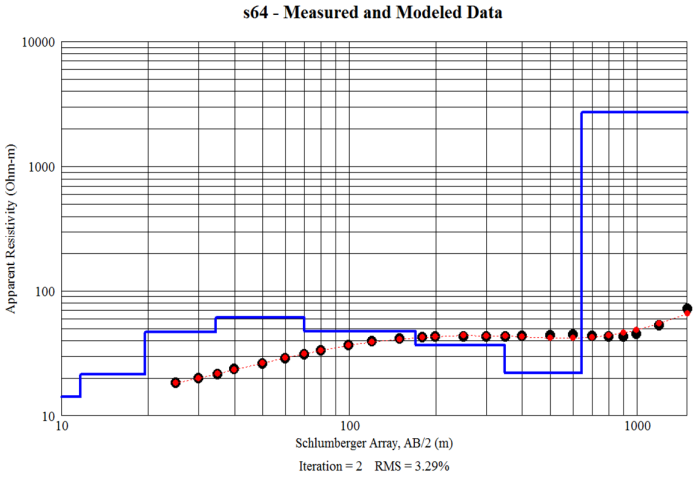
s64 - Measured and Modeled Data
Apparent Resistivity (Ohm-m)
10000
1000
100
10
10
100
1000
Schlumberger Array, AB/2 (m)
Iteration = 2 RMS = 3.29%

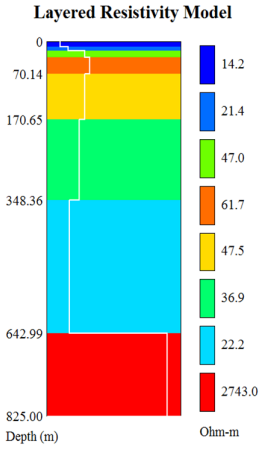
Layered Resistivity Model
0
70.14
170.65
348.36
642.99
825.00
Depth (m)
14.2
21.4
47.0
61.7
47.5
36.9
22.2
2743.0
Ohm-m

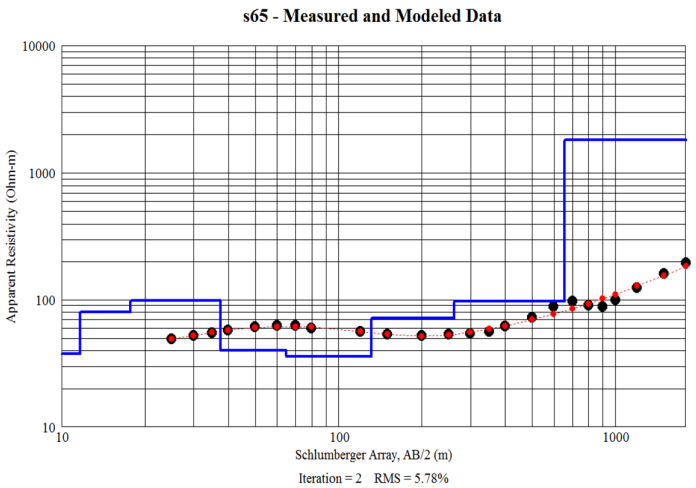
s65 - Measured and Modeled Data
Apparent Resistivity (Ohm-m)
10000
1000
100
10
10
100
1000
Schlumberger Array, AB/2 (m)
Iteration = 2 RMS = 5.78%

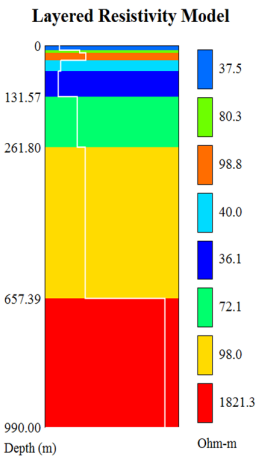
Layered Resistivity Model
0
131.57
261.80
657.39
990.00
Depth (m)
37.5
80.3
98.8
40.0
36.1
72.1
98.0
1821.3
Ohm-m

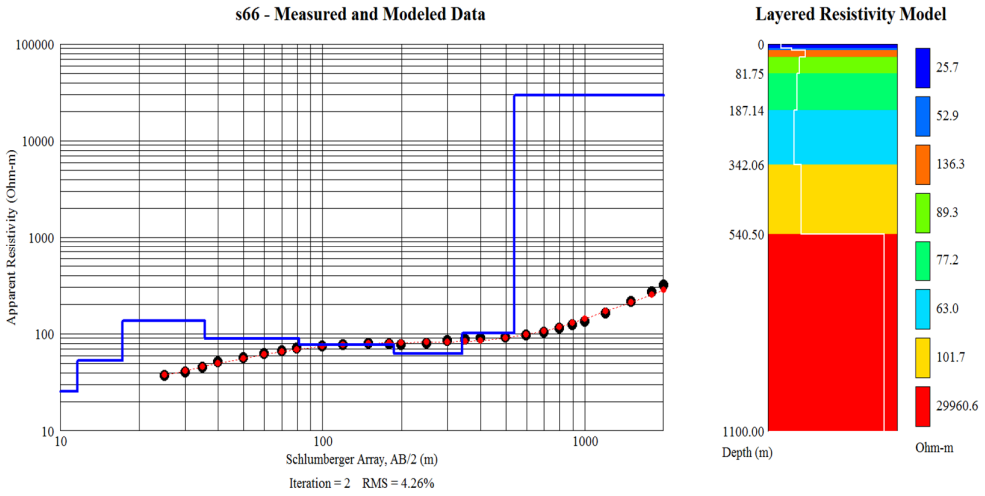
s66 - Measured and Modeled Data
Apparent Resistivity (Ohm-m)
100000
10000
1000
100
10
10
100
1000
Schlumberger Array, AB/2 (m)
Iteration = 2 RMS = 4.26%
Layered Resistivity Model
0
81.75
187.14
342.06
540.50
1100.00
Depth (m)
25.7
52.9
136.3
89.3
77.2
63.0
101.7
29960.6
Ohm-m

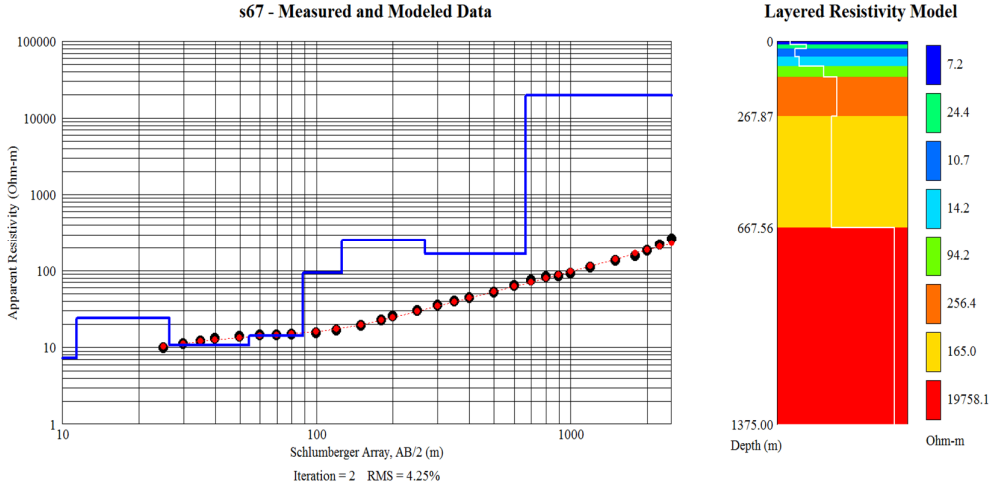
s67 - Measured and Modeled Data
Apparent Resistivity (Ohm-m)
100000
10000
1000
100
10
1
10
100
1000
Schlumberger Array, AB/2 (m)
Iteration = 2 RMS = 4.25%
Layered Resistivity Model
0
267.87
667.56
1375.00
Depth (m)
7.2
24.4
10.7
14.2
94.2
256.4
165.0
19758.1
Ohm-m

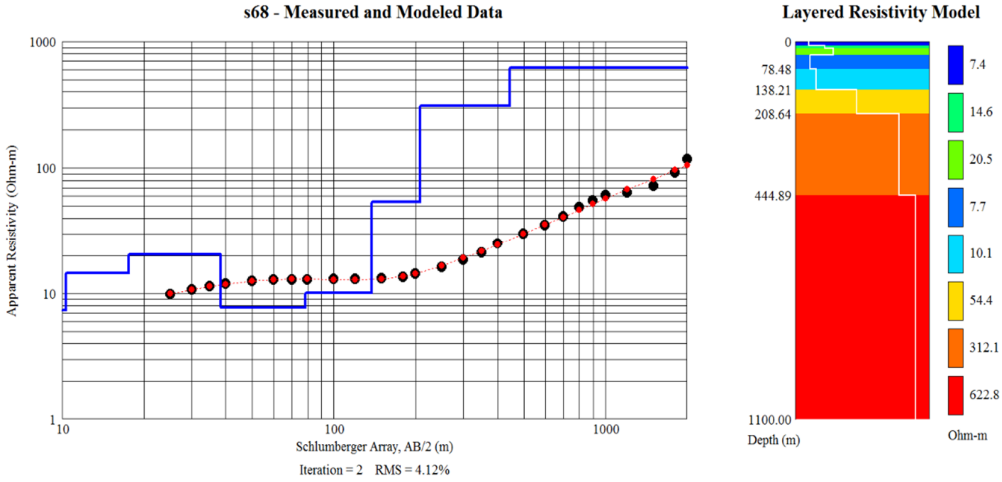
s68 - Measured and Modeled Data
Apparent Resistivity (Ohm-m)
1000
100
10
1
10
100
1000
Schlumberger Array, AB/2 (m)
Iteration = 2 RMS = 4.12%
Layered Resistivity Model
0
78.48
138.21
208.64
444.89
1100.00
Depth (m)
7.4
14.6
20.5
7.7
10.1
54.4
312.1
622.8
Ohm-m

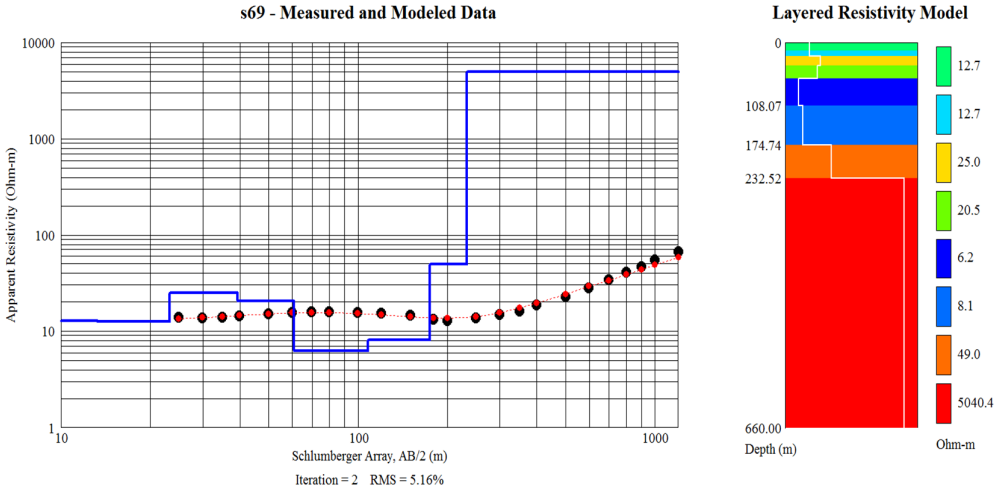
s69 - Measured and Modeled Data
Apparent Resistivity (Ohm-m)
10000
1000
100
10
1
10
100
1000
Schlumberger Array, AB/2 (m)
Iteration = 2 RMS = 5.16%
Layered Resistivity Model
0
108.07
174.74
232.52
660.00
Depth (m)
12.7
12.7
25.0
20.5
6.2
8.1
49.0
5040.4
Ohm-m

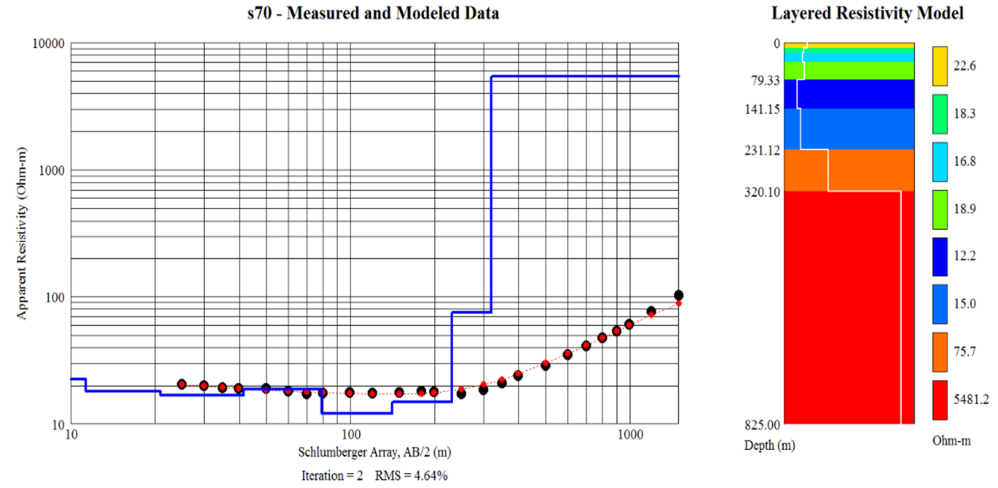
s70 - Measured and Modeled Data
Apparent Resistivity (Ohm-m)
10000
1000
100
10
10
100
1000
Schlumberger Array, AB/2 (m)
Iteration = 2 RMS = 4.64%
Layered Resistivity Model
0
79.33
141.15
231.12
320.10
825.00
Depth (m)
22.6
18.3
16.8
18.9
12.2
15.0
75.7
5481.2
Ohm-m

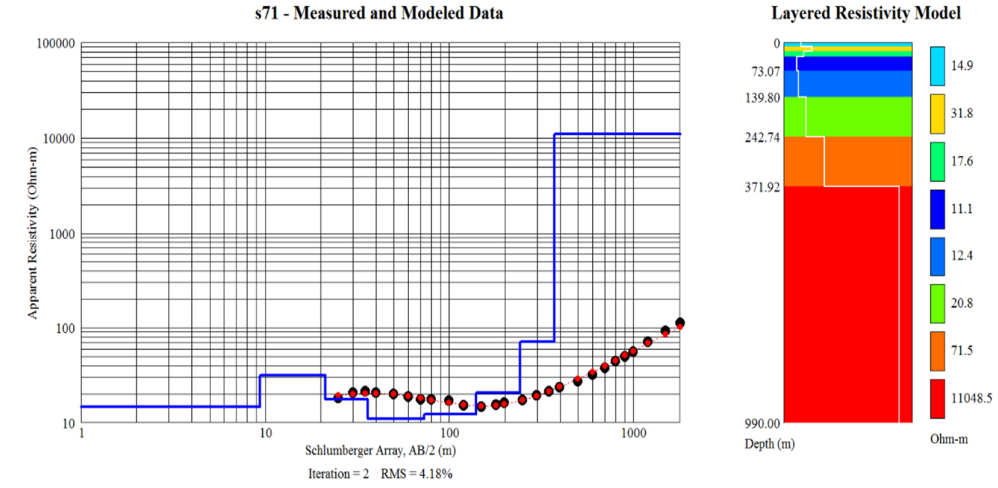
s71 - Measured and Modeled Data
Apparent Resistivity (Ohm-m)
100000
10000
1000
100
10
1
10
100
1000
Schlumberger Array, AB/2 (m)
Iteration = 2 RMS = 4.18%
Layered Resistivity Model
0
73.07
139.80
242.74
371.92
990.00
Depth (m)
14.9
31.8
17.6
11.1
12.4
20.8
71.5
11048.5
Ohm-m

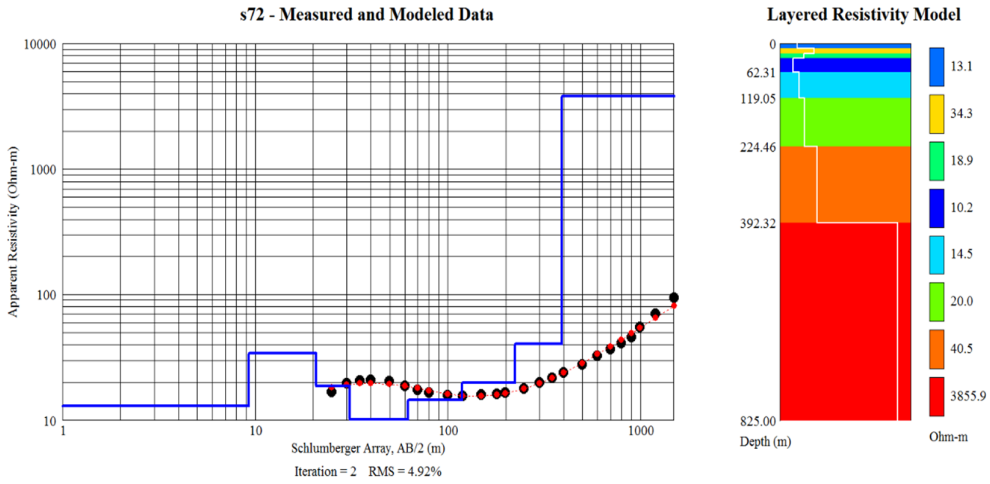
s72 - Measured and Modeled Data
Apparent Resistivity (Ohm-m)
10000
1000
100
10
1
10
100
1000
Schlumberger Array, AB/2 (m)
Iteration = 2 RMS = 4.92%
Layered Resistivity Model
0
62.31
119.05
224.46
392.32
825.00
Depth (m)
13.1
34.3
18.9
10.2
14.5
20.0
40.5
3855.9
Ohm-m

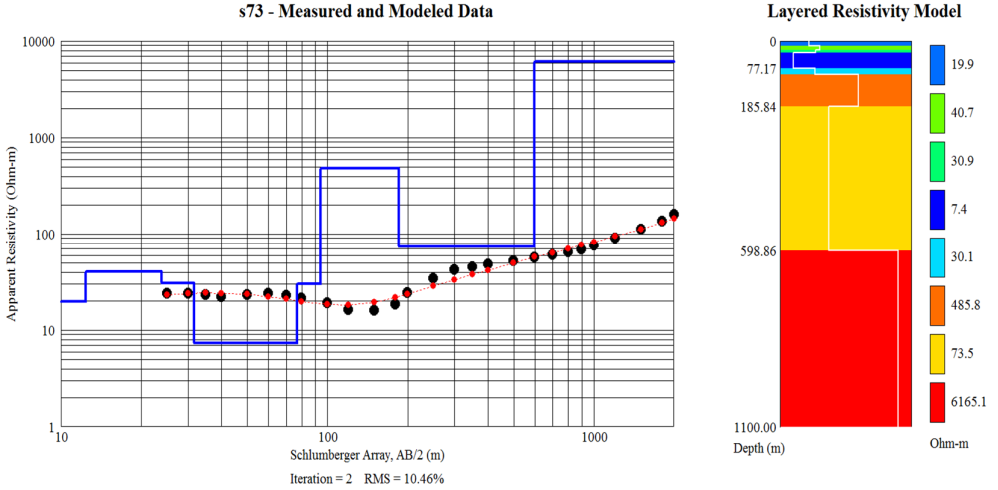
s73 - Measured and Modeled Data
Apparent Resistivity (Ohm-m)
10000
1000
100
10
1
10
100
1000
Schlumberger Array, AB/2 (m)
Iteration = 2 RMS = 10.46%
Layered Resistivity Model
0
77.17
185.84
598.86
1100.00
Depth (m)
19.9
40.7
30.9
7.4
30.1
485.8
73.5
6165.1
Ohm-m

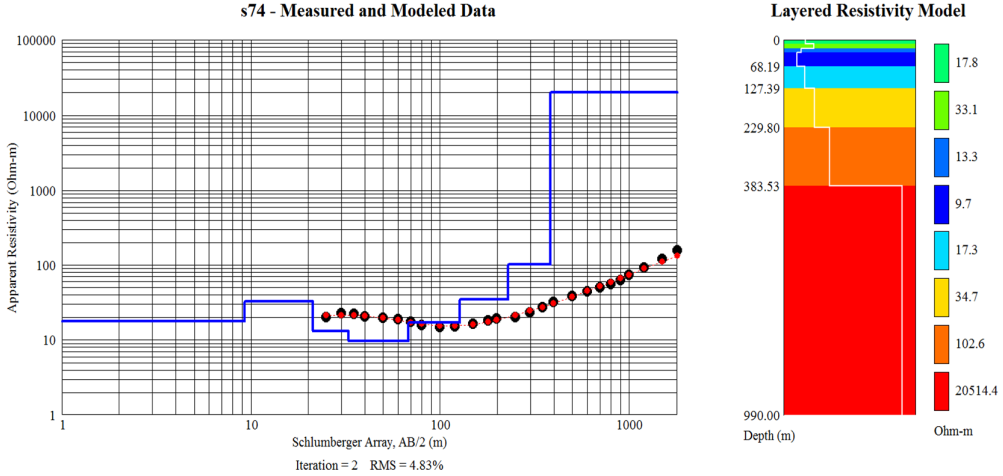
s74 - Measured and Modeled Data
Apparent Resistivity (Ohm-m)
100000
10000
1000
100
10
1
10
100
1000
Schlumberger Array, AB/2 (m)
Iteration = 2 RMS = 4.83%
Layered Resistivity Model
0
68.19
127.39
229.80
383.53
990.00
Depth (m)
17.8
33.1
13.3
9.7
17.3
34.7
102.6
20514.4
Ohm-m

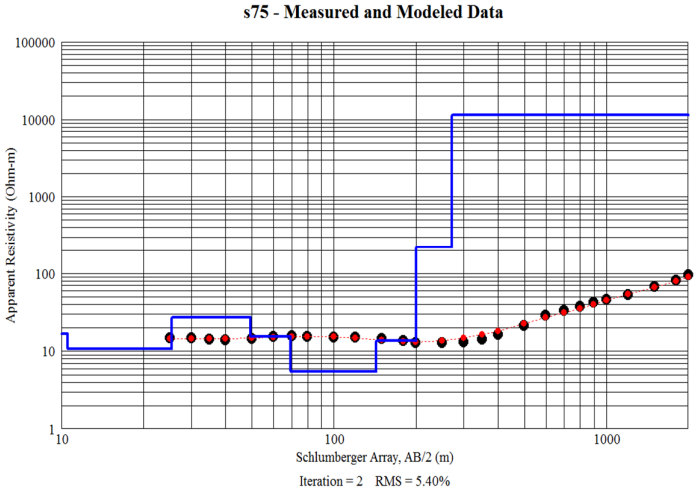
s75 - Measured and Modeled Data
Apparent Resistivity (Ohm-m)
100000
10000
1000
100
10
1
10
100
1000
Schlumberger Array, AB/2 (m)
Iteration = 2 RMS = 5.40%

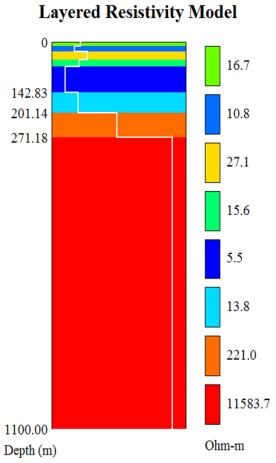
Layered Resistivity Model
0
142.83
201.14
271.18
1100.00
Depth (m)
16.7
10.8
27.1
15.6
5.5
13.8
221.0
11583.7
Ohm-m

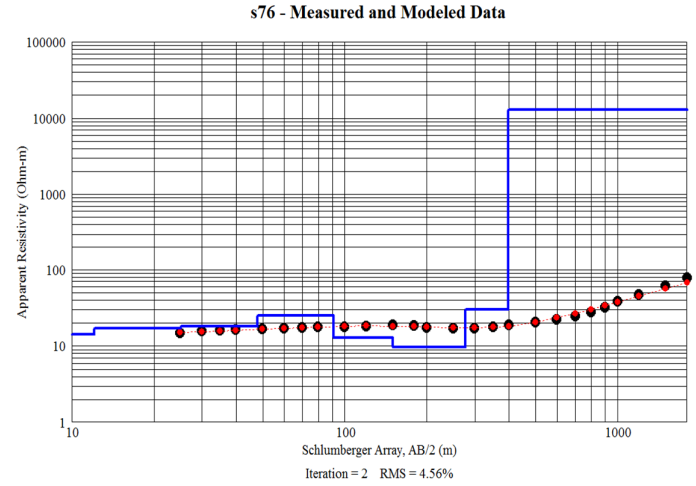
s76 - Measured and Modeled Data
Apparent Resistivity (Ohm-m)
100000
10000
1000
100
10
1
10
100
1000
Schlumberger Array, AB/2 (m)
Iteration = 2 RMS = 4.56%

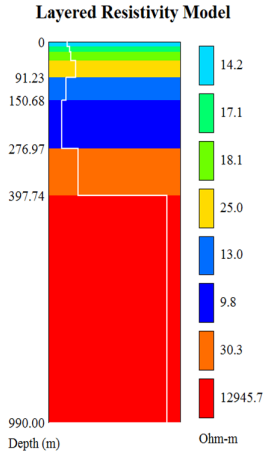
Layered Resistivity Model
0
91.23
150.68
276.97
397.74
990.00
Depth (m)
14.2
17.1
18.1
25.0
13.0
9.8
30.3
12945.7
Ohm-m

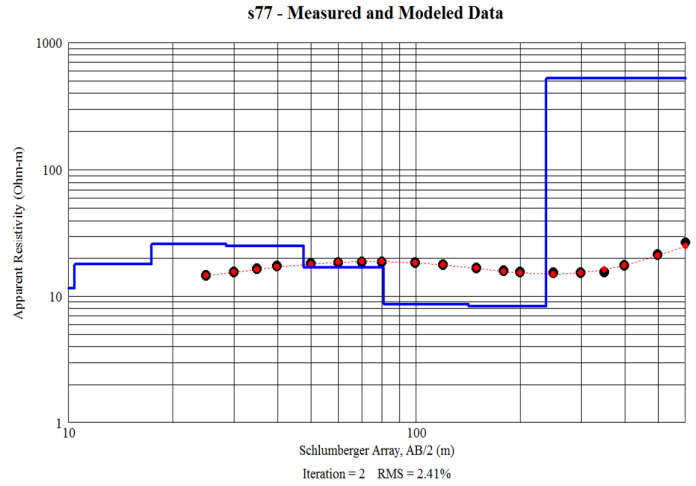
s77 - Measured and Modeled Data
Apparent Resistivity (Ohm-m)
1000
100
10
1
10
100
Schlumberger Array, AB/2 (m)
Iteration = 2 RMS = 2.41%

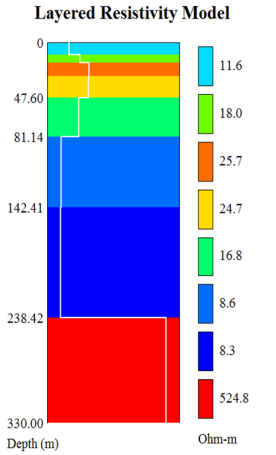
Layered Resistivity Model
0
47.60
81.14
142.41
238.42
330.00
Depth (m)
11.6
18.0
25.7
24.7
16.8
8.6
8.3
524.8
Ohm-m

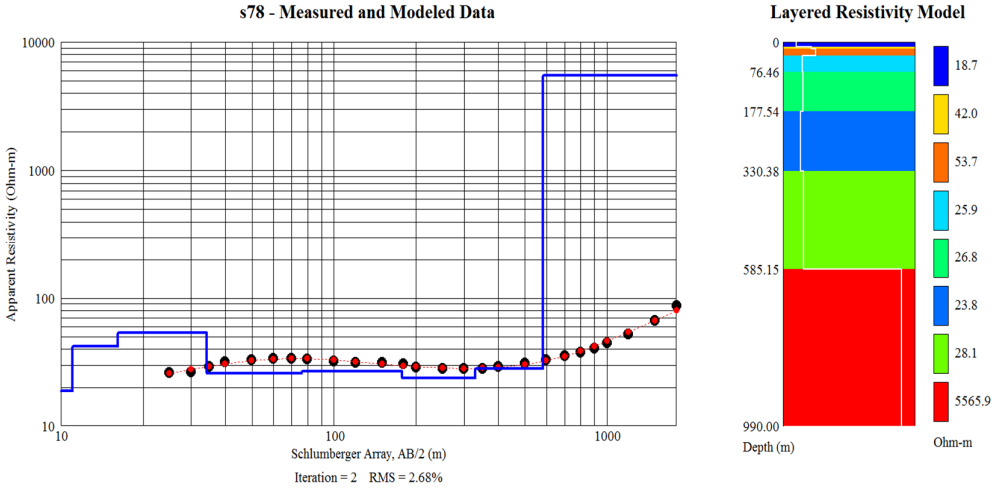
s78 - Measured and Modeled Data
Apparent Resistivity (Ohm-m)
10000
1000
100
10
10
100
1000
Schlumberger Array, AB/2 (m)
Iteration = 2 RMS = 2.68%
Layered Resistivity Model
0
76.46
177.54
330.38
585.15
990.00
Depth (m)
18.7
42.0
53.7
25.9
26.8
23.8
28.1
5565.9
Ohm-m

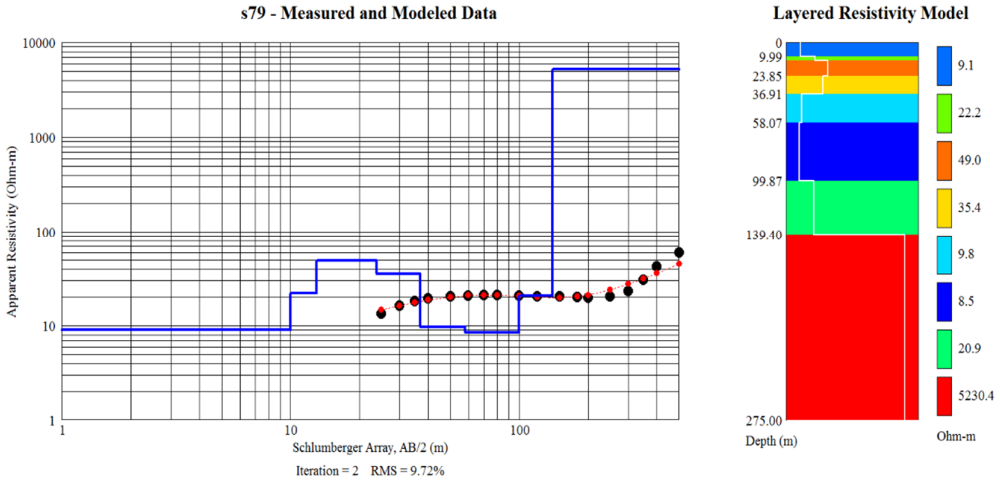
s79 - Measured and Modeled Data
Apparent Resistivity (Ohm-m)
10000
1000
100
10
1
1
10
100
Schlumberger Array, AB/2 (m)
Iteration = 2 RMS = 9.72%
Layered Resistivity Model
0
9.99
23.85
36.91
58.07
99.87
139.40
275.00
Depth (m)
9.1
22.2
49.0
35.4
9.8
8.5
20.9
5230.4
Ohm-m

Group 7

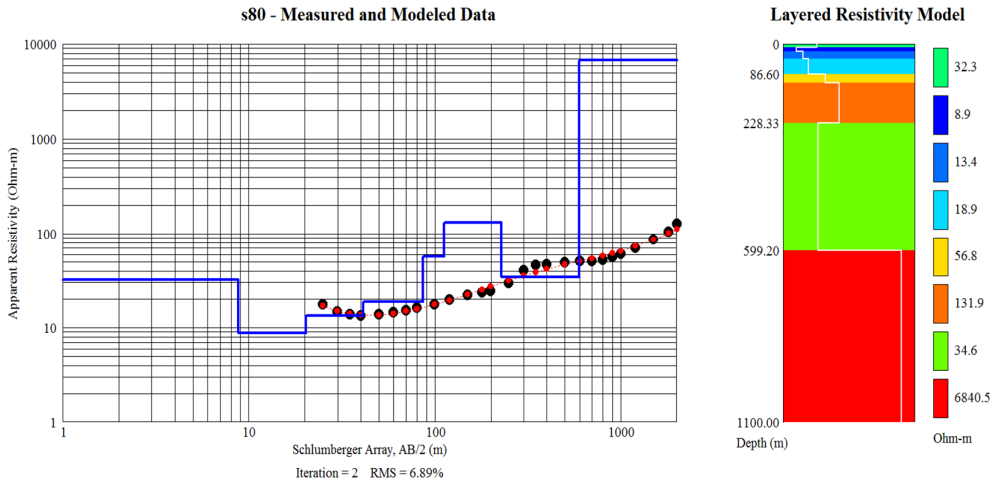
s80 - Measured and Modeled Data
Apparent Resistivity (Ohm-m)
10000
1000
100
10
1
1
10
100
1000
Schlumberger Array, AB/2 (m)
Iteration = 2 RMS = 6.89%
Layered Resistivity Model
0
86.60
228.33
599.20
1100.00
Depth (m)
32.3
8.9
13.4
18.9
56.8
131.9
34.6
6840.5
Ohm-m

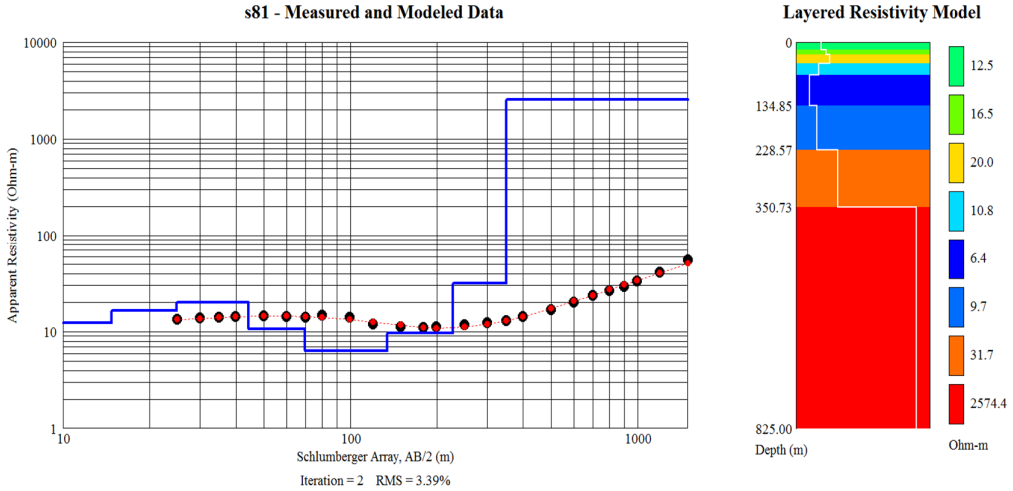
s81 - Measured and Modeled Data
Apparent Resistivity (Ohm-m)
10000
1000
100
10
1
10
100
1000
Schlumberger Array, AB/2 (m)
Iteration = 2 RMS = 3.39%
Layered Resistivity Model
0
134.85
228.57
350.73
825.00
Depth (m)
12.5
16.5
20.0
10.8
6.4
9.7
31.7
2574.4
Ohm-m

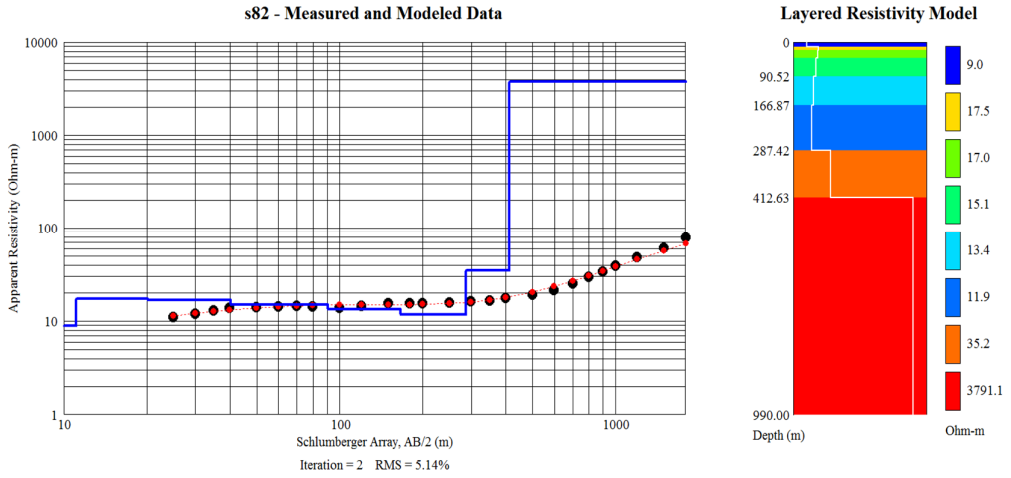
s82 - Measured and Modeled Data
Apparent Resistivity (Ohm-m)
10000
1000
100
10
1
10
100
1000
Schlumberger Array, AB/2 (m)
Iteration = 2 RMS = 5.14%
Layered Resistivity Model
0
90.52
166.87
287.42
412.63
990.00
Depth (m)
9.0
17.5
17.0
15.1
13.4
11.9
35.2
3791.1
Ohm-m

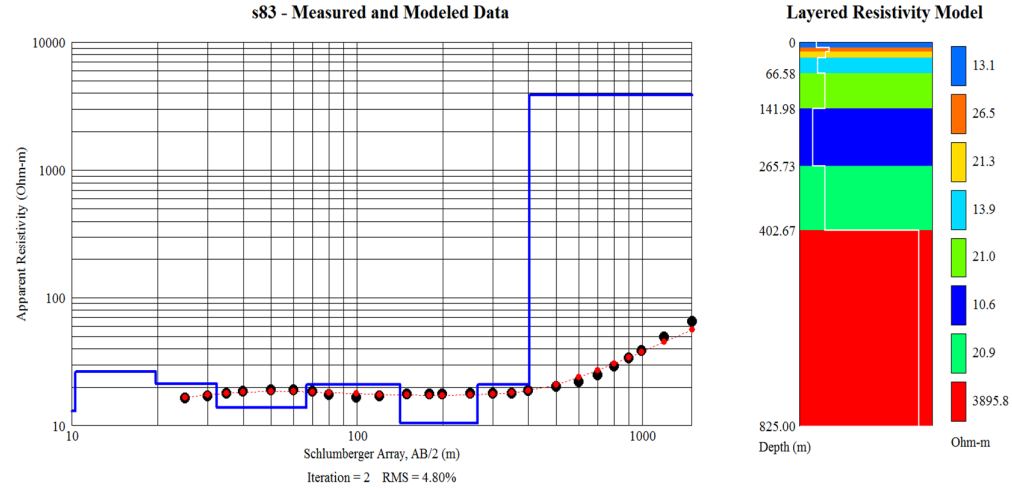
s83 - Measured and Modeled Data
Apparent Resistivity (Ohm-m)
10000
1000
100
10
10
100
1000
Schlumberger Array, AB/2 (m)
Iteration = 2 RMS = 4.80%
Layered Resistivity Model
0
66.58
141.98
265.73
402.67
825.00
Depth (m)
13.1
26.5
21.3
13.9
21.0
10.6
20.9
3895.8
Ohm-m

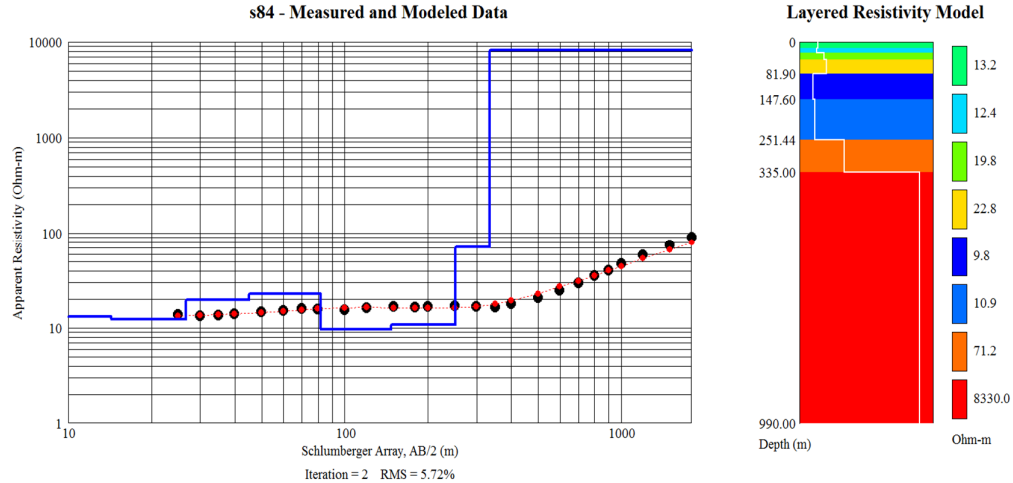
s84 - Measured and Modeled Data
Apparent Resistivity (Ohm-m)
10000
1000
100
10
1
10
100
1000
Schlumberger Array, AB/2 (m)
Iteration = 2 RMS = 5.72%
Layered Resistivity Model
0
81.90
147.60
251.44
335.00
990.00
Depth (m)
13.2
12.4
19.8
22.8
9.8
10.9
71.2
8330.0
Ohm-m

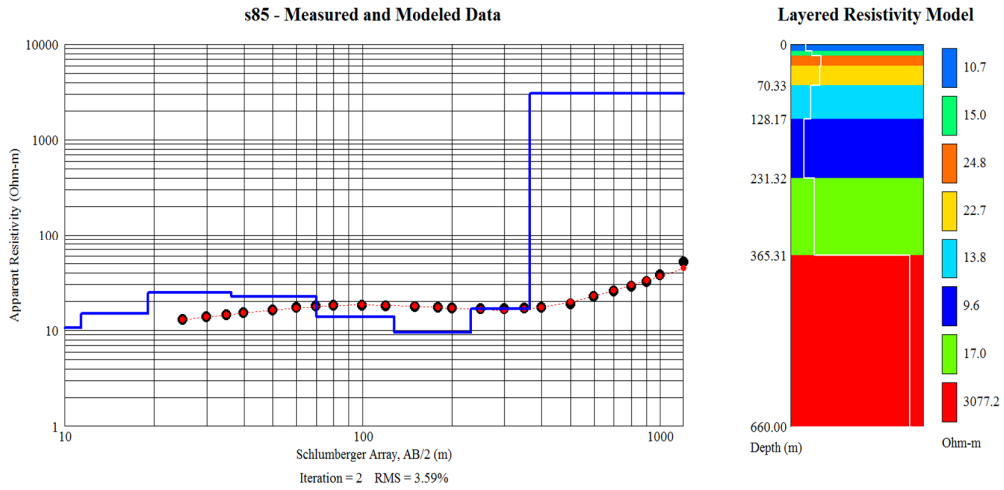
s85 - Measured and Modeled Data
Apparent Resistivity (Ohm-m)
10000
1000
100
10
1
10
100
1000
Schlumberger Array, AB/2 (m)
Iteration = 2 RMS = 3.59%
Layered Resistivity Model
0
70.33
128.17
231.32
365.31
660.00
Depth (m)
10.7
15.0
24.8
22.7
13.8
9.6
17.0
3077.2
Ohm-m

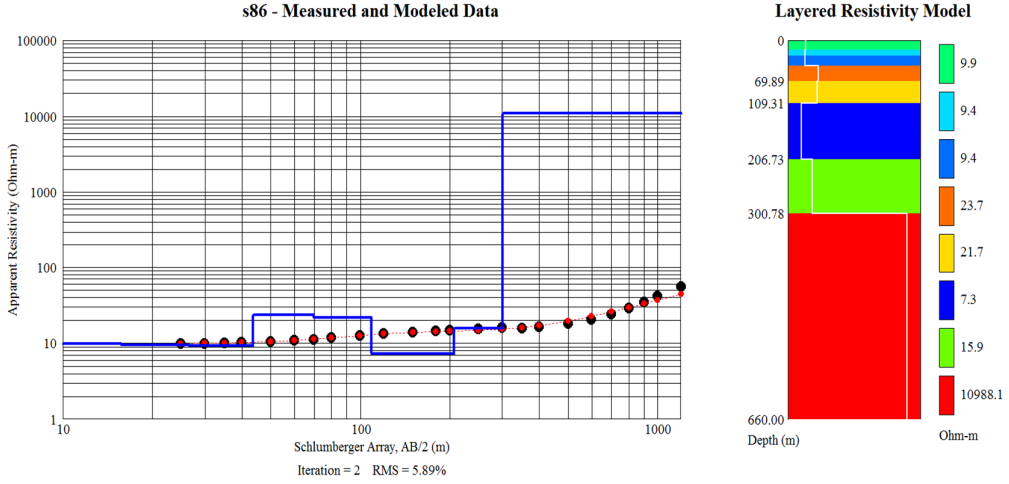
s86 - Measured and Modeled Data
Apparent Resistivity (Ohm-m)
100000
10000
1000
100
10
1
10
100
1000
Schlumberger Array, AB/2 (m)
Iteration = 2 RMS = 5.89%
Layered Resistivity Model
0
69.89
109.31
206.73
300.78
660.00
Depth (m)
9.9
9.4
9.4
23.7
21.7
7.3
15.9
10988.1
Ohm-m

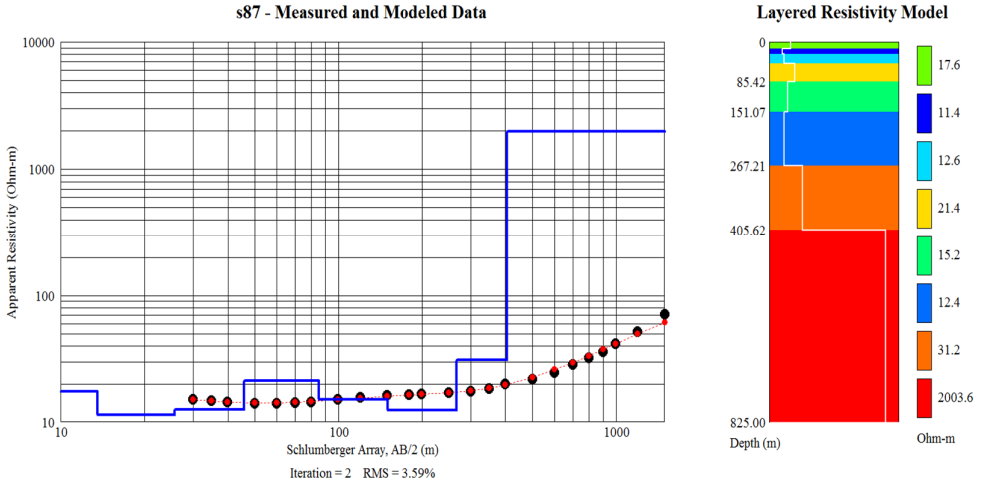
s87 - Measured and Modeled Data
Apparent Resistivity (Ohm-m)
10000
1000
100
10
10
100
1000
Schlumberger Array, AB/2 (m)
Iteration = 2 RMS = 3.59%
Layered Resistivity Model
0
85.42
151.07
267.21
405.62
825.00
Depth (m)
17.6
11.4
12.6
21.4
15.2
12.4
31.2
2003.6
Ohm-m

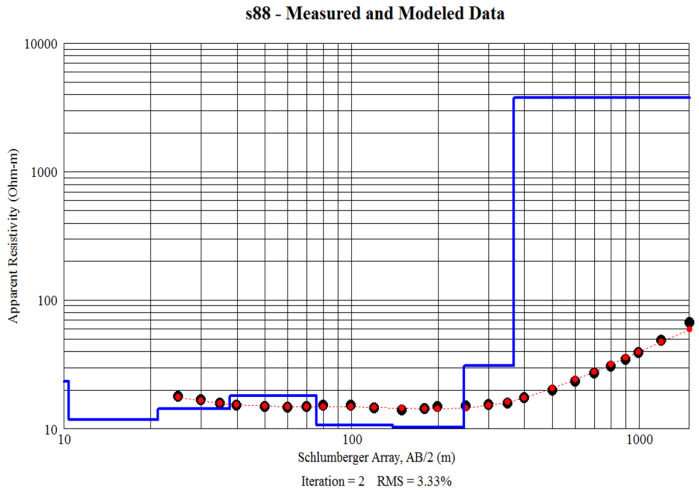
s88 - Measured and Modeled Data
Apparent Resistivity (Ohm-m)
10000
1000
100
10
10
100
1000
Schlumberger Array, AB/2 (m)
Iteration = 2 RMS = 3.33%

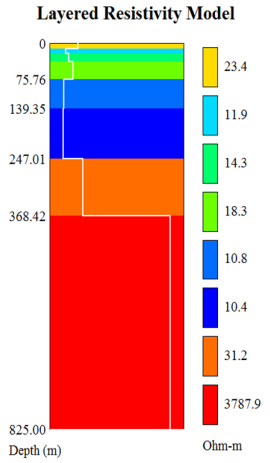
Layered Resistivity Model
0
75.76
139.35
247.01
368.42
825.00
Depth (m)
23.4
11.9
14.3
18.3
10.8
10.4
31.2
3787.9
Ohm-m

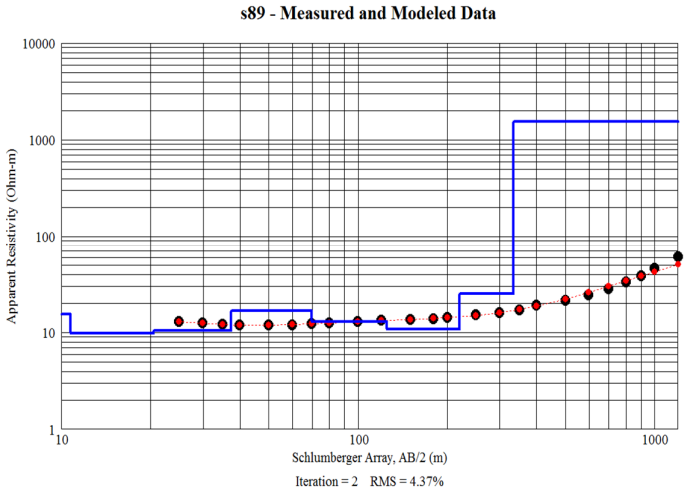
s89 - Measured and Modeled Data
Apparent Resistivity (Ohm-m)
10000
1000
100
10
1
10
100
1000
Schlumberger Array, AB/2 (m)
Iteration = 2 RMS = 4.37%

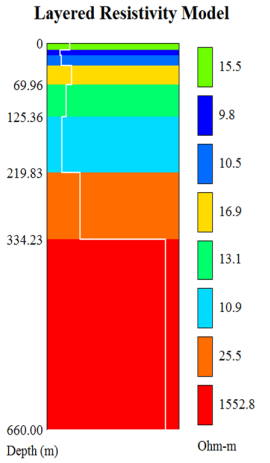
Layered Resistivity Model
0
69.96
125.36
219.83
334.23
660.00
Depth (m)
15.5
9.8
10.5
16.9
13.1
10.9
25.5
1552.8
Ohm-m

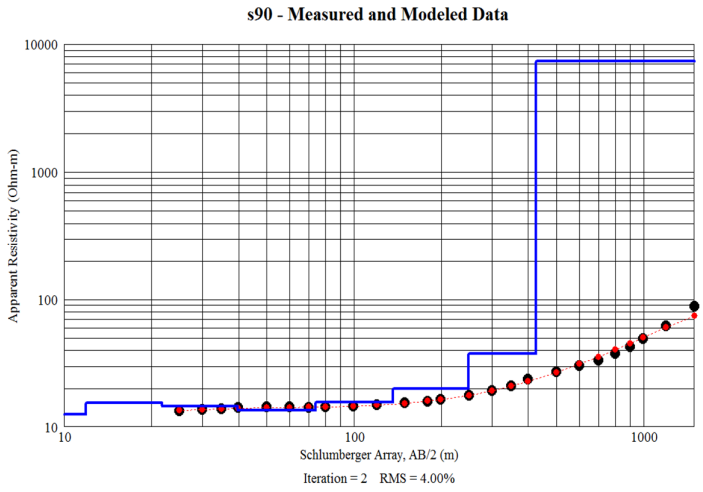
s90 - Measured and Modeled Data
Apparent Resistivity (Ohm-m)
10000
1000
100
10
10
100
1000
Schlumberger Array, AB/2 (m)
Iteration = 2 RMS = 4.00%

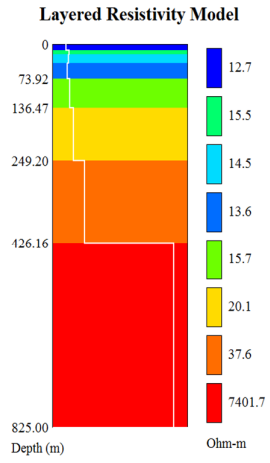
Layered Resistivity Model
0
73.92
136.47
249.20
426.16
825.00
Depth (m)
12.7
15.5
14.5
13.6
15.7
20.1
37.6
7401.7
Ohm-m

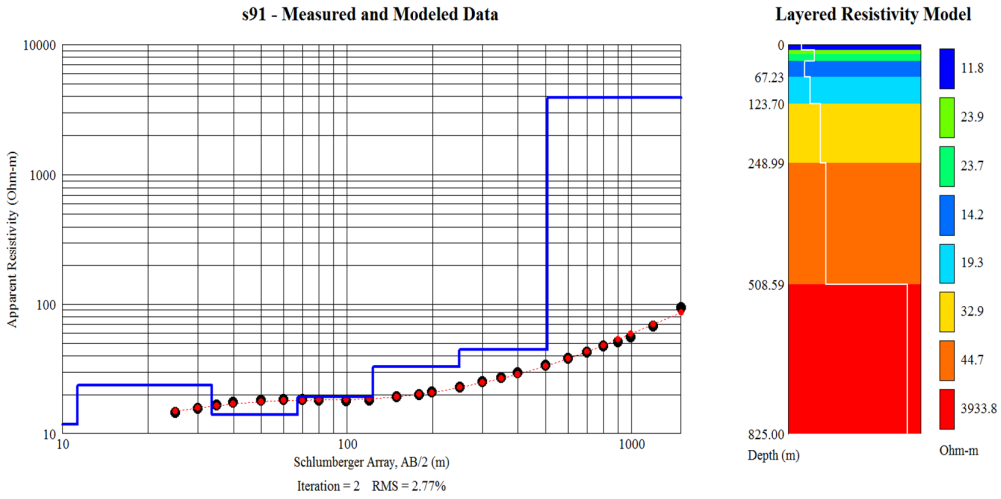
s91 - Measured and Modeled Data
Apparent Resistivity (Ohm-m)
10000
1000
100
10
10
100
1000
Schlumberger Array, AB/2 (m)
Iteration = 2 RMS = 2.77%
Layered Resistivity Model
0
67.23
123.70
248.99
508.59
825.00
Depth (m)
11.8
23.9
23.7
14.2
19.3
32.9
44.7
3933.8
Ohm-m

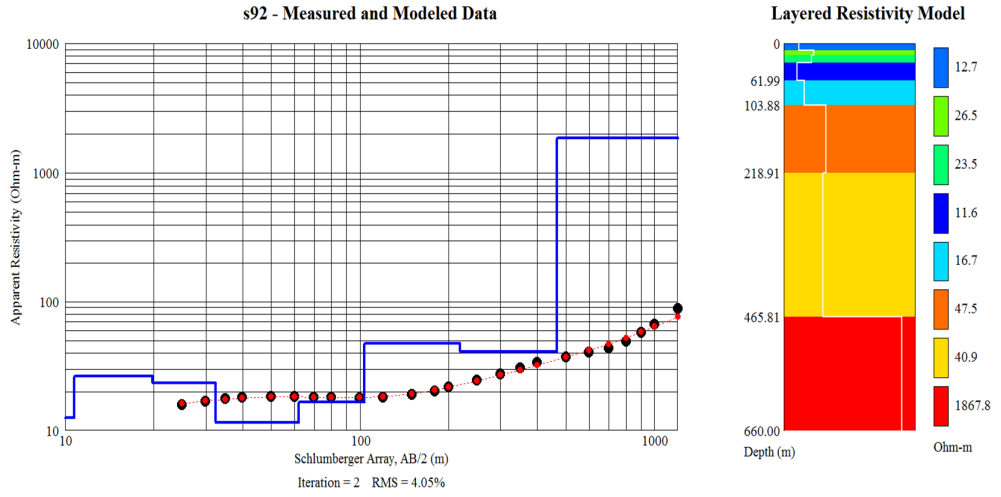
s92 - Measured and Modeled Data
Apparent Resistivity (Ohm-m)
10000
1000
100
10
10
100
1000
Schlumberger Array, AB/2 (m)
Iteration = 2 RMS = 4.05%
Layered Resistivity Model
0
61.99
103.88
218.91
465.81
660.00
Depth (m)
12.7
26.5
23.5
11.6
16.7
47.5
40.9
1867.8
Ohm-m

Group 8

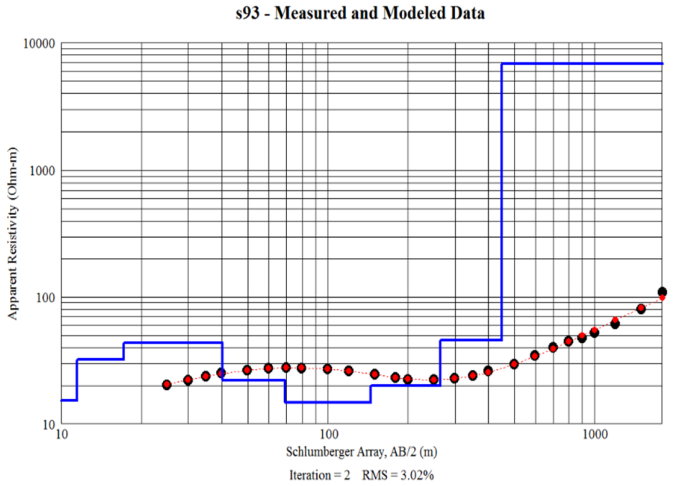
s93 - Measured and Modeled Data
Apparent Resistivity (Ohm-m)
10000
1000
100
10
10
100
1000
Schlumberger Array, AB/2 (m)
Iteration = 2 RMS = 3.02%

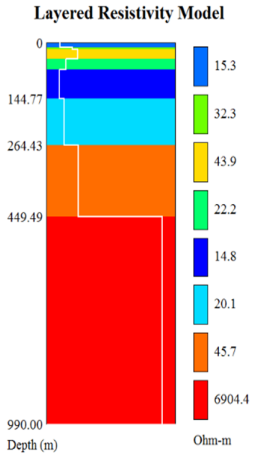
Layered Resistivity Model
0
144.77
264.43
449.49
990.00
Depth (m)
15.3
32.3
43.9
22.2
14.8
20.1
45.7
6904.4
Ohm-m

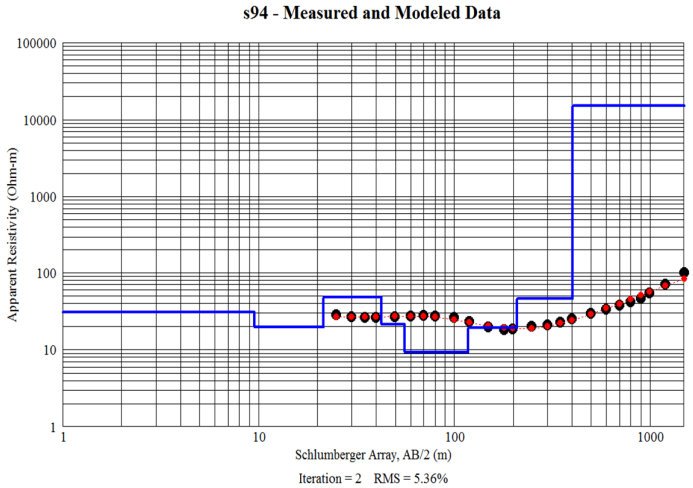
s94 - Measured and Modeled Data
Apparent Resistivity (Ohm-m)
100000
10000
1000
100
10
1
1
10
100
1000
Schlumberger Array, AB/2 (m)
Iteration = 2 RMS = 5.36%

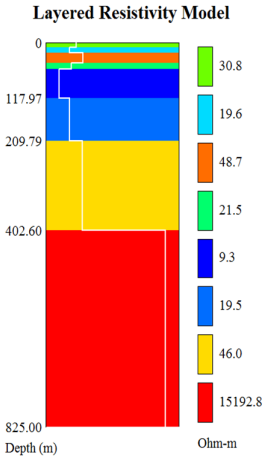
Layered Resistivity Model
0
117.97
209.79
402.60
825.00
Depth (m)
30.8
19.6
48.7
21.5
9.3
19.5
46.0
15192.8
Ohm-m

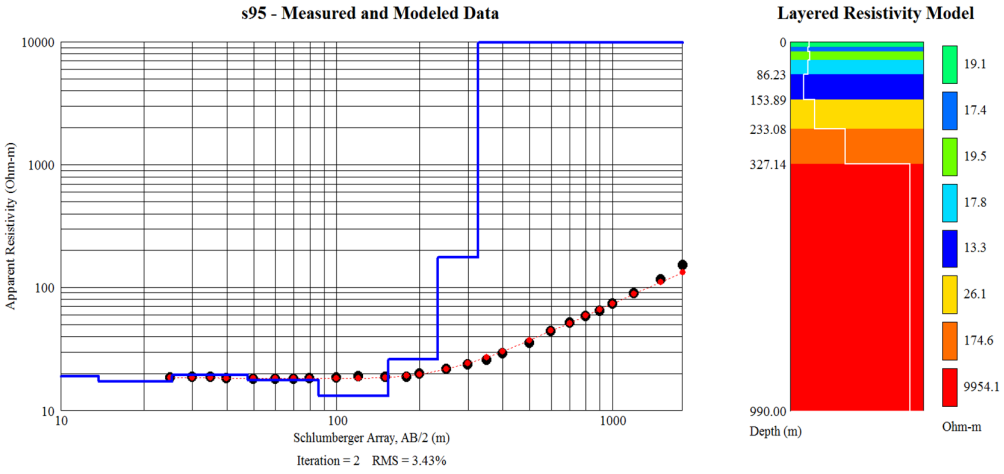
s95 - Measured and Modeled Data
Apparent Resistivity (Ohm-m)
10000
1000
100
10
10
100
1000
Schlumberger Array, AB/2 (m)
Iteration = 2 RMS = 3.43%
Layered Resistivity Model
0
86.23
153.89
233.08
327.14
990.00
Depth (m)
19.1
17.4
19.5
17.8
13.3
26.1
174.6
9954.1
Ohm-m

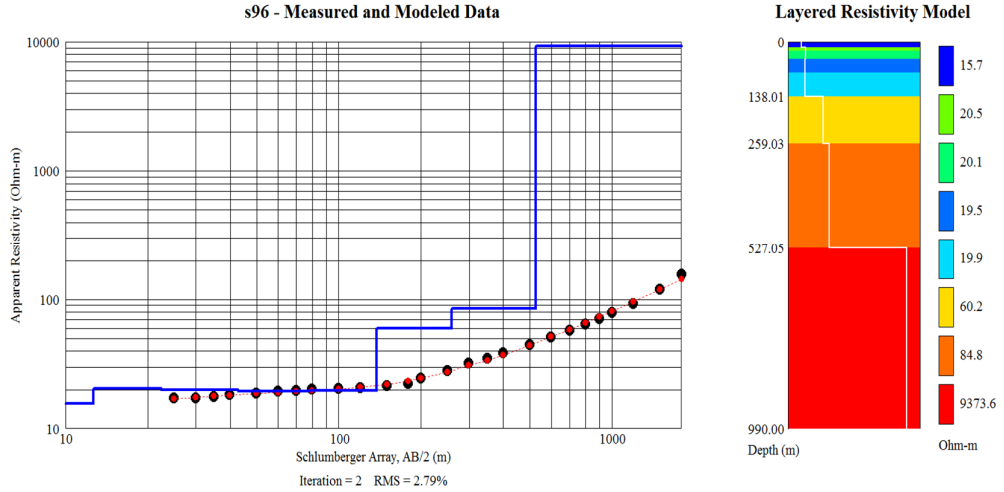
s96 - Measured and Modeled Data
Apparent Resistivity (Ohm-m)
10000
1000
100
10
10
100
1000
Schlumberger Array, AB/2 (m)
Iteration = 2 RMS = 2.79%
Layered Resistivity Model
0
138.01
259.03
527.05
990.00
Depth (m)
15.7
20.5
20.1
19.5
19.9
60.2
84.8
9373.6
Ohm-m

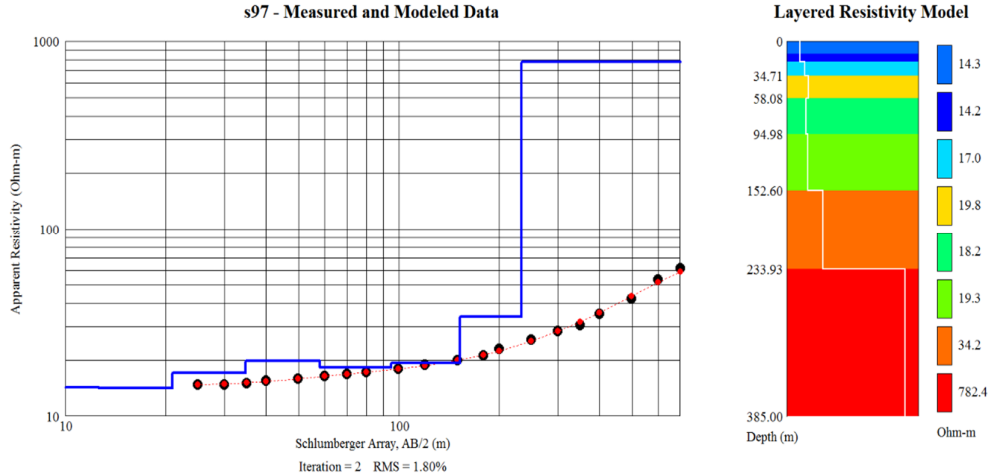
s97 - Measured and Modeled Data
Apparent Resistivity (Ohm-m)
1000
100
10
10
100
Schlumberger Array, AB/2 (m)
Iteration = 2 RMS = 1.80%
Layered Resistivity Model
0
34.71
58.08
94.98
152.60
233.93
385.00
Depth (m)
14.3
14.2
17.0
19.8
18.2
19.3
34.2
782.4
Ohm-m

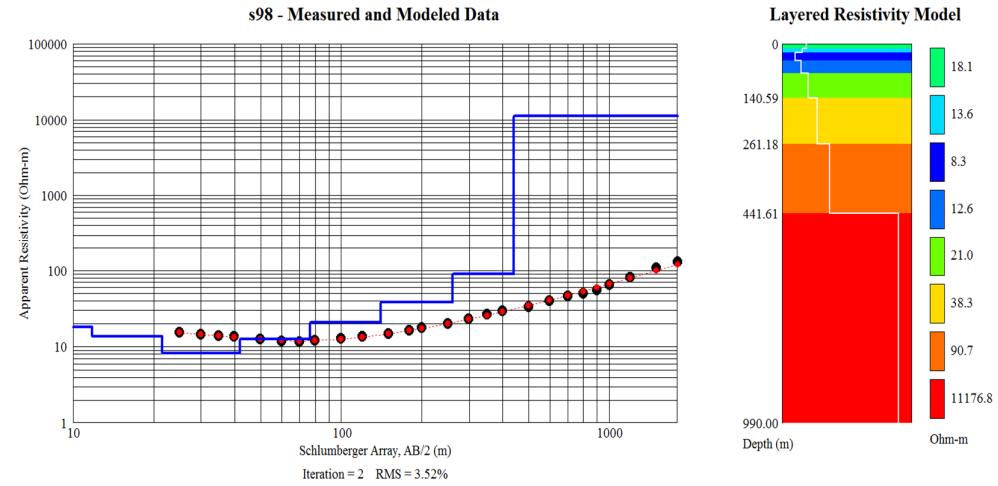
s98 - Measured and Modeled Data
Apparent Resistivity (Ohm-m)
100000
10000
1000
100
10
1
10
100
1000
Schlumberger Array, AB/2 (m)
Iteration = 2 RMS = 3.52%
Layered Resistivity Model
0
140.59
261.18
441.61
990.00
Depth (m)
18.1
13.6
8.3
12.6
21.0
38.3
90.7
11176.8
Ohm-m

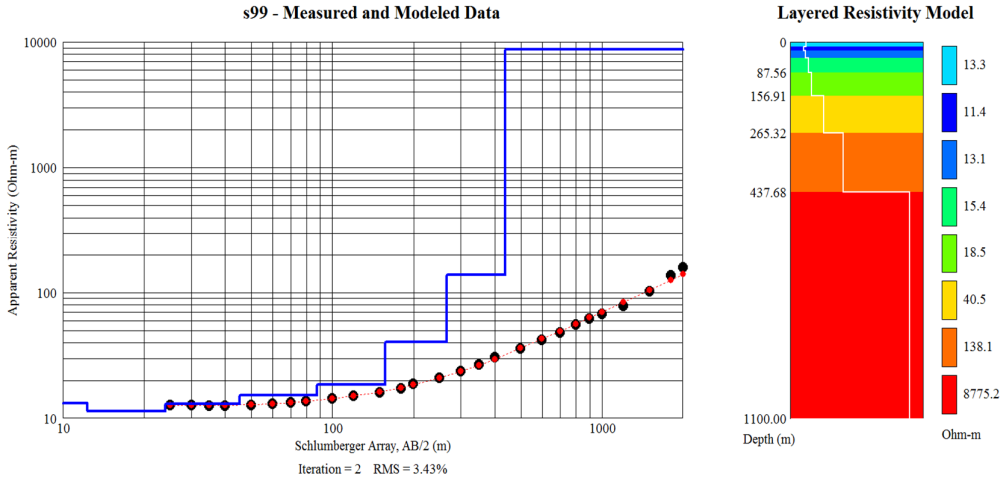
s99 - Measured and Modeled Data
Apparent Resistivity (Ohm-m)
10000
1000
100
10
10
100
1000
Schlumberger Array, AB/2 (m)
Iteration = 2 RMS = 3.43%
Layered Resistivity Model
0
87.56
156.91
265.32
437.68
1100.00
Depth (m)
13.3
11.4
13.1
15.4
18.5
40.5
138.1
8775.2
Ohm-m

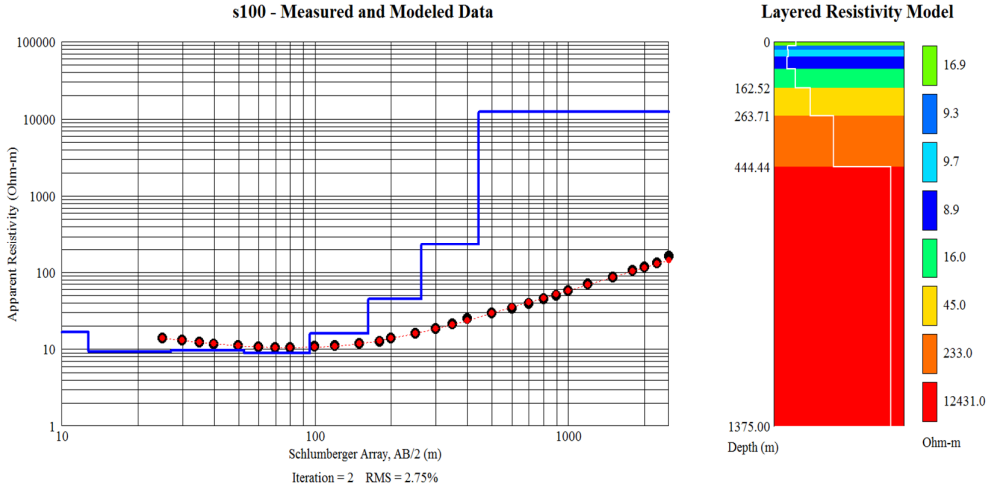
s100 - Measured and Modeled Data
Apparent Resistivity (Ohm-m)
100000
10000
1000
100
10
1
10
100
1000
Schlumberger Array, AB/2 (m)
Iteration = 2 RMS = 2.75%
Layered Resistivity Model
0
162.52
263.71
444.44
1375.00
Depth (m)
16.9
9.3
9.7
8.9
16.0
45.0
233.0
12431.0
Ohm-m

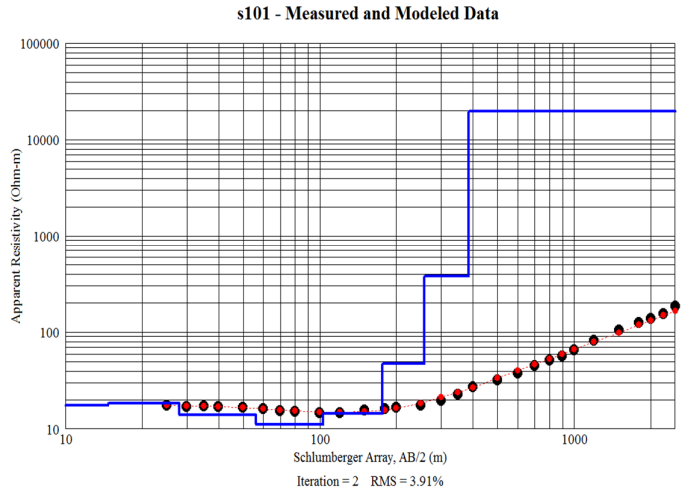
s101 - Measured and Modeled Data
Apparent Resistivity (Ohm-m)
100000
10000
1000
100
10
10
100
1000
Schlumberger Array, AB/2 (m)
Iteration = 2 RMS = 3.91%

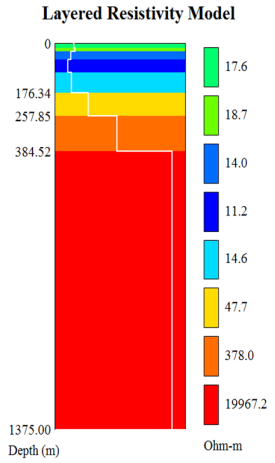
Layered Resistivity Model
0
176.34
257.85
384.52
1375.00
Depth (m)
17.6
18.7
14.0
11.2
14.6
47.7
378.0
19967.2
Ohm-m

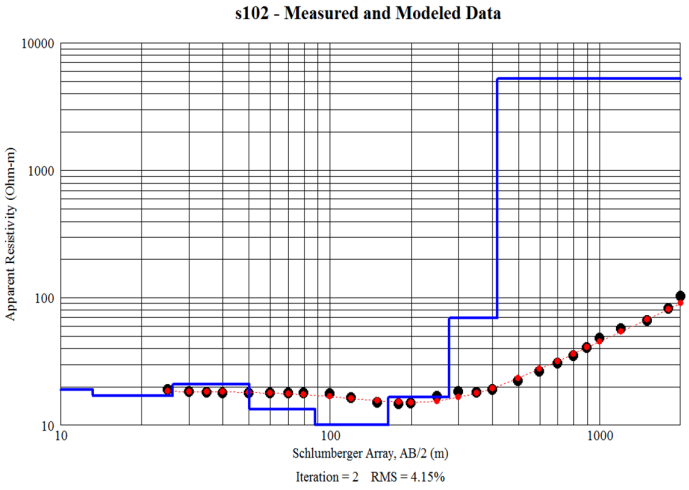
s102 - Measured and Modeled Data
Apparent Resistivity (Ohm-m)
10000
1000
100
10
10
100
1000
Schlumberger Array, AB/2 (m)
Iteration = 2 RMS = 4.15%

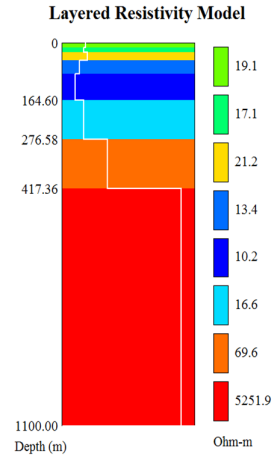
Layered Resistivity Model
0
164.60
276.58
417.36
1100.00
Depth (m)
19.1
17.1
21.2
13.4
10.2
16.6
69.6
5251.9
Ohm-m

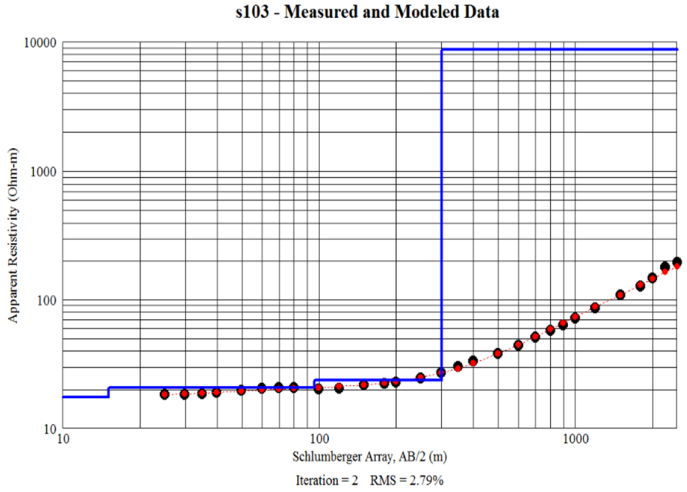
s103 - Measured and Modeled Data
Apparent Resistivity (Ohm-m)
10000
1000
100
10
10
100
1000
Schlumberger Array, AB/2 (m)
Iteration = 2 RMS = 2.79%

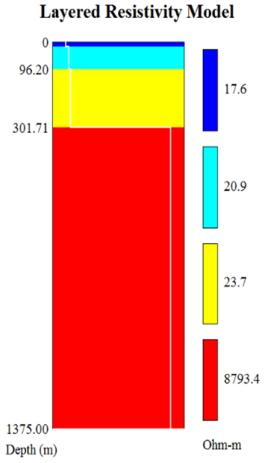
Layered Resistivity Model
0
96.20
301.71
1375.00
Depth (m)
17.6
20.9
23.7
8793.4
Ohm-m

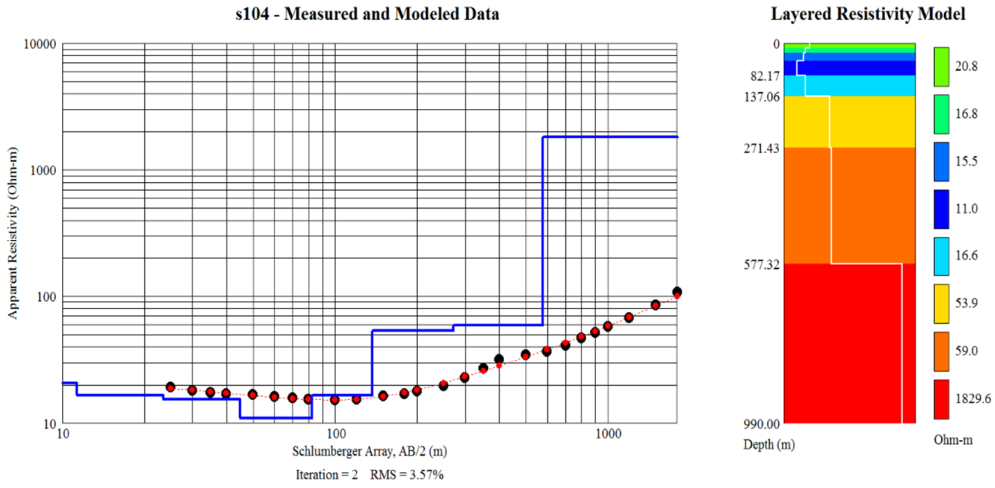
s104 - Measured and Modeled Data
Apparent Resistivity (Ohm-m)
10000
1000
100
10
10
100
1000
Schlumberger Array, AB/2 (m)
Iteration = 2 RMS = 3.57%
Layered Resistivity Model
0
82.17
137.06
271.43
577.32
990.00
Depth (m)
20.8
16.8
15.5
11.0
16.6
53.9
59.0
1829.6
Ohm-m

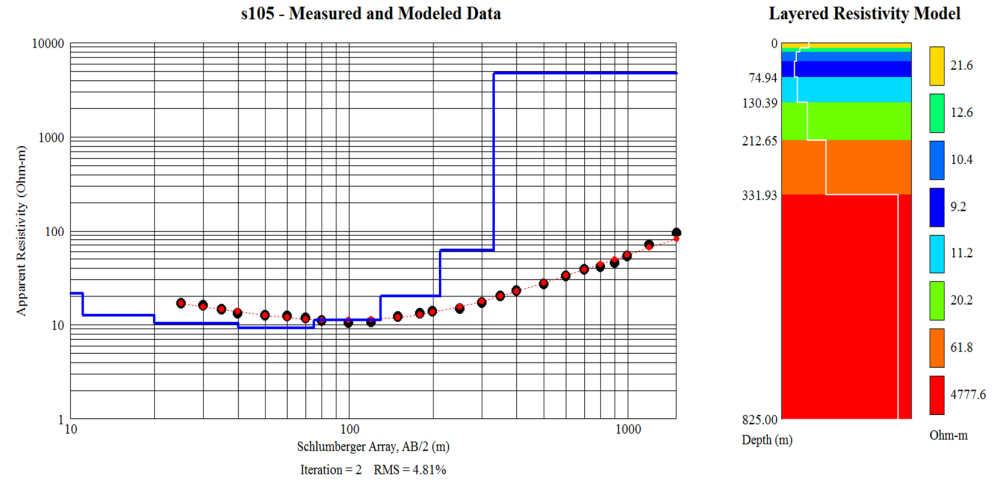
s105 - Measured and Modeled Data
Apparent Resistivity (Ohm-m)
10000
1000
100
10
1
10
100
1000
Schlumberger Array, AB/2 (m)
Iteration = 2 RMS = 4.81%
Layered Resistivity Model
0
74.94
130.39
212.65
331.93
825.00
Depth (m)
21.6
12.6
10.4
9.2
11.2
20.2
61.8
4777.6
Ohm-m

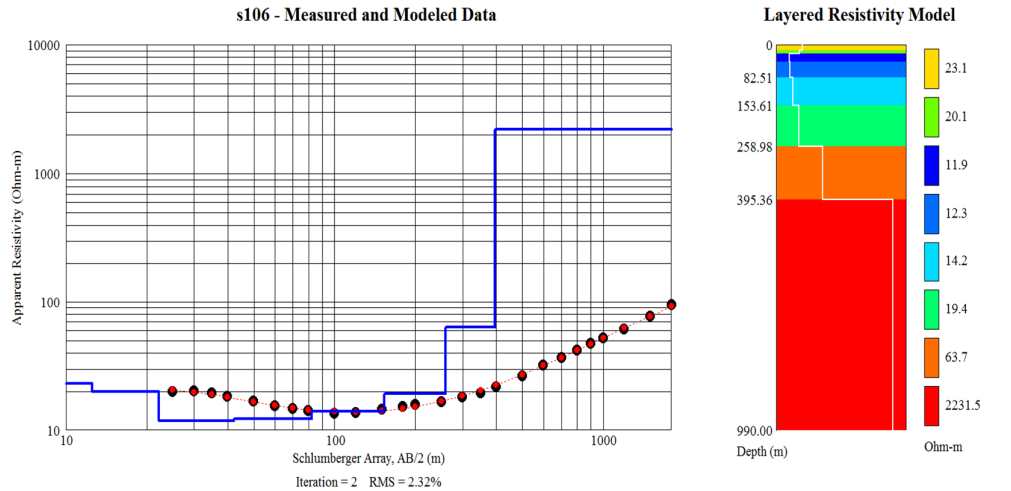
s106 - Measured and Modeled Data
Apparent Resistivity (Ohm-m)
10000
1000
100
10
10
100
1000
Schlumberger Array, AB/2 (m)
Iteration = 2 RMS = 2.32%
Layered Resistivity Model
0
82.51
153.61
258.98
395.36
990.00
Depth (m)
23.1
20.1
11.9
12.3
14.2
19.4
63.7
2231.5
Ohm-m

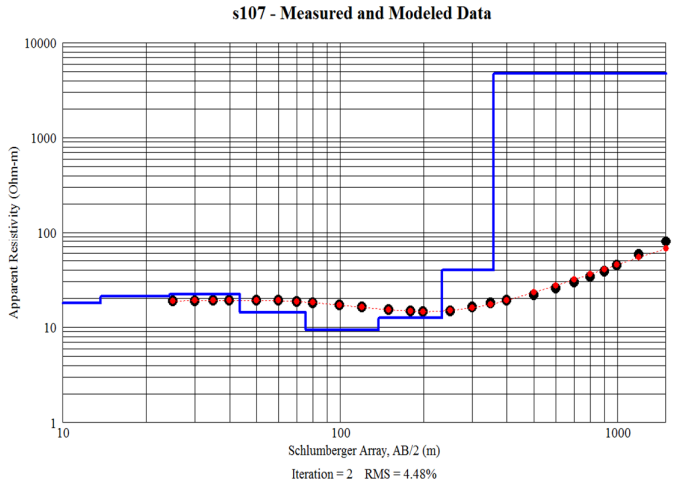
s107 - Measured and Modeled Data
Apparent Resistivity (Ohm-m)
10000
1000
100
10
1
10
100
1000
Schlumberger Array, AB/2 (m)
Iteration = 2 RMS = 4.48%

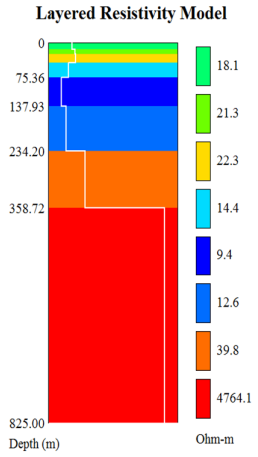
Layered Resistivity Model
0
75.36
137.93
234.20
358.72
825.00
Depth (m)
18.1
21.3
22.3
14.4
9.4
12.6
39.8
4764.1
Ohm-m

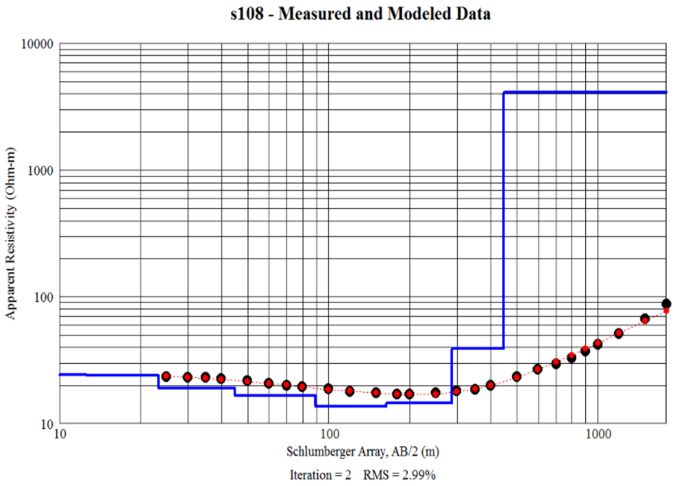
s108 - Measured and Modeled Data
Apparent Resistivity (Ohm-m)
10000
1000
100
10
10
100
1000
Schlumberger Array, AB/2 (m)
Iteration = 2 RMS = 2.99%

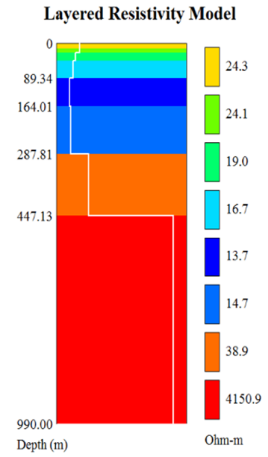
Layered Resistivity Model
0
89.34
164.01
287.81
447.13
990.00
Depth (m)
24.3
24.1
19.0
16.7
13.7
14.7
38.9
4150.9
Ohm-m

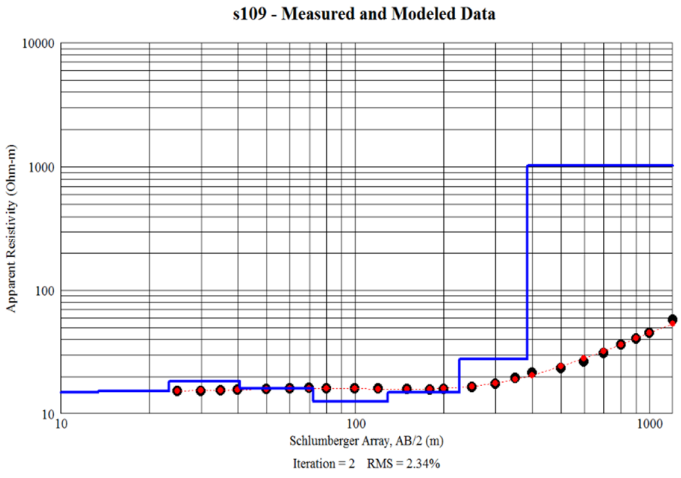
s109 - Measured and Modeled Data
Apparent Resistivity (Ohm-m)
10000
1000
100
10
10
100
1000
Schlumberger Array, AB/2 (m)
Iteration = 2 RMS = 2.34%

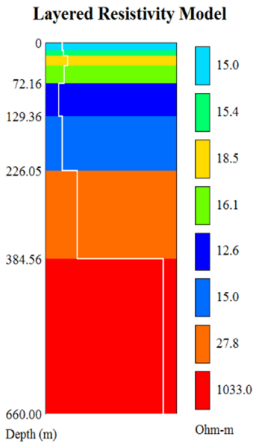
Layered Resistivity Model
0
72.16
129.36
226.05
384.56
660.00
Depth (m)
15.0
15.4
18.5
16.1
12.6
15.0
27.8
1033.0
Ohm-m

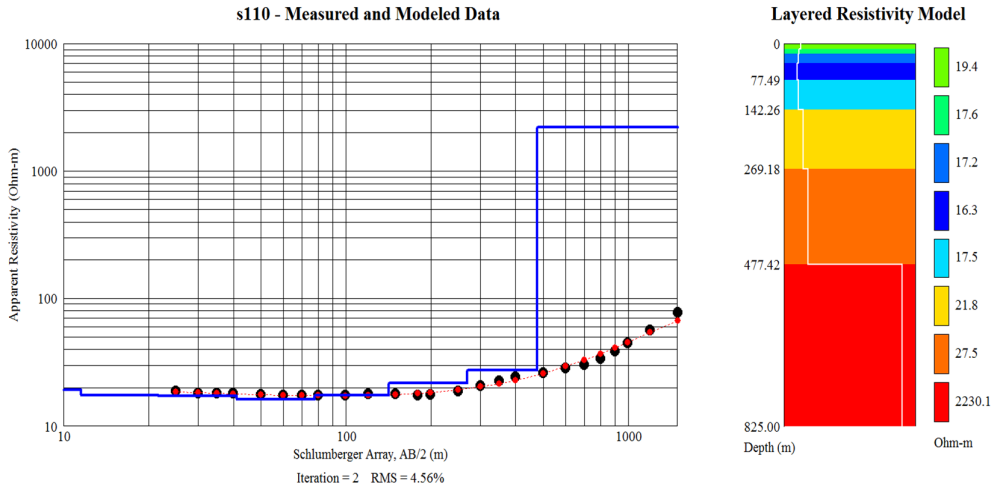
s110 - Measured and Modeled Data
Apparent Resistivity (Ohm-m)
10000
1000
100
10
10
100
1000
Schlumberger Array, AB/2 (m)
Iteration = 2 RMS = 4.56%
Layered Resistivity Model
0
77.49
142.26
269.18
477.42
825.00
Depth (m)
19.4
17.6
17.2
16.3
17.5
21.8
27.5
2230.1
Ohm-m

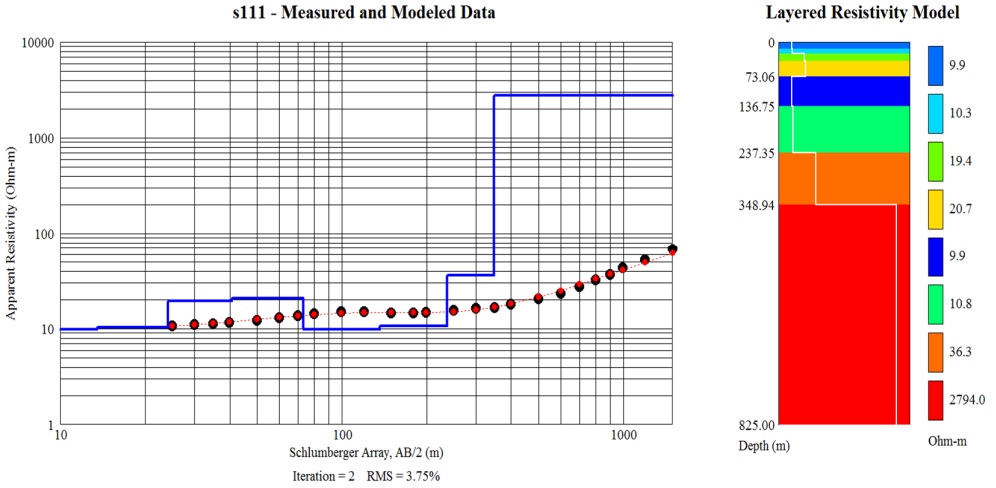
s111 - Measured and Modeled Data
Apparent Resistivity (Ohm-m)
10000
1000
100
10
1
10
100
1000
Schlumberger Array, AB/2 (m)
Iteration = 2 RMS = 3.75%
Layered Resistivity Model
0
73.06
136.75
237.35
348.94
825.00
Depth (m)
9.9
10.3
19.4
20.7
9.9
10.8
36.3
2794.0
Ohm-m

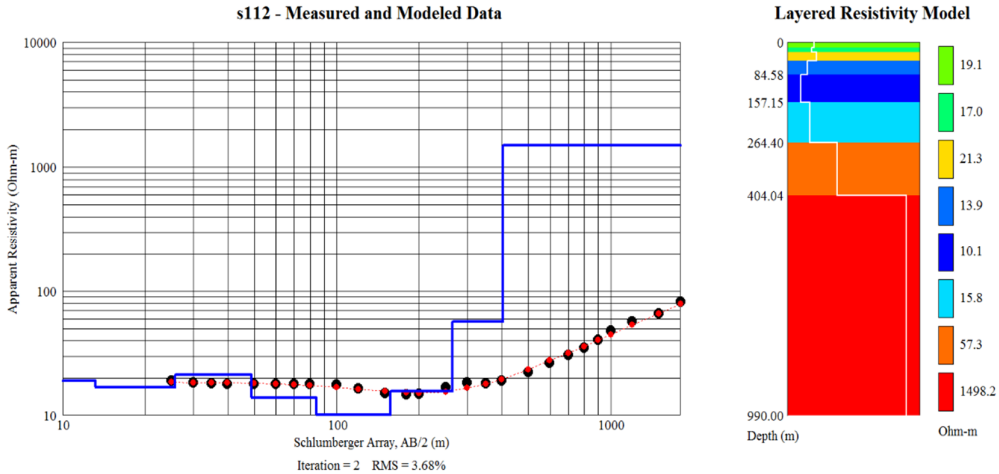
s112 - Measured and Modeled Data
Apparent Resistivity (Ohm-m)
10000
1000
100
10
10
100
1000
Schlumberger Array, AB/2 (m)
Iteration = 2 RMS = 3.68%
Layered Resistivity Model
0
84.58
157.15
264.40
404.04
990.00
Depth (m)
19.1
17.0
21.3
13.9
10.1
15.8
57.3
1498.2
Ohm-m

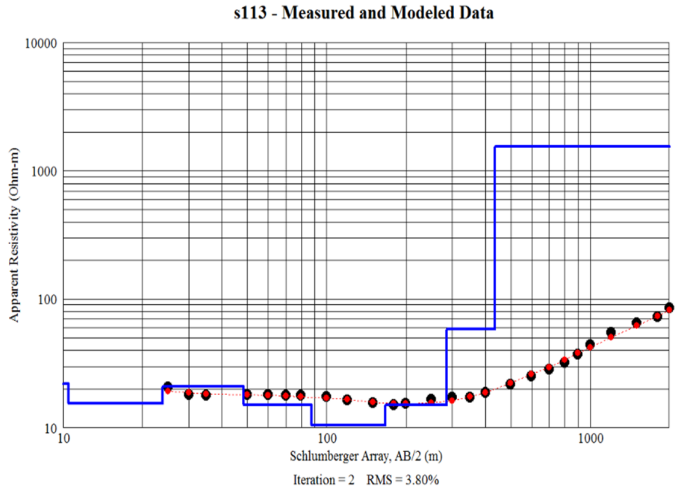
s113 - Measured and Modeled Data
Apparent Resistivity (Ohm-m)
10000
1000
100
10
10
100
1000
Schlumberger Array, AB/2 (m)
Iteration = 2 RMS = 3.80%

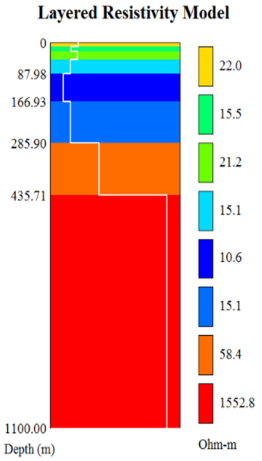
Layered Resistivity Model
0
87.98
166.93
285.90
435.71
1100.00
Depth (m)
22.0
15.5
21.2
15.1
10.6
15.1
58.4
1552.8
Ohm-m

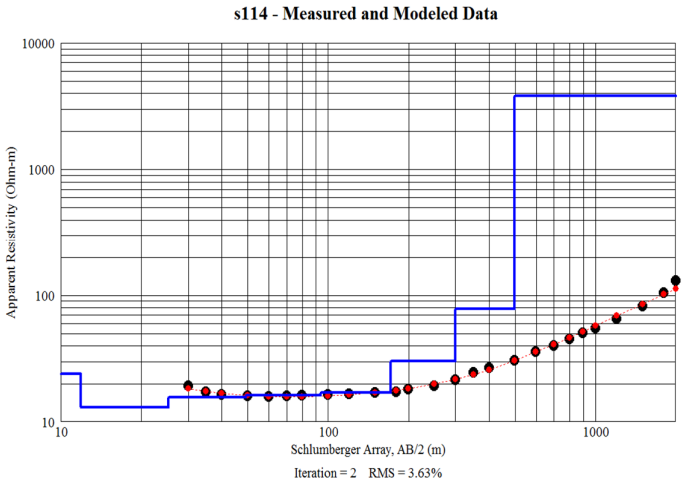
s114 - Measured and Modeled Data
Apparent Resistivity (Ohm-m)
10000
1000
100
10
10
100
1000
Schlumberger Array, AB/2 (m)
Iteration = 2 RMS = 3.63%

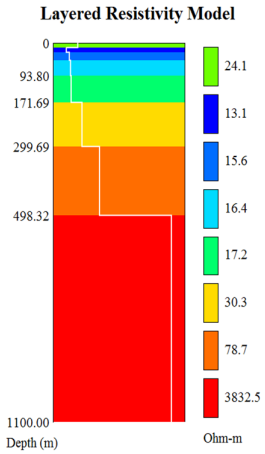
Layered Resistivity Model
0
93.80
171.69
299.69
498.32
1100.00
Depth (m)
24.1
13.1
15.6
16.4
17.2
30.3
78.7
3832.5
Ohm-m

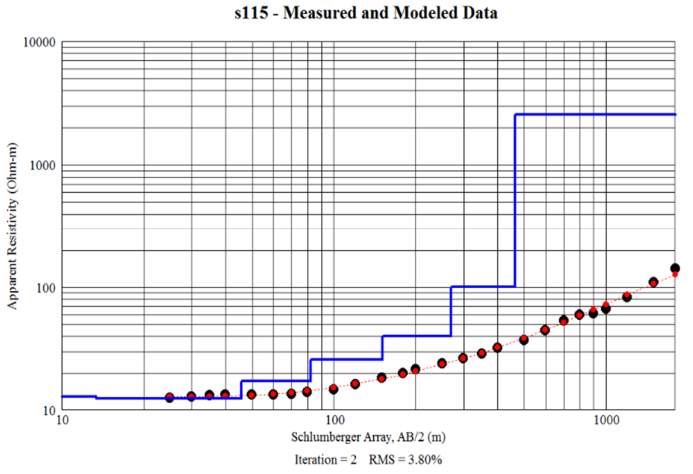
s115 - Measured and Modeled Data
Apparent Resistivity (Ohm-m)
10000
1000
100
10
10
100
1000
Schlumberger Array, AB/2 (m)
Iteration = 2 RMS = 3.80%

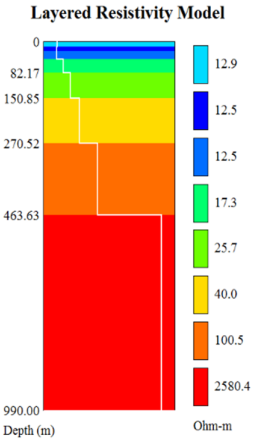
Layered Resistivity Model
0
82.17
150.85
270.52
463.63
990.00
Depth (m)
12.9
12.5
12.5
17.3
25.7
40.0
100.5
2580.4
Ohm-m

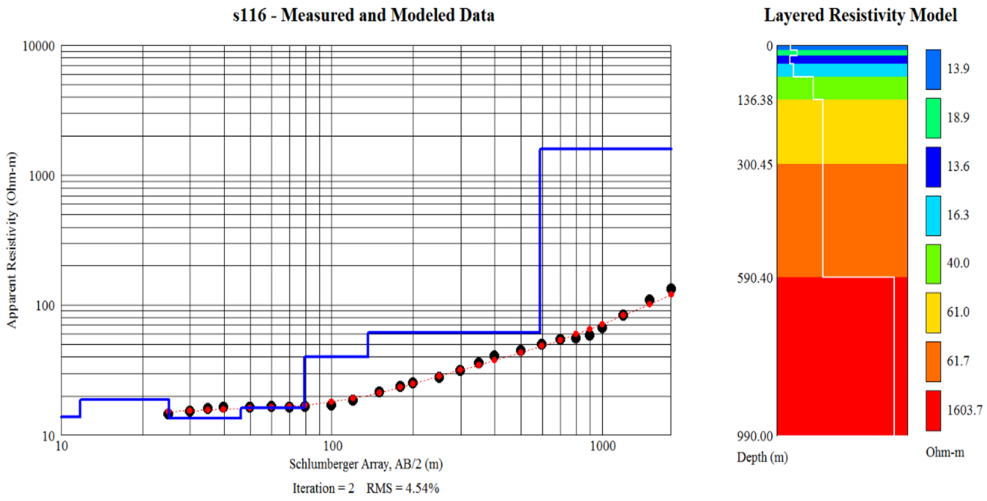
s116 - Measured and Modeled Data
Apparent Resistivity (Ohm-m)
10000
1000
100
10
10
100
1000
Schlumberger Array, AB/2 (m)
Iteration = 2 RMS = 4.54%
Layered Resistivity Model
0
136.38
300.45
590.40
990.00
Depth (m)
13.9
18.9
13.6
16.3
40.0
61.0
61.7
1603.7
Ohm-m

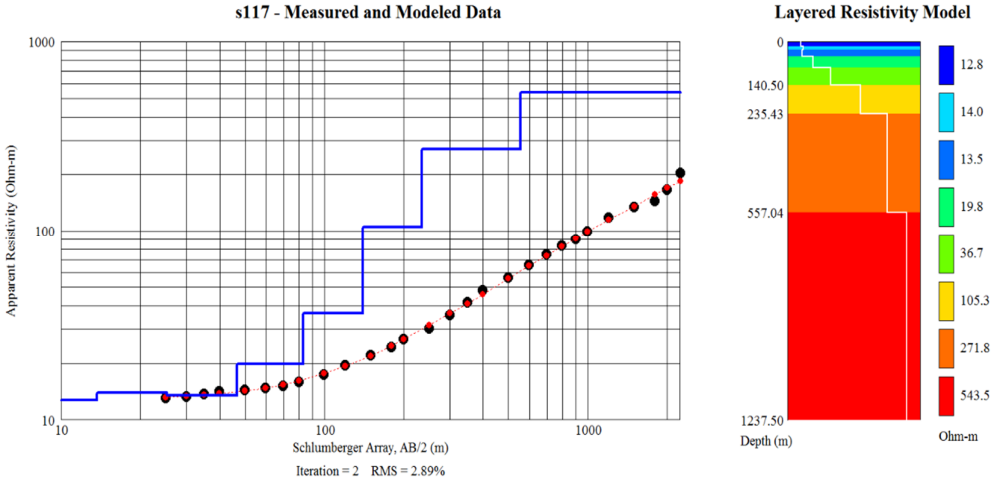
s117 - Measured and Modeled Data
Apparent Resistivity (Ohm-m)
1000
100
10
10
100
1000
Schlumberger Array, AB/2 (m)
Iteration = 2 RMS = 2.89%
Layered Resistivity Model
0
140.50
235.43
557.04
1237.50
Depth (m)
12.8
14.0
13.5
19.8
36.7
105.3
271.8
543.5
Ohm-m

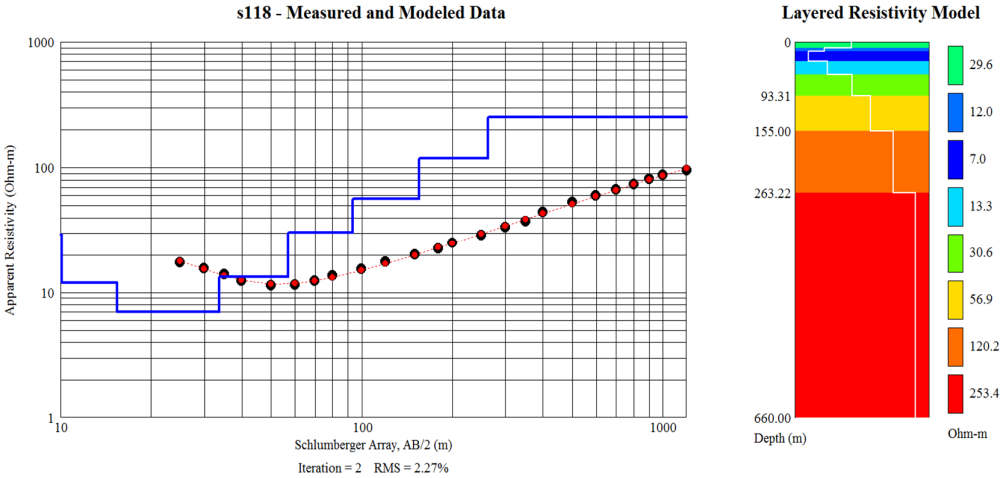
s118 - Measured and Modeled Data
Apparent Resistivity (Ohm-m)
1000
100
10
1
10
100
1000
Schlumberger Array, AB/2 (m)
Iteration = 2 RMS = 2.27%
Layered Resistivity Model
0
93.31
155.00
263.22
660.00
Depth (m)
29.6
12.0
7.0
13.3
30.6
56.9
120.2
253.4
Ohm-m

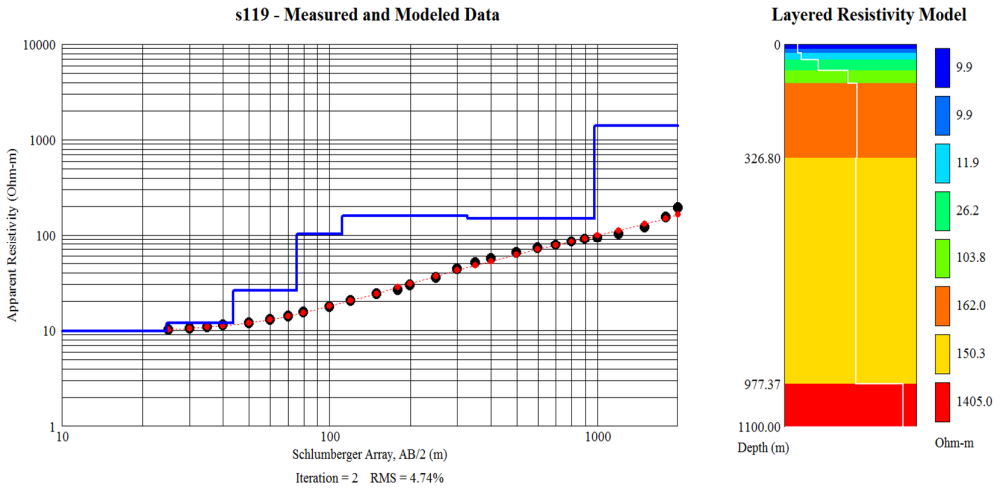
s119 - Measured and Modeled Data
Apparent Resistivity (Ohm-m)
10000
1000
100
10
1
10
100
1000
Schlumberger Array, AB/2 (m)
Iteration = 2 RMS = 4.74%
Layered Resistivity Model
0
326.80
977.37
1100.00
Depth (m)
9.9
9.9
11.9
26.2
103.8
162.0
150.3
1405.0
Ohm-m

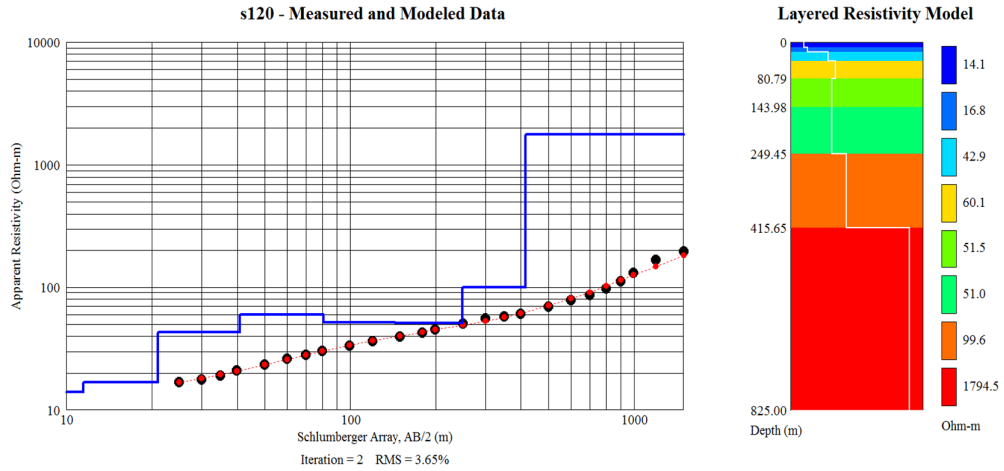
s120 - Measured and Modeled Data
Apparent Resistivity (Ohm-m)
10000
1000
100
10
10
100
1000
Schlumberger Array, AB/2 (m)
Iteration = 2 RMS = 3.65%
Layered Resistivity Model
0
80.79
143.98
249.45
415.65
825.00
Depth (m)
14.1
16.8
42.9
60.1
51.5
51.0
99.6
1794.5
Ohm-m

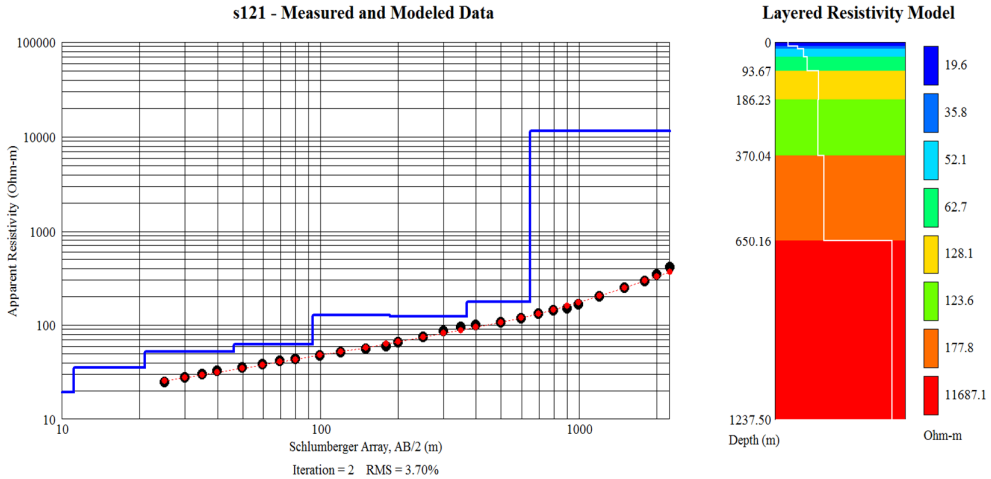
s121 - Measured and Modeled Data
Apparent Resistivity (Ohm-m)
100000
10000
1000
100
10
10
100
1000
Schlumberger Array, AB/2 (m)
Iteration = 2 RMS = 3.70%
Layered Resistivity Model
0
93.67
186.23
370.04
650.16
1237.50
Depth (m)
19.6
35.8
52.1
62.7
128.1
123.6
177.8
11687.1
Ohm-m

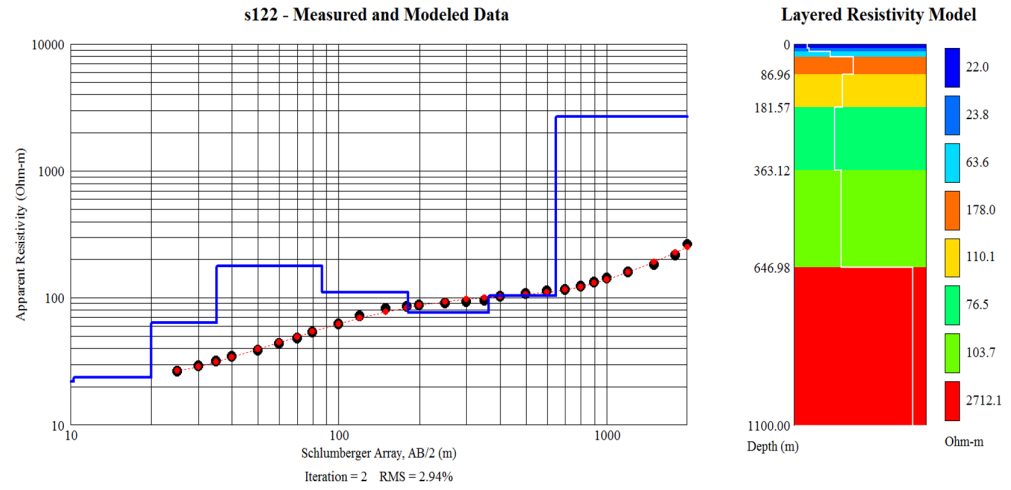
s122 - Measured and Modeled Data
Apparent Resistivity (Ohm-m)
10000
1000
100
10
10
100
1000
Schlumberger Array, AB/2 (m)
Iteration = 2 RMS = 2.94%
Layered Resistivity Model
0
86.96
181.57
363.12
646.98
1100.00
Depth (m)
22.0
23.8
63.6
178.0
110.1
76.5
103.7
2712.1
Ohm-m

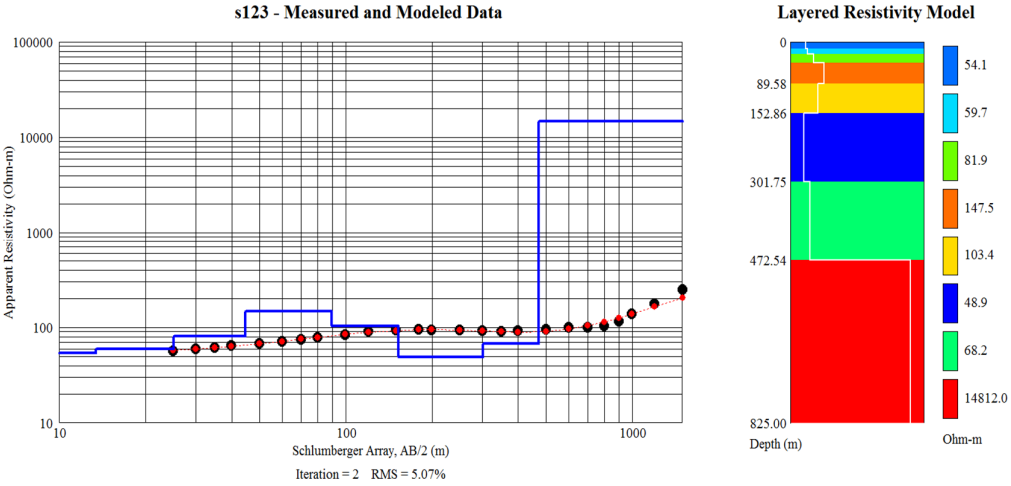
s123 - Measured and Modeled Data
Apparent Resistivity (Ohm-m)
100000
10000
1000
100
10
10
100
1000
Schlumberger Array, AB/2 (m)
Iteration = 2 RMS = 5.07%
Layered Resistivity Model
0
89.58
152.86
301.75
472.54
825.00
Depth (m)
54.1
59.7
81.9
147.5
103.4
48.9
68.2
14812.0
Ohm-m

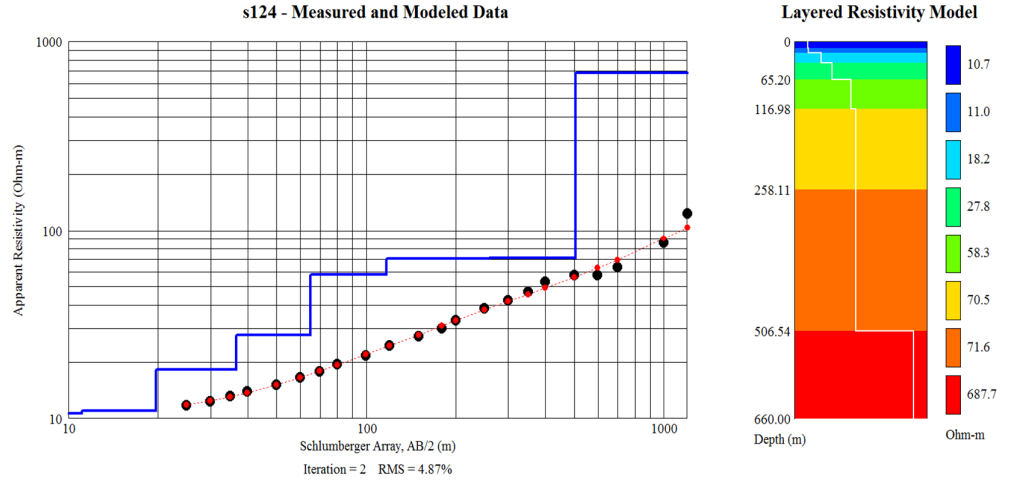
s124 - Measured and Modeled Data
Apparent Resistivity (Ohm-m)
1000
100
10
10
100
1000
Schlumberger Array, AB/2 (m)
Iteration = 2 RMS = 4.87%
Layered Resistivity Model
0
65.20
116.98
258.11
506.54
660.00
Depth (m)
10.7
11.0
18.2
27.8
58.3
70.5
71.6
687.7
Ohm-m

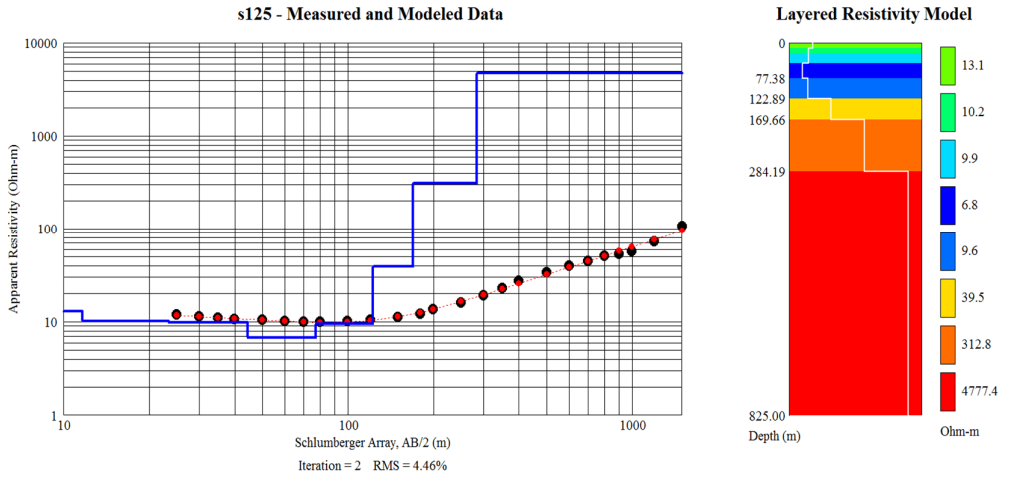
s125 - Measured and Modeled Data
Apparent Resistivity (Ohm-m)
10000
1000
100
10
1
10
100
1000
Schlumberger Array, AB/2 (m)
Iteration = 2 RMS = 4.46%
Layered Resistivity Model
0
77.38
122.89
169.66
284.19
825.00
Depth (m)
13.1
10.2
9.9
6.8
9.6
39.5
312.8
4777.4
Ohm-m

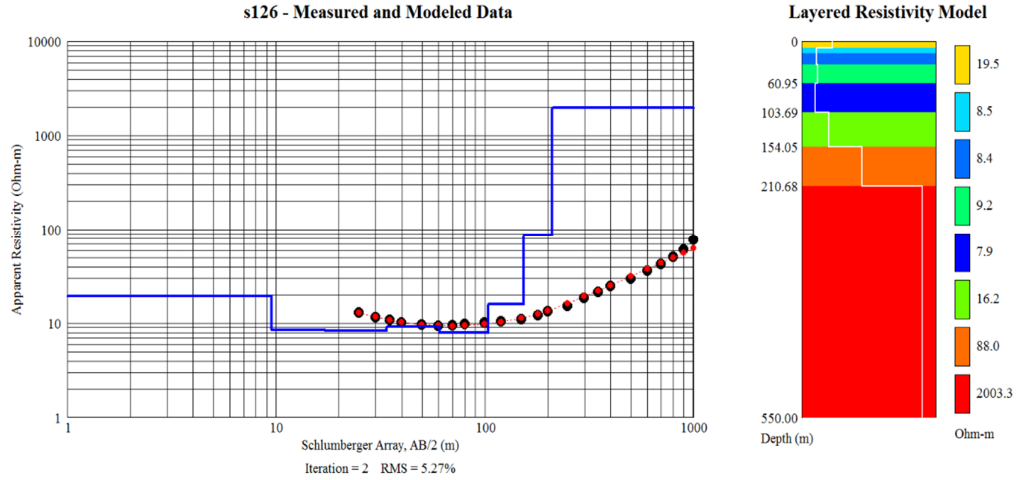
s126 - Measured and Modeled Data
Apparent Resistivity (Ohm-m)
10000
1000
100
10
1
1
10
100
1000
Schlumberger Array, AB/2 (m)
Iteration = 2 RMS = 5.27%
Layered Resistivity Model
0
60.95
103.69
154.05
210.68
550.00
Depth (m)
19.5
8.5
8.4
9.2
7.9
16.2
88.0
2003.3
Ohm-m

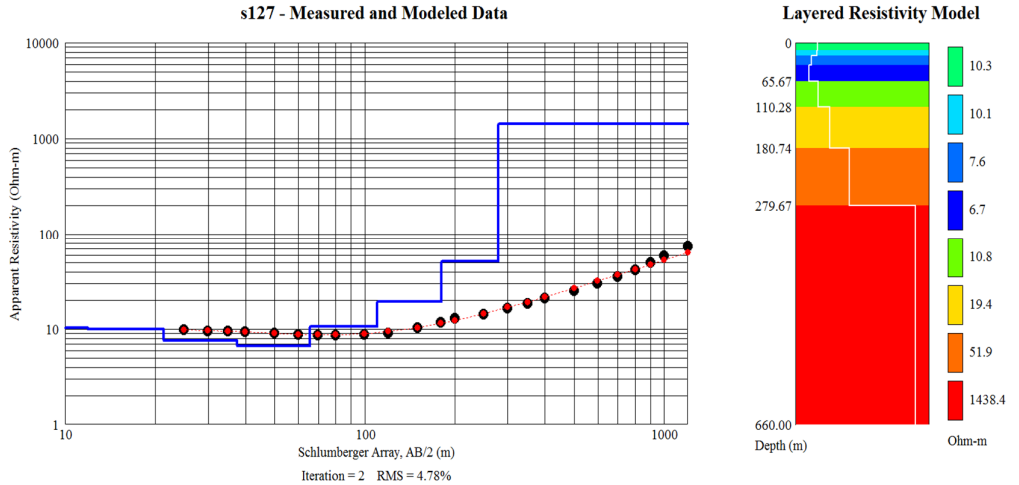
s127 - Measured and Modeled Data
Apparent Resistivity (Ohm-m)
10000
1000
100
10
1
10
100
1000
Schlumberger Array, AB/2 (m)
Iteration = 2 RMS = 4.78%
Layered Resistivity Model
0
65.67
110.28
180.74
279.67
660.00
Depth (m)
10.3
10.1
7.6
6.7
10.8
19.4
51.9
1438.4
Ohm-m

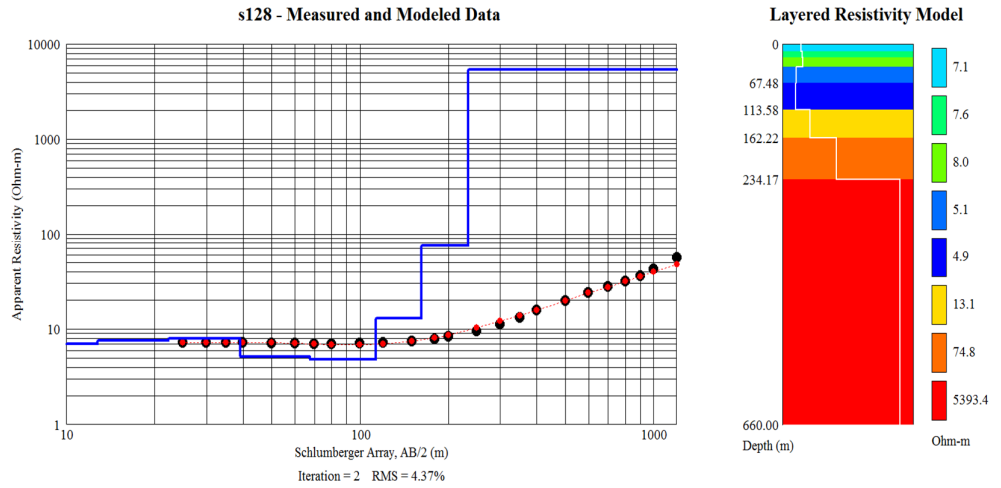
s128 - Measured and Modeled Data
Apparent Resistivity (Ohm-m)
10000
1000
100
10
1
10
100
1000
Schlumberger Array, AB/2 (m)
Iteration = 2 RMS = 4.37%
Layered Resistivity Model
0
67.48
113.58
162.22
234.17
660.00
Depth (m)
7.1
7.6
8.0
5.1
4.9
13.1
74.8
5393.4
Ohm-m

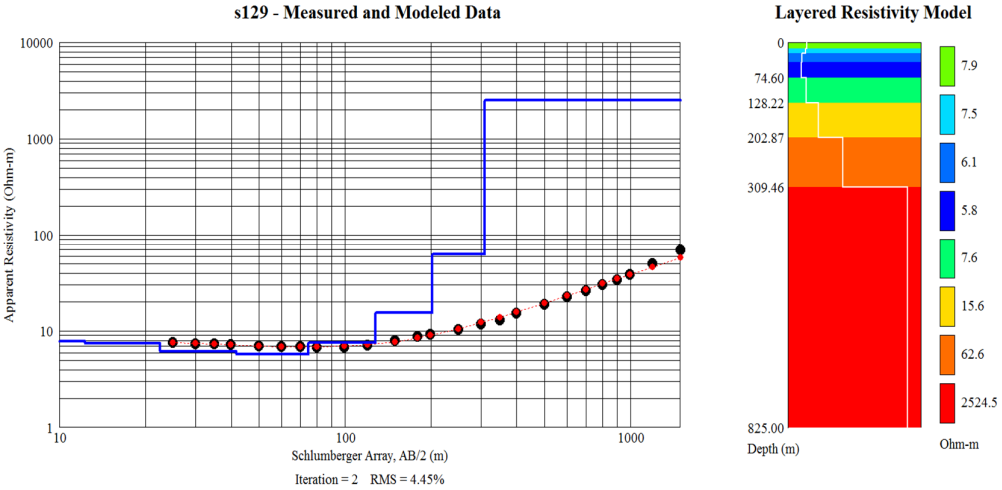
s129 - Measured and Modeled Data
Apparent Resistivity (Ohm-m)
10000
1000
100
10
1
10
100
1000
Schlumberger Array, AB/2 (m)
Iteration = 2 RMS = 4.45%
Layered Resistivity Model
0
74.60
128.22
202.87
309.46
825.00
Depth (m)
7.9
7.5
6.1
5.8
7.6
15.6
62.6
2524.5
Ohm-m

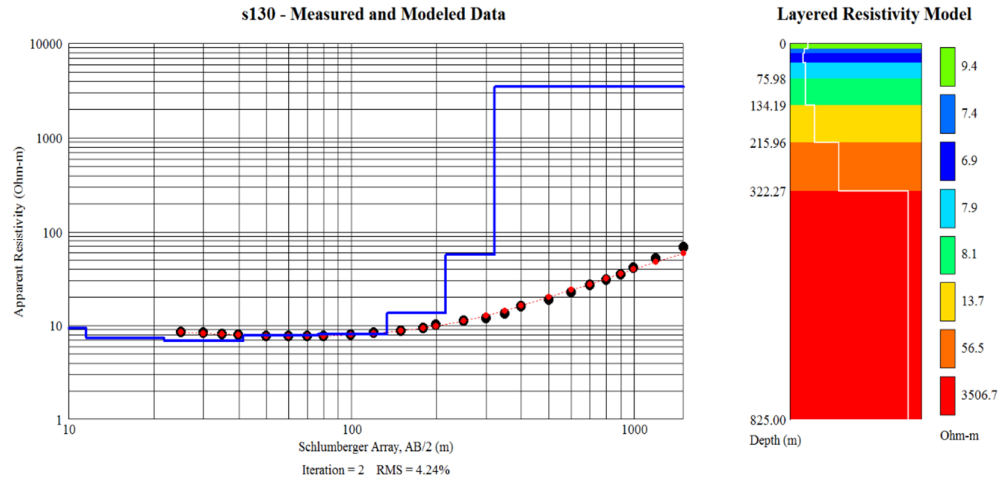
s130 - Measured and Modeled Data
Apparent Resistivity (Ohm-m)
10000
1000
100
10
1
10
100
1000
Schlumberger Array, AB/2 (m)
Iteration = 2 RMS = 4.24%
Layered Resistivity Model
0
75.98
134.19
215.96
322.27
825.00
Depth (m)
9.4
7.4
6.9
7.9
8.1
13.7
56.5
3506.7
Ohm-m

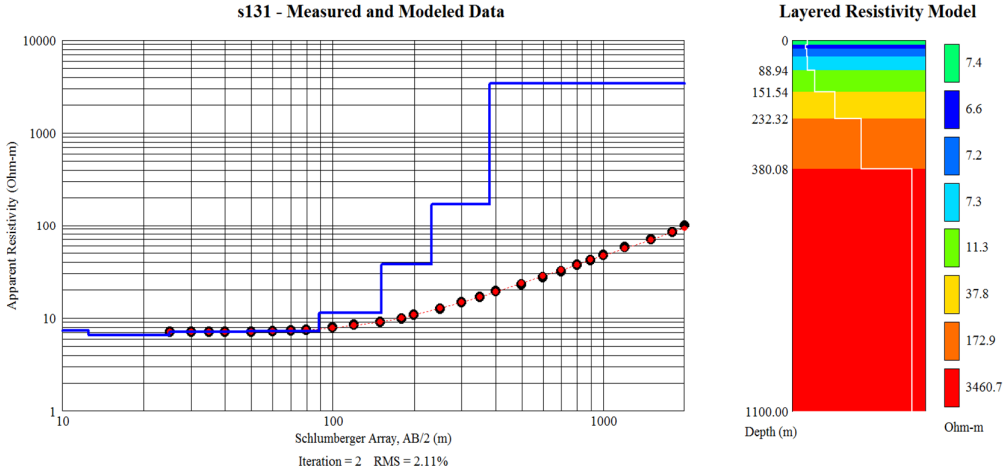
s131 - Measured and Modeled Data
Apparent Resistivity (Ohm-m)
10000
1000
100
10
1
10
100
1000
Schlumberger Array, AB/2 (m)
Iteration = 2 RMS = 2.11%
Layered Resistivity Model
0
88.94
151.54
232.32
380.08
1100.00
Depth (m)
7.4
6.6
7.2
7.3
11.3
37.8
172.9
3460.7
Ohm-m

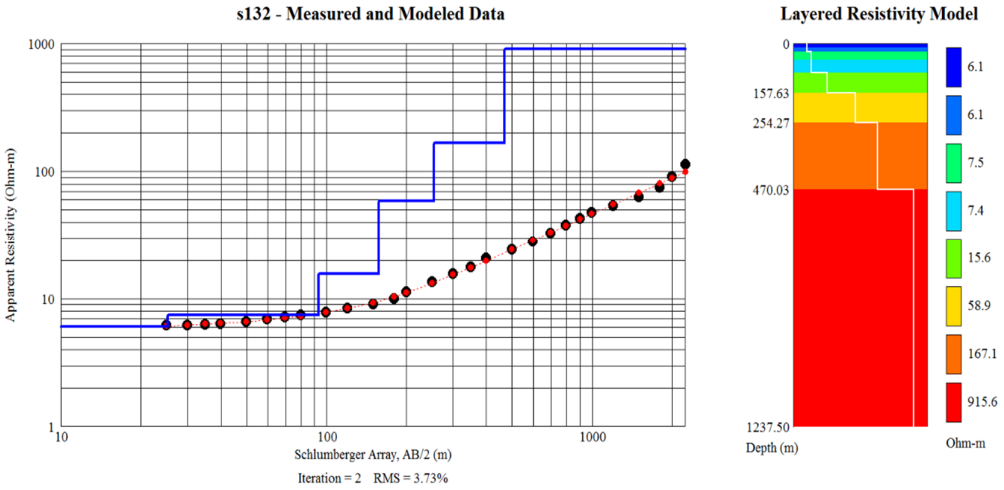
s132 - Measured and Modeled Data
Apparent Resistivity (Ohm-m)
1000
100
10
1
10
100
1000
Schlumberger Array, AB/2 (m)
Iteration = 2 RMS = 3.73%
Layered Resistivity Model
0
157.63
254.27
470.03
1237.50
Depth (m)
6.1
6.1
7.5
7.4
15.6
58.9
167.1
915.6
Ohm-m

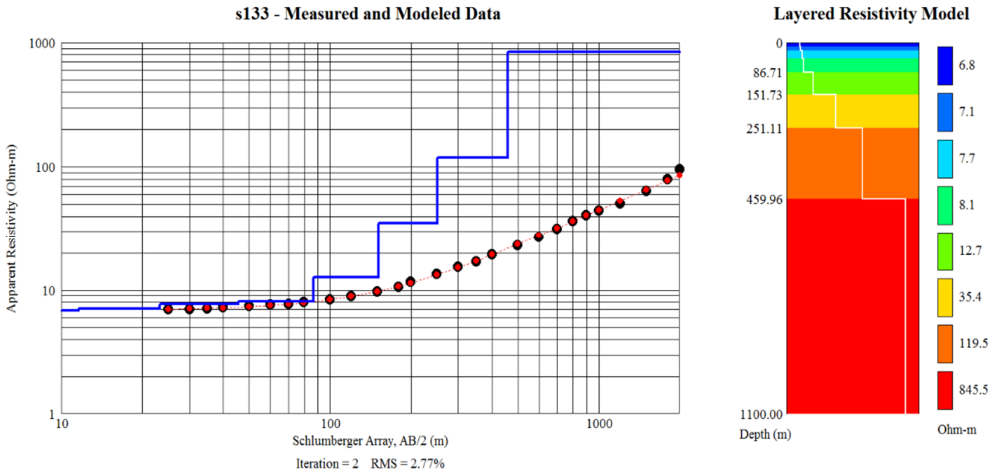
s133 - Measured and Modeled Data
Apparent Resistivity (Ohm-m)
1000
100
10
1
10
100
1000
Schlumberger Array, AB/2 (m)
Iteration = 2 RMS = 2.77%
Layered Resistivity Model
0
86.71
151.73
251.11
459.96
1100.00
Depth (m)
6.8
7.1
7.7
8.1
12.7
35.4
119.5
845.5
Ohm-m

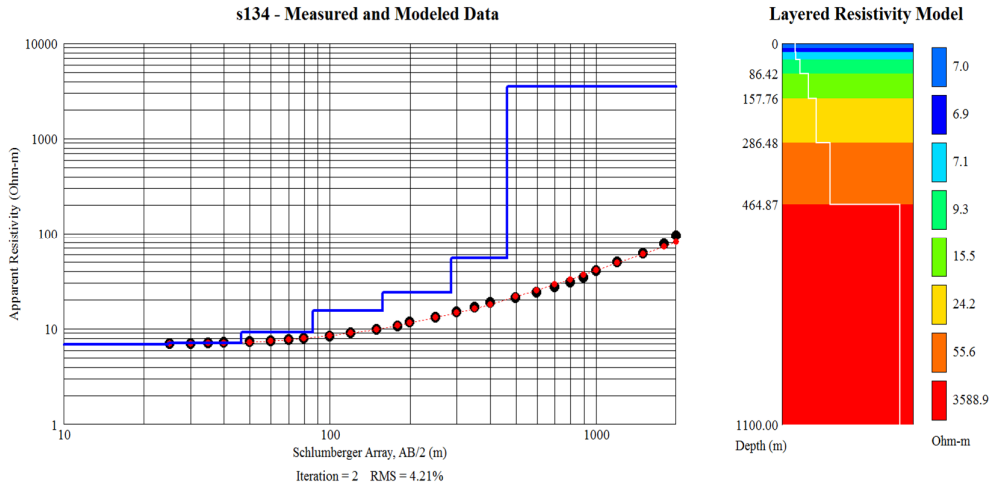
s134 - Measured and Modeled Data
Apparent Resistivity (Ohm-m)
10000
1000
100
10
1
10
100
1000
Schlumberger Array, AB/2 (m)
Iteration = 2 RMS = 4.21%
Layered Resistivity Model
0
86.42
157.76
286.48
464.87
1100.00
Depth (m)
7.0
6.9
7.1
9.3
15.5
24.2
55.6
3588.9
Ohm-m

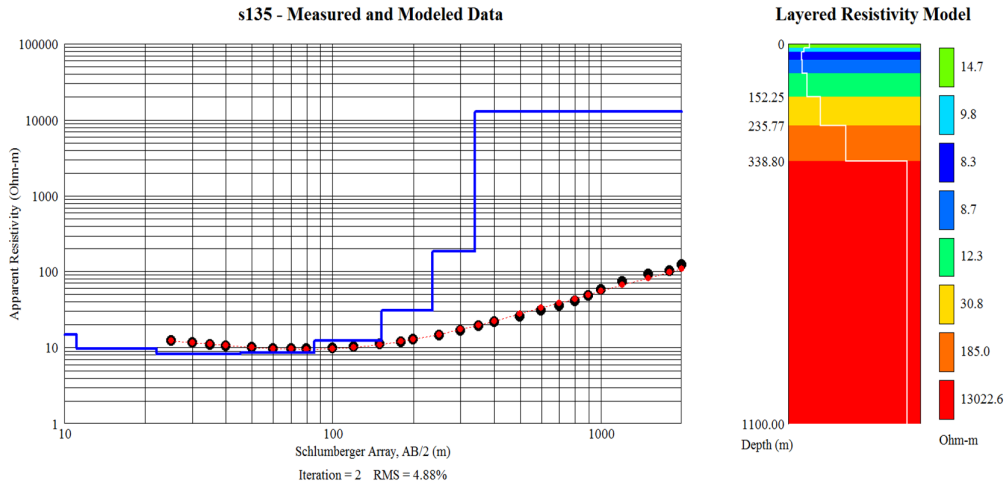
s135 - Measured and Modeled Data
Apparent Resistivity (Ohm-m)
100000
10000
1000
100
10
1
10
100
1000
Schlumberger Array, AB/2 (m)
Iteration = 2 RMS = 4.88%
Layered Resistivity Model
0
152.25
235.77
338.80
1100.00
Depth (m)
14.7
9.8
8.3
8.7
12.3
30.8
185.0
13022.6
Ohm-m

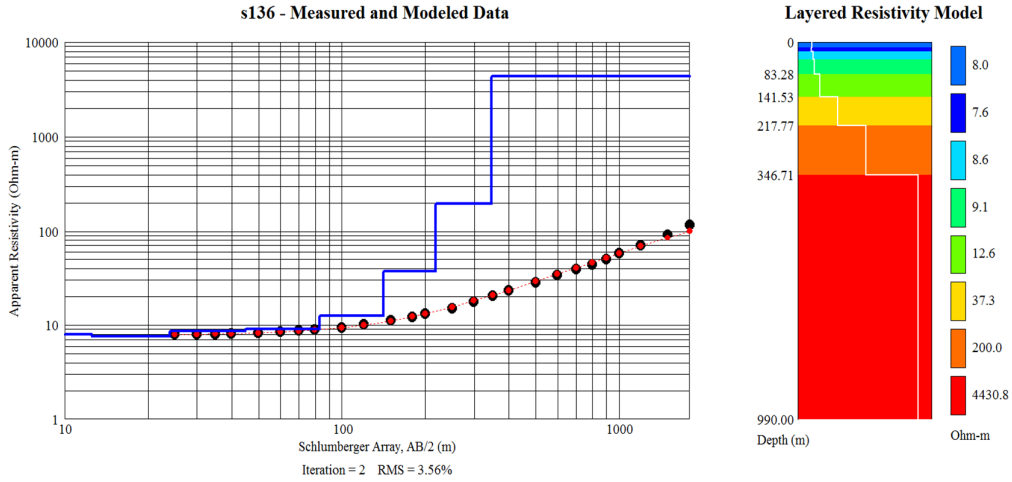
s136 - Measured and Modeled Data
Apparent Resistivity (Ohm-m)
10000
1000
100
10
1
10
100
1000
Schlumberger Array, AB/2 (m)
Iteration = 2 RMS = 3.56%
Layered Resistivity Model
0
83.28
141.53
217.77
346.71
990.00
Depth (m)
8.0
7.6
8.6
9.1
12.6
37.3
200.0
4430.8
Ohm-m

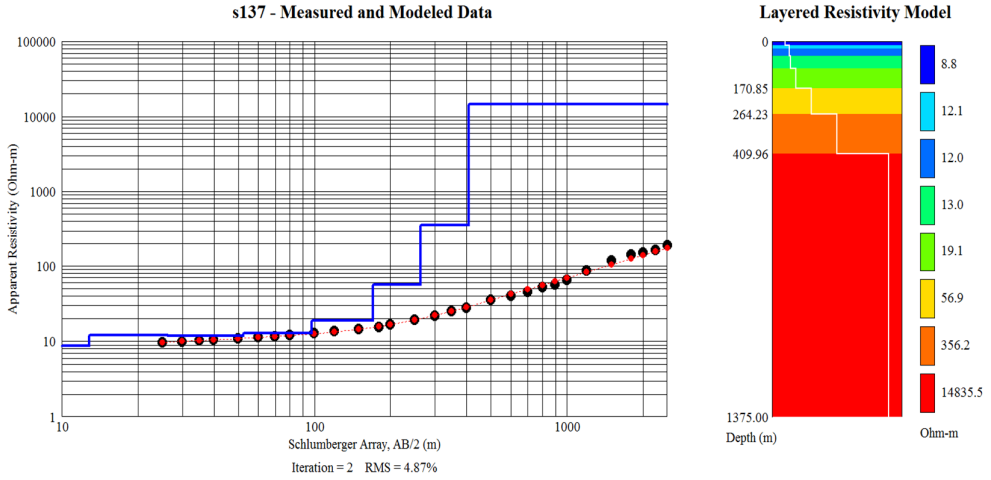
s137 - Measured and Modeled Data
Apparent Resistivity (Ohm-m)
100000
10000
1000
100
10
1
10
100
1000
Schlumberger Array, AB/2 (m)
Iteration = 2 RMS = 4.87%
Layered Resistivity Model
0
170.85
264.23
409.96
1375.00
Depth (m)
8.8
12.1
12.0
13.0
19.1
56.9
356.2
14835.5
Ohm-m

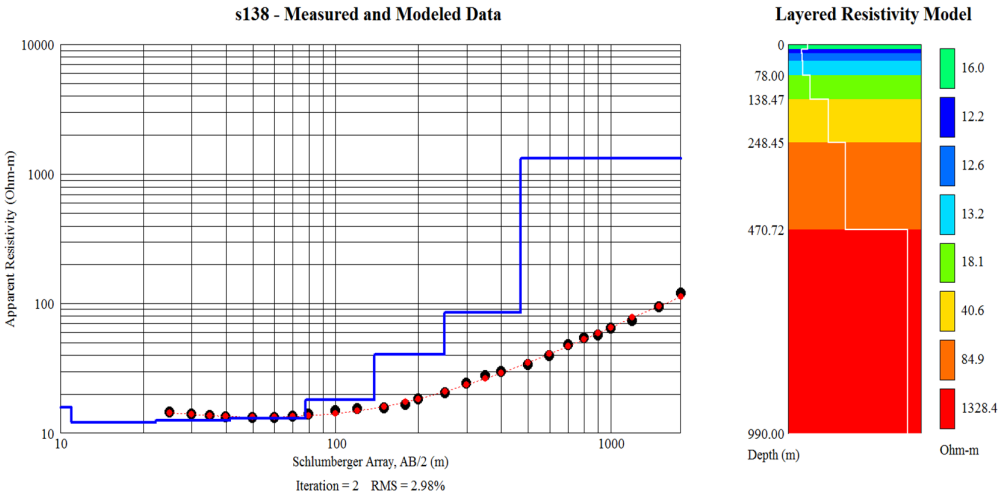
s138 - Measured and Modeled Data
Apparent Resistivity (Ohm-m)
10000
1000
100
10
10
100
1000
Schlumberger Array, AB/2 (m)
Iteration = 2 RMS = 2.98%
Layered Resistivity Model
0
78.00
138.47
248.45
470.72
990.00
Depth (m)
16.0
12.2
12.6
13.2
18.1
40.6
84.9
1328.4
Ohm-m

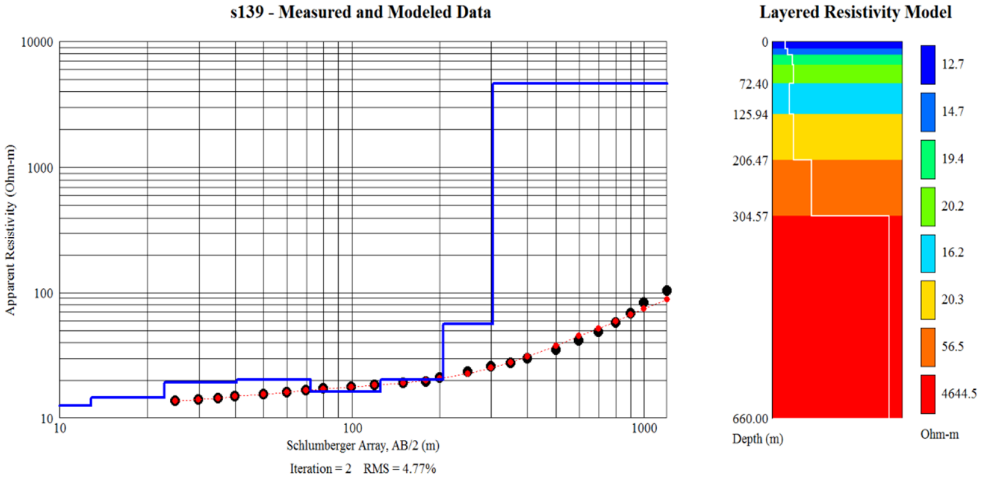
s139 - Measured and Modeled Data
Apparent Resistivity (Ohm-m)
10000
1000
100
10
10
100
1000
Schlumberger Array, AB/2 (m)
Iteration = 2 RMS = 4.77%
Layered Resistivity Model
0
72.40
125.94
206.47
304.57
660.00
Depth (m)
12.7
14.7
19.4
20.2
16.2
20.3
56.5
4644.5
Ohm-m

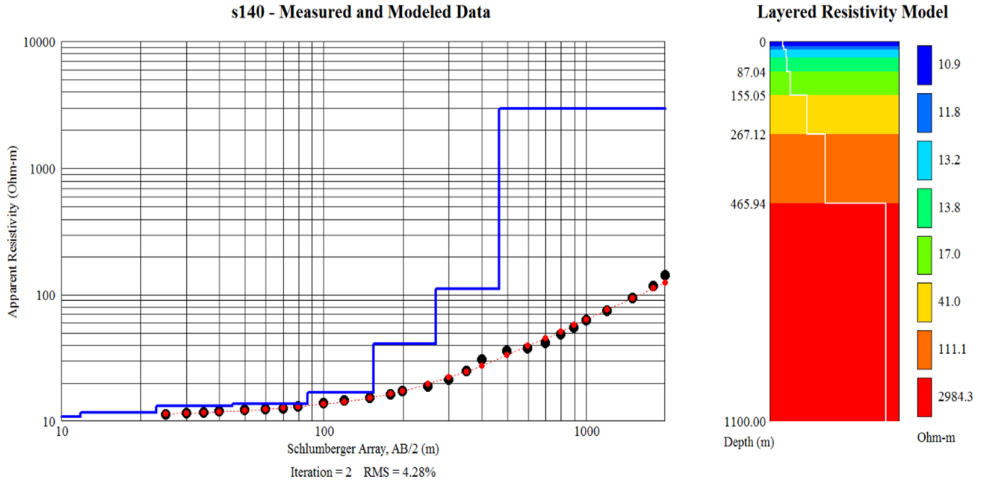
s140 - Measured and Modeled Data
Apparent Resistivity (Ohm-m)
10000
1000
100
10
10
100
1000
Schlumberger Array, AB/2 (m)
Iteration = 2 RMS = 4.28%
Layered Resistivity Model
0
87.04
155.05
267.12
465.94
1100.00
Depth (m)
10.9
11.8
13.2
13.8
17.0
41.0
111.1
2984.3
Ohm-m

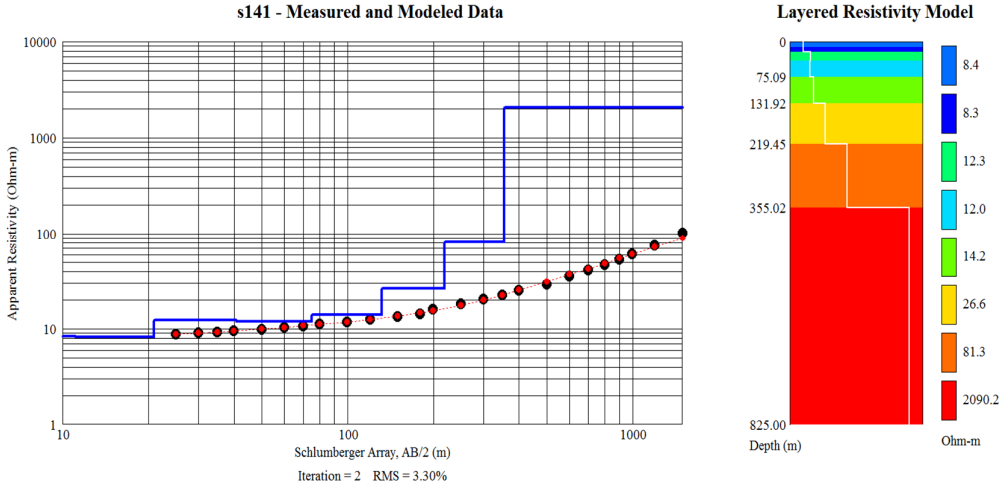
s141 - Measured and Modeled Data
Apparent Resistivity (Ohm-m)
10000
1000
100
10
1
10
100
1000
Schlumberger Array, AB/2 (m)
Iteration = 2 RMS = 3.30%
Layered Resistivity Model
0
75.09
131.92
219.45
355.02
825.00
Depth (m)
8.4
8.3
12.3
12.0
14.2
26.6
81.3
2090.2
Ohm-m

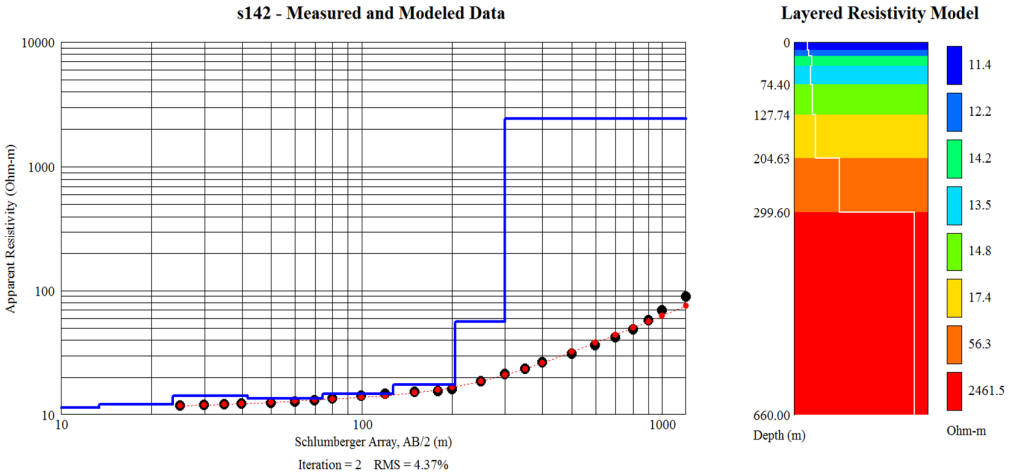
s142 - Measured and Modeled Data
Apparent Resistivity (Ohm-m)
10000
1000
100
10
10
100
1000
Schlumberger Array, AB/2 (m)
Iteration = 2 RMS = 4.37%
Layered Resistivity Model
0
74.40
127.74
204.63
299.60
660.00
Depth (m)
11.4
12.2
14.2
13.5
14.8
17.4
56.3
2461.5
Ohm-m

Group 9

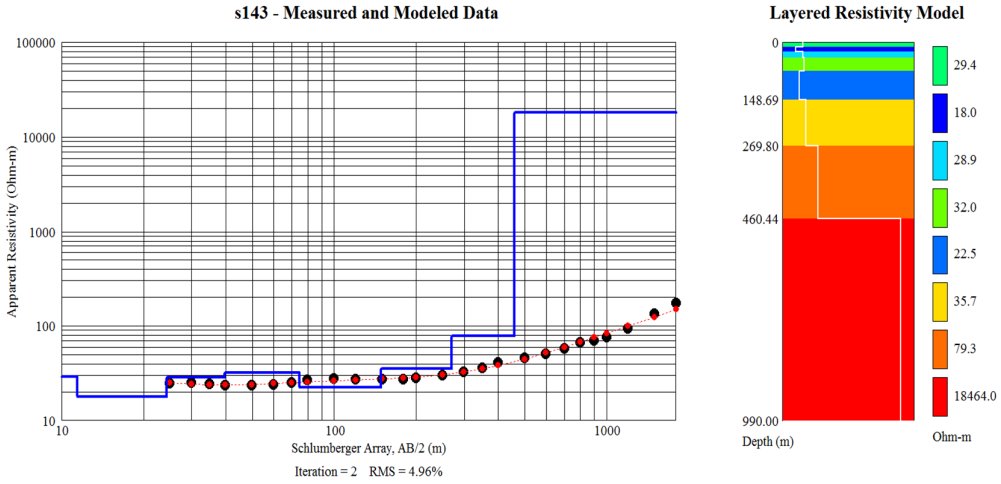
s143 - Measured and Modeled Data
Apparent Resistivity (Ohm-m)
100000
10000
1000
100
10
10
100
1000
Schlumberger Array, AB/2 (m)
Iteration = 2 RMS = 4.96%
Layered Resistivity Model
0
148.69
269.80
460.44
990.00
Depth (m)
29.4
18.0
28.9
32.0
22.5
35.7
79.3
18464.0
Ohm-m

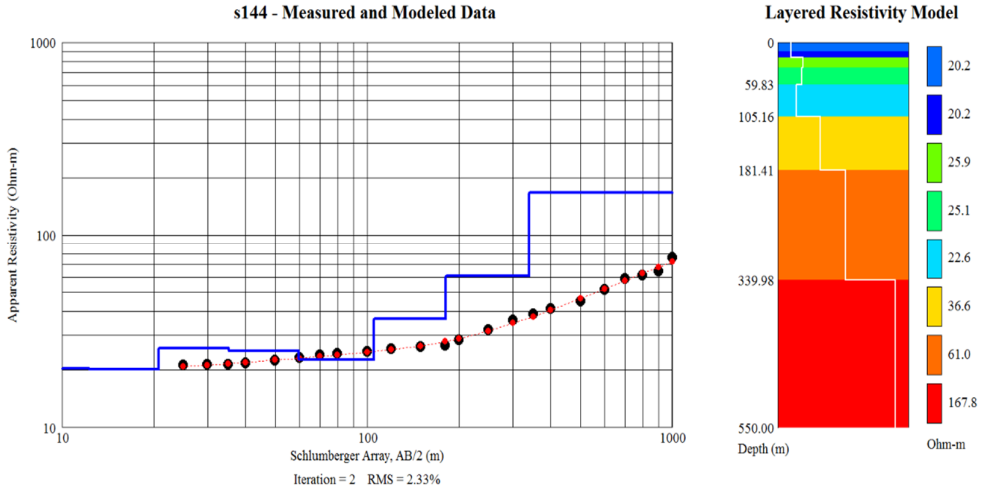
s144 - Measured and Modeled Data
Apparent Resistivity (Ohm-m)
1000
100
10
10
100
1000
Schlumberger Array, AB/2 (m)
Iteration = 2 RMS = 2.33%
Layered Resistivity Model
0
59.83
105.16
181.41
339.98
550.00
Depth (m)
20.2
20.2
25.9
25.1
22.6
36.6
61.0
167.8
Ohm-m

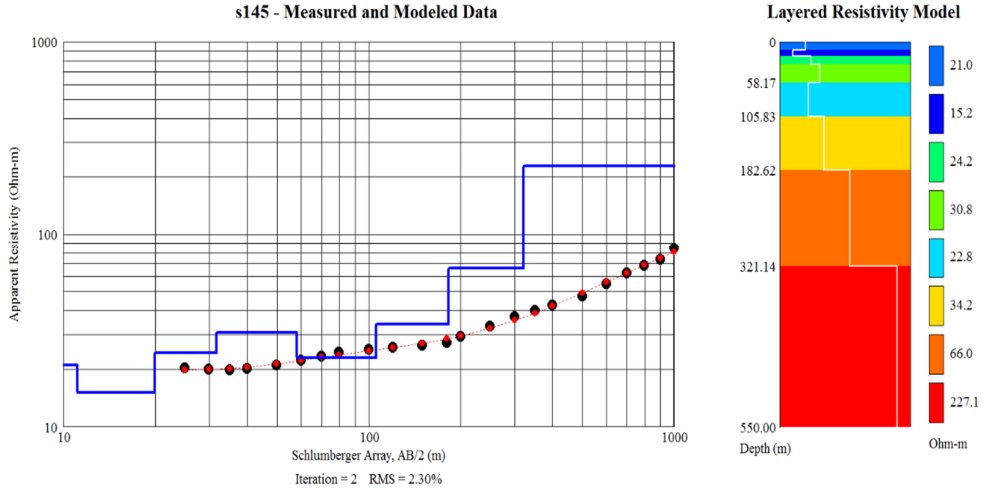
s145 - Measured and Modeled Data
Apparent Resistivity (Ohm-m)
1000
100
10
10
100
1000
Schlumberger Array, AB/2 (m)
Iteration = 2 RMS = 2.30%
Layered Resistivity Model
0
58.17
105.83
182.62
321.14
550.00
Depth (m)
21.0
15.2
24.2
30.8
22.8
34.2
66.0
227.1
Ohm-m

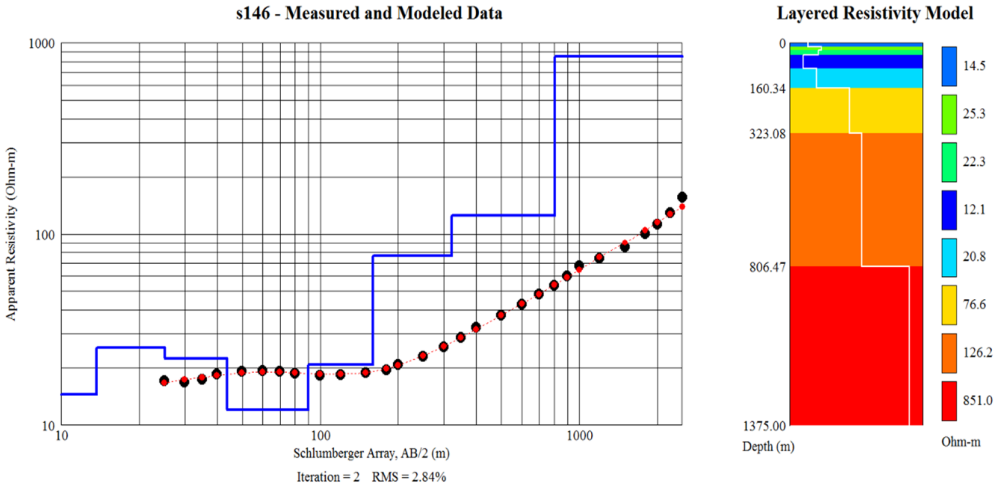
s146 - Measured and Modeled Data
Apparent Resistivity (Ohm-m)
1000
100
10
10
100
1000
Schlumberger Array, AB/2 (m)
Iteration = 2 RMS = 2.84%
Layered Resistivity Model
0
160.34
323.08
806.47
1375.00
Depth (m)
14.5
25.3
22.3
12.1
20.8
76.6
126.2
851.0
Ohm-m

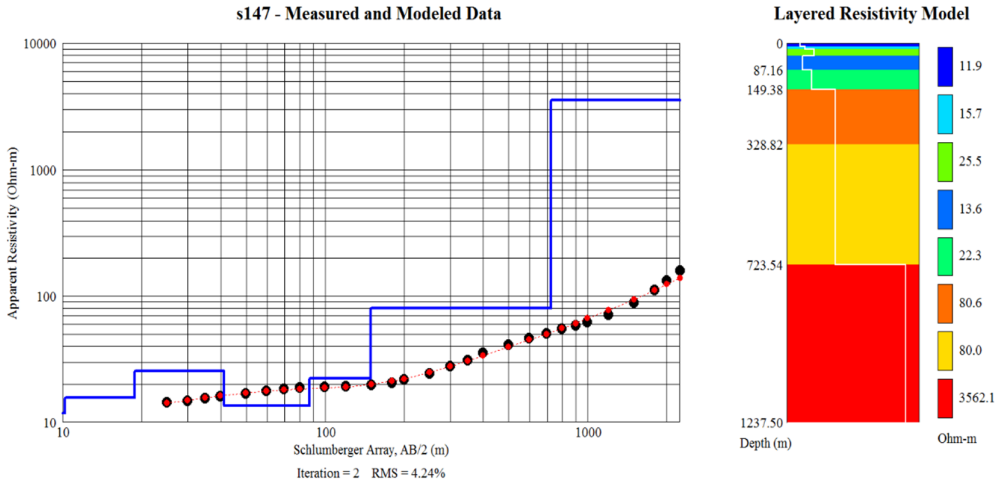
s147 - Measured and Modeled Data
Apparent Resistivity (Ohm-m)
10000
1000
100
10
10
100
1000
Schlumberger Array, AB/2 (m)
Iteration = 2 RMS = 4.24%
Layered Resistivity Model
0
87.16
149.38
328.82
723.54
1237.50
Depth (m)
11.9
15.7
25.5
13.6
22.3
80.6
80.0
3562.1
Ohm-m

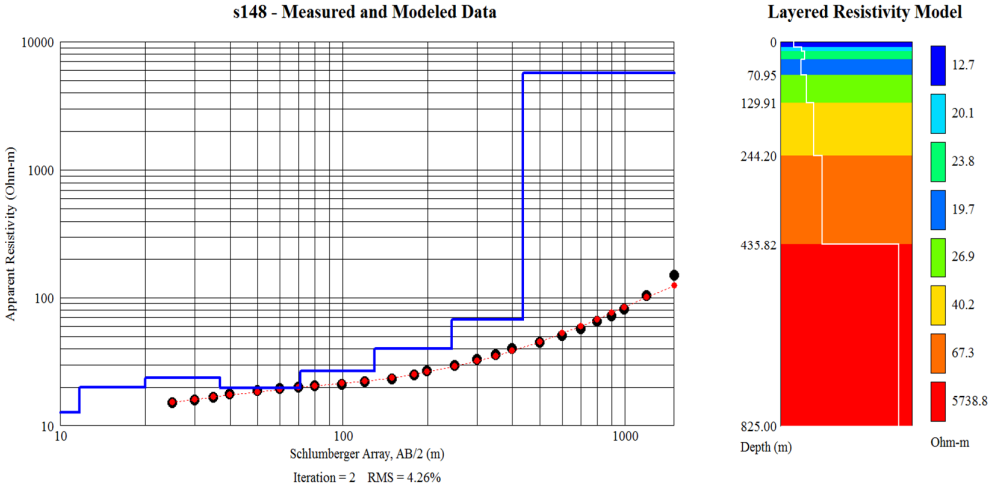
s148 - Measured and Modeled Data
Apparent Resistivity (Ohm-m)
10000
1000
100
10
10
100
1000
Schlumberger Array, AB/2 (m)
Iteration = 2 RMS = 4.26%
Layered Resistivity Model
0
70.95
129.91
244.20
435.82
825.00
Depth (m)
12.7
20.1
23.8
19.7
26.9
40.2
67.3
5738.8
Ohm-m

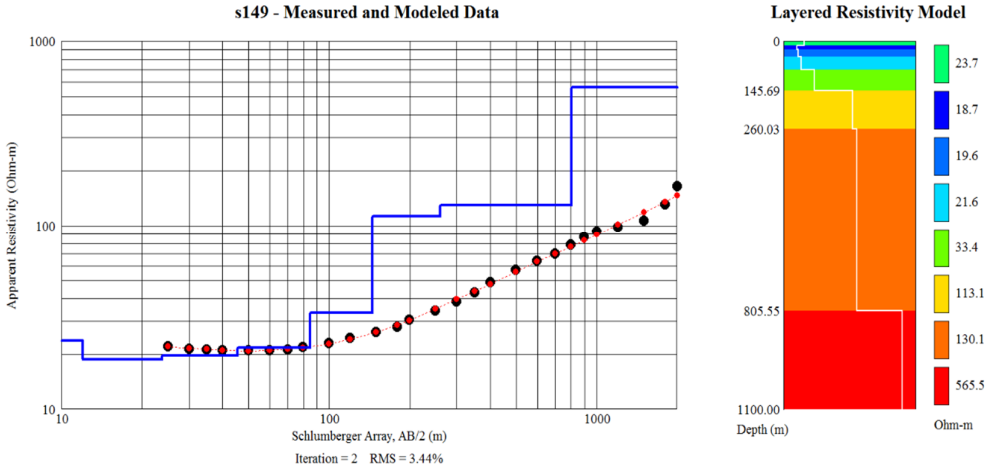
s149 - Measured and Modeled Data
Apparent Resistivity (Ohm-m)
1000
100
10
10
100
1000
Schlumberger Array, AB/2 (m)
Iteration = 2 RMS = 3.44%
Layered Resistivity Model
0
145.69
260.03
805.55
1100.00
Depth (m)
23.7
18.7
19.6
21.6
33.4
113.1
130.1
565.5
Ohm-m

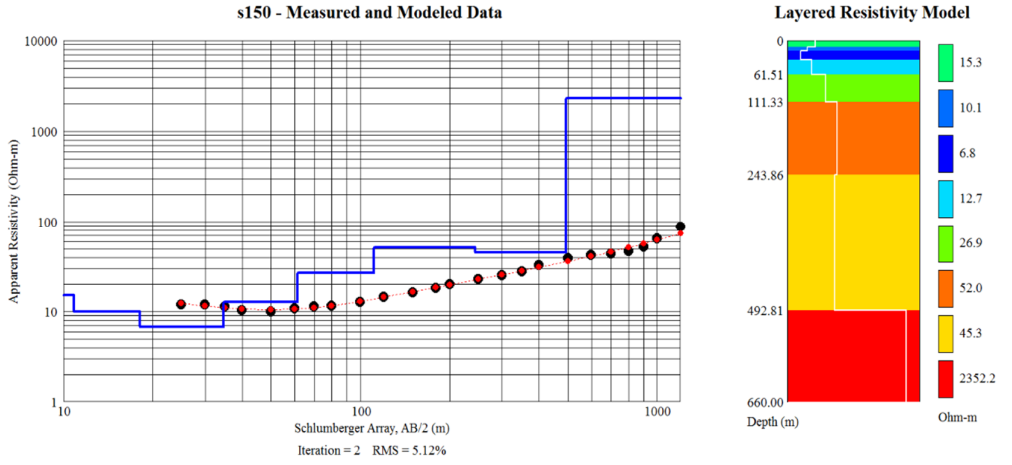
s150 - Measured and Modeled Data
Apparent Resistivity (Ohm-m)
10000
1000
100
10
1
10
100
1000
Schlumberger Array, AB/2 (m)
Iteration = 2 RMS = 5.12%
Layered Resistivity Model
0
61.51
111.33
243.86
492.81
660.00
Depth (m)
15.3
10.1
6.8
12.7
26.9
52.0
45.3
2352.2
Ohm-m

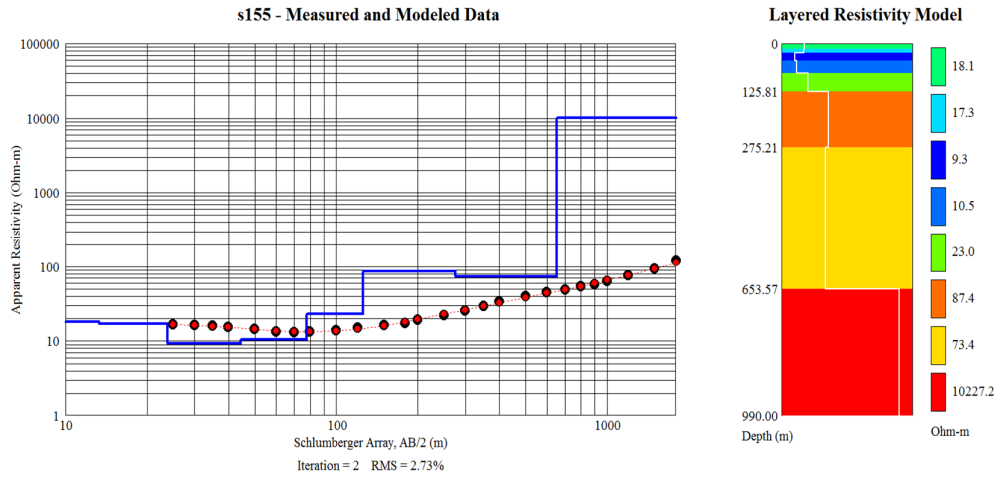
s155 - Measured and Modeled Data
Apparent Resistivity (Ohm-m)
100000
10000
1000
100
10
1
10
100
1000
Schlumberger Array, AB/2 (m)
Iteration = 2 RMS = 2.73%
Layered Resistivity Model
0
125.81
275.21
653.57
990.00
Depth (m)
18.1
17.3
9.3
10.5
23.0
87.4
73.4
10227.2
Ohm-m

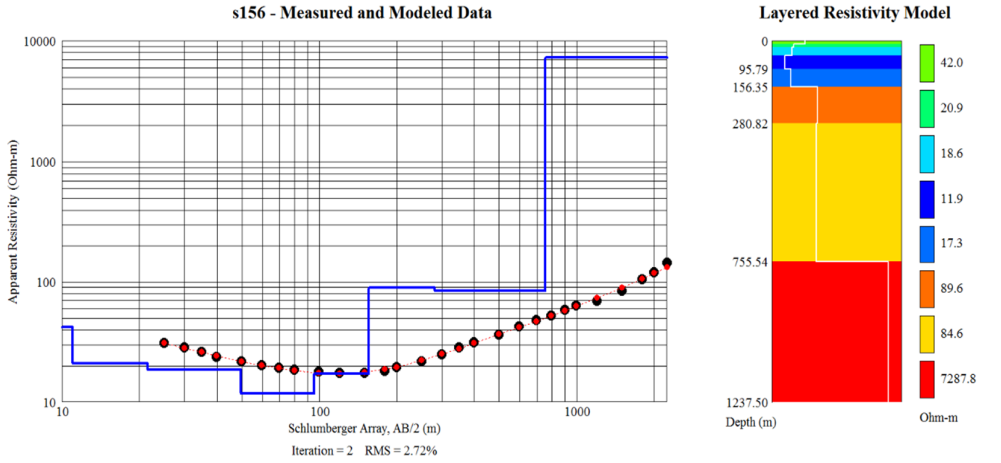
s156 - Measured and Modeled Data
Apparent Resistivity (Ohm-m)
10000
1000
100
10
10
100
1000
Schlumberger Array, AB/2 (m)
Iteration = 2 RMS = 2.72%
Layered Resistivity Model
0
95.79
156.35
280.82
755.54
1237.50
Depth (m)
42.0
20.9
18.6
11.9
17.3
89.6
84.6
7287.8
Ohm-m

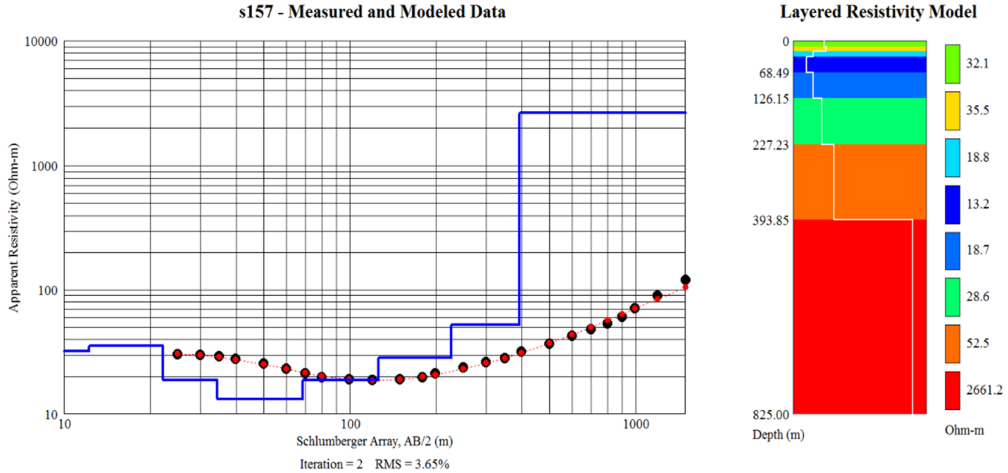
s157 - Measured and Modeled Data
Apparent Resistivity (Ohm-m)
10000
1000
100
10
10
100
1000
Schlumberger Array, AB/2 (m)
Iteration = 2 RMS = 3.65%
Layered Resistivity Model
0
68.49
126.15
227.23
393.85
825.00
Depth (m)
32.1
35.5
18.8
13.2
18.7
28.6
52.5
2661.2
Ohm-m

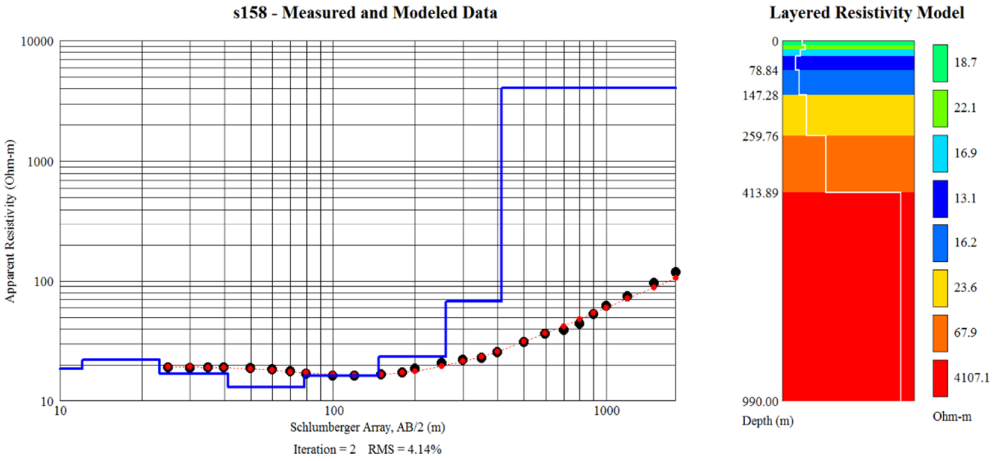
s158 - Measured and Modeled Data
Apparent Resistivity (Ohm-m)
10000
1000
100
10
10
100
1000
Schlumberger Array, AB/2 (m)
Iteration = 2 RMS = 4.14%
Layered Resistivity Model
0
78.84
147.28
259.76
413.89
990.00
Depth (m)
18.7
22.1
16.9
13.1
16.2
23.6
67.9
4107.1
Ohm-m

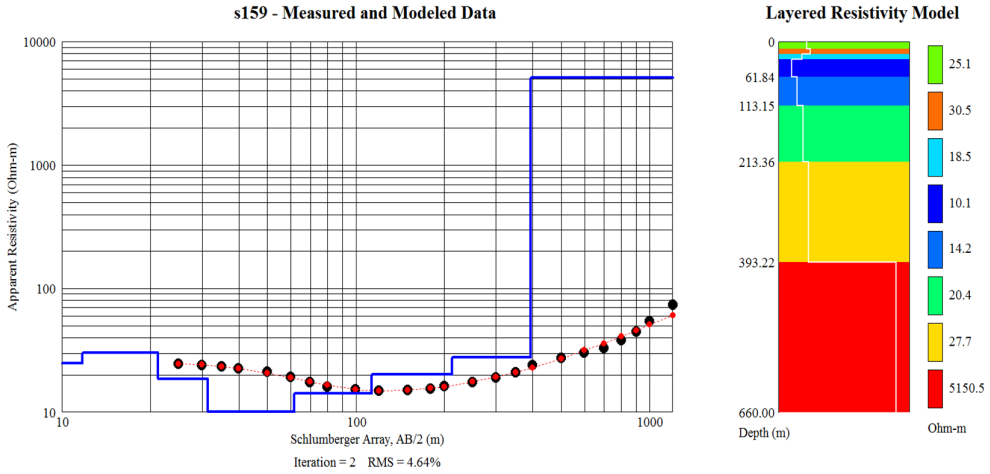
s159 - Measured and Modeled Data
Apparent Resistivity (Ohm-m)
10000
1000
100
10
10
100
1000
Schlumberger Array, AB/2 (m)
Iteration = 2 RMS = 4.64%
Layered Resistivity Model
0
61.84
113.15
213.36
393.22
660.00
Depth (m)
25.1
30.5
18.5
10.1
14.2
20.4
27.7
5150.5
Ohm-m

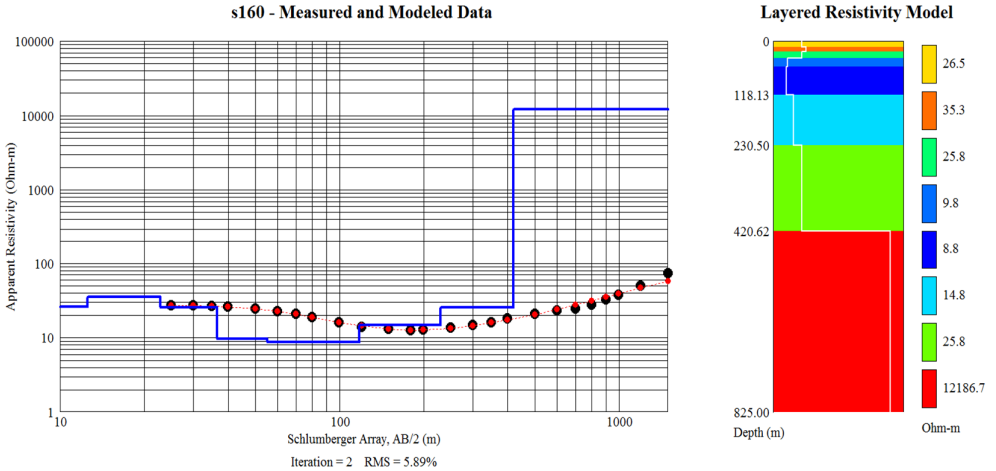
s160 - Measured and Modeled Data
Apparent Resistivity (Ohm-m)
100000
10000
1000
100
10
1
10
100
1000
Schlumberger Array, AB/2 (m)
Iteration = 2 RMS = 5.89%
Layered Resistivity Model
0
118.13
230.50
420.62
825.00
Depth (m)
26.5
35.3
25.8
9.8
8.8
14.8
25.8
12186.7
Ohm-m

Group 10

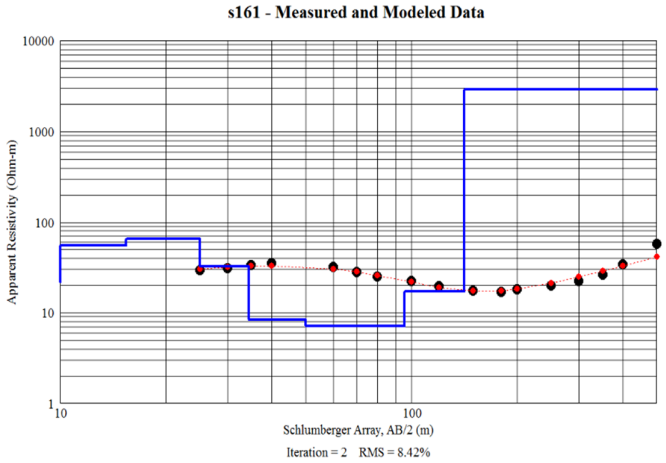
s161 - Measured and Modeled Data
Apparent Resistivity (Ohm-m)
10000
1000
100
10
1
10
100
Schlumberger Array, AB/2 (m)
Iteration = 2 RMS = 8.42%

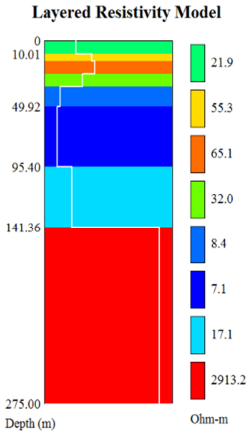
Layered Resistivity Model
0
10.01
49.92
95.40
141.36
275.00
Depth (m)
21.9
55.3
65.1
32.0
8.4
7.1
17.1
2913.2
Ohm-m

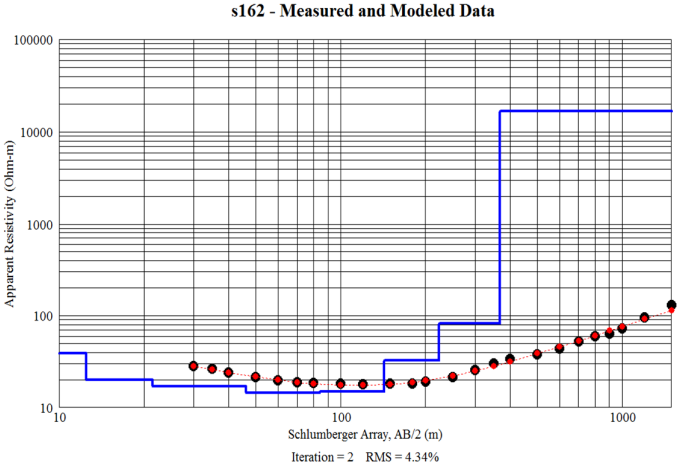
s162 - Measured and Modeled Data
Apparent Resistivity (Ohm-m)
100000
10000
1000
100
10
10
100
1000
Schlumberger Array, AB/2 (m)
Iteration = 2 RMS = 4.34%

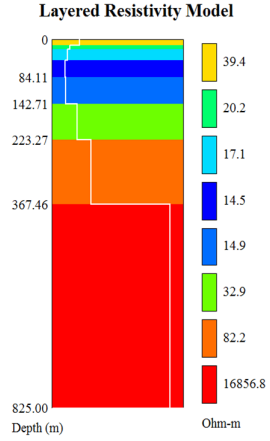
Layered Resistivity Model
0
84.11
142.71
223.27
367.46
825.00
Depth (m)
39.4
20.2
17.1
14.5
14.9
32.9
82.2
16856.8
Ohm-m

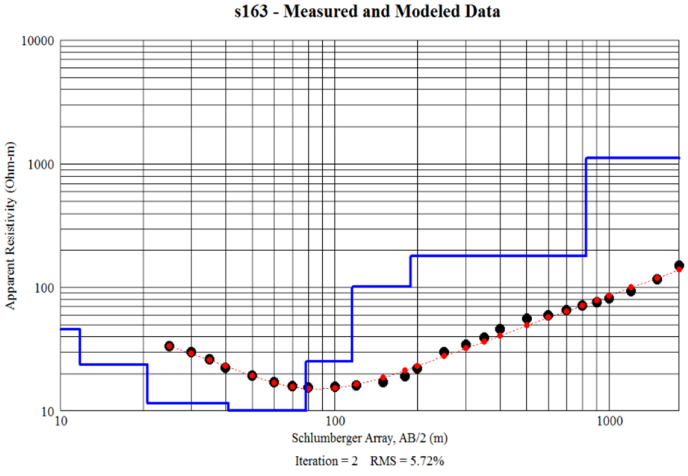
s163 - Measured and Modeled Data
Apparent Resistivity (Ohm-m)
10000
1000
100
10
10
100
1000
Schlumberger Array, AB/2 (m)
Iteration = 2 RMS = 5.72%

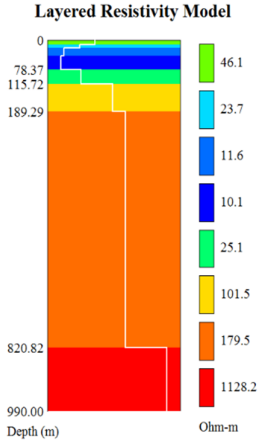
Layered Resistivity Model
0
78.37
115.72
189.29
820.82
990.00
Depth (m)
46.1
23.7
11.6
10.1
25.1
101.5
179.5
1128.2
Ohm-m

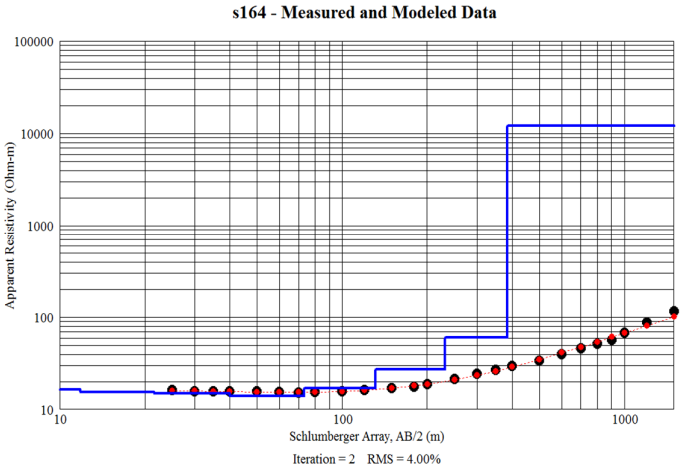
s164 - Measured and Modeled Data
Apparent Resistivity (Ohm-m)
100000
10000
1000
100
10
10
100
1000
Schlumberger Array, AB/2 (m)
Iteration = 2 RMS = 4.00%

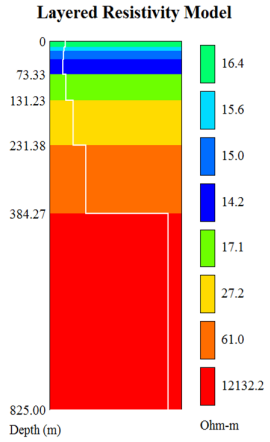
Layered Resistivity Model
0
73.33
131.23
231.38
384.27
825.00
Depth (m)
16.4
15.6
15.0
14.2
17.1
27.2
61.0
12132.2
Ohm-m

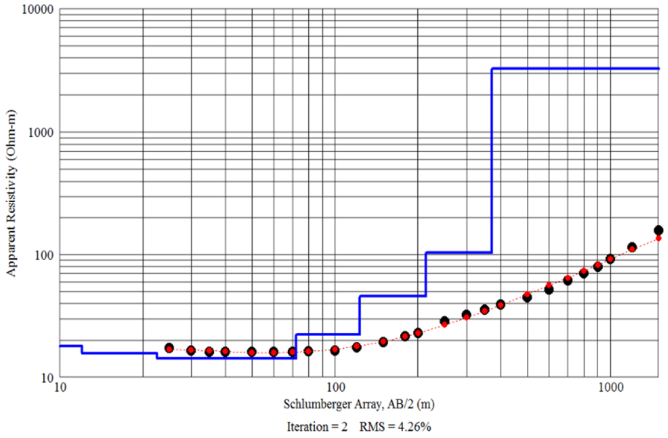
s165 - Measured and Modeled Data
Apparent Resistivity (Ohm-m)
10000
1000
100
10
10
100
1000
Schlumberger Array, AB/2 (m)
Iteration = 2 RMS = 4.26%

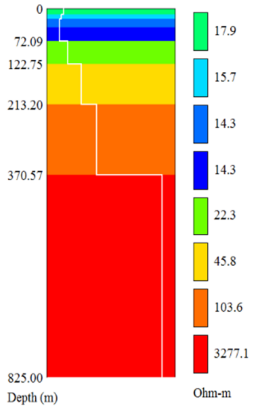
Layered Resistivity Model
0
72.09
122.75
213.20
370.57
825.00
Depth (m)
17.9
15.7
14.3
14.3
22.3
45.8
103.6
3277.1
Ohm-m

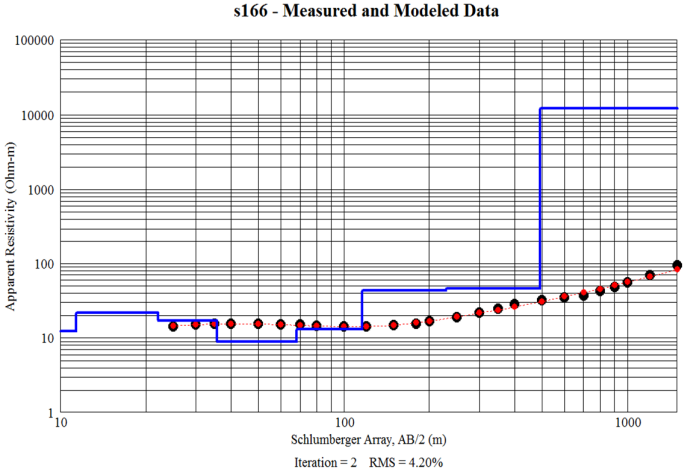
s166 - Measured and Modeled Data
Apparent Resistivity (Ohm-m)
100000
10000
1000
100
10
1
10
100
1000
Schlumberger Array, AB/2 (m)
Iteration = 2 RMS = 4.20%

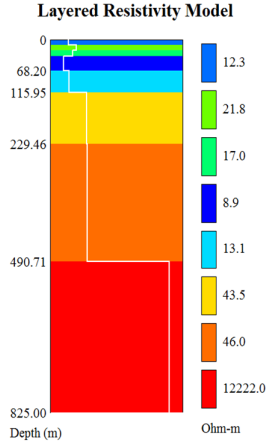
Layered Resistivity Model
0
68.20
115.95
229.46
490.71
825.00
Depth (m)
12.3
21.8
17.0
8.9
13.1
43.5
46.0
12222.0
Ohm-m

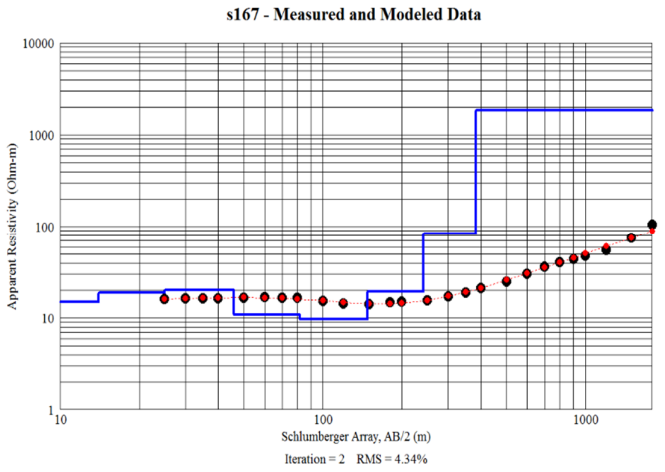
s167 - Measured and Modeled Data
Apparent Resistivity (Ohm-m)
10000
1000
100
10
1
10
100
1000
Schlumberger Array, AB/2 (m)
Iteration = 2 RMS = 4.34%

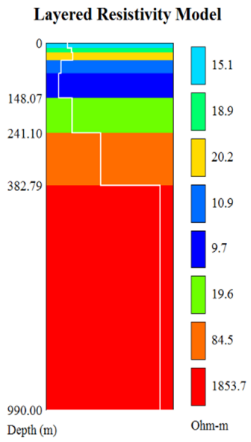
Layered Resistivity Model
0
148.07
241.10
382.79
990.00
Depth (m)
15.1
18.9
20.2
10.9
9.7
19.6
84.5
1853.7
Ohm-m

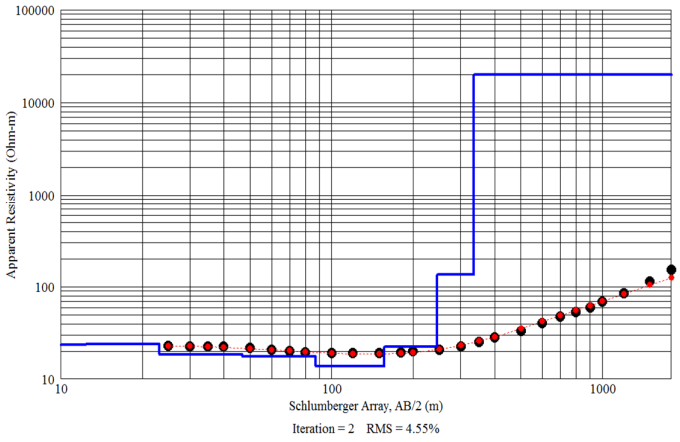
s168 - Measured and Modeled Data
Apparent Resistivity (Ohm-m)
100000
10000
1000
100
10
10
100
1000
Schlumberger Array, AB/2 (m)
Iteration = 2 RMS = 4.55%

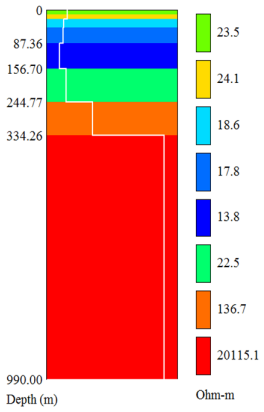
Layered Resistivity Model
0
87.36
156.70
244.77
334.26
990.00
Depth (m)
23.5
24.1
18.6
17.8
13.8
22.5
136.7
20115.1
Ohm-m

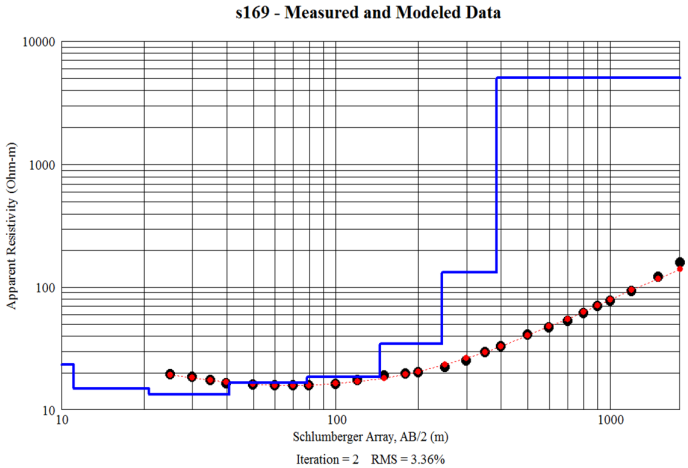
s169 - Measured and Modeled Data
Apparent Resistivity (Ohm-m)
10000
1000
100
10
10
100
1000
Schlumberger Array, AB/2 (m)
Iteration = 2 RMS = 3.36%

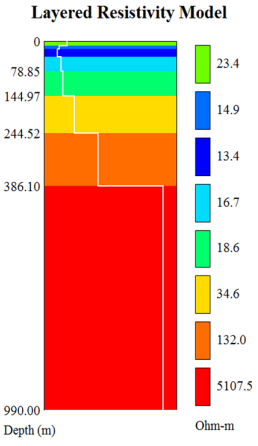
Layered Resistivity Model
0
78.85
144.97
244.52
386.10
990.00
Depth (m)
23.4
14.9
13.4
16.7
18.6
34.6
132.0
5107.5
Ohm-m

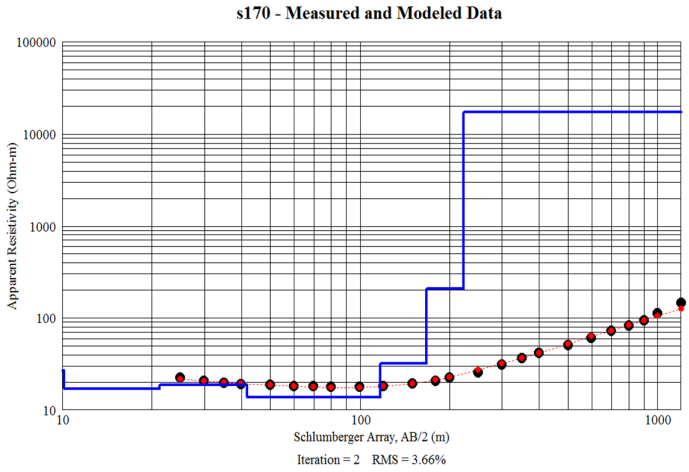
s170 - Measured and Modeled Data
Apparent Resistivity (Ohm-m)
100000
10000
1000
100
10
10
100
1000
Schlumberger Array, AB/2 (m)
Iteration = 2 RMS = 3.66%

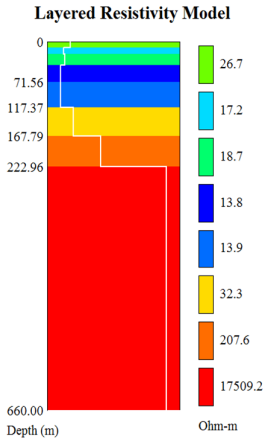
Layered Resistivity Model
0
71.56
117.37
167.79
222.96
660.00
Depth (m)
26.7
17.2
18.7
13.8
13.9
32.3
207.6
17509.2
Ohm-m

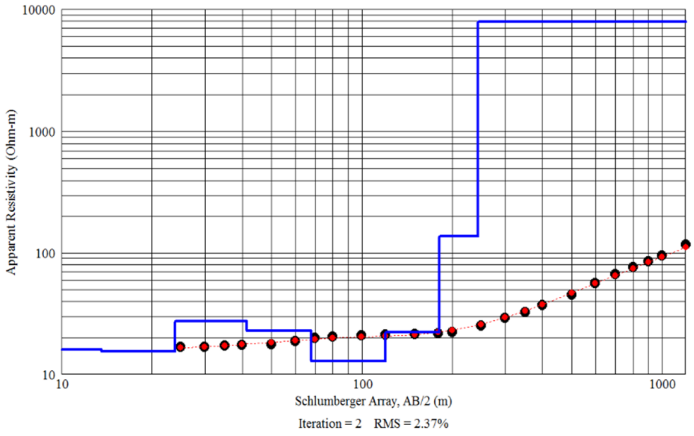
s171 - Measured and Modeled Data
Apparent Resistivity (Ohm-m)
10000
1000
100
10
10
100
1000
Schlumberger Array, AB/2 (m)
Iteration = 2 RMS = 2.37%

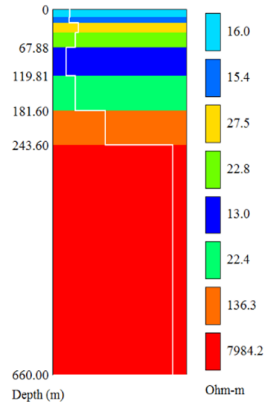
Layered Resistivity Model
0
67.88
119.81
181.60
243.60
660.00
Depth (m)
16.0
15.4
27.5
22.8
13.0
22.4
136.3
7984.2
Ohm-m

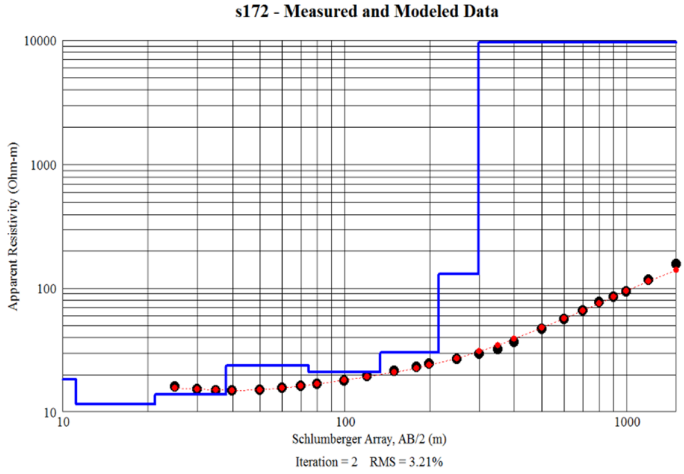
s172 - Measured and Modeled Data
Apparent Resistivity (Ohm-m)
10000
1000
100
10
10
100
1000
Schlumberger Array, AB/2 (m)
Iteration = 2 RMS = 3.21%

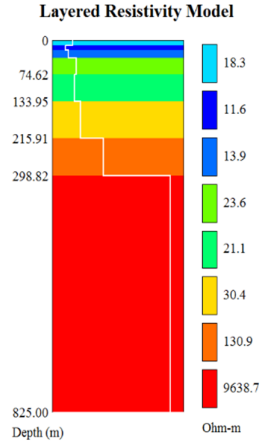
Layered Resistivity Model
0
74.62
133.95
215.91
298.82
825.00
Depth (m)
18.3
11.6
13.9
23.6
21.1
30.4
130.9
9638.7
Ohm-m

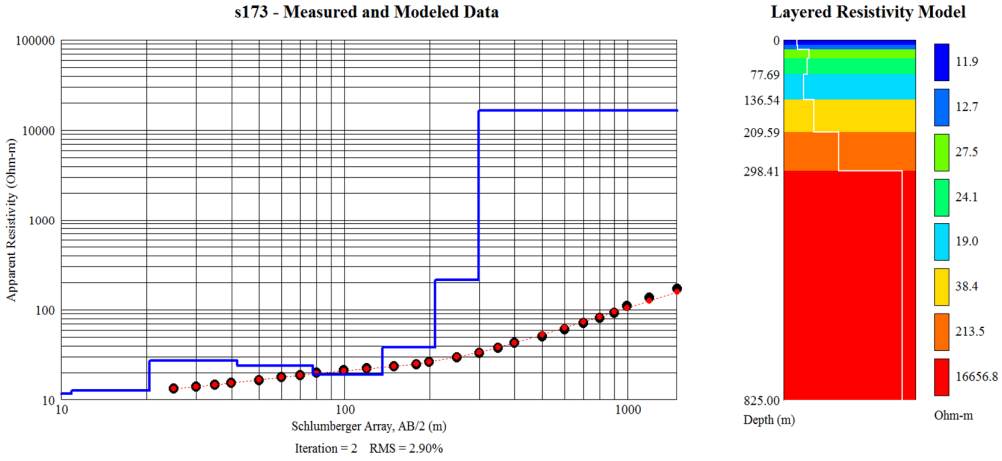
s173 - Measured and Modeled Data
Apparent Resistivity (Ohm-m)
100000
10000
1000
100
10
10
100
1000
Schlumberger Array, AB/2 (m)
Iteration = 2 RMS = 2.90%
Layered Resistivity Model
0
77.69
136.54
209.59
298.41
825.00
Depth (m)
11.9
12.7
27.5
24.1
19.0
38.4
213.5
16656.8
Ohm-m

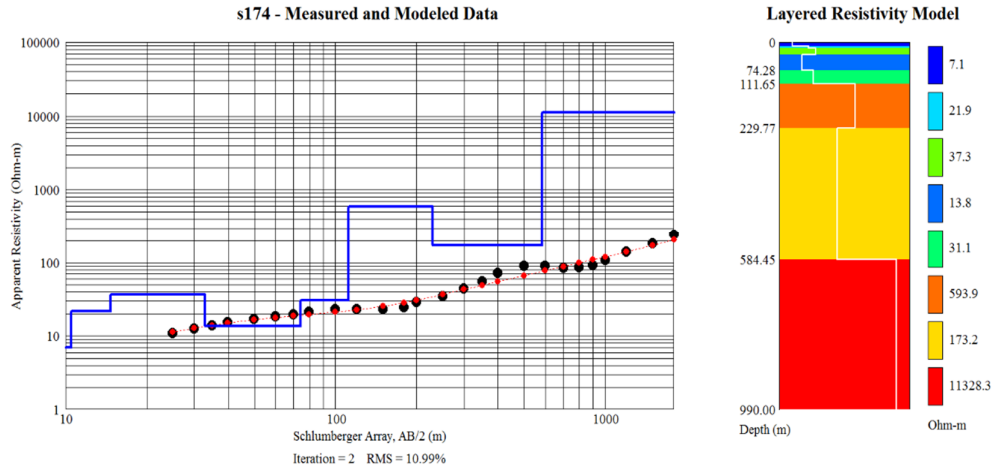
s174 - Measured and Modeled Data
Apparent Resistivity (Ohm-m)
100000
10000
1000
100
10
1
10
100
1000
Schlumberger Array, AB/2 (m)
Iteration = 2 RMS = 10.99%
Layered Resistivity Model
0
74.28
111.65
229.77
584.45
990.00
Depth (m)
7.1
21.9
37.3
13.8
31.1
593.9
173.2
11328.3
Ohm-m

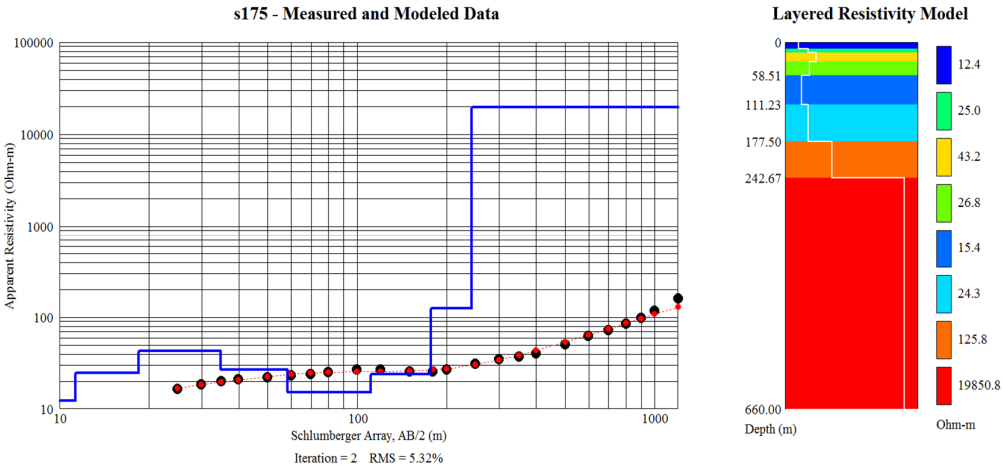
s175 - Measured and Modeled Data
Apparent Resistivity (Ohm-m)
100000
10000
1000
100
10
10
100
1000
Schlumberger Array, AB/2 (m)
Iteration = 2 RMS = 5.32%
Layered Resistivity Model
0
58.51
111.23
177.50
242.67
660.00
Depth (m)
12.4
25.0
43.2
26.8
15.4
24.3
125.8
19850.8
Ohm-m

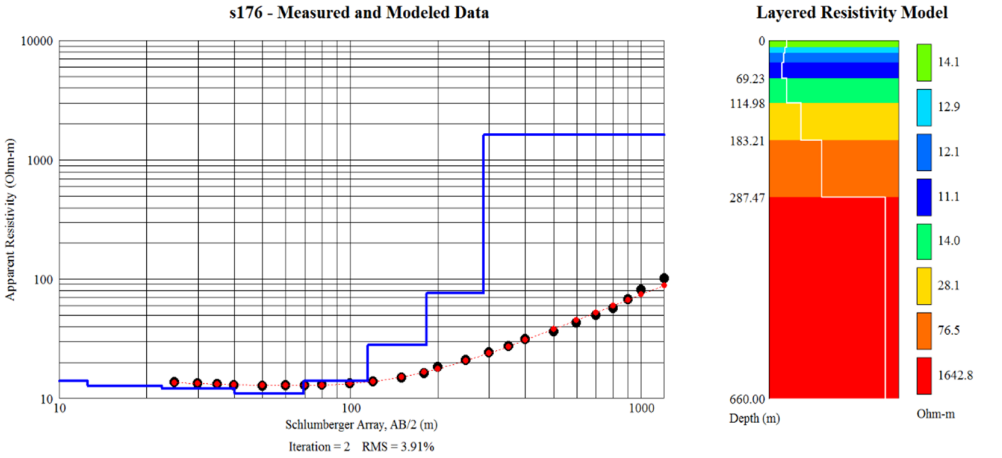
s176 - Measured and Modeled Data
Apparent Resistivity (Ohm-m)
10000
1000
100
10
10
100
1000
Schlumberger Array, AB/2 (m)
Iteration = 2 RMS = 3.91%
Layered Resistivity Model
0
69.23
114.98
183.21
287.47
660.00
Depth (m)
14.1
12.9
12.1
11.1
14.0
28.1
76.5
1642.8
Ohm-m

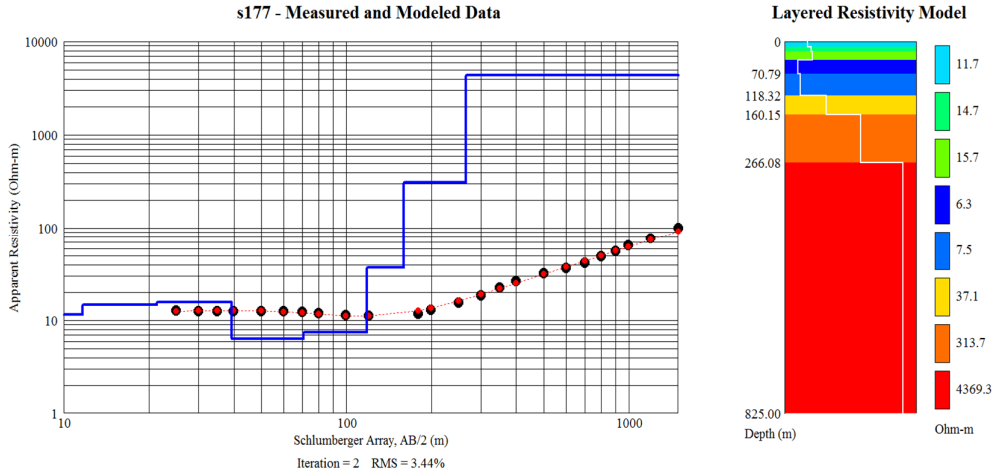
s177 - Measured and Modeled Data
Apparent Resistivity (Ohm-m)
10000
1000
100
10
1
10
100
1000
Schlumberger Array, AB/2 (m)
Iteration = 2 RMS = 3.44%
Layered Resistivity Model
0
70.79
118.32
160.15
266.08
825.00
Depth (m)
11.7
14.7
15.7
6.3
7.5
37.1
313.7
4369.3
Ohm-m

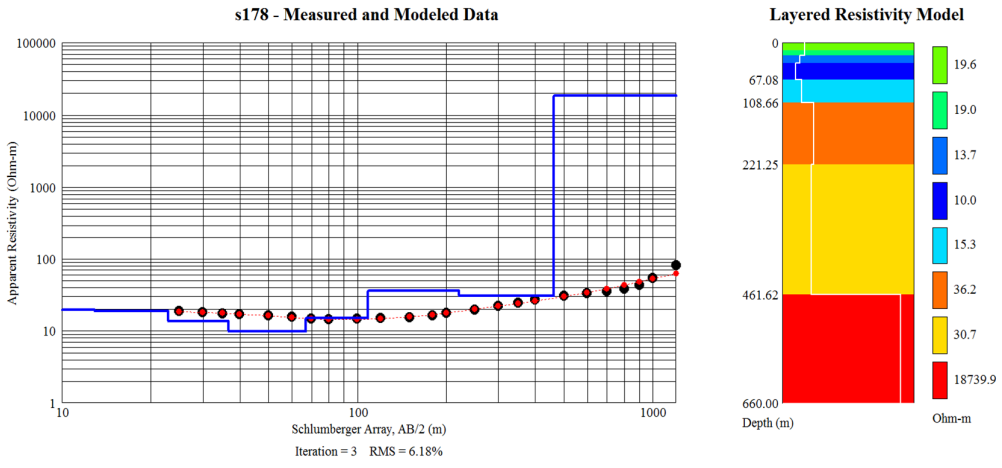
s178 - Measured and Modeled Data
Apparent Resistivity (Ohm-m)
100000
10000
1000
100
10
1
10
100
1000
Schlumberger Array, AB/2 (m)
Iteration = 3 RMS = 6.18%
Layered Resistivity Model
0
67.08
108.66
221.25
461.62
660.00
Depth (m)
19.6
19.0
13.7
10.0
15.3
36.2
30.7
18739.9
Ohm-m

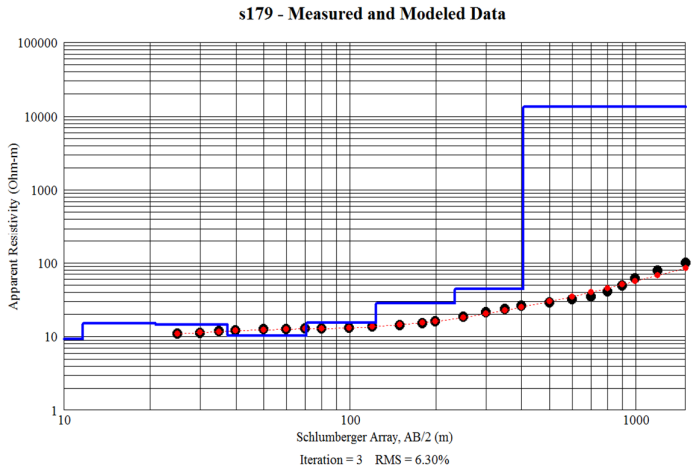
s179 - Measured and Modeled Data
Apparent Resistivity (Ohm-m)
100000
10000
1000
100
10
1
10
100
1000
Schlumberger Array, AB/2 (m)
Iteration = 3 RMS = 6.30%

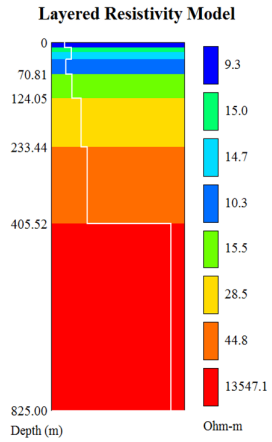
Layered Resistivity Model
0
70.81
124.05
233.44
405.52
825.00
Depth (m)
9.3
15.0
14.7
10.3
15.5
28.5
44.8
13547.1
Ohm-m

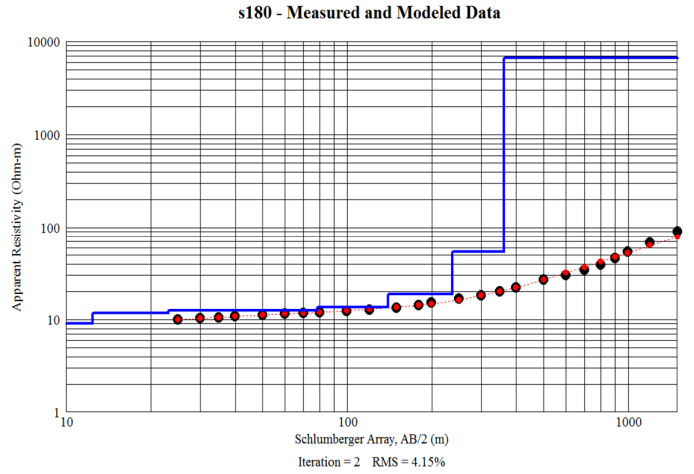
s180 - Measured and Modeled Data
Apparent Resistivity (Ohm-m)
10000
1000
100
10
1
10
100
1000
Schlumberger Array, AB/2 (m)
Iteration = 2 RMS = 4.15%

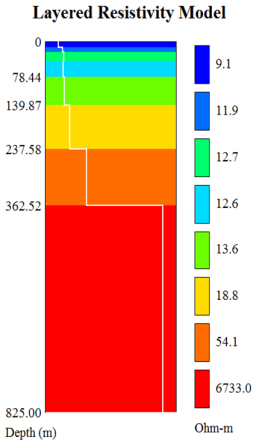
Layered Resistivity Model
0
78.44
139.87
237.58
362.52
825.00
Depth (m)
9.1
11.9
12.7
12.6
13.6
18.8
54.1
6733.0
Ohm-m

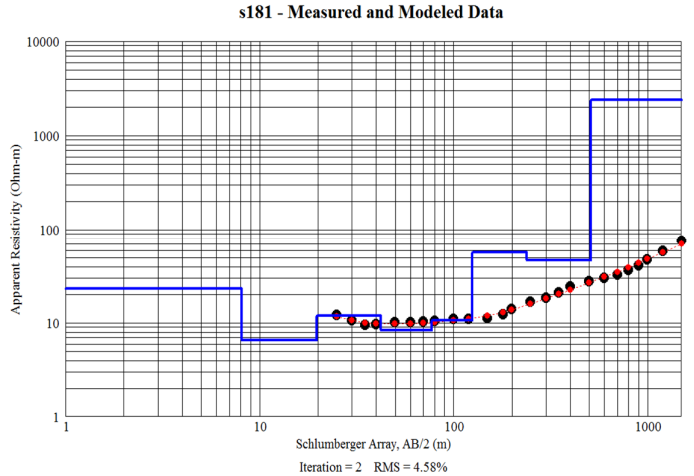
s181 - Measured and Modeled Data
Apparent Resistivity (Ohm-m)
10000
1000
100
10
1
1
10
100
1000
Schlumberger Array, AB/2 (m)
Iteration = 2 RMS = 4.58%

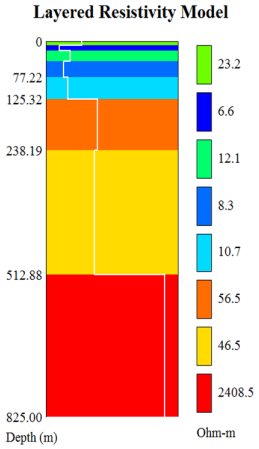
Layered Resistivity Model
0
77.22
125.32
238.19
512.88
825.00
Depth (m)
23.2
6.6
12.1
8.3
10.7
56.5
46.5
2408.5
Ohm-m

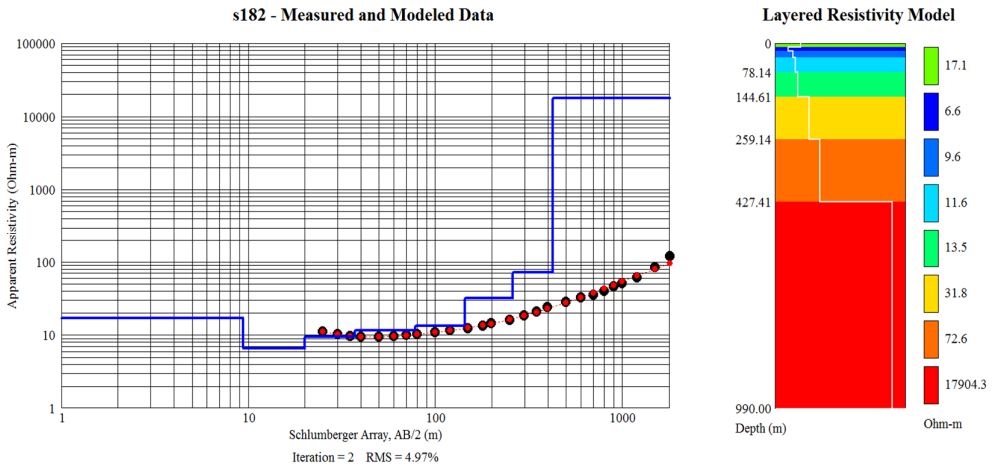
s182 - Measured and Modeled Data
Apparent Resistivity (Ohm-m)
100000
10000
1000
100
10
1
1
10
100
1000
Schlumberger Array, AB/2 (m)
Iteration = 2 RMS = 4.97%
Layered Resistivity Model
0
78.14
144.61
259.14
427.41
990.00
Depth (m)
17.1
6.6
9.6
11.6
13.5
31.8
72.6
17904.3
Ohm-m

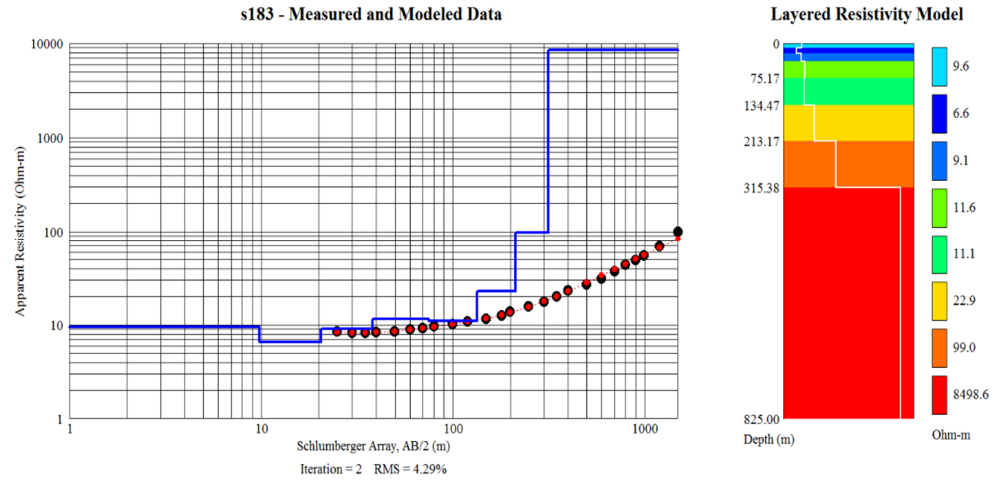
s183 - Measured and Modeled Data
Apparent Resistivity (Ohm-m)
10000
1000
100
10
1
1
10
100
1000
Schlumberger Array, AB/2 (m)
Iteration = 2 RMS = 4.29%
Layered Resistivity Model
0
75.17
134.47
213.17
315.38
825.00
Depth (m)
9.6
6.6
9.1
11.6
11.1
22.9
99.0
8498.6
Ohm-m

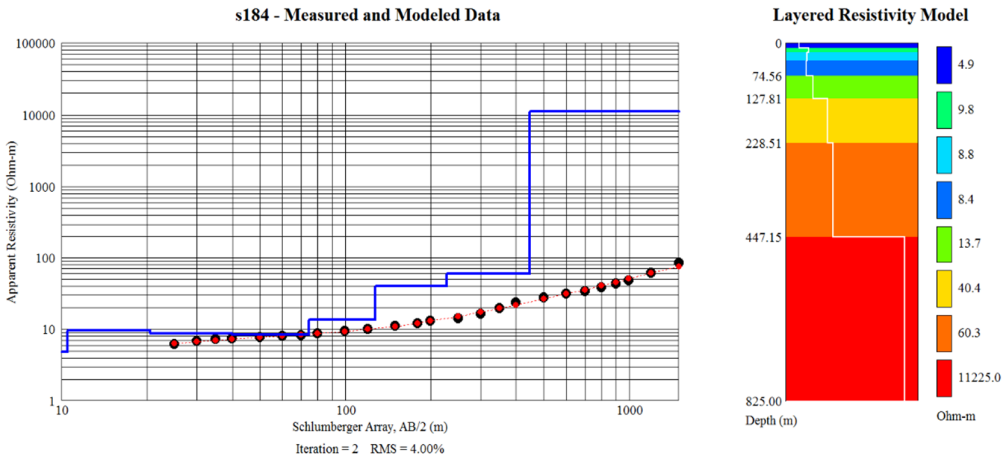
s184 - Measured and Modeled Data
Apparent Resistivity (Ohm-m)
100000
10000
1000
100
10
1
10
100
1000
Schlumberger Array, AB/2 (m)
Iteration = 2 RMS = 4.00%
Layered Resistivity Model
0
74.56
127.81
228.51
447.15
825.00
Depth (m)
4.9
9.8
8.8
8.4
13.7
40.4
60.3
11225.0
Ohm-m

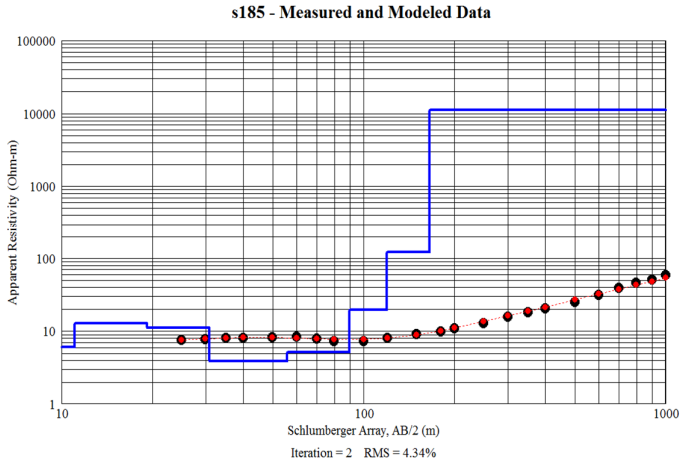
s185 - Measured and Modeled Data
Apparent Resistivity (Ohm-m)
100000
10000
1000
100
10
1
10
100
1000
Schlumberger Array, AB/2 (m)
Iteration = 2 RMS = 4.34%

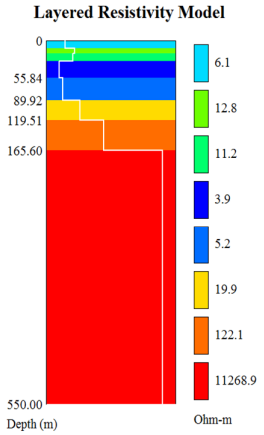
Layered Resistivity Model
0
55.84
89.92
119.51
165.60
550.00
Depth (m)
6.1
12.8
11.2
3.9
5.2
19.9
122.1
11268.9
Ohm-m

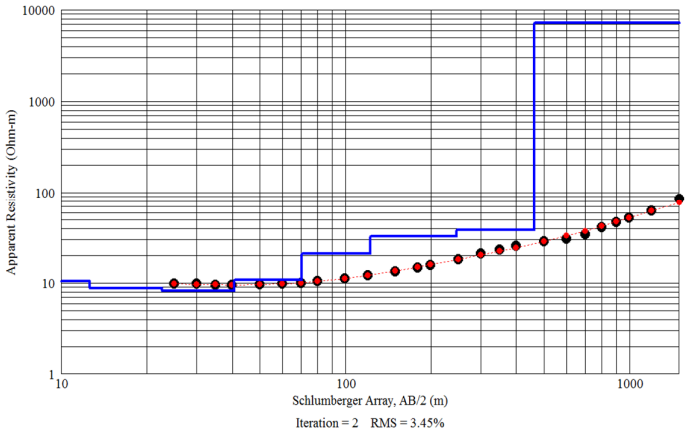
s186 - Measured and Modeled Data
Apparent Resistivity (Ohm-m)
10000
1000
100
10
1
10
100
1000
Schlumberger Array, AB/2 (m)
Iteration = 2 RMS = 3.45%

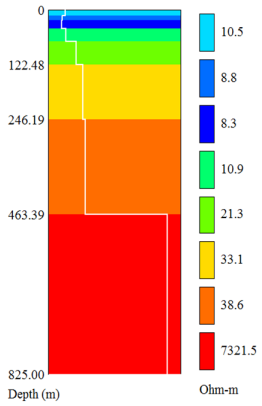
Layered Resistivity Model
0
122.48
246.19
463.39
825.00
Depth (m)
10.5
8.8
8.3
10.9
21.3
33.1
38.6
7321.5
Ohm-m

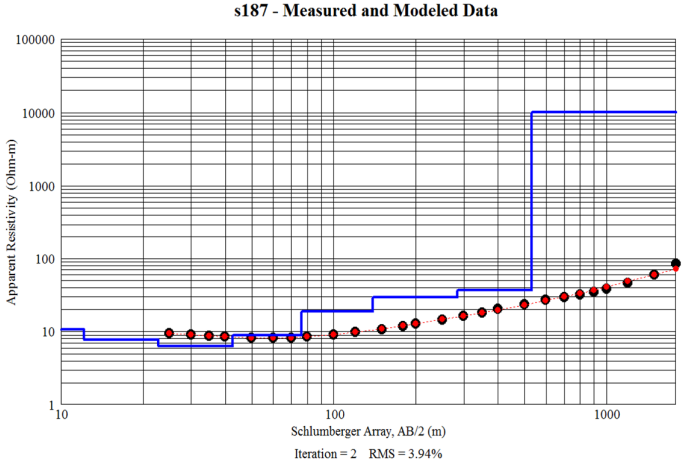
s187 - Measured and Modeled Data
Apparent Resistivity (Ohm-m)
100000
10000
1000
100
10
1
10
100
1000
Schlumberger Array, AB/2 (m)
Iteration = 2 RMS = 3.94%

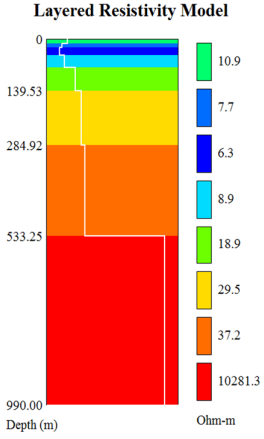
Layered Resistivity Model
0
139.53
284.92
533.25
990.00
Depth (m)
10.9
7.7
6.3
8.9
18.9
29.5
37.2
10281.3
Ohm-m

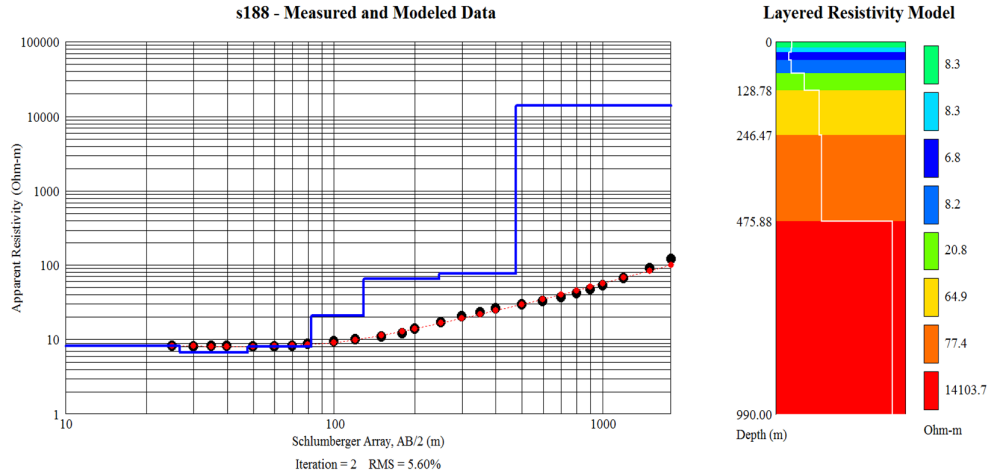
s188 - Measured and Modeled Data
Apparent Resistivity (Ohm-m)
100000
10000
1000
100
10
1
10
100
1000
Schlumberger Array, AB/2 (m)
Iteration = 2 RMS = 5.60%
Layered Resistivity Model
0
128.78
246.47
475.88
990.00
Depth (m)
8.3
8.3
6.8
8.2
20.8
64.9
77.4
14103.7
Ohm-m

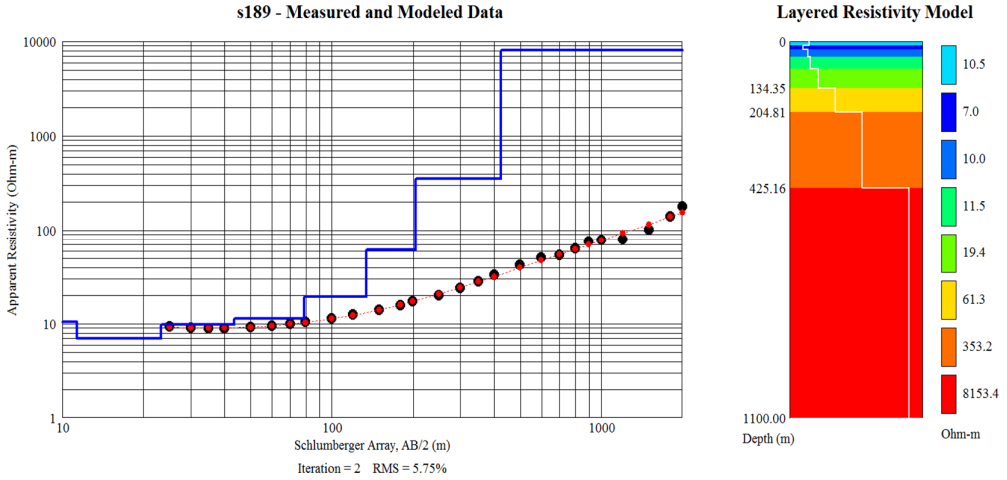
s189 - Measured and Modeled Data
Apparent Resistivity (Ohm-m)
10000
1000
100
10
1
10
100
1000
Schlumberger Array, AB/2 (m)
Iteration = 2 RMS = 5.75%
Layered Resistivity Model
0
134.35
204.81
425.16
1100.00
Depth (m)
10.5
7.0
10.0
11.5
19.4
61.3
353.2
8153.4
Ohm-m

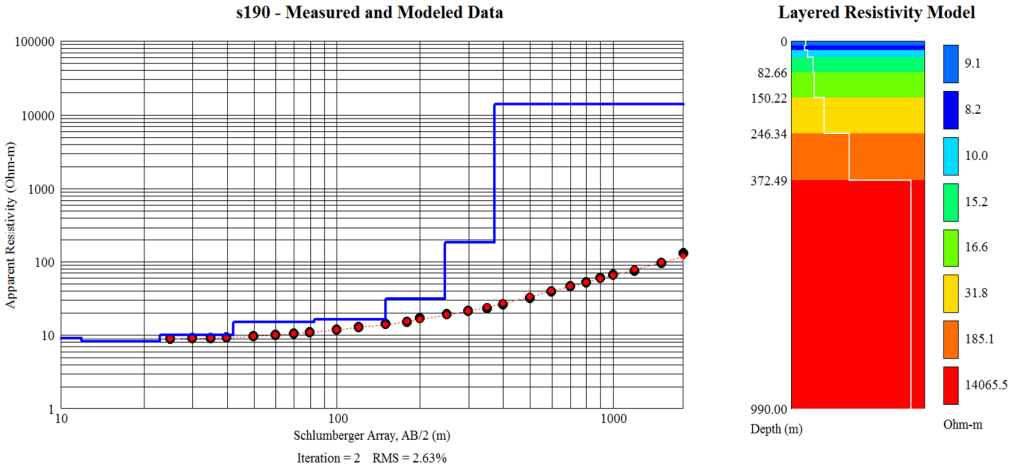
s190 - Measured and Modeled Data
Apparent Resistivity (Ohm-m)
100000
10000
1000
100
10
1
10
100
1000
Schlumberger Array, AB/2 (m)
Iteration = 2 RMS = 2.63%
Layered Resistivity Model
0
82.66
150.22
246.34
372.49
990.00
Depth (m)
9.1
8.2
10.0
15.2
16.6
31.8
185.1
14065.5
Ohm-m

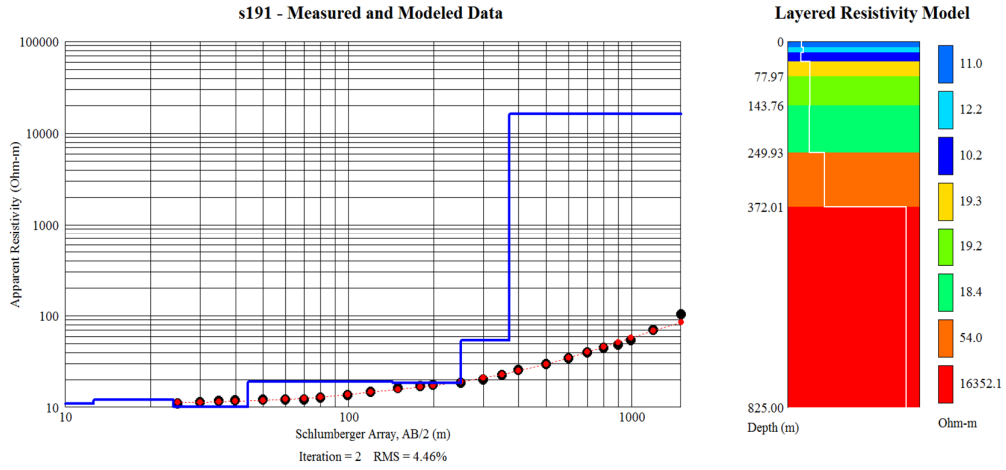
s191 - Measured and Modeled Data
Apparent Resistivity (Ohm-m)
100000
10000
1000
100
10
10
100
1000
Schlumberger Array, AB/2 (m)
Iteration = 2 RMS = 4.46%
Layered Resistivity Model
0
77.97
143.76
249.93
372.01
825.00
Depth (m)
11.0
12.2
10.2
19.3
19.2
18.4
54.0
16352.1
Ohm-m

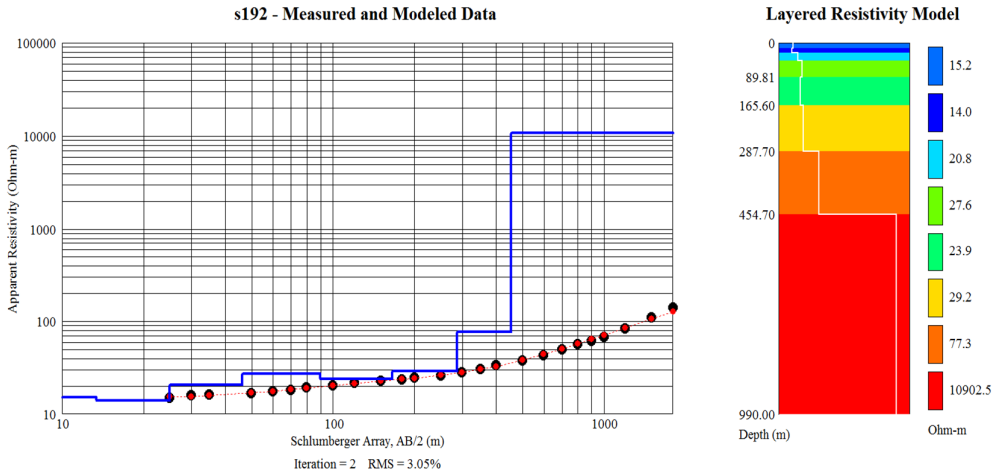
s192 - Measured and Modeled Data
Apparent Resistivity (Ohm-m)
100000
10000
1000
100
10
10
100
1000
Schlumberger Array, AB/2 (m)
Iteration = 2 RMS = 3.05%
Layered Resistivity Model
0
89.81
165.60
287.70
454.70
990.00
Depth (m)
15.2
14.0
20.8
27.6
23.9
29.2
77.3
10902.5
Ohm-m

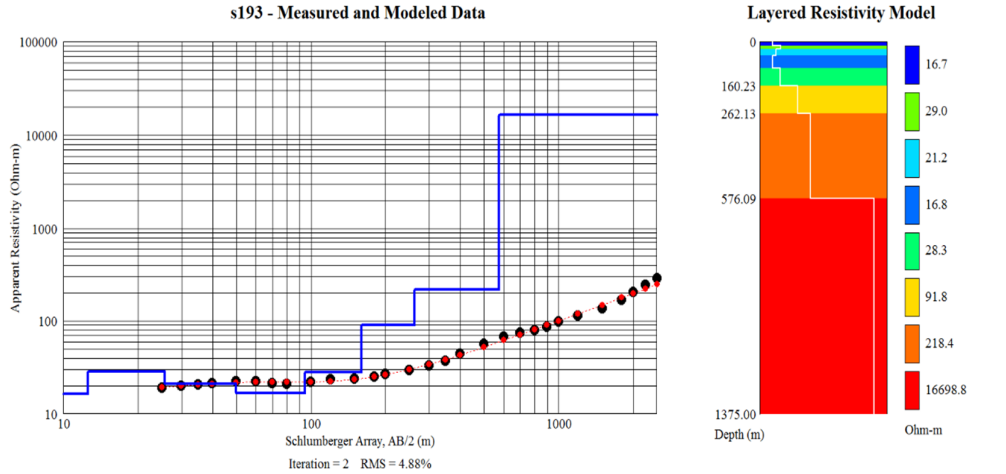
s193 - Measured and Modeled Data
Apparent Resistivity (Ohm-m)
100000
10000
1000
100
10
10
100
1000
Schlumberger Array, AB/2 (m)
Iteration = 2 RMS = 4.88%
Layered Resistivity Model
0
160.23
262.13
576.09
1375.00
Depth (m)
16.7
29.0
21.2
16.8
28.3
91.8
218.4
16698.8
Ohm-m

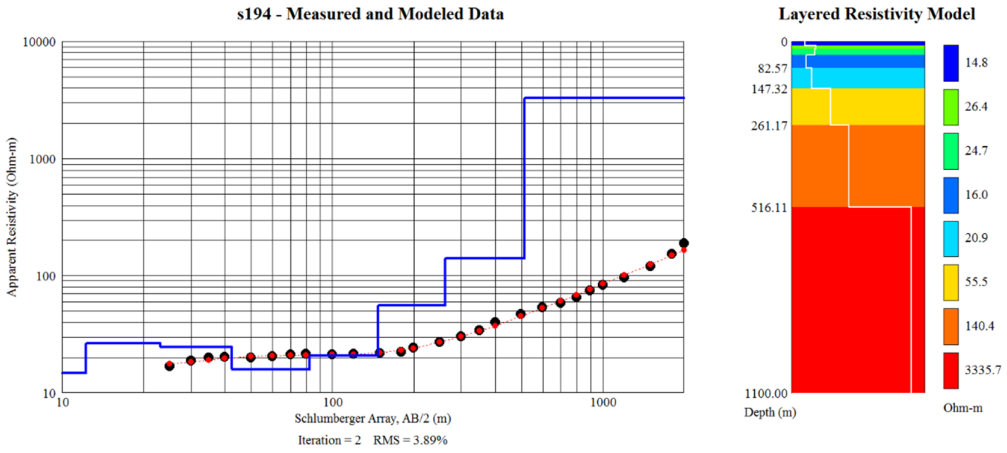
s194 - Measured and Modeled Data
Apparent Resistivity (Ohm-m)
10000
1000
100
10
10
100
1000
Schlumberger Array, AB/2 (m)
Iteration = 2 RMS = 3.89%
Layered Resistivity Model
0
82.57
147.32
261.17
516.11
1100.00
Depth (m)
14.8
26.4
24.7
16.0
20.9
55.5
140.4
3335.7
Ohm-m

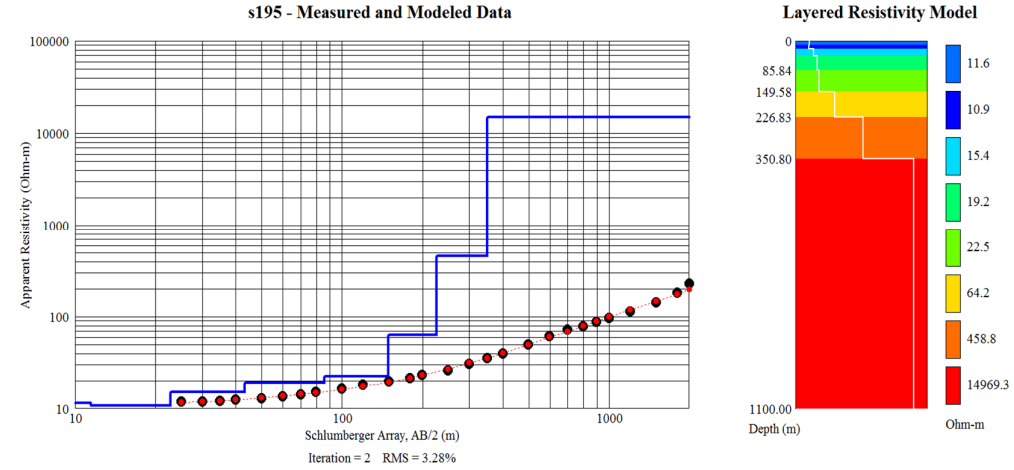
s195 - Measured and Modeled Data
Apparent Resistivity (Ohm-m)
100000
10000
1000
100
10
10
100
1000
Schlumberger Array, AB/2 (m)
Iteration = 2 RMS = 3.28%
Layered Resistivity Model
0
85.84
149.58
226.83
350.80
1100.00
Depth (m)
11.6
10.9
15.4
19.2
22.5
64.2
458.8
14969.3
Ohm-m

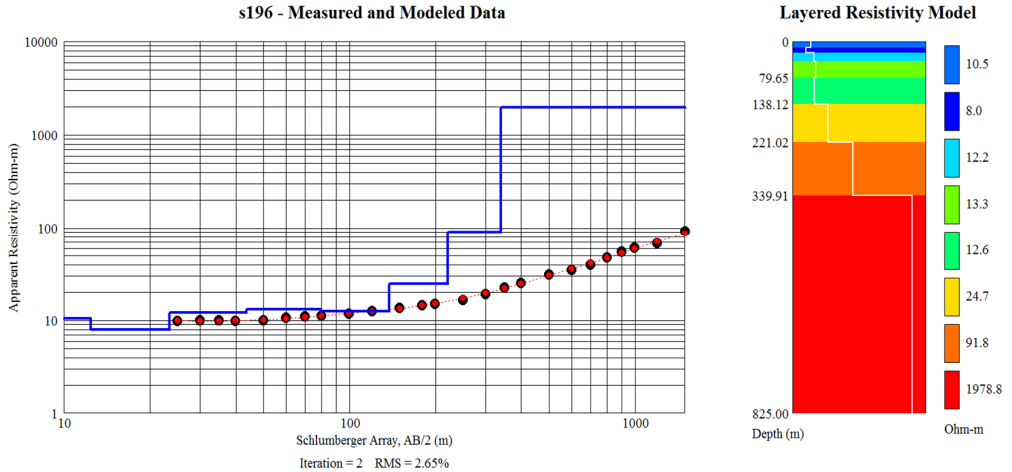
s196 - Measured and Modeled Data
Apparent Resistivity (Ohm-m)
10000
1000
100
10
1
10
100
1000
Schlumberger Array, AB/2 (m)
Iteration = 2 RMS = 2.65%
Layered Resistivity Model
0
79.65
138.12
221.02
339.91
825.00
Depth (m)
10.5
8.0
12.2
13.3
12.6
24.7
91.8
1978.8
Ohm-m

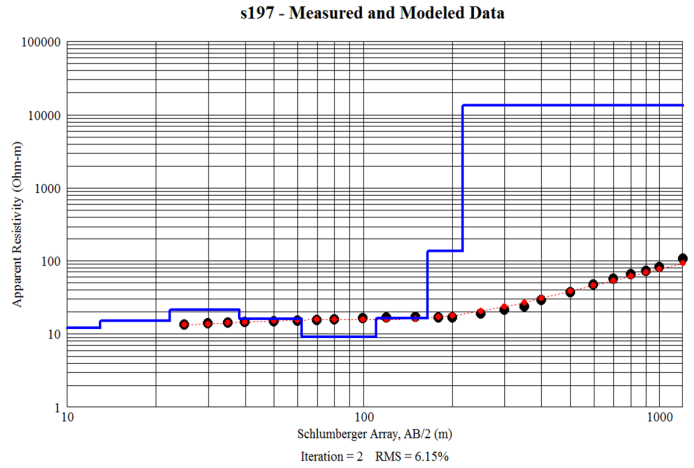
s197 - Measured and Modeled Data
Apparent Resistivity (Ohm-m)
100000
10000
1000
100
10
1
10
100
1000
Schlumberger Array, AB/2 (m)
Iteration = 2 RMS = 6.15%

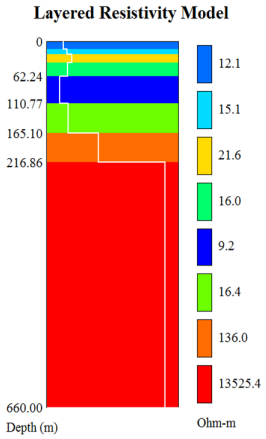
Layered Resistivity Model
0
62.24
110.77
165.10
216.86
660.00
Depth (m)
12.1
15.1
21.6
16.0
9.2
16.4
136.0
13525.4
Ohm-m

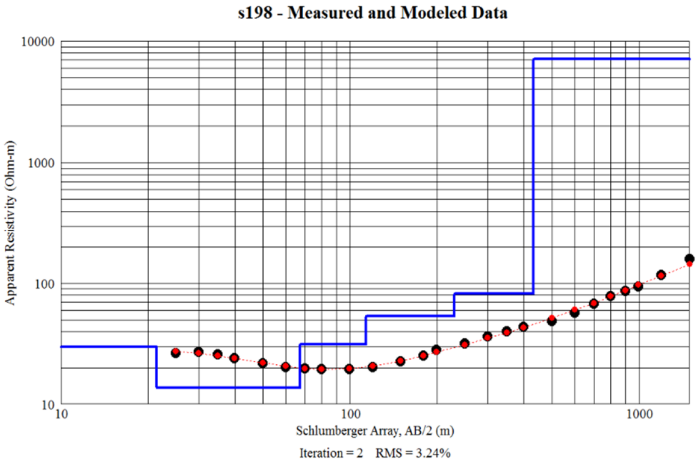
s198 - Measured and Modeled Data
Apparent Resistivity (Ohm-m)
10000
1000
100
10
10
100
1000
Schlumberger Array, AB/2 (m)
Iteration = 2 RMS = 3.24%

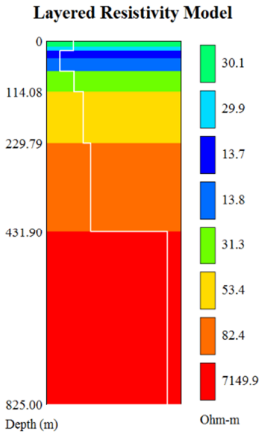
Layered Resistivity Model
0
114.08
229.79
431.90
825.00
Depth (m)
30.1
29.9
13.7
13.8
31.3
53.4
82.4
7149.9
Ohm-m

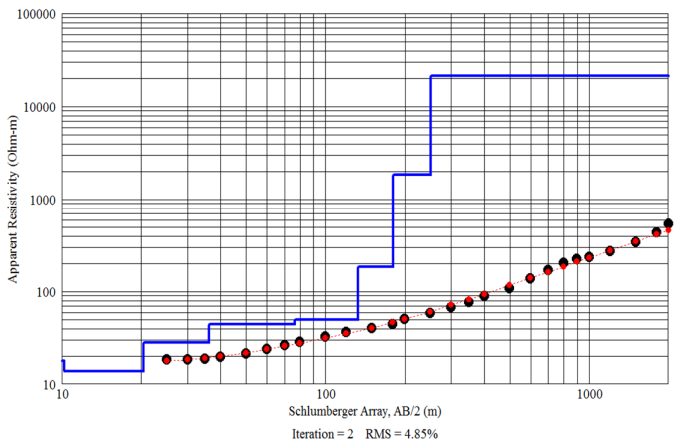
s199 - Measured and Modeled Data
Apparent Resistivity (Ohm-m)
100000
10000
1000
100
10
10
100
1000
Schlumberger Array, AB/2 (m)
Iteration = 2 RMS = 4.85%

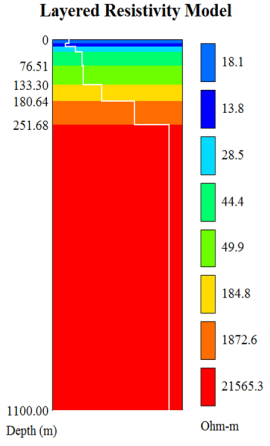
Layered Resistivity Model
0
76.51
133.30
180.64
251.68
1100.00
Depth (m)
18.1
13.8
28.5
44.4
49.9
184.8
1872.6
21565.3
Ohm-m

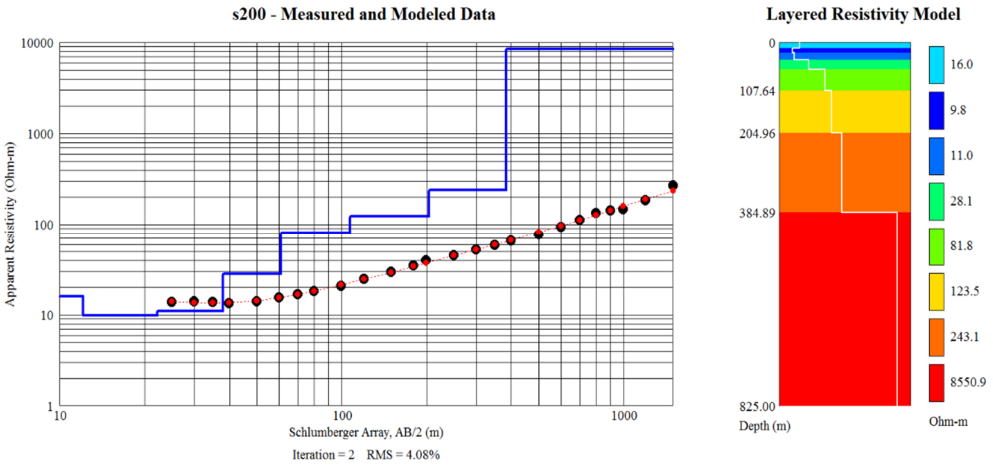
s200 - Measured and Modeled Data
Apparent Resistivity (Ohm-m)
10000
1000
100
10
1
10
100
1000
Schlumberger Array, AB/2 (m)
Iteration = 2 RMS = 4.08%
Layered Resistivity Model
0
107.64
204.96
384.89
825.00
Depth (m)
16.0
9.8
11.0
28.1
81.8
123.5
243.1
8550.9
Ohm-m

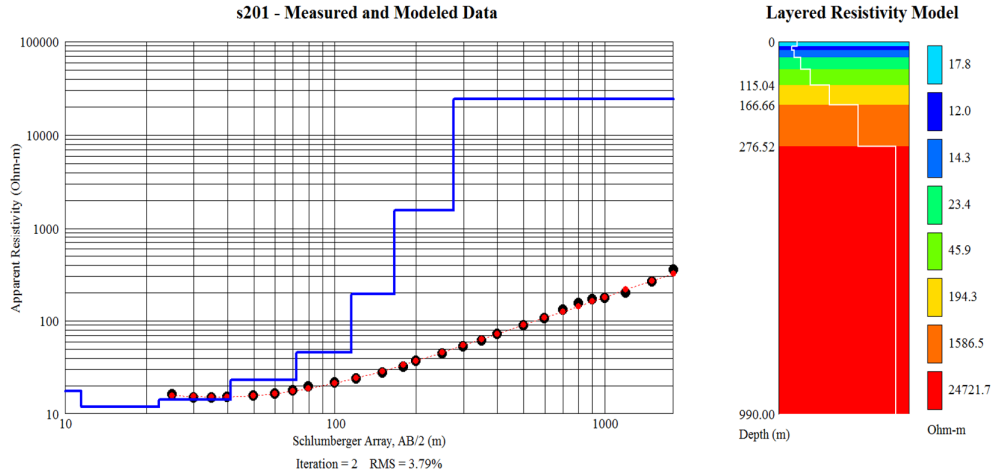
s201 - Measured and Modeled Data
Apparent Resistivity (Ohm-m)
100000
10000
1000
100
10
10
100
1000
Schlumberger Array, AB/2 (m)
Iteration = 2 RMS = 3.79%
Layered Resistivity Model
0
115.04
166.66
276.52
990.00
Depth (m)
17.8
12.0
14.3
23.4
45.9
194.3
1586.5
24721.7
Ohm-m

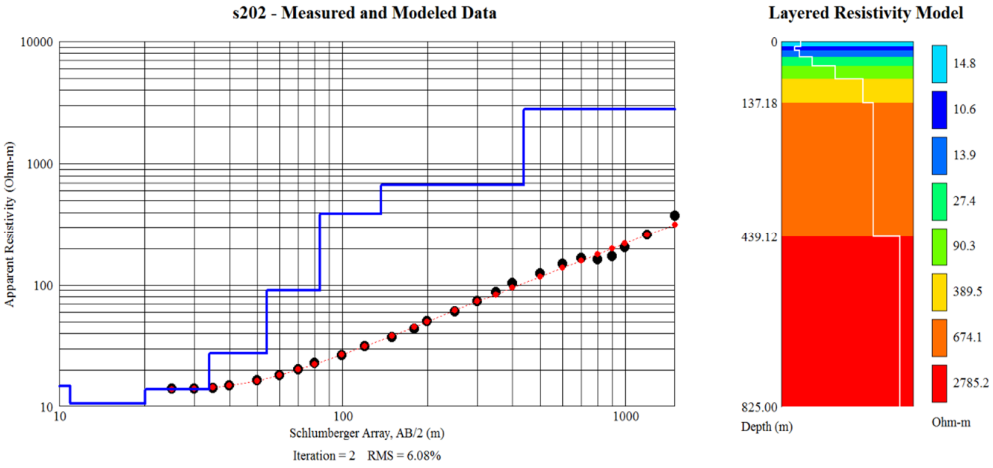
s202 - Measured and Modeled Data
Apparent Resistivity (Ohm-m)
10000
1000
100
10
10
100
1000
Schlumberger Array, AB/2 (m)
Iteration = 2 RMS = 6.08%
Layered Resistivity Model
0
137.18
439.12
825.00
Depth (m)
14.8
10.6
13.9
27.4
90.3
389.5
674.1
2785.2
Ohm-m

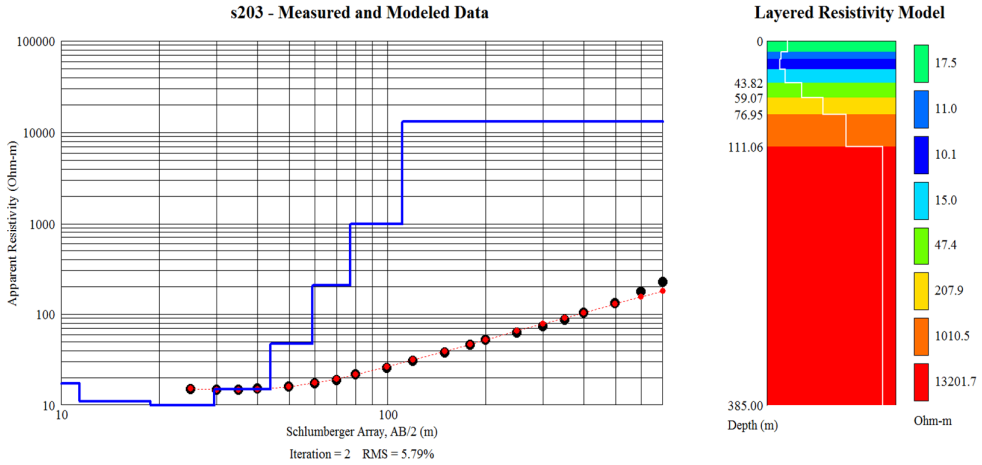
s203 - Measured and Modeled Data
Apparent Resistivity (Ohm-m)
100000
10000
1000
100
10
10
100
Schlumberger Array, AB/2 (m)
Iteration = 2 RMS = 5.79%
Layered Resistivity Model
0
43.82
59.07
76.95
111.06
385.00
Depth (m)
17.5
11.0
10.1
15.0
47.4
207.9
1010.5
13201.7
Ohm-m

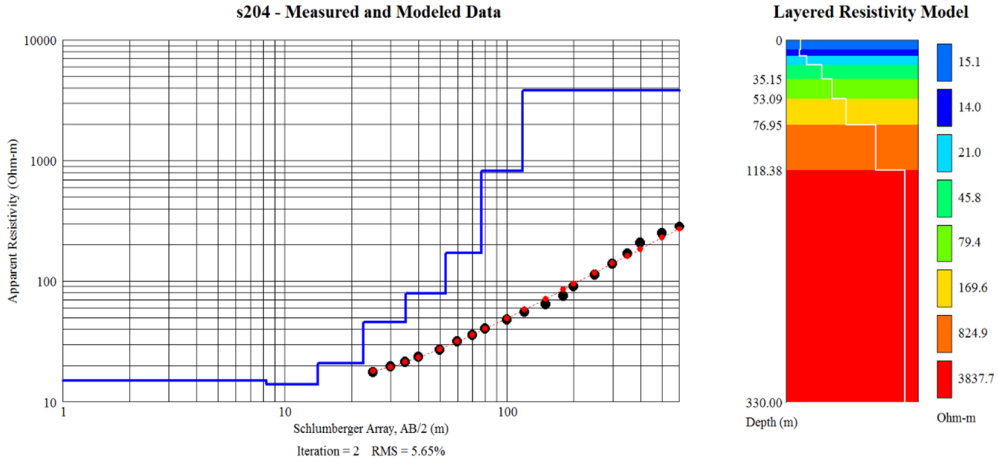
s204 - Measured and Modeled Data
Apparent Resistivity (Ohm-m)
10000
1000
100
10
1
10
100
Schlumberger Array, AB/2 (m)
Iteration = 2 RMS = 5.65%
Layered Resistivity Model
0
35.15
53.09
76.95
118.38
330.00
Depth (m)
15.1
14.0
21.0
45.8
79.4
169.6
824.9
3837.7
Ohm-m

Group 11

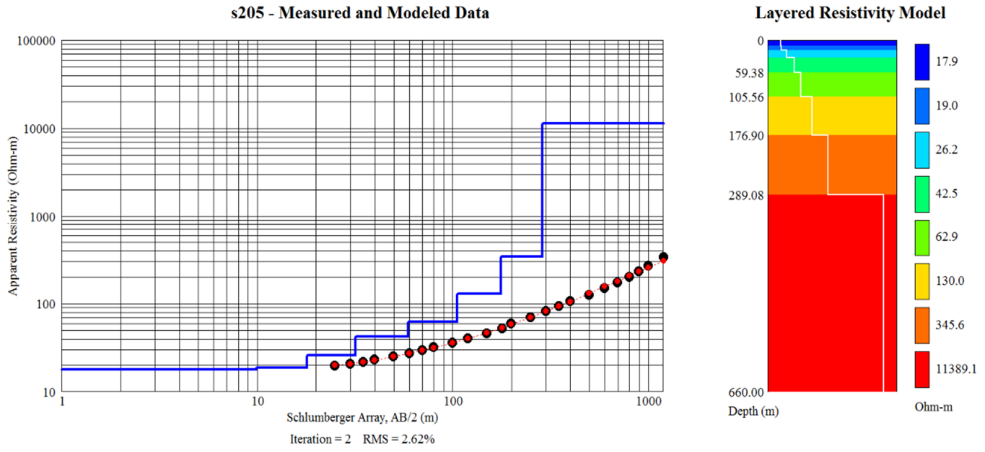
s205 - Measured and Modeled Data
Apparent Resistivity (Ohm-m)
100000
10000
1000
100
10
1
10
100
1000
Schlumberger Array, AB/2 (m)
Iteration = 2 RMS = 2.62%
Layered Resistivity Model
0
59.38
105.56
176.90
289.08
660.00
Depth (m)
17.9
19.0
26.2
42.5
62.9
130.0
345.6
11389.1
Ohm-m

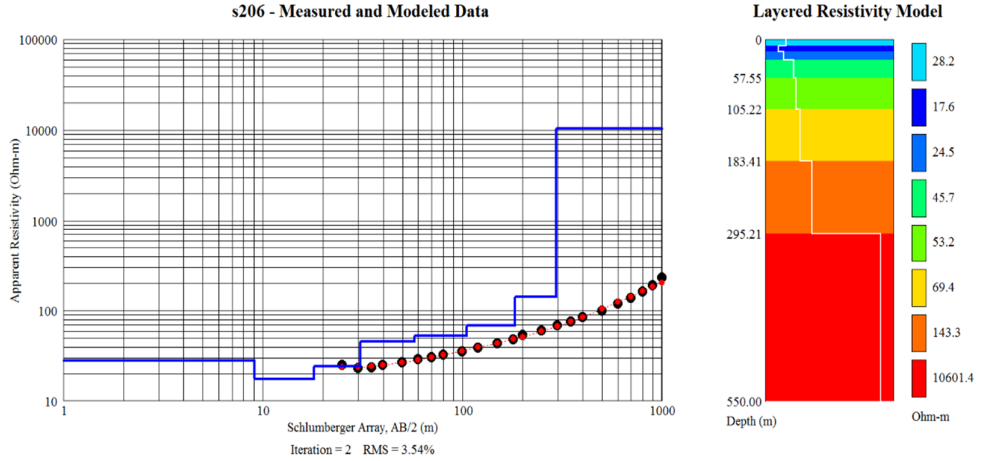
s206 - Measured and Modeled Data
Apparent Resistivity (Ohm-m)
100000
10000
1000
100
10
1
10
100
1000
Schlumberger Array, AB/2 (m)
Iteration = 2 RMS = 3.54%
Layered Resistivity Model
0
57.55
105.22
183.41
295.21
550.00
Depth (m)
28.2
17.6
24.5
45.7
53.2
69.4
143.3
10601.4
Ohm-m

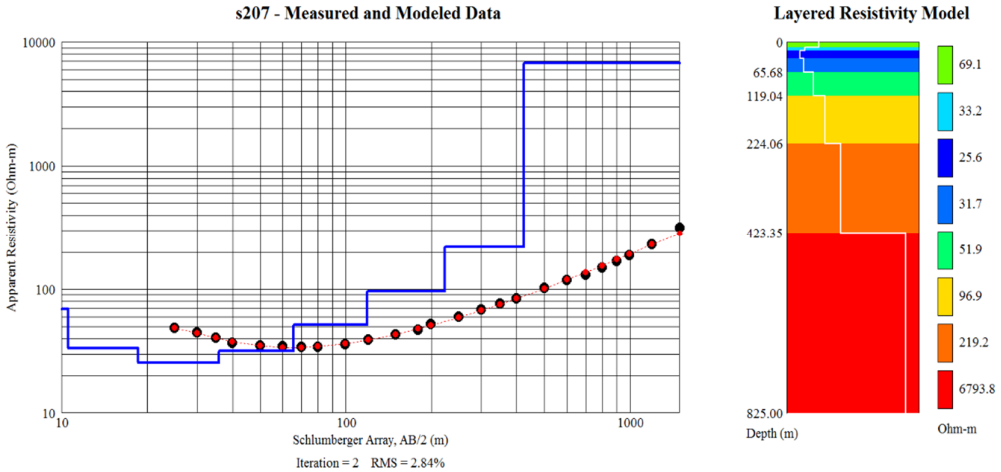
s207 - Measured and Modeled Data
Apparent Resistivity (Ohm-m)
10000
1000
100
10
10
100
1000
Schlumberger Array, AB/2 (m)
Iteration = 2 RMS = 2.84%
Layered Resistivity Model
0
65.68
119.04
224.06
423.35
825.00
Depth (m)
69.1
33.2
25.6
31.7
51.9
96.9
219.2
6793.8
Ohm-m

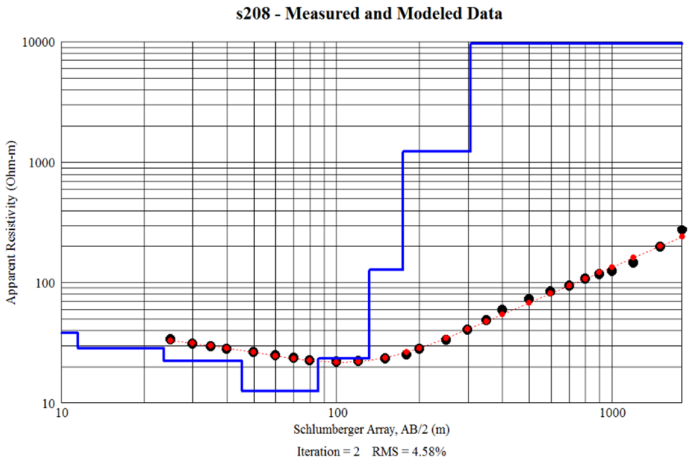
s208 - Measured and Modeled Data
Apparent Resistivity (Ohm-m)
10000
1000
100
10
10
100
1000
Schlumberger Array, AB/2 (m)
Iteration = 2 RMS = 4.58%

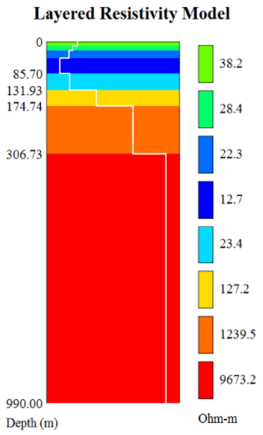
Layered Resistivity Model
0
85.70
131.93
174.74
306.73
990.00
Depth (m)
38.2
28.4
22.3
12.7
23.4
127.2
1239.5
9673.2
Ohm-m

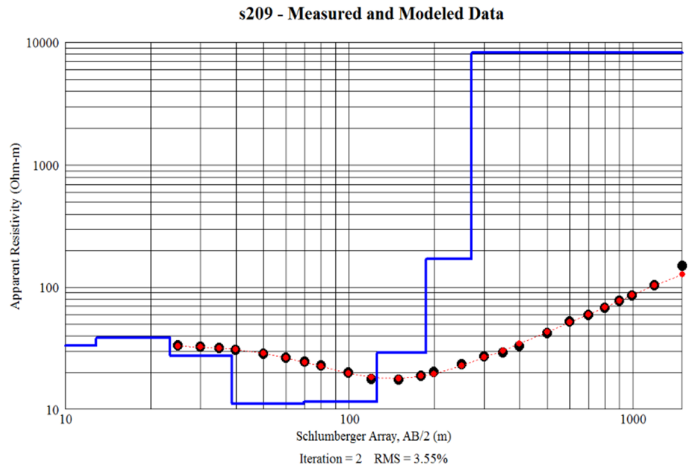
s209 - Measured and Modeled Data
Apparent Resistivity (Ohm-m)
10000
1000
100
10
10
100
1000
Schlumberger Array, AB/2 (m)
Iteration = 2 RMS = 3.55%

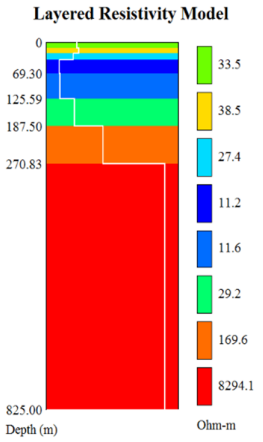
Layered Resistivity Model
0
69.30
125.59
187.50
270.83
825.00
Depth (m)
33.5
38.5
27.4
11.2
11.6
29.2
169.6
8294.1
Ohm-m

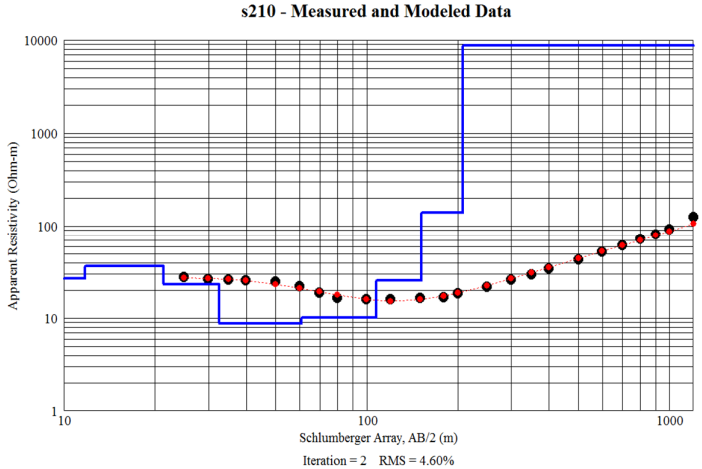
s210 - Measured and Modeled Data
Apparent Resistivity (Ohm-m)
10000
1000
100
10
1
10
100
1000
Schlumberger Array, AB/2 (m)
Iteration = 2 RMS = 4.60%

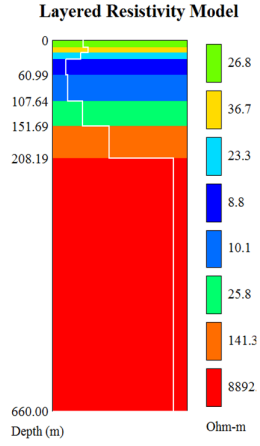
Layered Resistivity Model
0
60.99
107.64
151.69
208.19
660.00
Depth (m)
26.8
36.7
23.3
8.8
10.1
25.8
141.3
8892
Ohm-m

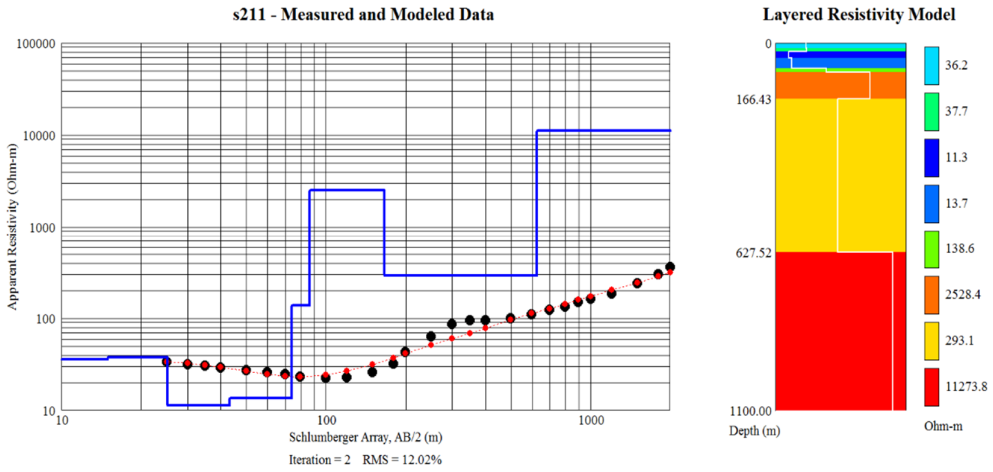
s211 - Measured and Modeled Data
Apparent Resistivity (Ohm-m)
100000
10000
1000
100
10
10
100
1000
Schlumberger Array, AB/2 (m)
Iteration = 2 RMS = 12.02%
Layered Resistivity Model
0
166.43
627.52
1100.00
Depth (m)
36.2
37.7
11.3
13.7
138.6
2528.4
293.1
11273.8
Ohm-m

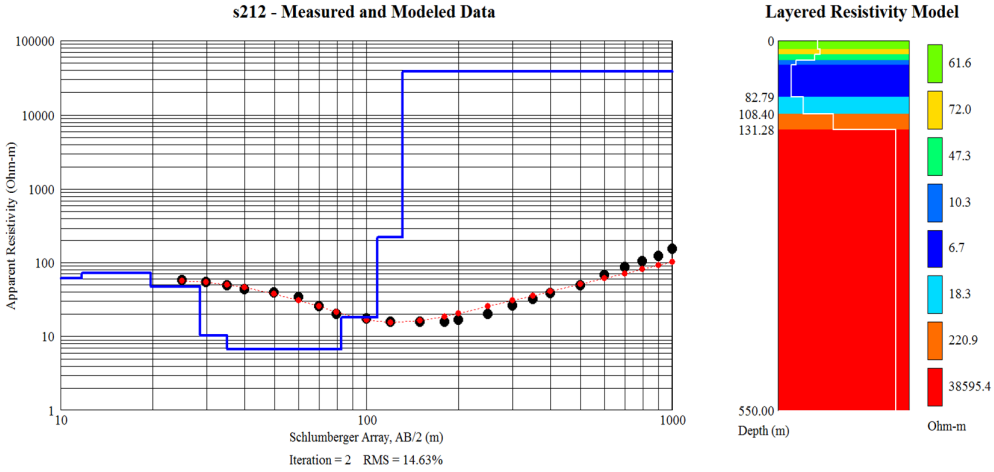
s212 - Measured and Modeled Data
Apparent Resistivity (Ohm-m)
100000
10000
1000
100
10
1
10
100
1000
Schlumberger Array, AB/2 (m)
Iteration = 2 RMS = 14.63%
Layered Resistivity Model
0
82.79
108.40
131.28
550.00
Depth (m)
61.6
72.0
47.3
10.3
6.7
18.3
220.9
38595.4
Ohm-m

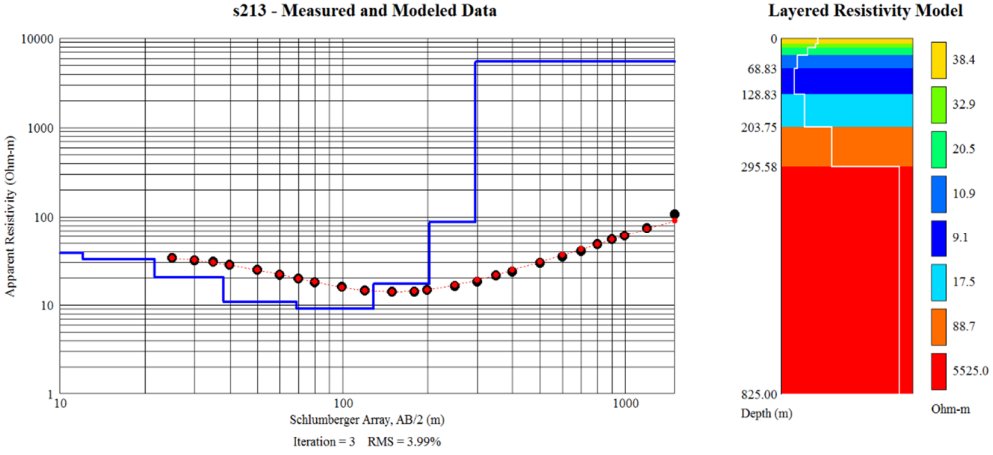
s213 - Measured and Modeled Data
Apparent Resistivity (Ohm-m)
10000
1000
100
10
1
10
100
1000
Schlumberger Array, AB/2 (m)
Iteration = 3 RMS = 3.99%
Layered Resistivity Model
0
68.83
128.83
203.75
295.58
825.00
Depth (m)
38.4
32.9
20.5
10.9
9.1
17.5
88.7
5525.0
Ohm-m

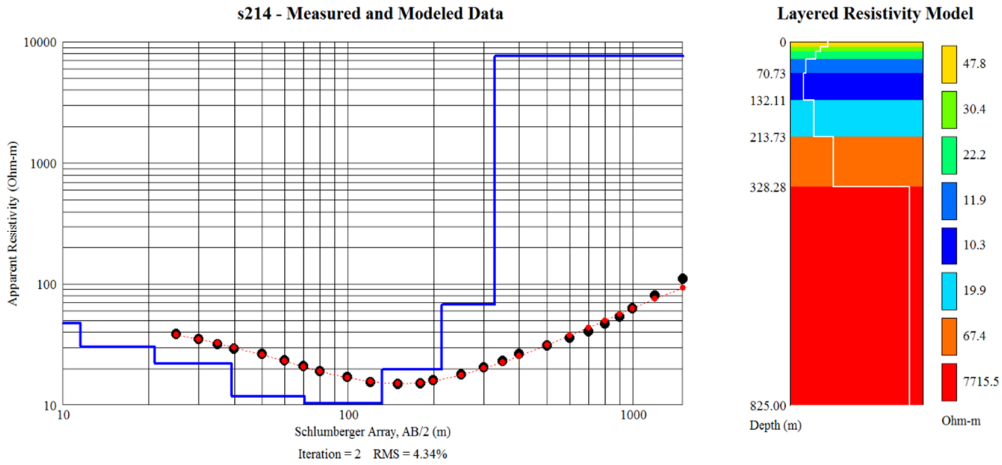
s214 - Measured and Modeled Data
Apparent Resistivity (Ohm-m)
10000
1000
100
10
10
100
1000
Schlumberger Array, AB/2 (m)
Iteration = 2 RMS = 4.34%
Layered Resistivity Model
0
70.73
132.11
213.73
328.28
825.00
Depth (m)
47.8
30.4
22.2
11.9
10.3
19.9
67.4
7715.5
Ohm-m

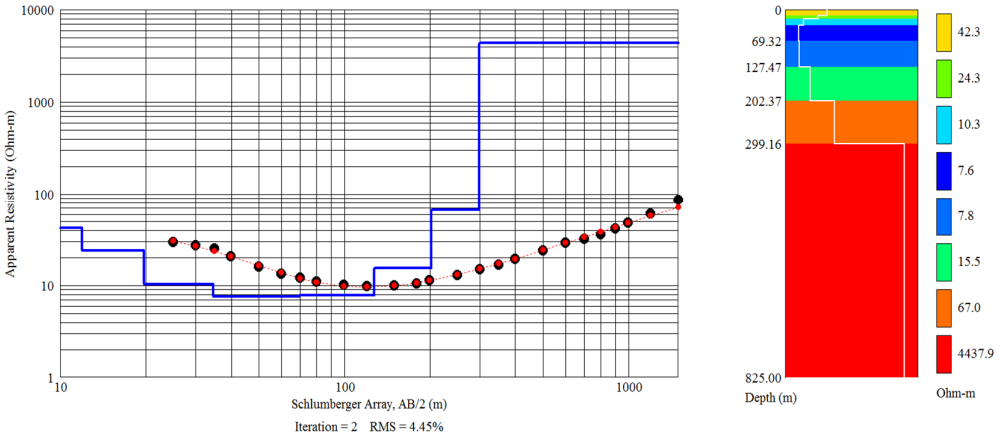
s215 - Measured and Modeled Data
Apparent Resistivity (Ohm-m)
10000
1000
100
10
1
10
100
1000
Schlumberger Array, AB/2 (m)
Iteration = 2 RMS = 4.45%
Layered Resistivity Model
0
69.32
127.47
202.37
299.16
825.00
Depth (m)
42.3
24.3
10.3
7.6
7.8
15.5
67.0
4437.9
Ohm-m

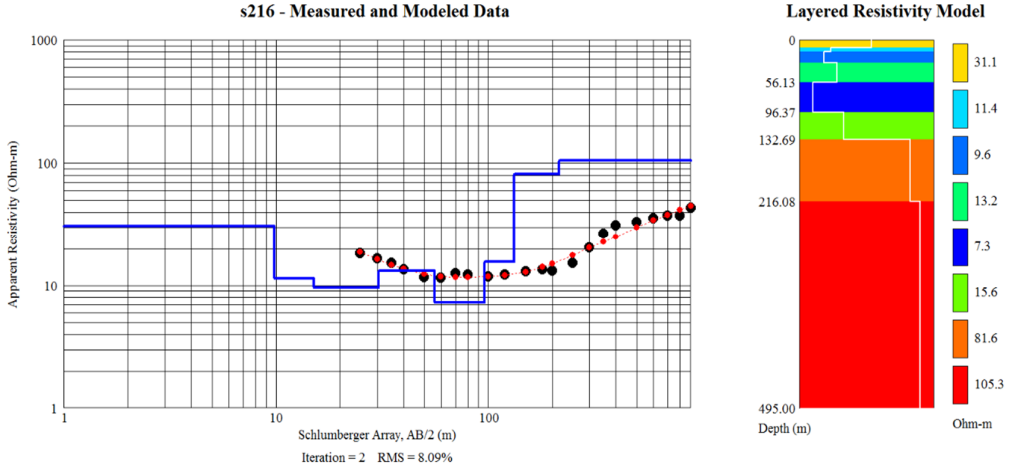
s216 - Measured and Modeled Data
Apparent Resistivity (Ohm-m)
1000
100
10
1
1
10
100
Schlumberger Array, AB/2 (m)
Iteration = 2 RMS = 8.09%
Layered Resistivity Model
0
56.13
96.37
132.69
216.08
495.00
Depth (m)
31.1
11.4
9.6
13.2
7.3
15.6
81.6
105.3
Ohm-m

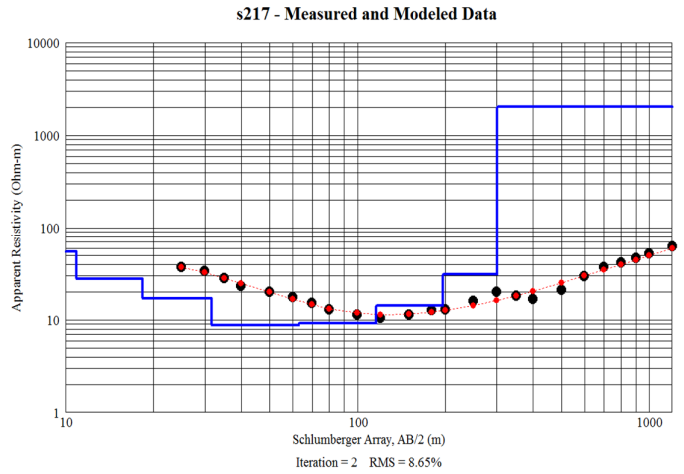
s217 - Measured and Modeled Data
Apparent Resistivity (Ohm-m)
10000
1000
100
10
1
10
100
1000
Schlumberger Array, AB/2 (m)
Iteration = 2 RMS = 8.65%

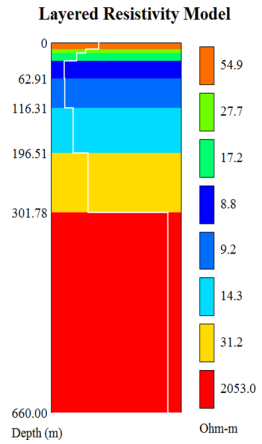
Layered Resistivity Model
0
62.91
116.31
196.51
301.78
660.00
Depth (m)
54.9
27.7
17.2
8.8
9.2
14.3
31.2
2053.0
Ohm-m

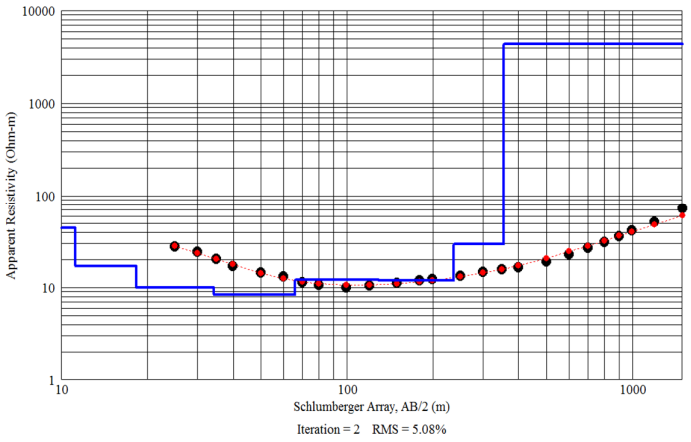
s218 - Measured and Modeled Data
Apparent Resistivity (Ohm-m)
10000
1000
100
10
1
10
100
1000
Schlumberger Array, AB/2 (m)
Iteration = 2 RMS = 5.08%

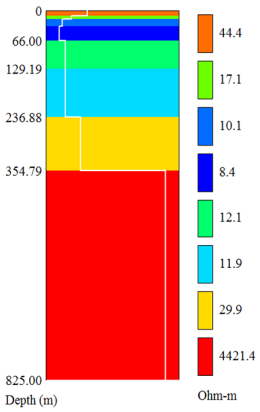
Layered Resistivity Model
0
66.00
129.19
236.88
354.79
825.00
Depth (m)
44.4
17.1
10.1
8.4
12.1
11.9
29.9
4421.4
Ohm-m

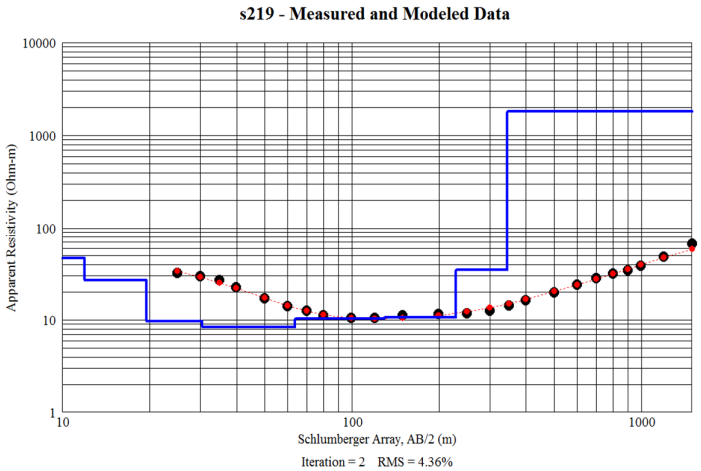
s219 - Measured and Modeled Data
Apparent Resistivity (Ohm-m)
10000
1000
100
10
1
10
100
1000
Schlumberger Array, AB/2 (m)
Iteration = 2 RMS = 4.36%

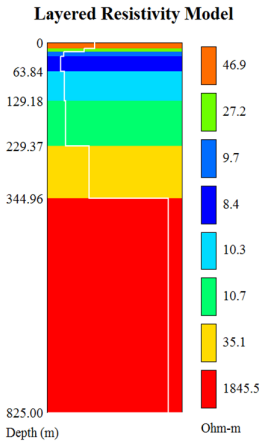
Layered Resistivity Model
0
63.84
129.18
229.37
344.96
825.00
Depth (m)
46.9
27.2
9.7
8.4
10.3
10.7
35.1
1845.5
Ohm-m

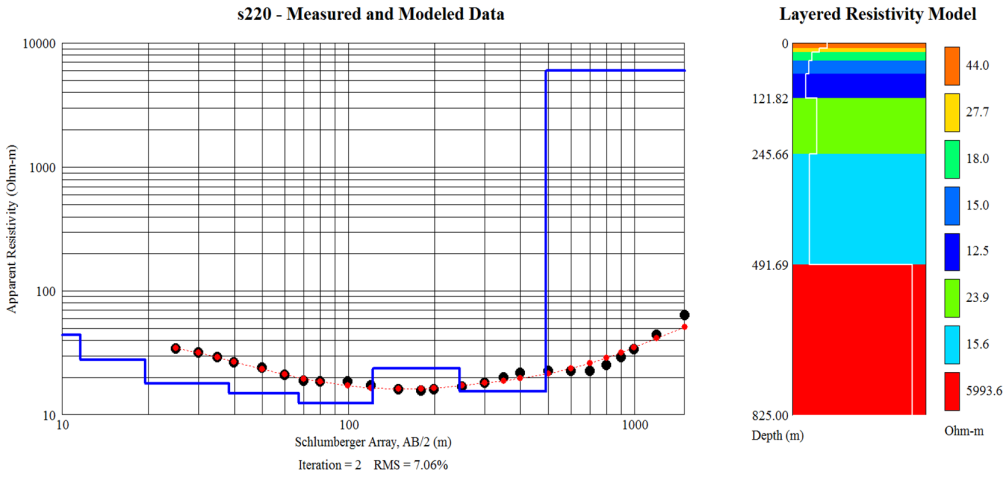
s220 - Measured and Modeled Data
Apparent Resistivity (Ohm-m)
10000
1000
100
10
10
100
1000
Schlumberger Array, AB/2 (m)
Iteration = 2 RMS = 7.06%
Layered Resistivity Model
0
121.82
245.66
491.69
825.00
Depth (m)
44.0
27.7
18.0
15.0
12.5
23.9
15.6
5993.6
Ohm-m

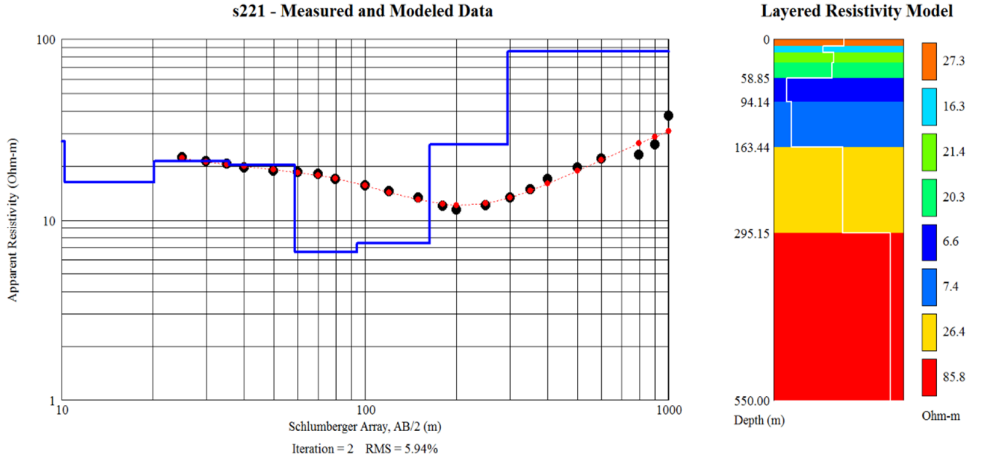
s221 - Measured and Modeled Data
Apparent Resistivity (Ohm-m)
100
10
1
10
100
1000
Schlumberger Array, AB/2 (m)
Iteration = 2 RMS = 5.94%
Layered Resistivity Model
0
58.85
94.14
163.44
295.15
550.00
Depth (m)
27.3
16.3
21.4
20.3
6.6
7.4
26.4
85.8
Ohm-m

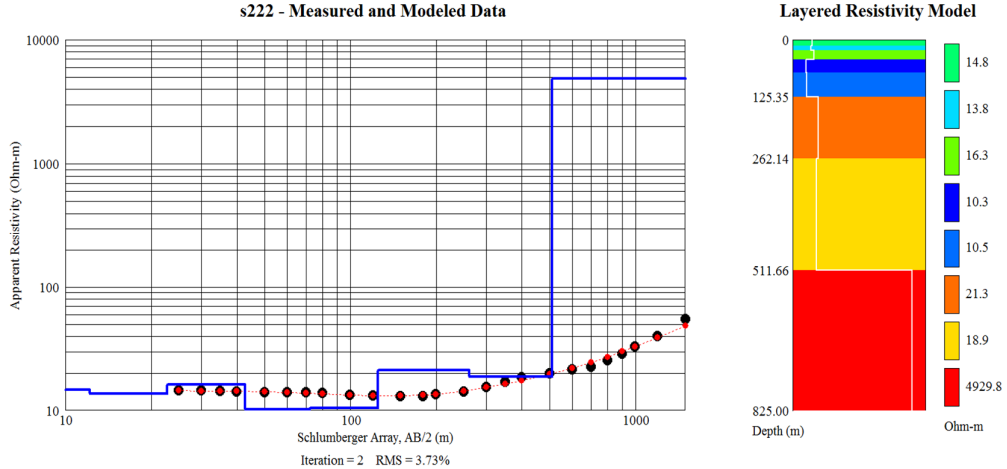
s222 - Measured and Modeled Data
Apparent Resistivity (Ohm-m)
10000
1000
100
10
10
100
1000
Schlumberger Array, AB/2 (m)
Iteration = 2 RMS = 3.73%
Layered Resistivity Model
0
125.35
262.14
511.66
825.00
Depth (m)
14.8
13.8
16.3
10.3
10.5
21.3
18.9
4929.8
Ohm-m

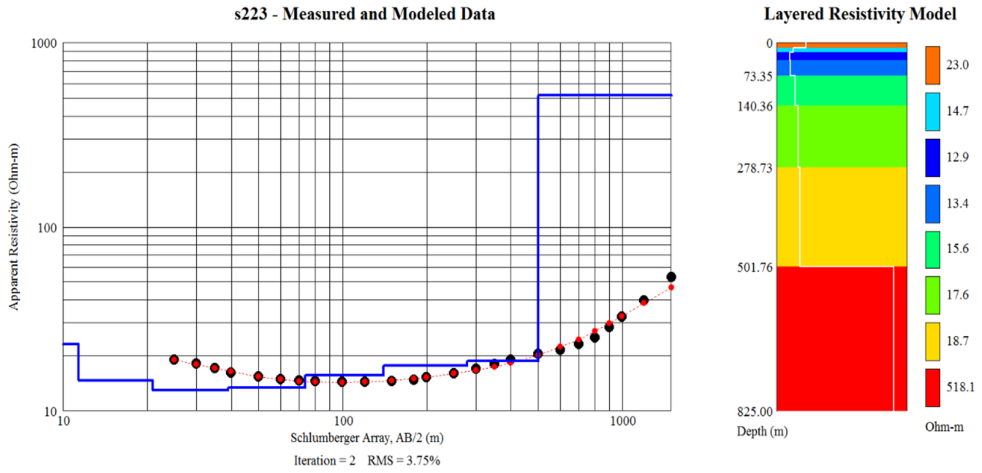
s223 - Measured and Modeled Data
Apparent Resistivity (Ohm-m)
1000
100
10
10
100
1000
Schlumberger Array, AB/2 (m)
Iteration = 2 RMS = 3.75%
Layered Resistivity Model
0
73.35
140.36
278.73
501.76
825.00
Depth (m)
23.0
14.7
12.9
13.4
15.6
17.6
18.7
518.1
Ohm-m

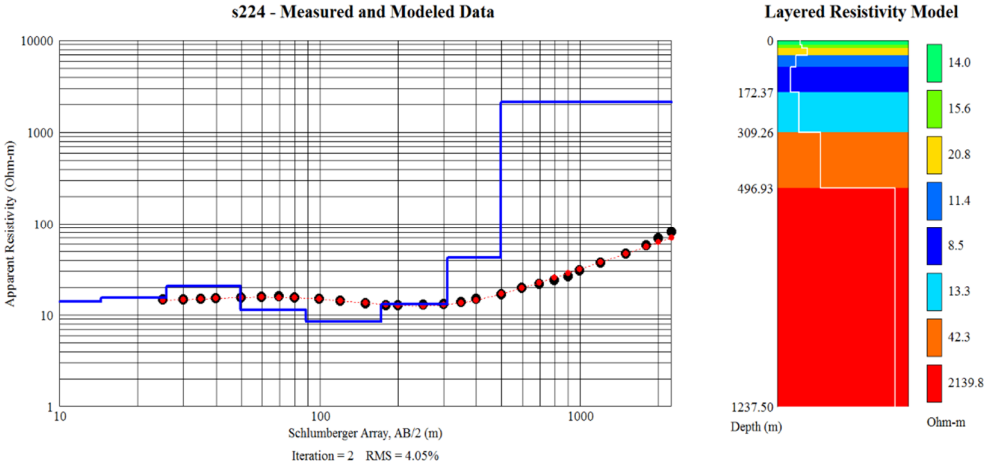
s224 - Measured and Modeled Data
Apparent Resistivity (Ohm-m)
10000
1000
100
10
1
10
100
1000
Schlumberger Array, AB/2 (m)
Iteration = 2 RMS = 4.05%
Layered Resistivity Model
0
172.37
309.26
496.93
1237.50
Depth (m)
14.0
15.6
20.8
11.4
8.5
13.3
42.3
2139.8
Ohm-m

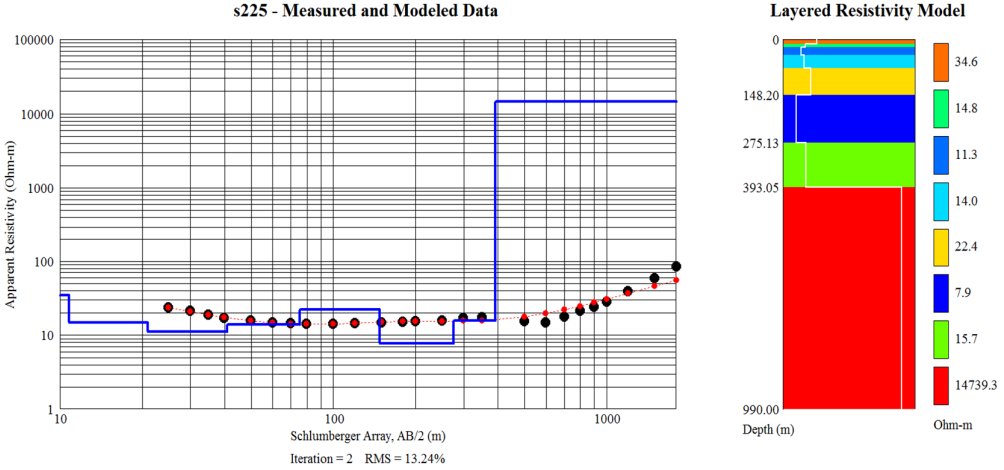
s225 - Measured and Modeled Data
Apparent Resistivity (Ohm-m)
100000
10000
1000
100
10
1
10
100
1000
Schlumberger Array, AB/2 (m)
Iteration = 2 RMS = 13.24%
Layered Resistivity Model
0
148.20
275.13
393.05
990.00
Depth (m)
34.6
14.8
11.3
14.0
22.4
7.9
15.7
14739.3
Ohm-m

s226 - Measured and Modeled Data

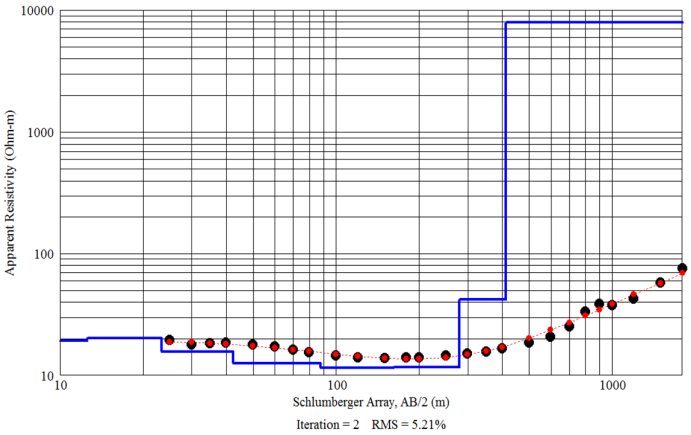

Iteration = 2 RMS = 5.21%

Layered Resistivity Model

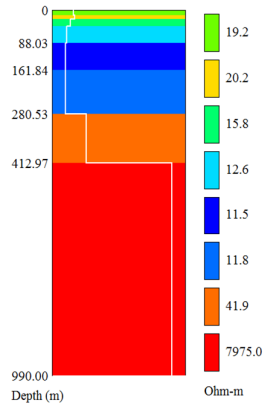

s227 - Measured and Modeled Data

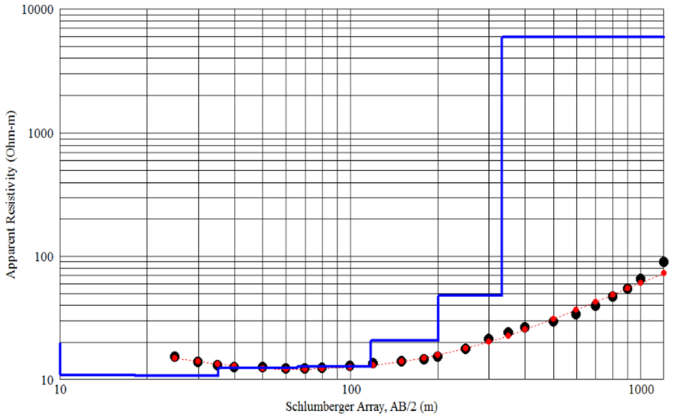

Iteration = 2 RMS = 5.25%

Layered Resistivity Model

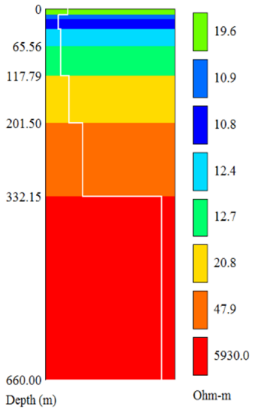

s228 - Measured and Modeled Data

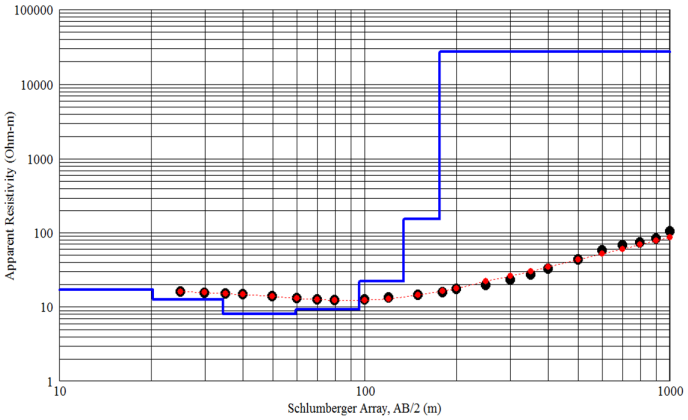

Iteration = 2 RMS = 6.70%

Layered Resistivity Model

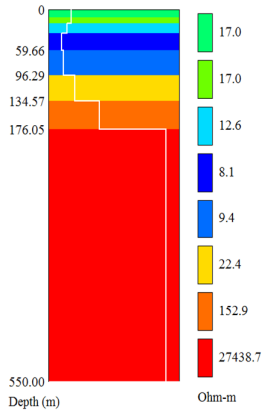

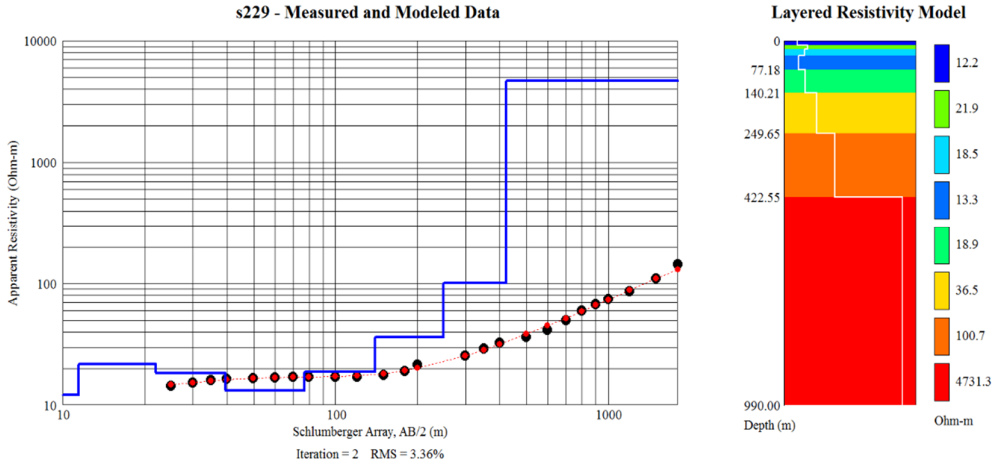
s229 - Measured and Modeled Data
Apparent Resistivity (Ohm-m)
10000
1000
100
10
10
100
1000
Schlumberger Array, AB/2 (m)
Iteration = 2 RMS = 3.36%
Layered Resistivity Model
0
77.18
140.21
249.65
422.55
990.00
Depth (m)
12.2
21.9
18.5
13.3
18.9
36.5
100.7
4731.3
Ohm-m

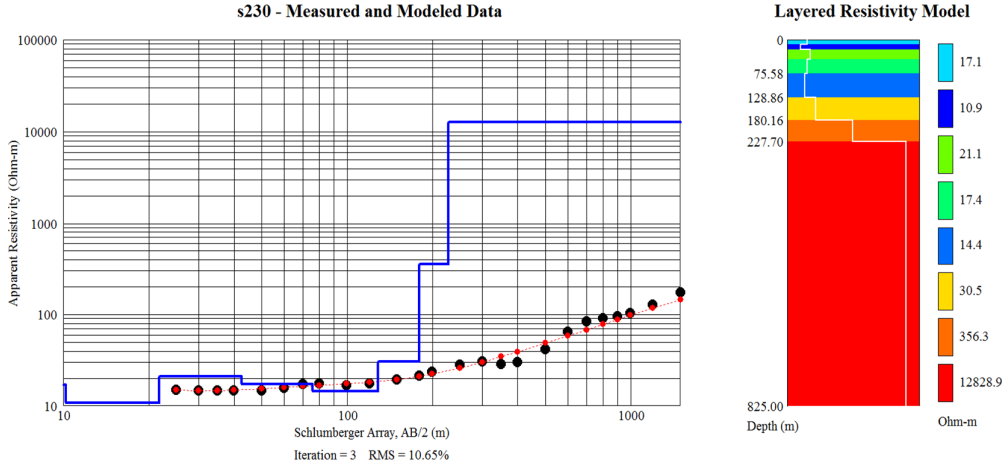
s230 - Measured and Modeled Data
Apparent Resistivity (Ohm-m)
100000
10000
1000
100
10
10
100
1000
Schlumberger Array, AB/2 (m)
Iteration = 3 RMS = 10.65%
Layered Resistivity Model
0
75.58
128.86
180.16
227.70
825.00
Depth (m)
17.1
10.9
21.1
17.4
14.4
30.5
356.3
12828.9
Ohm-m

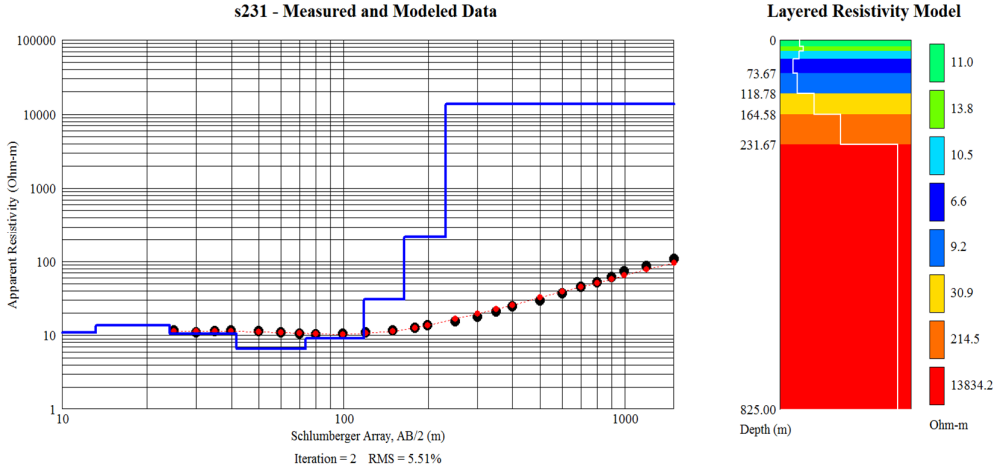
s231 - Measured and Modeled Data
Apparent Resistivity (Ohm-m)
100000
10000
1000
100
10
1
10
100
1000
Schlumberger Array, AB/2 (m)
Iteration = 2 RMS = 5.51%
Layered Resistivity Model
0
73.67
118.78
164.58
231.67
825.00
Depth (m)
11.0
13.8
10.5
6.6
9.2
30.9
214.5
13834.2
Ohm-m

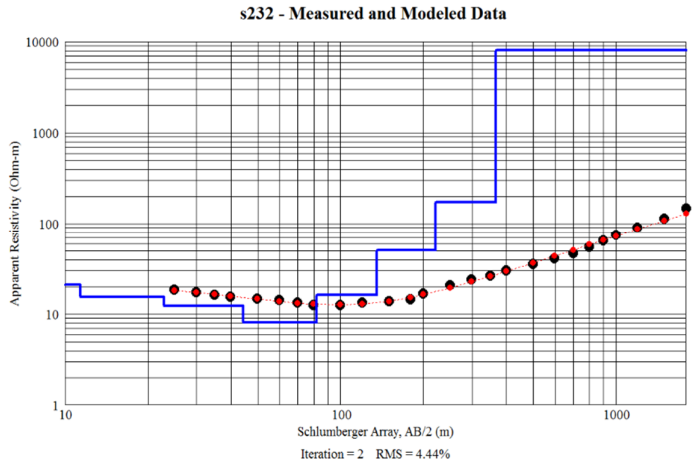
s232 - Measured and Modeled Data
Apparent Resistivity (Ohm-m)
10000
1000
100
10
1
10
100
1000
Schlumberger Array, AB/2 (m)
Iteration = 2 RMS = 4.44%

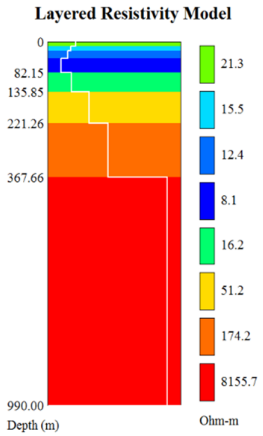
Layered Resistivity Model
0
82.15
135.85
221.26
367.66
990.00
Depth (m)
21.3
15.5
12.4
8.1
16.2
51.2
174.2
8155.7
Ohm-m

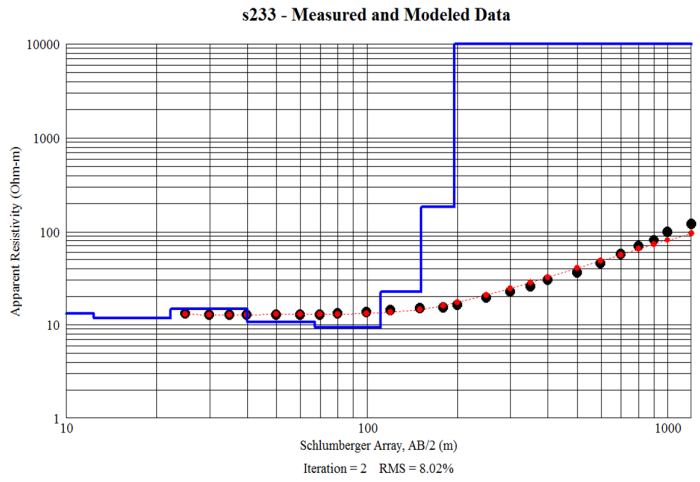
s233 - Measured and Modeled Data
Apparent Resistivity (Ohm-m)
10000
1000
100
10
1
10
100
1000
Schlumberger Array, AB/2 (m)
Iteration = 2 RMS = 8.02%

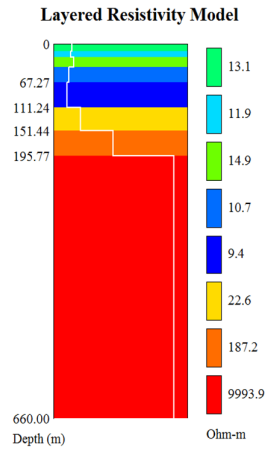
Layered Resistivity Model
0
67.27
111.24
151.44
195.77
660.00
Depth (m)
13.1
11.9
14.9
10.7
9.4
22.6
187.2
9993.9
Ohm-m

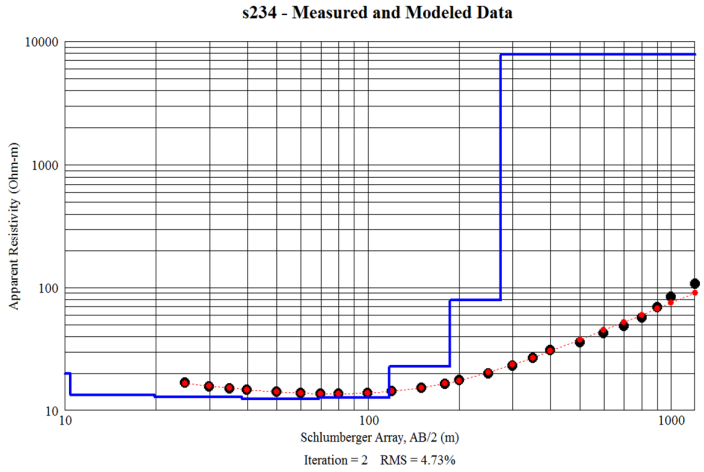
s234 - Measured and Modeled Data
Apparent Resistivity (Ohm-m)
10000
1000
100
10
10
100
1000
Schlumberger Array, AB/2 (m)
Iteration = 2 RMS = 4.73%

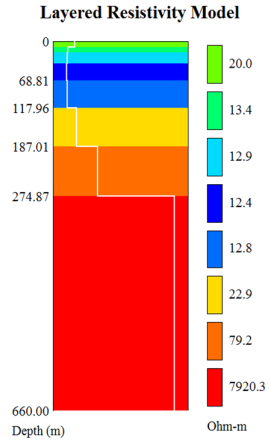
Layered Resistivity Model
0
68.81
117.96
187.01
274.87
660.00
Depth (m)
20.0
13.4
12.9
12.4
12.8
22.9
79.2
7920.3
Ohm-m

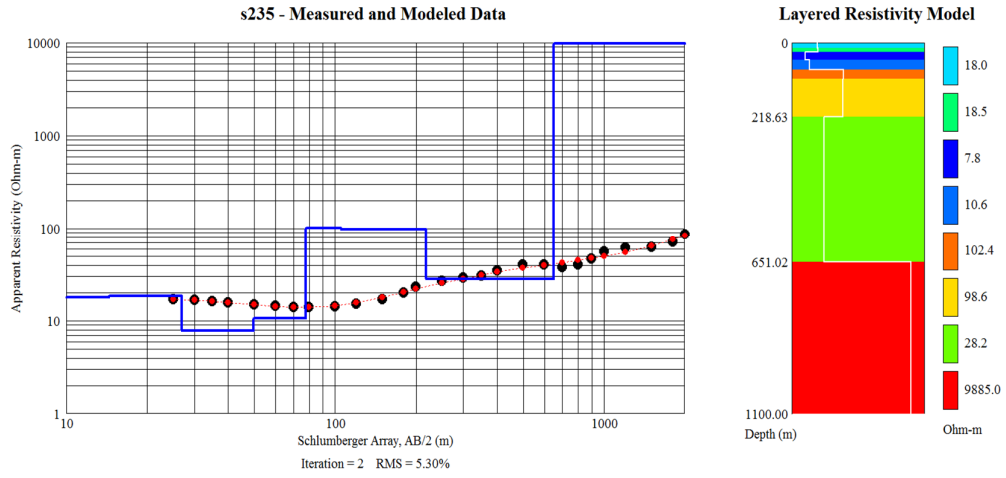
s235 - Measured and Modeled Data
Apparent Resistivity (Ohm-m)
10000
1000
100
10
1
10
100
1000
Schlumberger Array, AB/2 (m)
Iteration = 2 RMS = 5.30%
Layered Resistivity Model
0
218.63
651.02
1100.00
Depth (m)
18.0
18.5
7.8
10.6
102.4
98.6
28.2
9885.0
Ohm-m

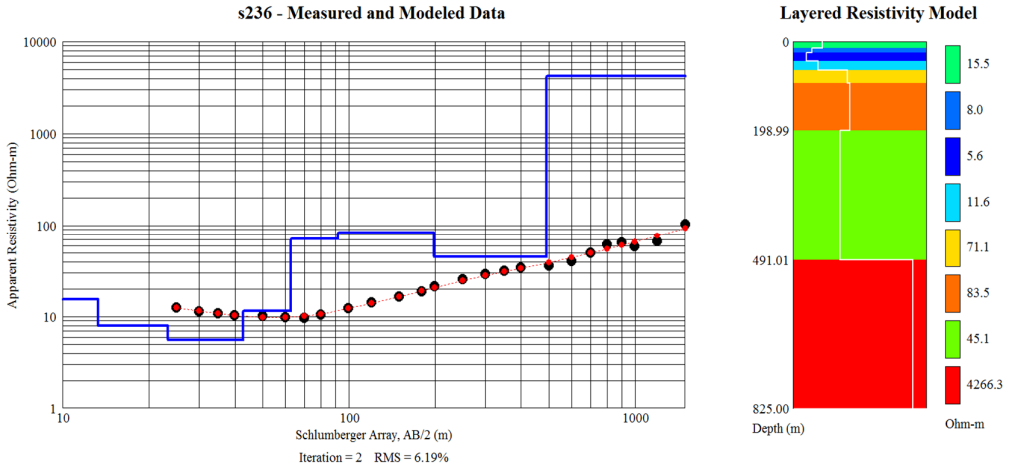
s236 - Measured and Modeled Data
Apparent Resistivity (Ohm-m)
10000
1000
100
10
1
10
100
1000
Schlumberger Array, AB/2 (m)
Iteration = 2 RMS = 6.19%
Layered Resistivity Model
0
198.99
491.01
825.00
Depth (m)
15.5
8.0
5.6
11.6
71.1
83.5
45.1
4266.3
Ohm-m

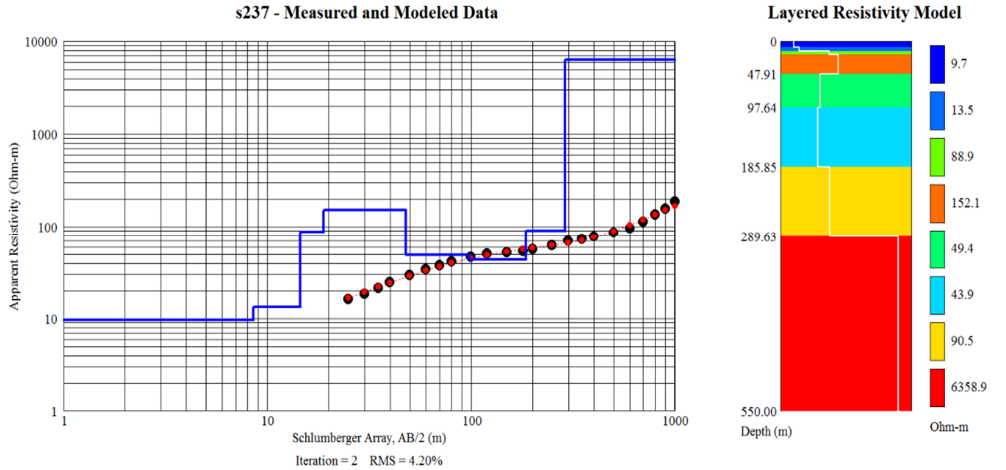
s237 - Measured and Modeled Data
Apparent Resistivity (Ohm-m)
10000
1000
100
10
1
1
10
100
1000
Schlumberger Array, AB/2 (m)
Iteration = 2 RMS = 4.20%
Layered Resistivity Model
0
47.91
97.64
185.85
289.63
550.00
Depth (m)
9.7
13.5
88.9
152.1
49.4
43.9
90.5
6358.9
Ohm-m

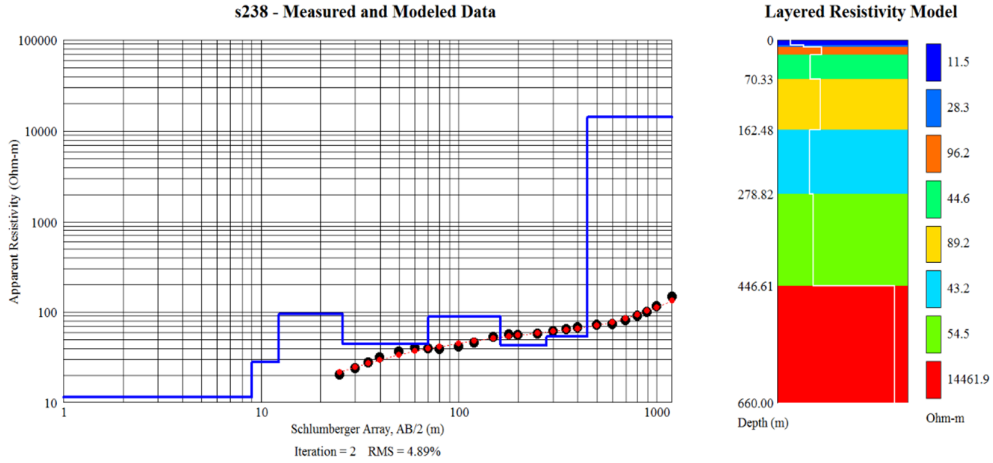
s238 - Measured and Modeled Data
Apparent Resistivity (Ohm-m)
100000
10000
1000
100
10
1
10
100
1000
Schlumberger Array, AB/2 (m)
Iteration = 2 RMS = 4.89%
Layered Resistivity Model
0
70.33
162.48
278.82
446.61
660.00
Depth (m)
11.5
28.3
96.2
44.6
89.2
43.2
54.5
14461.9
Ohm-m

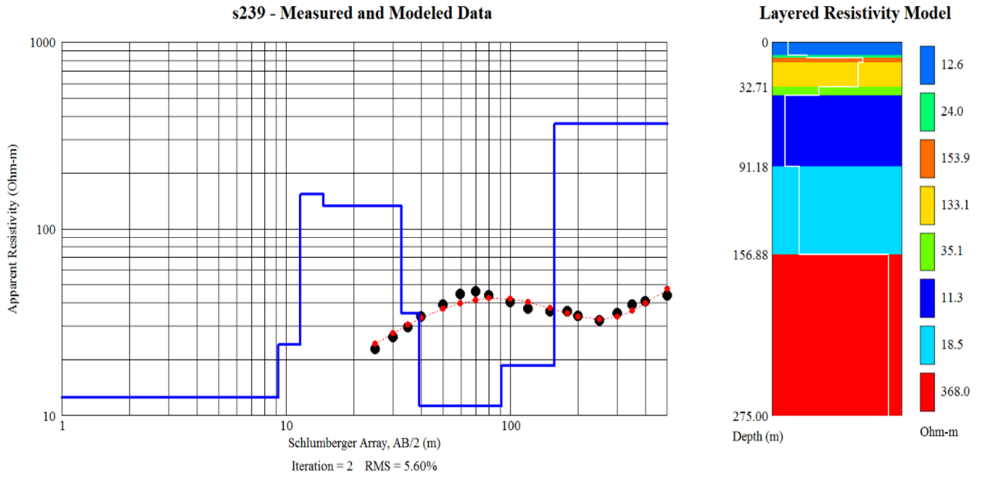
s239 - Measured and Modeled Data
Apparent Resistivity (Ohm-m)
1000
100
10
1
10
100
Schlumberger Array, AB/2 (m)
Iteration = 2 RMS = 5.60%
Layered Resistivity Model
0
32.71
91.18
156.88
275.00
Depth (m)
12.6
24.0
153.9
133.1
35.1
11.3
18.5
368.0
Ohm-m

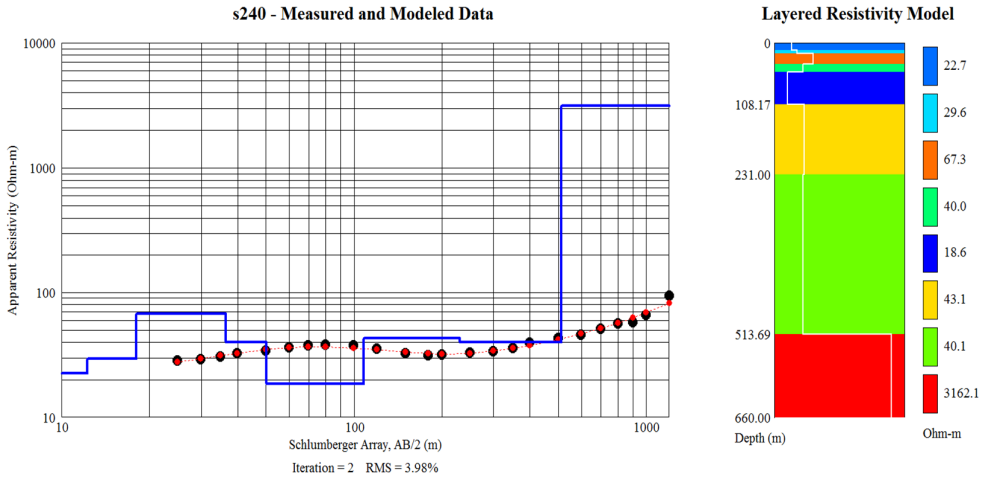
s240 - Measured and Modeled Data
Apparent Resistivity (Ohm-m)
10000
1000
100
10
10
100
1000
Schlumberger Array, AB/2 (m)
Iteration = 2 RMS = 3.98%
Layered Resistivity Model
0
108.17
231.00
513.69
660.00
Depth (m)
22.7
29.6
67.3
40.0
18.6
43.1
40.1
3162.1
Ohm-m

Group 12

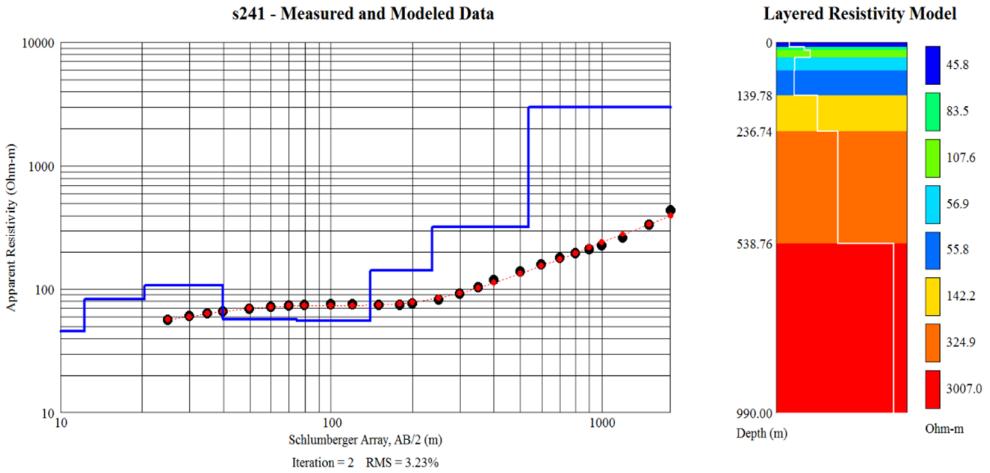
s241 - Measured and Modeled Data
Apparent Resistivity (Ohm-m)
10000
1000
100
10
10
100
1000
Schlumberger Array, AB/2 (m)
Iteration = 2 RMS = 3.23%
Layered Resistivity Model
0
139.78
236.74
538.76
990.00
Depth (m)
45.8
83.5
107.6
56.9
55.8
142.2
324.9
3007.0
Ohm-m

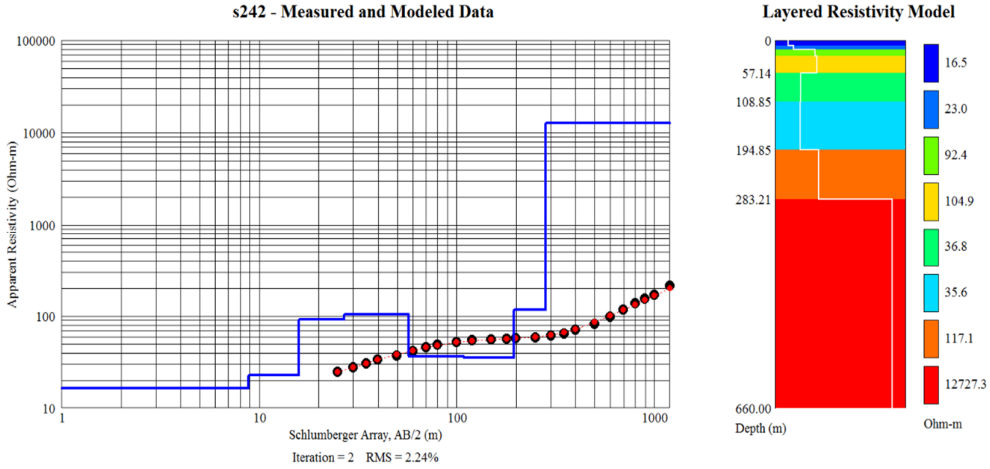
s242 - Measured and Modeled Data
Apparent Resistivity (Ohm-m)
100000
10000
1000
100
10
1
10
100
1000
Schlumberger Array, AB/2 (m)
Iteration = 2 RMS = 2.24%
Layered Resistivity Model
0
57.14
108.85
194.85
283.21
660.00
Depth (m)
16.5
23.0
92.4
104.9
36.8
35.6
117.1
12727.3
Ohm-m

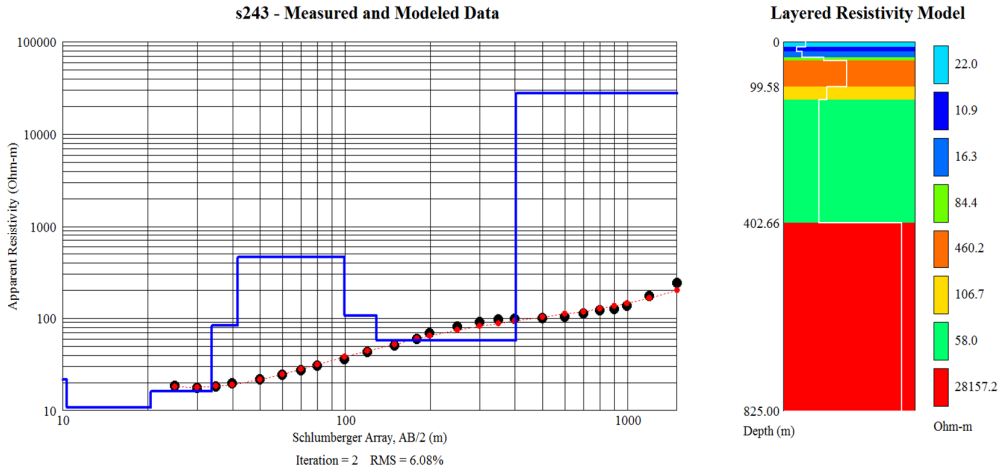
s243 - Measured and Modeled Data
Apparent Resistivity (Ohm-m)
100000
10000
1000
100
10
10
100
1000
Schlumberger Array, AB/2 (m)
Iteration = 2 RMS = 6.08%
Layered Resistivity Model
0
99.58
402.66
825.00
Depth (m)
22.0
10.9
16.3
84.4
460.2
106.7
58.0
28157.2
Ohm-m

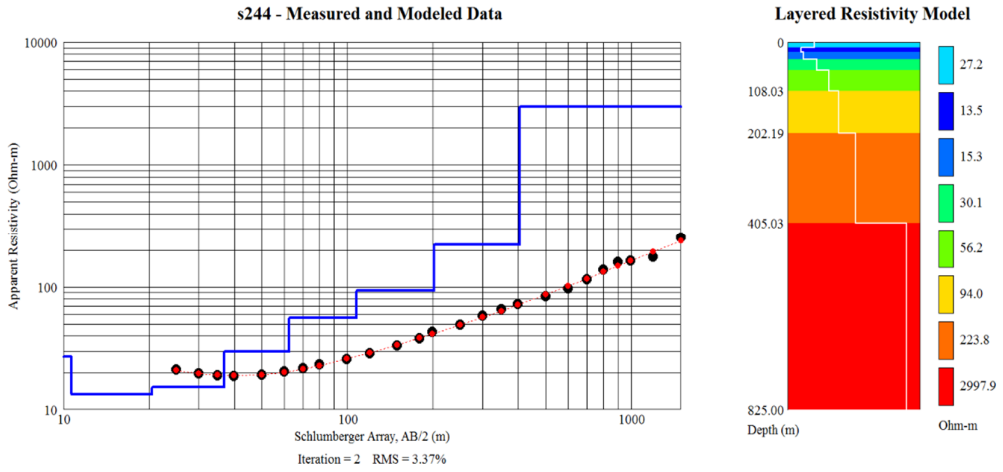
s244 - Measured and Modeled Data
Apparent Resistivity (Ohm-m)
10000
1000
100
10
10
100
1000
Schlumberger Array, AB/2 (m)
Iteration = 2 RMS = 3.37%
Layered Resistivity Model
0
108.03
202.19
405.03
825.00
Depth (m)
27.2
13.5
15.3
30.1
56.2
94.0
223.8
2997.9
Ohm-m

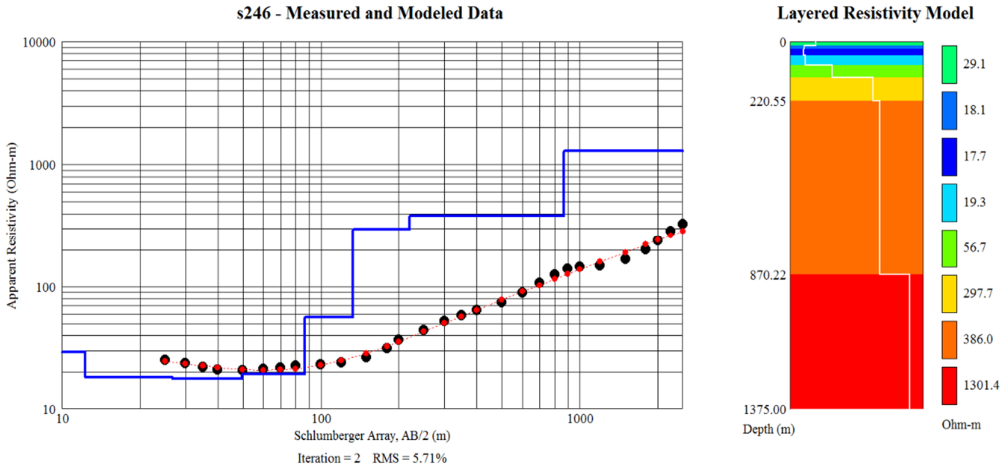
s246 - Measured and Modeled Data
Apparent Resistivity (Ohm-m)
10000
1000
100
10
10
100
1000
Schlumberger Array, AB/2 (m)
Iteration = 2 RMS = 5.71%
Layered Resistivity Model
0
220.55
870.22
1375.00
Depth (m)
29.1
18.1
17.7
19.3
56.7
297.7
386.0
1301.4
Ohm-m

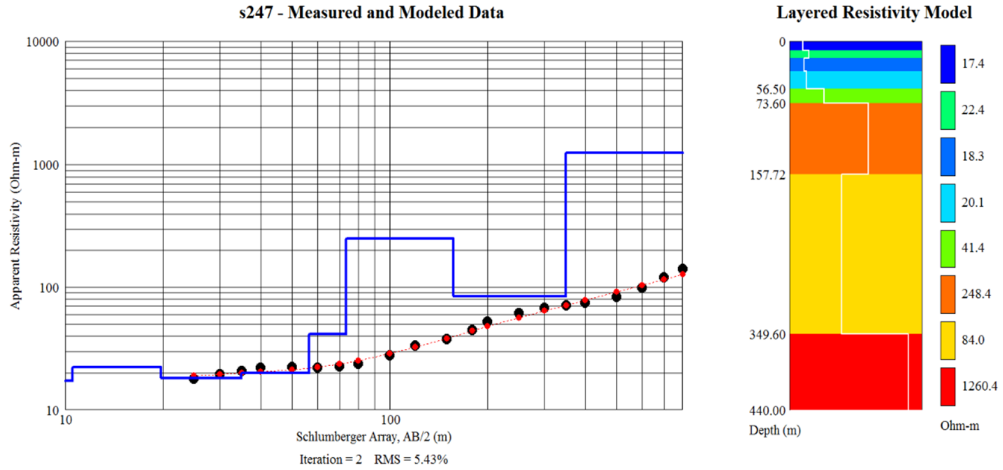
s247 - Measured and Modeled Data
Apparent Resistivity (Ohm-m)
10000
1000
100
10
10
100
Schlumberger Array, AB/2 (m)
Iteration = 2 RMS = 5.43%
Layered Resistivity Model
0
56.50
73.60
157.72
349.60
440.00
Depth (m)
17.4
22.4
18.3
20.1
41.4
248.4
84.0
1260.4
Ohm-m

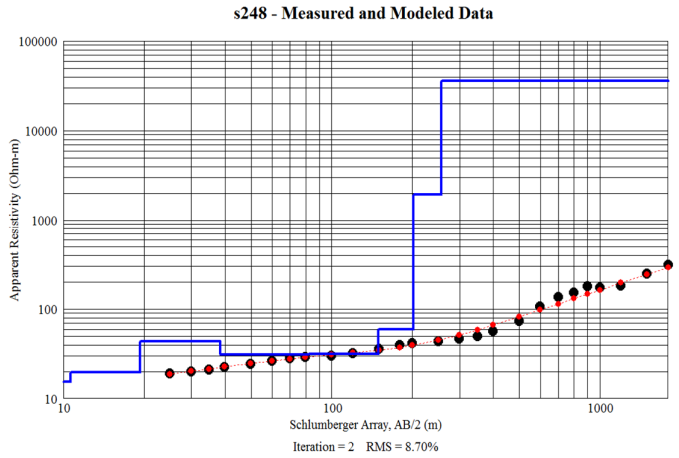
s248 - Measured and Modeled Data
Apparent Resistivity (Ohm-m)
100000
10000
1000
100
10
10
100
1000
Schlumberger Array, AB/2 (m)
Iteration = 2 RMS = 8.70%

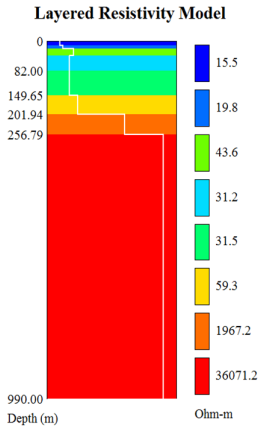
Layered Resistivity Model
0
82.00
149.65
201.94
256.79
990.00
Depth (m)
15.5
19.8
43.6
31.2
31.5
59.3
1967.2
36071.2
Ohm-m

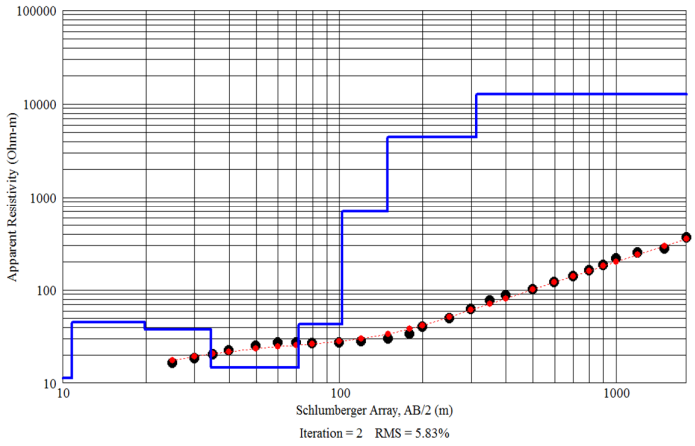
s249 - Measured and Modeled Data
Apparent Resistivity (Ohm-m)
100000
10000
1000
100
10
10
100
1000
Schlumberger Array, AB/2 (m)
Iteration = 2 RMS = 5.83%

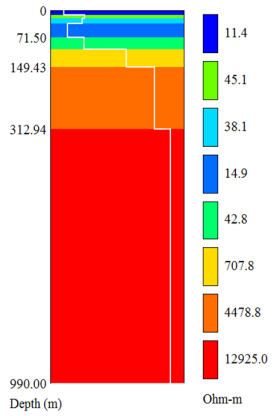
Layered Resistivity Model
0
71.50
149.43
312.94
990.00
Depth (m)
11.4
45.1
38.1
14.9
42.8
707.8
4478.8
12925.0
Ohm-m

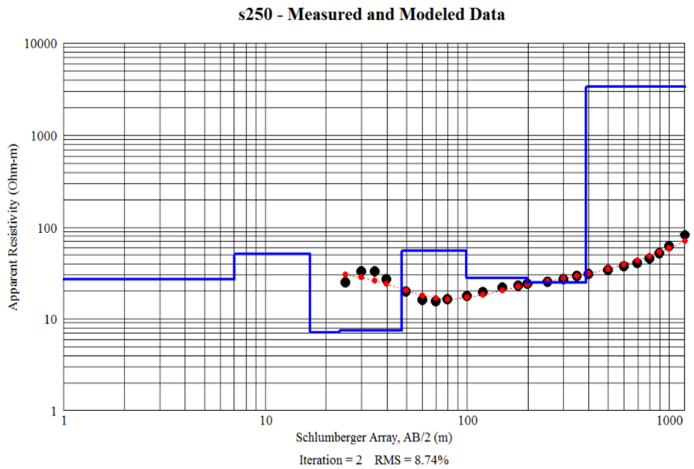
s250 - Measured and Modeled Data
Apparent Resistivity (Ohm-m)
10000
1000
100
10
1
1
10
100
1000
Schlumberger Array, AB/2 (m)
Iteration = 2 RMS = 8.74%

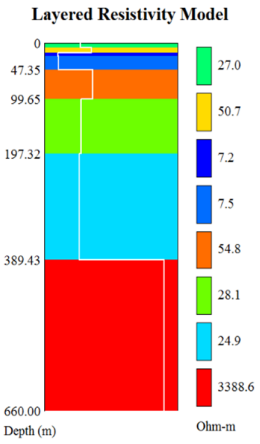
Layered Resistivity Model
0
47.35
99.65
197.32
389.43
660.00
Depth (m)
27.0
50.7
7.2
7.5
54.8
28.1
24.9
3388.6
Ohm-m

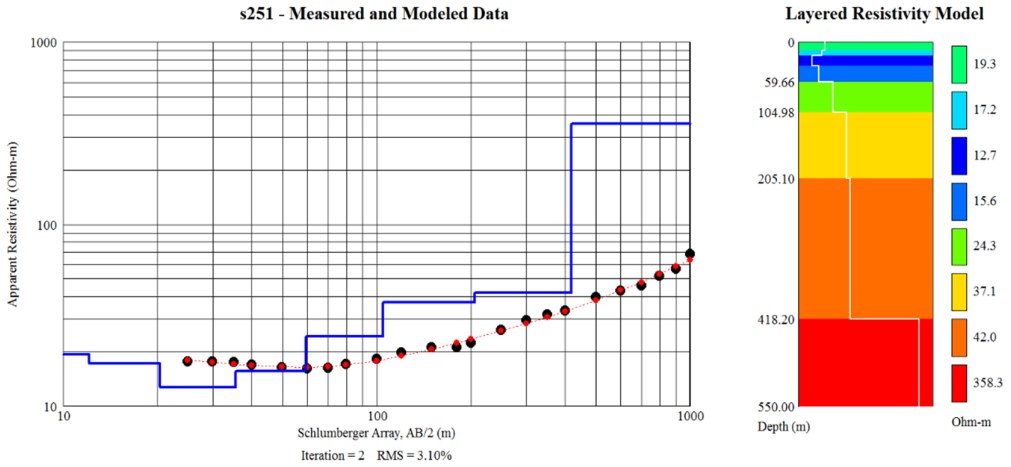
s251 - Measured and Modeled Data
Apparent Resistivity (Ohm-m)
1000
100
10
10
100
1000
Schlumberger Array, AB/2 (m)
Iteration = 2 RMS = 3.10%
Layered Resistivity Model
0
59.66
104.98
205.10
418.20
550.00
Depth (m)
19.3
17.2
12.7
15.6
24.3
37.1
42.0
358.3
Ohm-m

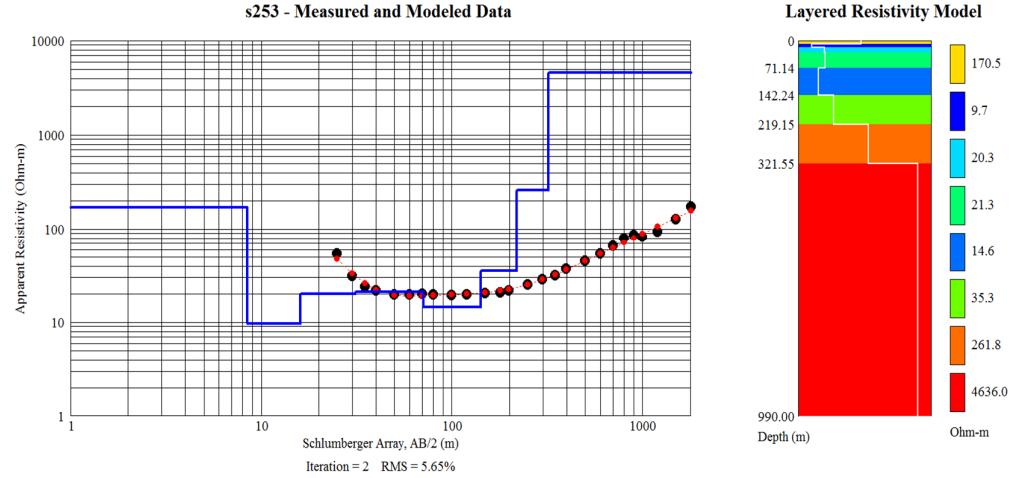
s253 - Measured and Modeled Data
Apparent Resistivity (Ohm-m)
10000
1000
100
10
1
1
10
100
1000
Schlumberger Array, AB/2 (m)
Iteration = 2 RMS = 5.65%
Layered Resistivity Model
0
71.14
142.24
219.15
321.55
990.00
Depth (m)
170.5
9.7
20.3
21.3
14.6
35.3
261.8
4636.0
Ohm-m

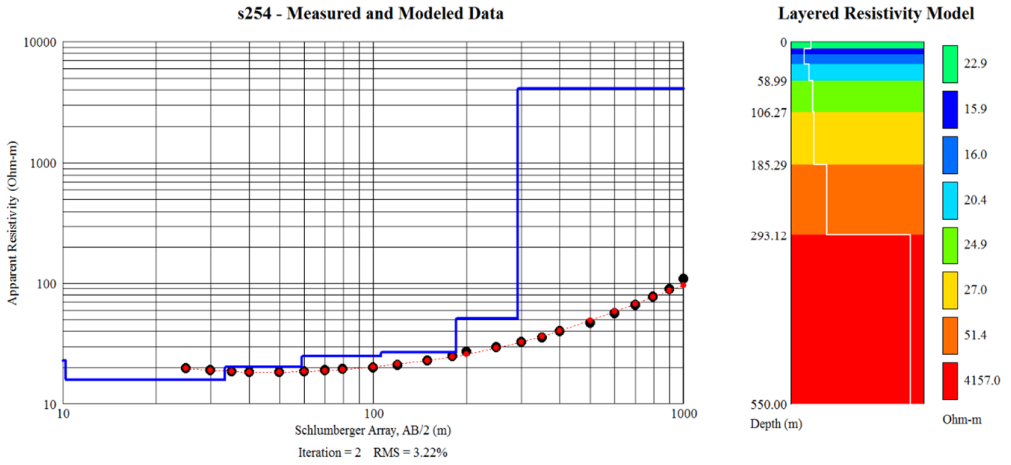
s254 - Measured and Modeled Data
Apparent Resistivity (Ohm-m)
10000
1000
100
10
10
100
1000
Schlumberger Array, AB/2 (m)
Iteration = 2 RMS = 3.22%
Layered Resistivity Model
0
58.99
106.27
185.29
293.12
550.00
Depth (m)
22.9
15.9
16.0
20.4
24.9
27.0
51.4
4157.0
Ohm-m

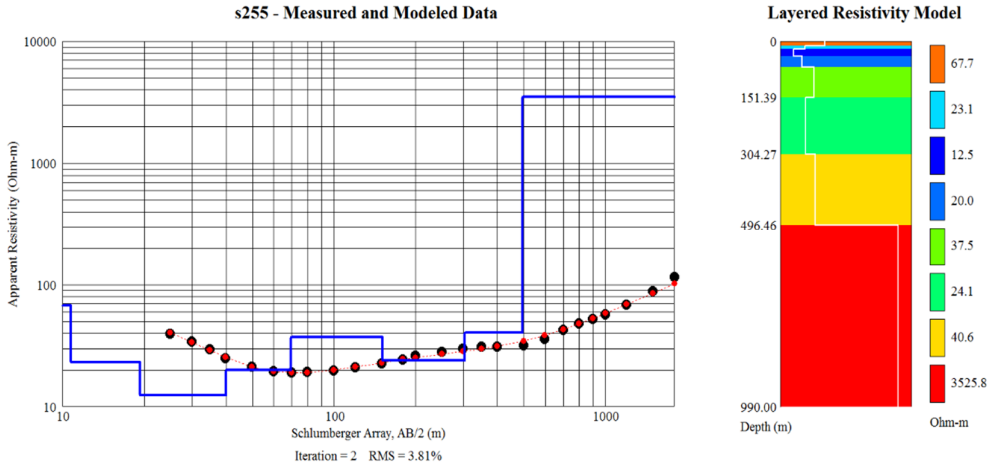
s255 - Measured and Modeled Data
Apparent Resistivity (Ohm-m)
10000
1000
100
10
10
100
1000
Schlumberger Array, AB/2 (m)
Iteration = 2 RMS = 3.81%
Layered Resistivity Model
0
151.39
304.27
496.46
990.00
Depth (m)
67.7
23.1
12.5
20.0
37.5
24.1
40.6
3525.8
Ohm-m

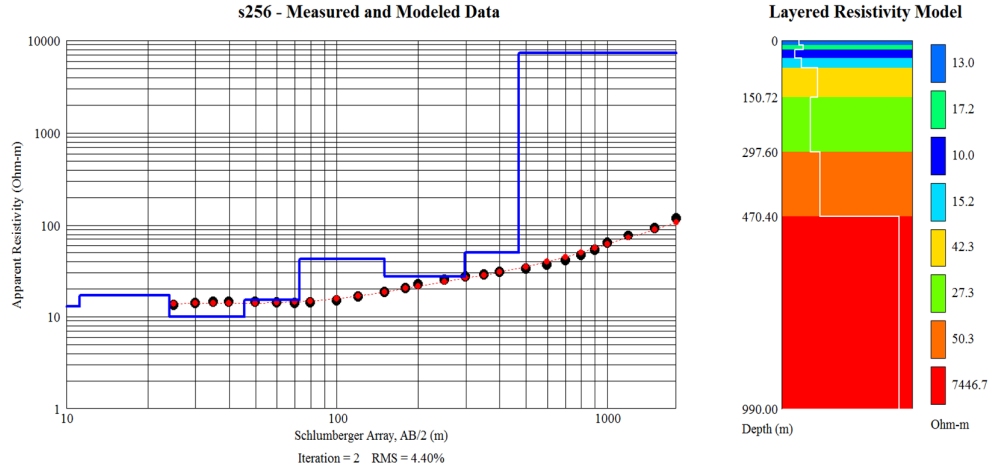
s256 - Measured and Modeled Data
Apparent Resistivity (Ohm-m)
10000
1000
100
10
1
10
100
1000
Schlumberger Array, AB/2 (m)
Iteration = 2 RMS = 4.40%
Layered Resistivity Model
0
150.72
297.60
470.40
990.00
Depth (m)
13.0
17.2
10.0
15.2
42.3
27.3
50.3
7446.7
Ohm-m

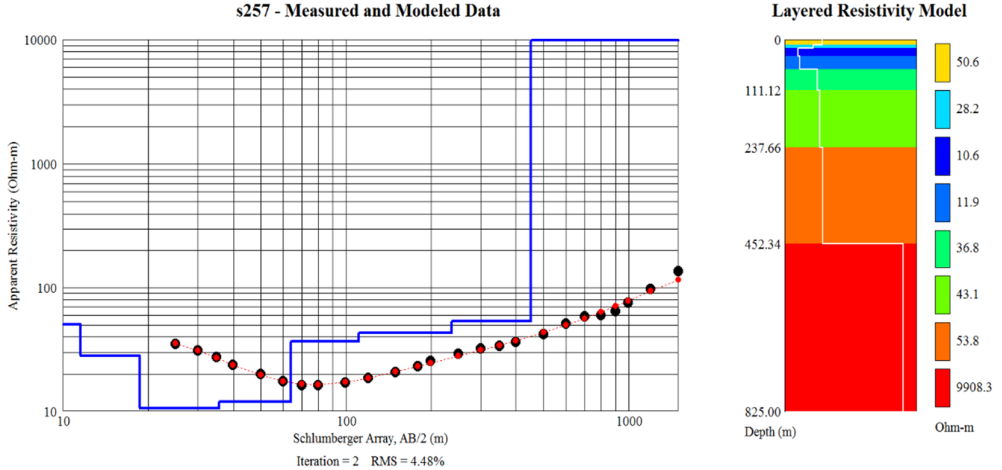
s257 - Measured and Modeled Data
Apparent Resistivity (Ohm-m)
10000
1000
100
10
10
100
1000
Schlumberger Array, AB/2 (m)
Iteration = 2 RMS = 4.48%
Layered Resistivity Model
0
111.12
237.66
452.34
825.00
Depth (m)
50.6
28.2
10.6
11.9
36.8
43.1
53.8
9908.3
Ohm-m

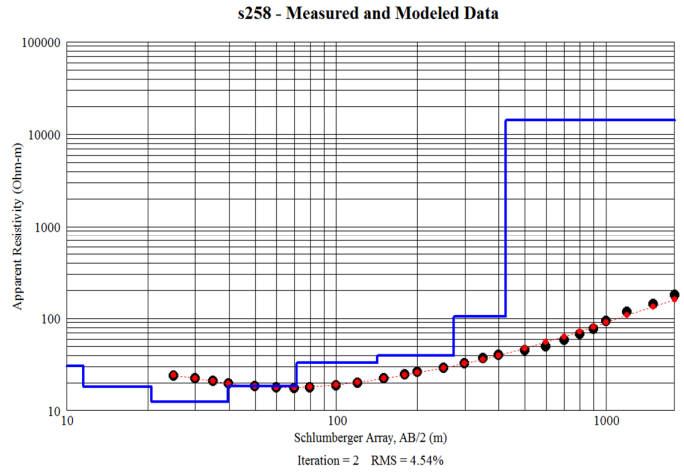
s258 - Measured and Modeled Data
Apparent Resistivity (Ohm-m)
100000
10000
1000
100
10
10
100
1000
Schlumberger Array, AB/2 (m)
Iteration = 2 RMS = 4.54%

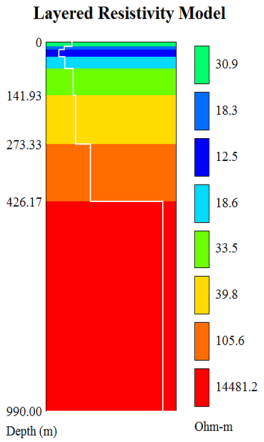
Layered Resistivity Model
0
141.93
273.33
426.17
990.00
Depth (m)
30.9
18.3
12.5
18.6
33.5
39.8
105.6
14481.2
Ohm-m

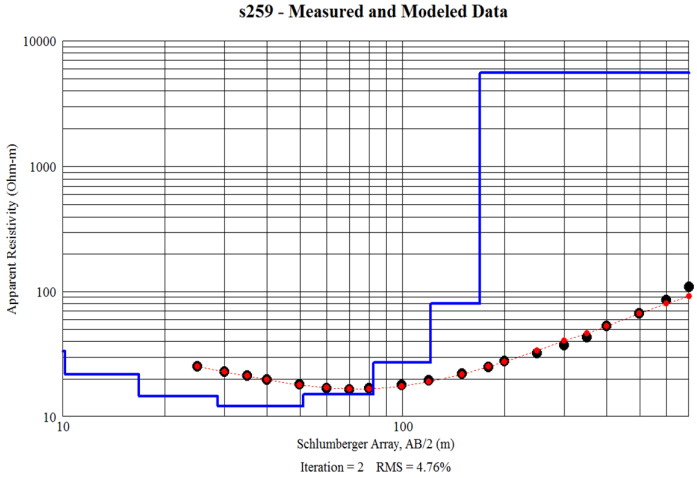
s259 - Measured and Modeled Data
Apparent Resistivity (Ohm-m)
10000
1000
100
10
10
100
Schlumberger Array, AB/2 (m)
Iteration = 2 RMS = 4.76%

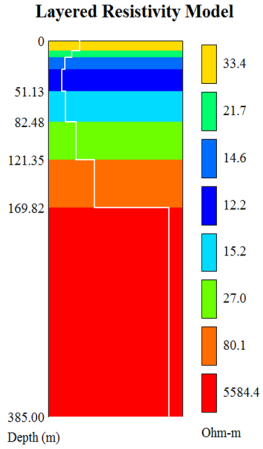
Layered Resistivity Model
0
51.13
82.48
121.35
169.82
385.00
Depth (m)
33.4
21.7
14.6
12.2
15.2
27.0
80.1
5584.4
Ohm-m

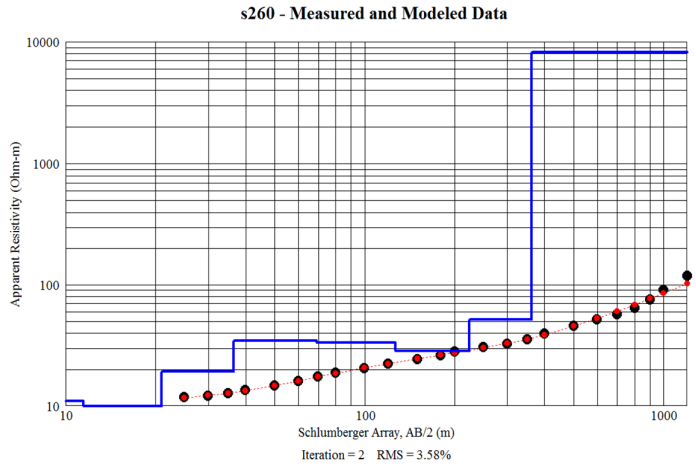
s260 - Measured and Modeled Data
Apparent Resistivity (Ohm-m)
10000
1000
100
10
10
100
1000
Schlumberger Array, AB/2 (m)
Iteration = 2 RMS = 3.58%

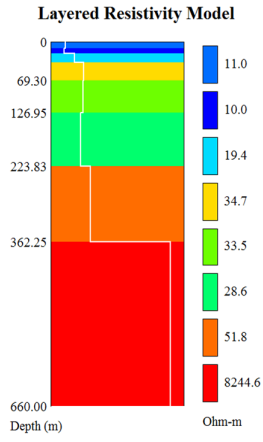
Layered Resistivity Model
0
69.30
126.95
223.83
362.25
660.00
Depth (m)
11.0
10.0
19.4
34.7
33.5
28.6
51.8
8244.6
Ohm-m

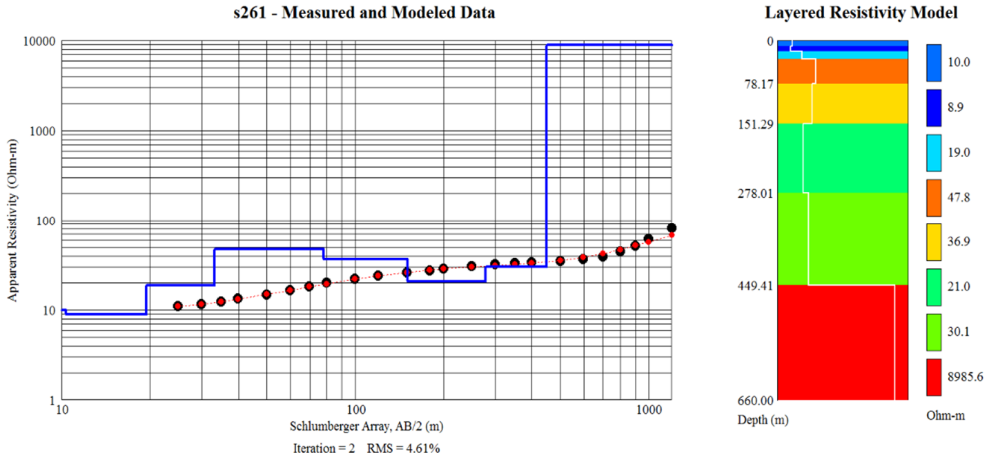
s261 - Measured and Modeled Data
Apparent Resistivity (Ohm-m)
10000
1000
100
10
1
10
100
1000
Schlumberger Array, AB/2 (m)
Iteration = 2 RMS = 4.61%
Layered Resistivity Model
0
78.17
151.29
278.01
449.41
660.00
Depth (m)
10.0
8.9
19.0
47.8
36.9
21.0
30.1
8985.6
Ohm-m

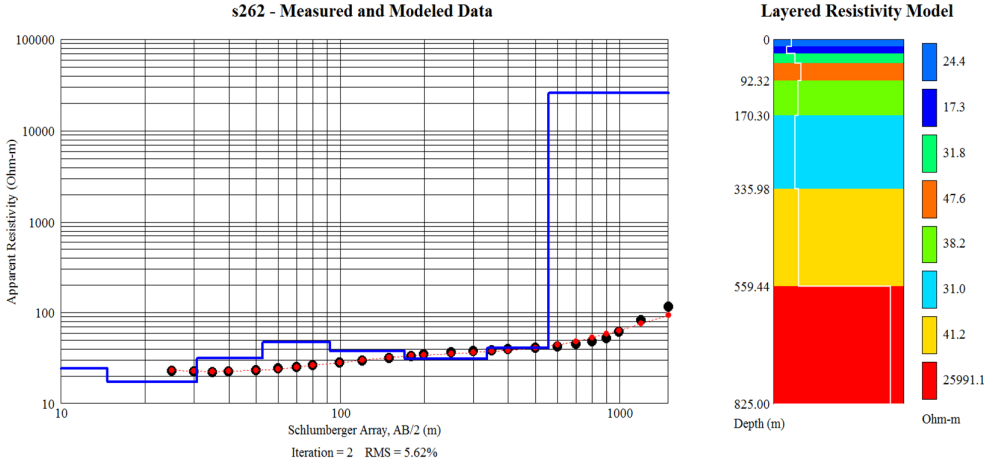
s262 - Measured and Modeled Data
Apparent Resistivity (Ohm-m)
100000
10000
1000
100
10
10
100
1000
Schlumberger Array, AB/2 (m)
Iteration = 2 RMS = 5.62%
Layered Resistivity Model
0
92.32
170.30
335.98
559.44
825.00
Depth (m)
24.4
17.3
31.8
47.6
38.2
31.0
41.2
25991.1
Ohm-m

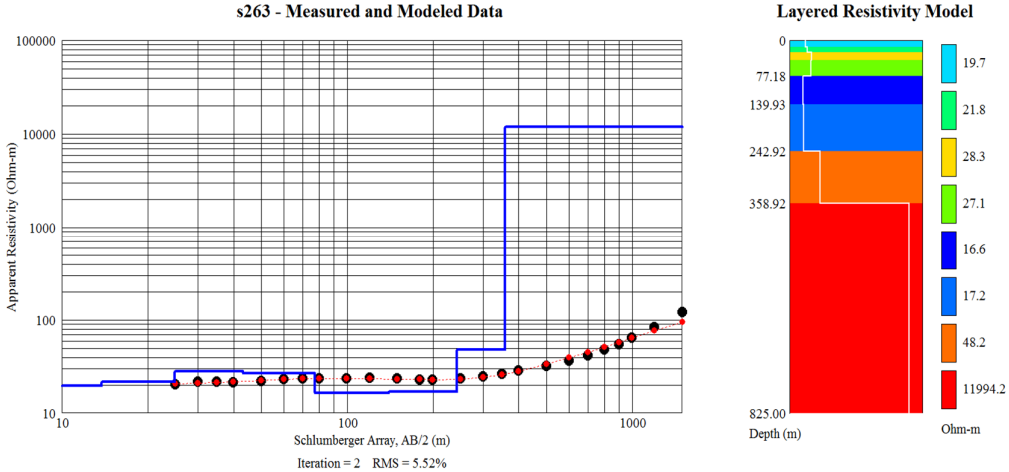
s263 - Measured and Modeled Data
Apparent Resistivity (Ohm-m)
100000
10000
1000
100
10
10
100
1000
Schlumberger Array, AB/2 (m)
Iteration = 2 RMS = 5.52%
Layered Resistivity Model
0
77.18
139.93
242.92
358.92
825.00
Depth (m)
19.7
21.8
28.3
27.1
16.6
17.2
48.2
11994.2
Ohm-m

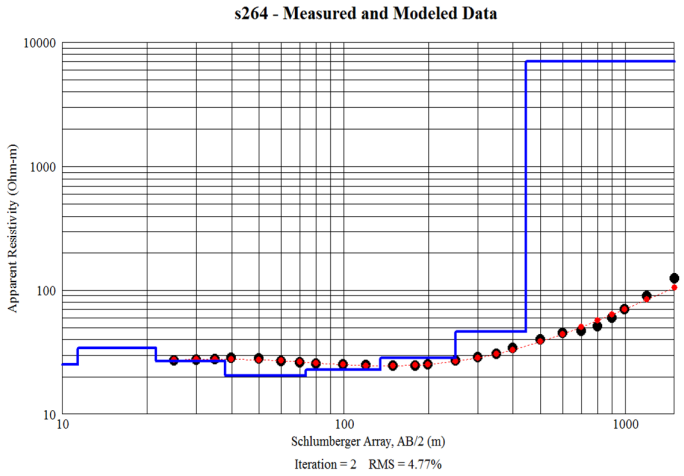
s264 - Measured and Modeled Data
Apparent Resistivity (Ohm-m)
10000
1000
100
10
10
100
1000
Schlumberger Array, AB/2 (m)
Iteration = 2 RMS = 4.77%

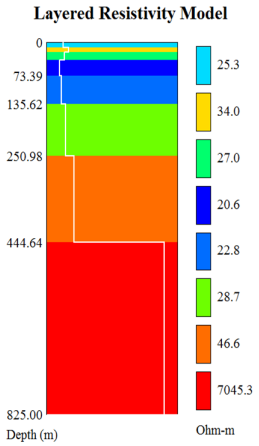
Layered Resistivity Model
0
73.39
135.62
250.98
444.64
825.00
Depth (m)
25.3
34.0
27.0
20.6
22.8
28.7
46.6
7045.3
Ohm-m

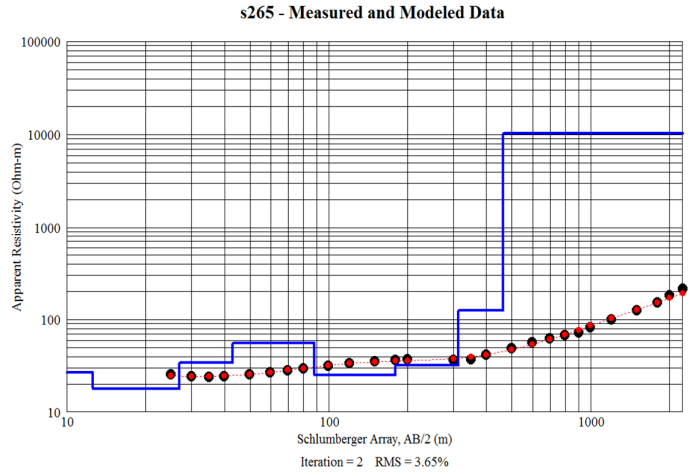
s265 - Measured and Modeled Data
Apparent Resistivity (Ohm-m)
100000
10000
1000
100
10
10
100
1000
Schlumberger Array, AB/2 (m)
Iteration = 2 RMS = 3.65%

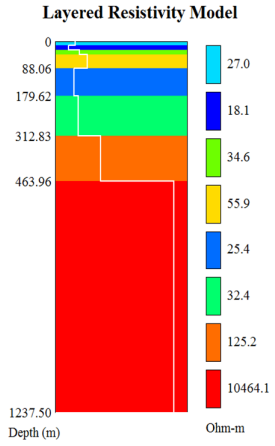
Layered Resistivity Model
0
88.06
179.62
312.83
463.96
1237.50
Depth (m)
27.0
18.1
34.6
55.9
25.4
32.4
125.2
10464.1
Ohm-m

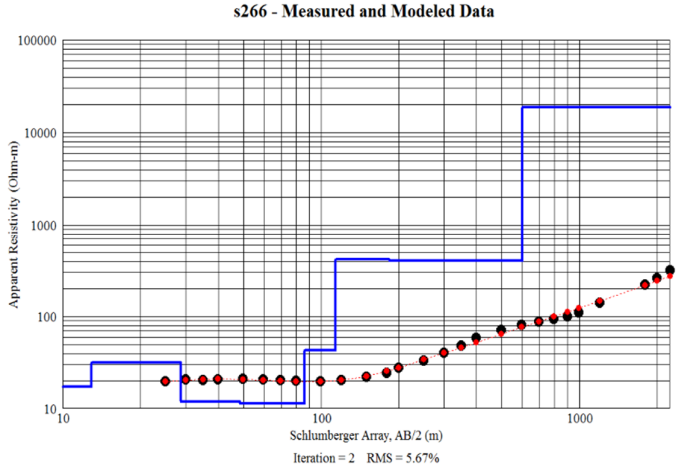
s266 - Measured and Modeled Data
Apparent Resistivity (Ohm-m)
100000
10000
1000
100
10
10
100
1000
Schlumberger Array, AB/2 (m)
Iteration = 2 RMS = 5.67%

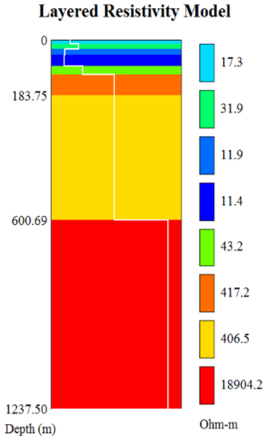
Layered Resistivity Model
0
183.75
600.69
1237.50
Depth (m)
17.3
31.9
11.9
11.4
43.2
417.2
406.5
18904.2
Ohm-m

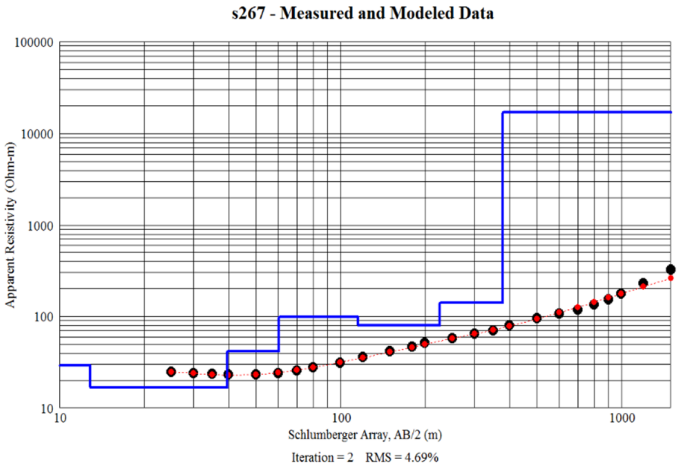
s267 - Measured and Modeled Data
Apparent Resistivity (Ohm-m)
100000
10000
1000
100
10
10
100
1000
Schlumberger Array, AB/2 (m)
Iteration = 2 RMS = 4.69%

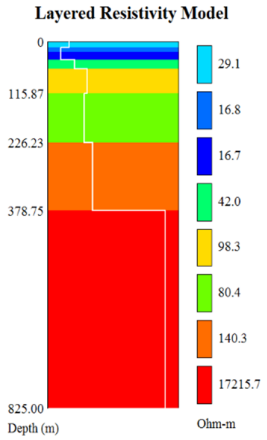
Layered Resistivity Model
0
115.87
226.23
378.75
825.00
Depth (m)
29.1
16.8
16.7
42.0
98.3
80.4
140.3
17215.7
Ohm-m

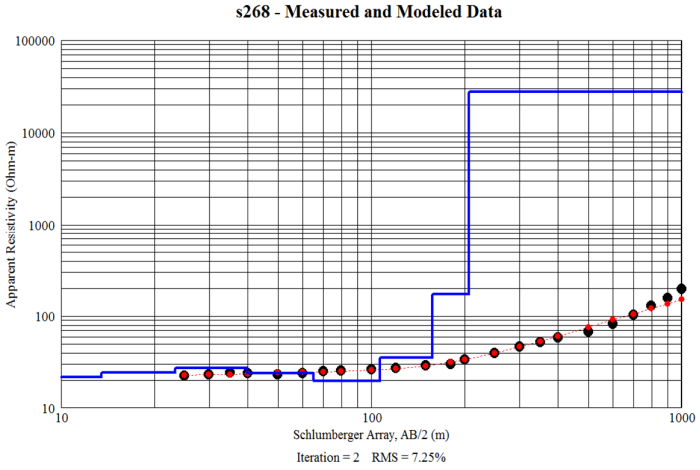
s268 - Measured and Modeled Data
Apparent Resistivity (Ohm-m)
100000
10000
1000
100
10
10
100
1000
Schlumberger Array, AB/2 (m)
Iteration = 2 RMS = 7.25%

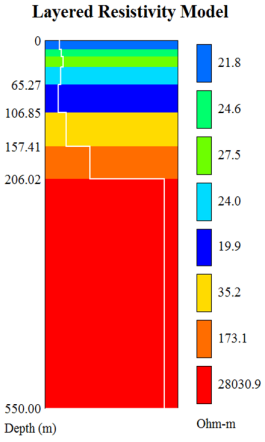
Layered Resistivity Model
0
65.27
106.85
157.41
206.02
550.00
Depth (m)
21.8
24.6
27.5
24.0
19.9
35.2
173.1
28030.9
Ohm-m

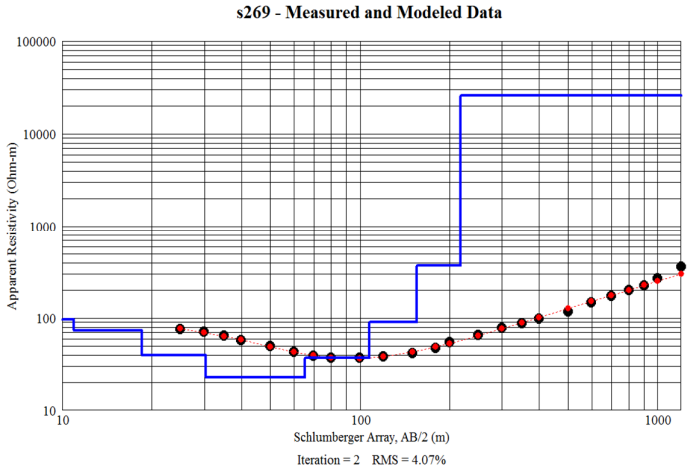
s269 - Measured and Modeled Data
Apparent Resistivity (Ohm-m)
100000
10000
1000
100
10
10
100
1000
Schlumberger Array, AB/2 (m)
Iteration = 2 RMS = 4.07%

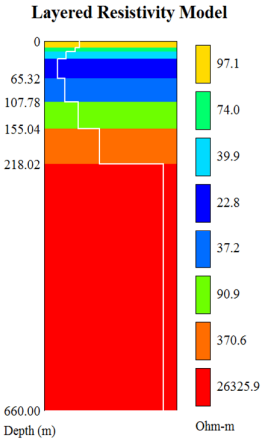
Layered Resistivity Model
0
65.32
107.78
155.04
218.02
660.00
Depth (m)
97.1
74.0
39.9
22.8
37.2
90.9
370.6
26325.9
Ohm-m

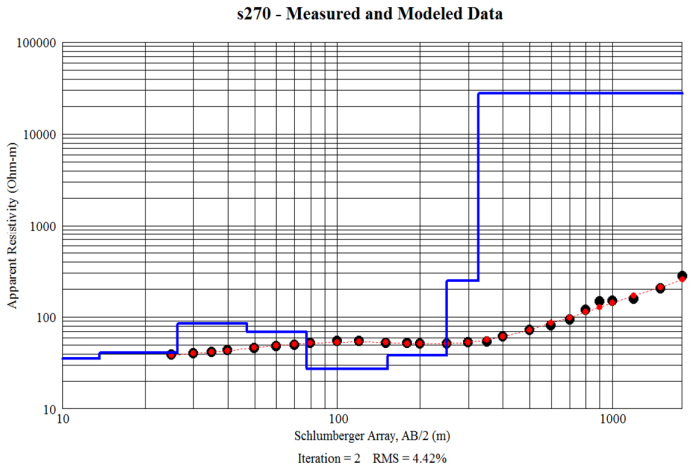
s270 - Measured and Modeled Data
Apparent Resistivity (Ohm-m)
100000
10000
1000
100
10
10
100
1000
Schlumberger Array, AB/2 (m)
Iteration = 2 RMS = 4.42%

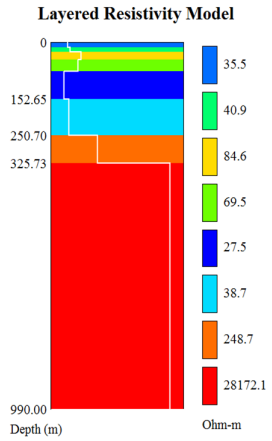
Layered Resistivity Model
0
152.65
250.70
325.73
990.00
Depth (m)
35.5
40.9
84.6
69.5
27.5
38.7
248.7
28172.1
Ohm-m

Group 13

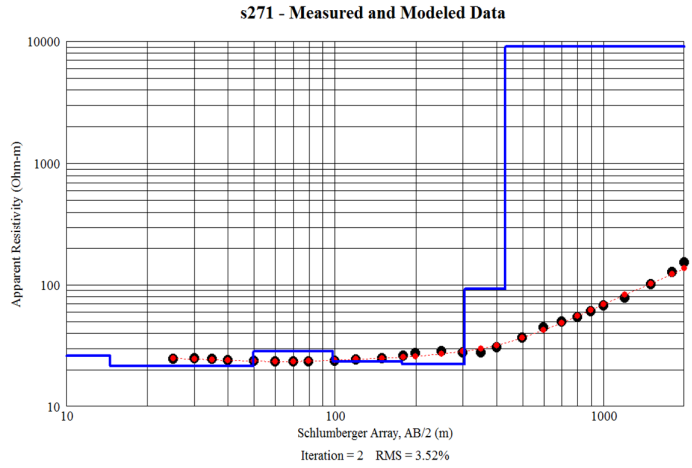
s271 - Measured and Modeled Data
Apparent Resistivity (Ohm-m)
10000
1000
100
10
10
100
1000
Schlumberger Array, AB/2 (m)
Iteration = 2 RMS = 3.52%

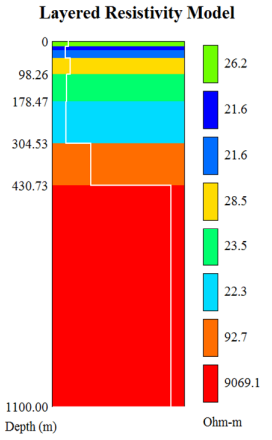
Layered Resistivity Model
0
98.26
178.47
304.53
430.73
1100.00
Depth (m)
26.2
21.6
21.6
28.5
23.5
22.3
92.7
9069.1
Ohm-m

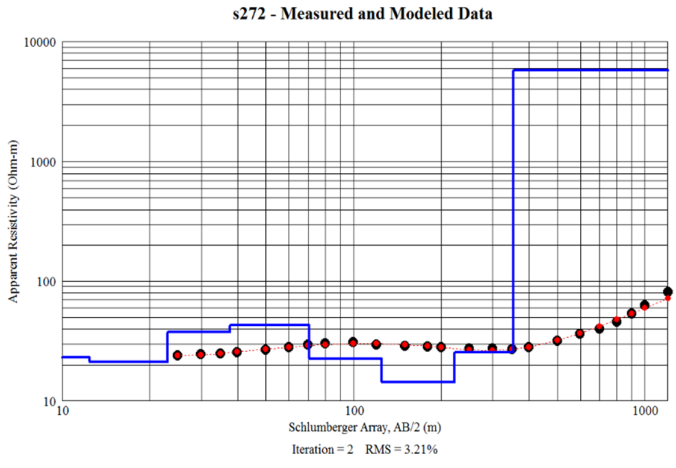
s272 - Measured and Modeled Data
Apparent Resistivity (Ohm-m)
10000
1000
100
10
10
100
1000
Schlumberger Array, AB/2 (m)
Iteration = 2 RMS = 3.21%

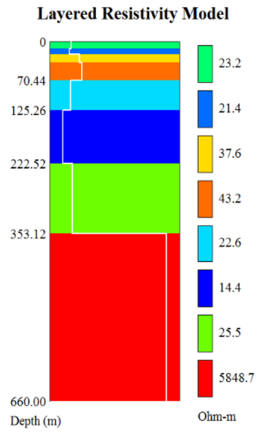
Layered Resistivity Model
0
70.44
125.26
222.52
353.12
660.00
Depth (m)
23.2
21.4
37.6
43.2
22.6
14.4
25.5
5848.7
Ohm-m

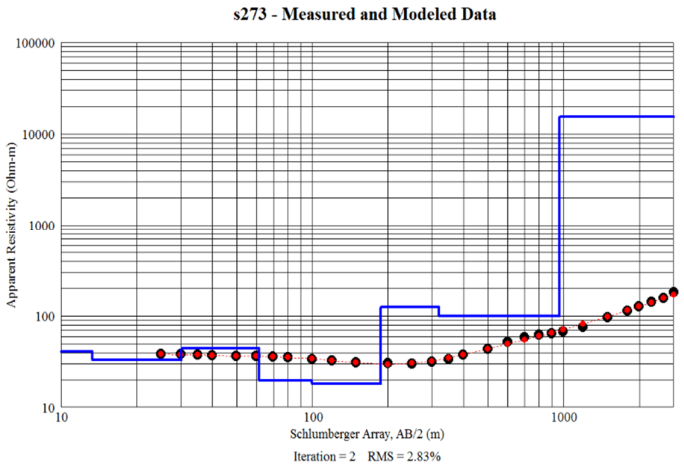
s273 - Measured and Modeled Data
Apparent Resistivity (Ohm-m)
100000
10000
1000
100
10
10
100
1000
Schlumberger Array, AB/2 (m)
Iteration = 2 RMS = 2.83%

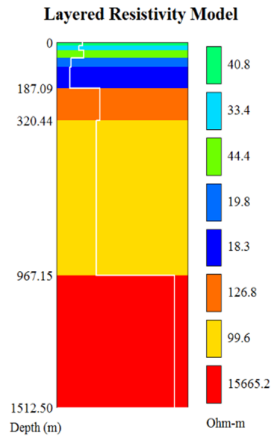
Layered Resistivity Model
0
187.09
320.44
967.15
1512.50
Depth (m)
40.8
33.4
44.4
19.8
18.3
126.8
99.6
15665.2
Ohm-m

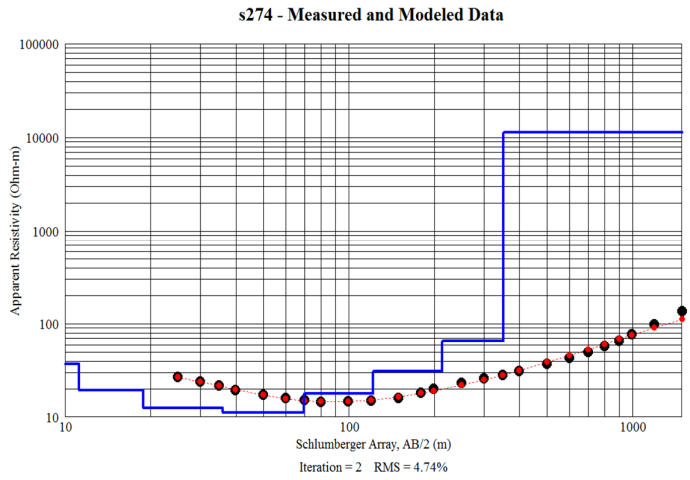
s274 - Measured and Modeled Data
Apparent Resistivity (Ohm-m)
100000
10000
1000
100
10
10
100
1000
Schlumberger Array, AB/2 (m)
Iteration = 2 RMS = 4.74%

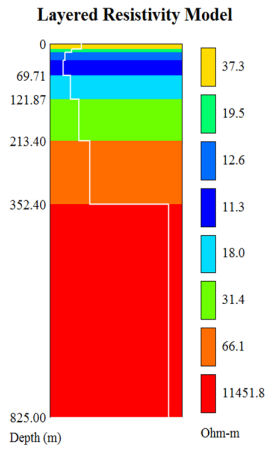
Layered Resistivity Model
0
69.71
121.87
213.40
352.40
825.00
Depth (m)
37.3
19.5
12.6
11.3
18.0
31.4
66.1
11451.8
Ohm-m

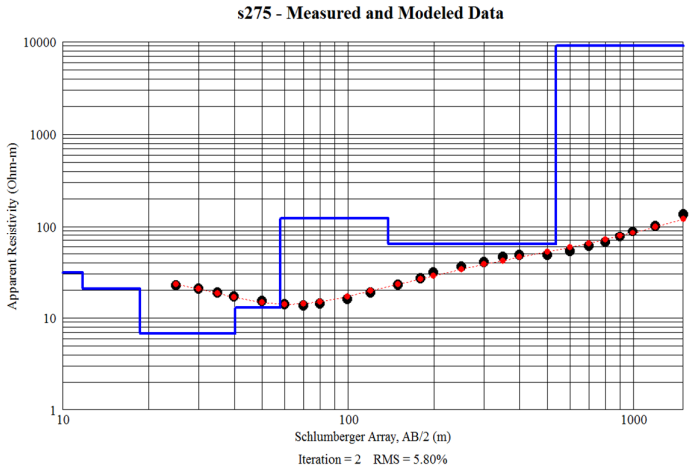
s275 - Measured and Modeled Data
Apparent Resistivity (Ohm-m)
10000
1000
100
10
1
10
100
1000
Schlumberger Array, AB/2 (m)
Iteration = 2 RMS = 5.80%

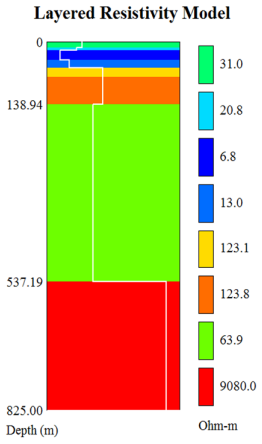
Layered Resistivity Model
0
138.94
537.19
825.00
Depth (m)
31.0
20.8
6.8
13.0
123.1
123.8
63.9
9080.0
Ohm-m

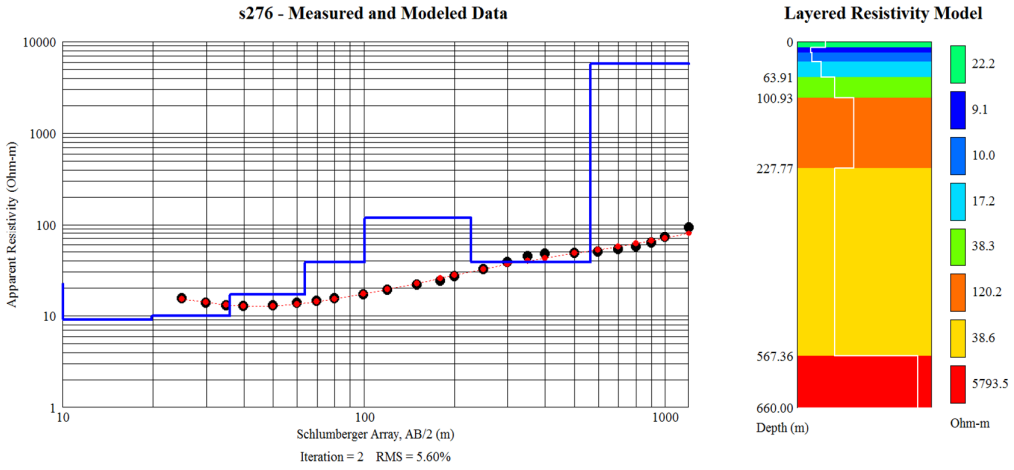
s276 - Measured and Modeled Data
Apparent Resistivity (Ohm-m)
10000
1000
100
10
1
10
100
1000
Schlumberger Array, AB/2 (m)
Iteration = 2 RMS = 5.60%
Layered Resistivity Model
0
63.91
100.93
227.77
567.36
660.00
Depth (m)
22.2
9.1
10.0
17.2
38.3
120.2
38.6
5793.5
Ohm-m

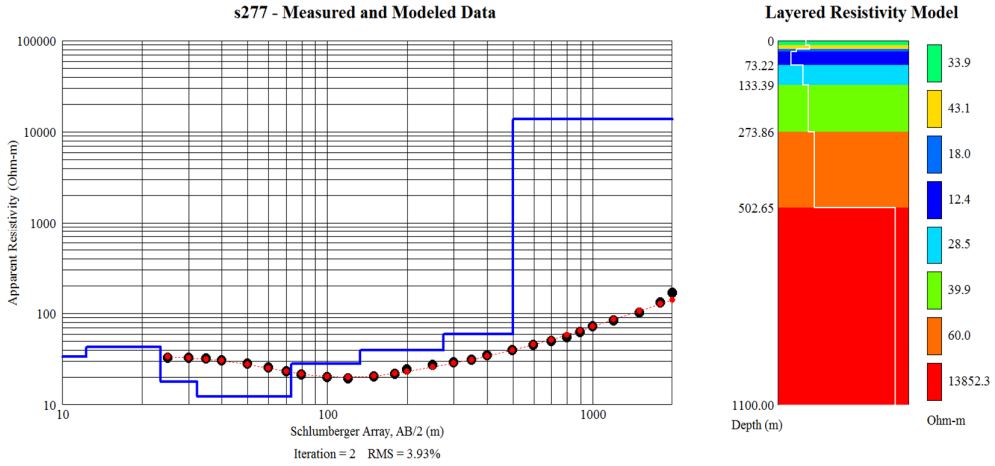
s277 - Measured and Modeled Data
Apparent Resistivity (Ohm-m)
100000
10000
1000
100
10
10
100
1000
Schlumberger Array, AB/2 (m)
Iteration = 2 RMS = 3.93%
Layered Resistivity Model
0
73.22
133.39
273.86
502.65
1100.00
Depth (m)
33.9
43.1
18.0
12.4
28.5
39.9
60.0
13852.3
Ohm-m

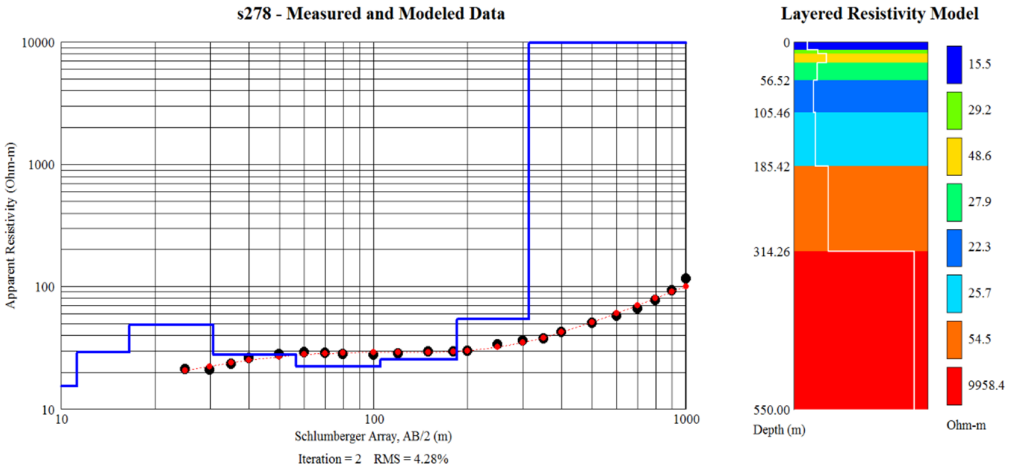
s278 - Measured and Modeled Data
Apparent Resistivity (Ohm-m)
10000
1000
100
10
10
100
1000
Schlumberger Array, AB/2 (m)
Iteration = 2 RMS = 4.28%
Layered Resistivity Model
0
56.52
105.46
185.42
314.26
550.00
Depth (m)
15.5
29.2
48.6
27.9
22.3
25.7
54.5
9958.4
Ohm-m

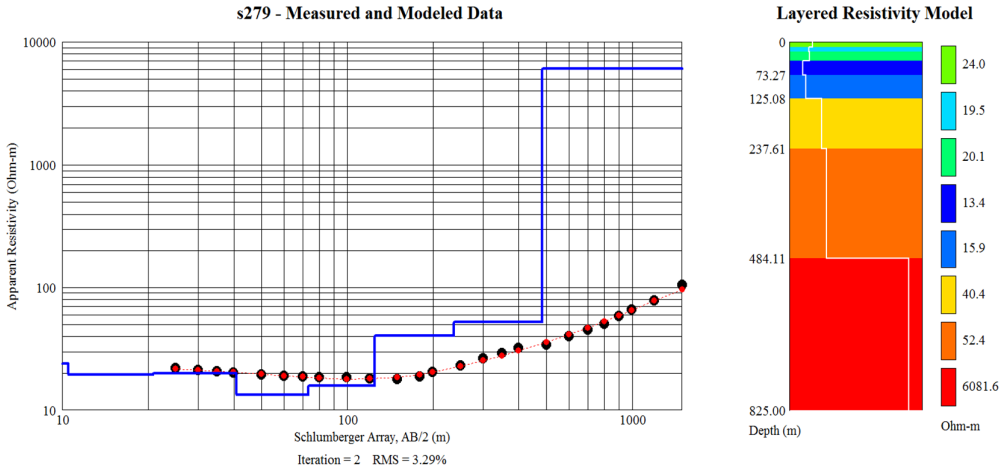
s279 - Measured and Modeled Data
Apparent Resistivity (Ohm-m)
10000
1000
100
10
10
100
1000
Schlumberger Array, AB/2 (m)
Iteration = 2 RMS = 3.29%
Layered Resistivity Model
0
73.27
125.08
237.61
484.11
825.00
Depth (m)
24.0
19.5
20.1
13.4
15.9
40.4
52.4
6081.6
Ohm-m

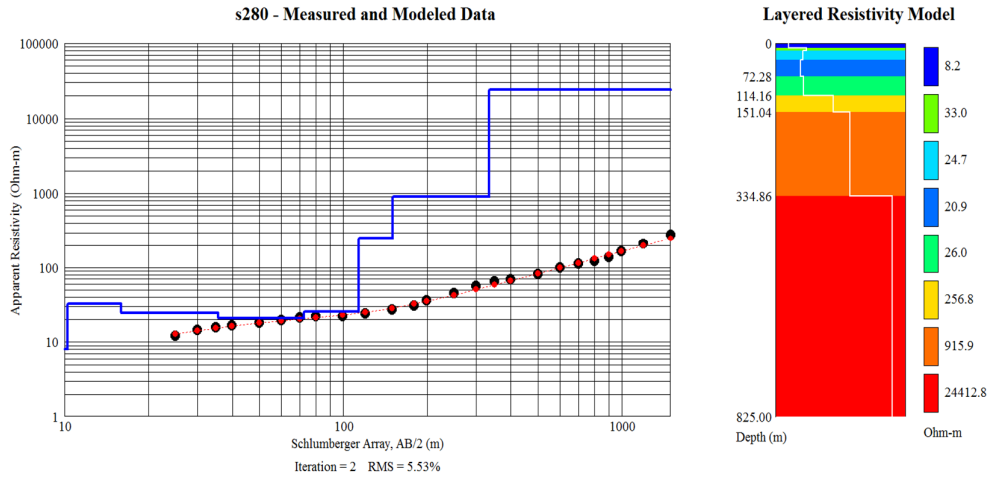
s280 - Measured and Modeled Data
Apparent Resistivity (Ohm-m)
100000
10000
1000
100
10
1
10
100
1000
Schlumberger Array, AB/2 (m)
Iteration = 2 RMS = 5.53%
Layered Resistivity Model
0
72.28
114.16
151.04
334.86
825.00
Depth (m)
8.2
33.0
24.7
20.9
26.0
256.8
915.9
24412.8
Ohm-m

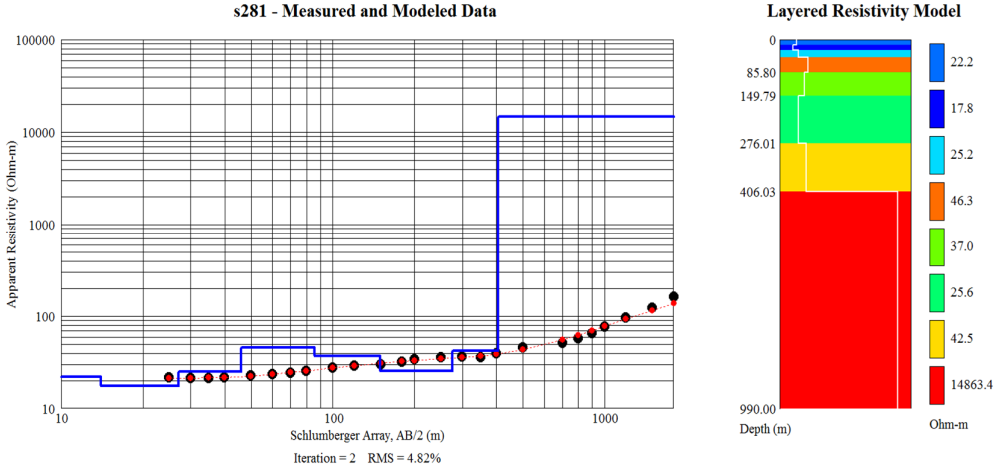
s281 - Measured and Modeled Data
Apparent Resistivity (Ohm-m)
100000
10000
1000
100
10
10
100
1000
Schlumberger Array, AB/2 (m)
Iteration = 2 RMS = 4.82%
Layered Resistivity Model
0
85.80
149.79
276.01
406.03
990.00
Depth (m)
22.2
17.8
25.2
46.3
37.0
25.6
42.5
14863.4
Ohm-m

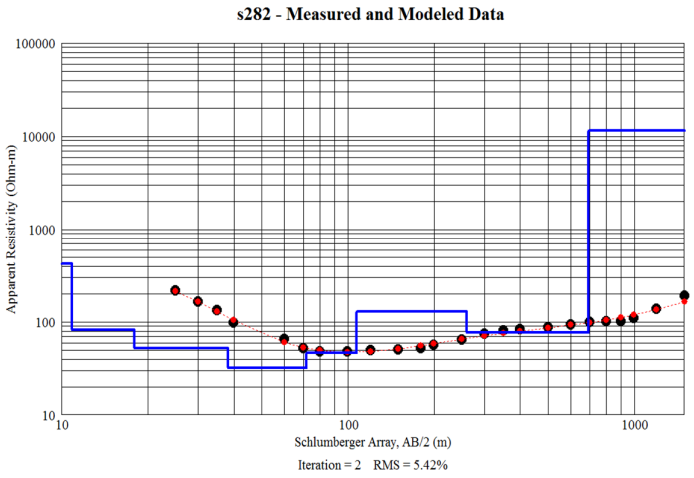
s282 - Measured and Modeled Data
Apparent Resistivity (Ohm-m)
100000
10000
1000
100
10
10
100
1000
Schlumberger Array, AB/2 (m)
Iteration = 2 RMS = 5.42%

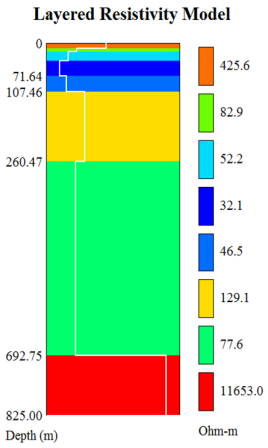
Layered Resistivity Model
0
71.64
107.46
260.47
692.75
825.00
Depth (m)
425.6
82.9
52.2
32.1
46.5
129.1
77.6
11653.0
Ohm-m

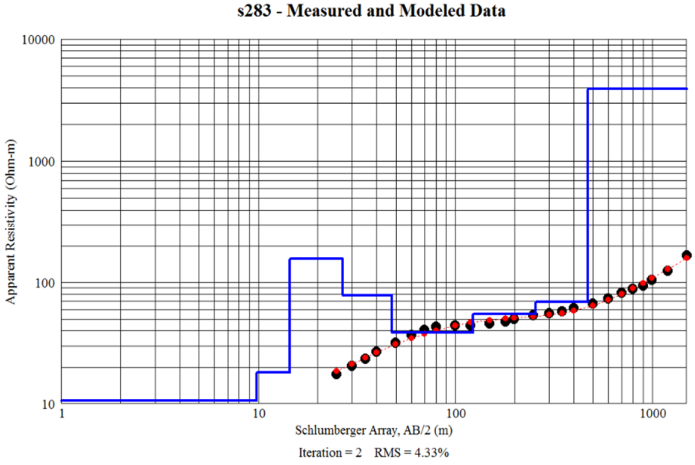
s283 - Measured and Modeled Data
Apparent Resistivity (Ohm-m)
10000
1000
100
10
1
10
100
1000
Schlumberger Array, AB/2 (m)
Iteration = 2 RMS = 4.33%

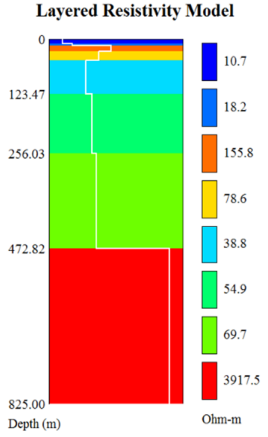
Layered Resistivity Model
0
123.47
256.03
472.82
825.00
Depth (m)
10.7
18.2
155.8
78.6
38.8
54.9
69.7
3917.5
Ohm-m

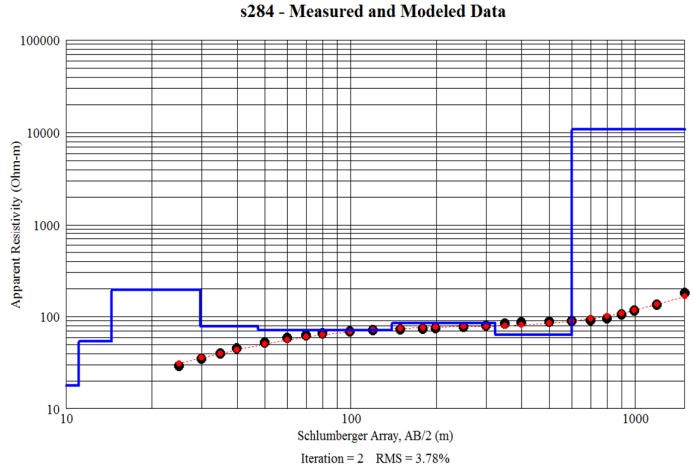
s284 - Measured and Modeled Data
Apparent Resistivity (Ohm-m)
100000
10000
1000
100
10
10
100
1000
Schlumberger Array, AB/2 (m)
Iteration = 2 RMS = 3.78%

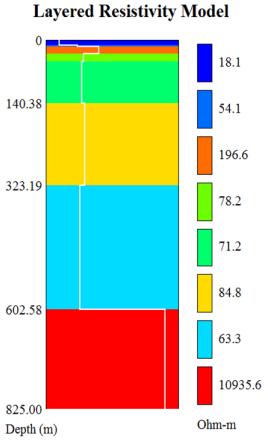
Layered Resistivity Model
0
140.38
323.19
602.58
825.00
Depth (m)
18.1
54.1
196.6
78.2
71.2
84.8
63.3
10935.6
Ohm-m

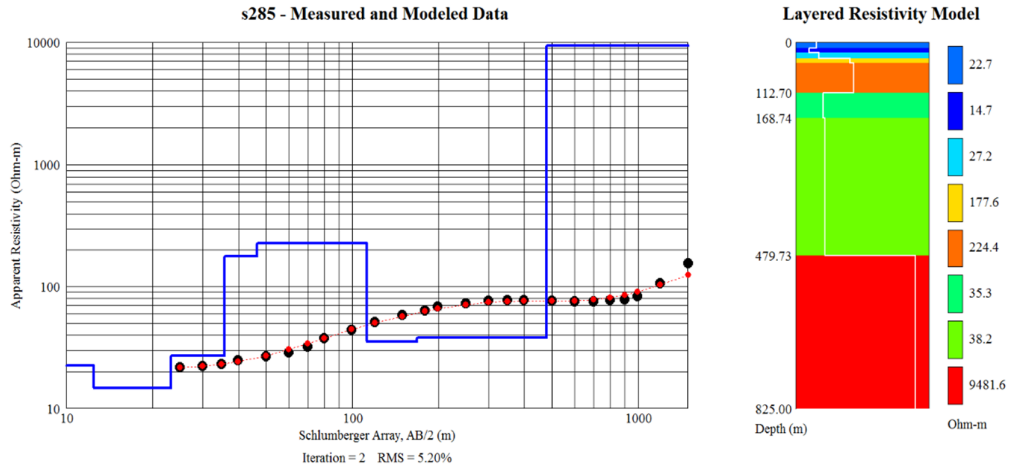
s285 - Measured and Modeled Data
Apparent Resistivity (Ohm-m)
10000
1000
100
10
10
100
1000
Schlumberger Array, AB/2 (m)
Iteration = 2 RMS = 5.20%
Layered Resistivity Model
0
112.70
168.74
479.73
825.00
Depth (m)
22.7
14.7
27.2
177.6
224.4
35.3
38.2
9481.6
Ohm-m

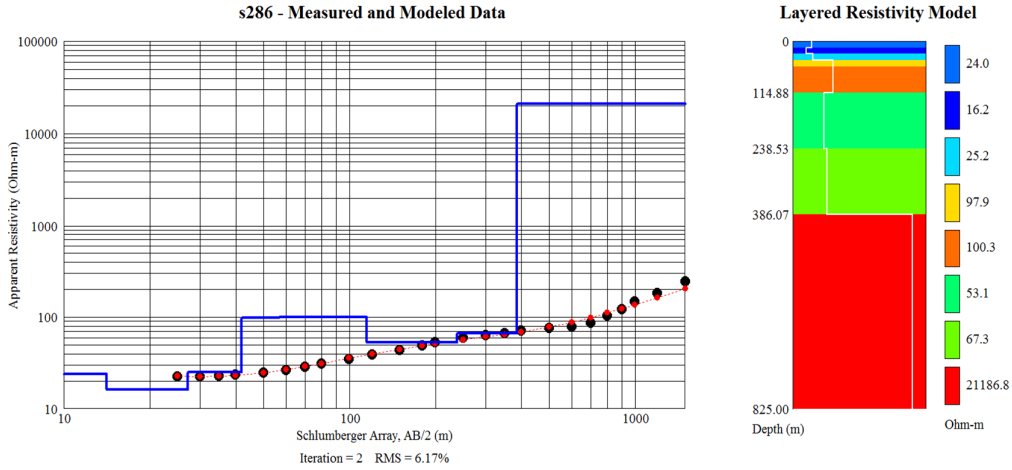
s286 - Measured and Modeled Data
Apparent Resistivity (Ohm-m)
100000
10000
1000
100
10
10
100
1000
Schlumberger Array, AB/2 (m)
Iteration = 2 RMS = 6.17%
Layered Resistivity Model
0
114.88
238.53
386.07
825.00
Depth (m)
24.0
16.2
25.2
97.9
100.3
53.1
67.3
21186.8
Ohm-m

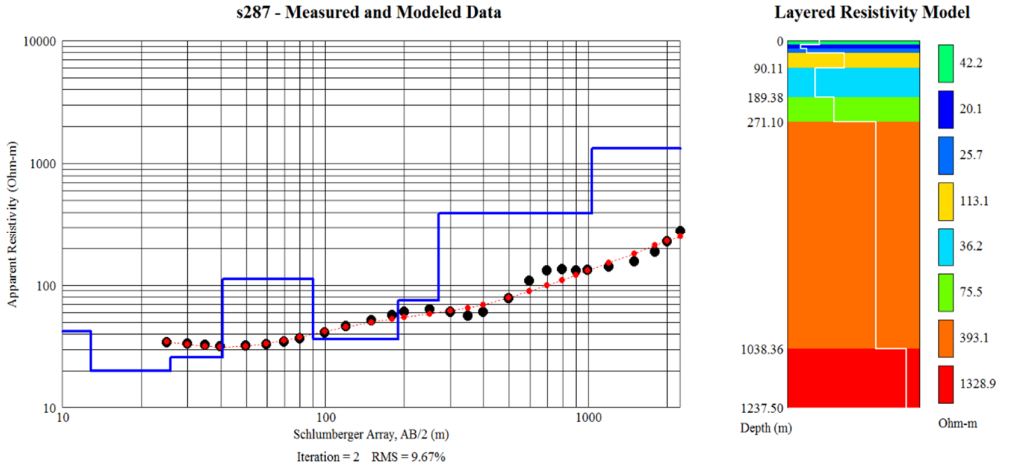
s287 - Measured and Modeled Data
Apparent Resistivity (Ohm-m)
10000
1000
100
10
10
100
1000
Schlumberger Array, AB/2 (m)
Iteration = 2 RMS = 9.67%
Layered Resistivity Model
0
90.11
189.38
271.10
1038.36
1237.50
Depth (m)
42.2
20.1
25.7
113.1
36.2
75.5
393.1
1328.9
Ohm-m

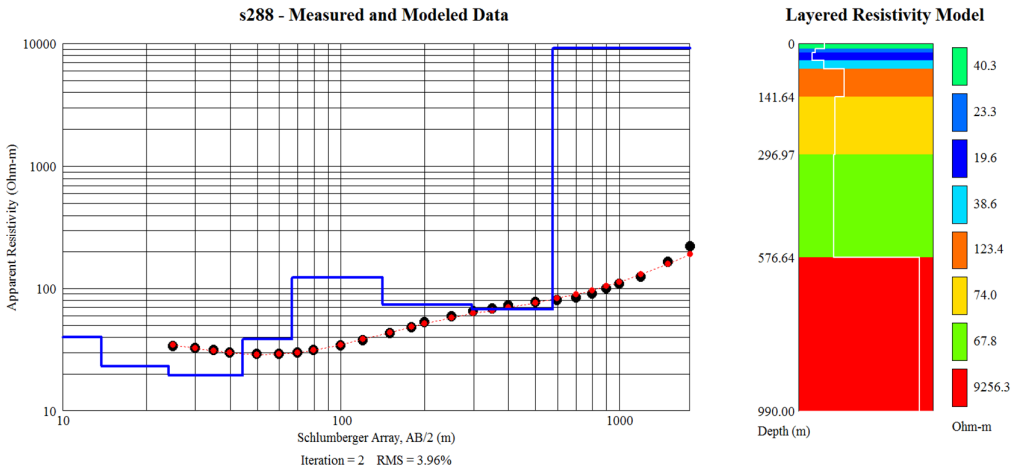
s288 - Measured and Modeled Data
Apparent Resistivity (Ohm-m)
10000
1000
100
10
10
100
1000
Schlumberger Array, AB/2 (m)
Iteration = 2 RMS = 3.96%
Layered Resistivity Model
0
141.64
296.97
576.64
990.00
Depth (m)
40.3
23.3
19.6
38.6
123.4
74.0
67.8
9256.3
Ohm-m

Group 14

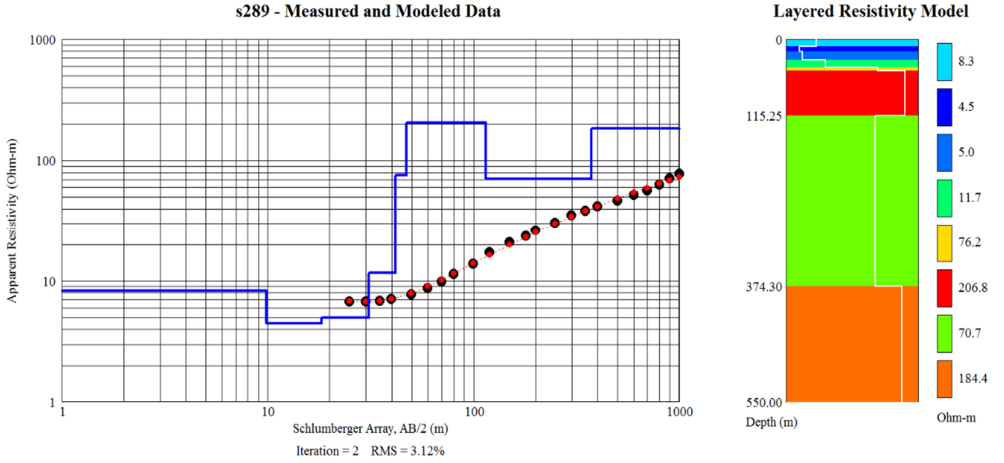
s289 - Measured and Modeled Data
Apparent Resistivity (Ohm-m)
1000
100
10
1
1
10
100
1000
Schlumberger Array, AB/2 (m)
Iteration = 2 RMS = 3.12%
Layered Resistivity Model
0
115.25
374.30
550.00
Depth (m)
8.3
4.5
5.0
11.7
76.2
206.8
70.7
184.4
Ohm-m

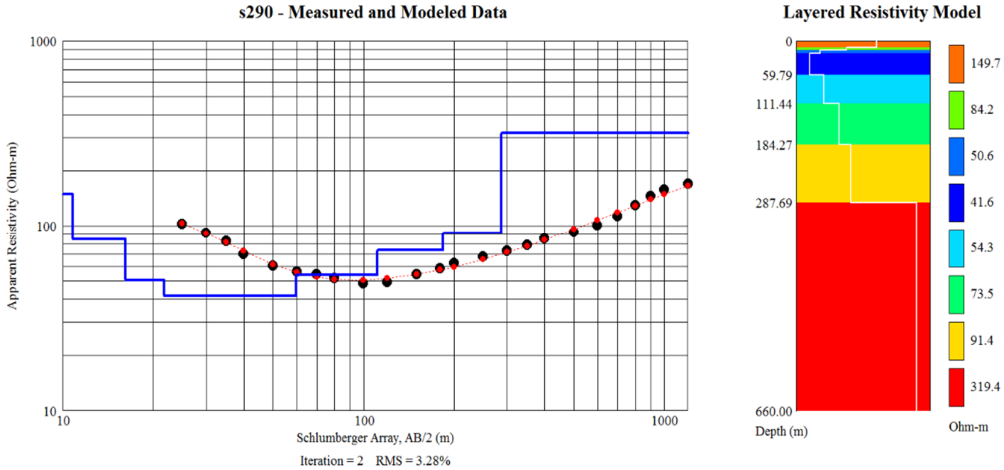
s290 - Measured and Modeled Data
Apparent Resistivity (Ohm-m)
1000
100
10
10
100
1000
Schlumberger Array, AB/2 (m)
Iteration = 2 RMS = 3.28%
Layered Resistivity Model
0
59.79
111.44
184.27
287.69
660.00
Depth (m)
149.7
84.2
50.6
41.6
54.3
73.5
91.4
319.4
Ohm-m

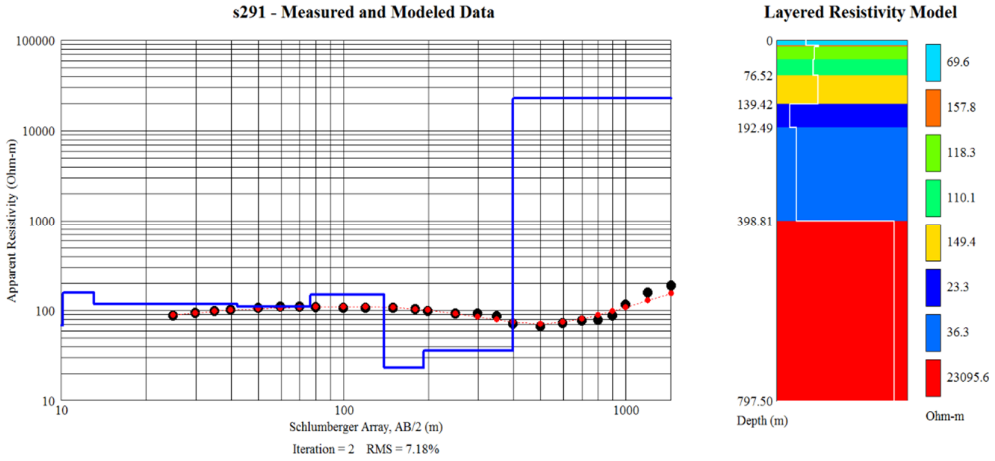
s291 - Measured and Modeled Data
Apparent Resistivity (Ohm-m)
100000
10000
1000
100
10
10
100
1000
Schlumberger Array, AB/2 (m)
Iteration = 2 RMS = 7.18%
Layered Resistivity Model
0
76.52
139.42
192.49
398.81
797.50
Depth (m)
69.6
157.8
118.3
110.1
149.4
23.3
36.3
23095.6
Ohm-m

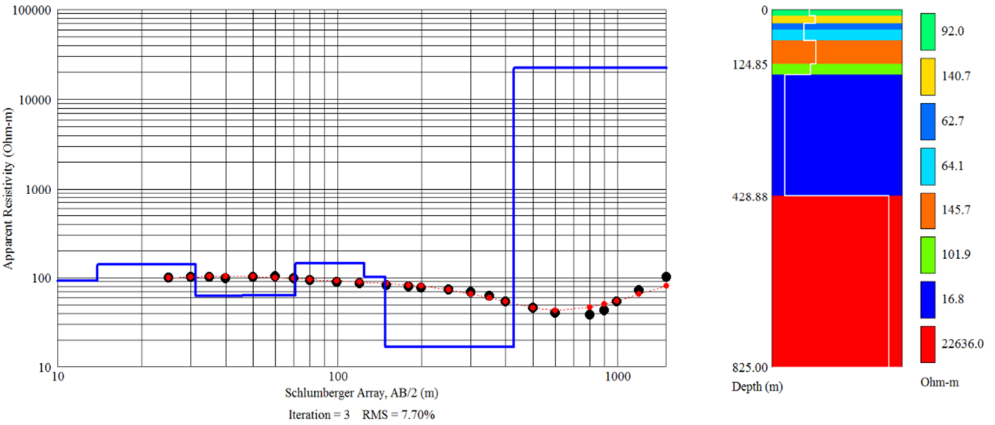
s292 - Measured and Modeled Data
Apparent Resistivity (Ohm-m)
100000
10000
1000
100
10
10
100
1000
Schlumberger Array, AB/2 (m)
Iteration = 3 RMS = 7.70%
Layered Resistivity Model
0
124.85
428.88
825.00
Depth (m)
92.0
140.7
62.7
64.1
145.7
101.9
16.8
22636.0
Ohm-m

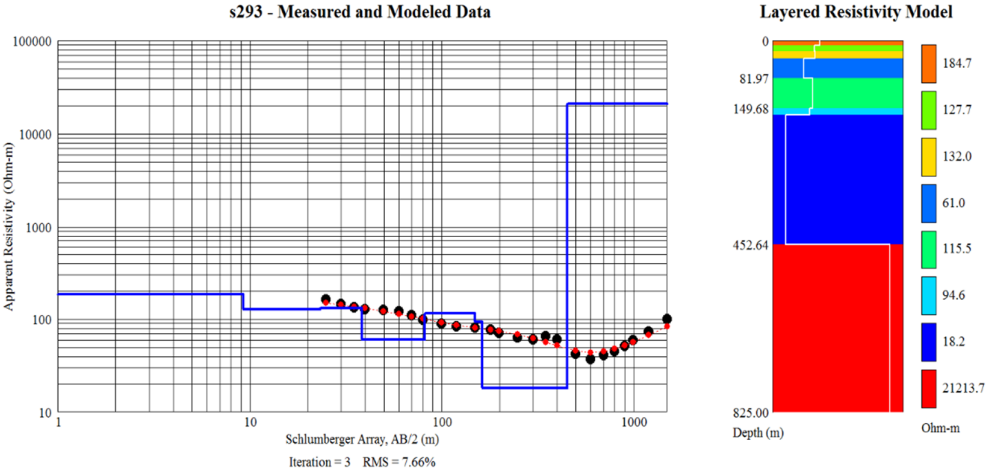
s293 - Measured and Modeled Data
Apparent Resistivity (Ohm-m)
100000
10000
1000
100
10
1
10
100
1000
Schlumberger Array, AB/2 (m)
Iteration = 3 RMS = 7.66%
Layered Resistivity Model
0
81.97
149.68
452.64
825.00
Depth (m)
184.7
127.7
132.0
61.0
115.5
94.6
18.2
21213.7
Ohm-m

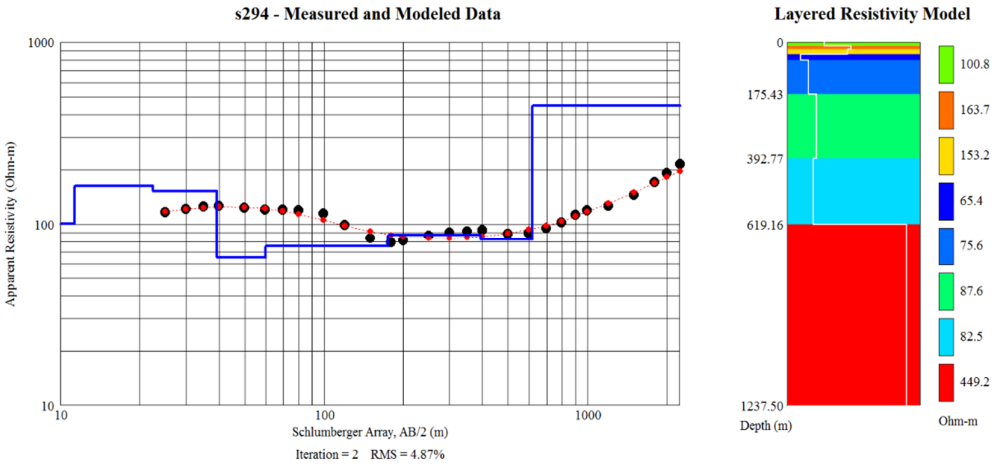
s294 - Measured and Modeled Data
Apparent Resistivity (Ohm-m)
1000
100
10
10
100
1000
Schlumberger Array, AB/2 (m)
Iteration = 2 RMS = 4.87%
Layered Resistivity Model
0
175.43
392.77
619.16
1237.50
Depth (m)
100.8
163.7
153.2
65.4
75.6
87.6
82.5
449.2
Ohm-m

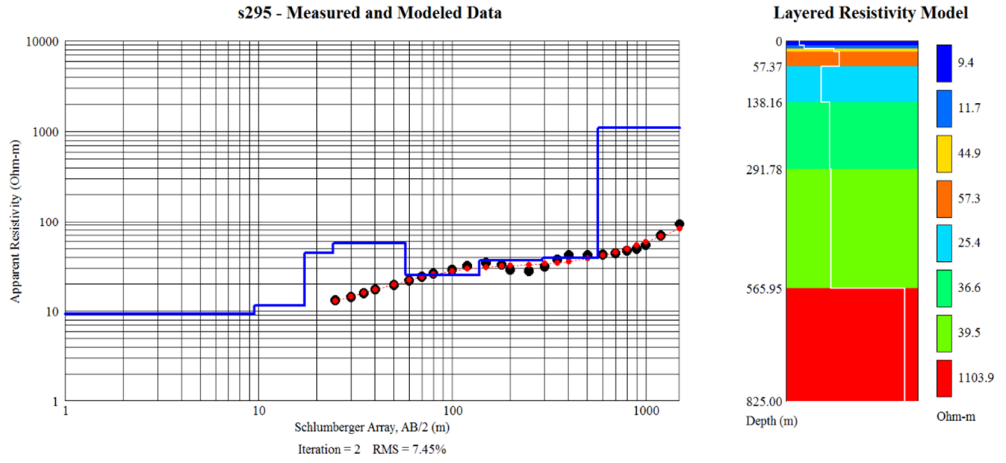
s295 - Measured and Modeled Data
Apparent Resistivity (Ohm-m)
10000
1000
100
10
1
1
10
100
1000
Schlumberger Array, AB/2 (m)
Iteration = 2 RMS = 7.45%
Layered Resistivity Model
0
57.37
138.16
291.78
565.95
825.00
Depth (m)
9.4
11.7
44.9
57.3
25.4
36.6
39.5
1103.9
Ohm-m

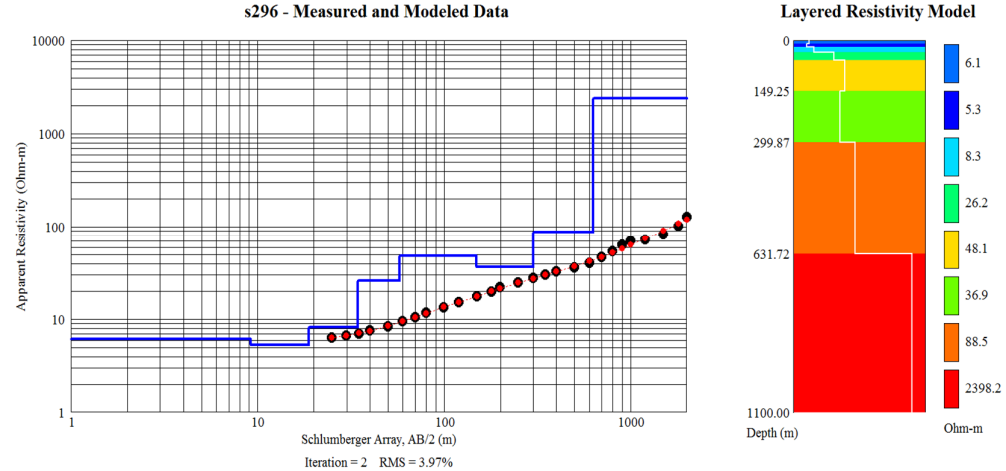
s296 - Measured and Modeled Data
Apparent Resistivity (Ohm-m)
10000
1000
100
10
1
1
10
100
1000
Schlumberger Array, AB/2 (m)
Iteration = 2 RMS = 3.97%
Layered Resistivity Model
0
149.25
299.87
631.72
1100.00
Depth (m)
6.1
5.3
8.3
26.2
48.1
36.9
88.5
2398.2
Ohm-m

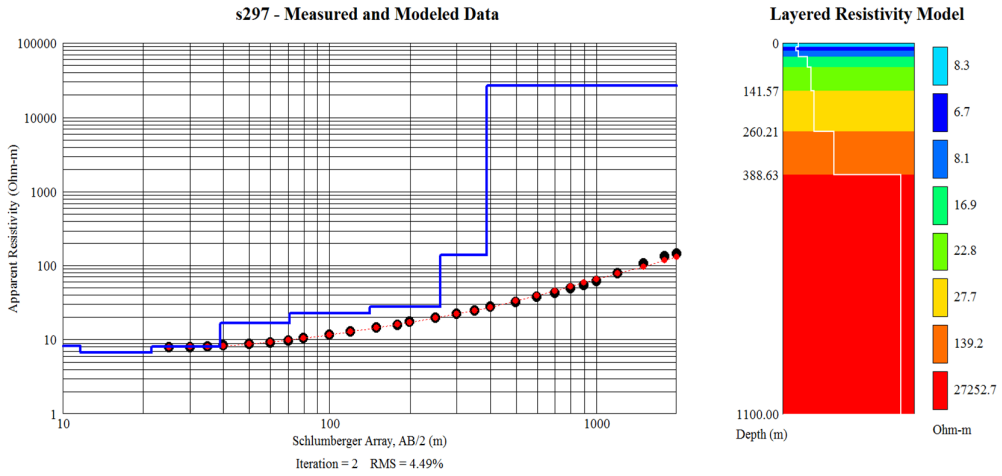
s297 - Measured and Modeled Data
Apparent Resistivity (Ohm-m)
100000
10000
1000
100
10
1
10
100
1000
Schlumberger Array, AB/2 (m)
Iteration = 2 RMS = 4.49%
Layered Resistivity Model
0
141.57
260.21
388.63
1100.00
Depth (m)
8.3
6.7
8.1
16.9
22.8
27.7
139.2
27252.7
Ohm-m

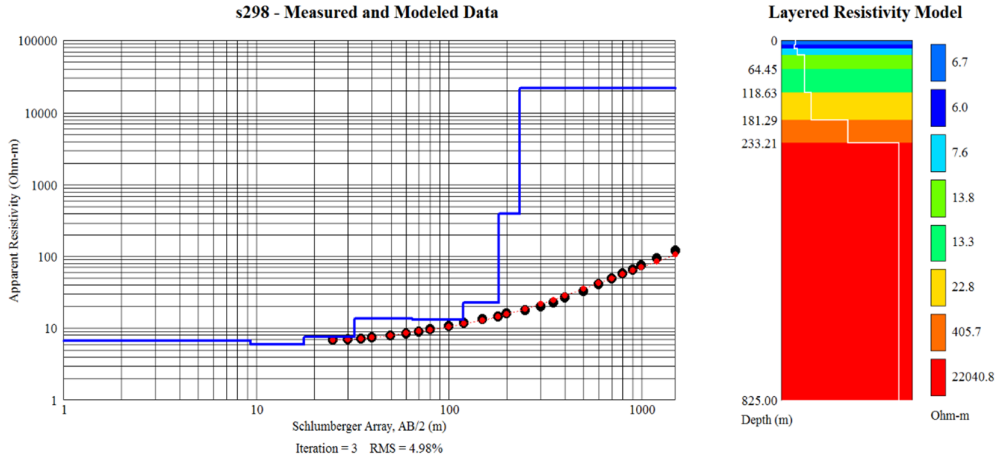
s298 - Measured and Modeled Data
Apparent Resistivity (Ohm-m)
100000
10000
1000
100
10
1
1
10
100
1000
Schlumberger Array, AB/2 (m)
Iteration = 3 RMS = 4.98%
Layered Resistivity Model
0
64.45
118.63
181.29
233.21
825.00
Depth (m)
6.7
6.0
7.6
13.8
13.3
22.8
405.7
22040.8
Ohm-m

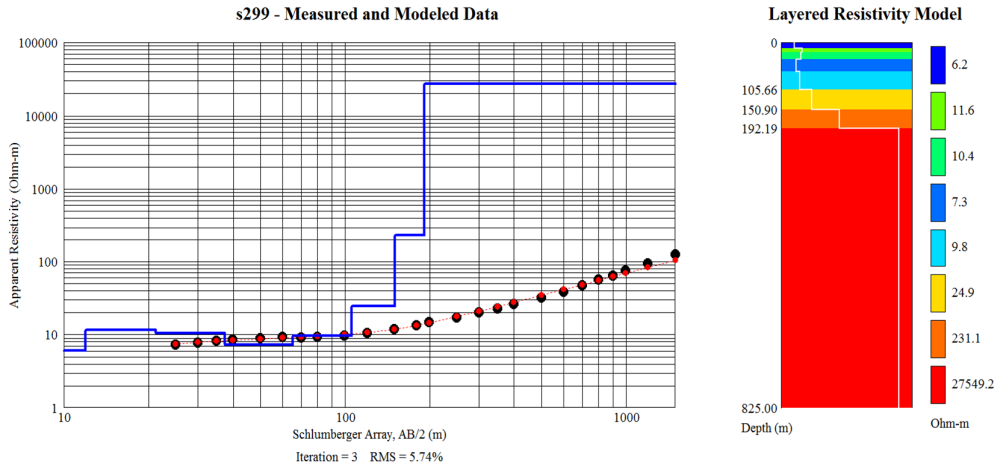
s299 - Measured and Modeled Data
Apparent Resistivity (Ohm-m)
100000
10000
1000
100
10
1
10
100
1000
Schlumberger Array, AB/2 (m)
Iteration = 3 RMS = 5.74%
Layered Resistivity Model
0
105.66
150.90
192.19
825.00
Depth (m)
6.2
11.6
10.4
7.3
9.8
24.9
231.1
27549.2
Ohm-m

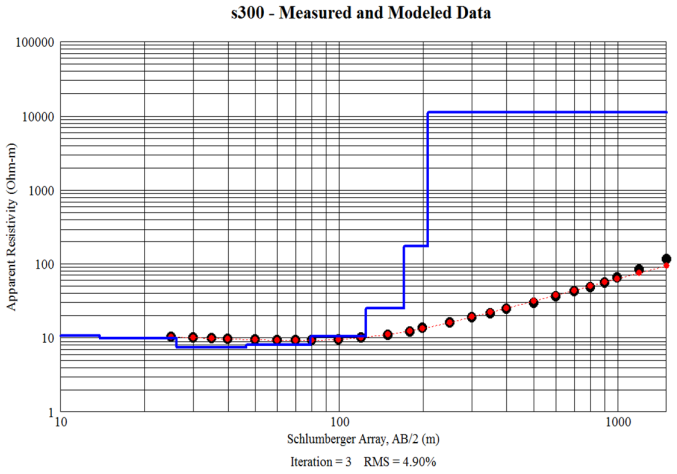
s300 - Measured and Modeled Data
Apparent Resistivity (Ohm-m)
100000
10000
1000
100
10
1
10
100
1000
Schlumberger Array, AB/2 (m)
Iteration = 3 RMS = 4.90%

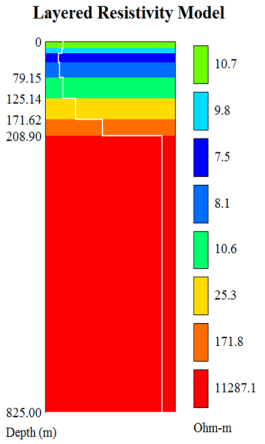
Layered Resistivity Model
0
79.15
125.14
171.62
208.90
825.00
Depth (m)
10.7
9.8
7.5
8.1
10.6
25.3
171.8
11287.1
Ohm-m

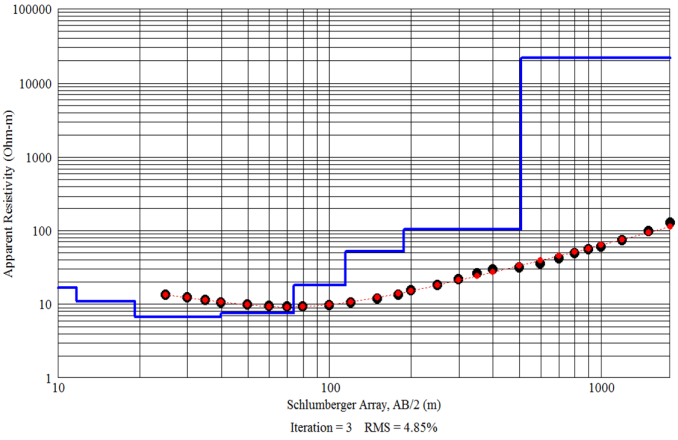
s301 - Measured and Modeled Data
Apparent Resistivity (Ohm-m)
100000
10000
1000
100
10
1
10
100
1000
Schlumberger Array, AB/2 (m)
Iteration = 3 RMS = 4.85%

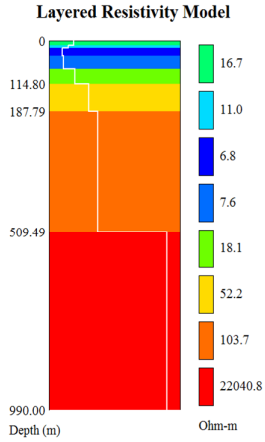
Layered Resistivity Model
0
114.80
187.79
509.49
990.00
Depth (m)
16.7
11.0
6.8
7.6
18.1
52.2
103.7
22040.8
Ohm-m

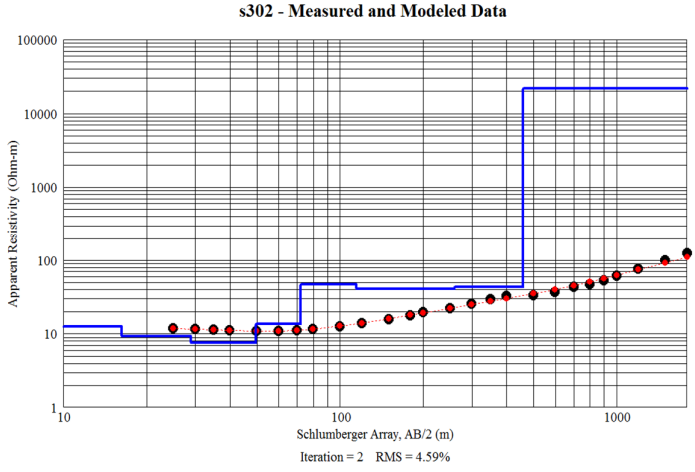
s302 - Measured and Modeled Data
Apparent Resistivity (Ohm-m)
100000
10000
1000
100
10
1
10
100
1000
Schlumberger Array, AB/2 (m)
Iteration = 2 RMS = 4.59%

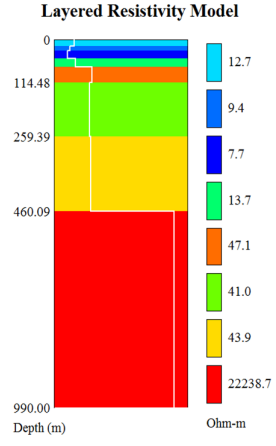
Layered Resistivity Model
0
114.48
259.39
460.09
990.00
Depth (m)
12.7
9.4
7.7
13.7
47.1
41.0
43.9
22238.7
Ohm-m

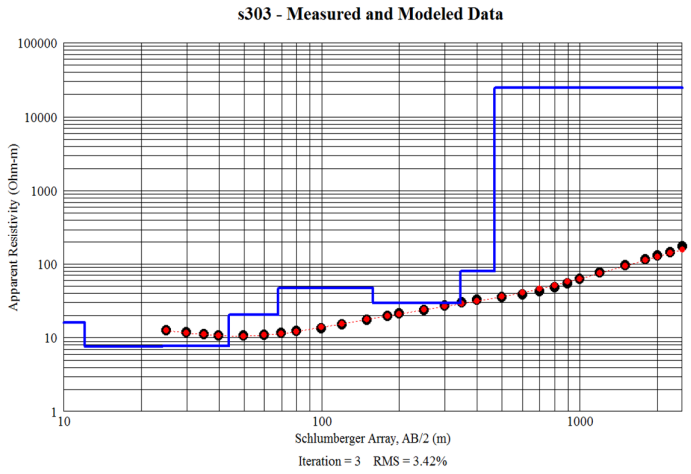
s303 - Measured and Modeled Data
Apparent Resistivity (Ohm-m)
100000
10000
1000
100
10
1
10
100
1000
Schlumberger Array, AB/2 (m)
Iteration = 3 RMS = 3.42%

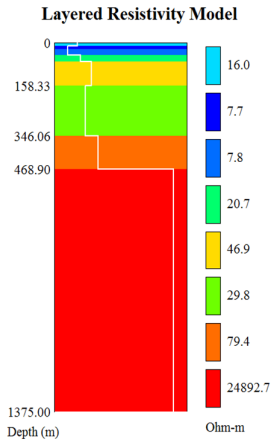
Layered Resistivity Model
0
158.33
346.06
468.90
1375.00
Depth (m)
16.0
7.7
7.8
20.7
46.9
29.8
79.4
24892.7
Ohm-m

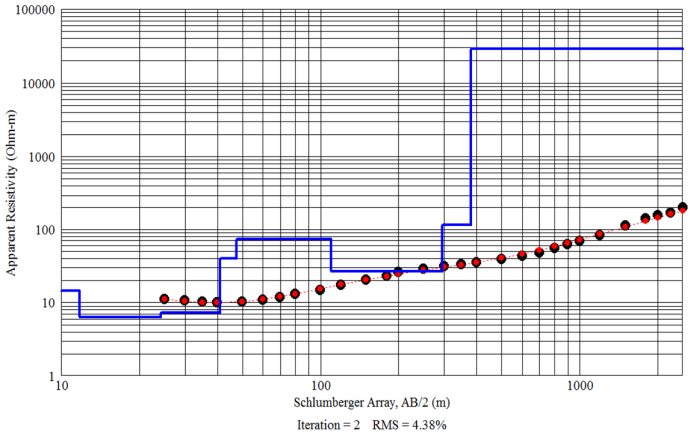
s304 - Measured and Modeled Data
Apparent Resistivity (Ohm-m)
100000
10000
1000
100
10
1
10
100
1000
Schlumberger Array, AB/2 (m)
Iteration = 2 RMS = 4.38%

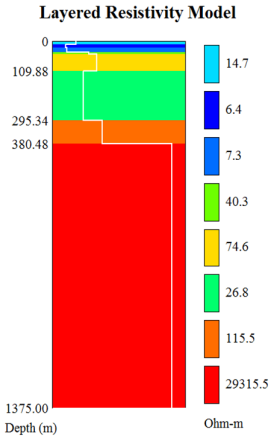
Layered Resistivity Model
0
109.88
295.34
380.48
1375.00
Depth (m)
14.7
6.4
7.3
40.3
74.6
26.8
115.5
29315.5
Ohm-m

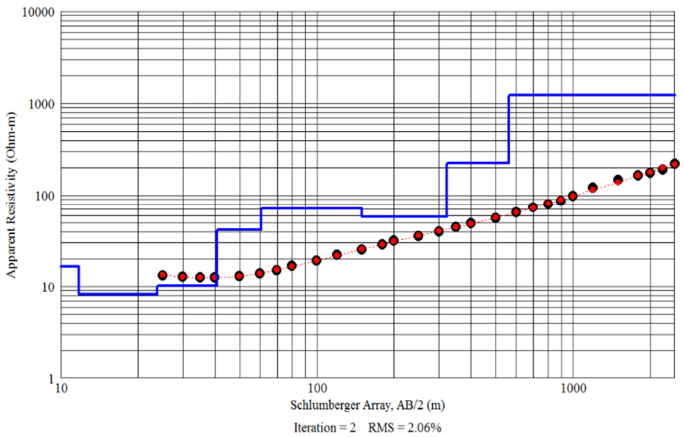
s305 - Measured and Modeled Data
Apparent Resistivity (Ohm-m)
10000
1000
100
10
1
10
100
1000
Schlumberger Array, AB/2 (m)
Iteration = 2 RMS = 2.06%

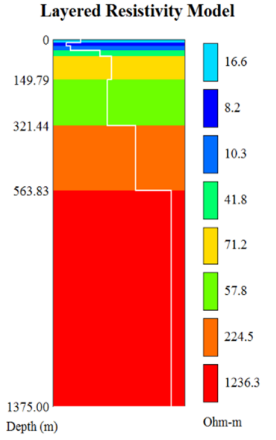
Layered Resistivity Model
0
149.79
321.44
563.83
1375.00
Depth (m)
16.6
8.2
10.3
41.8
71.2
57.8
224.5
1236.3
Ohm-m

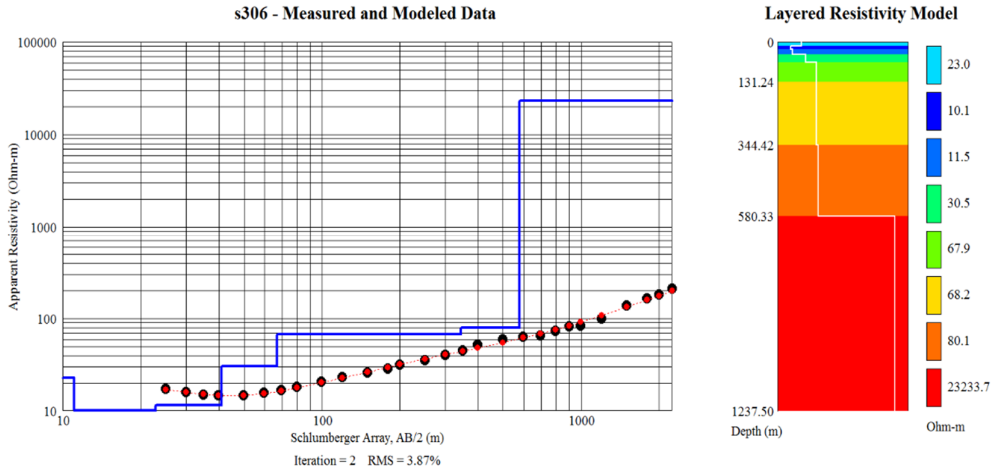
s306 - Measured and Modeled Data
Apparent Resistivity (Ohm-m)
100000
10000
1000
100
10
10
100
1000
Schlumberger Array, AB/2 (m)
Iteration = 2 RMS = 3.87%
Layered Resistivity Model
0
131.24
344.42
580.33
1237.50
Depth (m)
23.0
10.1
11.5
30.5
67.9
68.2
80.1
23233.7
Ohm-m

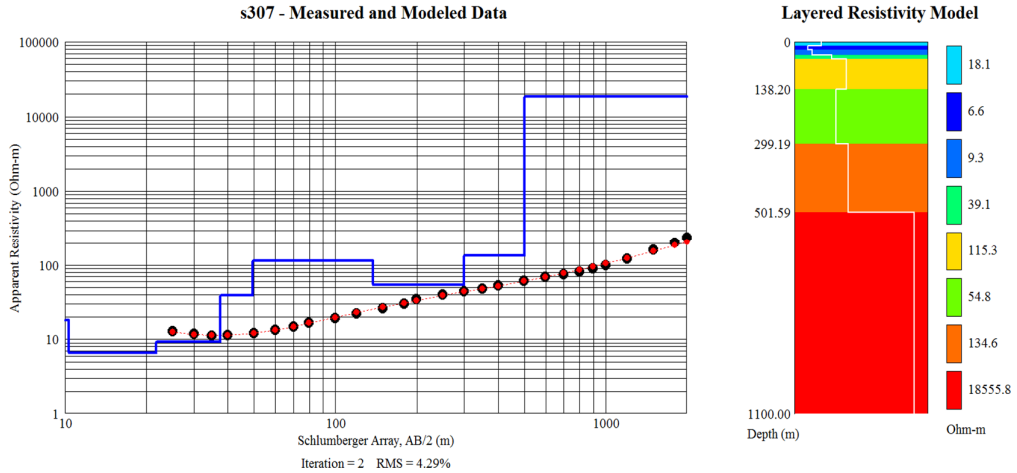
s307 - Measured and Modeled Data
Apparent Resistivity (Ohm-m)
100000
10000
1000
100
10
1
10
100
1000
Schlumberger Array, AB/2 (m)
Iteration = 2 RMS = 4.29%
Layered Resistivity Model
0
138.20
299.19
501.59
1100.00
Depth (m)
18.1
6.6
9.3
39.1
115.3
54.8
134.6
18555.8
Ohm-m

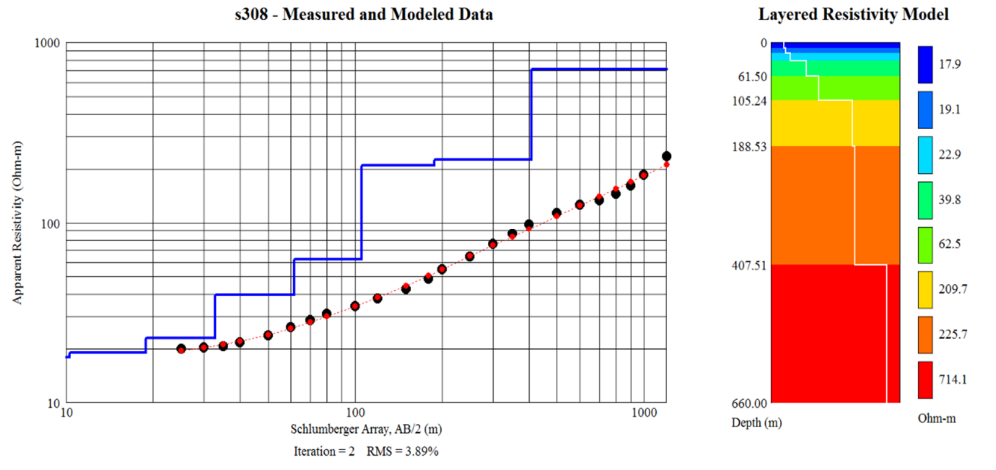
s308 - Measured and Modeled Data
Apparent Resistivity (Ohm-m)
1000
100
10
10
100
1000
Schlumberger Array, AB/2 (m)
Iteration = 2 RMS = 3.89%
Layered Resistivity Model
0
61.50
105.24
188.53
407.51
660.00
Depth (m)
17.9
19.1
22.9
39.8
62.5
209.7
225.7
714.1
Ohm-m

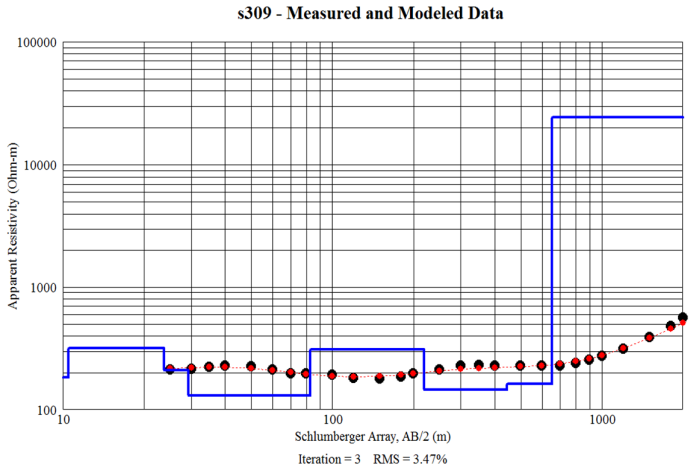
s309 - Measured and Modeled Data
Apparent Resistivity (Ohm-m)
100000
10000
1000
100
10
100
1000
Schlumberger Array, AB/2 (m)
Iteration = 3 RMS = 3.47%

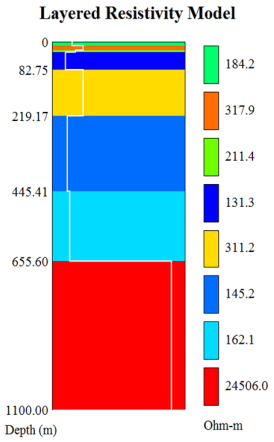
Layered Resistivity Model
0
82.75
219.17
445.41
655.60
1100.00
Depth (m)
184.2
317.9
211.4
131.3
311.2
145.2
162.1
24506.0
Ohm-m

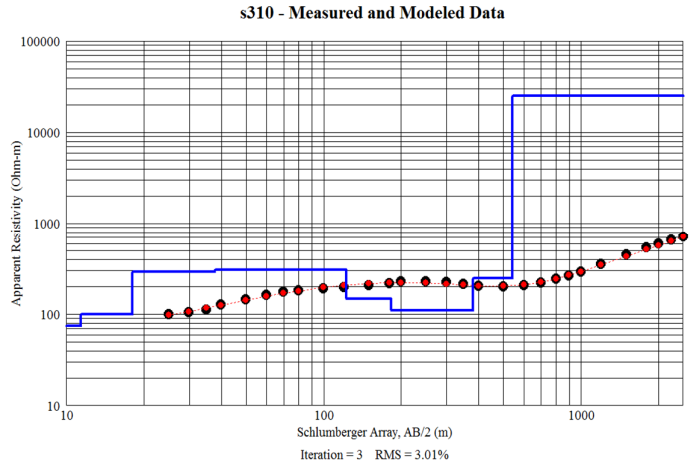
s310 - Measured and Modeled Data
Apparent Resistivity (Ohm-m)
100000
10000
1000
100
10
100
1000
Schlumberger Array, AB/2 (m)
Iteration = 3 RMS = 3.01%

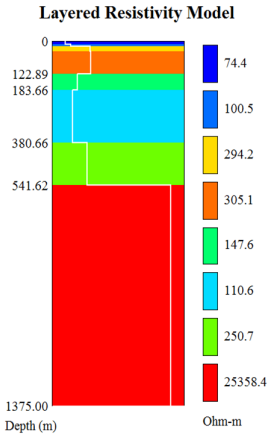
Layered Resistivity Model
0
122.89
183.66
380.66
541.62
1375.00
Depth (m)
74.4
100.5
294.2
305.1
147.6
110.6
250.7
25358.4
Ohm-m

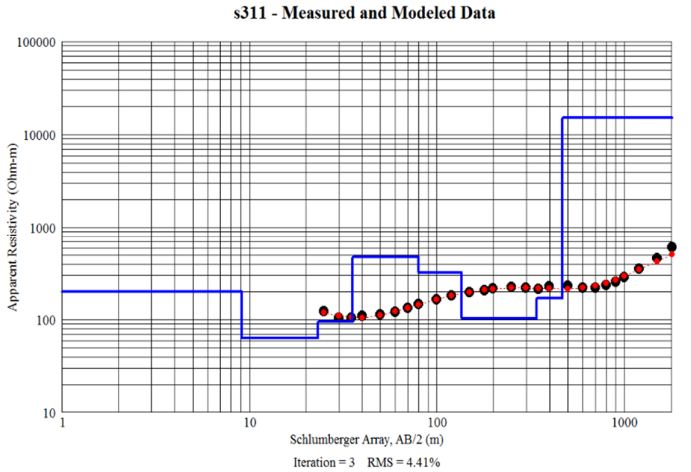
s311 - Measured and Modeled Data
Apparent Resistivity (Ohm-m)
100000
10000
1000
100
10
1
10
100
1000
Schlumberger Array, AB/2 (m)
Iteration = 3 RMS = 4.41%

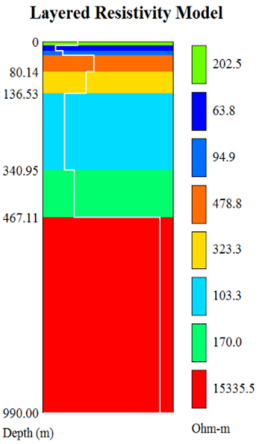
Layered Resistivity Model
0
80.14
136.53
340.95
467.11
990.00
Depth (m)
202.5
63.8
94.9
478.8
323.3
103.3
170.0
15335.5
Ohm-m

Group 15

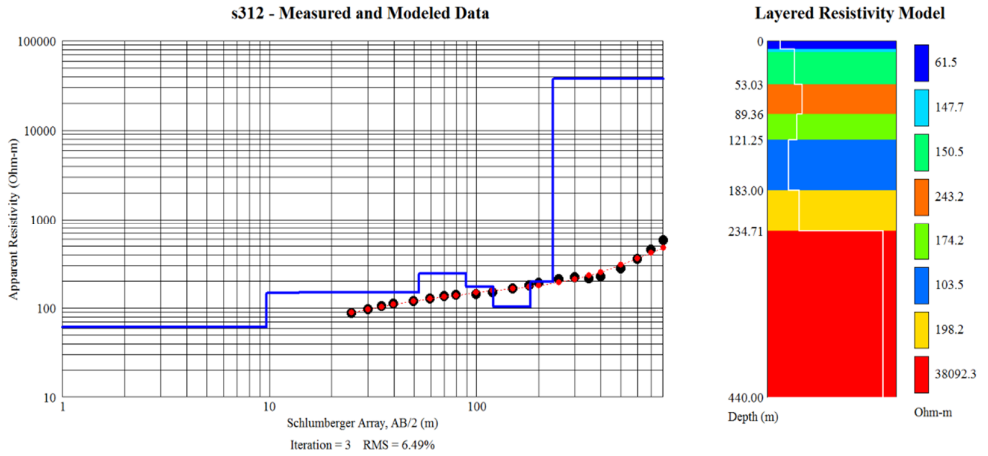
s312 - Measured and Modeled Data
Apparent Resistivity (Ohm-m)
100000
10000
1000
100
10
1
10
100
Schlumberger Array, AB/2 (m)
Iteration = 3 RMS = 6.49%
Layered Resistivity Model
0
53.03
89.36
121.25
183.00
234.71
440.00
Depth (m)
61.5
147.7
150.5
243.2
174.2
103.5
198.2
38092.3
Ohm-m

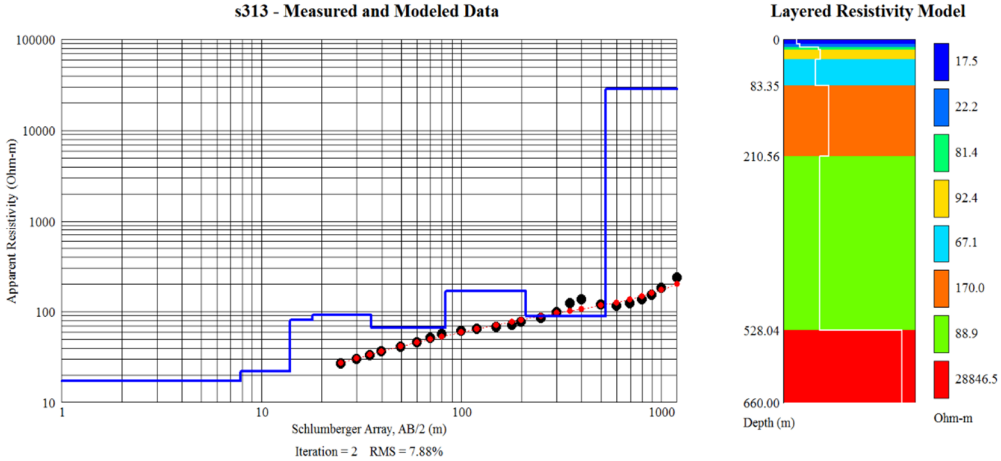
s313 - Measured and Modeled Data
Apparent Resistivity (Ohm-m)
100000
10000
1000
100
10
1
10
100
1000
Schlumberger Array, AB/2 (m)
Iteration = 2 RMS = 7.88%
Layered Resistivity Model
0
83.35
210.56
528.04
660.00
Depth (m)
17.5
22.2
81.4
92.4
67.1
170.0
88.9
28846.5
Ohm-m

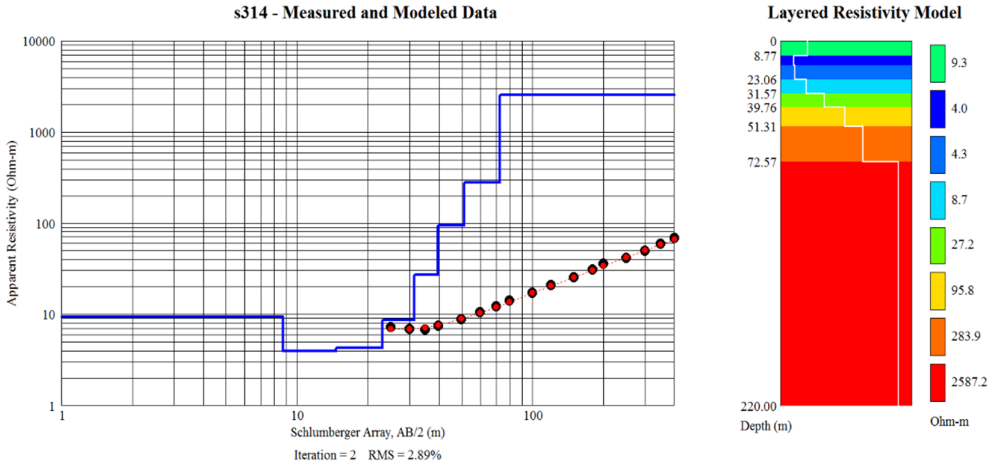
s314 - Measured and Modeled Data
Apparent Resistivity (Ohm-m)
10000
1000
100
10
1
10
100
Schlumberger Array, AB/2 (m)
Iteration = 2 RMS = 2.89%
Layered Resistivity Model
0
8.77
23.06
31.57
39.76
51.31
72.57
220.00
Depth (m)
9.3
4.0
4.3
8.7
27.2
95.8
283.9
2587.2
Ohm-m

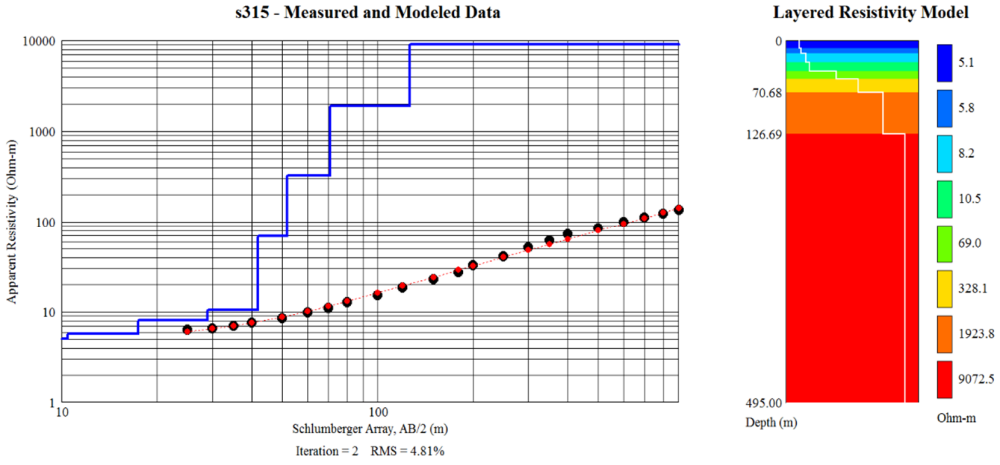
s315 - Measured and Modeled Data
Apparent Resistivity (Ohm-m)
10000
1000
100
10
1
10
100
Schlumberger Array, AB/2 (m)
Iteration = 2 RMS = 4.81%
Layered Resistivity Model
0
70.68
126.69
495.00
Depth (m)
5.1
5.8
8.2
10.5
69.0
328.1
1923.8
9072.5
Ohm-m

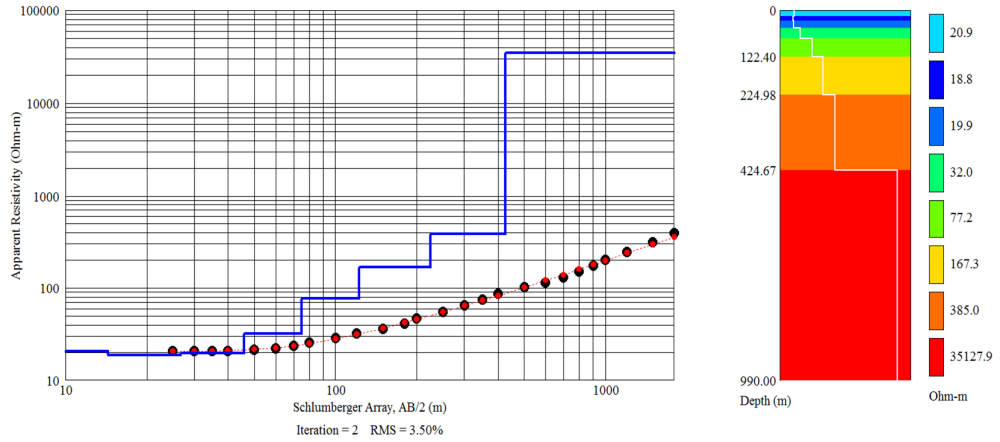
s316 - Measured and Modeled Data
Apparent Resistivity (Ohm-m)
100000
10000
1000
100
10
10
100
1000
Schlumberger Array, AB/2 (m)
Iteration = 2 RMS = 3.50%
Layered Resistivity Model
0
122.40
224.98
424.67
990.00
Depth (m)
20.9
18.8
19.9
32.0
77.2
167.3
385.0
35127.9
Ohm-m

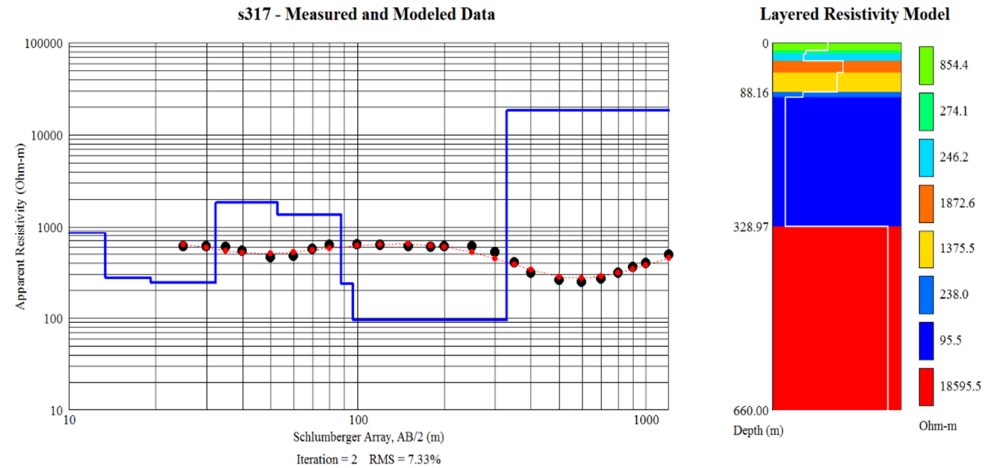
s317 - Measured and Modeled Data
Apparent Resistivity (Ohm-m)
100000
10000
1000
100
10
10
100
1000
Schlumberger Array, AB/2 (m)
Iteration = 2 RMS = 7.33%
Layered Resistivity Model
0
88.16
328.97
660.00
Depth (m)
854.4
274.1
246.2
1872.6
1375.5
238.0
95.5
18595.5
Ohm-m

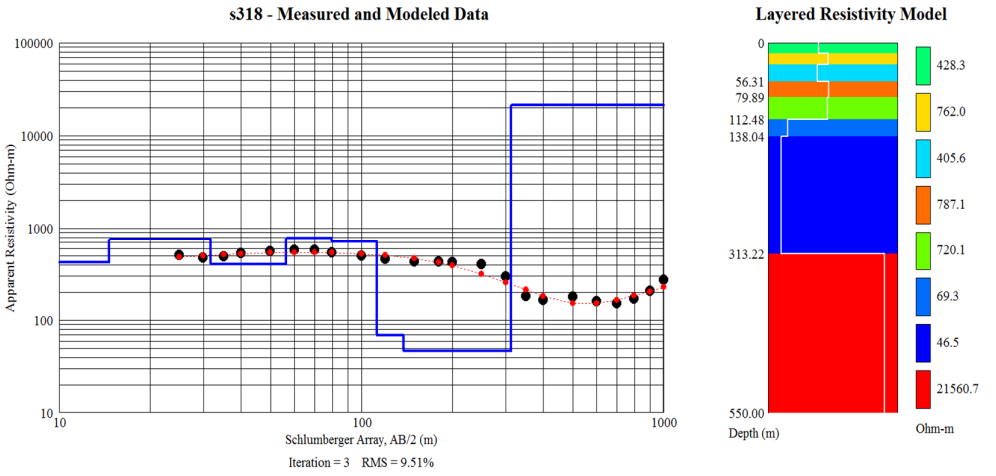
s318 - Measured and Modeled Data
Apparent Resistivity (Ohm-m)
100000
10000
1000
100
10
10
100
1000
Schlumberger Array, AB/2 (m)
Iteration = 3 RMS = 9.51%
Layered Resistivity Model
0
56.31
79.89
112.48
138.04
313.22
550.00
Depth (m)
428.3
762.0
405.6
787.1
720.1
69.3
46.5
21560.7
Ohm-m

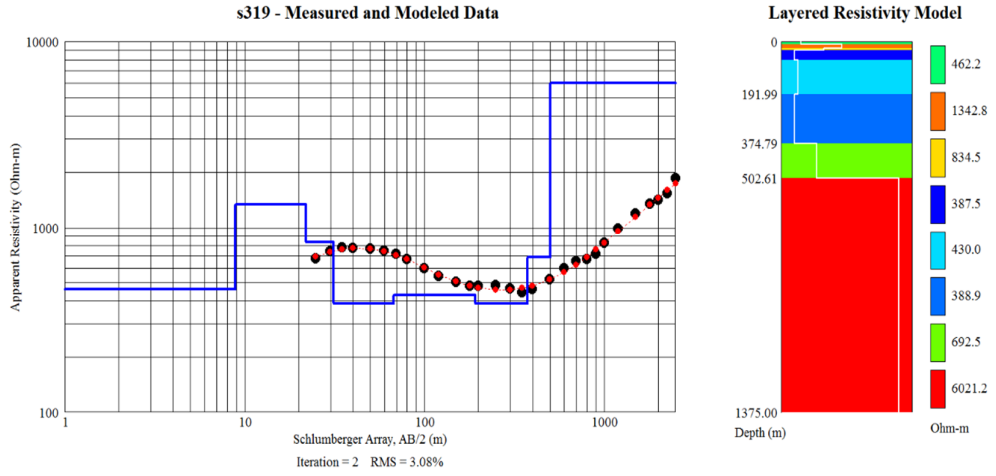
s319 - Measured and Modeled Data
Apparent Resistivity (Ohm-m)
10000
1000
100
1
10
100
1000
Schlumberger Array, AB/2 (m)
Iteration = 2 RMS = 3.08%
Layered Resistivity Model
0
191.99
374.79
502.61
1375.00
Depth (m)
462.2
1342.8
834.5
387.5
430.0
388.9
692.5
6021.2
Ohm-m

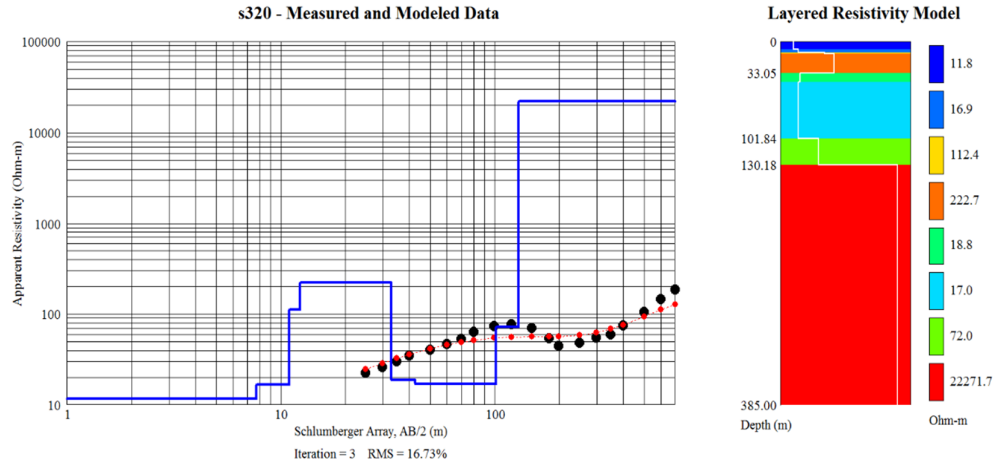
s320 - Measured and Modeled Data
Apparent Resistivity (Ohm-m)
100000
10000
1000
100
10
1
10
100
Schlumberger Array, AB/2 (m)
Iteration = 3 RMS = 16.73%
Layered Resistivity Model
0
33.05
101.84
130.18
385.00
Depth (m)
11.8
16.9
112.4
222.7
18.8
17.0
72.0
22271.7
Ohm-m

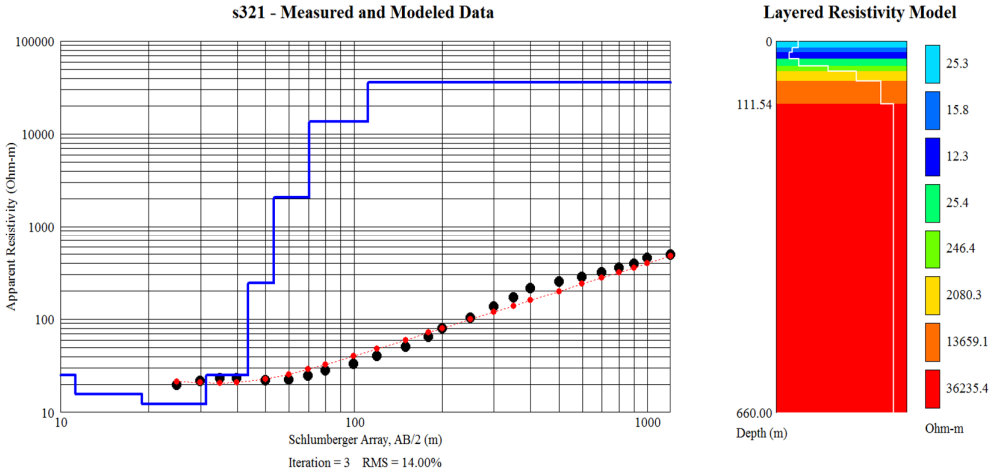
s321 - Measured and Modeled Data
Apparent Resistivity (Ohm-m)
100000
10000
1000
100
10
10
100
1000
Schlumberger Array, AB/2 (m)
Iteration = 3 RMS = 14.00%
Layered Resistivity Model
0
111.54
660.00
Depth (m)
25.3
15.8
12.3
25.4
246.4
2080.3
13659.1
36235.4
Ohm-m

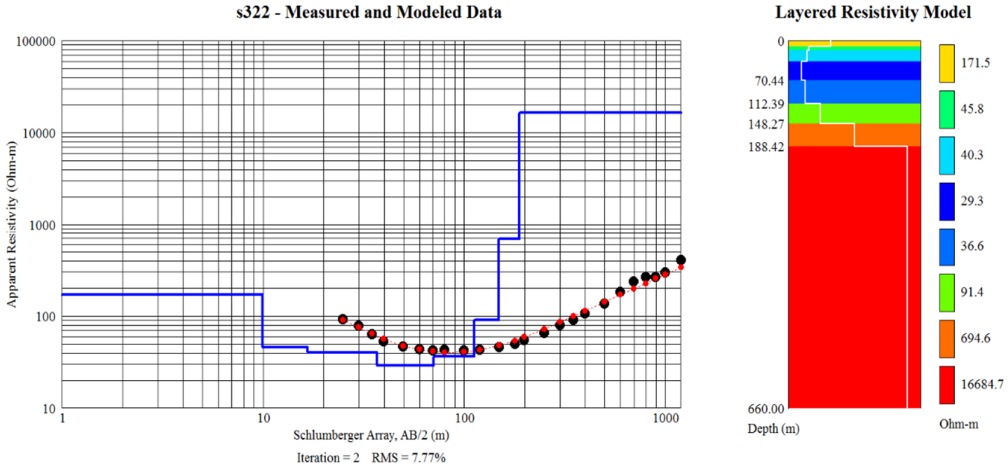
s322 - Measured and Modeled Data
Apparent Resistivity (Ohm-m)
100000
10000
1000
100
10
1
10
100
1000
Schlumberger Array, AB/2 (m)
Iteration = 2 RMS = 7.77%
Layered Resistivity Model
0
70.44
112.39
148.27
188.42
660.00
Depth (m)
171.5
45.8
40.3
29.3
36.6
91.4
694.6
16684.7
Ohm-m

Group 16

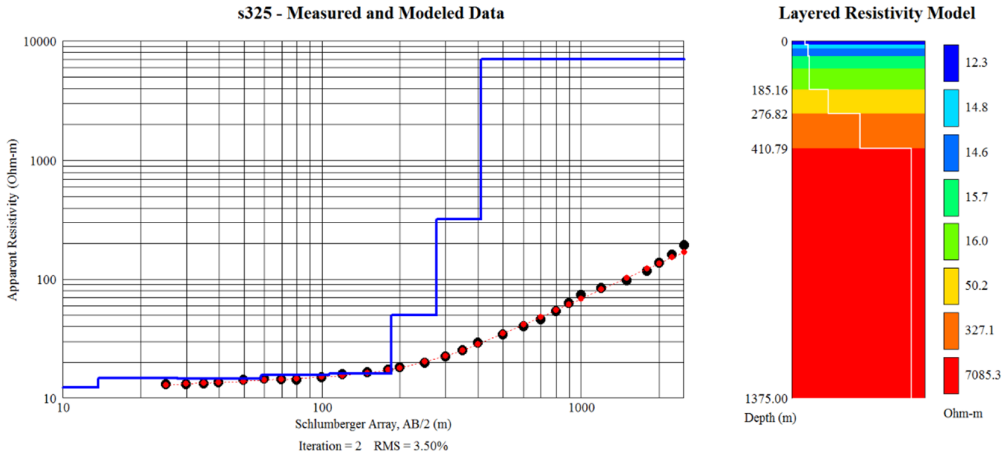
s325 - Measured and Modeled Data
Apparent Resistivity (Ohm-m)
10000
1000
100
10
10
100
1000
Schlumberger Array, AB/2 (m)
Iteration = 2 RMS = 3.50%
Layered Resistivity Model
0
185.16
276.82
410.79
1375.00
Depth (m)
12.3
14.8
14.6
15.7
16.0
50.2
327.1
7085.3
Ohm-m

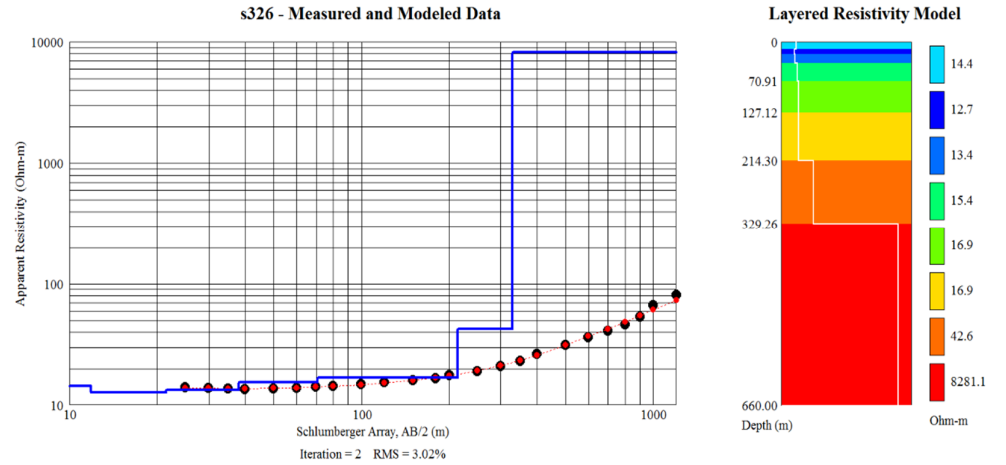
s326 - Measured and Modeled Data
Apparent Resistivity (Ohm-m)
10000
1000
100
10
10
100
1000
Schlumberger Array, AB/2 (m)
Iteration = 2 RMS = 3.02%
Layered Resistivity Model
0
70.91
127.12
214.30
329.26
660.00
Depth (m)
14.4
12.7
13.4
15.4
16.9
16.9
42.6
8281.1
Ohm-m

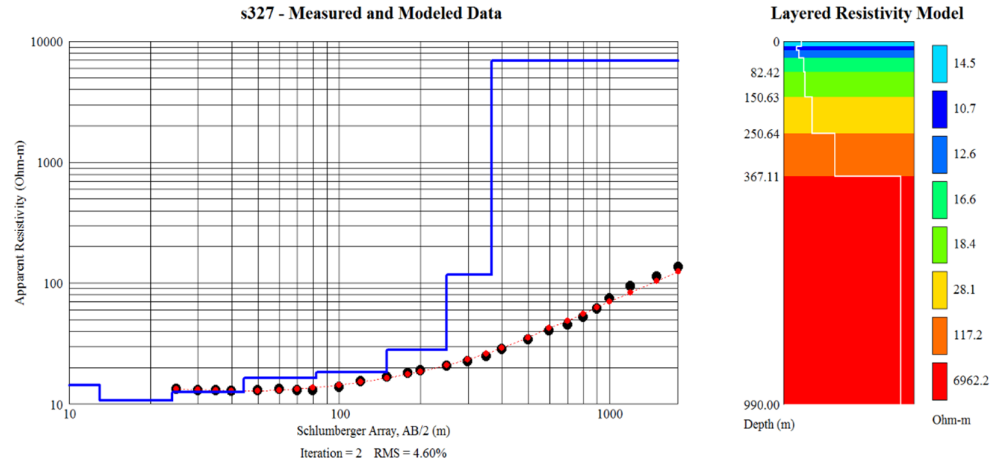
s327 - Measured and Modeled Data
Apparent Resistivity (Ohm-m)
10000
1000
100
10
10
100
1000
Schlumberger Array, AB/2 (m)
Iteration = 2 RMS = 4.60%
Layered Resistivity Model
0
82.42
150.63
250.64
367.11
990.00
Depth (m)
14.5
10.7
12.6
16.6
18.4
28.1
117.2
6962.2
Ohm-m

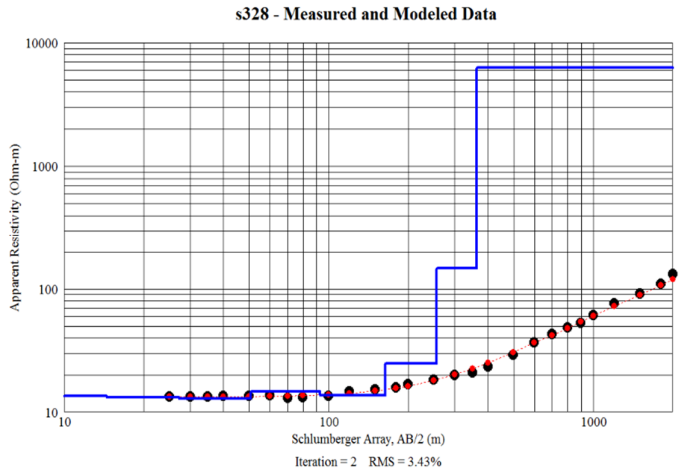
s328 - Measured and Modeled Data
Apparent Resistivity (Ohm-m)
10000
1000
100
10
10
100
1000
Schlumberger Array, AB/2 (m)
Iteration = 2 RMS = 3.43%

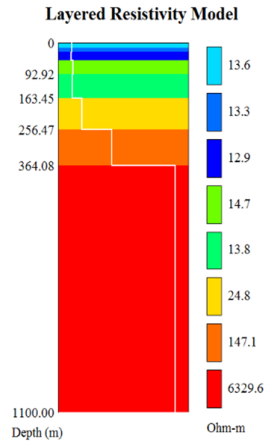
Layered Resistivity Model
0
92.92
163.45
256.47
364.08
1100.00
Depth (m)
13.6
13.3
12.9
14.7
13.8
24.8
147.1
6329.6
Ohm-m

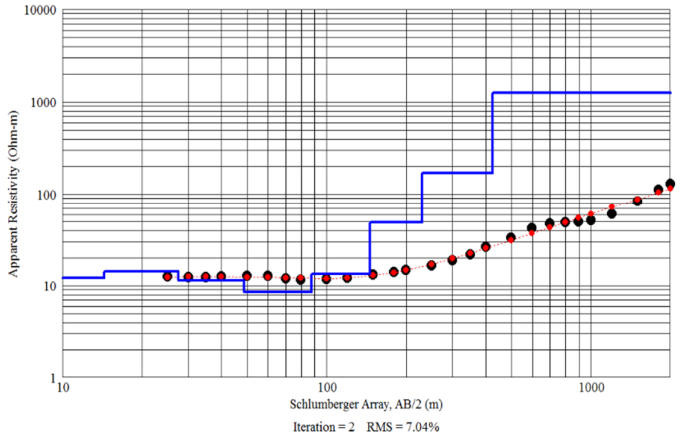
s329 - Measured and Modeled Data
Apparent Resistivity (Ohm-m)
10000
1000
100
10
1
10
100
1000
Schlumberger Array, AB/2 (m)
Iteration = 2 RMS = 7.04%

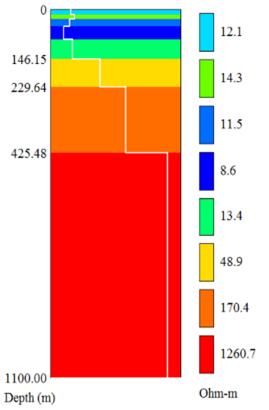
Layered Resistivity Model
0
146.15
229.64
425.48
1100.00
Depth (m)
12.1
14.3
11.5
8.6
13.4
48.9
170.4
1260.7
Ohm-m

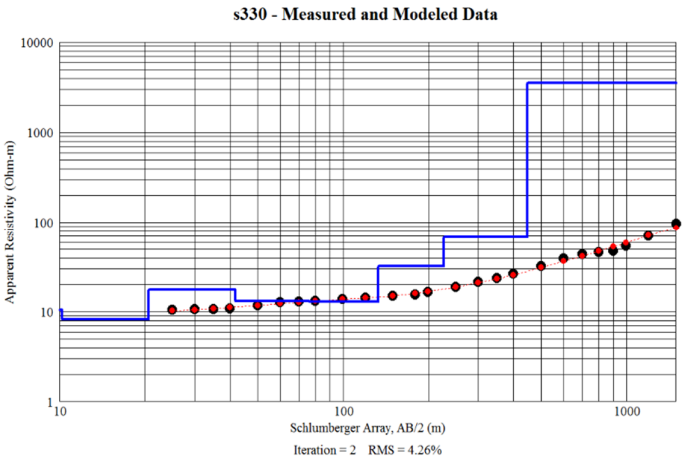
s330 - Measured and Modeled Data
Apparent Resistivity (Ohm-m)
10000
1000
100
10
1
10
100
1000
Schlumberger Array, AB/2 (m)
Iteration = 2 RMS = 4.26%

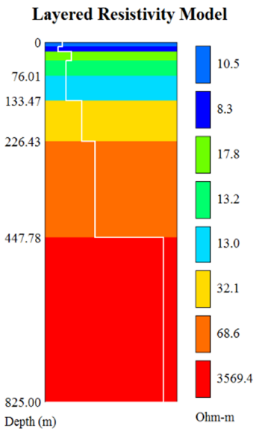
Layered Resistivity Model
0
76.01
133.47
226.43
447.78
825.00
Depth (m)
10.5
8.3
17.8
13.2
13.0
32.1
68.6
3569.4
Ohm-m

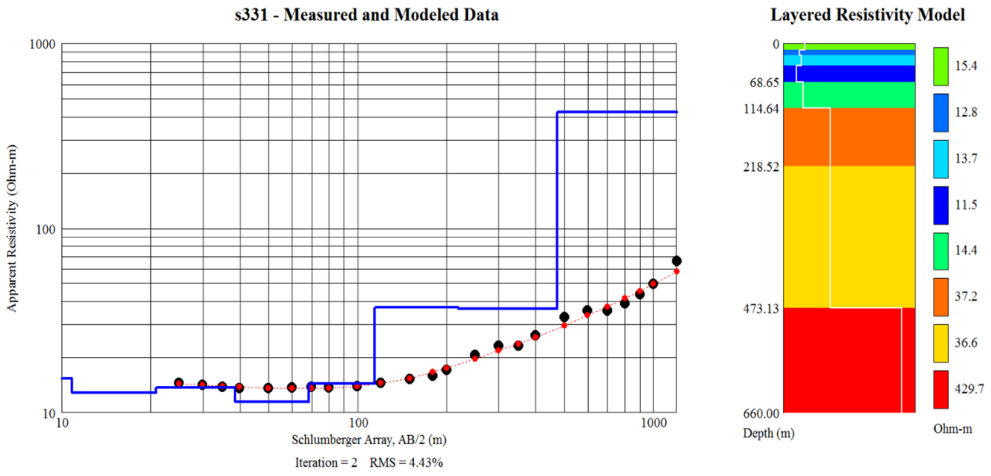
s331 - Measured and Modeled Data
Apparent Resistivity (Ohm-m)
1000
100
10
10
100
1000
Schlumberger Array, AB/2 (m)
Iteration = 2 RMS = 4.43%
Layered Resistivity Model
0
68.65
114.64
218.52
473.13
660.00
Depth (m)
15.4
12.8
13.7
11.5
14.4
37.2
36.6
429.7
Ohm-m

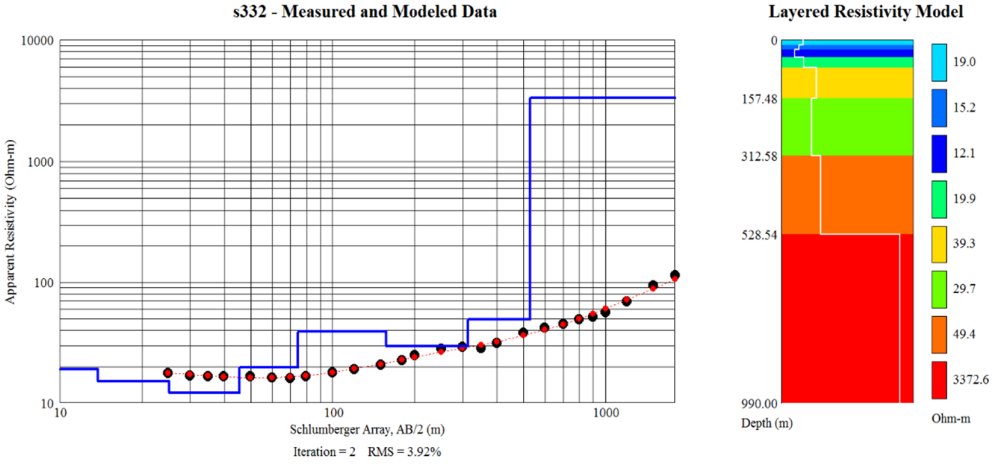
s332 - Measured and Modeled Data
Apparent Resistivity (Ohm-m)
10000
1000
100
10
10
100
1000
Schlumberger Array, AB/2 (m)
Iteration = 2 RMS = 3.92%
Layered Resistivity Model
0
157.48
312.58
528.54
990.00
Depth (m)
19.0
15.2
12.1
19.9
39.3
29.7
49.4
3372.6
Ohm-m

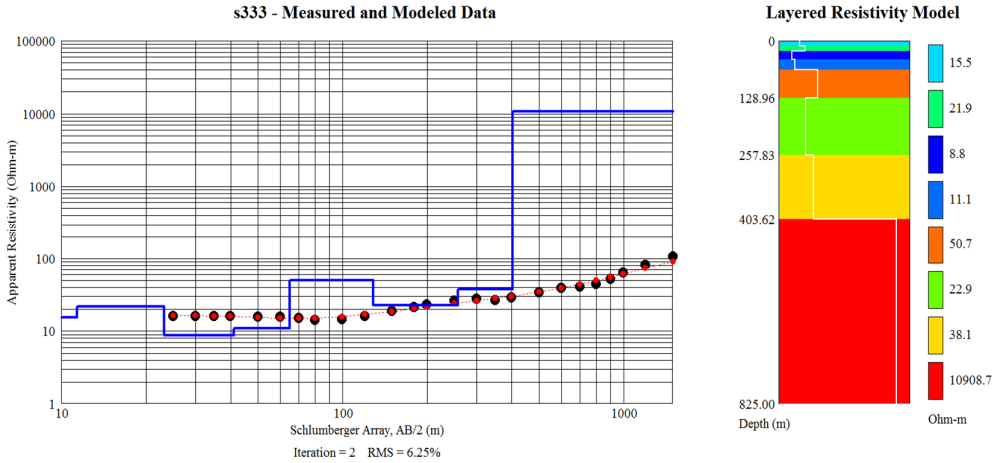
s333 - Measured and Modeled Data
Apparent Resistivity (Ohm-m)
100000
10000
1000
100
10
1
10
100
1000
Schlumberger Array, AB/2 (m)
Iteration = 2 RMS = 6.25%
Layered Resistivity Model
0
128.96
257.83
403.62
825.00
Depth (m)
15.5
21.9
8.8
11.1
50.7
22.9
38.1
10908.7
Ohm-m

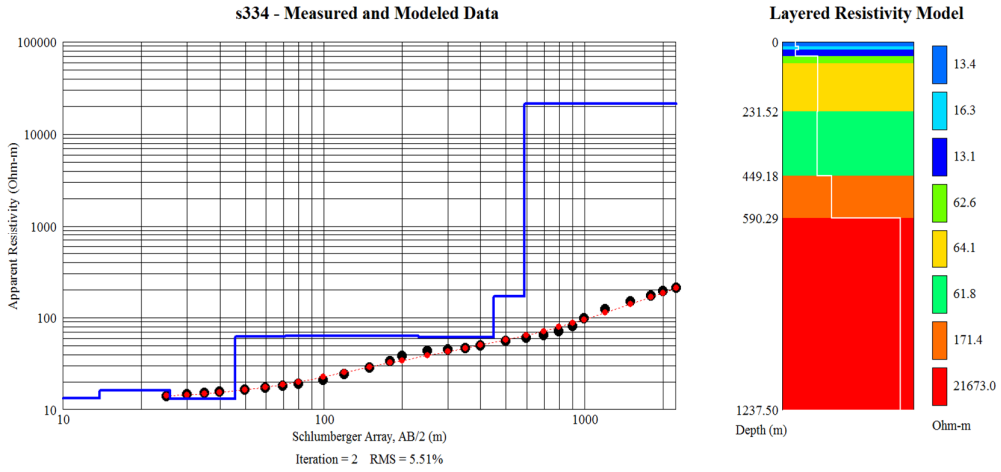
s334 - Measured and Modeled Data
Apparent Resistivity (Ohm-m)
100000
10000
1000
100
10
10
100
1000
Schlumberger Array, AB/2 (m)
Iteration = 2 RMS = 5.51%
Layered Resistivity Model
0
231.52
449.18
590.29
1237.50
Depth (m)
13.4
16.3
13.1
62.6
64.1
61.8
171.4
21673.0
Ohm-m

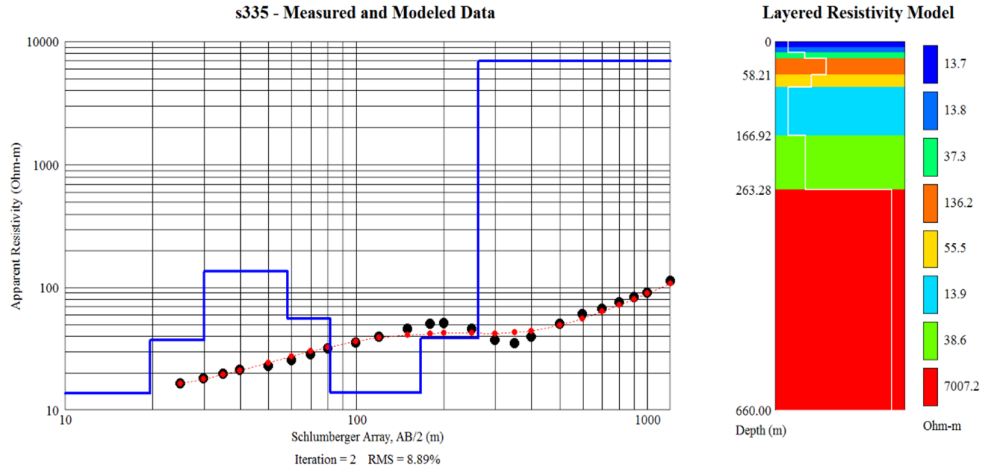
s335 - Measured and Modeled Data
Apparent Resistivity (Ohm-m)
10000
1000
100
10
10
100
1000
Schlumberger Array, AB/2 (m)
Iteration = 2 RMS = 8.89%
Layered Resistivity Model
0
58.21
166.92
263.28
660.00
Depth (m)
13.7
13.8
37.3
136.2
55.5
13.9
38.6
7007.2
Ohm-m

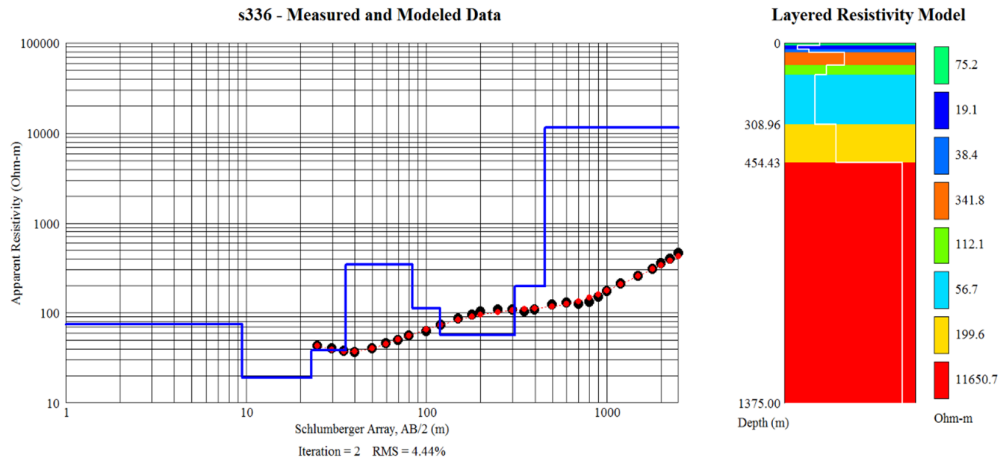
s336 - Measured and Modeled Data
Apparent Resistivity (Ohm-m)
100000
10000
1000
100
10
1
10
100
1000
Schlumberger Array, AB/2 (m)
Iteration = 2 RMS = 4.44%
Layered Resistivity Model
0
308.96
454.43
1375.00
Depth (m)
75.2
19.1
38.4
341.8
112.1
56.7
199.6
11650.7
Ohm-m

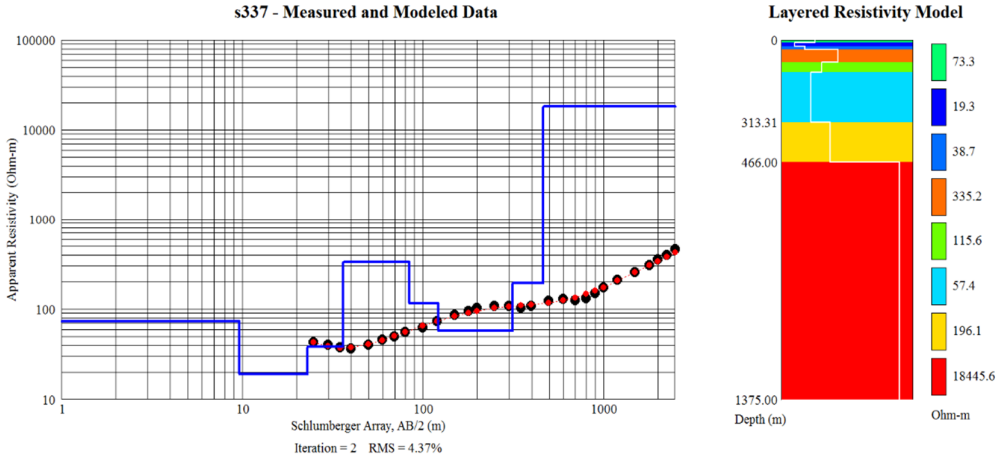
s337 - Measured and Modeled Data
Apparent Resistivity (Ohm-m)
100000
10000
1000
100
10
1
10
100
1000
Schlumberger Array, AB/2 (m)
Iteration = 2 RMS = 4.37%
Layered Resistivity Model
0
313.31
466.00
1375.00
Depth (m)
73.3
19.3
38.7
335.2
115.6
57.4
196.1
18445.6
Ohm-m

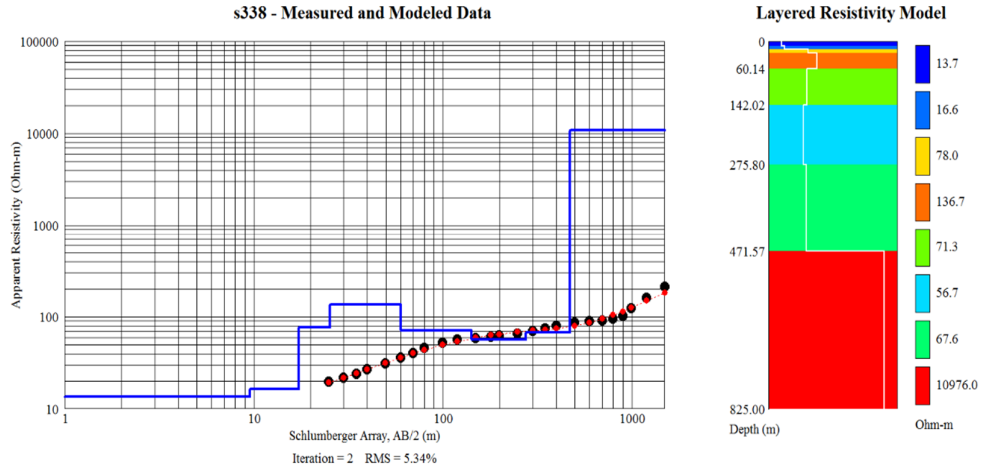
s338 - Measured and Modeled Data
Apparent Resistivity (Ohm-m)
100000
10000
1000
100
10
1
10
100
1000
Schlumberger Array, AB/2 (m)
Iteration = 2 RMS = 5.34%
Layered Resistivity Model
0
60.14
142.02
275.80
471.57
825.00
Depth (m)
13.7
16.6
78.0
136.7
71.3
56.7
67.6
10976.0
Ohm-m

Group 17

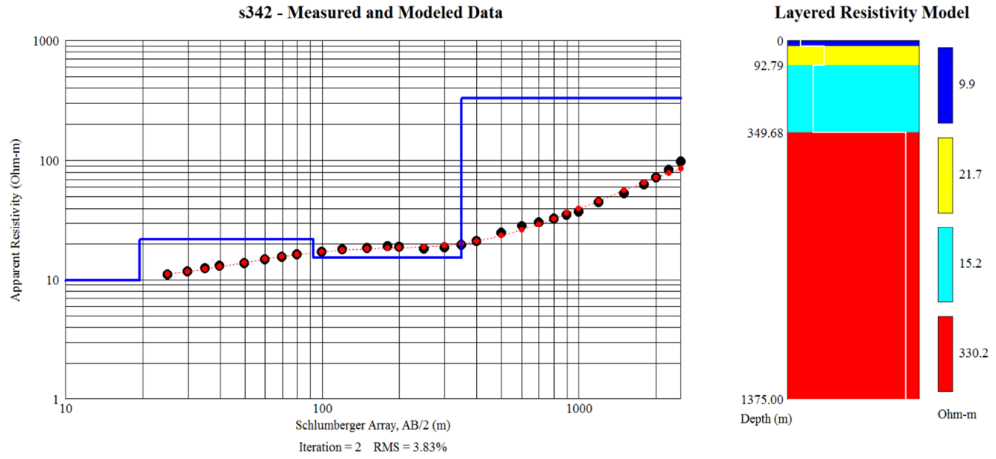
s342 - Measured and Modeled Data
Apparent Resistivity (Ohm-m)
1000
100
10
1
10
100
1000
Schlumberger Array, AB/2 (m)
Iteration = 2 RMS = 3.83%
Layered Resistivity Model
0
92.79
349.68
1375.00
Depth (m)
9.9
21.7
15.2
330.2
Ohm-m

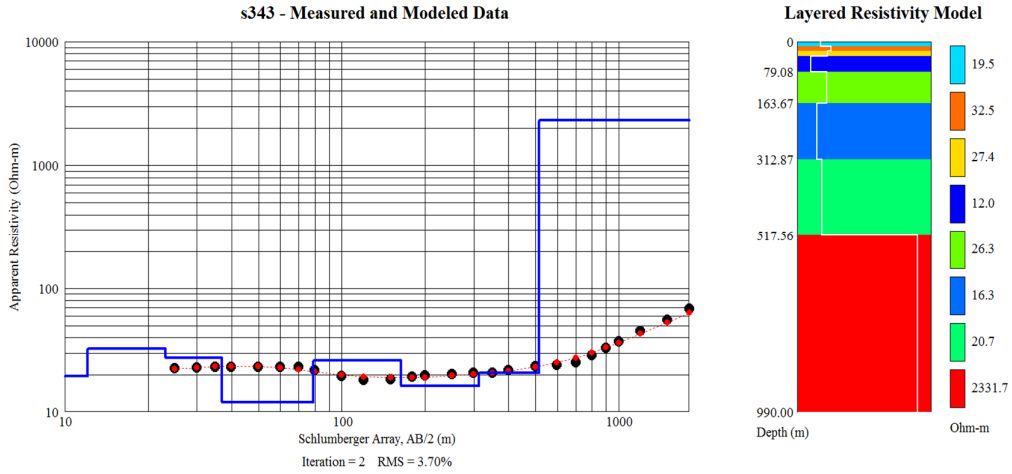
s343 - Measured and Modeled Data
Apparent Resistivity (Ohm-m)
10000
1000
100
10
10
100
1000
Schlumberger Array, AB/2 (m)
Iteration = 2 RMS = 3.70%
Layered Resistivity Model
0
79.08
163.67
312.87
517.56
990.00
Depth (m)
19.5
32.5
27.4
12.0
26.3
16.3
20.7
2331.7
Ohm-m

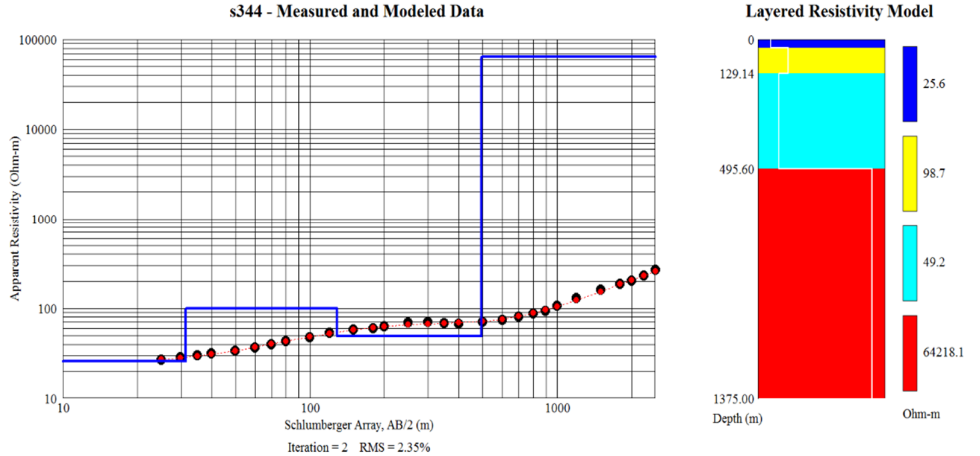
s344 - Measured and Modeled Data
Apparent Resistivity (Ohm-m)
100000
10000
1000
100
10
10
100
1000
Schlumberger Array, AB/2 (m)
Iteration = 2 RMS = 2.35%
Layered Resistivity Model
0
129.14
495.60
1375.00
Depth (m)
25.6
98.7
49.2
64218.1
Ohm-m

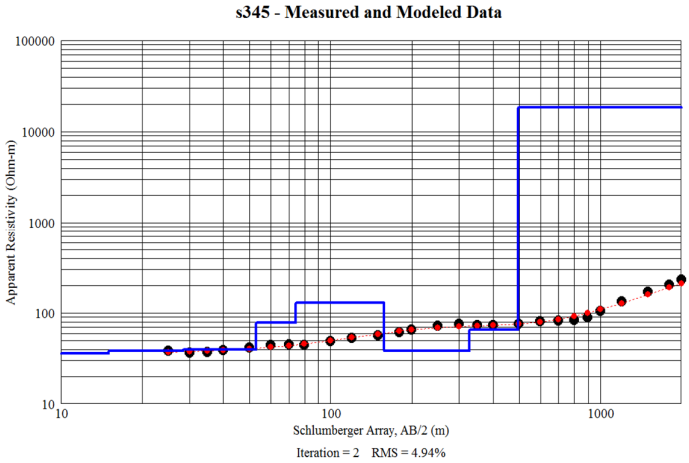
s345 - Measured and Modeled Data
Apparent Resistivity (Ohm-m)
100000
10000
1000
100
10
10
100
1000
Schlumberger Array, AB/2 (m)
Iteration = 2 RMS = 4.94%

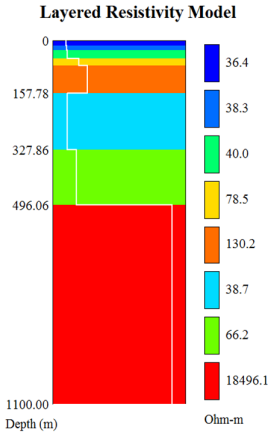
Layered Resistivity Model
0
157.78
327.86
496.06
1100.00
Depth (m)
36.4
38.3
40.0
78.5
130.2
38.7
66.2
18496.1
Ohm-m

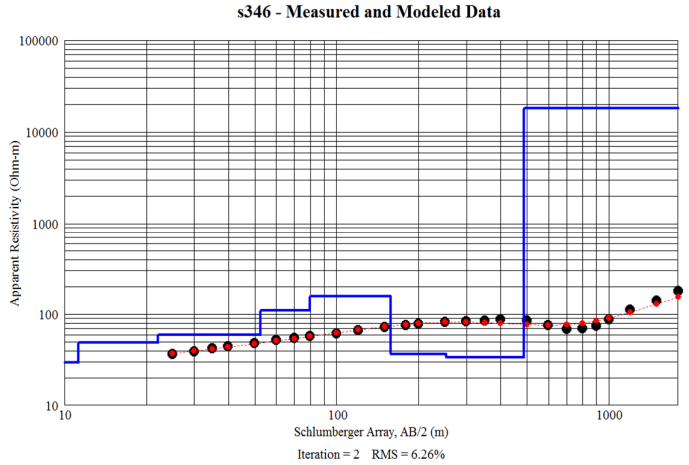
s346 - Measured and Modeled Data
Apparent Resistivity (Ohm-m)
100000
10000
1000
100
10
10
100
1000
Schlumberger Array, AB/2 (m)
Iteration = 2 RMS = 6.26%

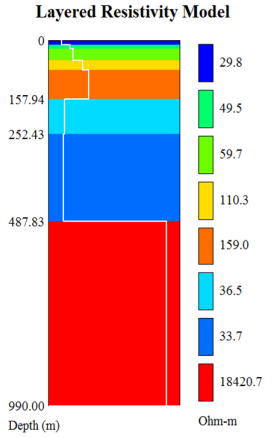
Layered Resistivity Model
0
157.94
252.43
487.83
990.00
Depth (m)
29.8
49.5
59.7
110.3
159.0
36.5
33.7
18420.7
Ohm-m

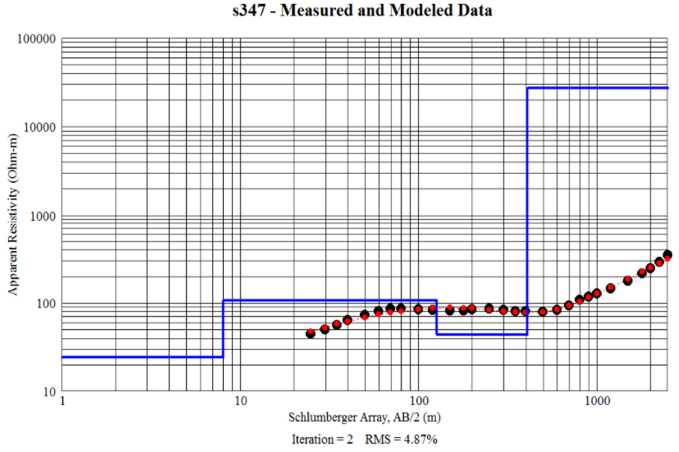
s347 - Measured and Modeled Data
Apparent Resistivity (Ohm-m)
100000
10000
1000
100
10
1
10
100
1000
Schlumberger Array, AB/2 (m)
Iteration = 2 RMS = 4.87%

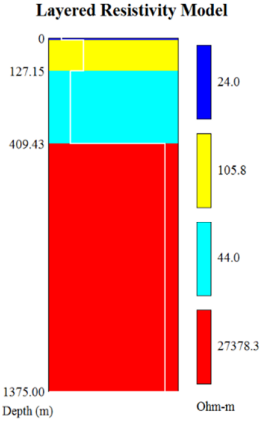
Layered Resistivity Model
0
127.15
409.43
1375.00
Depth (m)
24.0
105.8
44.0
27378.3
Ohm-m

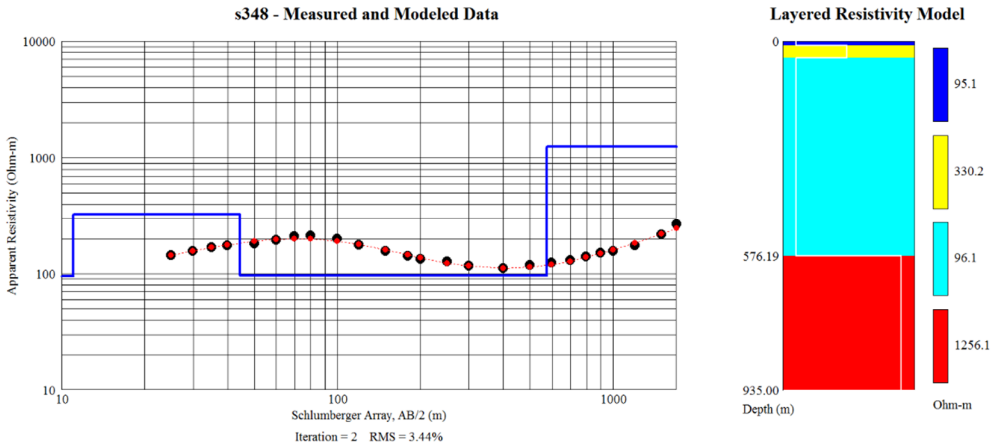
s348 - Measured and Modeled Data
Apparent Resistivity (Ohm-m)
10000
1000
100
10
10
100
1000
Schlumberger Array, AB/2 (m)
Iteration = 2 RMS = 3.44%
Layered Resistivity Model
0
576.19
935.00
Depth (m)
95.1
330.2
96.1
1256.1
Ohm-m

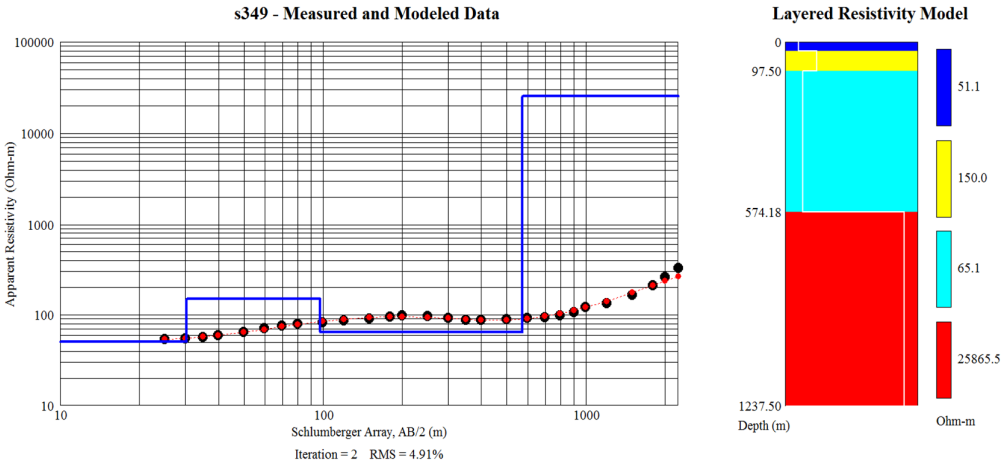
s349 - Measured and Modeled Data
Apparent Resistivity (Ohm-m)
100000
10000
1000
100
10
10
100
1000
Schlumberger Array, AB/2 (m)
Iteration = 2 RMS = 4.91%
Layered Resistivity Model
0
97.50
574.18
1237.50
Depth (m)
51.1
150.0
65.1
25865.5
Ohm-m

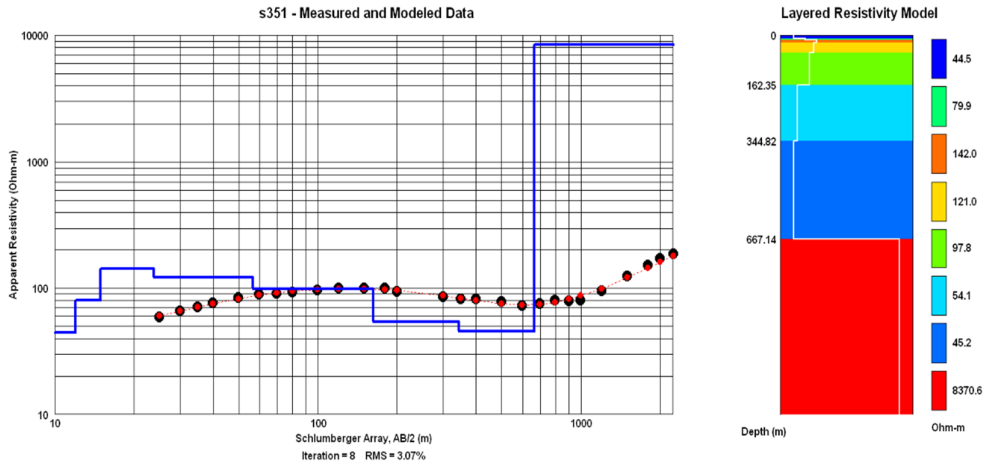
s351 - Measured and Modeled Data
Apparent Resistivity (Ohm-m)
10000
1000
100
10
10
100
1000
Schlumberger Array, AB/2 (m)
Iteration = 8 RMS = 3.07%
Layered Resistivity Model
0
162.35
344.82
667.14
Depth (m)
44.5
79.9
142.0
121.0
97.8
54.1
45.2
8370.6
Ohm-m

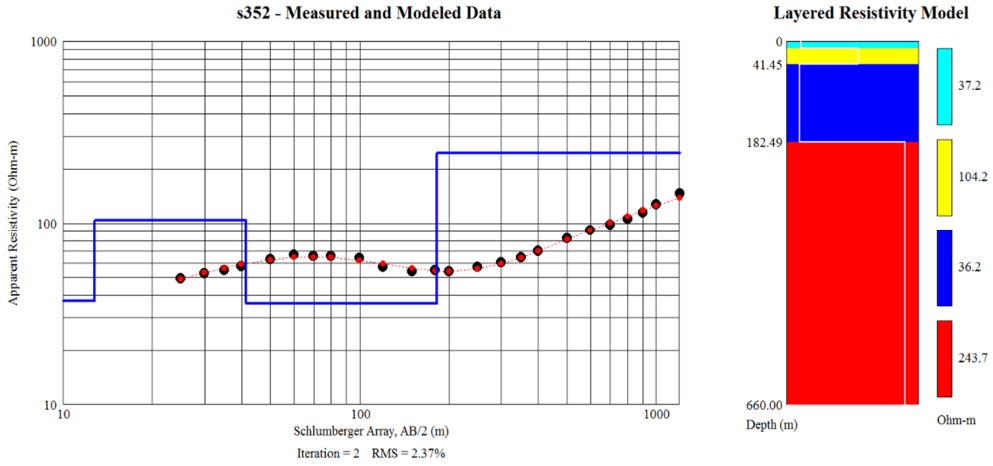
s352 - Measured and Modeled Data
Apparent Resistivity (Ohm-m)
1000
100
10
10
100
1000
Schlumberger Array, AB/2 (m)
Iteration = 2 RMS = 2.37%
Layered Resistivity Model
0
41.45
182.49
660.00
Depth (m)
37.2
104.2
36.2
243.7
Ohm-m

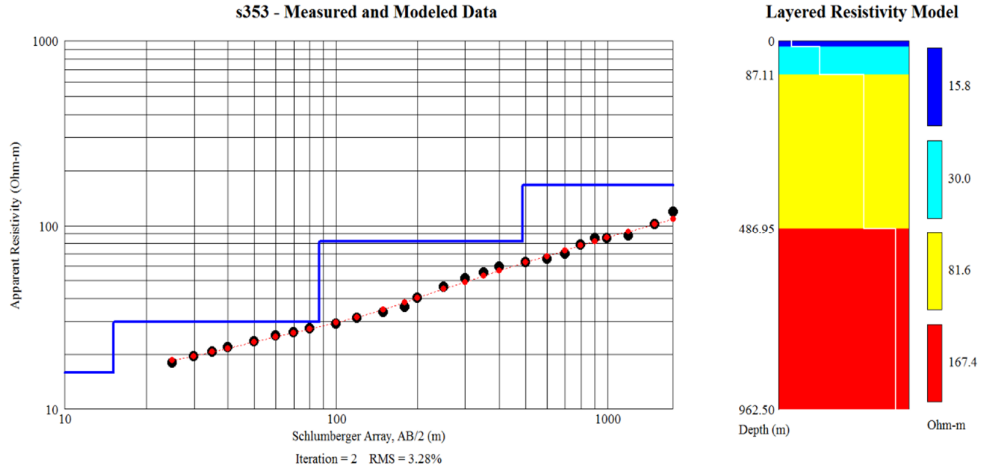
s353 - Measured and Modeled Data
Apparent Resistivity (Ohm-m)
1000
100
10
10
100
1000
Schlumberger Array, AB/2 (m)
Iteration = 2 RMS = 3.28%
Layered Resistivity Model
0
87.11
486.95
962.50
Depth (m)
15.8
30.0
81.6
167.4
Ohm-m

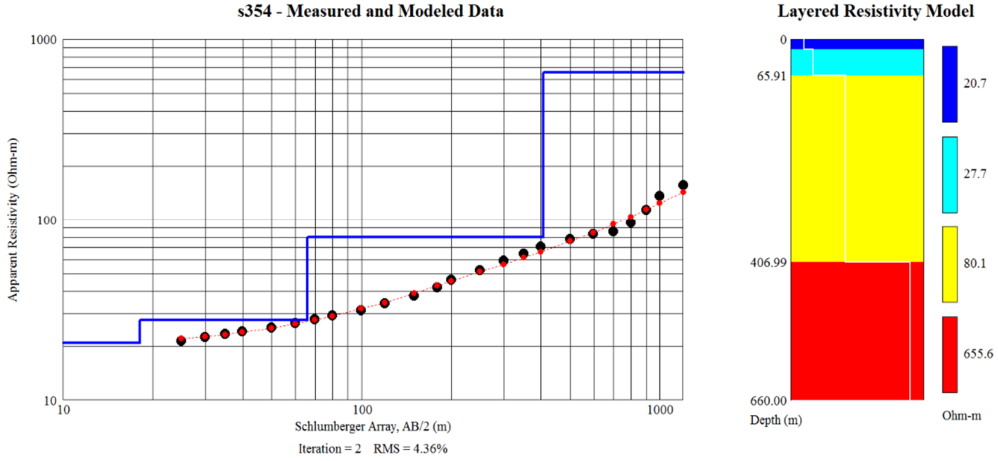
s354 - Measured and Modeled Data
Apparent Resistivity (Ohm-m)
1000
100
10
10
100
1000
Schlumberger Array, AB/2 (m)
Iteration = 2 RMS = 4.36%
Layered Resistivity Model
0
65.91
406.99
660.00
Depth (m)
20.7
27.7
80.1
655.6
Ohm-m

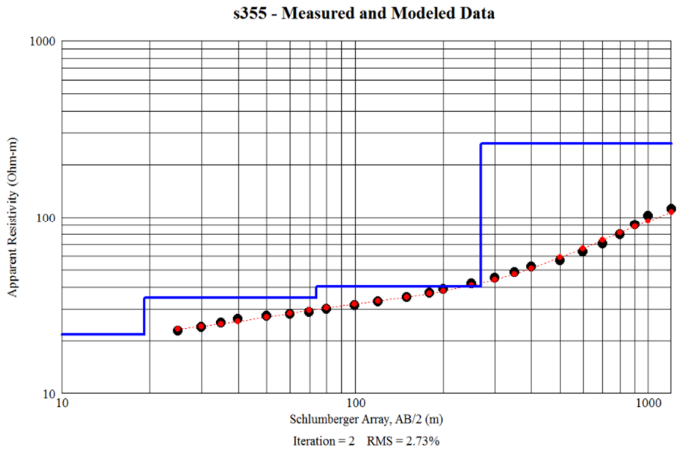
s355 - Measured and Modeled Data
Apparent Resistivity (Ohm-m)
1000
100
10
10
100
1000
Schlumberger Array, AB/2 (m)
Iteration = 2 RMS = 2.73%

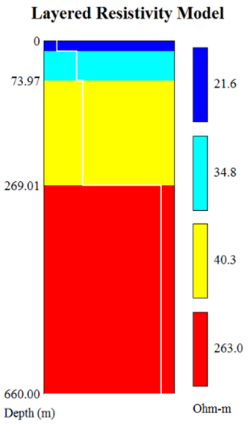
Layered Resistivity Model
0
73.97
269.01
660.00
Depth (m)
21.6
34.8
40.3
263.0
Ohm-m

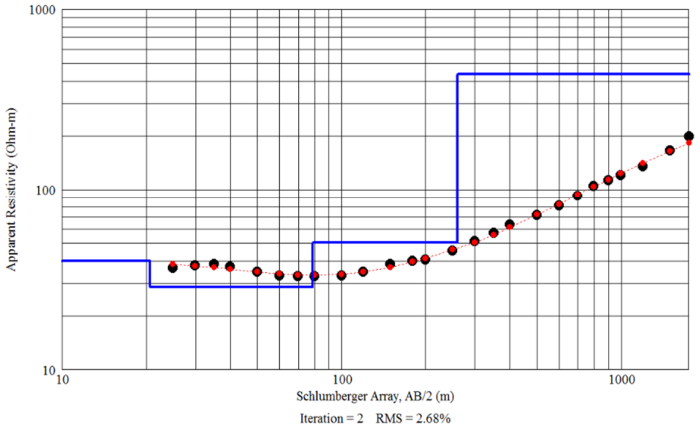
s356 - Measured and Modeled Data
Apparent Resistivity (Ohm-m)
1000
100
10
10
100
1000
Schlumberger Array, AB/2 (m)
Iteration = 2 RMS = 2.68%

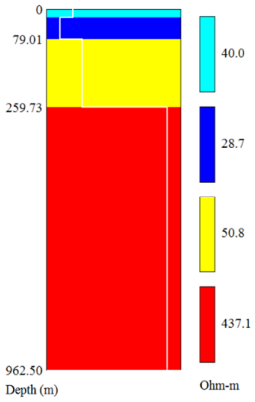
Layered Resistivity Model
0
79.01
259.73
962.50
Depth (m)
40.0
28.7
50.8
437.1
Ohm-m

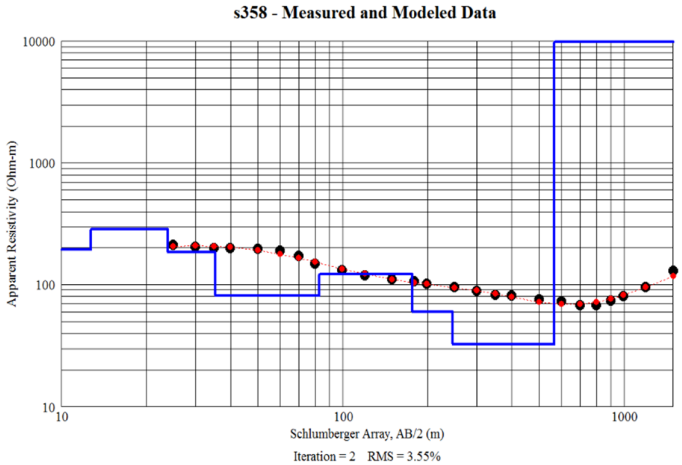
s358 - Measured and Modeled Data
Apparent Resistivity (Ohm-m)
10000
1000
100
10
10
100
1000
Schlumberger Array, AB/2 (m)
Iteration = 2 RMS = 3.55%

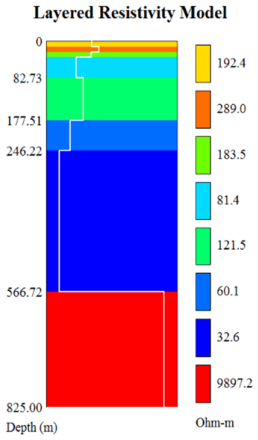
Layered Resistivity Model
0
82.73
177.51
246.22
566.72
825.00
Depth (m)
192.4
289.0
183.5
81.4
121.5
60.1
32.6
9897.2
Ohm-m

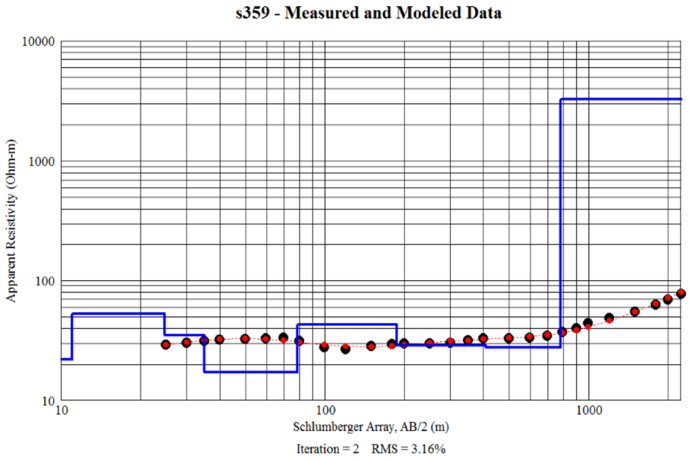
s359 - Measured and Modeled Data
Apparent Resistivity (Ohm-m)
10000
1000
100
10
10
100
1000
Schlumberger Array, AB/2 (m)
Iteration = 2 RMS = 3.16%

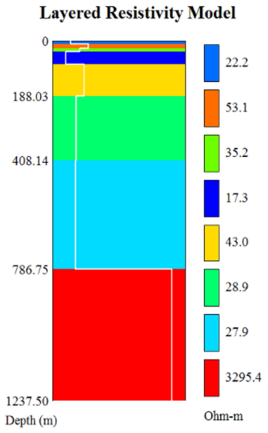
Layered Resistivity Model
0
188.03
408.14
786.75
1237.50
Depth (m)
22.2
53.1
35.2
17.3
43.0
28.9
27.9
3295.4
Ohm-m

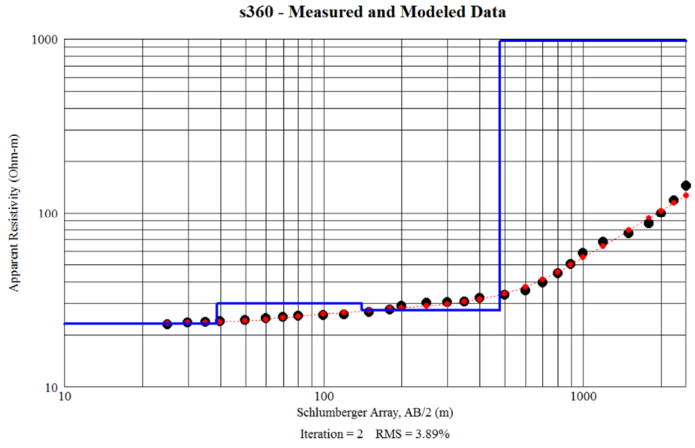
s360 - Measured and Modeled Data
Apparent Resistivity (Ohm-m)
1000
100
10
10
100
1000
Schlumberger Array, AB/2 (m)
Iteration = 2 RMS = 3.89%

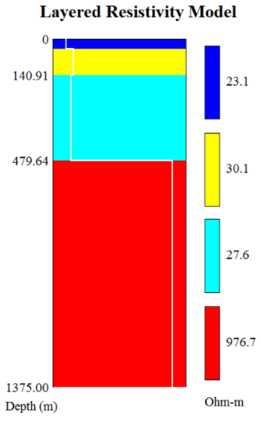
Layered Resistivity Model
0
140.91
479.64
1375.00
Depth (m)
23.1
30.1
27.6
976.7
Ohm-m

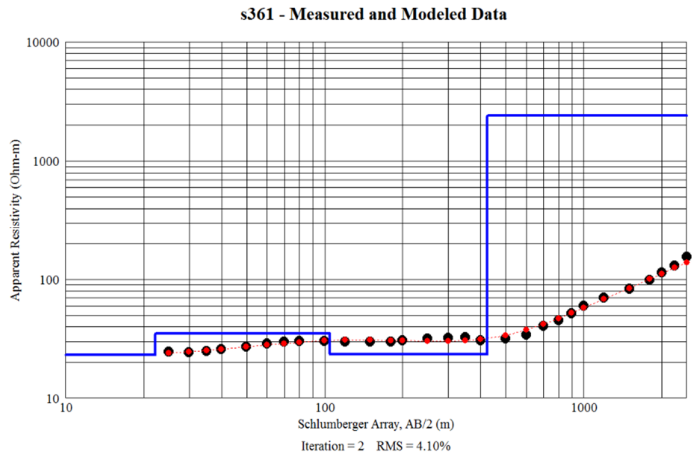
s361 - Measured and Modeled Data
Apparent Resistivity (Ohm-m)
10000
1000
100
10
10
100
1000
Schlumberger Array, AB/2 (m)
Iteration = 2 RMS = 4.10%

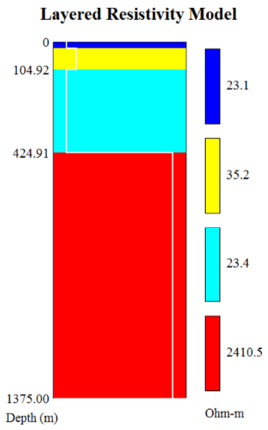
Layered Resistivity Model
0
104.92
424.91
1375.00
Depth (m)
23.1
35.2
23.4
2410.5
Ohm-m

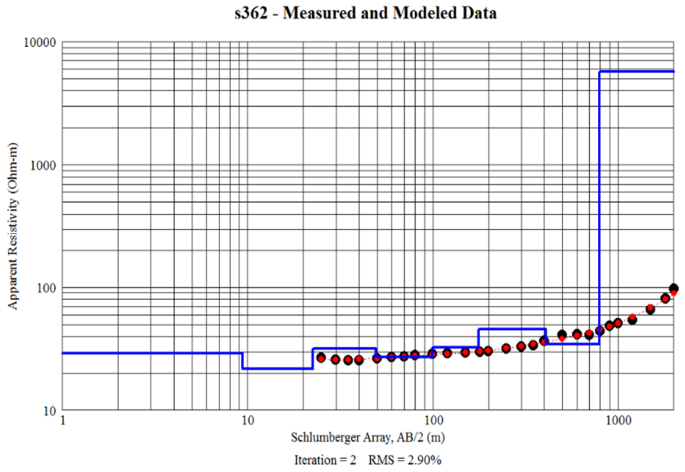
s362 - Measured and Modeled Data
Apparent Resistivity (Ohm-m)
10000
1000
100
10
1
10
100
1000
Schlumberger Array, AB/2 (m)
Iteration = 2 RMS = 2.90%

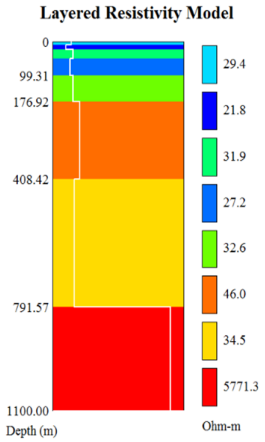
Layered Resistivity Model
0
99.31
176.92
408.42
791.57
1100.00
Depth (m)
29.4
21.8
31.9
27.2
32.6
46.0
34.5
5771.3
Ohm-m

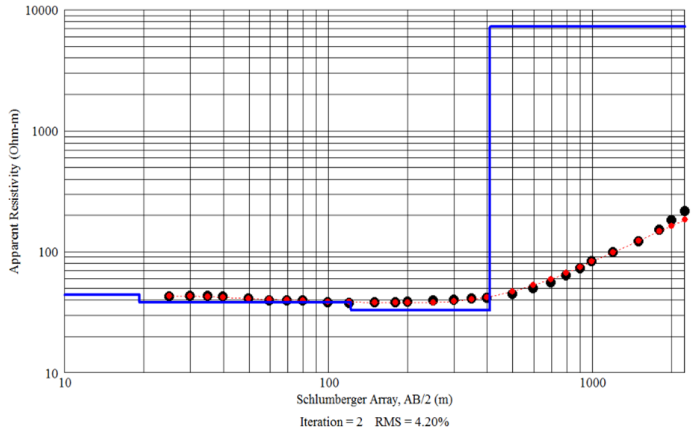
s363 - Measured and Modeled Data
Apparent Resistivity (Ohm-m)
10000
1000
100
10
10
100
1000
Schlumberger Array, AB/2 (m)
Iteration = 2 RMS = 4.20%

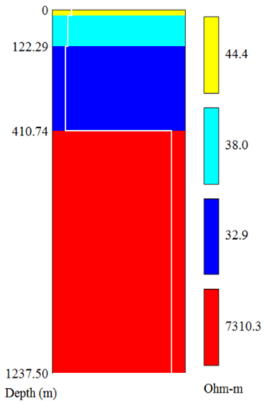
Layered Resistivity Model
0
122.29
410.74
1237.50
Depth (m)
44.4
38.0
32.9
7310.3
Ohm-m

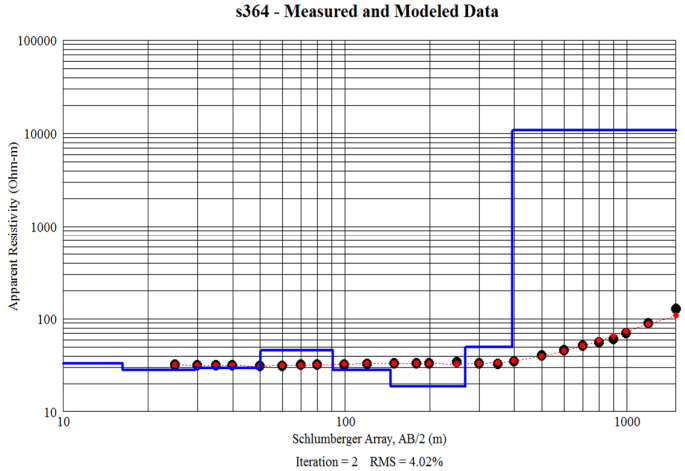
s364 - Measured and Modeled Data
Apparent Resistivity (Ohm-m)
100000
10000
1000
100
10
10
100
1000
Schlumberger Array, AB/2 (m)
Iteration = 2 RMS = 4.02%

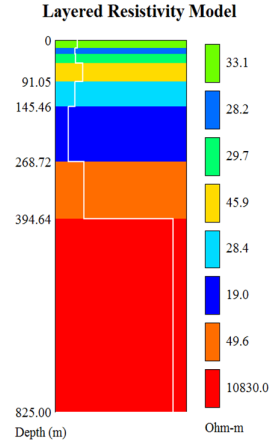
Layered Resistivity Model
0
91.05
145.46
268.72
394.64
825.00
Depth (m)
33.1
28.2
29.7
45.9
28.4
19.0
49.6
10830.0
Ohm-m

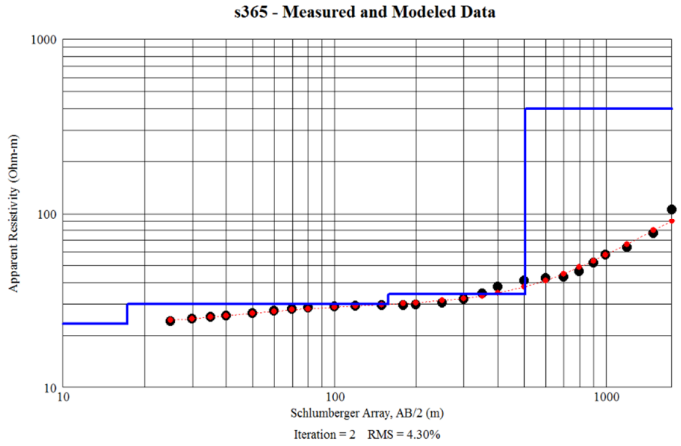
s365 - Measured and Modeled Data
Apparent Resistivity (Ohm-m)
1000
100
10
10
100
1000
Schlumberger Array, AB/2 (m)
Iteration = 2 RMS = 4.30%

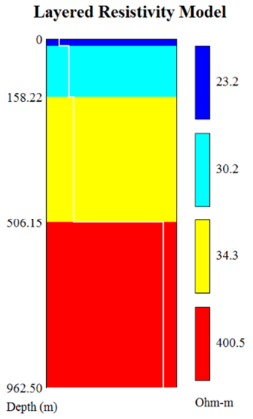
Layered Resistivity Model
0
158.22
506.15
962.50
Depth (m)
23.2
30.2
34.3
400.5
Ohm-m

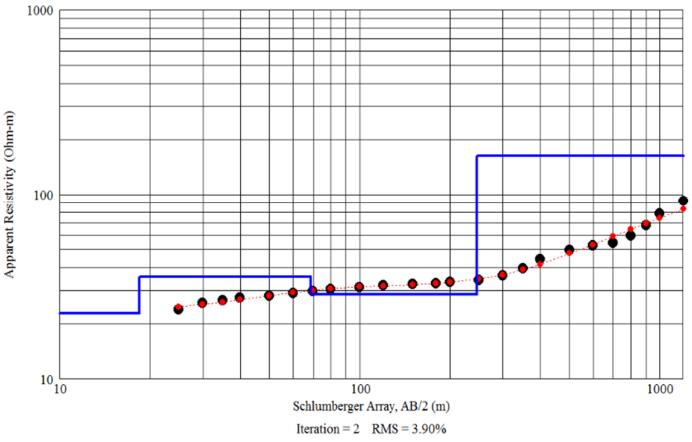
s366 - Measured and Modeled Data
Apparent Resistivity (Ohm-m)
1000
100
10
10
100
1000
Schlumberger Array, AB/2 (m)
Iteration = 2 RMS = 3.90%

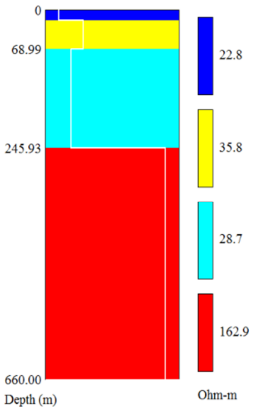
Layered Resistivity Model
0
68.99
245.93
660.00
Depth (m)
22.8
35.8
28.7
162.9
Ohm-m

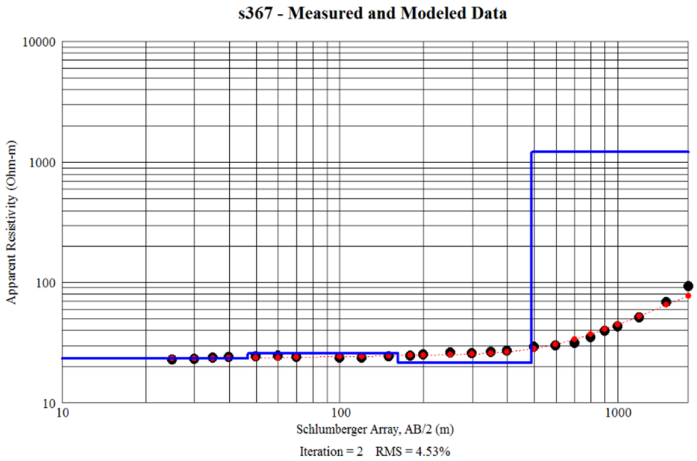
s367 - Measured and Modeled Data
Apparent Resistivity (Ohm-m)
10000
1000
100
10
10
100
1000
Schlumberger Array, AB/2 (m)
Iteration = 2 RMS = 4.53%

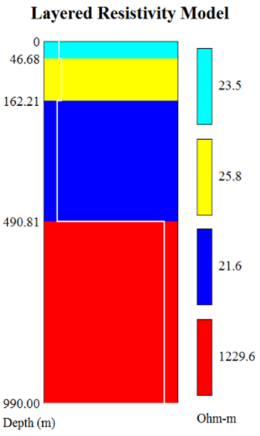
Layered Resistivity Model
0
46.68
162.21
490.81
990.00
Depth (m)
23.5
25.8
21.6
1229.6
Ohm-m

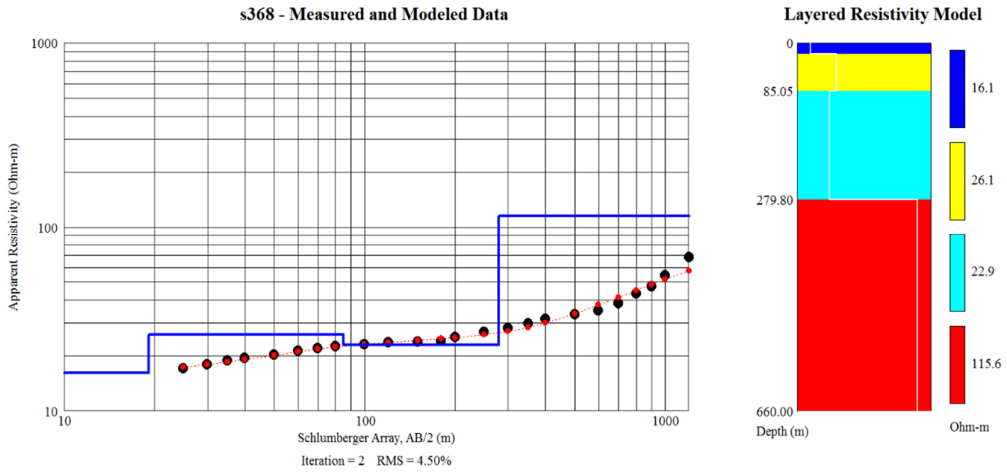
s368 - Measured and Modeled Data
Apparent Resistivity (Ohm-m)
1000
100
10
10
100
1000
Schlumberger Array, AB/2 (m)
Iteration = 2 RMS = 4.50%
Layered Resistivity Model
0
85.05
279.80
660.00
Depth (m)
16.1
26.1
22.9
115.6
Ohm-m

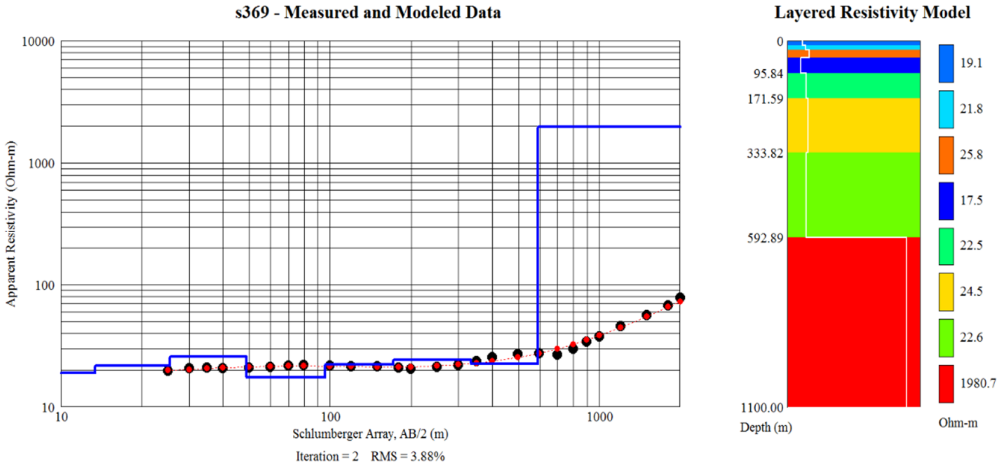
s369 - Measured and Modeled Data
Apparent Resistivity (Ohm-m)
10000
1000
100
10
10
100
1000
Schlumberger Array, AB/2 (m)
Iteration = 2 RMS = 3.88%
Layered Resistivity Model
0
95.84
171.59
333.82
592.89
1100.00
Depth (m)
19.1
21.8
25.8
17.5
22.5
24.5
22.6
1980.7
Ohm-m

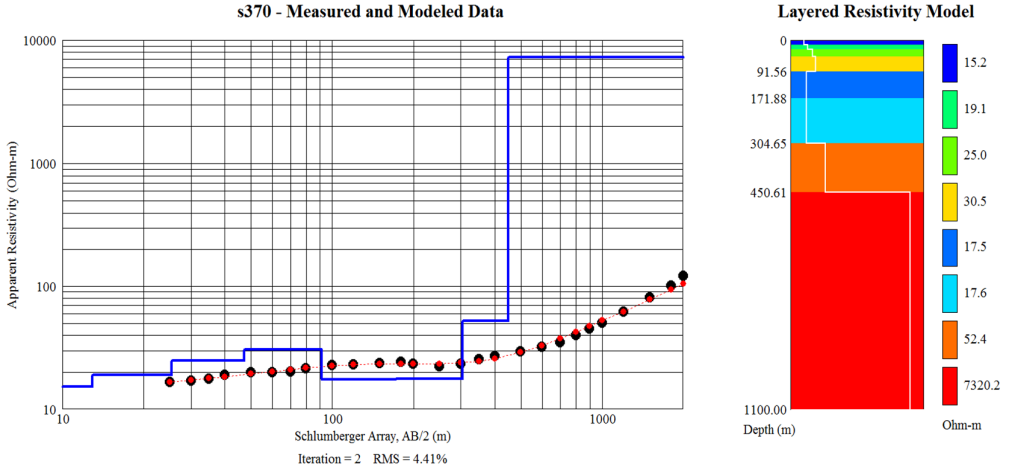
s370 - Measured and Modeled Data
Apparent Resistivity (Ohm-m)
10000
1000
100
10
10
100
1000
Schlumberger Array, AB/2 (m)
Iteration = 2 RMS = 4.41%
Layered Resistivity Model
0
91.56
171.88
304.65
450.61
1100.00
Depth (m)
15.2
19.1
25.0
30.5
17.5
17.6
52.4
7320.2
Ohm-m

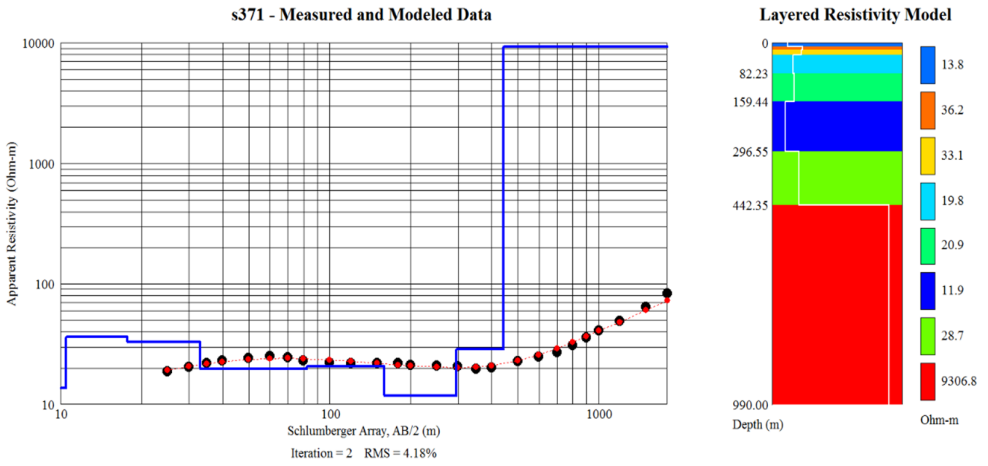
s371 - Measured and Modeled Data
Apparent Resistivity (Ohm-m)
10000
1000
100
10
10
100
1000
Schlumberger Array, AB/2 (m)
Iteration = 2 RMS = 4.18%
Layered Resistivity Model
0
82.23
159.44
296.55
442.35
990.00
Depth (m)
13.8
36.2
33.1
19.8
20.9
11.9
28.7
9306.8
Ohm-m

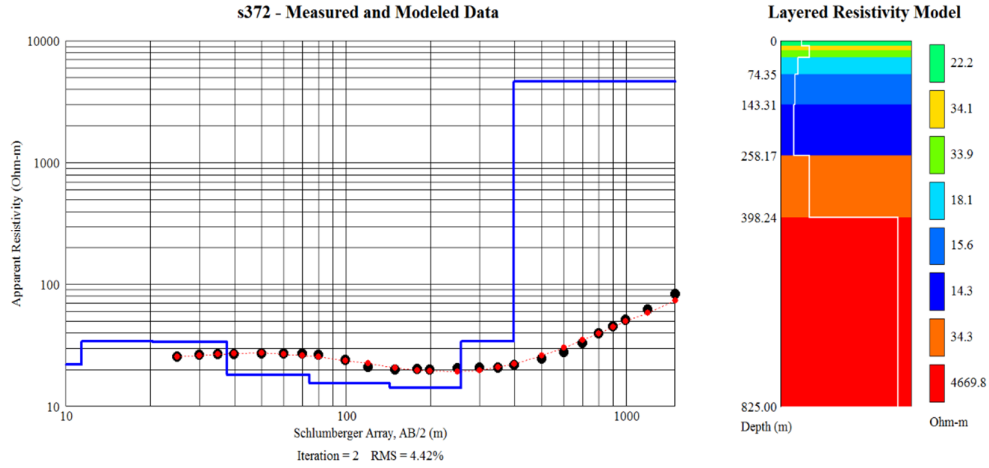
s372 - Measured and Modeled Data
Apparent Resistivity (Ohm-m)
10000
1000
100
10
10
100
1000
Schlumberger Array, AB/2 (m)
Iteration = 2 RMS = 4.42%
Layered Resistivity Model
0
74.35
143.31
258.17
398.24
825.00
Depth (m)
22.2
34.1
33.9
18.1
15.6
14.3
34.3
4669.8
Ohm-m

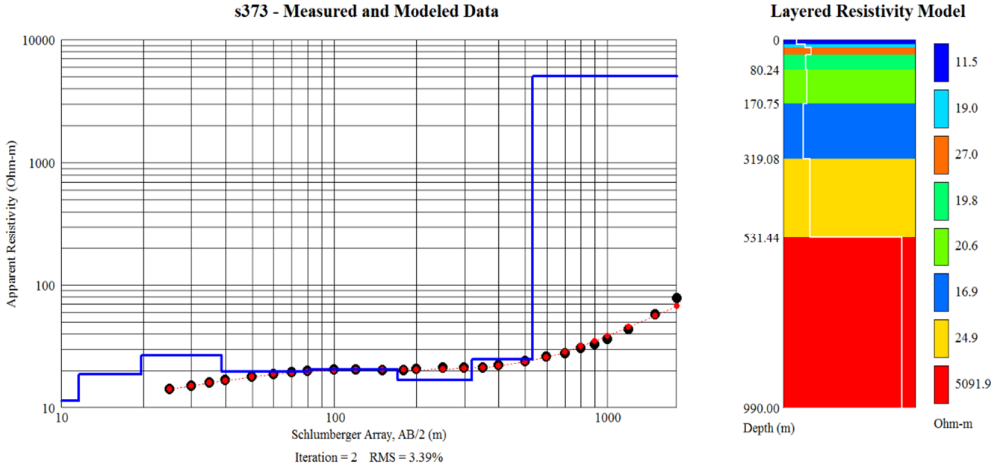
s373 - Measured and Modeled Data
Apparent Resistivity (Ohm-m)
10000
1000
100
10
10
100
1000
Schlumberger Array, AB/2 (m)
Iteration = 2 RMS = 3.39%
Layered Resistivity Model
0
80.24
170.75
319.08
531.44
990.00
Depth (m)
11.5
19.0
27.0
19.8
20.6
16.9
24.9
5091.9
Ohm-m

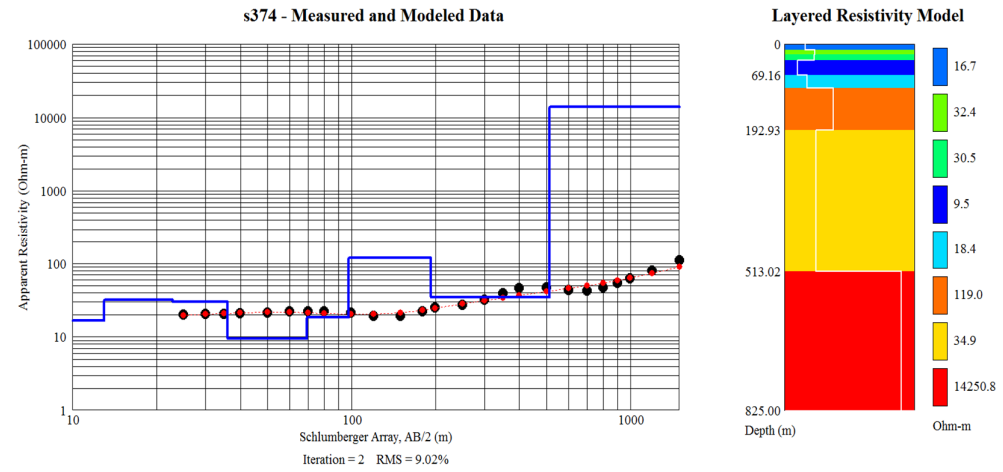
s374 - Measured and Modeled Data
Apparent Resistivity (Ohm-m)
100000
10000
1000
100
10
1
10
100
1000
Schlumberger Array, AB/2 (m)
Iteration = 2 RMS = 9.02%
Layered Resistivity Model
0
69.16
192.93
513.02
825.00
Depth (m)
16.7
32.4
30.5
9.5
18.4
119.0
34.9
14250.8
Ohm-m

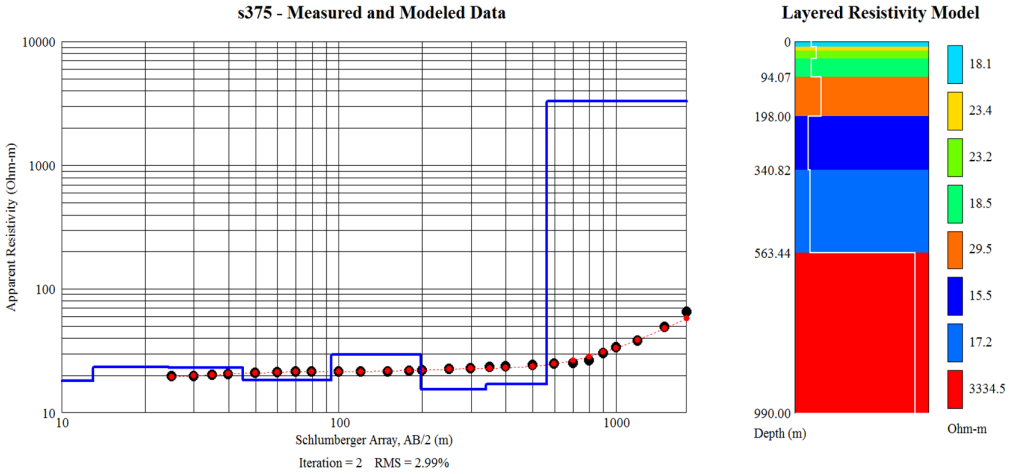
s375 - Measured and Modeled Data
Apparent Resistivity (Ohm-m)
10000
1000
100
10
10
100
1000
Schlumberger Array, AB/2 (m)
Iteration = 2 RMS = 2.99%
Layered Resistivity Model
0
94.07
198.00
340.82
563.44
990.00
Depth (m)
18.1
23.4
23.2
18.5
29.5
15.5
17.2
3334.5
Ohm-m

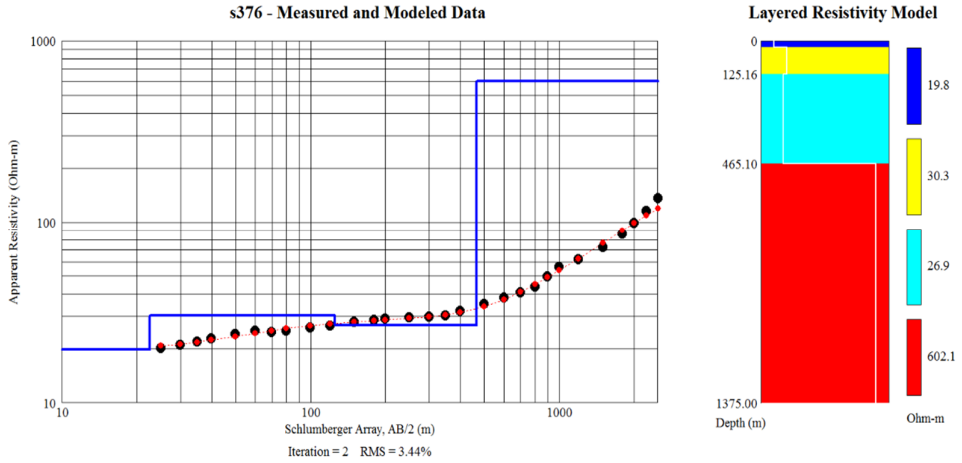
s376 - Measured and Modeled Data
Apparent Resistivity (Ohm-m)
1000
100
10
10
100
1000
Schlumberger Array, AB/2 (m)
Iteration = 2 RMS = 3.44%
Layered Resistivity Model
0
125.16
465.10
1375.00
Depth (m)
19.8
30.3
26.9
602.1
Ohm-m

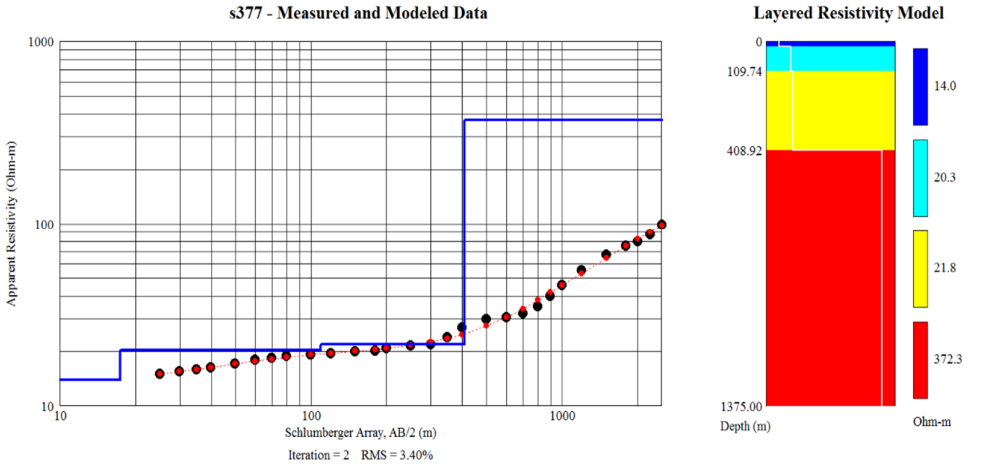
s377 - Measured and Modeled Data
Apparent Resistivity (Ohm-m)
1000
100
10
10
100
1000
Schlumberger Array, AB/2 (m)
Iteration = 2 RMS = 3.40%
Layered Resistivity Model
0
109.74
408.92
1375.00
Depth (m)
14.0
20.3
21.8
372.3
Ohm-m

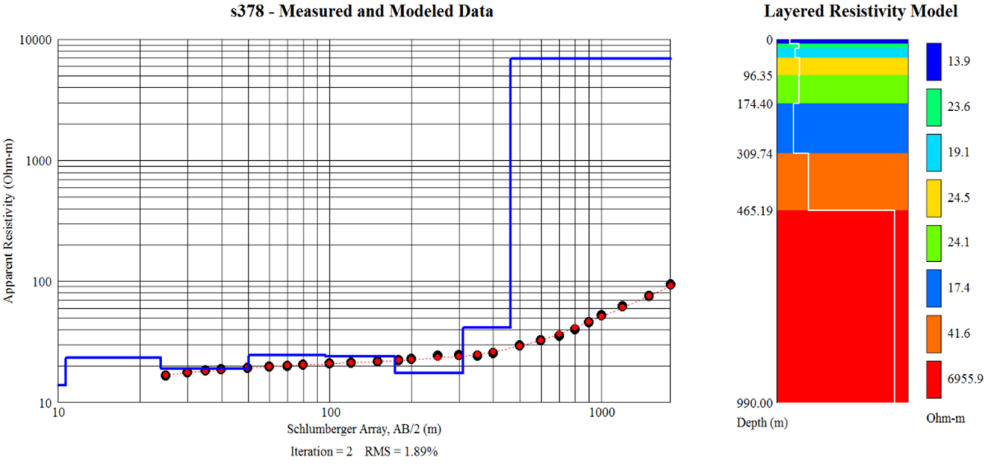
s378 - Measured and Modeled Data
Apparent Resistivity (Ohm-m)
10000
1000
100
10
10
100
1000
Schlumberger Array, AB/2 (m)
Iteration = 2 RMS = 1.89%
Layered Resistivity Model
0
96.35
174.40
309.74
465.19
990.00
Depth (m)
13.9
23.6
19.1
24.5
24.1
17.4
41.6
6955.9
Ohm-m

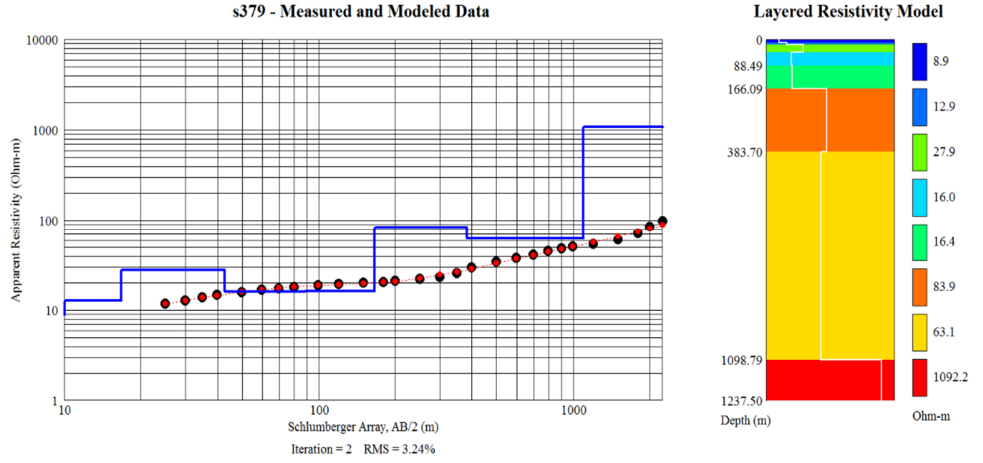
s379 - Measured and Modeled Data
Apparent Resistivity (Ohm-m)
10000
1000
100
10
1
10
100
1000
Schlumberger Array, AB/2 (m)
Iteration = 2 RMS = 3.24%
Layered Resistivity Model
0
88.49
166.09
383.70
1098.79
1237.50
Depth (m)
8.9
12.9
27.9
16.0
16.4
83.9
63.1
1092.2
Ohm-m

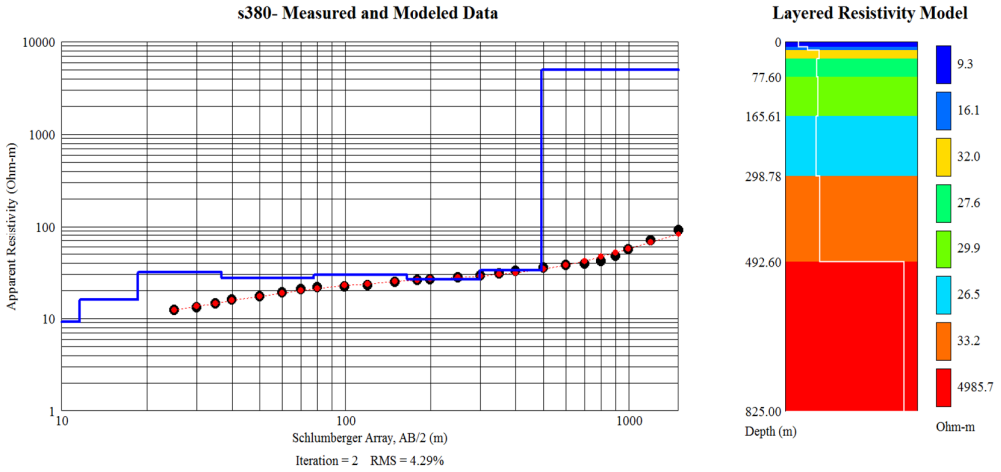
s380- Measured and Modeled Data
Apparent Resistivity (Ohm-m)
10000
1000
100
10
1
10
100
1000
Schlumberger Array, AB/2 (m)
Iteration = 2 RMS = 4.29%
Layered Resistivity Model
0
77.60
165.61
298.78
492.60
825.00
Depth (m)
9.3
16.1
32.0
27.6
29.9
26.5
33.2
4985.7
Ohm-m

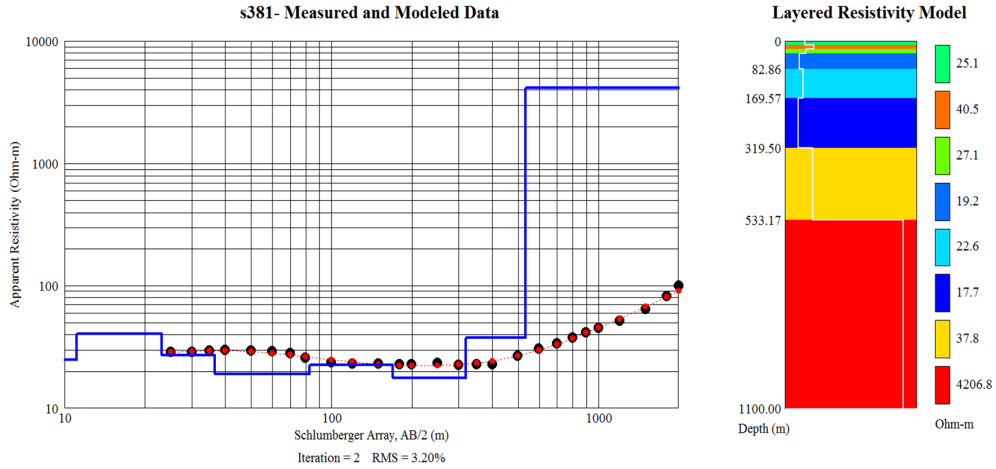
s381- Measured and Modeled Data
Apparent Resistivity (Ohm-m)
10000
1000
100
10
10
100
1000
Schlumberger Array, AB/2 (m)
Iteration = 2 RMS = 3.20%
Layered Resistivity Model
0
82.86
169.57
319.50
533.17
1100.00
Depth (m)
25.1
40.5
27.1
19.2
22.6
17.7
37.8
4206.8
Ohm-m

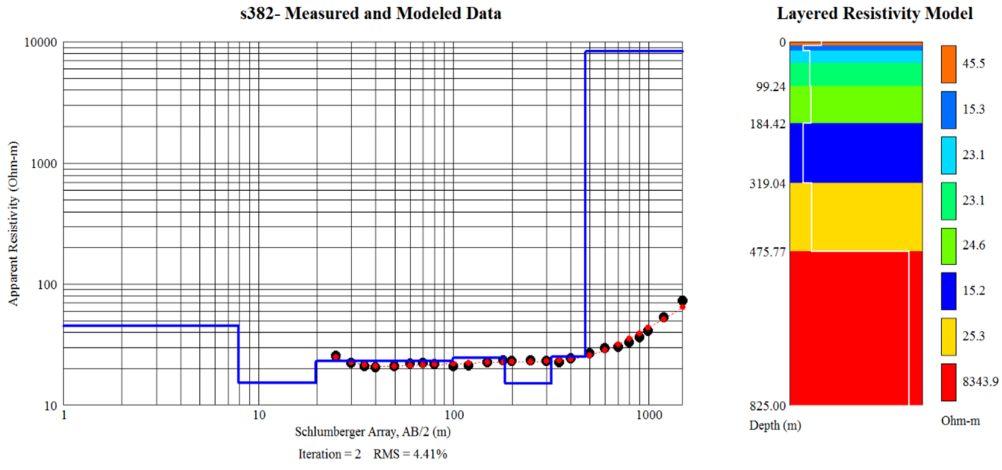
s382- Measured and Modeled Data
Apparent Resistivity (Ohm-m)
10000
1000
100
10
1
10
100
1000
Schlumberger Array, AB/2 (m)
Iteration = 2 RMS = 4.41%
Layered Resistivity Model
0
99.24
184.42
319.04
475.77
825.00
Depth (m)
45.5
15.3
23.1
23.1
24.6
15.2
25.3
8343.9
Ohm-m

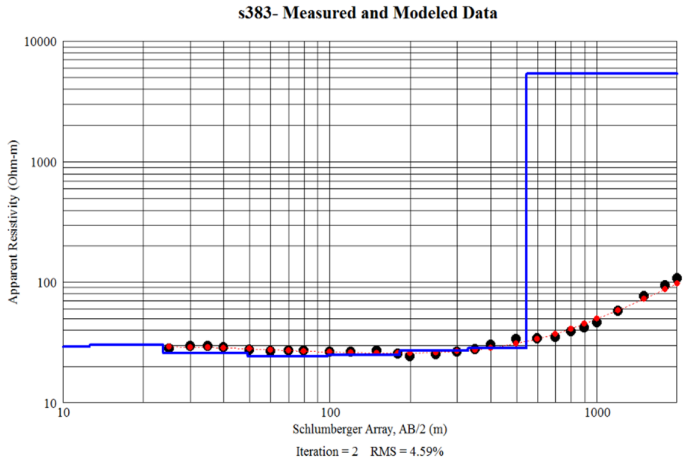
s383- Measured and Modeled Data
Apparent Resistivity (Ohm-m)
10000
1000
100
10
10
100
1000
Schlumberger Array, AB/2 (m)
Iteration = 2 RMS = 4.59%

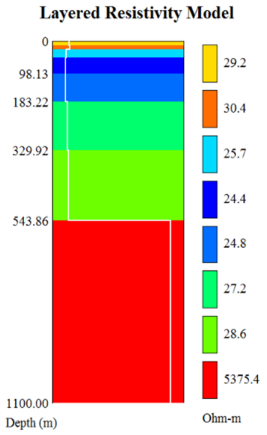
Layered Resistivity Model
0
98.13
183.22
329.92
543.86
1100.00
Depth (m)
29.2
30.4
25.7
24.4
24.8
27.2
28.6
5375.4
Ohm-m

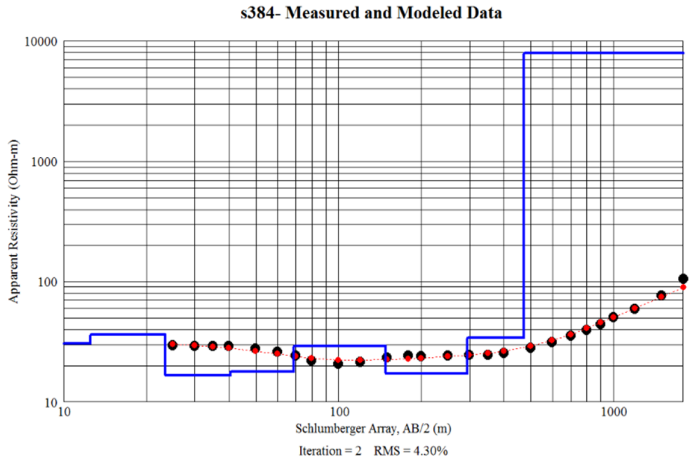
s384- Measured and Modeled Data
Apparent Resistivity (Ohm-m)
10000
1000
100
10
10
100
1000
Schlumberger Array, AB/2 (m)
Iteration = 2 RMS = 4.30%

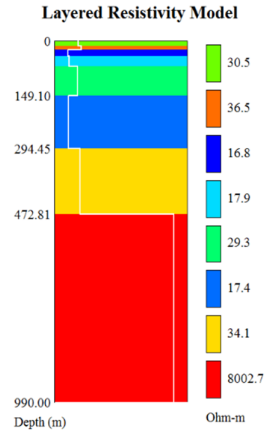
Layered Resistivity Model
0
149.10
294.45
472.81
990.00
Depth (m)
30.5
36.5
16.8
17.9
29.3
17.4
34.1
8002.7
Ohm-m

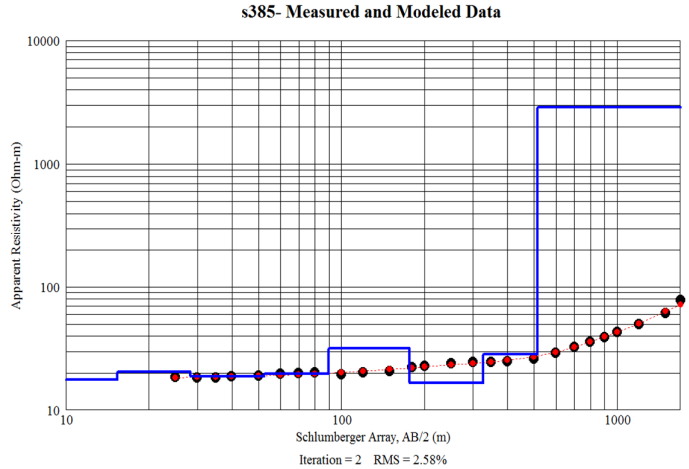
s385- Measured and Modeled Data
Apparent Resistivity (Ohm-m)
10000
1000
100
10
10
100
1000
Schlumberger Array, AB/2 (m)
Iteration = 2 RMS = 2.58%

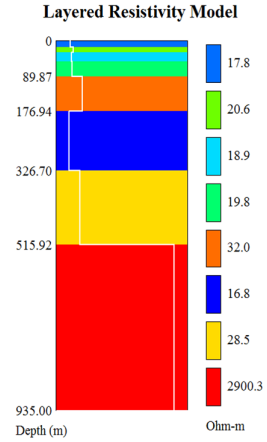
Layered Resistivity Model
0
89.87
176.94
326.70
515.92
935.00
Depth (m)
17.8
20.6
18.9
19.8
32.0
16.8
28.5
2900.3
Ohm-m

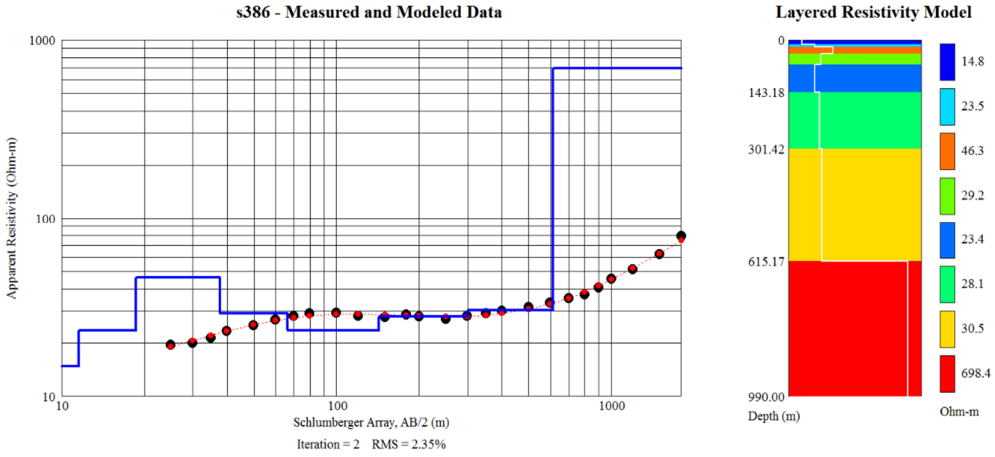
s386 - Measured and Modeled Data
Apparent Resistivity (Ohm-m)
1000
100
10
10
100
1000
Schlumberger Array, AB/2 (m)
Iteration = 2 RMS = 2.35%
Layered Resistivity Model
0
143.18
301.42
615.17
990.00
Depth (m)
14.8
23.5
46.3
29.2
23.4
28.1
30.5
698.4
Ohm-m

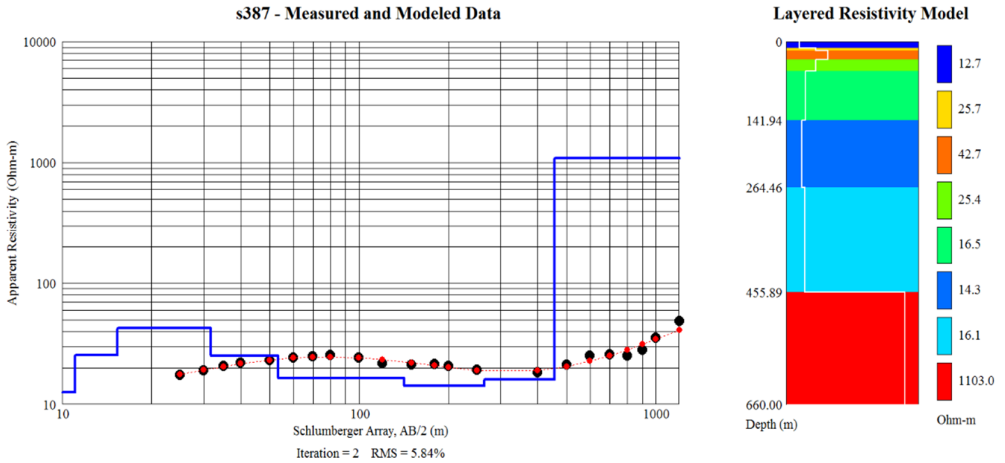
s387 - Measured and Modeled Data
Apparent Resistivity (Ohm-m)
10000
1000
100
10
10
100
1000
Schlumberger Array, AB/2 (m)
Iteration = 2 RMS = 5.84%
Layered Resistivity Model
0
141.94
264.46
455.89
660.00
Depth (m)
12.7
25.7
42.7
25.4
16.5
14.3
16.1
1103.0
Ohm-m

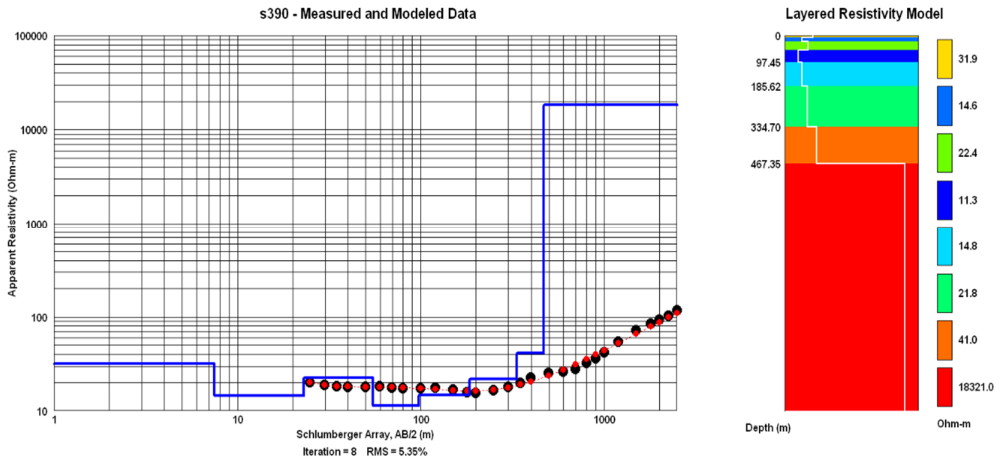
s390 - Measured and Modeled Data
Apparent Resistivity (Ohm-m)
100000
10000
1000
100
10
1
10
100
1000
Schlumberger Array, AB/2 (m)
Iteration = 8 RMS = 5.35%
Layered Resistivity Model
0
97.45
185.62
334.70
467.35
Depth (m)
31.9
14.6
22.4
11.3
14.8
21.8
41.0
18321.0
Ohm-m

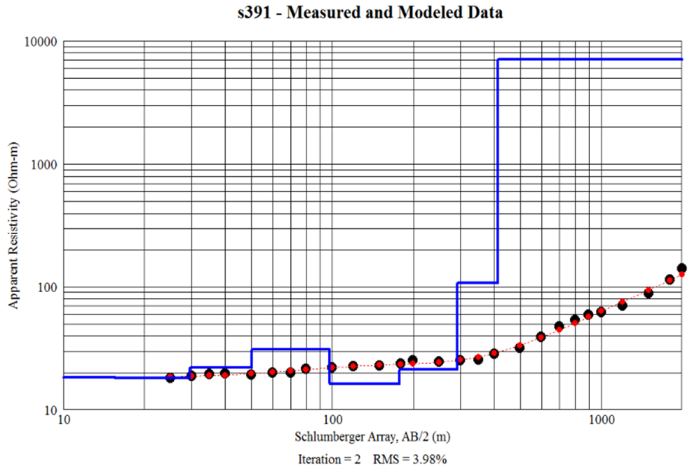
s391 - Measured and Modeled Data
Apparent Resistivity (Ohm-m)
10000
1000
100
10
10
100
1000
Schlumberger Array, AB/2 (m)
Iteration = 2 RMS = 3.98%

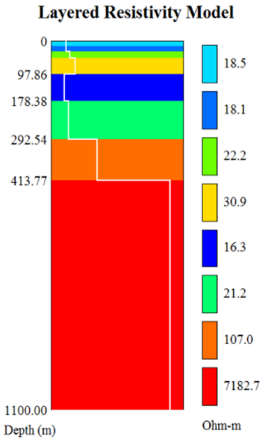
Layered Resistivity Model
0
97.86
178.38
292.54
413.77
1100.00
Depth (m)
18.5
18.1
22.2
30.9
16.3
21.2
107.0
7182.7
Ohm-m

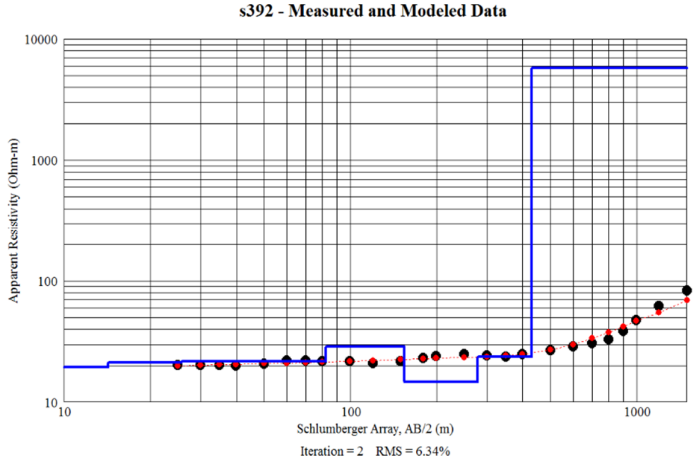
s392 - Measured and Modeled Data
Apparent Resistivity (Ohm-m)
10000
1000
100
10
10
100
1000
Schlumberger Array, AB/2 (m)
Iteration = 2 RMS = 6.34%

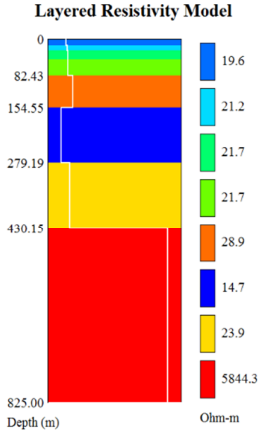
Layered Resistivity Model
0
82.43
154.55
279.19
430.15
825.00
Depth (m)
19.6
21.2
21.7
21.7
28.9
14.7
23.9
5844.3
Ohm-m

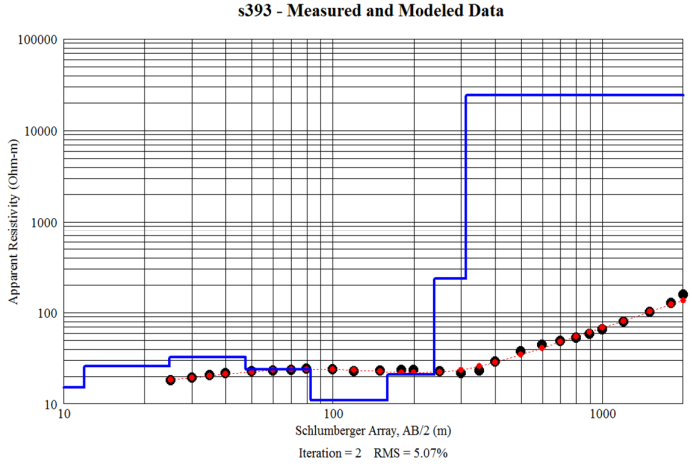
s393 - Measured and Modeled Data
Apparent Resistivity (Ohm-m)
100000
10000
1000
100
10
10
100
1000
Schlumberger Array, AB/2 (m)
Iteration = 2 RMS = 5.07%

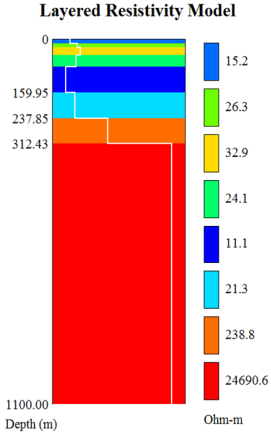
Layered Resistivity Model
0
159.95
237.85
312.43
1100.00
Depth (m)
15.2
26.3
32.9
24.1
11.1
21.3
238.8
24690.6
Ohm-m

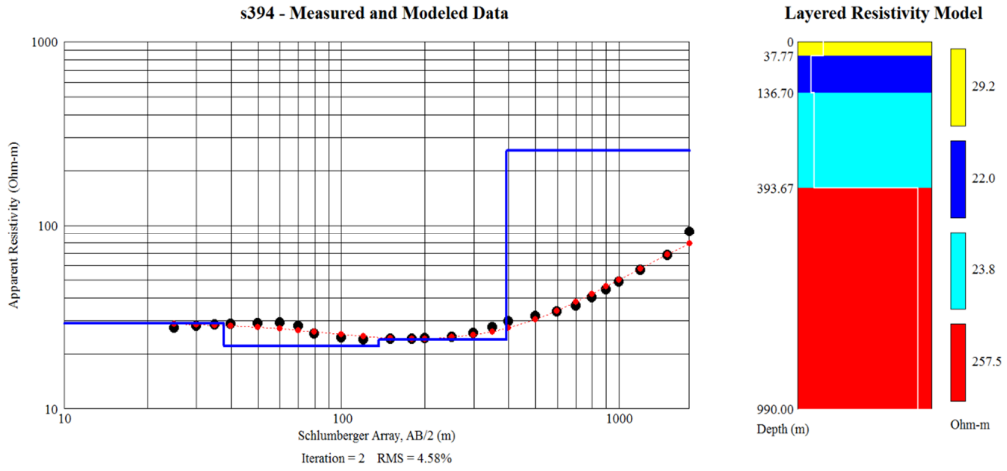
s394 - Measured and Modeled Data
Apparent Resistivity (Ohm-m)
1000
100
10
10
100
1000
Schlumberger Array, AB/2 (m)
Iteration = 2 RMS = 4.58%
Layered Resistivity Model
0
37.77
136.70
393.67
990.00
Depth (m)
29.2
22.0
23.8
257.5
Ohm-m

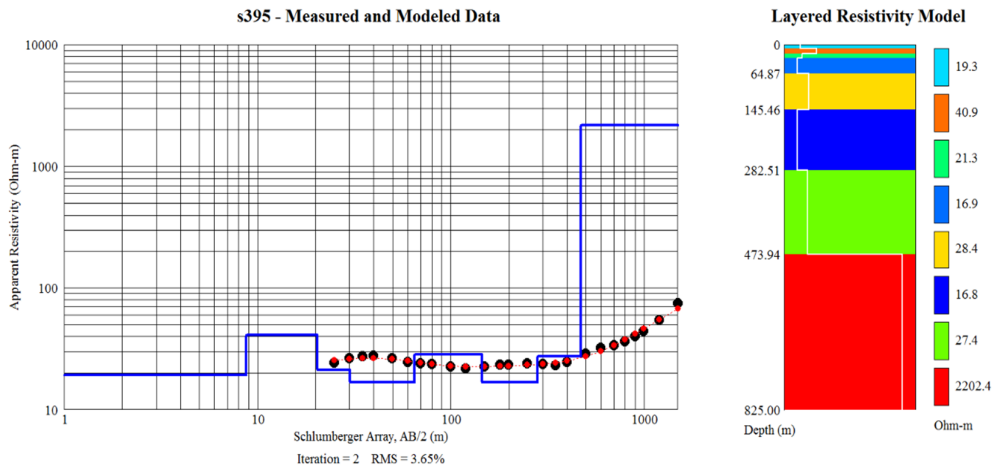
s395 - Measured and Modeled Data
Apparent Resistivity (Ohm-m)
10000
1000
100
10
1
10
100
1000
Schlumberger Array, AB/2 (m)
Iteration = 2 RMS = 3.65%
Layered Resistivity Model
0
64.87
145.46
282.51
473.94
825.00
Depth (m)
19.3
40.9
21.3
16.9
28.4
16.8
27.4
2202.4
Ohm-m

Appendix F: 1D Rolling Inversion and 2D Inversion Models

AREA 1:

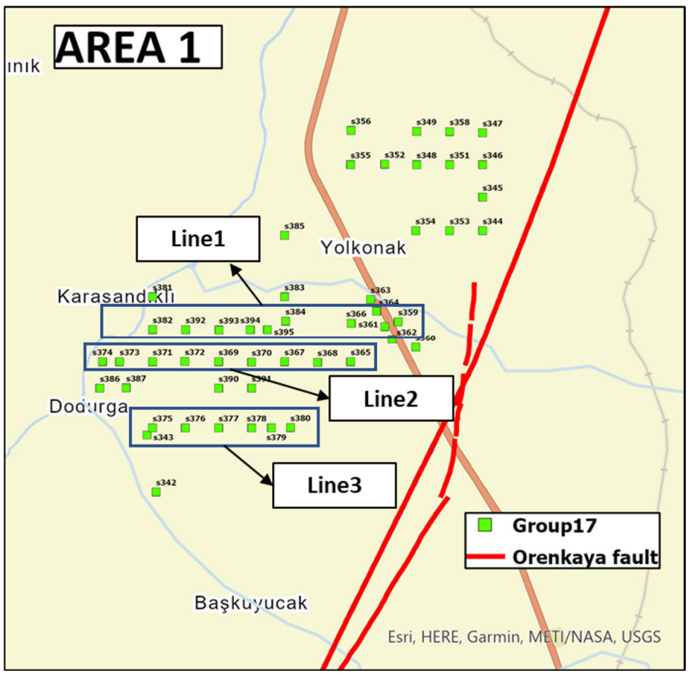

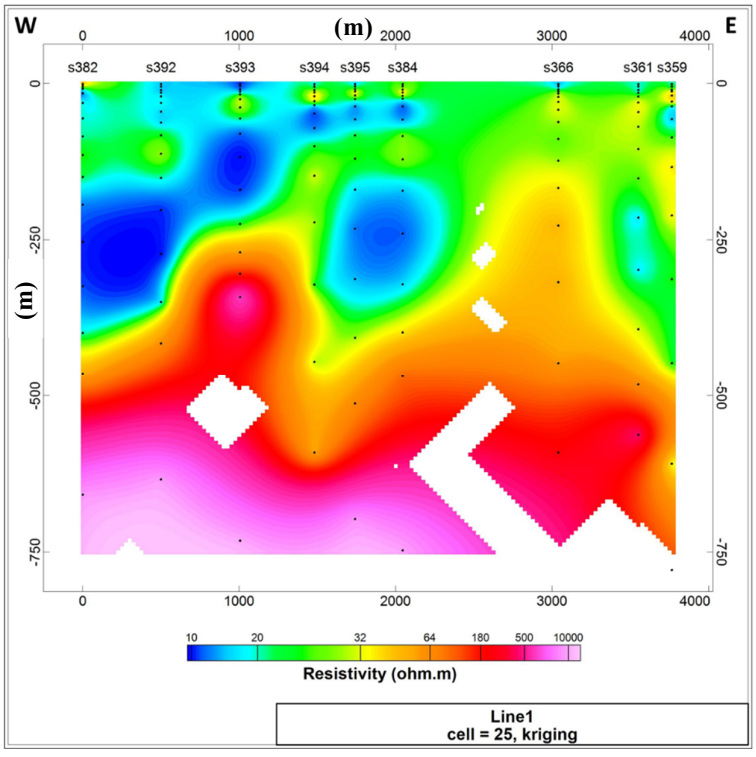

1D rolling inversion model of Line1.

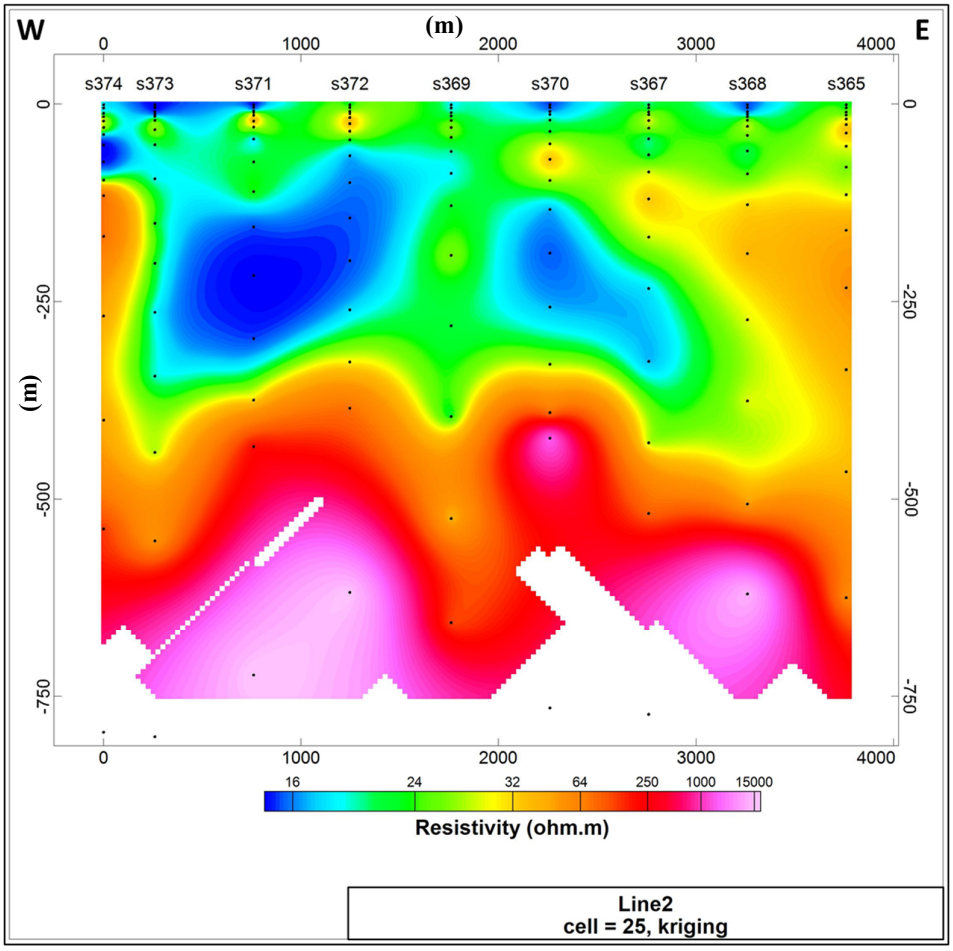

1D rolling inversion model of Line2.

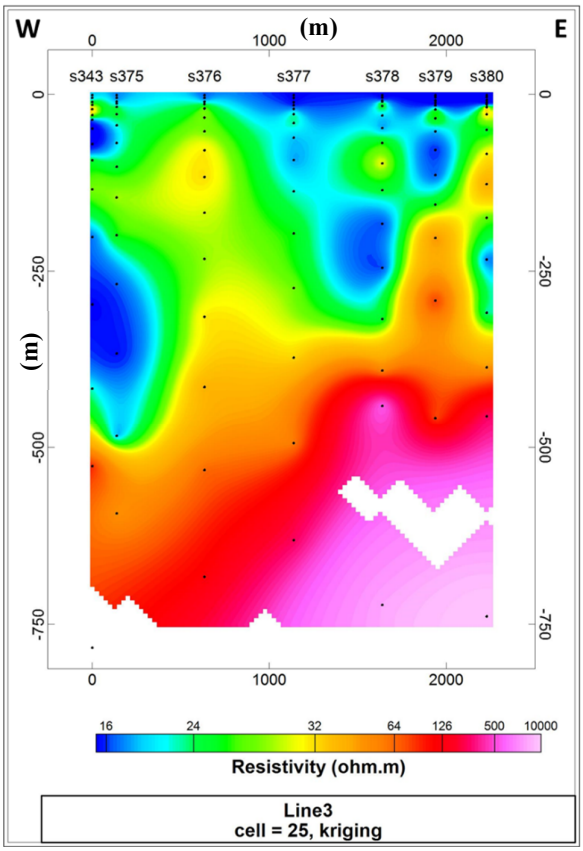

1D rolling inversion model of Line3.

AREA 2:

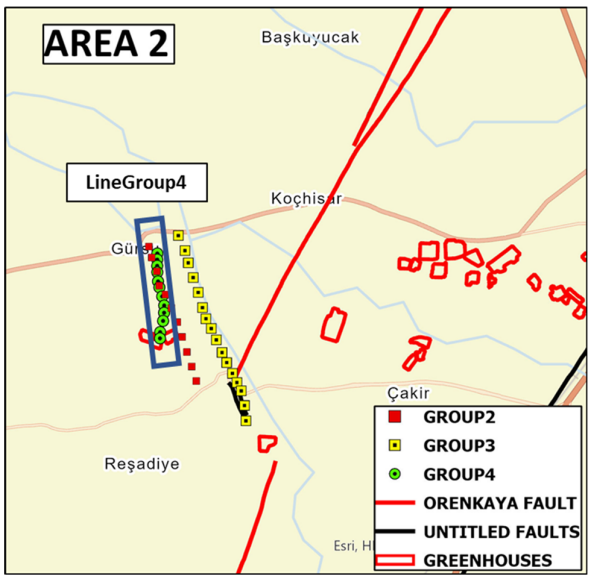

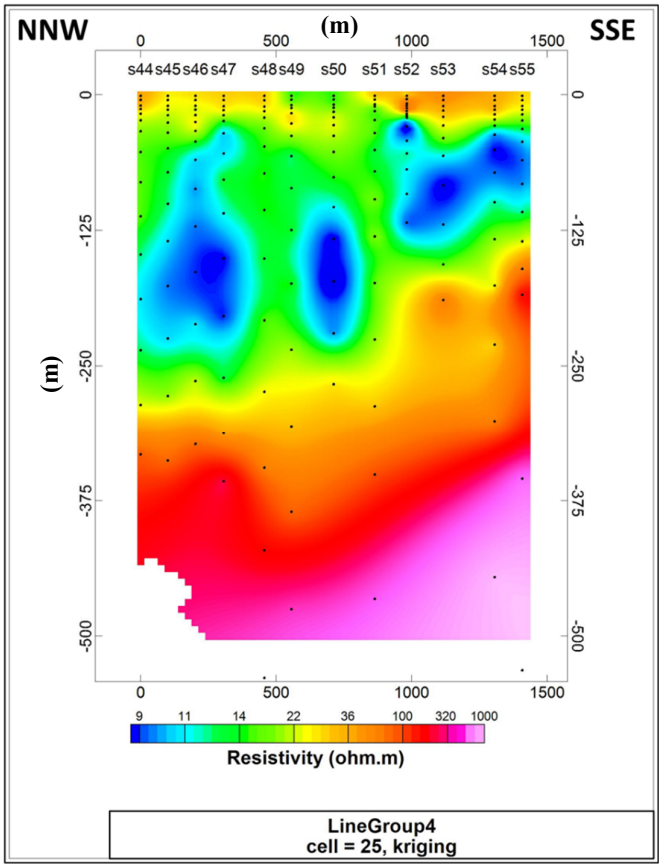

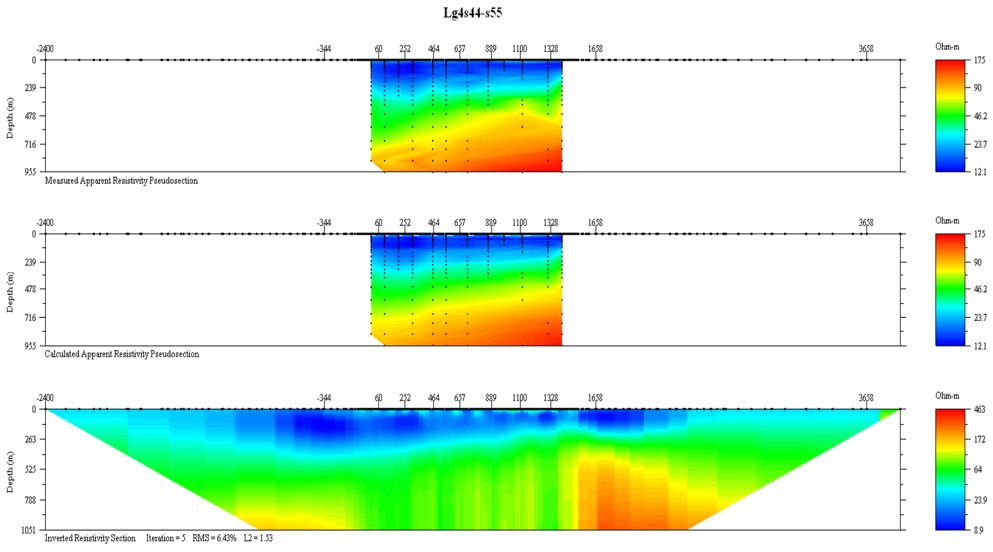

1D rolling and 2D inversion models of LineGroup4.

AREA 3:

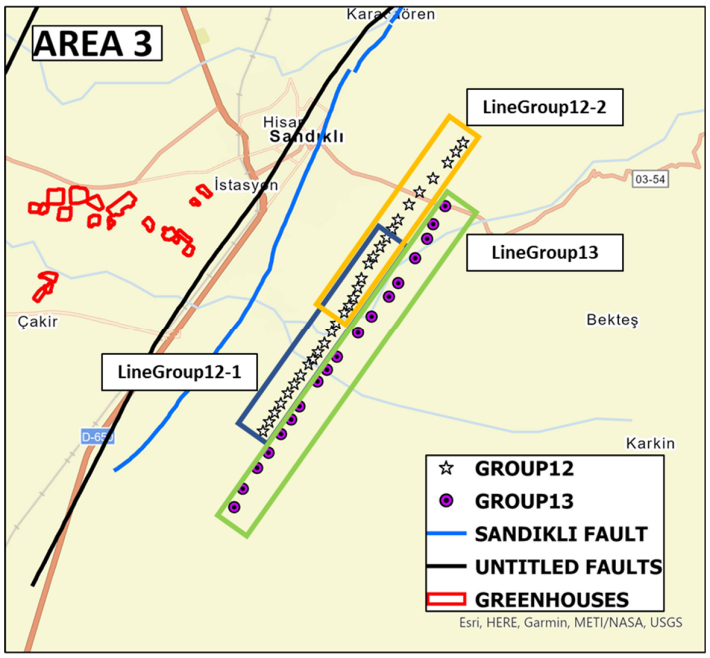
AREA 3
Karaören
Hisar
Sandıklı
İstasyon
Çakir
Bekteş
Karkin
03-54
D-65
LineGroup12-2
LineGroup13
LineGroup12-1
GROUP12
GROUP13
SANDIKLI FAULT
UNTITLED FAULTS
GREENHOUSES
Esri, HERE, Garmin, METI/NASA, USGS

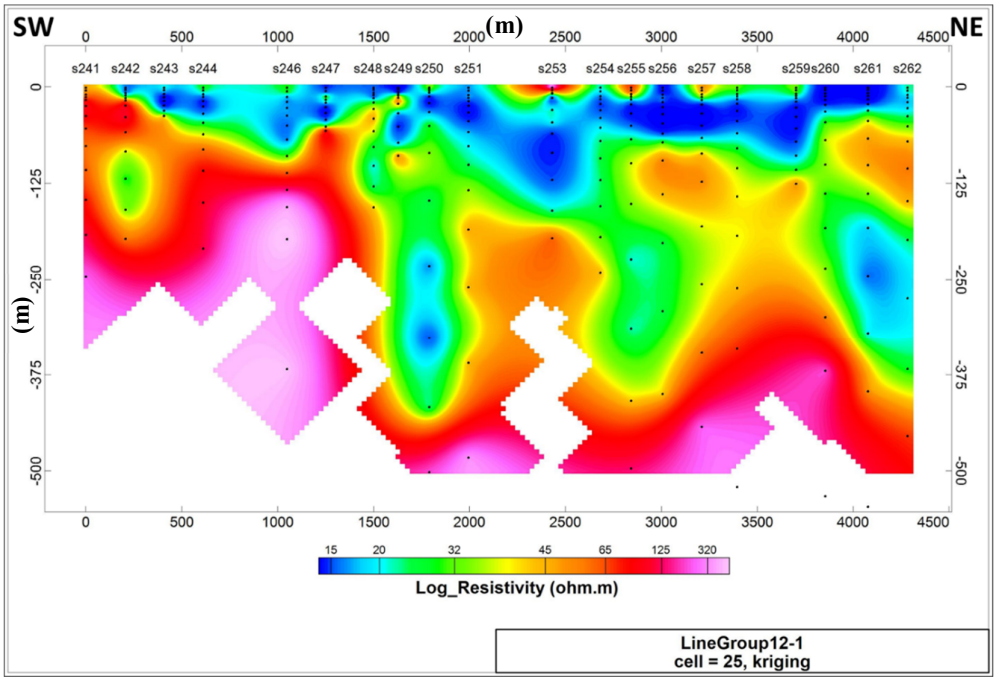
SW
NE
(m)
0 500 1000 1500 2000 2500 3000 3500 4000 4500
s241 s242 s243 s244 s246 s247 s248 s249 s250 s251 s253 s254 s255 s256 s257 s258 s259 s260 s261 s262
0 -125 -250 -375 -500
15 20 32 45 65 125 320
Log_Resistivity (ohm.m)
LineGroup12-1
cell = 25, kriging

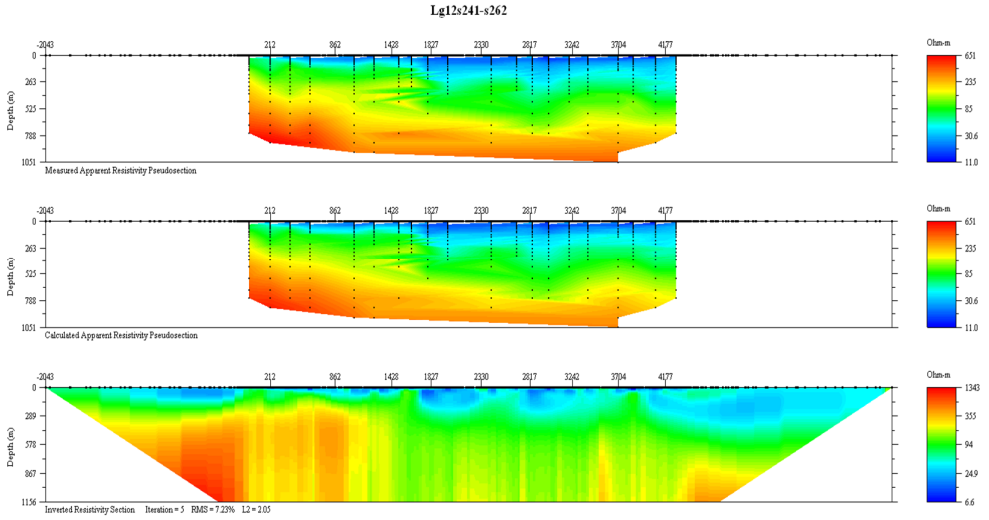

1D rolling and 2D inversion models of LineGroup12-1.

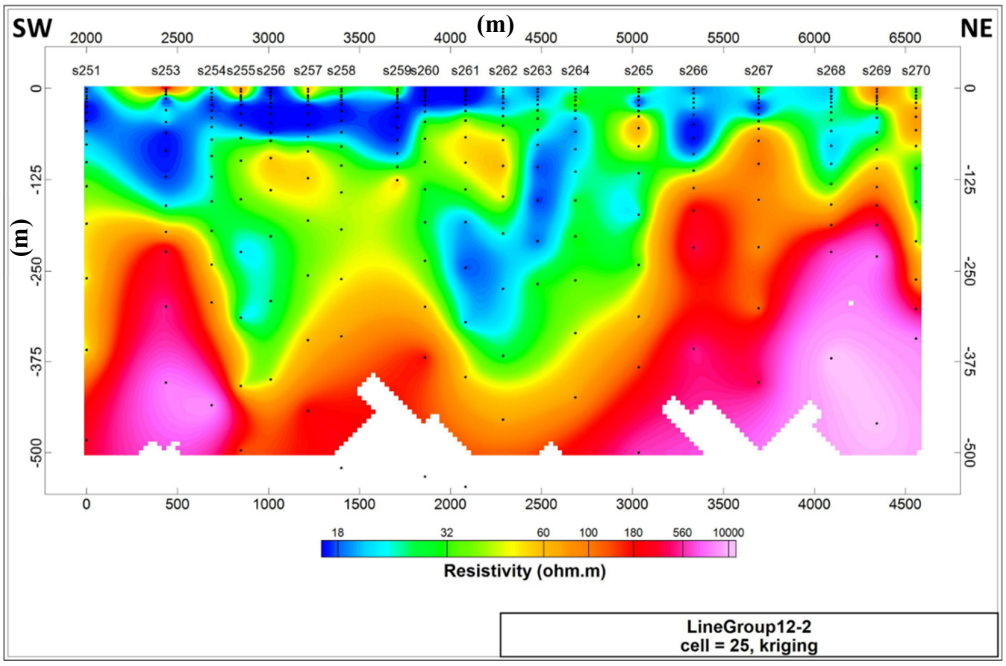

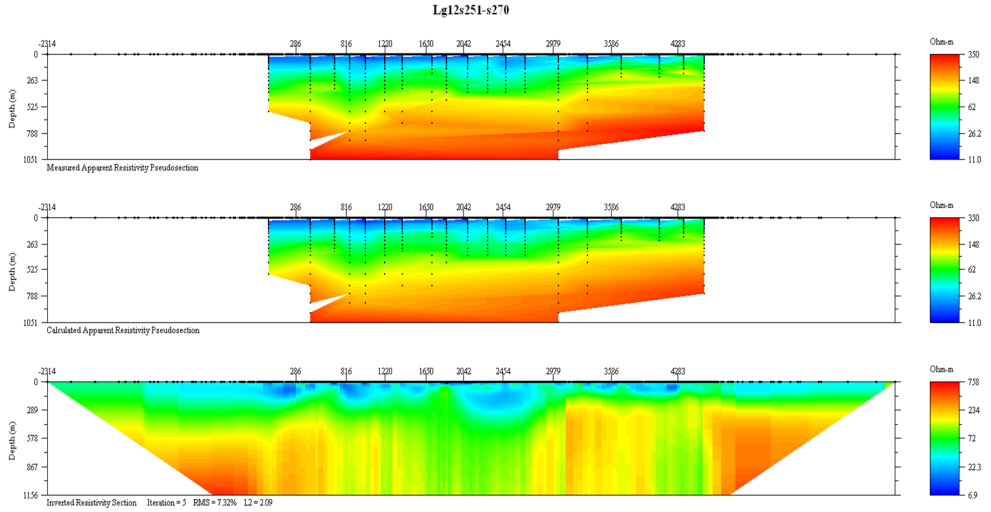

1D rolling and 2D inversion models of LineGroup12-2.

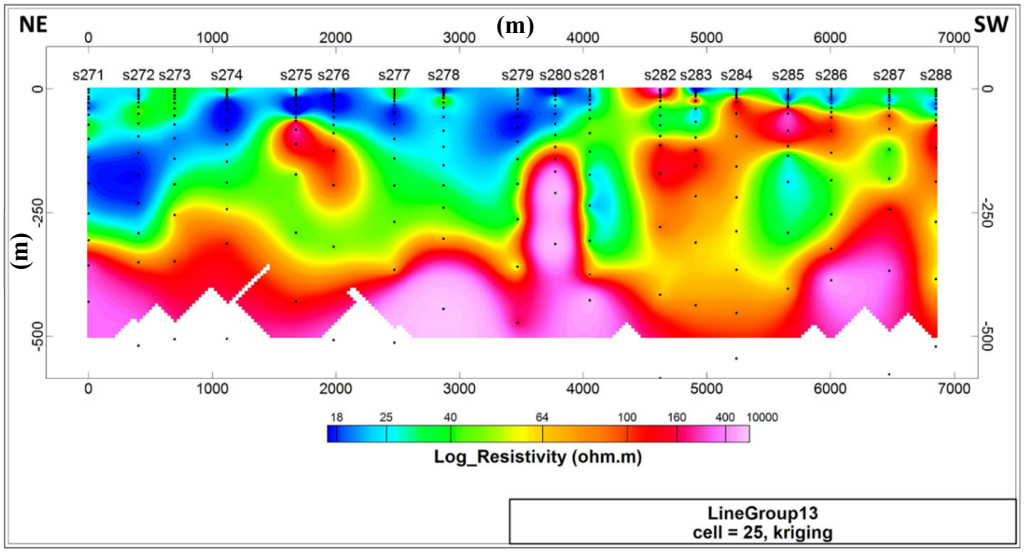

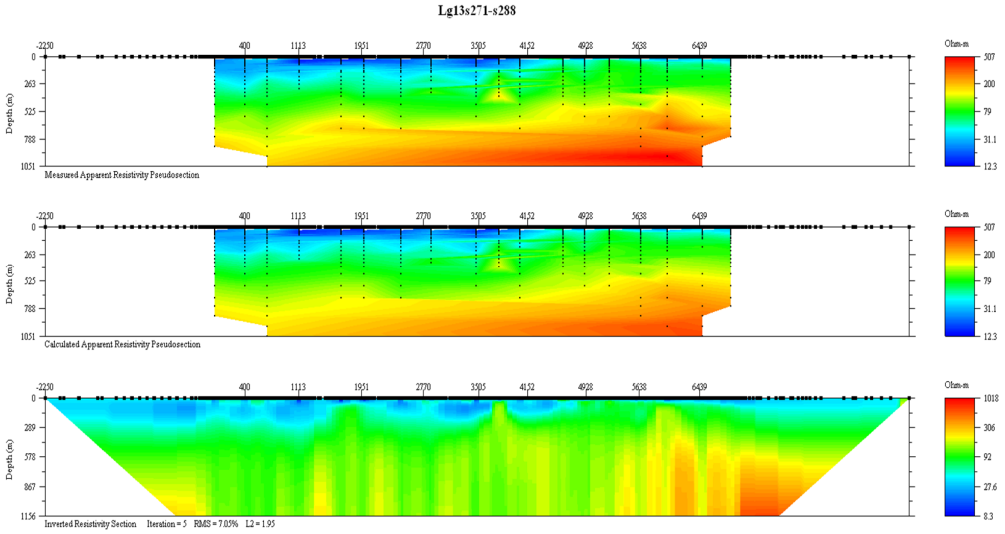

1D rolling and 2D inversion models of LineGroup13.

AREA 4:

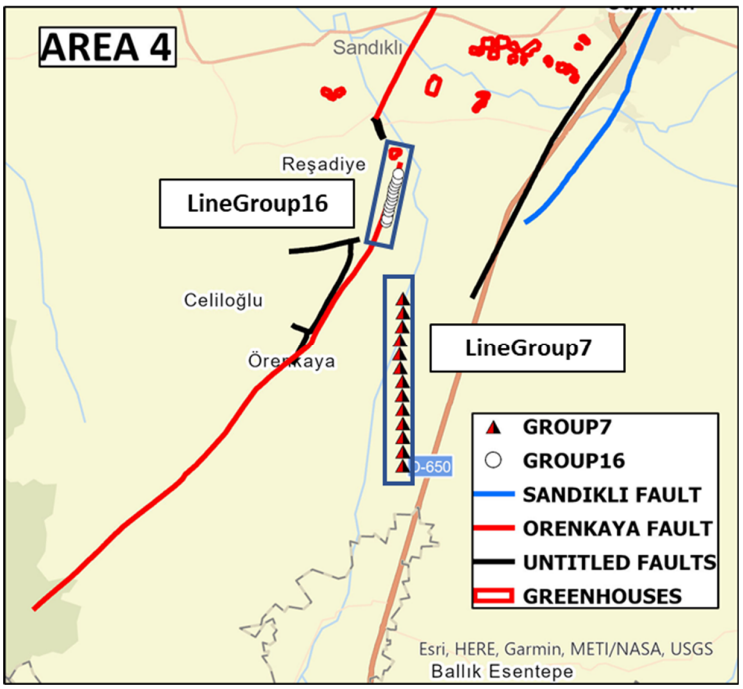

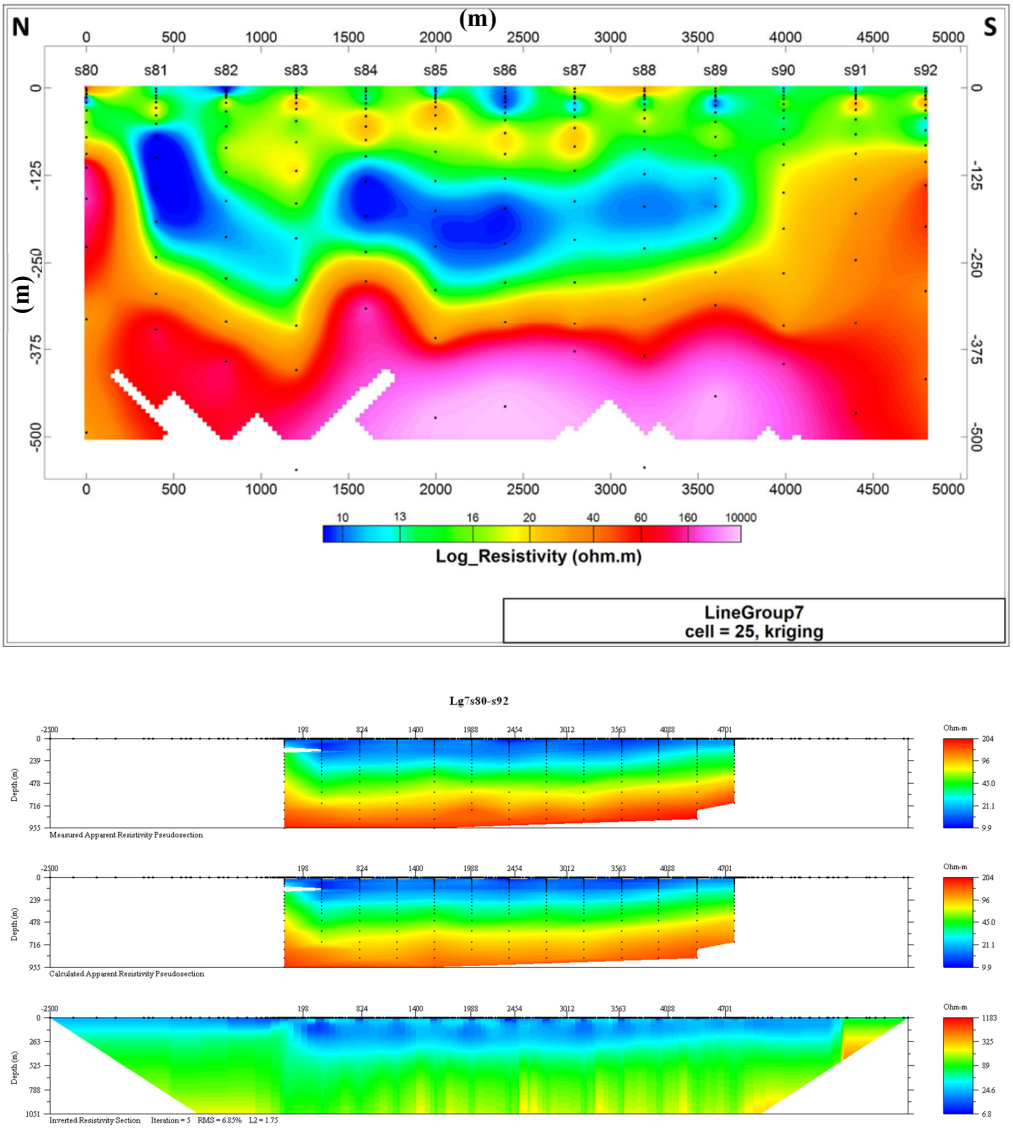

1D rolling and 2D inversion models of LineGroup7.

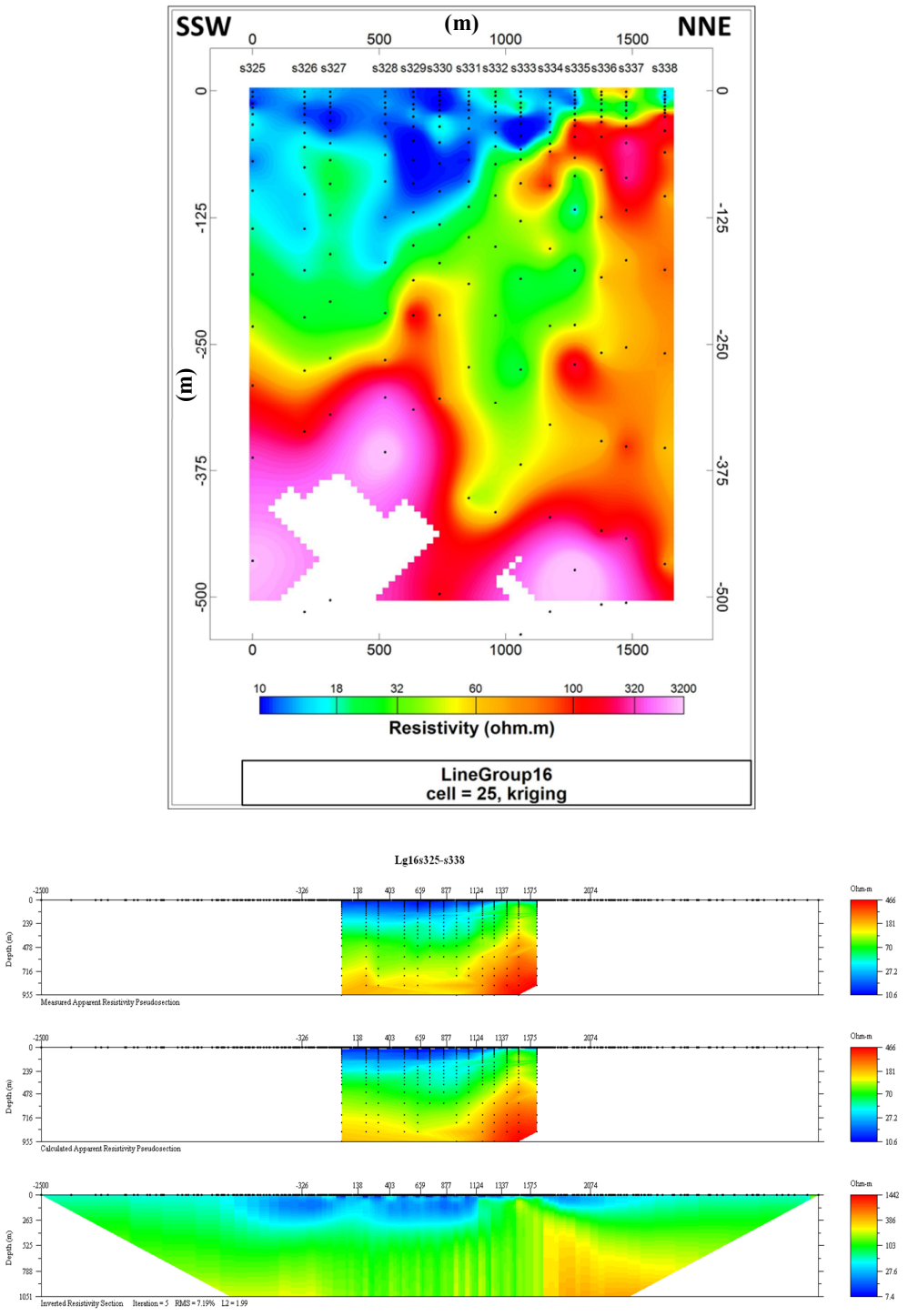

1D rolling and 2D inversion models of LineGroup16.

AREA 5:

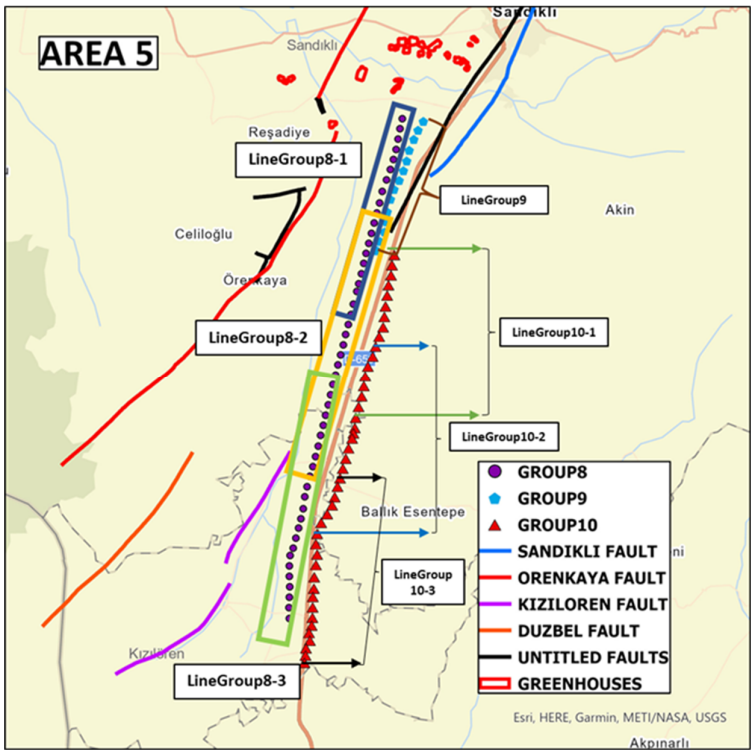
AREA 5
Sandıklı
Reşadiye
LineGroup8-1
LineGroup9
Akin
Celiloğlu
LineGroup8-2
LineGroup10-1
LineGroup10-2
GROUP8
GROUP9
GROUP10
SANDIKLI FAULT
ORENKAYA FAULT
KIZILOREN FAULT
DUZBEL FAULT
UNTITLED FAULTS
GREENHOUSES
Balık Esentepe
LineGroup 10-3
LineGroup8-3
Esri, HERE, Garmin, METI/NASA, USGS
Akpınarlı

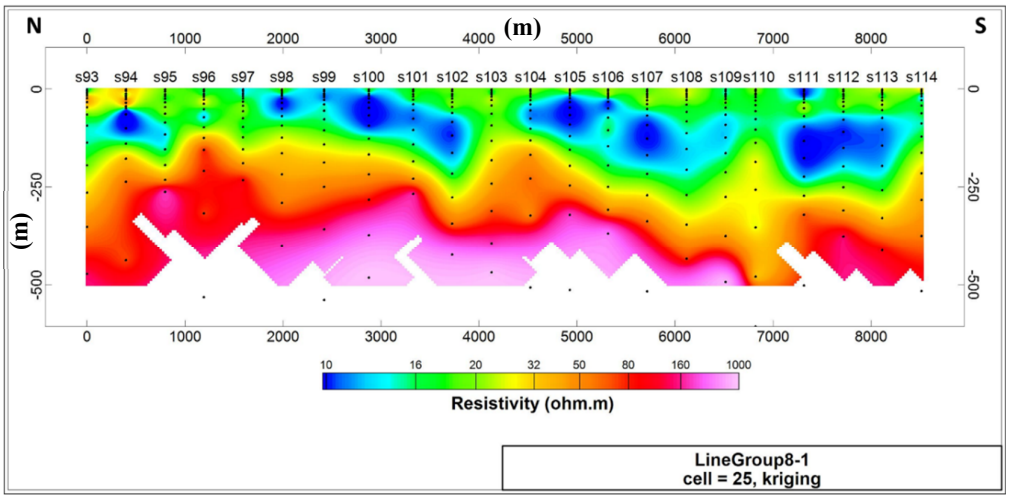
N
S
(m)
0
1000
2000
3000
4000
5000
6000
7000
8000
s93 s94 s95 s96 s97 s98 s99 s100 s101 s102 s103 s104 s105 s106 s107 s108 s109 s110 s111 s112 s113 s114
-250
-500
10
16
20
32
50
80
160
1000
Resistivity (ohm.m)
LineGroup8-1
cell = 25, kriging

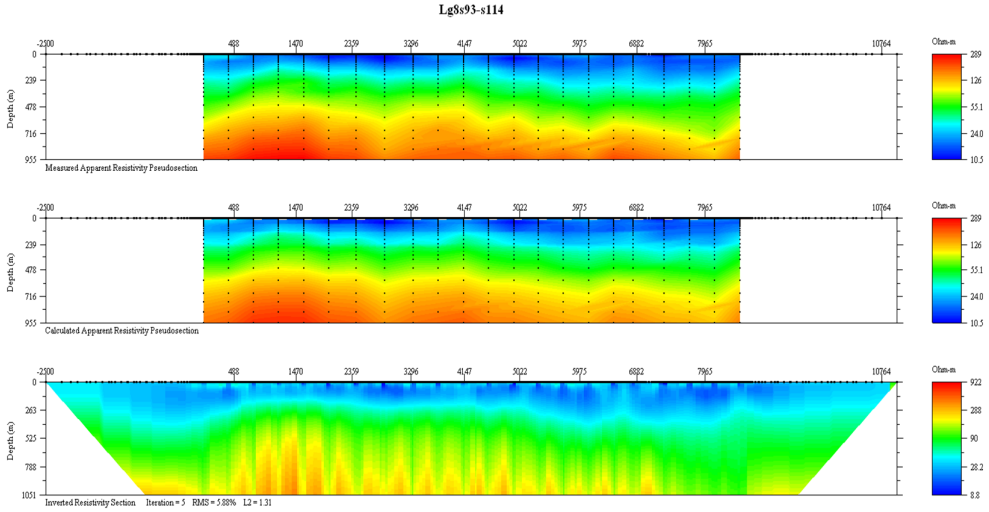

1D rolling and 2D inversion models of LineGroup8-1.

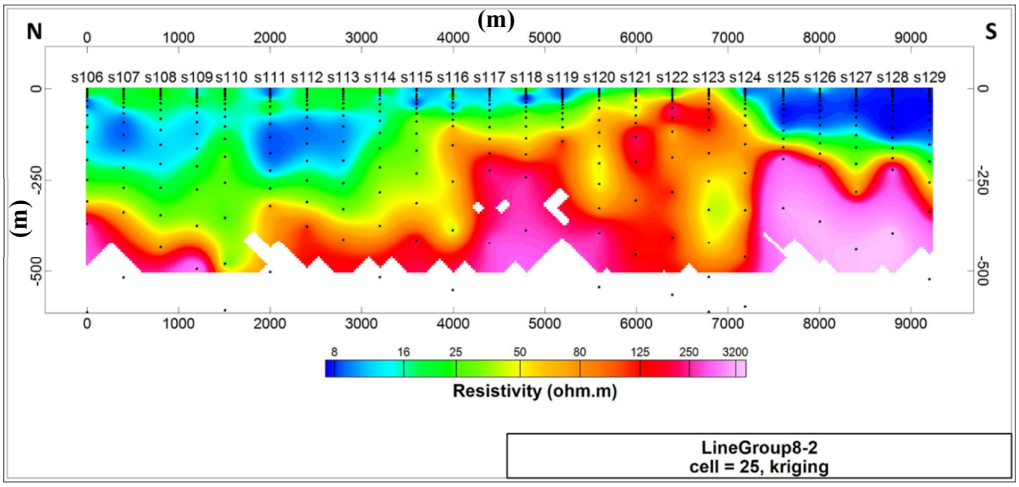

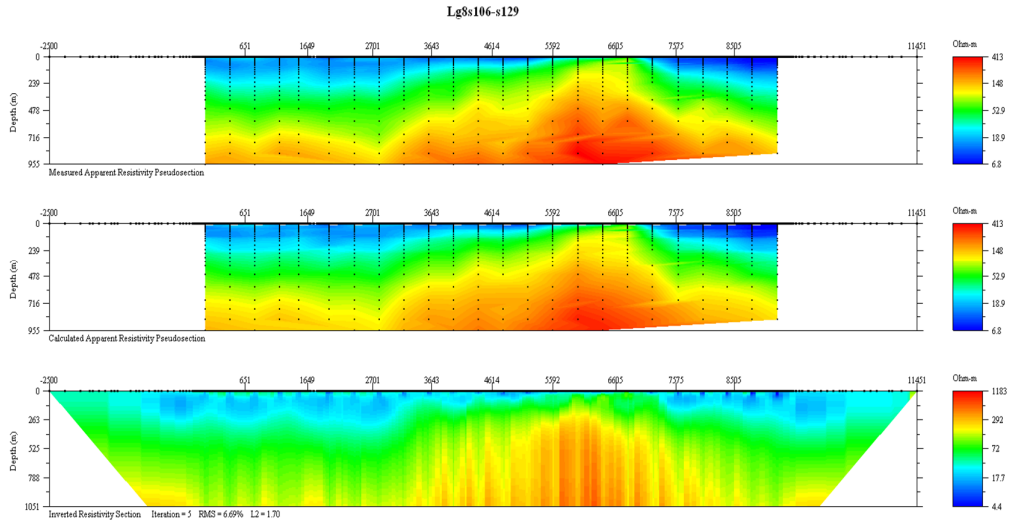

1D rolling and 2D inversion models of LineGroup8-2.

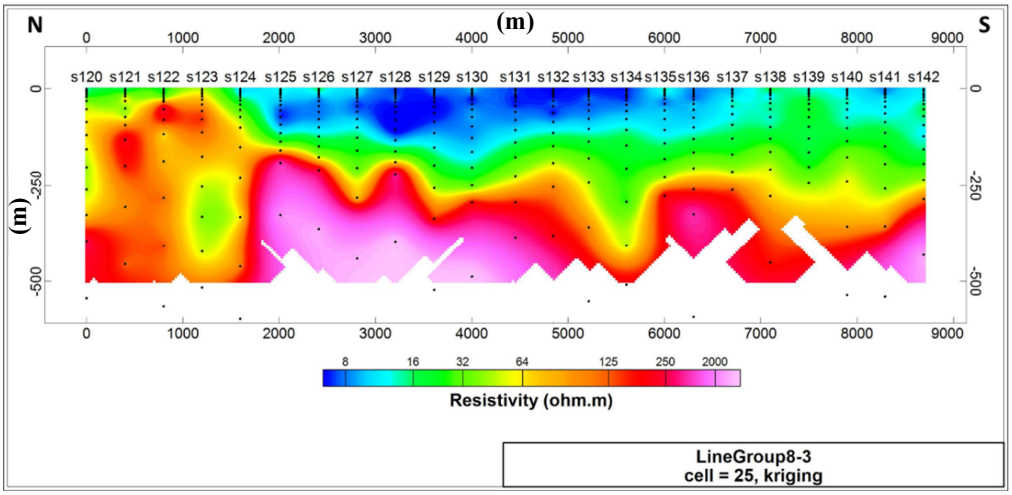

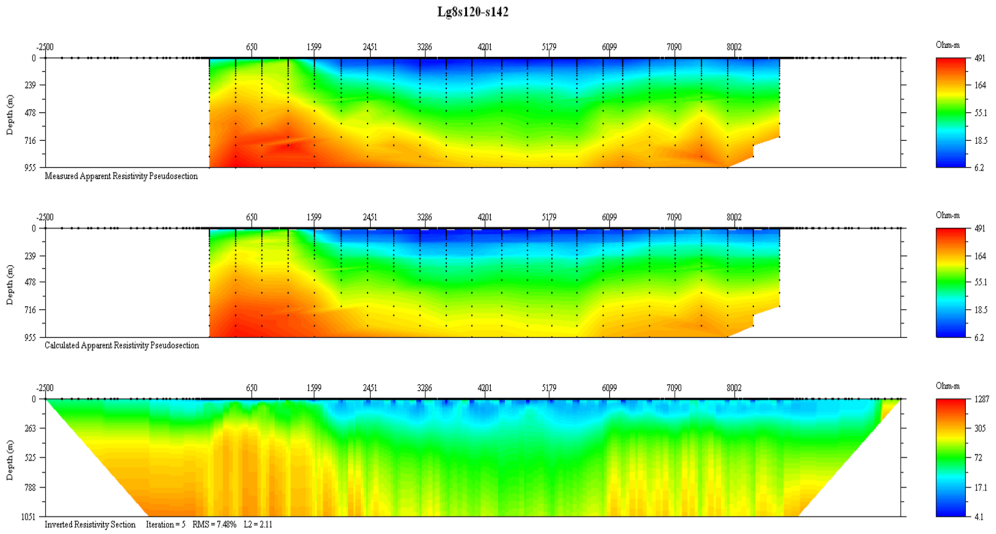

1D rolling and 2D inversion models of LineGroup8-3.

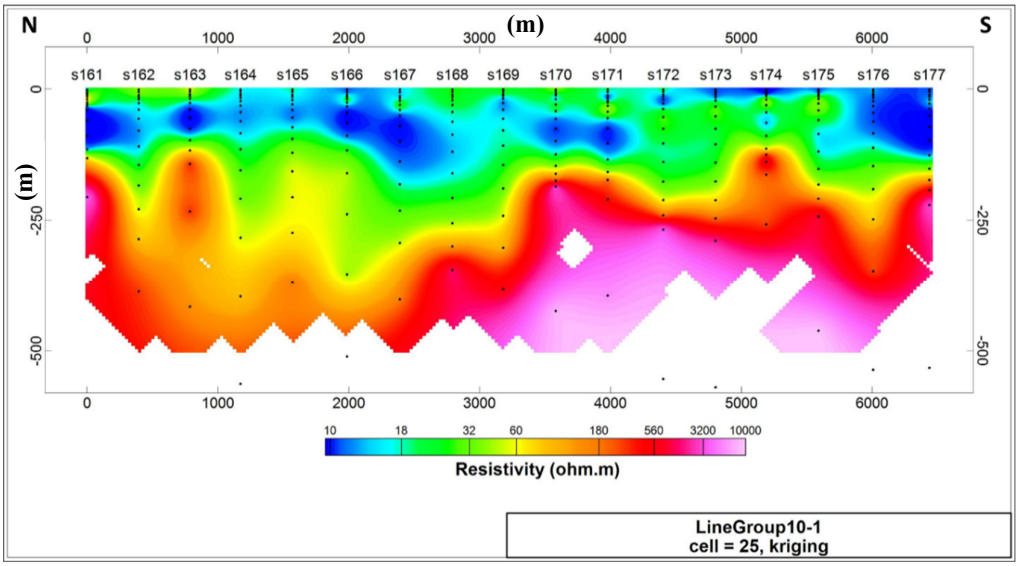

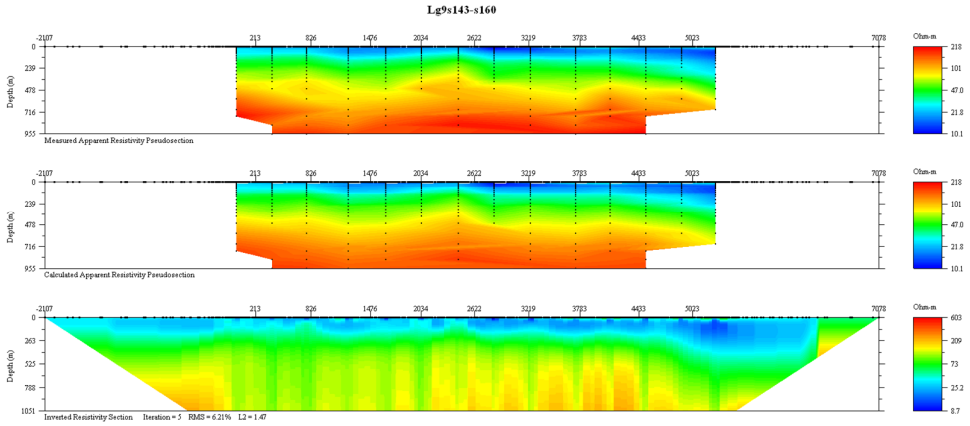

1D rolling and 2D inversion models of LineGroup10-1.

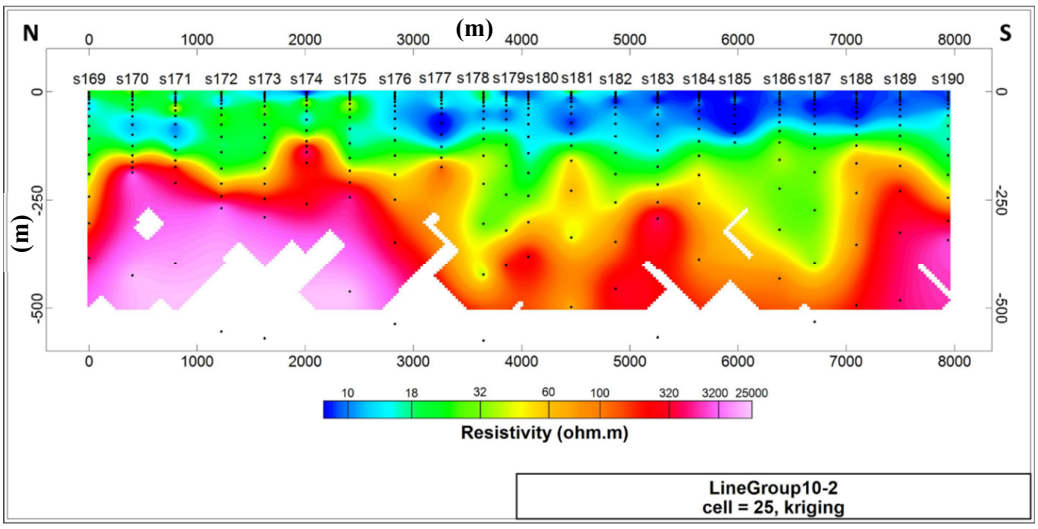

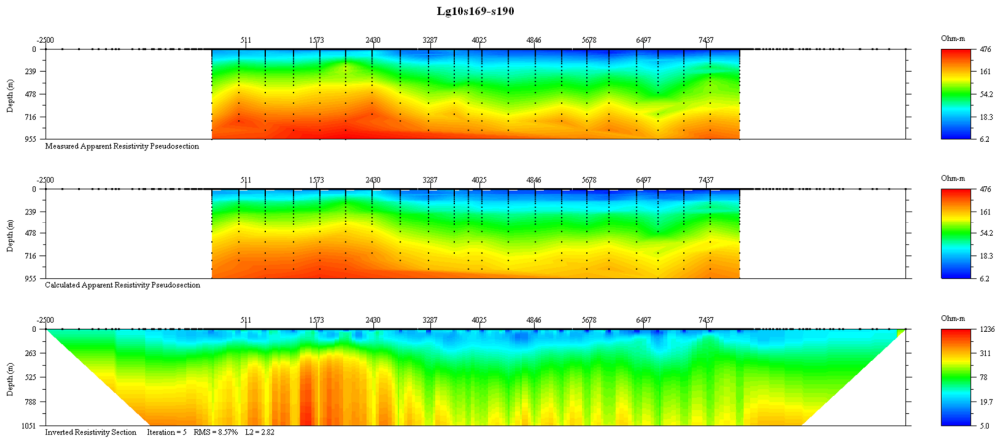

1D rolling and 2D inversion models of LineGroup10-2.

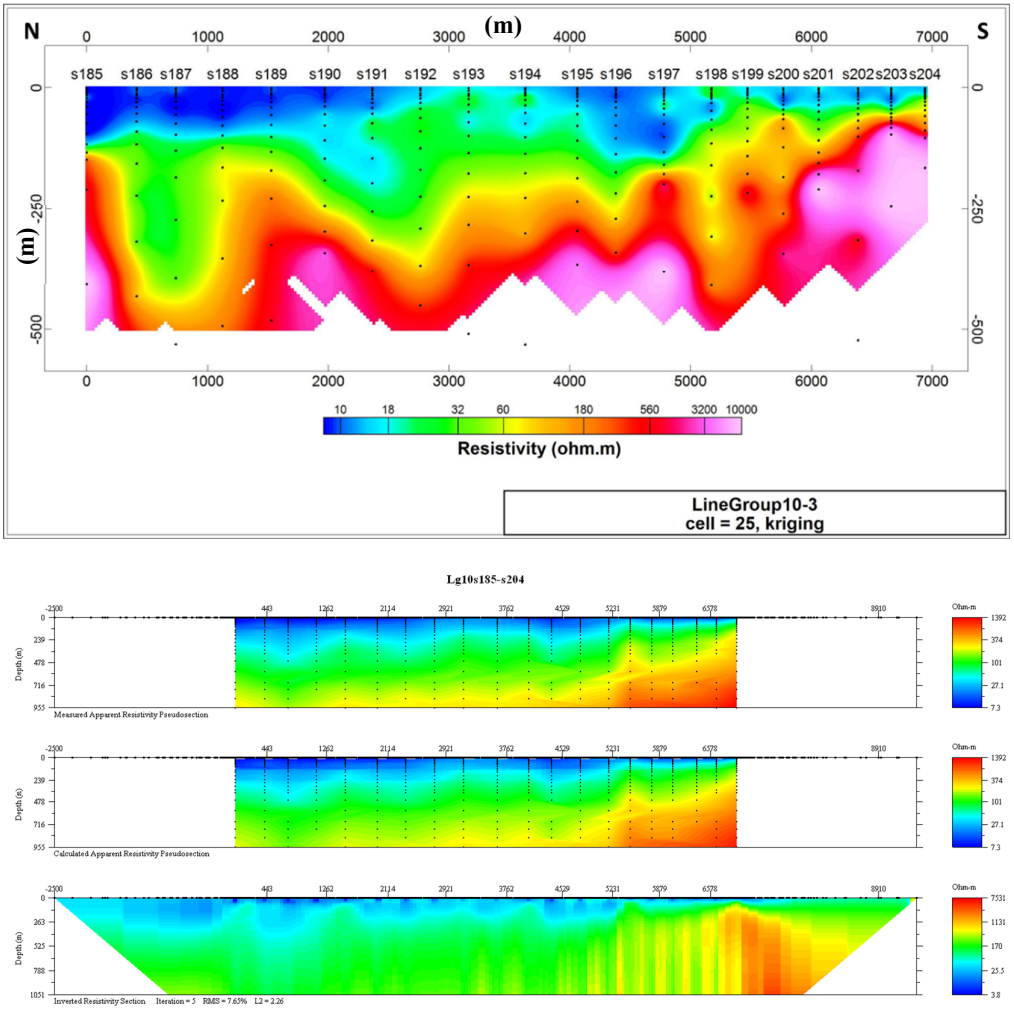

1D rolling and 2D inversion models of LineGroup10-3.

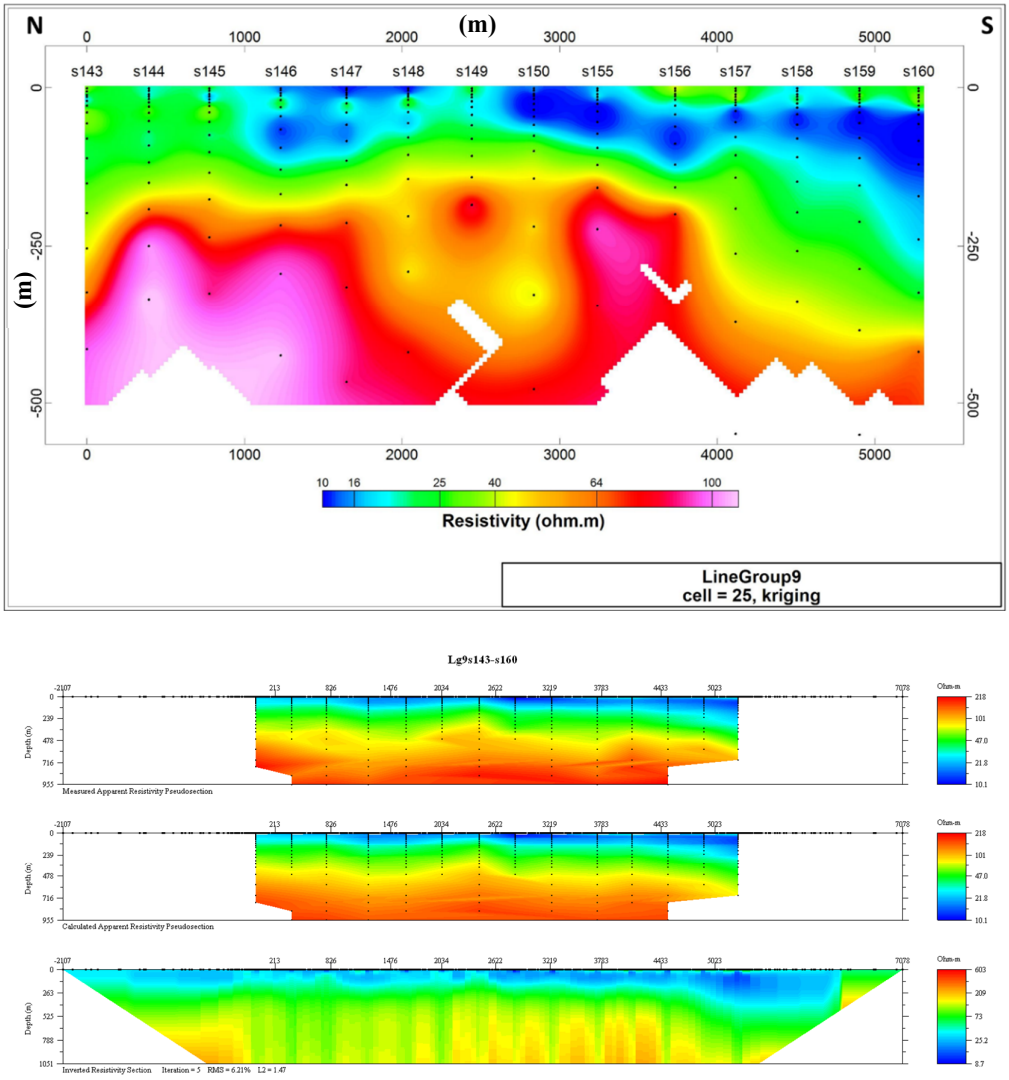

1D rolling and 2D inversion models of LineGroup9.